# THE PROTEROZOIC GRANULITE FACIES TERRANE AROUND KLIPRAND, NAMAQUALAND METAMORPHIC COMPLEX

by

HANS-MARTIN ALBAT

Thesis submitted in fulfilment of the requirements for the degree of Doctor of Philosophy in the Faculty of Science of the University of Cape Town

Department of Geology

1983

## ABSTRACT

The basement rocks of an area of some 8000 $km^2$ around the village of Kliprand in Namaqualand have been geologically mapped. These form part of the extensive Proterozoic Namaqualand Metamorphic Complex and comprise a supracrustal sequence of metavolcanics and metasediments (calcareous, pelitic, semipelitic, quartzose, quartzo-feldspathic, ferruginous and mafic rock units) and a variety of intrusive rocks of differing ages and ranging in composition from granitic to ultramafic. Charnockite and charno-enderbite feature prominently amongst the most commonly recorded intrusive rocks. There is at present no consensus regarding the actual ages of the various rock types, but the ages between 1200-2000 Ma are consistent with current geochronology and lithostratigraphic correlations.

Three episodes of folding ($D_2$-$D_4$) deform the regionally developed gneissic banding which itself may be of tectonic origin ($D_1$). The superimposition of these folds created a complex interference pattern in which modified basin-and-dome-type structures feature prominently. Folding was accompanied and followed by shearing yielding tectonic slides and discrete shear zones formed by dextral and sinistral shear couples. The dextral shear zones strike west-northwest and east-northeast, while their sinistral equivalents strike east, northeast and north-northwest to north.

Deformation was accompanied by regional metamorphism attaining granulite facies grade and transforming the pre-existing lithologies into gneisses. The metamorphism appears to involve one major thermal event comprising several episodes of recrystallisation which are closely related to the deformation. This event culminated during $D_2$ deformation and progressively younger structures appear to have associated mineral assemblages indicative of progressively lower grade metamorphism.

Two major prograde metamorphic zones are recognised; a southern granulite facies zone covering the bulk of the area and a northern zone characterised by amphibolite facies mineralogy. The transition between these zones is largely concealed, but the available evidence suggests that the facies boundary coincides approximately with 29° 49'S latitude. The metamorphic zonation is defined by the mineral assemblages recorded in metamorphosed basic rocks with two pyroxene-bearing granolites giving way to clinopyroxene and/or sphene-bearing amphibolites in the north. Evidence supporting a decreasing metamorphic grade across the area from the south to the north is further documented by the change in Z-absorption colour of hornblende from brown/brownish-green to green, the changing chemistry of hornblende and the change in Z-absorption

colour of biotite from red/red-brown to brown.

Extensive quantitative geothermometry indicates that the peak temperatures attained in the granulite facies zone fall into the range of 700-900°C. Attention is drawn to the fact that the temperatures derived from compositions of coexisting pyroxenes are somewhat higher that those determined for the pelitic rocks and it appears that the pyroxene geothermometers are not very sensitive on the lower temperature side, indicating temperatures that are too high. Feldspar geothermometry on the other hand, yields unrealistically low results.

Regional metamorphism took place under relatively low pressures as suggested by the stable coexistence of "orthopyroxene + plagioclase" in metabasites, the coexistence of "plagioclase + olivine" in mafic/ultramafic rocks, and the abundance of cordierite in addition to the lack of kyanite in pelitic rocks. The chemistry of hornblende, in particular the $Al^{VI}/Si$ ratio, and the chemical compositions of garnet ($almandine_{57-68}$ $pyrope_{27-38}$ $grossular_{2-4}$ $spessartine_{1-4}$) in pelitic rocks support this conclusion. Quantitative geobarometry utilising garnet-plagioclase and garnet-cordierite equilibria indicates a maximum pressure of the order of 5-6 Kb for the granulite facies zone.

Some of the metamorphic minerals are characterised by a compositional zonation related to retrogression. This feature has major implications to quantitative geothermometry/geobarometry and applies particularly to garnet.

Under the high temperature conditions prevailing during metamorphism gneisses with appropriate composition were subjected to *in situ* partial melting generating migmatites. The leucosomes are garnet-bearing and are recorded over an extensive part of the area, but are most conspicuous in the granulite facies zone. In such a relatively "dry" environment the breakdown of hydrous minerals may aid the melting process through their release of water. The temperatures estimated have certainly exceeded the vapour-absent muscovite melting curve and they were also high enough to initiate melting in biotite-bearing assemblages in the absence of free water.

By way of discussion it is established to what extent, if at all, the evolution of the Namaqualand Metamorphic Complex can be modelled in terms of the plate tectonic theory. It appears that the most characteristic signatures related to the convergence phase of the Wilson cycle (trench sediments, ophiolites and high pressure-low temperature metamorphism) are not recognised in the exposed part of the mobile belt. This does not imply that a plate tectonic model is not applicable to the evolution of the Namaqualand Metamorphic Complex as the signatures may be concealed by Cape and Karoo sediments. An ensialic model is considered a possible alternative.

CONTENTS

## PREFACE

The mineral abbreviations used in the text are shown in the following table:

| | | | | | |
|---|---|---|---|---|---|
| Ab | - | Albite | Hy | - | Hypersthene |
| Ad | - | Andalusite | Il | - | Ilmenite |
| Al | - | Almandine | Kf | - | K-feldspar |
| Am | - | Amphibole | Ky | - | Kyanite |
| An | - | Anorthite | M | - | Melt |
| Ap | - | Apatite | Ma | - | Magnetite |
| At | - | Anthophyllite | Mu | - | Muscovite |
| Bi | - | Biotite | Ol | - | Olivine |
| Cc | - | Calcite | Op | - | Orthopyroxene |
| Cd | - | Cordierite | Om | - | Opaque Minerals |
| Ch | - | Chlorite | Par | - | Pargasite |
| Co | - | Corundum | Pg | - | Plagioclase |
| Cp | - | Clinopyroxene | Qz | - | Quartz |
| Cz | - | Clinozoisite | Ru | - | Rutile |
| Di | - | Diopside | Sa | - | Sapphirine |
| Do | - | Dolomite | Se | - | Sericite |
| En | - | Enstatite | Si | - | Sillimanite |
| Ep | - | Epidote | Sn | - | Sphene |
| F | - | Fluorite | Sp | - | Spinel |
| Fo | - | Forsterite | St | - | Staurolite |
| Ga | - | Garnet | Tr | - | Tremolite |
| Gr | - | Grossular | V | - | Vapour |
| Hb | - | Hornblende | Wo | - | Wollastonite |
| He | - | Hercynite | Zc | - | Zircon |
| | | | Zo | - | Zoisite |

OTHER SYMBOLS USED:

| | | |
|---|---|---|
| $K_D$ | = | distribution coefficient |
| K | = | equilibrium constant |
| R | = | gas constant |
| G | = | Gibbs energy |
| S | = | entropy |
| H | = | enthalpy |
| V | = | volume |
| $a_1^A$ | = | activity of end-member molecule 1 in phase A |
| $\gamma_1^A$ | = | activity coefficient of end-member molecule 1 in phase A |
| $X_1^A$ | = | mole fraction of end-member molecule 1 in phase A |
| $\Delta$ | = | prefix for change in some property for a balanced reaction (e.g. $\Delta V$ = volume change of a reaction) |
| o | = | superscript for a standard state property |
| T | = | temperature |
| P | = | pressure ($P_{total}$ = total pressure) |
| $P_{H_2O}$ | = | partial pressure of $H_2O$ |
| $P_{fluid}$ | = | fluid pressure |
| f | = | fugacity ($fO_2$ = oxygen fugacity) |
| s | = | sample standard deviation |
| $\bar{x}$ | = | sample mean |
| $\Sigma$ | = | sum of (e.g. $\Sigma$ Fe = $Fe^{+2}$ + $Fe^{+3}$) |
| ln | = | natural logarithm |
| $A^o$ | = | angstrom unit |
| Kb | = | kilobar |
| $^oC$ | = | degrees centigrade |
| $^oK$ | = | degrees kelvin |
| eu | = | entropy unit |

Where an "X" is shown in tables, the presence of a particular mineral is implied without specification of its abundance.

# I INTRODUCTION

## A Regional Tectonic Setting

The area on which this study is based is situated in the north-western part of the Cape Province of South Africa and is generally referred to as Namaqualand and Bushmanland. Latitudes 29°30'S and 31°00'S form the northern and southern boundaries of the study area and on the western and eastern sides the area is bounded by longitudes 18°30'E and 19°00'E respectively. The aerial extent comprises approximately 8000 km$^2$ of which only a small portion contains outcrops of basement gneisses and intrusive rocks, while the remaining parts are covered by Karoo sediments and various types of superficial deposits.

In Fig. 1, the crustal segment studied is shown in relation to the broad tectonic framework of southern Africa. It forms part of a granite-migmatite-gneiss terrane which has been referred to as the Namaqua Mobile Belt (Truswell, 1977), the Namaqua Province (Kröner and Blignault, 1976) or as the Namaqualand Metamorphic Complex (SACS, 1980). The term "province" describes a geographic region which contrasts from the adjacent area(s) in lithology, structure, grade of metamorphism and radiometric age (Kröner and Blignault, *op.cit.*)while "mobile belt" in the sense of Wynne-Edwards (1972) comprises the entire region affected by the Namaqua tectogenesis.

Along the coastal region of Natal, comparable metamorphites are exposed to the north of Port Edward (Truswell, *op.cit.*; Matthews, 1981). These rocks have been thrust northwards onto the southern flank of the Kaapvaal craton (Matthews, 1972) and are considered to form part of a continuous tectonic zone extending from Natal and continuing beneath the Karoo cover to Namaqualand and Bushmanland, the whole being referred to as the Namaqua-Natal Mobile Belt (Anhaeusser *et al.*, 1968). This view is substantiated by similar radiometric ages of ~900 to 1200 Ma (Nicolaysen and Burger, 1965; Burger and Coertze, 1973; Clifford *et al.*, 1975a, 1981; Matthews, *op.cit.*) which characterise the Kibaran orogeny (Clifford, 1970) and is also supported by geophysical investigations (Meyer, 1981) and deep drilling (Truswell, *op.cit.*).

The Namaqualand Metamorphic Complex generally has an east-west structural grain, but recent studies have shown that in the Orange River region between Goodhouse and Upington the Namaqualand Metamorphic Complex bifurcates and yields a smaller northwest-trending belt extending towards Aus and Lüderitz in SWA/Namibia (Blignault *et al.*, 1974).

Polyphase tectonism associated with regional metamorphism (largely of granulite facies grade) and large-scale plutonism are characteristic of the complex (Joubert, 1971a, 1974c; Blignault *et al.*, *op.cit.*) and manifest the

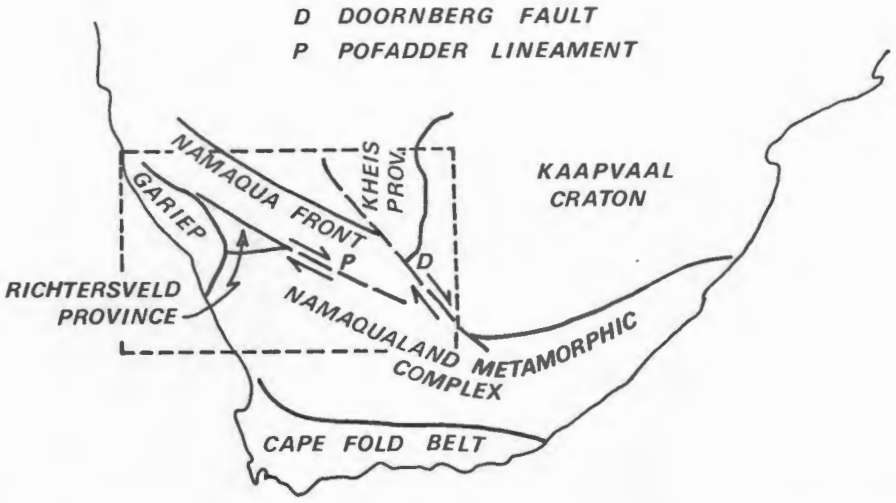


Fig. 1a: The Namaqualand Metamorphic Complex in relation to other tectonic provinces in Southern Africa (after Kröner and Blignault, 1976; Stowe, 1982).

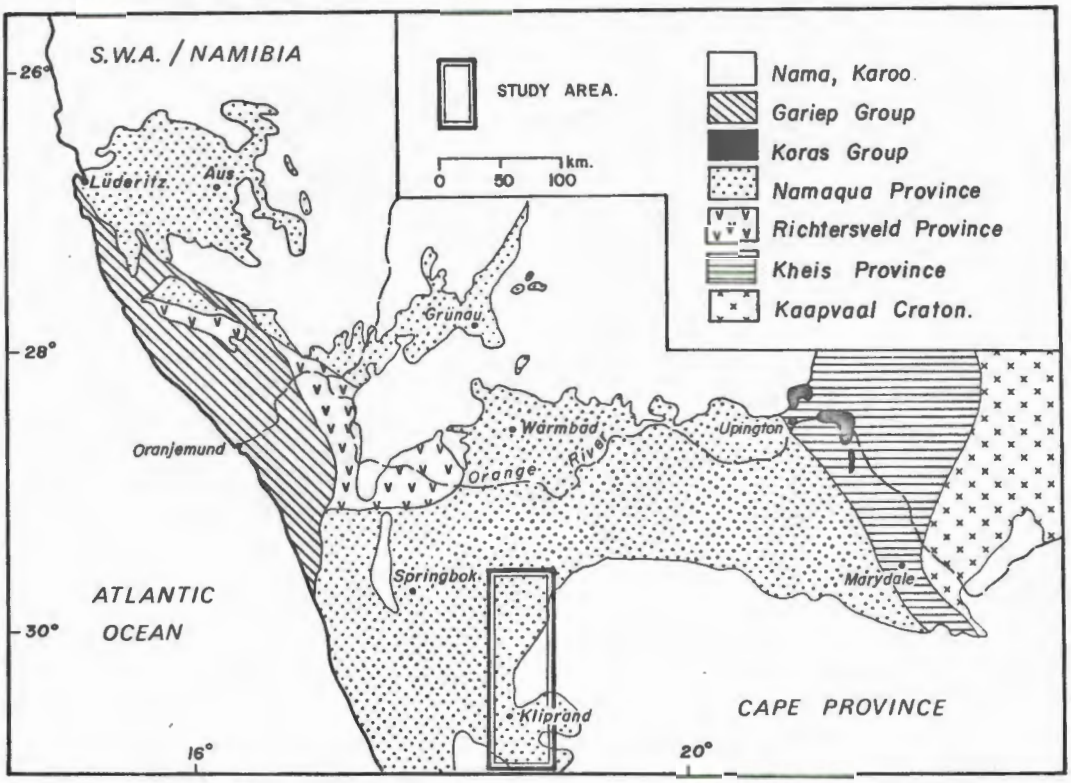


Fig. 1b: Enlarged sketch of the rectangular section in Fig. 1a showing the regional setting of the study area.

unstable nature of this belt in the past.

The Namaqualand Metamorphic Complex encloses a wedge-shaped crustal segment in the lower Orange River region (Vioolsdrif area) which comprises the Orange River Group - a volcano (calc-alkaline) - sedimentary succession (Blignault, 1977; Reid, 1977; Ritter, 1980) intruded by the Vioolsdrif Suite, a fully differentiated and apparently genetically related basic to acid igneous sequence attaining batholithic dimensions (Blignault, *op.cit.*). These rocks display distinctly different structural, geochemical and radiometric age patterns to the surrounding gneisses and are, therefore, considered to constitute a separate tectonic province - the Richtersveld Province (Blignault, 1974a,b; Kröner and Blignault, *op.cit.*). Its southern boundary is an intensely foliated zone which could represent a thrust zone (Theart, 1980) and the northern boundary is complicated by major northwest-trending shear zones (Blignault *et al.*, *op.cit.*; Toogood, 1976). Regional metamorphism within the Richtersveld Province is low to medium grade (Blignault, 1974b; Ward, 1974; Ritter, *op.cit.*) and increases across the boundary with the Namaqua Province both in a southerly and northeasterly direction (van Aswegen, 1981; Blignault *et al.*, *op.cit.*). The volcanic rocks of the Haib Subgroup are considered to have extruded about 2000 Ma ago (Reid, 1979a) and the Vioolsdrif batholith yields Rb-Sr and Pb/Pb isotopic data suggesting an age of emplacement between 1700 and 1900 Ma (Reid, 1979b).

A younger volcano-sedimentary sequence (Gariep-Group) of late Precambrian age is exposed along the west coast where it unconformably overlies the Namaqua and Richtersveld Provinces. These rocks apparently were deposited in a trough (geosyncline) formed by subvertical shear movements (Joubert, 1971a; Joubert and Kröner, 1972; Kröner, 1974) which could be related to tension caused by the late Precambrian break-up of the Kalahari-Brazil plate (Kröner *et al.*, 1973; Kroner, *op.cit.*) and subsequently these rocks were deformed during the Pan-African orogeny (Kröner, *op.cit.*). They are considered to be younger than the 1000 Ma-old pegmatites (Martin, 1965), but the age of the basal part of the Gariep Group is still controversial. Kröner (*op.cit.*) and Allsopp *et al.*, (1979) have argued in favour of a 900 Ma age for the lower Stinkfontein Formation, while Ritter (1980) advocates a 700 Ma age on account of petrographic and field relationships.

The eastern boundary of the Namaqua Province lies in sheared contact with the Kaapvaal craton (Pretorius, 1974), a crustal segment that was relatively stable since the end of the Archaean apart from gentle vertical tectonics during the Proterozoic, leading to the formation of intracratonic basins in which vast amounts of sediments accumulated with extensive intrusive and extrusive igneous activity (Truswell, *op.cit.*).

In the Upington-Marydale area the marginal position between the Namaqua Province and the Kaapvaal craton is occupied by the Kheis Province (Kröner and Blignault, *op.cit.*)which is essentially underlain by metasediments and metavolcanics (Vajner, 1974). The inter-relationships between these tectonic provinces have recently been elucidated within the frame of the National Geodynamics Project (Upington Geotraverse) (Vajner, *op.cit.*) van Bever Donker, 1980; van Zyl, 1981; Stowe, 1979, 1980, 1981). Considerable controversy

revolves around the age of these rocks. Vajner (*op.cit.*) considered the "Kheis Group" to pre-date the Archaean Skalkseput and Draghoender granites on account of their intrusive relationship with the "Marydale Formation", but the antiquity of the overlying Kaaien Group has subsequently been questioned (Botha *et al.*, 1976; Linström, 1977; Smit, 1977). It is now known that the Marydale and Kaaien Groups are separated by an unconformity (Stowe *pers.comm.*). A Pb/Pb isochron age of ~3000 Ma for the Modderfontein iron formation (Cornell and Barton, 1979) is considered to be a minimum age for the Marydale Group. The overlying Kheis Group in contrast is regarded to be younger than 2100 Ma (SACS, 1980) and most probably of comparable age to the Richtersveld Province. The metamorphism in the Kheis Province is of fairly low grade, but increases rapidly westwards towards the Namaqua Province (Vajner, *op.cit.*; Linström, *op.cit.*; Smit, *op.cit.*; Botha and Grobler, 1979; van Zyl, *op.cit.*) across a zone which is complicated by overprinting and extensive shearing (Vajner, *op.cit.*).

East of Upington a virtually unmetamorphosed volcano-sedimentary sequence (Koras Group) unconformably overlies the folded Kheis Group and according to Grobler *et al.*, (1977) the calc-alkaline volcanics and immature sediments accumulated in graben-like troughs that formed subsequent to the Namaqua tectogenesis. The volcanic rocks have yielded radiometric ages in the region of 1100-1200 Ma (van Niekerk and Burger, 1967; Kröner *et al.*, 1977; Botha *et al.*, 1979a).

The southern boundary of the Namaqualand Metamorphic Complex is concealed by a cover of younger sediments involving correlates of the Nama Group, the Cape Supergroup and the Karoo Sequence.

## B. Previous Work

Geological literature on the study area is virtually non-existent and the available publications are either concerned with areas of economic interest as, for example, the Steenkampskraal monazite deposit (Pike, 1959) which has been dated at 1180 ± 40 Ma (Nicolaysen and Burger, 1965) or with aspects of the post-Mokolian geology involving the Nama Group (Rogers, 1913; Kröner, 1968), the Karoo Sequence (Hälbich, 1962), kimberlites and post-kimberlite sediments (Reuning, 1931; Cornelissen and Verwoerd, 1973, 1975), melilite basalts (Rogers, 1912; Taljaard, 1937; Moore, 1979) and erosion surfaces (Mabutt, 1955). The literature on other parts of the Namaqualand Metamorphic Complex surrounding the area investigated is, however, voluminous and aids in conveying the broad regional tectono-thermal development of this terrane.

Initial interest in the area between the lower Orange River and Bitterfontein was focused on the copper deposits in the Nababeep district (Rogers, 1916). Mining operations and detailed mapping by geologists of the O'okiep Copper Company (Benedict *et al.*, 1964; Marais *et al.*, 1975) have contributed considerably to our understanding of Namaqualand geology. Much of the current research revolves around the Nababeep district (Clifford *et al.*, 1975a,b, 1978, 1981; McCarthy, 1976, 1978).

The Nuwerus-Bitterfontein area and further eastwards has previously been investigated by Brink (1950), Pike (1959), Jansen (1960) and Kröner (1968). Systematic regional mapping, however, only started with Joubert (1971a) who covered some 12 000 km$^2$ adjacent to and west of the study area and who for the first time outlines the broad tectonic and metamorphic framework of Western Namaqualand. Subsequent studies south of Springbok (Zelt, 1975, 1978, 1980), however, demand some adjustments to the original metamorphic zonation model suggested by Joubert (*op.cit.*). Jack (1980) has investigated a large area west of Garies, while Theart (1980) and van Aswegen (1981) have concentrated on the geological aspects north of Springbok. The geology of the Richtersveld Province is also well documented (de Villers and Söhnge, 1959; von Backström and de Villiers, 1972; Ward, 1973, 1974, 1977; Bertrand, 1975; Reid, 1977; Ritter, 1980).

Bordering onto the study area in the north is the terrane between Pofadder, Onseepkans, Goodhouse and Aggeneys which is largely underlain by a supracrustal sequence of metasediments and metavolcanics collectively referred to as the Bushmanland Group (SACS, 1980). Initially, this area had been studied by Coetzee (1942a,b) who concentrated on a small portion west of Pella along the Orange River and the work was extended by von Backström and de Villiers (1972). Joubert mapped an extensive area between Pofadder and Aggeneys (the map was released at the 16th Geocongress of the Geological Society of South Africa) and outlines various geological aspects (Joubert, 1971b, 1973, 1974a,b,c, 1976). Certain parts of the area were investigated in more detail, for example, the Namiesberg (Moore, 1977), Gamsberg (Rozendaal, 1978) and the Aggeneysberge (Lipson, 1978). An extensive area south of Pofadder has also been studied by Paizes (1975).

Further east towards the margin of the Kaapvaal craton in the Kakamas-Kenhardt-Upington-Prieska area the early geological investigations by Rogers and Schwarz (1900) and Rogers and du Toit (1910) were extended by Poldervaart and von Backström (1949) and von Backström (1962, 1964, 1967) and in recent years this area forms the focal point of discussion concerning the craton-mobile belt relationships (Geringer, 1973; Vajner, 1974; Pretorius, 1974; Cornell, 1975; Botha *et al.*, 1976, 1977, 1979b; Geringer and Botha, 1977; Linström, 1977; Smit, 1977; Grobler *et al.*, 1977; Joubert, 1978; Botha and Grobler, 1979; Stowe, 1979, 1980, 1981; van Bever Donker, 1980; van Zyl, 1981).

Across the border into southern SWA/Namibia, Namaqualand-type rocks have been traced all the way to Lüderitz (Beukes, 1973; McDaid, 1975, 1978; Blignault *et al.*, 1974; Jackson, 1976; Toogood, 1976; Blignault, 1977).

From the economic point of view, the Namaqualand Metamorphic Complex has proved to be of considerable potential and this is reflected in many publications. The famous cupriferous "noritoid" bodies of the Nababeep district (Rogers, 1916; Benedict *et al.*, 1964) were the first significant economic discoveries. Intensive prospecting in recent years has revealed several other major base metal deposits and these include Broken Hill at Aggeneys (Lipson, 1978; Wilson, 1981), Gamsberg (Rozendaal, 1978) and the Prieska Copper Mine at Copperton (Middleton, 1976). Besides these, other

mineral deposits have attracted interest such as alluvial diamonds, monazite on Steenkampskraal (Pike, 1959), tungsten at Nababeep and Upington (Söhnge, 1950; von Backström, 1950), barite at Gamsberg (Mathias, 1940; Coetzee, 1958), sillimanite and corundum-sillimanite near Pella (Coetzee, 1940; de Jager and von Backström, 1961; de Jager, 1963; Frick and Coetzee, 1974), wollastonite near Garies (de Jager and Simpson, 1962) and various pegmatite minerals (beryl, spodumene, scheelite, tantalite/columbite and rare earth minerals) encountered within the pegmatite belt of the north-western Cape Province (Gevers *et al.*, 1937; Hugo, 1969; von Backström, 1973).

Geophysical studies on the Namaqualand Metamorphic Complex have contributed to reveal some of the deep-seated crustal phenomena. Van Zijl (1978) has studied the deep electrical resistivity structure of the crust along a traverse between Upington and Kamieskroon and this has disclosed a rather interesting crustal zonation pattern. An east-west conductor underlying the deep Karoo trough in the southern Cape Province has been detected by means of magnetometer array studies (de Beer, 1978; de Beer and Gough, 1980) and is considered to represent oceanic crust which makes it tempting to speculate that this could coincide with the southern margin of the Namaqualand Metamorphic Complex and accordingly represents a potential subduction zone during the Namaqua tectogenesis (*ibid.*). Related geophysical anomalies are discussed by de Beer *et al.* (1974). A regional gravity survey of the region to the east of the study area has recently been released by Meyer and Duvenhage (1981).

Despite some controversial results, geochronology has aided tremendously in elucidating the timing of various events within and around the Namaqualand Metamorphic Complex. The approximate 2000 Ma age of the Haib volcanics (Reid, 1979a) and the 1900-1700 Ma Rb-Sr and Pb-Pb whole rock isotopic ages of the Vioolsdrif composite batholith (Reid, 1979b) point toward the greater antiquity of the Richtersveld Province compared to the surrounding Namaqualand gneisses, which in the Nababeep district have yielded much younger ages in the approximate range of 1100-1200 Ma (Clifford *et al.*, 1975, 1978, 1981) which are similar to those previously recorded (Nicolaysen and Burger, 1965; Burger and Coertze, 1973). Ages comparable to those of the Vioolsdrif batholith (1700-1800 Ma) have recently been determined for grey gneisses (Gladkop suite) in the Steinkopf area (Barton *et al.*, 1981; Reid and Barton, 1982).

Along the northeastern boundary of the Namaqualand Metamorphic Complex a minimum age for the deformation and metamorphism is provided by the post-tectonic Koras Group dated at 1180-1150 Ma (Kröner *et al.* 1977; Botha *et al.* 1979a).

Gamsberg, Aggeneys and Copperton ore deposits have yielded Pb-Pb ages in the range of 1200-1500 Ma (Köppel, 1978, 1980; Cornell, 1975, 1978) and Köppel (*op.cit.*) has concluded that provided the ore bodies dated are syngenetic, the Bushmanland Group cannot be older than 1500 Ma. This conclusion is subsequently challenged by Reid (1981) who, on the basis of Sm-Nd isotopic studies on a large variety of rock types from widely separated localities, demonstrates the preponderance of 1900-2000 Ma model ages and

suggests a temporal equivalence between the Namaqua and Richtersveld Provinces. Apparently, the Sm-Nd system has the advantage over other conventional isotopic systems in that it tends to remain undisturbed even during quite intense metamorphism (*ibid.*).

## C Present Investigation

This study forms part of a mapping project of the Precambrian Research Unit under contract to the Geological Survey of South Africa and is aimed at completing the regional mapping of the Namaqualand Metamorphic Complex on a reconnaissance basis.

The regional geology of the study area was virtually unknown prior to the commencement of this survey. Only a few scattered localities, some of economic interest, were previously investigated. These circumstances demand a rather broad scope of the present investigation which involves the following aspects:

1. Mapping of the basement rocks over an area of approximately 8000 $km^2$.

2. A careful study of the mineral assemblages in potentially useful rock types with the aim to elucidate the metamorphic history and metamorphic zonation of the terrane.

3. To determine chemical compositions as well as chemical zonations of a variety of minerals in order to establish regional changes in mineral chemistry and to quantify the P-T conditions of regional metamorphism by applying thermodynamic principles in modern geobarometry and geothermometry.

4. To investigate the structural history of the area and to establish the relationship between deformation and metamorphism.

Field mapping was carried out during two consecutive periods. The southernmost two thirds of the area was completed during the months of March, 1978 to February, 1979 and the remainder was mapped between April, 1980 and June, 1980. Monochrome aerial photographs of an approximate 1:60 000 scale were provided by the Geological Survey and the mapping was done initially on transparent overlays, three of which were used per photograph for lithology, structural data and sample localities respectively. The geology was subsequently transferred by optical projection onto twelve 1:50 000 scale topographic map sheets published by the Government Printer. These maps were then reduced to a scale of 1:100 000 and redrawn onto a stable-base film with a fixed co-ordinate grid.

Systematic mapping was preceded by a photogeological interpretation and some reconnaissance in the vicinity of Kliprand, the major settlement in the area. The field work was aided by the availability of a Land Rover, the high density of roads and tracks providing good access and the magnificent co-operation of the local farmers. Unfortunately, the enormous size of the

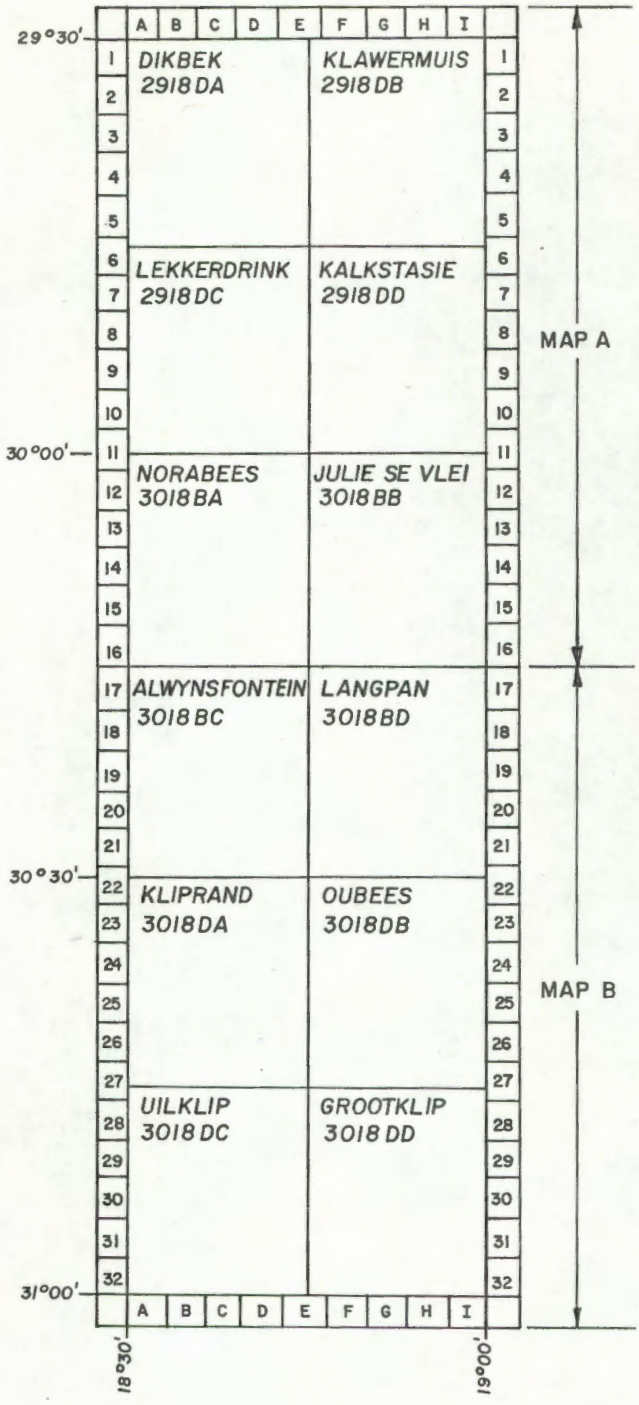


Fig. 2: Sketch showing the twelve 1:50 000 topographic sheets with names and numbers split into two sections, map A and map B.

area and the short time period available placed considerable limitations on detailed studies and demanded the mapping to be carried out at great speed. For the sake of convenience, the map has been split up into a northern and southern sheet, each covering the area of six 1:50 000 topographic maps and these will be referred to, respectively, as map A and map B (Fig. 2) throughout the thesis.

Laboratory work involved various aspects. Thin sections of all the rock units were studied microscopically to establish the general petrology. As previous studies in adjacent areas have indicated a pronounced north-south metamorphic zonation pointing towards a transition from the granulite facies to amphibolite facies terrane somewhere within the study area, the sampling programme was aimed at locating this boundary and involved the careful microscopic study of the mineral assemblages recorded in potentially useful rock types collected at relatively close intervals (where outcrop permitted) throughout the entire region. A large number of thin sections of a variety of quartzo-feldspathic rocks were stained by the method outlined in Appendix 1A and this aided in the rapid identification of the feldspars during modal analyses. Chemical compositions of minerals was established with the aid of the Cambridge 5 electron microprobe of the Geochemistry Department at the University of Cape Town and was largely utilised in the quantitative evaluation of the P-T conditions attained during regional metamorphism.

The mapping revealed an extensive terrane of lower crustal materials and it is, therefore, not unexpected that the main thrust of this study is directed towards the elucidation of some of the geological phenomena recorded in the deeply eroded crust of the Namaqualand Metamorphic Complex. At the same time, it was considered desirable to describe the various rock types in view of the fact that the area had not been studied previously.

## D Acknowledgements

Professor A. J. Erlank played a vital role during my initial application as a Ph.D. candidate and his recommendation is sincerely appreciated. The project was initiated and supervised by Professor P. Joubert, Director of the Chamber of Mines Precambrian Research Unit, and for his patience, reading of the manuscript and constructive and helpful criticism, I am much obliged.

My understanding of metamorphic petrology would still be latent if it was not for the valuable contribution made by Dr. D. J. Waters of the Department of Earth Sciences, University of Cape Town, who introduced me to the application of thermodynamics to metamorphic petrology and for his stimulating lecture course and many subsequent discussions, I am most grateful.

During the course of study, I received considerable help from my colleagues Dr. N. E. Odling, Dr. C. W. Stowe, Dr. C. J. H. Hartnady, Dr. C. Z. van Zyl, Dr. U. Ritter, Mr. J. M. Moore, Mr. A. M. Jack and Mr. H. F. J. Theart, to whom I express my appreciation. In particular, I am

indebted to Dr. K. W. Kasch for his constructive help, stimulating discussions and moral support.

Research facilities were made available by the Precambrian Research Unit and the Department of Geochemistry at the University of Cape Town and in this connection I am thankful to Professors P. Joubert, A. J. Erlank, A. M. Reid and A. O. Fuller. Without the teaching ability of Mr. R. S. Rickard, the electron microprobe would still be a mystery to me and I appreciate his skilful instructions and his incredible patience and helping hand during the course of analytical sessions. I am also indebted to Dr. C. J. Hartnady for instruction on the operation of the X-ray diffraction equipment.

The technical staff at the University of Cape Town and in particular, Mr. R. J. Oliver, Mr. D. Wilson, Mr. P. Sieas, Mr. E. Stout and Mr. H. C. F. Hendriks spent many weeks preparing thin sections and for this I am most thankful. I also received help from Mr. S. B. Lawrence and Mr. P. Meyer which I acknowledge.

On the production side I express my sincere appreciation for the skilful efforts of Mrs. E. A. Phillips and Mrs. A. Bateman who kindly typed the manuscripts and tables. The drafting of the figures in the text and the geological map was largely the effort of Mrs. R. M. E. Kovats, but some of the figures were drafted by Miss P. Eloff. I also thank Ms. M. van den Meiracker for her work on the colour separation for the maps.

To all the farmers in the Kliprand area, I express my gratitude for their cooperation and hospitality during fieldwork. In particular, I am thankful to Mr. S. Lazarus of Kliprand for providing free of charge accommodation on his farm Dood Drink. The warming welcome and hospitality by my friends Renate and Jürgen Reck on Gal Puts were also very much appreciated.

Meiner geliebten Frau, Lenchen, gilt mein besonderer Dank für ihre treue Unterstützung und endlosen Ermutigungen während meines Studiums. Danken möchte ich auch meiner Mutter and meinen Schwiegereltern, Ruth and Hans Behr, für ihren Beitrag zum Erfolg. In grosser Dankbarkeit gedenke ich meines verstorbenen Vaters der das Interesse an der Geologie in mir erweckt und gefördert hat.

# II LITHOLOGIC UNITS

## A Introduction

The lithostratigraphic designation Namaqualand Metamorphic Complex includes metasedimentary, metavolcanic and intrusive rocks (SACS, 1980). In the first part of this chapter the petrography of the pre-tectonic volcano-sedimentary sequence is described. Following Turner (1968) and Jackson (1976) these gneisses are grouped on a mineralogical basis into calcareous, pelitic, semipelitic, quartzose, quartzo-feldspathic, ferruginous and mafic metamorphites. The intrusive rocks of Mokolian age are considered next and the remaining part of this chapter deals briefly with the sediments unconformably overlying the gneisses of the Namaqualand Metamorphic Complex as well as intrusives of Phanerozoic age.

## B Namaqualand Metamorphic Complex (Pre-Tectonic Volcano-Sedimentary Sequence)

### 1. Calcareous Metamorphites (Map units Mc, Mm)

These rocks can be classified into two categories namely those that consist essentially of calc-silicate minerals with little or no carbonates as opposed to the second group comprising rocks containing abundant carbonate minerals. These two rock types are respectively referred to as calc-silicate gneiss and marble.

South of latitude 30° 15'S outcrops of calc-silicate gneiss are rare and generally too small to be shown separately on the accompanying geological map. A very small outcrop on the farm Dabidas (407) requires special mention as this represents the only occurrence of a wollastonite-bearing gneiss found during the field examination. This rock occurs as a small body which is completely enclosed by a semipelitic biotite and garnet-bearing migmatite. The interbanding of thin calc-silicate gneiss units and semi-pelitic units is commonly recorded in the area.

North of latitude 30° 00' S calc-silicate gneisses are very abundant and feature prominently on the farms Banken (91), Struisbult (94), Diep Vlei (102) and Koumis (103).

Marble is very rare and the only outcrops encountered during the period of field mapping are recorded on the farm Kat Vlei (235) where boulders and

TABLE 1

Estimated modal compositions (in volume per cent) of calc-silicate gneiss. Retrograde minerals in parenthesis. The epidote group minerals comprise primary and secondary phase. Abbreviations as in preface. (m = <1%)

| Sample No. | clino-pyroxene | plagio-clase | quartz | grandite | epidote group minerals | amphibole | sphene | scapolite | wollas-tonite | calcite | opaque minerals | other = m | locality |
|---|---|---|---|---|---|---|---|---|---|---|---|---|---|
| HA 1105 | 7 | 81 | 11 | | m | | 1 | | | | | | C1 |
| HA 1102 | 10 | 60 | | 29 | m | | 1 | | | | | Ap | D1 |
| HA 1103 | 10 | 66 | 11 | 13 | m | | m | | | | | | D1 |
| HA 1107 | 13 | 29 | 22 | 30 | 1 | | 5 | | | | | | E1 |
| HA 1108 | | 84 | | 12 | 2 | | 2 | | | m | m | Ap | F1 |
| HA 1142 | 5 | 60 | | 30 | 4 | | m | | | m | 1 | | F1 |
| HA 1144 | 7 | 60 | | 32 | m | | m | | | | 1 | Ap | G1 |
| HA 1126 | 13 | 64 | | 22 | m | | 1 | | | | m | Zc | G1 |
| HA 1093 | 3 | 56 | 25 | 12 | 2 | | 1 | m | | | 1 | | D2 |
| HA 1114 | 12 | 22 | 64 | | m | | m | | | | 2 | Ap | I2 |
| HA 1124 | | 72 | 10 | 15 | 3 | | m | | | | m | (Se) | H2 |
| HA 1094 | 41 | 28 | 3 | 20 | | | m | 8 | | | | | D3 |
| HA 1097 | 38 | 11 | 3 | 22 | m | | m | 26 | | | m | | D3 |
| HA 1117 | 60 | 39 | | m | m | | 1 | | | | | (Se) | H3 |
| HA 1132 | 15 | 78 | | 3 | 1 | | 1 | | | | 2 | Ap Zc | C4 |
| HA 1101 | 5 | 79 | | 15 | m | | m | | | | 1 | Ap | D4 |
| HA 1090 | 17 | 24 | 58 | | | | m | | | | 1 | (Se) | E4 |
| HA 1148 | 10 | 55 | | 14 | 20 | | 1 | | | | m | | F4 |
| HA 1085 | 9 | 31 | 60 | m | m | | m | | | | m | Ap (Mu) | H4 |
| HA 1122 | 6 | 61 | | 30 | m | | m | m | | | 3 | Ap | I4 |
| HA 1087 | 5 | 62 | 3 | 28 | m | | 2 | | | | | Ap | F5 |
| HA 1076 | 3 | 86 | 8 | | m | | | | | | 3 | | H5 |
| HA 1078 | 42 | 45 | m | | | m | m | | | | 3 | (Mu) | H5 |
| HA 1140 | 8 | 52 | 21 | 18 | | | 1 | | | | m | Ap Zc | A6 |
| HA 1073 | | 99 | | | m | | | | | | m | (Bi)(Ch)=1% | D6 |
| HA 1009 | 15 | 45 | 39 | | | | m | | | | 1 | (Se) | F6 |
| HA 1082 | 4 | 56 | | 40 | | | | | | m | m | (Mu) | H6 |
| HA 1003 | 10 | 41 | 45 | | | | 1 | | | | 3 | Ap (Mu) | F7 |
| HA 1004 | 26 | 43 | 29 | | | | 1 | | | | 1 | Ap (Se) | F7 |
| HA 1013 | 18 | | 18 | 18 | | | m | 44 | | 2 | m | Ap | F8 |
| HA 1021 | 8 | 15 | 76 | | m | | m | | | | 1 | Ap (Mu) | G8 |
| HA 1027 | 48 | 37 | 14 | m | m | | m | | | m | | Ap (Mu)(Ch) | G8 |
| HA 1061 | 95 | | | | | m | m | 3 | | 1 | m | | C9 |
| HA 1062 | 46 | | | | | | 2 | 52 | | m | | | C9 |
| HA 1022 | 21 | 18 | 59 | | | | | | | | 2 | Zc | I9 |
| HA 1052 | 40 | 60 | m | | | | m | | | | m | (Se) | E10 |
| HA 1031 | 33 | 37 | 21 | 6 | | | 3 | | | | | Ap (Mu) | F10 |
| HA 1038 | 66 | 21 | | 7 | | | m | 6 | | | | | F10 |
| HA 1054 | 72 | 28 | | | | | m | | | | m | | D11 |
| HA 1055 | 46 | 29 | | 25 | | | | | | | m | | D11 |
| HA 1049 | 11 | 12 | 76 | m | | | m | | | | 1 | (Se) | E11 |
| HA 1048 | 6 | 70 | 24 | m | | | m | | | | | | E11 |
| HA 1047 | 16 | 25 | 53 | 6 | m | | | | | m | m | (Se) | E11 |

TABLE 1 (Cont.)

Estimated modal compositions (in volume per cent) of calc-silicate gneiss. Retrograde minerals in parenthesis. The epidote group minerals comprise pri primary and secondary phases. Abbreviations as in preface. (m = <1%)

| Sample No. | clinopyroxene | plagioclase | quartz | grandite | epidote group minerals | amphibole | sphene | scapolite | wollas-tonite | calcite | opaque minerals | other = m | locality |
|---|---|---|---|---|---|---|---|---|---|---|---|---|---|
| HA 1034 | 62 | 33 | 5 | | | | m | | | | | | E11 |
| HA 1033 | 60 | 38 | | | | m | m | | | | 2 | Zc | E11 |
| HA 1035 | 63 | 34 | | | m | | 1 | | | | 2 | (Mu) | E11 |
| HA 1043 | 51 | 46 | m | | | | m | | | | 3 | (Se)(Ch) | F11 |
| HA 459 | 6 | | m | 4 | m | | 1 | 89 | | m | m | Ap (Ch) | B21 |
| HA 438 | 15 | 80 | m | | | | 3 | | | | 1 | Ap Zc Kf=1% | B21 |
| HA 439 | 7 | 83 | 8 | | | | 1 | | | | 1 | (Ch)(Se) | B21 |
| HA 979 | 10 | 80 | 9 | | | | 1 | | | m | m | (Se) | C21 |
| HA 44 | | | | | 8 | 92 | | | | m | | | C22 |
| HA 1150 | | | 10 | | 8 | 82 | | | | | | | C22 |
| HA 1151 | 83 | 7 | 10 | | | | m | | | | | | C22 |
| HA 1152 | 30 | 54 | 10 | 3 | | | 3 | | | | | | C22 |
| HA 1153 | 40 | 50 | | 10 | m | | 3 | | | | | (Se) | C22 |
| HA 1156 | 50 | 15 | 35 | | | m | m | | | m | | (Se)(Mu) | C22 |
| HA 263 | 84 | 12 | 4 | | | m | m | | | m | m | Ap (Se) | D22 |
| HA 997 | | | 1 | | | 99 | | | | | | | D22 |
| HA 1155 | 2 | m | 1 | | m | | m | 2 | 95 | m | | Ap | D22 |
| HA 1157 | 99 | | 1 | | | | m | | | | | | D22 |
| HA 376 | 32 | 67 | m | | | | 1 | | | | m | Ap (Ch) | B24 |
| HA 930 | 10 | 59 | 30 | | | | 1 | | | | m | Ap | A25 |
| HA 314 | 15 | 20 | 63 | | m | | 1 | 1 | | m | | Ap (Mu) | C25 |
| HA 604 | 53 | 35 | | 7 | m | | 5 | | | m | | (Se) | H25 |
| HA 618 | 30 | 29 | | | | m | 8 | 32 | | m | m | | H25 |
| HA 917 | 9 | 12 | 79 | | | | m | | | m | | Ap(Se)(Ch) | B26 |
| HA 691 | | 82 | 1 | 7 | | | m | | | | | | F27 |
| HA 694 | 34 | 60 | 5 | | m | | m | | | | 1 | Zc (Mu) | F29 |

suboutcrops of marble are found amongst secondary surface limestone (calcrete) along a small topographic rise trending east-northeast between the farm house at Kat Vlei and the windmill near Geelvlei. The marble unit is at most a few tens of metres thick and forms part of a sequence involving pink quartzo-feldspathic gneiss, hypersthene-pyroclase granolite, clinopyroxene-scapolite-bearing rocks and a thin band of quartzite.

(a) Petrography of the Calc-silicate Gneisses - Generally the calc-silicate rocks display some type of banding in outcrop which often results from alternating garnet-rich and clinopyroxene-rich layers. Their colour varies considerably due to compositional differences, but pale grey, dark green, black and orange-brown colours are common and the grain size varies from fine to very coarse.

A number of 69 specimens have been studied under the petrographic microscope and the range of modal compositions encountered in these specimens is shown in Table 1. All the thin sections studied display a granoblastic texture, but in some specimens superimposed secondary corona textures occur and are described in more detail in Chapter III.D. The following minerals are recorded in varying proportions : garnet, clinopyroxene, plagioclase, quartz, scapolite, wollastonite, amphibole, calcite, sphene, epidote group minerals, opaque minerals (largely magnetite), apatite, zircon, muscovite/sericite, chlorite, $\pm$ biotite and $\pm$ K-feldspar.

The *garnet* is generally of a dark orange-brown colour, but in some specimens (e.g. HA 604) the mineral is pale yellow. Microprobe analyses of the orange-brown garnets indicate that this mineral is composed essentially of the andradite and grossular molecules (Chapter III.D.). These garnets occur either as rounded grains (often poikiloblastic) of variable size, but frequently less than 1 mm in diameter, although large crystals up to 15 cm across have been observed in isolated outcrops, or alternatively, garnet forms a corona mineral. These garnet coronas have been recorded in a number of specimens (HA 1140, HA 1082, HA 1047, HA 1048, HA 1049, HA 1031) where grandite forms rims around clinopyroxene and edging the clinopyroxene-quartz and clinopyroxene-plagioclase contacts. Garnet rimming opaque minerals is very rare, but has also been observed. The garnet in the granulite facies terrane is generally free of inclusions, but there is a tendency for garnet to become more poikiloblastic in specimens from the amphibolite facies terrane where the mineral is frequently seen to enclose small rounded grains of quartz, plagioclase, clinopyroxene and sphene.

*Clinopyroxene* is encountered in the majority of the specimens studied. The mineral generally has a dark green colour and is pleochroic in shades of green and yellow-green. Microprobe analyses show that these minerals are solid solutions of the diopside-hedenbergite series. All the compositions plot into the fields of salite and ferrosalite on the diopside-hedenbergite join (Chapter III.D.). Although less poikiloblastic than garnet, the mineral is occasionally seen to contain inclusions of quartz, plagioclase and sphene, but only rarely is garnet observed amongst these inclusions.

*Plagioclase*, when dominant, produces a granoblastic polygonal texture with straight grain boundaries meeting in triple points. The mineral is generally free of inclusions, but poikiloblastic plagioclase is recorded in two specimens (HA 1140 and HA 1103), both of which are from the amphibolite facies terrane. Plagioclase compositions have been determined optically and by means of microprobe analyses and are found to vary between $An_{51}$ and $An_{96}$. Most grains display either a continuous gradual zonation or they are optically uniform. In some specimens, however, the zonation is abrupt and discontinuous along a sharp boundary, on either side of which, the mineral has markedly different optical properties. The zonation in the latter grains is often concentric and the cores are of a more sodic composition compared to the enclosing rims (Chapter III.D.). Within a particular thin section not all the grains display this abrupt zonation and it is suggested that the cores of such grains represent remnants of a pre-existing plagioclase phase. Crystals displaying abrupt discontinuous zonation are recorded in specimens HA 1101, HA 1093, HA 1124 and HA 1082, all of which have been collected in the amphibolite facies terrane. Most plagioclase grains are remarkably fresh, but extensive or complete saussuritisation is observed in some specimens.

*Quartz*, if present in larger amounts, has an influence on the texture, as grain boundaries tend to become interlobate. The mineral is generally in a strained state.

*Scapolite* is recorded in 12 of the specimens studied. It occurs as equant grains with straight grain boundaries meeting in triple junctions and when abundant creates a granoblastic polygonal texture. Judging by the birefringence (upper first-order to lower second-order) the mineral has a high Ca-content (Deer *et.al.*, 1971). Although commonly fresh, in some specimens the mineral is altered partly to muscovite along the grain margins and cleavage traces.

*Wollastonite* is very rare and has only been recorded in one specimen (HA 1155), collected on the farm Dabidas (407), well within the granulite facies terrane. The wollastonite-bearing rock occurs as a small lens-shaped body ($\pm$ 2 square metres in outcrop area) within grey migmatitic biotite-garnet gneisses. In outcrop the host rock has a very dark colour and displays a peculiar rough and pitted weathered surface.

*Amphiboles* are recorded in some of the specimens in accessory amounts and only in three of the specimens studied are amphiboles major constituents. The one specimen (HA 997) has been collected on the farm Dabidas (407) in close proximity to the wollastonite occurrence and microprobe analyses have proved an amphibole composition close to the tremolite-actinolite field boundary (Chapter III.D.). The other two amphibole-bearing rocks (HA 44 and HA 1150) are also encountered on the farm Dabidas (407) and the amphibole composition as determined by microprobe analyses, plot into the field of magnesio-hornblende (Chapter III.D.).

*Sphene* occurs in small amounts in the majority of the specimens examined. Two optically similar varieties are recorded: a light-brown type with the typical sphene colour and a more orange-brown variety with distinct pleochroism. The colour of the second type is very similar to that of the associated grandite garnet from which it is almost indistinguishable in plane polarised light. The mineral forms rounded equant grains dispersed evenly throughout the rock or sometimes it occurs concentrated in layers. Partial rims of sphene around opaque minerals have also been observed. Throughout the entire study area (including the granulite facies terrane), sphene in calc-silicate gneisses appears to be in textural equilibrium with grandite and clinopyroxene. This suggests that sphene in these rocks is a stable phase even at the highest grades of regional metamorphism. The two optically similar minerals have not been analysed and it is quite conceivable that they represent different minerals.

*Epidote* group minerals are abundant in some specimens where they are frequently observed as secondary retrograde coronas surrounding grandite along the interface between the garnet and plagioclase. These epidote rims are, in fact, double coronas with epidote always developed nearer the grandite while zoisite forms a thin rim along the epidote-plagioclase contact (Chapter III.D.). Clinozoisite is also commonly observed in accessory amounts as a secondary alteration product. In some specimens (HA 1124, HA 1105, HA 1126, HA 1093, HA 1132) small equant grains of epidote group minerals have polygonal outlines (Fig. 3) and appear to be in textural equilibrium with the other associated calc-silicate minerals. These grains frequently display a concentric zonation with dark-brown cores which are generally pleochroic in shades of brown, greenish-brown and yellow-brown and are biaxial negative with a large 2V. The cores are surrounded by lighter coloured weakly pleochroic rims. Expansion cracks are always observed around these zoned grains. The optical properties and expansion cracks suggest that the mineral is very likely to be allanite, the rare-earth member of the epidote family. According to Deer *et al.* (1971) the hydration of allanite causes expansion leading to the formation of radiating cracks in the surrounding minerals. It is often not possible to obtain a meaningful interference figure from these grains. Polygonal grains of allanite (?) have only been recorded in specimens collected in the amphibolite facies terrane and the textural relationships between this mineral and associated calc-silicate phases suggests that it was a stable phase during upper amphibolite facies metamorphism.

*Calcite* is occasionally recorded in accessory amounts. It occurs closely associated with grandite and clinopyroxene, often forming an intergrowth with these minerals. *Opaque minerals* occur as rounded, equant or irregularly shaped grains closely associated with clinopyroxene and grandite. In some outcrops large ovoid magnetite grains up to 3 cm across have been observed, but more commonly these grains are less than a few mm in diameter. *Apatite* and *zircon* are common accessory minerals and *sericite, muscovite* and *chlorite* are recorded as lateration products.

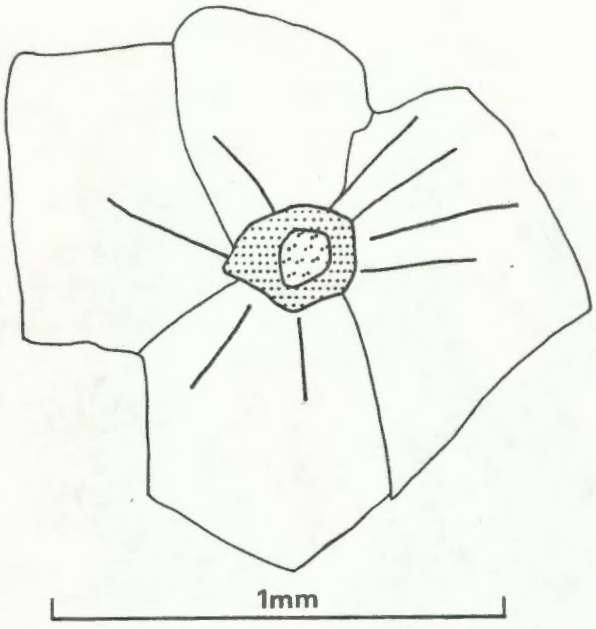


Fig. 3 Textural relationships between an epidote group mineral (allanite?) (stippled) and plagioclase (clear) in calc-silicate rock specimen HA 1132 from the amphibolite facies terrane. The grain of allanite displays concentric zoning; the polygonal outlines suggest textural equilibrium between allanite and plagioclase. Also note the radial cracks surrounding the grain of allanite, which probably result from expansion during hydration (Deer *et al.*, 1971).

(b) Petrography of the Marble - The marbles are medium to coarse grained and in hand specimens are seen to contain abundant orange and green coloured grains. The darker minerals are often concentrated in small lenses and stringers. Fresh specimens either have a white or pale orange-brown colour. Microscopic examination of two specimens reveal the presence of the following minerals arranged in order of decreasing abundance: dolomite, calcite, olivine (serpentine), chondrodite/clinohumite, spinel, phlogopite, opaque minerals and apatite.

*Dolomite* occurs as colourless, twinned grains and is generally of slightly coarser grain size than the associated *calcite*. The calcite is slightly less abundant than dolomite and together the two minerals make up the bulk of the rock. Both minerals are easily distinguished from each other in plane polarised light, because calcite is always crowded with tiny inclusions (exsolution) resulting in a dusty appearance of the mineral.

*Olivine* forms round or ovoid grains with serpentine replacement along cleavage traces and grain boundaries. In many grains the alteration has gone to completion, leaving pale yellow serpentine spherules with fibro-lamellar structure. Some of these spherules contain brownish dust-like fine-grained micaceous minerals with higher birefringence than serpentine. The olivine has the optical properties of forsterite.

*Humite group minerals* occur as ovoid grains with golden, orange-yellow to pale yellow pleochroism. These grains are fresh with minor alteration restricted to grain boundaries and the optical properties are consistent with those of the chondrodite-clinohumite series.

*Spinel* has a pale green colour and is represented as small rounded grains generally free from alteration, although some grains are edged by a narrow rim. Larger crystals show imperfect cleavage. *Phlogopite* is not very abundant, but a few flakes have been observed. In one of the specimens a single grain of *tremolite* was recorded. *Opaque minerals* occupy tiny patches amongst the alteration products of olivine and *apatite* is a rare accessory mineral.

## 2 Pelitic Metamorphites (Map units Mal, Mhal, Ms)

(a) Aluminous (pelitic) Gneisses - These rocks contain variable proportions and combinations of the minerals cordierite, almandine-rich garnet, sillimanite, biotite, hypersthene (anthophyllite), alkali-feldspar, plagioclase, quartz, spinel, magnetite, ilmenite and corundum. In the literature similar rock types have been described as metapelites or kinzigites (Büsch *et al.*, 1980).

Outcrops of these rocks feature prominently in the southern part of the area where a close spatial association of these pelitic gneisses and feldspathic quartzites are noted. Frequently the quartzites occur as thin bands within the pelitic units in a manner suggesting that both rock types form part of a sedimentary sequence.

In the field the aluminous gneisses are easily recognisable by their dark brown colour. Fresh specimens are generally greenish-grey, a colour which is probably related to the abundance of cordierite. The coarse grain size is characteristic and large porphyroblasts of garnet and cordierite are common. Large sillimanite needles are generally well orientated within the gneissic banding and define a pronounced linear fabric. Radiating randomly orientated aggregates of sillimanite "roses", however, are also frequently

Table 2 Minerals recorded in hypersthene-free pelitic gneisses. Abbreviations as in preface.

a < 1%, b = 1-5%, c = 5-10%, d = 10-20%, e >20%

| Sample No. | cordierite | garnet | sillimanite | biotite | quartz | plagioclase | K-feldspar | opaque minerals | other (a) | locality |
|---|---|---|---|---|---|---|---|---|---|---|
| HA 1026 | e | d | a | b | e | d | d | a | He Zc | H10 |
| HA 1029 | d | d | b | a | d | d | e | a | He Zc | F10 |
| HA 1036 | e | d | a | a | e | c | d | a | Co He Zc | E11 |
| HA 514 | b | d | b | a | e | c | e | b | Co He Zc | B19 |
| HA 515 | d | - | b | a | e | c | e | b | He Zc | B19 |
| HA 507 | c | - | b | b | e | d | e | a | He Zc | A20 |
| HA 456 | a | - | a | b | e | b | d | a | He Zc | A21 |
| HA 505 | e | b | a | a | d | d | e | b | Co He Zc | A21 |
| HA 981 | e | - | a | - | e | c | e | b | Co He Zc | B21 |
| HA 982A | d | c | b | b | e | d | e | a | He Zc | C22 |
| HA 982B | c | b | b | b | e | d | e | b | He Zc | C22 |
| HA 267 | b | b | c | b | e | b | e | b | Co He Zc | C22 |
| HA 143 | c | d | b | a | d | b | e | a | He Zc | E24 |
| HA 164 | d | b | a | b | e | c | e | b | He Zc | E24 |
| HA 148 | b | b | a | b | e | b | c | a | He Zc | E24 |
| HA 652 | - | b | b | a | e | a | b | a | Zc | F25 |
| HA 338 | d | - | c | a | e | d | e | b | He Zc | B26 |
| HA 339 | c | b | - | a | e | e | e | a | Co He Zc | B26 |
| HA 329 | b | b | b | a | e | b | e | a | Co He Zc | C26 |
| HA 995 | d | - | b | a | e | d | e | b | He Zc | C26 |
| HA 632 | b | b | b | b | e | d | d | b | He Zc | H26 |
| HA 901 | d | - | a | a | e | e | e | b | He Zc | D27 |
| HA 681 | d | a | - | a | e | b | e | a | Co He Zc | F27 |
| HA 686 | b | d | a | a | e | e | d | a | Co He Zc | F27 |
| HA 687 | d | - | - | a | e | e | e | a | He Zc | F27 |
| HA 869A | d | b | a | b | e | d | e | a | He Zc | A28 |
| HA 869B | b | d | a | b | e | d | e | a | He Zc | A28 |
| HA 870 | d | e | b | b | d | d | e | a | He Zc | A28 |
| HA 871A | b | c | c | c | d | c | e | b | He Zc | A28 |
| HA 871B | d | b | b | b | e | b | e | b | He Zc | A28 |
| HA 903 | b | a | c | b | e | d | e | a | He Zc | D28 |
| HA 708 | d | a | a | - | e | e | c | b | Co He Zc | H28 |
| HA 717 | d | a | a | a | e | e | d | b | Co He Zc | I28 |
| HA 800 | d | - | b | b | e | e | d | a | He Zc | C29 |
| HA 697 | b | - | a | a | e | c | e | a | Co He Zc | F29 |
| HA 821 | e | - | c | - | b | d | e | b | Co He Zc | A31 |
| HA 841 | c | c | a | a | e | d | e | b | He Zc | A32 |
| HA 827 | d | - | - | a | e | e | e | b | He Zc | A32 |

recorded within the foliation plane. In the majority of the outcrops these rocks are banded and display alternating leucocratic and melanocratic layers, which, on a regional scale are more or less concordant and define a planar fabric. The leucocratic layers are pegmatitic and consist essentially of quartz and feldspars with scattered porphyroblasts of garnet and the melanocratic layers are composed of cordierite, garnet, biotite and sillimanite. The relationship of the two types of layers is that of *in situ* migmatites (Mehnert, 1968). At some localities banding is not observed and instead the rocks are extremely coarse grained and have a granitic appearance. The relative abundance of the minerals recorded in the hypersthene-free pelitic gneiss specimens are indicated in Table 2 and the minerals encountered in cordierite-hypersthene (anthophyllite) gneisses are listed in Table 3.

Table 3 Minerals recorded in cordierite-hypersthene (anthophyllite) gneisses.
Abbreviations as in preface.

| Sample No. | cordierite | orthopyroxene | anthophyllite | biotite | garnet | quartz | K-feldspar/ plagioclase | opaque minerals | other | locality |
|---|---|---|---|---|---|---|---|---|---|---|
| HA 1120 | x | x | x | x | | x | x | x | Ch Zc | I3 |
| HA 1119 | x | | x | x | x | x | x | x | Ch Zc | I3 |
| HA 826 | x | x | | x | | x | x | | He Zc | A32 |

*Cordierite* is the dominant ferromagnesian mineral and it occurs in two different habits, namely, as porphyroblasts which are locally as much as 2 cm across, and as a corona mineral surrounding other minerals. Cordierite porphyroblasts frequently display multiple twins resembling albite twins in plagioclase or more complex interpenetrating twin sets. According to Deer *et al.* (1971) complex twins are generally restricted to the high temperature environment. Most porphyroblasts are remarkably fresh with alteration restricted to the grain boundaries and cracks, but in some specimens cordierite has been completely replaced by greenish-yellow micaceous minerals. The mineral has a dusty appearance resulting from numerous minute opaque inclusions. Also present amongst these inclusions are small zircon grains surrounded by pleochroic haloes. Where biotite and cordierite are in contact in hypersthene-free rocks, the boundary between the two minerals is generally ragged and microscopic examination indicates textural disequilibrium between the two minerals. A rather peculiar myrmekitic cordierite-quartz intergrowth in which hypersthene is also involved has been recorded in one of the specimens (HA 826). Identical intergrowths are described in detail by Brink (1950, p., 131) from the Hoedkop-Hartseerkop area.

Cordierite coronas feature prominently in the majority of the specimens studied and are most frequently developed around opaque minerals and grains of hercynite-spinel. Sillimanite is often involved in the coronas. The matrix surrounding these corona textures is generally composed of quartz and feldspars, but in some specimens the cordierite coronas around hercynite are enclosed by large garnet porphyroblasts. Because cordierite commonly occurs in coronas completely surrounding other minerals, and thus post dating them, it is suggested that at least some of the cordierite has developed at a late stage in the tectono-thermal evolution of the Namaqualand Metamorphic Complex.

*Sillimanite* occurs as long, prismatic crystals, large enough to be recognised with the unaided eye in the field. Like cordierite, sillimanite forms in two different habits namely as prismatic, euhedral crystals and as coronas surrounding other minerals. In the field the sillimanite needles are generally observed to be well orientated defining a pronounced linear fabric but they are also seen to form radiating aggregates within the plane of the foliation. Complete random orientation also occurs, particularly in proximity to syntectonic intrusive rocks, indicating that mineral growth outlasted deformation.

Under the microscope euhedral sillimanite grains are often seen to be enclosed by spinel and opaque minerals, while tiny sillimanite needles occur as inclusions in garnet and cordierite porphyroblasts. In some garnet grains these sillimanite needles are arranged in a manner resembling small-scale tight isoclinal folds. If these are relict textures the folded sillimanite needles must represent the oldest recognisable s-surface, which predates the regional gneissic banding in which the garnet has developed. In other garnet grains, however, the needle-like sillimanite inclusions have random orientation.

Sillimanite coronas are commonly recorded around opaque minerals and grains of hercynite-spinel. These coronas or partial coronas are either surrounded by quartz and feldspar, by cordierite or in some specimens by garnet.

*Garnet* is recorded at the majority of the outcrop localities of pelitic gneisses, but some cordierite-rich rocks apparently lack this mineral. Porphyroblasts are common and occasionally can be as much as 4 cm across. The mineral has irregular grain boundaries with large embayments and is generally elongated parallel to the gneissic banding. Opaque minerals, spinel, quartz, sillimanite and biotite are common inclusions. Garnet coronas are not common, but in some specimens partial rims of garnet around opaque minerals and spinel are seen.

*Biotite* is commonly present in accessory amounts only, while phlogopite is more abundant in some of the cordierite-rich and cordierite-hypersthene gneisses. Some of the biotite grains have a red-brown maximum absorption colour, while in others the colour is dark brown with a slight greenish tinge. Small biotite flakes armour larger garnet grains in some specimens and zircon inclusions are surrounded by pleochroic haloes.

*Orthopyroxene* is very rare and occurs as minute grains (<0,01 mm across) in specimen HA 826 (collected on the farm Brandewynskraal (69)) where it occurs in association with a myrmekitic cordierite-quartz intergrowth and is also seen to partially rim opaque minerals. On the farm Gal-Puts (104) the orthopyroxene has developed as large porphyroblasts and the mineral is invariably surrounded by a rim of retrograde orthoamphibole (anthophyllite) and is also partially replaced by chlorite. The pleochroism of the mineral is intense and varies from a deep pink colour to pale green.

*Quartz* is present in all the specimens examined and occurs as irregularly shaped interlobate to amoeboid grains displaying variable strain features.

*Alkali feldspar* is the most abundant leucocratic mineral and features prominently in the leucosomes. The mineral is invariably microperthitic with fine stringers and beads of albite. Microcline microperthite forms large xenoblastic grains with embayed contacts. It is generally fresh, but minor sericitisation does occur, particularly along cleavage traces.

*Plagioclase* is less abundant than alkali feldspar and in the majority of the specimens this mineral is of andesine composition. The twin lamellae are generally deformed and many grains display compositional zoning. A myrmekitic quartz-plagioclase intergrowth is frequently developed particularly at the contact with alkali feldspar. Antiperthite has also been recorded.

A dark green *spinel* of the hercynite-spinel solid solution series is present in small amounts in most of the specimens studied. It is closely associated with sillimanite and opaque minerals with which it frequently forms an intergrowth. Many spinel grains display considerable exsolution of an opaque phase. In some specimens *corundum* occurs together with the spinel.

*Opaque minerals* are recorded in small amounts and *zircon* occurs as minute

grains (<0,01 mm) in accessory amounts and when enclosed by biotite and cordierite, is surrounded by pleochroic haloes.

*Pinite* and *chlorite* are common alteration products of primary minerals.

(b) Quartz-biotite-muscovite Schists and Quartz-muscovite Schists - Outcrops of these schists have only been found in the area to the north of latitude 29°.45'S (map A), always in association with the metaquartzites. On the farm Banken (91) at Banke se Kop quartz-biotite-muscovite schists, frequently garnetiferous, underlie the quartzites and are in turn underlain by pink quartzo-feldspathic gneisses. Along strike further west on the same farm these schists are also interbedded with the quartzites. Similar schists have been intersected in a borehole on the farm Struisbult (94) at a locality where quartzites appear in outcrop (F1). The quartzite-schist association has also been seen on the farm Koeris (78) where the rocks are dominated by quartz-muscovite schists.

These rocks are strongly foliated and sheared and appear to have acted as tectonic slides during deformation. Very commonly the schists have a rusty brown coloured coating of iron oxides particularly where ferruginous bands are recorded.

Miscroscopic examination reveals well-orientated brown *biotite flakes* defining a pronounced planar fabric. Grain contacts between biotite and *muscovite* are generally ragged and in contrast to the well orientated biotite crystals, the muscovite flakes occur in clusters in which individual crystals have random orientation, frequently at a high angle to the biotite foliation. The muscovite grains, on average, are very much smaller than the associated biotite flakes which they commonly penetrate. *Quartz* is an additional major constituent and is frequently in a strained state. *Opaque minerals* and *zircon* occur in accessory amounts. Although garnet has not been recorded in the specimens studied, it has been observed in outcrop.

### 3 Semipelitic Metamorphites (Map units Mbg, Mpal)

(a) Migmatitic Biotite-garnet Gneiss - Major outcrops of the migmatites are encountered in the southern part of the study area (map B). These rocks are considered to represent metasediments, a view point supported by their close spatial association and interbanding with other gneisses of undoubtedly sedimentary origin. Frequently they contain thin bands of feldspathic quartzite (often garnetiferous)(e.g. on Obeeb (8) and Nuwefontein (6)), bands of calc-silicate gneisses (a phenomenon well illustrated by the outcrops on the farms Dabidas (407) and Dooddrink (406) where calc-silicate rocks containing wollastonite, clinopyroxene, scapolite, calcic plagioclase and amphibole occur as lenses and bands in the semipelitic migmatites), lenses of pelitic gneiss and ferruginous layers (iron formation), while on Obees (402) the semipelitic rocks occur intimately associated with graphitic quartzite, sillimanite-bearing quartzo-feldspathic rocks and iron formation amongst other rock types.

One of the most striking features of these rocks is their banded nature (Plate 7). They contain numerous stringers, lenses and bands (generally discontinuous) composed of leucocratic pegmatitic garnetiferous quartzo-feldspathic material. Large garnet porphyroblasts yield the spotted appearance recorded on Plate 7. The leucocratic stringers are interpreted as leucosomes (Mehnert, 1968) produced by *in situ* partial melting accompanying a major high-grade regional thermal event. In some outcrops the leucosomes account for as much as 50 per cent of the rock volume and frequently form wide zones of white quartz-feldspar-garnet mobilisate.

Several specimens have been studied microscopically, but only one of which has been collected within the amphibolite facies terrane farm Leeuw Klip (112) while all other specimens studied are from the granulite facies terrane. Variable proportions of the following minerals are recorded: quartz, alkali-feldspar, plagioclase, biotite, almandine-rich garnet and accessory amounts of opaque minerals and zircon.

*Quartz* is present as a major constituent in all the specimens studied.

*Alkali feldspar* is particularly abundant in specimens collected in the southern part of the area where leucosomes feature prominently in outcrop. The mineral occurs as microperthite which forms a major component of the quartzo-feldspathic leucosomes. In contrast the specimens from the northern part of the area (map A), contain much less or no alkali feldspar.

*Plagioclase* is recorded in all the specimens studied. The mineral is generally zoned and in some of the specimens forms a myrmekitic intergrowth with quartz.

*Biotite* in specimens from the granulite facies terrane typically has a dark red-brown maximum absorption colour as opposed to the brown colour displayed by the mineral in the one specimen collected within the amphibolite facies terrane. This mineral accounts for 8 to 15 per cent of the modal composition and individual grains are well orientated defining a pronounced planar fabric.

In specimens from the migmatitic terrane (map B) *garnet* generally occurs as irregular-shaped poikiloblasts enclosing grains of quartz and minor biotite while in the northern part of the area (map A), the garnet grains tend to be more euhedral. Several garnet grains have been analysed with the aid of the electron microprobe and they are invariably almandine-rich and display a typically retrograde zonation pattern (Chapter IV).

(b) Semipelitic Quartzo-feldspathic Gneiss - Prominent outcrops of semi-pelitic quartzo-feldspathic gneisses occur on the farm Wielspoor (73) where a thin band of migmatitic aluminous gneiss grades into quartzo-feldspathic gneiss containing small amounts of aluminous minerals. Interbanded with these are migmatitic quartzo-feldspathic gneisses in which garnet and biotite are the ferromagnesian phases. Both the migmatitic gneisses and the semi-

pelitic quartzo-feldspathic gneisses have been grouped together on the accompanying geological map. The latter are generally light brown weathering, but fresh specimens have either a pinkish or a pale grey colour.

*Quartz, plagioclase* and *alkali feldspar* (microperthite) are the dominant minerals in the semipelitic gneisses. The other minerals recorded in small amounts include *cordierite, biotite, garnet, sillimanite, hercynite* and *opaque minerals*, while *corundum* and *zircon* occur in trace amounts.

The cordierite is largely altered to *pinite* and frequently forms a partial rim around opaque minerals and hercynite. Similar corona textures are recorded in the pelitic gneiss specimens. Where cordierite and biotite occur in contact, the boundary is much serrated and it appears that these two minerals are in a state of reaction.

These rocks are considered to represent metasediments of an intermediate type between metashales (aluminous gneiss proper) and meta-quartzo-feldspathic sediments.

### 4 Quartzose Metamorphites (Map units Mq, Mfq, Mgq)

(a) Metaquartzites - Pure, white glassy quartzites consisting of more than 95 per cent quartz are restricted to the area north of latitude 30° 00'S (map A). The southernmost outcrops found during field mapping are located on the farm Kat Vlei(235) where a thin quartzite band appears between pink quartzo-feldspathic gneiss and marble. The quartzite ridges account for the majority of the topographic rises in the otherwise flat lying Bushmanland Plateau. It is common to find schists and calc-silicate gneiss units interbanded with these rocks.

The quartzites are invariably white or pale grey in colour and are generally fairly coarse grained. They represent mature sediments devoid of feldspars and this feature distinguishes the metaquartzites which are restricted to the northern part of the area, from their feldspathic equivalents encountered and restricted to the area further south.

(b) Feldspathic Quartzites - These rocks contain abundant pink porphyroblasts of microcline-microperthite and they feature prominently in the southwestern corner of the study area. They occur in close association with and are frequently interbanded with pelitic and semipelitic gneisses. It appears that these rocks reach their maximum stratigraphic thickness in the south and become less voluminous to the north where they eventually fade out.

The colour of the feldspathic quartzites varies from white, grey to pinkish or sometimes greenish grey if epidote is abundant and ferruginous varieties are brown weathering. These rocks are frequently banded and in

some outcrops contain layers rich in aluminous and opaque minerals. Their grain size varies from medium to coarse.

*Quartz* is by far the dominant mineral followed by *microcline-microperthite*. Quartz grains frequently contain small inclusions and under high magnification tiny needles can often be observed. Strain effects and polygonisation of larger crystals are common features. In specimens which have been intensely sheared (mylonitic textures), the larger quartz crystals have been completely replaced by smaller strain-free grains.

K-feldspar occurs as microcline-micropethite generally displaying a well-developed tartan twinning. Exsolution lamellae are seen as tiny beads and stringlets and in mylonitic rocks in which the quartz has been completely recrystallised, the microcline has often survived deformation as large ovoid grains. *Plagioclase* has only been recorded in one specimen and it has the composition of $An_{38}$.

Other minerals that are recorded in small amounts (<5 per cent) include *cordierite, biotite, hypersthene, garnet, sillimanite, opaque minerals* (frequently specks of *haematite*) and *zircon*. *Chlorite, muscovite/sericite* and rarely *epidote* occur as alteration products.

The textures of the feldspathic quartzites are generally granoblastic interlobate but in intensely sheared specimens the texture is mylonitic.

(c) Graphitic Quartzites - An interesting occurrence of graphitic quartzite is encountered on the farm Obees (402) in the core of a $D_3$ synform. These quartzites are characterised by a dark grey colour and on freshly broken surfaces abundant graphite is apparent. The rocks are coarse grained and porous. Presumably the pore spaces were once filled with minerals since leached out of the rock and in fact iron oxides can still be recognised in some of the pores and it seems likely that they have replaced sulfides.

One specimen studied microscopically has revealed that the dominant minerals comprise strained quartz with graphite, amounting to between 10 and 15 per cent. Iron oxides (haematite) and apatite are also found and a yellow isotropic mineral with fairly high relief occurs in accessory amounts.

The graphitic quartzites are very closely associated with granolites(mafic volcanics?) semipelitic biotite-garnet gneisses, sillimanite-bearing quartzo-feldspathic rocks which contain specks of iron oxides and are frequently coated with iron oxides (largely haematite), iron formation with large garnets some of which are up to 15 cm across, and yellow-weathering calc-silicate rocks. Certainly these rock associations make this particular area an attractive prospecting target for base metals. Ultramafic rocks consisting of amphibole, olivine, orthopyroxene and spinel are also present at the same locality.

## 5 Quartzo-Feldspathic Metamorphites (Map units Mp, Mpl, Mpb, Mpa, Mw, Mmg, Mt)

These rocks consist essentially of quartz and feldspars with mafic minerals generally amounting to less than 5 per cent. Several different types of quartzo-feldspathic gneisses are recognised.

(a) Pink Quartzo-feldspathic Rocks - Of all the rock types encountered in the study area these gneisses are the most abundant and widespread. In the southern part of the area (Map B) an attempt has been made to distinguish between pink gneisses in which biotite is either absent or occurs only in trace amounts and a biotite-richer variety. On the accompanying geological map these two rock types are symbolised Mpl and Mpb respectively. Such a distinction has not been made in the northern area (Map A) where the symbol Mp has been used for all the pink gneisses.

In the adjacent area Joubert (1971a) referred to these rocks as pink gneiss, leptynite and leptite. They are easily distinguished from the surrounding gneisses by their deep red-brown weathering colour which is particularly characteristic for rocks with a low mafic mineral content. Grain size varies considerably. Some outcrops are equigranular and fine grained or contain poorly developed feldspar augen while others are porphyroblastic with subhedral to euhedral feldspar crystals. Very coarse grained outcrops with a granitic appearance are also common. In fact locally these rocks have been remobilised and display intrusive relationships.

A compositional banding is commonly recorded. Some outcrops contain thin white weathering bands and microscopic examination has revealed that these consist essentially of plagioclase and quartz. In other outcrops the banding is brought about by a variation in the mafic mineral content.

Microscopic studies of several specimens has shown that *quartz* and perthitic *alkali feldspar* are the dominant minerals while *plagioclase* is considerably less abundant. *Garnet* is generally present in small amounts and occurs as poikiloblasts enclosing rounded quartz grains. Other minerals encountered include brown to red-brown *biotite* (frequently marginally altered to chlorite), *opaque minerals, zircon, sphene* and *apatite*. *Calcite, chlorite* and *sericite* are recorded as alteration products.

Only rarely these rocks contain quartz-sillimanite nodules and these have previously been described from the Namiesberg area (Moore, 1977). Rocks superficially resembling the common pink quartzo-feldspathic gneisses but containing trace amounts of amphibole instead of garnet are encountered in the southwestern part of the study area and are designated by the symbol Mpa on the accompanying geological map. The amphibole is generally replaced by chlorite and calcite but some of the specimens studied still contain remnants of the pre-existing brown hornblende.

Kröner (1968) and Joubert (*op.cit.*) suggest that the pink quartzo-feldspathic gneisses represent metasediments. In the study area these rocks are frequently interbanded with pelitic, semipelitic and calcareous metamorphites with sharp or gradational contacts and it seems likely that they represent either metamorphosed sediments or acid volcanics.

(b) White Quartzo-feldspathic Rocks - Outcrops of the white quartzo-feldspathic rocks are restricted to the southern part of the area (map B) and comprise quartz-feldspar rocks, quartz-feldspar-garnet rocks and quartz-feldspar-garnet-biotite gneisses that are characterised by a snow-white colour. The varieties containing minor biotite generally have an off-white to pale grey colour. The northernmost prominent outcrops are encountered on the farms Skimmelkop (377), Daas Daap (378) and Roode Mond (392) where white garnetiferous quartzo-feldspathic rocks grade into pink quartzo-feldspathic gneisses.

Besides their close spatial association with pink quartzo-feldspathic gneisses into which they grade, the white quartzo-feldspathic rocks are also found in association with semipelitic migmatitic biotite-garnet gneisses and, when lacking biotite, are mineralogically indistinguishable from the garnetiferous leucosomes within the migmatites. Some outcrops are distinctly banded with alternating biotite-rich and biotite-free layers while others are rather massive with a spotted appearance caused by abundant pink garnet porphyroblasts.

Their grain size varies from medium to very coarse and they are inequigranular with porphyroblasts of garnet and frequently also augen-shaped feldspar crystals which can be up to a few cm across.

Microscopic examination reveals that the mineralogy comprises essentially quartz and alkali feldspar with subordinate amounts of plagioclase. Garnet occurs in small amounts in most of the specimens while biotite is also recorded in some of the outcrops.

*Quartz* is generally in a strained state and has irregular grain boundaries with large embayments. Alkali feldspar is recorded as *microcline microperthite* with bead texture and *plagioclase* occasionally forms a myrmekitic intergrowth with quartz. *Garnet* grains are frequently only a few mm in diameter, but in several outcrops this mineral forms large porphyroblasts 1-2 cm across. The mineral is poikiloblastically enclosing small rounded grains of quartz and is marginally altered to chlorite in places. *Biotite* is frequently present only in accessory amounts, but in some specimens accounts for a few per cent of the modal composition. *Zircon* and *opaque minerals* occur as accessory phases.

The mode of origin of these rocks is controversial. Gradational contacts with pink garnetiferous quartzo-feldspathic gneisses (believed to be part of the metasedimentary/metavolcanic sequence) suggests that they belong to the supracrustal pile. On the other hand, their general

appearance and mineralogy does not exclude the possibility that they could represent large *in situ* leucosomes produced by partial melting of pre-existing gneisses. There are, however, often no corresponding melanosomes along the contacts.

(c) Migmatitic Quartzo-feldspathic Gneiss - Migmatisation has affected a broad compositional range of lithologies and is a widespread phenomenon in the southern part of the study area. Several of the rock types described previously are migmatitic and like these, many outcrops of quartzo-feldspathic gneiss contain abundant leucosomes. *Alkali feldspar, quartz* and *plagioclase* form the major minerals within the leucocratic bands in which *garnet* porphyroblasts also feature prominently. The leucosomes generally have dark coloured border zones (melanosomes) in which mafic minerals (mainly *biotite*) are concentrated. Accompanying minerals include *quartz, alkali feldspar, plagioclase* (myrmekite), *opaque minerals, zircon* and *apatite*. Some of the outcrops appear to contain additional amphibole but this mineral has not been recorded in the thin sections studied.

These rocks resemble the *in situ* migmatites described by Mehnert (1968) and it seems likely that they have originated by a process involving partial melting during high grade regional metamorphism. In some outcrops the number of leucosomes per unit area increases considerably and the rocks become increasingly homogenised and have a granitic appearance. This is particularly well illustrated on the farm Haarbeen (23).

(d) Plagioclase-quartz-biotite Gneiss - Medium-grained grey gneisses are associated with calc-silicate rocks and pink quartzo-feldspathic gneisses on the farm Suurwater (242). These rocks are peculiar in the sense that they are frequently nodular with numerous round and oval-shaped quartz grains that tend to form positive features on the weathered surface and somewhat resemble amygdales in volcanic rocks.

Mineralogically these rocks are also anomalous because they do not contain alkali feldspar. The dominant minerals are plagioclase and quartz. In the two specimens studied petrographically the *plagioclase* (*andesine*) accounts for 49 to 58 per cent of the modal composition, while *quartz* is slightly less abundant and varies between 35 and 45 per cent. A brown-coloured *biotite* is also present in amounts between 5 and 7 per cent. *Opaque minerals, zircon, apatite* and *calcite* are accessory phases while *chlorite* and *sericite* are recorded as alteration products of biotite and plagioclase respectively.

## 6 Ferruginous Rocks (Map unit MFe)

This group comprises all rocks in which iron oxides (magnetite and haematite) from major constituents. The iron formations are interlayered

with other metasediments. Some of the occurrences are worth mentioning as they could be of economic interest.

Malachite-coated ferruginous rocks occur on the farm Kraalbosch Vlei (99)(map A). Further south (map B) several interesting outcrops are recorded. On the farm Dabidas (407) along the Dabidas-Klipfontein road a small dark brown gossan (?) outcrop is associated with a thin lens of ferruginous quartzite situated in proximity to the contact between aluminous cordierite-garnet-sillimanite gneiss and a finely laminated grey gneiss. Minor calc-silicate gneiss and a black manganiferous rock are also present. The latter is composed of the following minerals (in order of decreasing abundance): ferroaugite, quartz, opaque minerals (mainly magnetite), manganiferous garnet and pyroxmangite. The chemical compositions of these minerals are described in Chapter III E.4.

More spectacular gossans (?) occur on the farms Nuwefontein (6) and Uitkyk (9) where iron-rich rocks are interbanded with a sequence of semi-pelitic biotite-garnet gneiss and associated garnetiferous feldspathic quartzite. Some of the specimens display prominent boxwork structures and others are rather massive and banded.

On the farm Obees (402) iron formation forms part of a sequence involving haematite-rich aluminous quartzo-feldspathic rocks, graphitic quartzite, semipelitic and mafic rocks. Some outcrops contain abundant garnet porphyroblasts and graphite.

## 7 Mafic Metamorphites (Map units Mh, Ma)

(a) Hypersthene-pyroclase Granolite and Hypersthene-plagioclase Granolite - The literature concerning the terminology applicable to metamorphosed mafic rocks is considerably confused. For the purpose of this study the nomenclature proposed by Winkler and Sen (1973) and Winkler (1976, page 258) is adopted and accordingly the term "granolite" is applied to a hypersthene-bearing rock. By definition the term "granolite" applies to all metamorphosed rocks that contain orthopyroxene, but in this study the term is restricted to basic rocks. If the granolite specimen contains both clinopyroxene and plagioclase in addition to orthopyroxene the rock is referred to as a hypersthene-pyroclase granolite (clinopyroxene + plagioclase abbreviated to "pyroclase") and if clinopyroxene is absent, the term hypersthene-plagioclase granolite is applicable (Winkler and Sen, *op.cit.*). Of the 37 specimens studied, only two lack clinopyroxene and therefore the greater majority of these qualify as hypersthene-pyroclase granolite.

On the weathered surface these rocks generally display a rusty brown colour while fresh specimens invariably appear black. Banding is seen in

Table 4 Estimated modal compositions (in volume per cent) of hypersthene-pyroclase granolites and hypersthene - plagioclase
Retrograde minerals in parenthesis. Abbreviations as in preface.
(m = <1%)

| Sample No. | hypersthene | salite | plagioclase | quartz | hornblende | biotite | garnet | opaque minerals | other = m | locality |
|---|---|---|---|---|---|---|---|---|---|---|
| HA 1005 | 26 | 4 | 45 | 24 | | | | | (Mu) | F7 |
| HA 1064 | 3 | 7 | 44 | 3 | 41 | 2 | | m | Ap (Cc) (Ch) | C9 |
| HA 1025 | 24 | 5 | 52 | | 18 | m | | 1 | Ap | H9 |
| HA 1024 | 20 | 9 | 56 | | 15 | m | | m | | H9 |
| HA 1051 | 15 | 18 | 47 | | 20 | | | - | | E10 |
| HA 1030 | 11 | 7 | 36 | 43 | | m | 3 | m | Ap | F10 |
| HA 1046 | 25 | 22 | 48 | 5 | | m | | m | Ap | E11 |
| HA 1045 | 21 | 15 | 39 | 25 | | | | m | Ap | E11 |
| HA 1050 | 17 | 7 | 66 | | 6 | m | | 4 | Ap | F11 |
| HA 443 | 15 | 7 | 45 | | 32 | m | | 1 | Ap Zc | A21 |
| HA 444 | 30 | 8 | 60 | | | | | 2 | Ap | A21 |
| HA 472 | 13 | 4 | 55 | | 27 | m | | 1 | | A21 |
| HA 980 | 22 | 1 | 49 | | 24 | m | | 4 | | C21 |
| HA 972 | 20 | 10 | 54 | 15 | | m | | 1 | Ap (Se) | D21 |
| HA 239 | 18 | 2 | 49 | | 29 | m | | 2 | Ap | A22 |
| HA 983 | 4 | 50 | 24 | | 21 | | | 1 | | C22 |
| HA 973 | 26 | 13 | 49 | 7 | | | | 5 | Ap Zc | D22 |
| HA 412 | 9 | m | 40 | | 51 | m | | m | Ap | A23 |
| HA 385 | 10 | 10 | 35 | | 45 | m | | | Ap | B23 |
| HA 987A | 14 | 12 | 45 | | | 28 | | 1 | | B23 |
| HA 987B | 22 | | 44 | | 30 | | | 4 | | B23 |
| HA 269 | 11 | 15 | 56 | | 20 | m | | 3 | Ap | E23 |
| HA 939A | 24 | 11 | 53 | 7 | m | m | | 5 | Zc | B24 |
| HA 939B | | 31 | 61 | 2 | m | m | | 6 | | B24 |
| HA 929 | 5 | 3 | 58 | 7 | 22 | m | | 5 | Zc | B24 |
| HA 955 | 10 | 14 | 59 | 4 | | 12 | | 1 | Ap Zc | C24 |
| HA 951 | 15 | 7 | 75 | 1 | | 2 | | m | Ap | C24 |
| HA 127 | 17 | 12 | 67 | 1 | | 3 | | m | Ap | D24 |
| HA 957 | 15 | 10 | 55 | 7 | | 10 | | 3 | Ap Zc | D24 |
| HA 931 | 10 | 3 | 56 | 9 | 17 | m | | 5 | Ap Zc | B25 |
| HA 306 | 18 | 12 | 50 | 5 | 14 | m | | 1 | Ap | B25 |
| HA 926 | 13 | 16 | 51 | 7 | 10 | 1 | | 2 | Zc | A26 |

Table 4 (cont.) Estimated modal compositions (in volume per cent) of hypersthene - pyroclase granolites and hypersthene - plagioclase granolites. Retrograde minerals in parenthesis. Abbreviations as in preface. (m = <1%)

| Sample No. | hypersthene | salite | plagioclase | quartz | hornblende | biotite | opaque minerals | other = m | locality |
|---|---|---|---|---|---|---|---|---|---|
| HA 366 | 10 | 16 | 60 | 2 | | 10 | 2 | Ap Zc | B26 |
| HA 622 | 13 | 3 | 66 | 17 | | m | 1 | Ap Zc | H26 |
| HA 923 | X | X | X | | X | m | 2 | Zc | A27 |
| HA 888 | 8 | 6 | 62 | 10 | 10 | m | 4 | Ap Zc | B27 |
| HA 721 | 10 | m | 70 | 12 | 7 | | 1 | Ap Zc | H28 |
| HA 1128 | 16 | | 40 | 7 | 36 | 1 | m | | I3 |
| HA 1069 | 3 | | 29 | 2 | 66 | m | m | Ap (Cc) | C9 |

some outcrops as alternating hornblende-rich and pyroxene-rich layers.

The estimated modal compositions of the granolites are listed in Table 4.

*Orthopyroxene* accounts for about 14 per cent (by volume) of the modal composition of the average granolite specimen. The mineral occurs as small equidimensional xenoblastic grains and is always pleochroic ($\alpha$ = pink and $\gamma$ = pale green), but the intensity of the pleochroism varies from weak to very strong. Microprobe analyses indicate that the compositions of the orthopyroxenes range from bronzite to ferrohypersthene with hypersthene being most common. Larger crystals are sometimes observed to include small grains of clinopyroxene, biotite, plagioclase and hornblende, the latter mineral occurring as irregular fragments along cleavage planes and appear to be retrograde. Exsolution features have not been observed. Some grains are partly altered to chlorite particularly along the cleavage planes and grain boundaries, but generally the mineral is remarkably fresh.

*Clinopyroxene* has a pale-green colour and usually lacks pleochroism, but in some specimens it is weakly pleochroic. The mineral forms equidimensional xenoblastic grains with embayed contacts or occurs as poikiloblasts enclosing plagioclase, orthopyroxene, biotite, hornblende and opaque minerals. It is rarely twinned but no exsolution features have been detected. Microprobe analyses show that the mineral compositions plot mainly into the salite field close to the salite-augite field boundary, while augite and ferroaugite occur in some of the specimens. Hornblende is frequently observed along cleavage traces and grain boundaries, apparently as a retrograde phase, whilst in some grains calcite has

developed at the expense of salite. Where the mineral is in contact with hornblende, the grain boundaries are often serrated. Salite is generally less abundant than hypersthene and in only two of the specimens salite is absent.

*Hornblende* forms larger idioblastic polygonal grains. The mineral is intensely pleochroic and maximum absorption colours range from brown to brownish green. Grain boundaries are generally straight or slightly embayed and triple point junctions are common, indicating textural equilibrium with the pyroxenes. Hornblende also occurs as irregularly shaped fragments along pyroxene grain boundaries and penetrating the mineral along the cleavage planes apparently replacing the pyroxene presumably due to retrogression. Of all the specimens studied, only about 30 per cent contain no hornblende.

*Plagioclase* is the most abundant mineral, accounting for about 49 per cent of the modal composition of the average granolite specimen. The compositions of the mineral have been estimated optically utilising extinction angle techniques (Deer *et al.*, 1971) and some grains were analysed with the aid of the electron microprobe indicating a compositional variation between $An_{43}$ and $An_{90}$. Zoning is common, some grains are antiperthitic and they contain rectangular fragments of K-feldspar. Twin lamellae and cleavage planes are commonly bent, indicating later deformation. The mineral is generally fresh, but saussuritisation does occur.

*Biotite* is generally present in accessory amounts only, but in some specimens it is quite abundant. It occurs as idioblastic crystals with a moderate dimensional preferred orientation. The Z-absorption colour is always dark red-brown.

*Garnet* has only been recorded in one specimen (HA 1030) where it occurs as pale pinkish-coloured, ovoid grains closely associated with clinopyroxene, orthopyroxene and opaque minerals.

*Quartz* is present in some of the thin sections examined and occurs as more or less equant grains with undulose extinction and it is also observed in myrmekitic quartz-feldspar intergrowths.

*Opaque minerals* occupy the junctions between other grains, occur as a thin film of minute pellets along the edges of hornblende crystals, along contacts between individual pyroxene grains and along the interfaces between pyroxene and hornblende or frequently as trains of tiny specks along cleavage traces of hornblende and pyroxene. *Apatite* and *zircon* are encountered in accessory amounts, while minor *hercynite* is recorded in one of the specimens examined.

(b) Salite-bearing Amphibolites - These rocks are invariably dark, almost black in colour and of medium to coarse grain. Some outcrops are massive and relatively homogeneous with respect to composition, while banded varieties

have been recorded (e.g. on the farm Aasvogel Kop (403)). The alternating leucocratic and melanocratic bands consist of plagioclase with clinopyroxene and hornblende with clinopyroxene respectively.

Where contacts with the adjacent lithologies can be observed they are commonly concordant and no signs of intrusion are apparent suggesting that many of these mafic gneisses form part of the metavolcano-semimentary sequence. Salite-bearing amphibolites are encountered in the amphibolite facies as well as in the granulite facies terranes; their modal compositions are shown in Table 5.

*Hornblende* in specimens from the granulite facies terrane is characterised by a brown or brownish-green Z-absorption colour, while in specimens from the amphibolite facies terrane the hornblende is generally green or rarely bluish-green. Although the mineral is generally free of inclusions, some crystals are seen to enclose rounded grains of quartz, plagioclase and occasionally also clinopyroxene. Boundaries between individual hornblende crystals are straight and meet in triple point junctions, while contacts with clinopyroxene, plagioclase and quartz are either embayed or scalloped with the concave side towards the amphibole. The average salite-bearing amphibolite specimen contains 38 per cent hornblende.

In half of the specimens examined *clinopyroxene* accounts for less than 10 per cent of the modal composition. Microprobe analyses have shown that the clinopyroxene has the chemical composition of salite. The mineral occurs as xenoblastic equant grains and its colour varies from pale to fairly dark green. It is generally non-pleochroic, but in some specimens it is weakly pleochroic. Although generally free of inclusions, salite has been observed to poikiloblastically enclose plagioclase and sphene.

*Plagioclase* varies in abundance from 22 to 77 per cent. The mineral occurs as xenoblastic grains covering a compositional range of $An_{43}$ to $An_{89}$. Although plagioclase is generally fairly fresh, in some specimens the mineral is virtually completely saussuritised. Zoning is common and many grains display deformed twin lamellae.

*Quartz* occurs in small amounts in half of the specimens studied. When abundant the mineral forms fairly equant grains with interlobate boundaries and is generally in a strained state.

*Biotite* is absent from most specimens. Some rocks, however, contain this mineral in accessory amounts or rarely as much as 9 per cent (by volume). The maximum absorption colour varies from red-brown to brown.

*Sphene* is commonly seen and occurs as rims or partial rims around opaque minerals or as ovoid grains. The mineral is pleochroic and twinning is frequently observed. In two specimens (HA 606 and HA 615) sphene occurs associated with brown hornblende (characteristic of the granulite facies terrane) in apparent textural equilibrium with brown hornblende, salite and

Table 5 Estimated modal compositions (in volume per cent) of salite amphibolites. Retrograde minerals in parenthesis. Abbreviations as in preface. (m = <1%).

| Sample No. | hornblende | salite | plagio-clase | quartz | biotite | opaque minerals | other = m | locality |
|---|---|---|---|---|---|---|---|---|
| HA 1111 | 46 | m | 47 | 6 | m | 1 | Ap Sn Zc (Cc) | D2 |
| HA 1110 | 55 | 17 | 25 | 2 | | 1 | Sn Zc (Cz)(Se) | E2 |
| HA 1131 | 43 | 3 | 46 | 6 | | 2 | Ap(Cc)(Ch)(Se) | C3 |
| HA 1096 | 39 | 3 | 55 | 3 | | m | Ap Zc (Cz)(Mu) | D3 |
| HA 1016 | 51 | 9 | 40 | m | | m | Ap Zc (Se) | 13 |
| HA 1017 | 55 | 5 | 40 | m | | m | Ap Sn Zc (Se) (Cc) | 13 |
| HA 1129 | 30 | 41 | 29 | | | m | | 13 |
| HA 1092 | 42 | 2 | 31 | 25 | | | Ap Sn Zc (Se) | E5 |
| HA 1088 | 5 | 42 | 52 | | | 1 | Sn (Cc) (Cz) | F5 |
| HA 1136 | 30 | 1 | 50 | 10 | 5 | 4 | Ap Zc | A6 |
| HA 1137 | 45 | m | 53 | | | 2 | Ap | A6 |
| HA 1056 | 54 | 3 | 39 | 4 | m | m | Ap (Ch) | D9 |
| HA 1066 | 60 | 6 | 22 | 3 | 9 | m | Ap Zc | C10 |
| HA 391 | 51 | 15 | 34 | m | | m | Ap Zc | A23 |
| HA 577 | 28 | 2 | 69 | | | 1 | Ap Zc(Ch)(Cz)(Se) (Cc) | E23 |
| HA 548 | 19 | 1 | 77 | | 3 | m | Ap Zc (Ch) (Mu)(Ep) | F23 |
| HA 782 | 35 | 36 | 28 | | | 1 | Ap Zc (Se) | D24 |
| HA 606 | 32 | 41 | 27 | | | m | Ap Sn | H25 |
| HA 615 | 35 | 30 | 33 | | m | | Ap Sn = 2% | H25 |
| HA 625 | 22 | 36 | 42 | | | m | | H26 |
| HA 626 | 31 | 22 | 47 | | | m | Ap (Cc) | H26 |

plagioclase.

*Apatite* and *zircon* are common accessory phases, while *calcite*, *chlorite*, *clinozoisite*, *sericite* and *epidote* are the common alteration products.

(c) Amphibolites - Mafic rocks lacking salite are particularly common in the northern part of the area, a terrane characterised by amphibolite facies metamorphic grade. Amphibolites are not restricted to the amphibolite facies terrane, however, but they also occur occasionally associated with granulites. The estimated modal compositions of the amphibolites are listed in Table 6.

Table 6 Estimated modal compositions (in volume per cent) of salite - free amphibolites. Retrograde minerals in parenthesis. Abbreviations as in preface. (m = <1%).

| Sample No. | hornblende | plagio-clase | quartz | biotite | garnet | opaque minerals | other = m | locality |
|---|---|---|---|---|---|---|---|---|
| HA 1125 | 69 | 26 | 3 | m | | 2 | Ap Sn (Se)(Cz) | H1 |
| HA 1095 | 60 | 33 | 7 | | | m | Ap Sn Zc (Cz)(Ch) | D2 |
| HA 1104 | 65 | 29 | 6 | | | m | Ap Sn Zc | D2 |
| HA 1115 | 68 | 15 | 11 | m | 4 | 2 | Ap Zc (Se) | I2 |
| HA 1116 | 65 | 24 | 10 | m | | 1 | Ap Zc (Cz)(Ch) | 13 |
| HA 1121 | 68 | 23 | 8 | | | 1 | (Mu) | 13 |
| HA 1146 | 57 | 33 | 1 | 7 | | 2 | Ap Sn Zc | G4 |
| HA 1089 | 46 | 25 | 24 | m | | 5 | Ap Zc (Mu) | F5 |
| HA 1080 | 46 | 49 | 4 | 1 | | m | Ap (Ch) | G5 |
| HA 1079 | 47 | 40 | 13 | m | | m | Ap | H5 |
| HA 1134 | 25 | 30 | 33 | m | 10 | 2 | Ap (Ch) | A6 |
| HA 1084 | 69 | 28 | 2 | | | 1 | Ap Zc (Se)(Ch) | G6 |
| HA 1001 | 57 | 38 | | 5 | | m | Ap Zc (Ch)(Se) | D8 |
| HA 1015 | 32 | 31 | 13 | 18 | | 4 | Ap = 2% Zc | G8 |
| HA 1053 | 22 | 45 | 15 | 18 | | m | Ap Zc | C10 |
| HA 23 | 62 | 35 | | 1 | | 2 | Ap Zc | C21 |
| HA 141 | 22 | 77 | | | | 1 | Ap Zc (Ch) | E24 |
| HA 161 | 52 | 47 | | m | | 1 | Ap Zc | E24 |
| HA 542 | 59 | 39 | 1 | m | | 1 | Ap Zc | G24 |

*Hornblende* in amphibolites from the granulite facies terrane has a brown to brownish-green z-absorption colour and tiny opaque granules (probably ilmenite) are crowded along the crystal margins and cleavage traces. In contrast, the hornblende in specimens from the amphibolite facies terrane is characterised by a green or occasionally bluish-green Z-absorption colour and opaque granules are generally absent. Besides these opaque minerals, hornblende is generally free of inclusions.

Crystals often show a dimensional preferred orientation, becoming more pronounced in the amphibolite facies terrane. Marginal alteration to chlorite, biotite and occasionally calcite is seen around some crystals, but the majority of grains are fresh. The average amphibolite specimen contains 52 per cent hornblende.

*Plagioclase* forms equant grains with straight or curved grain boundaries. The mineral often displays symmetrical zonation and grain core compositions range between $An_{38}$ to $An_{86}$. On average the amphibolites contain about 35 per cent of this mineral, which is considerably less than in the case of hypersthene-pyroclase granolites. In most specimens the plagioclase is fresh, but occasionally sericite and epidote-group minerals have partially replaced the plagioclase.

*Quartz* is generally present in amounts ranging between 1 to 33 per cent. When quartz is abundant interlobate grain boundaries are common.

*Garnet* has not been observed in amphibolite specimens from the granulite facies terrane and is also very rare in specimens from the amphibolite facies area. Only two of the 19 specimens examined contain garnet.

*Biotite* is recorded in 14 of the 19 amphibolite specimens examined and occurs generally in accessory amounts only. When biotite is abundant it produces a lepidoblastic texture. In some specimens biotite is seen to be orientated at a high angle to the fabric defined by hornblende and is therefore considered to be of a late generation. The mineral has a red-brown maximum absorption colour and in some specimens biotite is marginally altered to chlorite.

*Sphene* has been recorded in minor amounts in four of the specimens where it occurs as ovoid grains or commonly forms a rim around opaque minerals while *apatite* and *zircon* are common accessory minerals.

## C Namaqualand Metamorphic Complex (Intrusive Rocks)

### 1 Augen Gneiss and Streaky Pink Quartzo-feldspathic Gneiss (Map unit Mg)

Gneisses of granitic composition and containing abundant augen of feldspar or aggregates of feldspar and quartz are widespread in the Namaqualand Metamorphic Complex (Joubert, 1971a). These are frequently referred to as the Nababeep Gneiss (Benedict *et al.*, 1964; van Zyl, 1967; Joubert, *op.cit.*) or Aroams Gneiss (Joubert, 1975). Mineralogically and texturally similar rocks are also encountered in the study area. In some of the outcrops the augen texture is poorly developed and only a few scattered

feldspar augen are apparent, the remaining being extremely stretched and resulting in a streaky gneiss. On the accompanying geological map the augen gneisses and streaky gneisses are grouped together under the same symbol.

These gneisses are invariably strongly foliated. The planar tectonic fabric is enhanced by the preferred orientation of feldspar augen and mafic minerals and also by a discontinuous banding which frequently appears to have developed by the intense flattening of megacrysts. A penetrative linear fabric has resulted from the extreme stretching of feldspar crystals and the preferred orientation of mafic minerals.

As a group these rocks display considerable variations in the abundance and sizes of the augen, the degree of banding and the type and abundance of the mafic mineral constituents. Weathered surfaces are either pink or light brown. Feldspar augen, when present, appear white or pink and generally have maximum dimensions of 1 to 3 cm.

Microscopic studies of several thin sections indicate that alkali feldspar, quartz and plagioclase are the dominant minerals. The alkali feldspar is generally *microperthite* but *microcline* is common in specimens from the amphibolite facies terrane. Most of the augen appear to be composed of alkali feldspar. *Plagioclase* commonly forms a myrmekitic intergrowth with quartz. *Antiperthite* is also recorded. Limited sericitisation of the plagioclase has been noticed in the majority of the thin sections studied. *Quartz* contains abundant minute inclusions and displays various strain features.

The mafic minerals include *biotite* (brown or red-brown variety and frequently partly altered to *chlorite*), *hornblende* (maximum absorption colour is green) and poikiloblasts of pink *garnet*. Biotite and garnet are by far the most common mafic minerals while hornblende is only recorded in some of the outcrops in the northern part of the study area (Map A).

The accessory minerals include *apatite, sphene, opaque minerals* and *zircon*.

Xenoliths of pink quartzo-feldspathic gneiss and cross-cutting contact relationships with adjacent gneisses suggest an igneous mode of origin for the augen gneiss and streaky gneisses. Frequently, however, the contacts with adjacent gneisses are sharp and apparently conformable creating the impression that these rocks from part of the supracrustal succession.

### 2 Bosluis and Nuwefontein Basic Bodies (Map unit Mh)

The general petrography of metagabbroids (hypersthene-pyroclase granolite) has been described (Chapter III B7). Some of the larger bodies

of definite intrusive origin have been assigned separate names. These include the Bosluis basic body (farm Bosluis (238), Map A) and the Nuwefontein basic bodies in the vicinity of Kliprand (Map B). The mineralogical compositions of several specimens collected from these basic intrusives are listed in Table 4, page 31. Two specimens from the poorly exposed Bosluis body (HA 1024 and HA 1025) consist of plagioclase, orthopyroxene, hornblende and salite as major constituents while the four specimens from the Nuwefontein bodies (HA 127, HA 951, HA 955 and HA 957) notably contain no hornblende but biotite and monor quartz instead. In two of the specimens biotite accounts for 10-12 per cent of the modal composition. In terms of the IUGS (1973) nomenclature for gabbroic rocks the Bosluis body can be described as a meta-pyroxene-hornblende gabbronite and the Nuwefontein bodies as biotite-bearing metagabbronorite and metagabbronorite.

From contact relationships with adjacent gneisses it has been deduced that the metagabbroids are intrusive rocks and their textures indicate that they have crystallised or recrystallised during granulite facies metamorphic conditions.

### 3 Charnockite and Related Alkali Feldspar-orthopyroxene-bearing Intrusive Rocks (Map units Mke, Mkc)

The term "charnockite" was introduced by Thomas Holland in 1892 to describe hypersthene-bearing granitic rocks in South India (Pichamuthu, 1953). Originally the term "charnockite series" covered a wide compositional range including hypersthene granite, norite and pyroxenite. De Waard (1969) defined charnockite as a metamorphic or magmatic rock of granitic bulk composition containing orthopyroxene (or fayalite and quartz) and perthite, and characterised by a dark grey-green colour. Most authorities on the subject seem to agree that the presence of orthopyroxene in a rock of granitic bulk composition is diagnostic. Orthopyroxene-bearing rocks whose modal compositions plot outside the granite field, as defined by Streckeisen (1967), should accordingly not be called charnockite. These have been assigned various names (Hødal, 1945; Giraud, 1964; Tobi, 1971, 1972; Torske, 1972), but so far no universally accepted classification has been published. Using the same subdivision of the alkali feldspar-plagioclase-quartz triangle proposed by Streckeisen (*op.cit.*), Tobi (1971) suggests an analgous nomenclature for orthopyroxene-bearing quartzo-feldspathic rocks. This nomenclature is subsequently criticised by Torske (*op.cit.*) and the revised version (Tobi, 1972) is used in this study (Fig. 4 ).

The orthopyroxene-bearing granitoids are characterised by variations in the abundance of the leucocratic minerals and in the type and abundance of ferromagnesian minerals present. It is therefore not surprising that they exhibit variable colours in outcrop as well as in fresh specimens. A large

number of texturally and mineralogically distinct charnockite bodies are recognised in the field but for the sake of simplicity all these are grouped together and collectively referred to as the Kliprand Charnockite Suite which includes charnockite, charno-enderbite and minor pyroxene-monzonite and monzonorite (Fig. 4). Separate status has only been assigned to a somewhat younger, dark brown weathering megacrystic rock, referred to as the Klein-Lieslap Megacrystic Charno-enderbite whose type area is situated south of Kliprand on the farm Uitkyk (9). Where texturally and/or mineralogically different charnockitic rocks occur in juxtaposition the approximate contact boundary is indicated by a broken line traversing the charnockite fields on the accompanying geological map.

Outcrops of charnockite and charno-enderbite feature prominently in the southern part of the study area in the vicinity of Kliprand (Map B) while only isolated occurrences are recorded north of latitude 30°00' S(Map A) on the farms Bosluis (238), Tauseb (237), Kat Vlei (235) and Lekker Drink (245). All the known outcrop localities are confined to the granulite facies terrane as defined by the presence of pyroxenes in metamorphosed mafic rocks.

In spite of their low mafic mineral content, these rocks are generally greenish grey, dark green to olive-brown in colour and weather in various tones of brown. They superficially resemble mafic rocks in some outcrops, their dark colour being a universally characteristic feature (Pichamuthu, 1953; Howie, 1964). According to Oliver and Schultz (1968) and Janardhan *et al.* (1979) the greenish colour is mainly due to chlorite occurring in an anastomising vein system.

The grain size is variable. Large megacrysts of feldspar commonly 6 to 7 cm in length and dimensionally orientated characterise the Klein-Lieslap Megacrystic Charno-enderbite. Augen-shaped feldspar crystals 1 to 2 cm across are common. The majority of the charnockites are inequigranular and coarse grained but some display uniform grain size distributions and are finer grained. Some varieties are characterised by a distinct lithological banding.

The estimated modal compositions of the 43 specimens studied are listed in Table 7.

*Alkali feldspar* is invariably perthitic and occurs as xenoblastic grains with large embayments. *Plagioclase* frequently forms a myrmekitic intergrowth with quartz. Individual crystals are commonly zoned. Compositions determined optically range between $An_{30}$ and $An_{45}$. Antiperthite is frequently recorded. *Quartz* is present in amounts ranging from 10 to 40 per cent (by volume). The mineral is generally strained.

Mafic minerals are not very abundant. *Orthopyroxene* occurs in small amounts (up to 12 per cent) accounting for about 3 per cent of the modal composition of the average specimen. Along grain boundaries, cleavage traces and irregular cracks the mineral is commonly partially altered to chlorite and/or amphibole and in two of the specimens examined (HA 1028, HA 749) the

alteration is complete and the former existence of orthopyroxene can only be inferred. Pleochroism of the mineral is moderate to very strong. *Clinopyroxene* is very rare and is only recorded in two specimens. *Biotite* is present in the majority of the thin sections examined, generally in small amounts (< 3 per cent). Only 7 of the 43 specimens contain biotite in excess of 3 per cent. The mineral is invariably of the red-brown variety. Only about half of the specimens studied contain *hornblende* generally accounting for less than 4 per cent of the modal composition. The maximum absorption colour of the mineral is dark brownish-green. *Garnet* is extremely rare and is recorded only in 2 of the specimens in amounts of less than 0,5 per cent.

Small amounts of *opaque minerals* occur and *apatite* and *zircon* are the main accessory phases. One of the specimens contains a trace of *green spinel* (probably hercynite). Amongst the secondary minerals *chlorite* is the most common while minor *calcite* is noted in some of the specimens studied.

The texture of these rocks can be described as granoblastic interlobate.

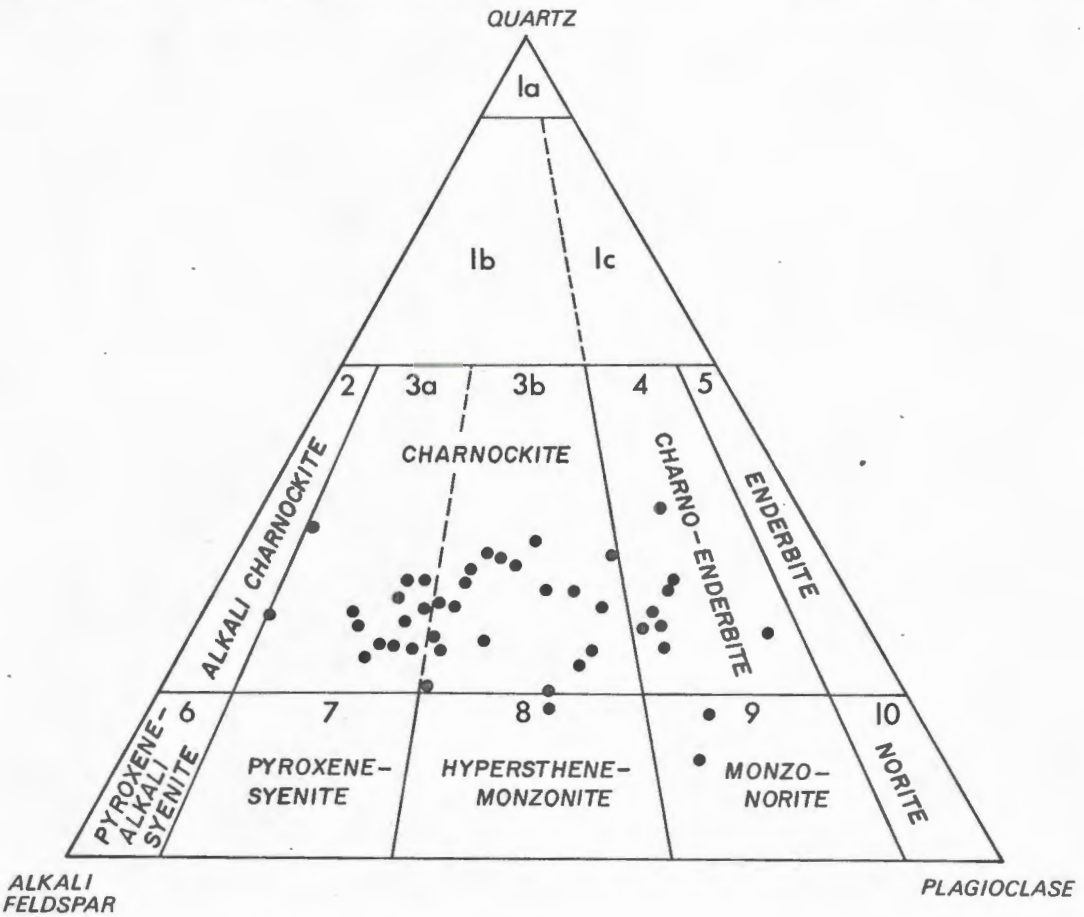


Fig. 4 Nomenclature of charnockites and related rock types from the Kliprand area in the classification of Tobi (1971, 1972). Plagioclase includes myrmekite.

TABLE 7

Estimated modal compositions (in volume per cent) of charnokites and related rocks. Retrograde minerals in parenthesis. Abbreviations as in preface. (m = <1%)

| Sample No. | K-feldspar perthite | quartz | plagioclase myrmekite | orthopyroxene | clinopyroxene | hornblende | biotite | garnet | opaque minerals | other = m | locality |
|---|---|---|---|---|---|---|---|---|---|---|---|
| HA 1075 | 16 | 25 | 27 | 12 | | m | 19 | | 1 | Ap Zc(Ch) | D7 |
| HA 1068 | 21 | 10 | 49 | 5 | 2 | m | 10 | | 3 | Ap Zc(Ch) | C9 |
| HA 1057 | 23 | 25 | 48 | m | | m | 1 | | 1 | Ap Zc(Ch)(Cc) | D9 |
| HA 1028 | 26 | 30 | 40 | | | m | 1 | | 1 | Ap Zc(Ch)(Cc) | F9 |
| HA 1065 | 20 | 26 | 44 | 4 | 1 | | 3 | | 2 | Ap Zc(Ch) | C10 |
| HA 499 | 29 | 37 | 30 | 3 | | | m | | m | Ap Zc(Ch) | A20 |
| HA 470 | 38 | 31 | 25 | 2 | | | 2 | | 2 | Ap Zc(Ch) | A21 |
| HA 985 | 33 | 35 | 29 | m | | | 2 | | 1 | Ap Zc(Ch) | B21 |
| HA 994 | 39 | 25 | 29 | 3 | | | 3 | | 1 | Ap Zc(Ch) | A22 |
| HA 933 | 46 | 25 | 23 | 2 | | 2 | 1 | | 1 | Ap Zc(Ch) | A24 |
| HA 936 | 27 | 30 | 35 | 3 | | 4 | m | | 1 | Ap Zc(Ch)(Cc) | A24 |
| HA 948 | 62 | 29 | 7 | 1 | | | 1 | | m | Ap Zc(Ch) | A24 |
| HA 947 | 34 | 16 | 36 | 4 | | 8 | m | | 2 | Ap Zc(Ch) | B24 |
| HA 953 | 9 | 22 | 48 | 7 | | | 13 | m | 1 | Ap Zc(Ch) | C24 |
| HA 788 | 35 | 18 | 38 | 6 | | 1 | | | 2 | Ap Zc(Ch)(Cc) | E24 |
| HA 581 | 18 | 31 | 44 | 3 | | | 3 | m | m | Ap Zc | G24 |
| HA 928 | 29 | 23 | 40 | 6 | | m | 1 | | 1 | Ap Zc(Ch) | A25 |
| HA 942 | 46 | 26 | 25 | 1 | | 1 | 1 | | m | Ap Zc(Ch) | B25 |
| HA 295 | 19 | 26 | 42 | 5 | | | 7 | | 1 | Ap Zc(Ch) | D25 |
| HA 649 | 51 | 25 | 21 | 3 | | | m | | | Ap Zc(Ch) | F25 |
| HA 950 | 30 | 31 | 33 | 2 | | 1 | 2 | | 1 | Ap Zc(Ch) | A26 |
| HA 927 | 45 | 33 | 21 | 1 | | m | m | | m | Zc(Ch) | A26 |
| HA 670 | 30 | 22 | 40 | 2 | | | 6 | | m | Ap Zc(Ch) | F26 |
| HA 666 | 19 | 16 | 52 | 6 | | | 6 | | 1 | Ap Zc(Ch) | F26 |
| HA 667 | 22 | 25 | 43 | 4 | | | 2 | | 4 | Ap Zc(Ch) | F26 |
| HA 654 | 34 | 40 | 18 | 5 | | | 2 | | 1 | Ap Zc(Ch) | G26 |
| HA 892 | 34 | 35 | 26 | 4 | | m | 1 | | m | Ap Zc(Ch) | B27 |
| HA 879 | 38 | 34 | 25 | 3 | | | m | | m | Ap Zc(Ch) | B27 |
| HA 883 | 45 | 30 | 23 | 2 | | | m | | m | Ap Zc(Ch) | B27 |
| HA 890 | 44 | 33 | 19 | m | | 4 | m | | m | Ap Zc(Ch) | B27 |
| HA 922 | 49 | 29 | 22 | m | | | m | | m | Ap Zc(Ch)(Mu) | B27 |
| HA 881 | 45 | 24 | 25 | 2 | | 4 | | | m | Ap Zc(Ch) | C27 |
| HA 896 | 52 | 40 | 6 | 1 | | | m | | 1 | Ap Zc(Ch) | D27 |
| HA 724 | 33 | 35 | 26 | 5 | | m | 1 | | m | Ap Zc(Ch) | H27 |
| HA 733 | 47 | 31 | 21 | m | | | 1 | | m | Ap Zc(Ch) | H27 |
| HA 722 | 40 | 29 | 25 | 5 | | m | m | | 1 | Ap Zc(Ch) | H27 |
| HA 747 | 14 | 39 | 38 | 2 | | | 6 | | 1 | Ap Zc He(Ch) | I27 |
| HA 872 | 52 | 28 | 15 | 2 | | | 2 | | 1 | Ap Zc(Ch) | A28 |
| HA 889 | 49 | 24 | 21 | 1 | | 5 | | | m | Ap Zc(Ch) | B28 |
| HA 749 | 50 | 21 | 27 | | | m | 2 | | m | Ap Zc(Ch)(Cc) | I28 |
| HA 862 | 43 | 30 | 25 | m | | | 2 | | m | Ap Zc(Ch) | B29 |
| HA 746 | 53 | 25 | 20 | 1 | | | 1 | | m | Ap Zc(Ch) | I29 |
| HA 742 | 53 | 29 | 17 | 1 | | m | | | m | Ap Zc(Ch) | I30 |

Charnockites invariably display a planar fabric in outcrop. This fabric is enhanced by the dimensional preferred orientation of feldspar megacrysts and in several outcrops by a pronounced banding. A weak linear fabric is often apparent within the foliation plane. Contacts with the surrounding gneisses vary from sharp to gradational and where the country rocks weather to a similar colour, considerable difficulty was experienced in locating contacts. Although the charnockites are often concordant within the surrounding gneisses there is ubiquitous evidence that they cross-cut adjacent lithologies. This together with the fact that they contain abundant xenoliths of the rock types comprising the volcano-sedimentary succession suggests that they are intrusive into and therefore post-date the paragneiss sequence.

The magmatic versus metamorphic modes of origin of charnockites is a controversial matter (Pichamuthu, 1953; Howie, 1955; Parras, 1958; Wilson, 1960; Cooray, 1969; de Waard, 1969; Bhattacharyya, 1972; Ramaswamy and Murty, 1973). Any one of the following processes can generate charnockite :

(a) Granulite facies metamorphism of pre-existing dry rocks of granitic bulk composition (sedimentary or magmatic).

(b) *In situ* dry melting during granulite facies metamorphism.

(c) Intrusion of a "dry" magma (undersaturated with respect to $H_2O$) into a dehydrated crust during granulite facies metamorphism with or without subsequently recrystallising under granulite facies conditions.

Field evidence supports a magmatic origin for the bulk of the charnockites in the study area, but there are several features indicating that these rocks recrystallised (or crystallised) under granulite facies metamorphic conditions. These include the following :

(a) Crystallisation in a stress field is indicated by the presence of a distinct planar fabric.

(b) Granoblastic textures resemble those in adjacent quartzo-feldspathic gneisses which have demonstrably been subjected to granulite facies metamorphism.

(c) Euhedral crystal outlines which are expected to result during crystallisation in a slowly cooling melt are absent.

(d) Hypersthene is frequently intensely pleochroic, which according to Howie (1955) is characteristic of high grade metamorphism.

Where in contact with augen gneiss and early syntectonic intrusive quartzo-feldspathic gneisses, (streaky gneisses) the charnockites always appear to be the younger intrusive phase. The Klein-Lieslap Megacrystic Charno-enderbite frequently contains xenoliths of other charnockites and

enderbites of the Kliprand Charnockite Suite. It is also demonstrably younger than many of the megacrystic (pyroxene-free) granitoids and it appears that the Klein-Lieslap Megacrystic Charno-enderbite is a relatively late syntectonic intrusive rock.

### 4 Karagas Hornblende-quartz Monzonite-gneiss (Map unit Mu)

On the farms Uitkyk (9) and Obeeb (8) a monzonitic gneiss crops out as an irregularly shaped amoeboid body approximately five km in length and on average about one km wide. In addition to this main body there are a few isolated occurrences within the Klein-Lieslap Megacrystic Charno-enderbite further south.

The characteristic features aiding in field identification include its grey colour, the presence of abundant hornblende, a pronounced mineral lineation caused by the alignment of hornblende crystals within a prominent planar tectonic fabric and its fairly homogeneous appearance with respect to mineralogical composition and grain size (the average sizes of individual grains range between one and two mm).

The mineralogical composition of the rock comprises alkali feldspar (45%), plagioclase (31%), quartz (13%), hornblende (10%) and opaque minerals (1%). In addition biotite, apatite and zircon occur in accessory amounts.

*Alkali feldspar* is generally untwinned and only a few grains display a poorly developed polysynthetic twinning. Fine exsolution lamellae can be detected optically in only some of the grains.

*Plagioclase* occurs as xenoblastic zoned grains and frequently forms a myrmekitic intergrowth with *quartz*. The latter mineral invariably displays undulose extinction and contains numerous tiny inclusions.

Apart from minor *biotite*, *hornblende* is the sole mafic mineral. It contains abundant small opaque inclusions and is characterised by a brownish-green Z- absorption colour.

The dominant internal structures of this gneiss are a penetrative planar fabric and a prominent mineral lineation, both of which are indistinguishable from similar structures in the adjacent gneisses.

Contacts with the surrounding pink quartzo-feldspathic gneisses are frequently discordant and xenoliths of pink gneiss are common suggesting that the Karagas Hornblende-quartz Monzonite-gneiss was emplaced as a magma.

From contact relationships it was deduced that the Klein-Lieslap Mega-

crystic Charno-enderbite and the Lepel Megacrystic Granite-gneiss are both younger than the Karagas Hornblende-quartz Monzonite Gneiss.

## 5 Syntectonic Granite/Granodiorite-gneiss

This section deals with a very brief description of the following rock units:

Klein Matjesfontein Alkali-feldspar Granite-gneiss (Map unit Mk)
Roode Kloof Granite-gneiss (Map unit Mr)
Burtons Puts Megacrystic Granite-gneiss (Map unit Mbs)
Daauws Megacrystic Granite-gneiss (Map unit Mag)
Uilklip Megacrystic Granite-gneiss (Map unit Mug)
Megacrystic Leucocratic Granite-gneiss (Map unit Mlg)
Lepel Megacrystic Granite-gneiss (Map unit Mub)
Banke Megacrystic Granodiorite-gneiss (Map unit Mb)
Klein Banken Megacrystic Granodiorite-gneiss (Map unit Mkg)
Ekstensie Megacrystic Granodiorite-gneiss (Map unit Mtg)

The criteria applied in the field to distinguish these granitoids involved grain size, the type and abundance of mafic minerals (biotite, garnet, hornblende) and the colour displayed on weathered and fresh surfaces. As a group these rocks are very coarse grained, inequigranular and generally containing abundant feldspar megacrysts, which in some of the granitoids (e.g. Lepel Megacrystic Granite-gneiss and Banke Megacrystic Granodiorite-gneiss are 5-7 cm long and almost 2 cm across. These megacrysts are dimensionally orientated and define a planar fabric suggesting that these rocks crystallised in a stress field.

Estimated modal compositions are listed in Table 8 and plotted in a Streckeisen diagram (Fig. 5). Too much reliance should not be placed on the actual figures (Table 8) as these are based on rather small samples (the area of a normal thin section) which may not yield a representative estimate of the abundance of minerals owing to the coarse grained nature of the specimens studied.

*Alkali feldspar* generally accounts for the bulk of the megacrysts. The mineral is invariably perthitic. In some of the granitoid specimens *plagioclase* features prominently amongst the megacrysts. Antiperthite is common and the composition ranges between oligoclase and andesine. Crystals are frequently zoned, display various strain features and commonly occur as myrmekitic intergrowth with quartz. Some grains are affected by sericitisation. *Quartz* invariably occurs in a strained state and individual grains often have amoeboid outlines. Quartz forms lenses and stringers in outcrops of the Roode Kloof Granite-gneiss.

The concentration of mafic minerals is variable from trace amounts to about 10-15 per cent. *Biotite* is the most common mafic mineral. Its Z-absorption colour varies between brown and red-brown suggesting a high temperature environment. In some of the specimens biotite is partly or completely altered to chlorite. The biotite is commonly accompanied by *garnet* poikiloblasts enclosing rounded grains of quartz. The size of garnet grains varies between less than 1 mm to several cm in diameter. Appreciable amounts of *hornblende* are recorded in specimens from the Banke Megacrystic Granodiorite-gneiss. The mineral has a green to greenish brown Z- absorption colour. In specimens from the Klein Banken Megacrystic Granodiorite gneiss the former presence of hornblende can only be inferred from the alteration products consisting essentially of chlorite, green biotite and calcite. The chlorite often forms an anastomising system of veins radiating into the adjacent feldspar matrix.

*Apatite, zircon* and *opaque minerals* are the common accessory phases while *hercynite* is recorded in one specimen. The alteration products of primary minerals are *chlorite, calcite, green biotite* and *sericite.*

There is little doubt that these granitoids reached their present position in a magmatic state. Evidence in support of this is furnished by the ubiquitously recorded xenoliths and their cross-cutting contact relationships with the gneisses they intrude. The absence of chilled margins and contact metamorphic phenomena suggests that these rocks were emplaced into a hot environment. From their coarse grain size it may be deduced that cooling was a slow process and probably took place at some depth.

On the farms Burtons Puts(408) and Banke (409) the Burtons Puts Megacrystic Granite-gneiss occurs in juxtaposition with a dark brown weathering orthopyroxene-bearing intrusive rock, which on account of its texture and mineralogy has been correlated with the Klein-Lieslap Megacrystic Charno-enderbite. The latter contains abundant xenoliths of the granite-gneiss suggesting (provided the correlation is correct) that the emplacement of the Burtons Puts Megacrystic Granite-gneiss pre-dates the intrusion of the charno-enderbite.

The Daauws Megacrystic Granite-gneiss contains xenoliths of and thus post-dates the Megacrystic Leucocratic Granite-gneiss. Its relationship to the Klein-Lieslap Megacrystic Charno-enderbite is not known. Difficulty was experienced in locating the contact between the two rock types on the farm Daauws(402) as both these rocks are brown weathering.

From contact relationships it has been deduced that the Uilklip Megacrystic Granite-gneiss is older than the Klein-Lieslap Megacrystic Charno-enderbite but younger than the Megacrystic Leucocratic Granite-gneiss.

On the farms Obeeb (8) and Uitkyk (9) there is good evidence that the Lepel Megacrystic Granite-gneiss pre-dates the emplacement of the Klein-Lieslap Megacrystic Charno-enderbite.

The relative ages of the remaining granitoids are uncertain. Very similar rocks have been described from the adjacent area by Joubert (1971a) as porphyroblastic granite-gneiss.

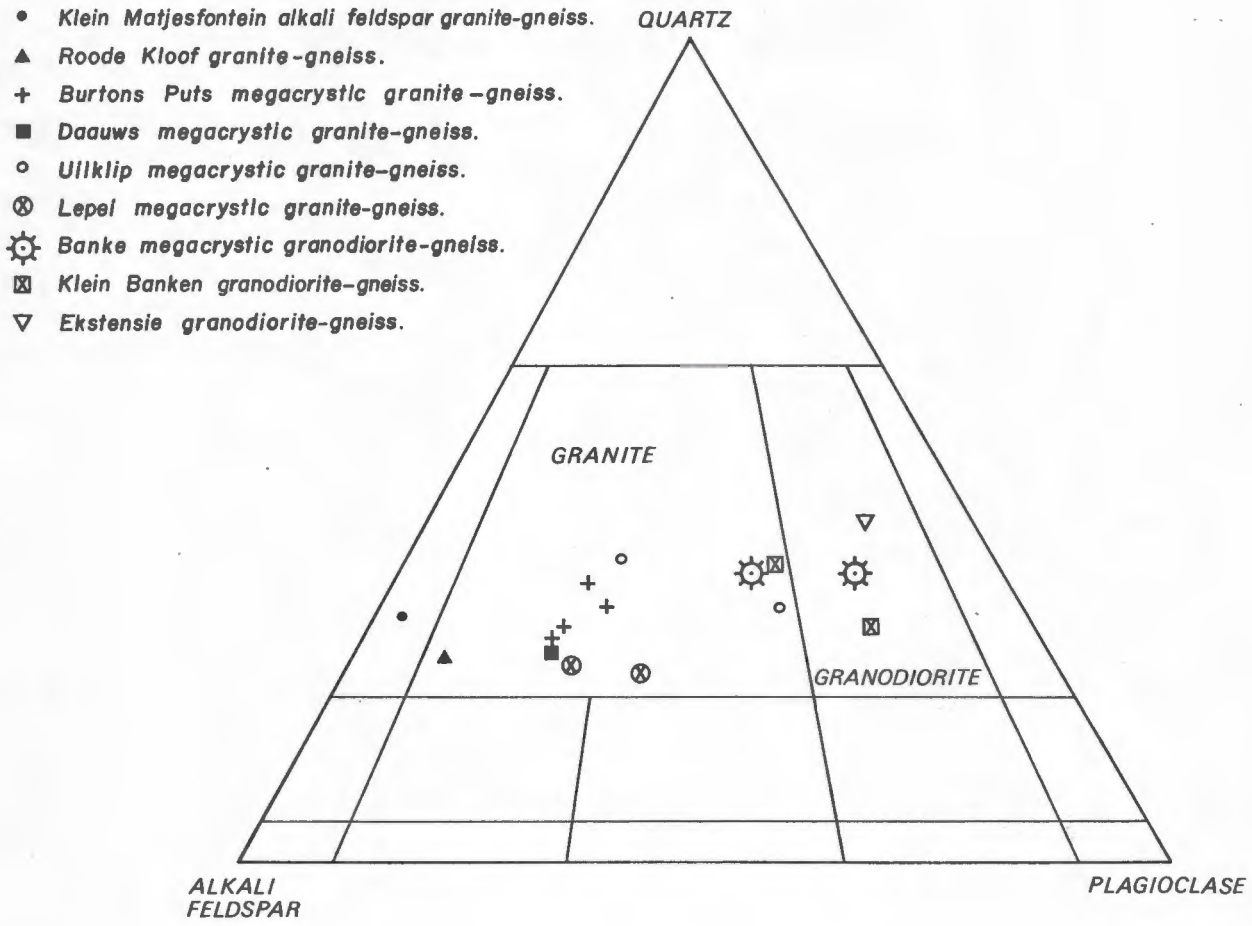


Fig. 5 Modal compositions of megacrystic granite/granodiorite gneisses plotted in a Streckeisan diagram.

Table 8 Estimated modal compositions of granite/granodiorite-gneisses. Abbreviations as in preface. (m = <1 per cent). Retrograde minerals in parenthesis.

| Sample No. | Map unit | quartz | K-feldspar | plagioclase/ myrmekite | biotite | garnet | hornblende | opaque minerals | other = m | locality |
|---|---|---|---|---|---|---|---|---|---|---|
| HA 372 | Mk | 30 | 67 | 3 | | | m | m | Zc | B23 |
| HA 736 | Mr | 25 | 65 | 10 | m | | | m m | Zc | H27 |
| HA 492 | Mbs | 28 | 48 | 21 | 3 | m | | m | Ap Zc (Ch Se) | B20 |
| HA 482 | Mbs | 30 | 43 | 24 | 3 | m m | | m | Ap Zc (Cc) | B20 |
| HA 488 | Mbs | 27 | 53 | 18 | 2 | m | | m | Zc | B20 |
| HA 519 | Mbs | 34 | 43 | 21 | 2 | m | | m | (Cc. Ch) | B20 |
| HA 644 | Mag | 26 | 50 | 21 | 3 | m | | m | Ap Zc | H26 |
| HA 798 | Mug | 31 | 26 | 43 | m | | | m | Zc | C30 |
| HA 683 | Mug | 37 | 38 | 23 | | | | | Ap Zc (Ch=2%) | F28 |
| HA 771 | Mub | 20 | 39 | 28 | 11 | 2 | | m | Ap Zc (Ch) | E26 |
| HA 599 | Mub | 21 | 46 | 21 | 8 | 4 | | | Ap Zc (Ch) | H25 |
| HA 512 | Mb | 29 | 14 | 41 | 8 | | 7 | 1 | Zc | A20 |
| HA 535 | Mb | 31 | 24 | 34 | 5 | | 6 | m | Zc | C20 |
| HA 818 | Mkg | 35 | 23 | 38 | 4 | m | | m | Ap Zc | A32 |
| HA 819 | Mkg | 24 | 15 | 46 | 3 | | | 2 | Ap He Zc (Ch/green Bi=10%) | A32 |
| HA 860 | Mtg | 38 | 10 | 45 | 6 | | | 1 | Ap Zc (Ch Se) | A29 |

# 6 Minor Intrusive Rocks

## (a) Obees Ultramafic Body (Map unit Mou)

The only outcrops of plagioclase-free ultramafic rocks found in the area occur on the farm Obees (402). These pitch black rocks are inhomogeneous with respect to grain size and composition. Amphibole crystals are up to 2 cm across.

Microscopic examination of one specimen (HA 601, Table 9 ) has revealed the presence of the following minerals (arranged in order of decreasing abundance): Amphibole, olivine, orthopyroxene, spinel and opaque minerals.

*Amphibole* forms large idioblastic crystals with straight grain boundaries meeting in triple points and yielding a granoblastic polygonal mosaic. The mineral has a greenish-brown colour and its chemical composition is that of magnesio-hornblende (Chapter III E).

*Olivine* is remarkably fresh and commonly occurs in clusters consisting of several crystals. Inclusions of opaque minerals and spinel are common. Hyalosiderite composition is indicated by microprobe analyses (Chapter III E).

*Orthopyroxene* has a pale pinkish colour and is weakly pleochroic. Its chemical composition is that of bronzite (Chapter III E).

A dark green *spinel* is present as small equidimensional grains. Its chemistry comprises essentially the hercynite-spinel solid solution series (Chapter III E). *Opaque minerals* occur in accessory amounts.

The metamorphic nature of this rock is documented in its granoblastic polygonal texture. Its strong, penetrative planar fabric is concordant with the gneissic banding in the adjacent paragneisses. Yellow-weathering calc-silicate rocks, graphitic quartzite, aluminous quartzo-feldspathic gneiss and iron formation occur in contact or in close proximity to the contacts with the ultramafic rocks. Although no xenoliths have been recorded, its cross-cutting contact relationship with the calc-silicate rocks suggests that the Obees Ultramafic Body has originally been emplaced as an igneous rock. The texture and mineralogy clearly demonstrate that this rock was subjected to conditions of high grade regional metamorphism subsequent to its emplacement.

## (b) Other Olivine-bearing Mafic/Ultramafic Bodies (Map unit Mo)

In addition to the Obees Ultramafic Body, which consists solely of mafic minerals, there are other small bodies with similar mineralogy but containing considerable amounts of plagioclase. Only two outcrop localities within the granulite facies terrane have been found during field work (farms Kamas (405)

and Uitkyk (9 )). Very similar rocks have also been sampled in the amphibolite facies terrane (farms Struisbult (94) and Donkerduispraat (95)). The specimens collected in the granulite facies terrane display granoblastic textures while corona textures feature prominently in the two specimens from the amphibolite facies terrane. It appears that the coronas overprint a pre-existing igneous texture.

The estimated modal compositions of these rocks are listed in Table 9.

*Amphibole* and *biotite* are the hydrous minerals encountered. In the specimens from the granulite facies terrane (HA 550 and HA 289) the maximum absorption colour of the amphibole is dark brown. The mineral occurs in two habits; as polygonal grains with straight grain boundaries meeting in triple points and as ragged small flakes edging pyroxene and apparently replacing it. Amphibole and olivine grains occur in contact in specimen HA 550 with no sign of reaction suggesting that both minerals were in stable coexistence during regional metamorphism. This also applies to specimen HA 289, but in the thin section studied smaller orthopyroxene grains frequently shield the olivine from the amphibole. In the two specimens from the amphibolite facies terrane (HA 1112 and HA 1145) the amphibole forms a symplectite with spinel in coronas separating olivine and plagioclase or ore minerals and plagioclase (Chapter III E). Biotite is only recorded in accessory amounts.

*Plagioclase* is frequently zoned and varies in abundance between 4 and 70 per cent. In one of the specimens (HA 550) the central parts of larger plagioclase crystals are crowded with numerous tiny spinel inclusions varying in shape from round to rod like. It is remarkable that not all the plagioclase grains contain these spinel inclusions, but where present, the spinel dust is restricted to the centres of the grains. The spinel clouded grain centres are surrounded by and occur in optical continuity with an inclusion-free plagioclase rim. Clouding of plagioclase by dust-like spinel inclusions in metagabbros is frequently recorded in the literature (Frodesen, 1968; Starmer, 1969; Whitney, 1972; Whitney and McLelland, 1973; McLelland and Whitney, 1980a,b).

*Olivine* occurs in small amounts (< 10 per cent) and forms rounded equant grains. The mineral is remarkably fresh. In the specimens from the amphibolite facies terrane olivine is invariably shielded from plagioclase by secondary corona minerals.

*Orthopyroxene* is moderately pleochroic and in most of the specimens studied forms the dominant mineral. Schiller textures and fine exsolution lamellae are present and the mineral occurs in two habits; as continuous rims (coronas) surrounding olivine (Chapter III E) and as primary equant grains which are often marginally retrogressed to amphibole.

*Clinopyroxene* is recorded in small amounts in the specimens collected in the amphibolite facies terrane.

*Opaque minerals*, dark green *spinel*, *biotite* and *zircon* occur in accessory amounts. The opaque minerals are occasionally rimmed by an amphibole-spinel symplectite along the ore-plagioclase contacts. The spinel occurs in different habits; as tiny vermicular rods intergrown with amphibole in coronas, as minute rod-like and round inclusions in plagioclase and as larger equant grains.

Contact relationships are generally obscured by superficial cover (the only evidence for the existence of these rocks on the farm Donkerduispraat (95) comprises several boulders penetrating the sand cover) but an original magmatic mode of origin of these rocks is considered to be most likely.

Table 9 Estimated modal compositions (in volume per cent) of olivine-bearing mafic and ultramafic rocks. Abbreviations as in preface. (m = 1%).

| Sample No. | Olivine | Orthopyroxene | Clinopyroxene | Hornblende | Plagioclase | Opaque minerals | Other = m | Locality |
|---|---|---|---|---|---|---|---|---|
| HA 1112 | 4 | 80 | 2 | 10 | 4 | m | Bi, Ch, Se, Sp, Zc | E1 |
| HA 1145 | 6 | 15 | 8 | 1 | 70 | m | Sp | G1 |
| HA 289 | 5 | 60 | | 10 | 25 | m | Bi, Sp | D24 |
| HA 550 | 10 | 55 | | 15 | 20 | m | Sp | F23 |
| HA 601 | 14 | 4 | | 80 | | m | Sp | H25 |

(c) Dyke-like Intrusive Bodies

Several occurrences of charnockite and hypersthene-pyroclase granolite assume dimensions of dyke or sill-like bodies emplaced concordantly along the regional foliation in the adjacent country rock. As these rocks have been described previously under the appropriate sections they are not considered here.

Besides these are some dyke-like bodies of intermediate to acid composition which have been emplaced along the regional foliation on the farms Banke (409) and Kamas (405). These rocks are distinctly banded and foliated and they frequently contain leucocratic quartzo-feldspathic seggregations which are discontinuous along strike. Other dykes are considerably younger and cut across the regional foliation and major folds. The latter are generally emplaced along younger shear zones and several of these dykes have been sheared subsequent to their emplacement and possess a distinct planar fabric. These younger dykes generally assume an east-west or east-southeast trend, but locally (e.g. on Bovenste Vlei (398) small dykes strike to the north-northwest.

Several specimens of these grey coloured medium to coarse-grained rocks have been studied petrographically and their modal compositions are listed in Table 10. One of the specimens (HA 558) collected on the farm Kamas (405) consists essentially of plagioclase and red biotite with minor amounts of quartz. Mineralogically, therefore, this rock is similar to some lamprophyres.

All other dyke rocks contain variable proportions of alkali feldspar, plagioclase and quartz and from Fig. 6 it is apparent that in terms of their mineral composition, they plot into the granite, quartz monzonite quartz monzo-diorite and diorite fields.

The alkali feldspar is *microcline microperthite* or *microcline*. In some specimens the *plagioclase* is antiperthitic and often forms a myrmekitic intergrowth with quartz. The latter mineral is frequently in a strained state.

The total mafic mineral content varies between 10 to 20 per cent by volume and comprises essentially biotite and hornblende. *Biotite* varies in maximum absorption colour from brown to red and in sheared rock is dimensionally orientated and defines a pronounced planar fabric. *Hornblende* is characterised by a green or greenish-brown Z-absorption colour, but in some specimens the amphibole is brown.

*Opaque minerals* are recorded in all the specimens studied and *apatite, fluorite, sphene* and *zircon* are common accessory phases. *Orthopyroxene* has only been recorded in small amounts in specimen HA 466.

Alteration of primary phases is common and consists of the sericitisation of plagioclase and the partial replacement of ferromagnesian phases by *calcite*, *chlorite* and *epidote group minerals*. It must be noted that there are also some east-west striking black mafic dykes, but they are not common. On the farm Tafelberg (64) for example, a small basic dyke is unconformably overlain by sediments of the Nama Group indicating that its emplacement must pre-date the deposition of these sediments. The largest mafic dyke recorded in the area traverses across the farms Matjes Fontein (1) (A21) and Middel Post (3) (B21) and has been emplaced into an east-west shear zone.

Table 10 Estimated modal compositions (in volume per cent) of various dyke-like bodies. Secondary alteration minerals are shown in brackets (m = < 1%)

| Sample No. | K-feldspar | plagioclase | quartz | biotite | hornblende | other | locality |
|---|---|---|---|---|---|---|---|
| HA 463 | 40 | 25 | 27 | 6 | | Ap F Om Sn (Ch) (Se) | B21 |
| HA 466 | 26 | 30 | 24 | 4 | 12 | Ap F Om Op (Ch) (Ep) (Se) | A21 |
| HA 476 | 34 | 28 | 25 | 7 | 2 | Ap Om Zc (Ch) (Ep) (Se) | A21 |
| HA 558 | | 75 | m | 25 | | Ap Om Zc (Se) | F24 |
| HA 561 | 33 | 44 | 15 | 2 | 5 | Ap Om Zc (Cc) (Ch) (Mu/Se) | G24 |
| HA 573 | 45 | 20 | 24 | 1 | 9 | Ap Om Sn Zc (Cc) (Ch) | F24 |
| HA 596 | 33 | 28 | 25 | 14 | | Ap Om Sn Zc (Ch) (Se) | H25 |
| HA 940 | 20 | 43 | 15 | 9 | 11 | Ap Om Zc (Ch) (Se) | B24 |
| HA 415 | 34 | 30 | 27 | 3 | 4 | Ap Om Zc (Cc) (Ch) (Se) | A23 |
| HA 496 | 42 | 24 | 22 | 4 | 7 | Ap Om Sn Zc (Cc) (Ch) | A20 |

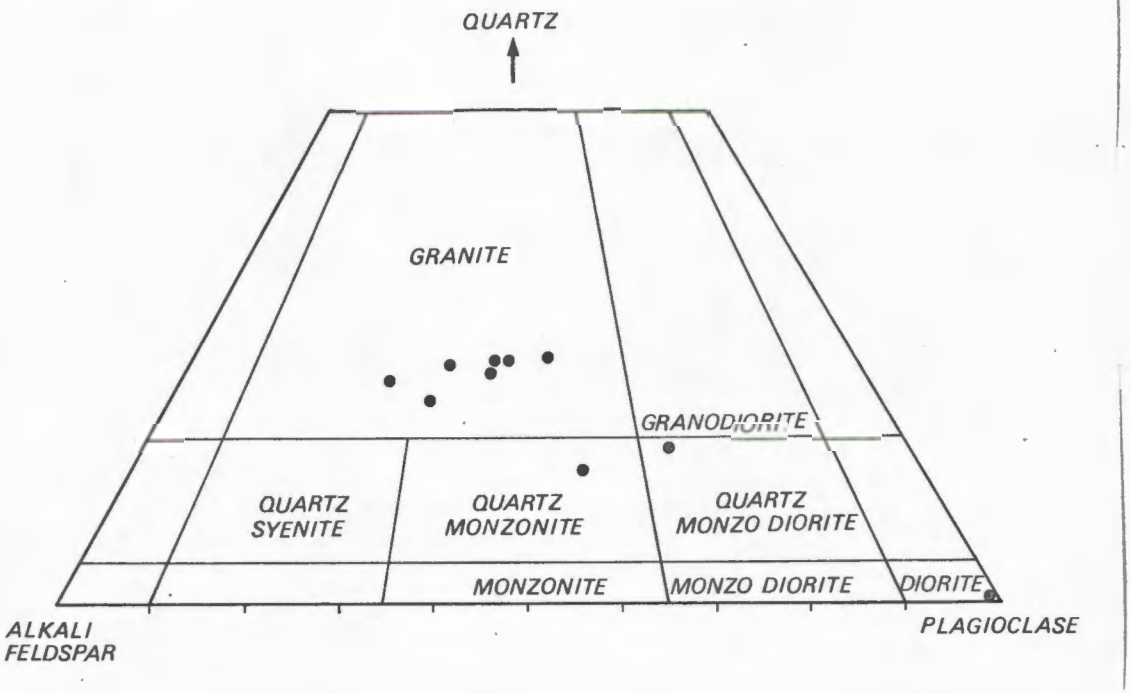


Fig. 6 Modal compositions of dyke-like intrusive rocks plotted in a Streckeisen diagram.

(d) Quartz Veins and Pegmatites

Major quartz veins large enough to be shown on the accompanying geological map generally trend west-northwest, west-southwest or east-west and they are recorded on the farms Dabidas (407), Dooddrink (406), Kamas (405) and Tafelberg (64). Smaller occurrences are, however, widespread throughout the area and frequently consist of an anastomising vein system in tectonic slides, shear zones and fault breccias.

Pegmatites are also commonly encountered throughout the area, but they are too small to be shown on the accompanying geological map. Several ages of pegmatitic veins are deduced from cross-cutting relationships. Two distinctly different compositional types have been found; ordinary leucocratic quartzo-feldspathic pegmatites, and magnetite-rich pegmatitic

rocks. The emplacement of these rocks frequently appears to be structurally controlled as they commonly occur along shear zones. Some of the pegmatites in the shear zones are bordered by mylonite but the pegmatite itself does not show any evidence of shearing and accordingly appears to post-date the shear deformation. In other shear zones the pegmatites contain ovoid augen-shaped crystals and their mylonitic texture indicates that they themselves were affected by the shear deformation.

## D Nama Group (Map units Nns, Nnq)

Arenaceous and argillaceous sediments correlated with the Nama Group in South West Africa/Namibia (Rogers, 1913; Kröner, 1968) of an age straddling the Precambrian-Cambrian boundary (Germs, 1972, 1974) are encountered in the extreme southwestern part of the study area. These sediments form part of the northernmost outcrop of a small basin in the Vanrhynsdorp-Niewoudtville-Nuwerus area.

According to Kröner (*op.cit.*) the stratigraphic sequence of these Nama sediments in the Rooiberg area to the southeast of Nuwerus comprises a basal unit of phyllite, grits, quartzite and limestone followed by a predominantly quartzitic unit which is feldspathic and frequently gritty and contains discontinuous layers of conglomerate, phyllite and shale and has been equated with the Kuibis "Series" (*ibid.*). Conformably overlying these quartzites are shales with discontinuous layers of mudstone and grit and these are correlated with the Schwarzrand "Series" (*ibid.*), now referred to as the Knersvlakte Formation (SACS, 1980).

In the study area the Nama sediments overlie the gneisses of the Namaqualand Metamorphic Complex with a marked angular unconformity. During the present investigation the basal member, correlates of the Mostertskop and Aties Formation (SACS, 1980) are not recognised. Instead the basal Nama comprises white feldspathic quartzites (Kuibis Formation - SACS, 1980) with coarse clastics (ferruginous feldspathic conglomerates) featuring prominently along the gneiss-sediment contact. In places the basal conglomerate contains as much as 50 per cent feldspar in the matrix. The quartzites overlying the basal conglomerate contain discontinuous bands of grit and conglomerate with well-rounded quartz pebbles. Isolated quartz pebbles are also recorded in the quartzites. On Bushmans Graaf Water (68) the quartzites are interbanded with a thin discontinuous lens of brecciated limestone. The northernmost occurrence of quartzites correlated with the Kuibis Formation are encountered on the farms Groot Klip (16) and Roode Sloot Vlakte(123)(G29) where these rocks are dipping gently (08-12 degrees) into a predominantly southerly to southeasterly direction.

Kröner (*op.cit.*) notes that the basal limestones are thickest in the central parts of the Nama basin, thinning out northwards and disappear in proximity of the Namaqualand gneisses. This is consistent with the absence of the pre-Kuibis Formation limestone-phyllite units in the study area.

Conformably overlying the quartzites are argillaceous rocks (shales and phyllites) with interbedded impure sandstones, grits, conglomerates and carbonates.

The coarse-grained nature (conglomerates and grits) and the immaturity of the sediments suggests that they represent a proximal facies close to the shoreline of the ancient Nama sea.

In the study area the Nama sediments strike dominantly in a north-northwest direction with generally southwesterly dips at angles ranging between 15 and 40 degrees. Across strike the succession is repetitive partly as a result of major fault displacements with northeasterly downthrow, but also due to rather gentle folding with plunges at shallow angles of 06 to 10 degrees towards the southeast or south-southeast. Further westwards in the Nuwerus area and also elsewhere in the Nama basin, Kröner (*op.cit.*) recognises two pulses of deformation, an older one yielding northwest-southeast folds plunging in either direction (these are certainly of the same generation as the major Nama folds in the study area) and a younger generation of northeast-southwest-trending folds which is responsible for the bimodal plunge directions of the earlier folds (*ibid.*). The younger folds are not well developed in the area investigated.

Although no thin sections of the Nama sediments have been studied it is evident from the outcrops that the metamorphic grade of these sediments is very low and according to Kröner (*op.cit.*) is largely confined to greenschist facies conditions.

## E Karoo Sequence

Large parts of the area studied are covered by Karoo sediments which are unconformably overlying the gneisses of the Namaqualand Metamorphic Complex. A detailed study of these sediments is beyond the scope of this thesis and the interested reader is referred to Hälbich (1962) and Theron and Blignault (1975) for stimulating discussions concerning these rocks in the adjoining area.

From the geological map of South Africa it is apparent that the outcrops encountered in the present area occupy the western most edge of an enormous sedimentary basin generally referred to as the "main Karoo basin" which covers a major part of the country.

In the study area the Karoo sequence comprises a basal rudaceous unit generally considered to be of glaciogenic origin. This diamictite (tillite) is succeeded by greenish-grey and black shaly and silty sediments. The black shales are carbonaceous and are confined to a narrow band characterised by a conspicuous white weathering which apparently results from gypsum released by reactions involving pyrite and carbonate. On account of its light colour tone it forms a prominent marker horizon which is easily spotted on aerial photographs. Previously this formation was known as the "white band" and the sediments underlying it were collectively referred to as the "Dwyka Series" which included both the diamictite and the upper Dwyka shales. The shales immediately overlying the "white band" were assigned to the "Ecca Series". In recent years, however, this arbitrary subdivision has fallen into disgrace and according to SACS (1980) the term "Dwyka" is now restricted to the basal glaciogenic sequence which has been assigned formation status while the previous "upper Dwyka shales" are now incorporated into the Ecca Group and are referred to as the Prince Albert Shale Formation and the "white band" has been renamed as the Whitehill Shale Formation.

By far the most prominent vertical profile of the entire sedimentary succession of Karoo sediments encountered in the study area is preserved in Langberg (I26/27), an "Inselberg" protected from erosion by thick dolerite sills, one of which forms a capping to the mountain. 250 to 300 metres of sediment (including some dolerite sills) comprising the entire record from the basal unconformity to the Whitehill Shale Formation are exposed in a vertical profile along the steep slopes of this mountain. In fact this is the only locality within the study area where outcrops of the Whitehill Shale Formation are recorded.

The basal diamictite is a massive, poorly sorted grey-green coloured rock with an argillaceous matrix. It contains a large compositional and textural variety of coarse angular rock fragments both of local and foreign derivation. These clasts are generally sparsely distributed and cover a wide range of sizes and shapes and it is not uncommon to find striated and faceted specimens. Common rock types recorded as erratics include: quartzite, feldspathic quartzite, arkose, various gneisses and granitoids, metamorphosed mafic rocks, jasper, chert, vein quartz, grey carbonate, banded and massive ironstone, porphyritic lava and green amygdaloidal lava with red and white amygdales. Particularly noteworthy are also the presence of round and oval shaped diamictite "balls" which range in diameter up to 25 cm and are quite abundant in places. These "balls" have an outer shell concentrically surrounding a somewhat softer core which frequently contains carbonate. These peculiar structures composed of diamictite have previously been described by Hälbich (*op.cit.*) with some discussion on their probable mode of origin.

Towards the top of the diamictite unit finely laminated shales with some clasts are alternating with thin bands of diamictite and with increasingly higher stratigraphic levels the glaciogenic sediments disappear and give way to greenish-grey shales and silty sediments interbanded with which are several dolerite sills.

Although there is general consensus regarding a glacial mode of origin for the diamictites, the ideas on ice-transport directions are diverse. Theron and Blignault (*op.cit.*), for example, believe that in the Loeriesfontein area the general ice advance was from east to west which is exactly opposite to the palaeo-ice movements envisaged by Crowell and Frakes (1972). for the same area.

Regarding the age of these rocks, it is generally believed that Karoo sedimentation commenced during the upper Carboniferous and according to Anderson (1977) the age of the Dwyka Formation is considered to be largely lower Permian.

## F Sediments of Post-Kimberlite Age

Driving along the main road between Platbakkies and Gamoep one is struck by the contrasting panorama on either side of the road. The area to the west is characterised by a rugged hilly topography underlain by gneisses of the Namaqualand Metamorphic Complex while to the east one faces an endless plain of unbroken monotony which is generally referred to as the Bushmanland Plateau, a peneplain with a gentle eastward dip and approximately 1000 metres above sea-level.

Extensive parts of this plateau are covered by a thin sequence of superficial sediments comprising unconsolidated wind blown sands, various types of soils, rubble, unconsolidated boulders and pebbles derived from weathering of Karoo tillite, silcrete, calcrete, conglomerate bands, various clays and opalised and kaolinised rocks and in restricted areas (pans) minor salt deposits. In the extreme southern part of the area similar superficial sediments form the cover to a plain which is locally referred to as the Knegsvlakte (or alternatively "Knersvlakte").

A valuable record of post-kimberlite sedimentation is preserved in many of the diatremes which according to some authors are occupied by lacustrine sediments overlying kimberlite pipes (Reuning, 1931; Cornelissen and Verwoerd, 1973, 1975). The sedimentary succession recorded in the "Boschjeslaagte" diatreme (Burtons Puts (408)) and the "Arnot" pipe (Banke (409)) have been described in detail by Reuning(*op.cit.*) and comprises from the bottom to the top a thick basal sequence of shales and carbonaceous shales with "Kieselguhr" and gypsum and silica concretions, clayey sandstones, silicified sands and rubble. The basal shaley sequence has yielded a variety of fossils including frogs ( Haughton,1931) various plant remains consisting of dicotyledonous leaves and wood remains as well as fern impressions (Rennie, 1931; Adamson, 1931). According to Haughton (*op.cit.*) these fossils point towards an early Tertiary age of the sediments and it may be deduced that fairly humid climactic conditions must have prevailed in this area during that time. These humid conditions are also reflected by the extent of *in situ* kaolinisation of the

gneisses belonging to the Namaqualand Metamorphic complex and evidence for which is quite common in the Banke-Platbakkies area. That this kaolinisation must have occurred over an extensive area is apparent from the numerous small remnants encountered at various topographic levels throughout the area.

Subsequent silicification of progressively younger sediments and fossil dunes clearly reflect a climatic change towards increasingly arid conditions that are still prevailing at the present day.

## G Intrusives of Phanerozoic Age

### 1 Karoo Dolerite

On the farm Lang Pan (395) small outcrops of dolerite occur over an extensive area which is underlain by sediments of the Karoo Sequence. Individual occurrences are too small to be shown on the accompanying geological map. Outcrops are generally encountered along the outer margins of small circular depressions (salt pans) probably indicative of diatremes of kimberlite and related volcanic rocks. The large frequency of dolerite outcrops on Lang Pan suggests the presence of a continuous sill within the Karoo Sequence.

Very similar rocks have been recorded on the farm Uitval (400) and also within rocks of the Namaqualand Metamorphic Complex on the farms Kamiebees (368) and Skimmelkop (377).

Petrographically these dolerites are very similar to the Karoo dolerites described by Walker and Poldervaart (1941) from the Calvinia District. They consist essentially of zoned *plagioclase, clinopyroxene, orthopyroxene, olivine* and *opaque minerals*. Olivine is frequently mantled by a rim of a greenish alteration generally referred to as bowlingite (Deer *et al.*, 1971). Some of the specimens studied contain minor secondary *biotite* and one of the specimens lacks olivine but contains glass with abundant microlites instead.

It seems likely that the dolerite bodies within the gneisses of the Namaqualand Metamorphic Complex represent feeder channels to the sills in the overlying Karoo sediments or sills intruded along the gneiss-sediment unconformity.

### 2 Plugs of Olivine Melilitite and Related Volcanic Rocks

The area between Gamoep, Platbakkies and Aggeneys is known to contain numerous small plugs of olivine melilitite and olivine nephelinites. The earliest petrographic descriptions of these volcanic rocks are provided by

Rogers (1912). Subsequently Taljaard (1937) studied the various melilite basalt occurrences in South Africa and describes several plugs in western Bushmanland with considerable petrographic detail. A detailed geochemical study of these volcanic rocks is provided by Moore (1979) who distinguishes three different types of volcanic pipes in the Gamoep-Garies area:

(a) Olivine melilitite and olivine nephelinite

(b) Pseudo-kimberlites which Moore (*op.cit.*) considers to be hydrothermally altered olivine melilitites. These frequently contain typical kimberlitic indicator minerals

(c) Sediment-filled kimberlite pipes and breccia necks

Taljaard (*op.cit.*) has considered individual outcrops of melilite basalts to represent isolated remnants of a once extensive sill that was emplaced between the gneisses of the Namaqualand Metamorphic Complex and the overlying Dwyka sediments. This idea is, however, no longer favoured and it is now considered that the individual occurrences form discrete bodies (pipes).

Moore (*op.cit.*) suggests that the volcanic activity was triggered off by stresses associated with epeirogenic upwarping of southern Africa.

During the present survey approximately twenty of these basaltic plugs were found. One of the largest of these forms a prominent hill on the farm Kliphakskeen (98) locally referred to as Spioenkop. Other farms on which these basalts occur include: Donkerduispraat (95), Tweeling (80), Kraalbosch Vlei (99), Klein Koumis (113), Welverdiend (120), Nam 7.33 (117), Kat Vlei (235), Lekker Drink (245), Gamoep (234) and Wolf Kraal (367)(along the Kliprand-Springbok road).

Some of these plugs are readily spotted on aerial photographs by their circular outline and dark colour, while others were only located during field mapping. The outcrops of these volcanic rocks are generally very poor and often their presence is indicated by rounded boulders or rubble forming mounds or small hills rising above the extensive sand cover of the Bushmanland Plateau. These bounders and outcrops typically have a black colour with an outer shell of a brown weathered surface. In hand specimens the rocks are seen to be porphyritic with phenocrysts generally 2 to 3 mm across (although some larger crystals do occur) set in a very fine-grained matrix. Some of the boulders contain fragments of country rock.

Only a few specimens of these rocks have been studied microscopically in thin section. It is beyond the scope of this study to describe them in detail, particularly in view of the published work listed above.

All the specimens studied contain euhedral *olivine* megacrysts, frequently 2 to 3 mm across, set in a fine-grained matrix. The olivine is of a magnesian composition and accounts for about 15 to 20 per cent of the modal composition.

Some of the olivine crystals are partly altered to *serpentine* and/or *phlogopite*.

*Melilite*, likewise, is frequently euhedral and forms much smaller phenocrysts. The mineral generally has a pale yellow colour and contains numerous small inclusions.

The matrix consists essentially of prismatic laths of *clinopyroxene* (augite), granules of *perovskite*, *opaque minerals* and interstitial *nepheline*. *Perovskite* and the opaque minerals commonly form larger anhedra.

## 3 Kimberlite Pipes

In addition to the melilite basalt plugs, the aerial photographs of the Kliprand, Gamoep, Aggeneys area reveal the presence of numerous circular features, generally in the form of small depressions and a large number of these are known to be underlain by kimberlite (Reuning, 1931; Cornelissen and Verwoerd, 1973, 1975).

For a considerable time the Bushmanland kimberlite pipes were considered to be the potential source for the alluvial diamonds along the Buffels River as well as the Koa River valley where diamonds are presently extracted from gravels exposed within the pans at Galputs and Bosluis. Intensive prospecting has, however, thus far failed to locate the source of the diamonds in the Bushmanland kimberlite province.

Drilling and prospecting pits have shown that a large number of these diatremes are filled with sediments to a considerable depth, recorded as being up to 260 metres thick (*ibid.*). The sediments generally dip towards the centre of the diatreme and include argillaceous and arenaceous rocks deposited in a lacustrine environment as indicated by the presence of various fossils including skeletons of frogs and dicotyledonous leaf impressions (*ibid.*).

In the field these circular features are seen to form shallow depressions frequently with a thick calcrete edge associated with which is ferruginous chalcedony silicified kaolin and frequently manganiferous material. Ferricrete is abundant in some of the depressions and gypsum has been exposed in many of the prospecting pits.

The exact age of these diatremes is still uncertain, but the fossil evidence points towards a late Cretaceous to early Tertiary age (Houghton, 1969).

The spatial and temporal association of melilite basalt and kimberlite in Bushmanland has led to considerable speculation on genetic interrelationships (Moore, *op.cit.*), particularly as some of the diatremes contain both rock types (Cornelissen and Verwoerd, (*op.cit.*).

# III METAMORPHISM AND MINERAL CHEMISTRY

## A Introduction

Mineral assemblages in the gneisses investigated are consistent with a model of decreasing metamorphic grade from south to north, ranging from granulite to upper amphibolite facies. In detail, the metamorphic history of the area is probably complex with the earliest record largely or completely destroyed by the dominant event of high grade regional metamorphism which leads to the formation of ubiquitous granoblastic textures. Due to the lack of conclusive evidence for an earlier metamorphic imprint, however, the regional thermal event responsible for the development of this granoblastic texture and associated high grade mineral assemblages is regarded to represent the oldest recognisable metamorphism and is referred to as $M_1$. The post-$M_1$ metamorphic path followed a trend of declining temperature and decreasing pressure as documented by secondary minerals frequently developed in corona textures.

The prime aim here concerns the study of some aspects of the dominant regional metamorphism of three rock groups, the mafic, pelitic and calcareous gneisses. The mineral assemblages in these rocks and the chemical compositions of coexisting minerals are studied in some detail to provide a record of the P-T conditions which have prevailed during regional metamorphism. In this chapter the physical conditions accompanying metamorphism will only be evaluated qualitatively and attempts to determine these parameters (pressure and temperature) quantitatively using appropriate thermodynamic models on experimentally calibrated equilibria are discussed in Chapter IV.

## B Metamorphism of Mafic Rocks

### 1 Mineral Parageneses in Mafic Rocks

The mineral assemblages in mafic lithologies provide vital information on metamorphic grade and regional variations in metamorphism. Considering only the ferromagnesian phases of the 80 specimens examined, the following mineral parageneses have been found in the area investigated (the frequency

of occurrence of each paragenesis is indicated in parentheses).

orthopyroxene + clinopyroxene + hornblende (19)
orthopyroxene + clinopyroxene + hornblende + biotite (3)
orthopyroxene + clinopyroxene + garnet (1)
orthopyroxene + clinopyroxene + biotite (4)
orthopyroxene + biotite (1)
orthopyroxene + clinopyroxene (8)
orthopyroxene + hornblende (2)

clinopyroxene + hornblende (18)
clinopyroxene + hornblende + biotite (2)
hornblende + garnet (2)
hornblende + biotite (7)
hornblende (13)

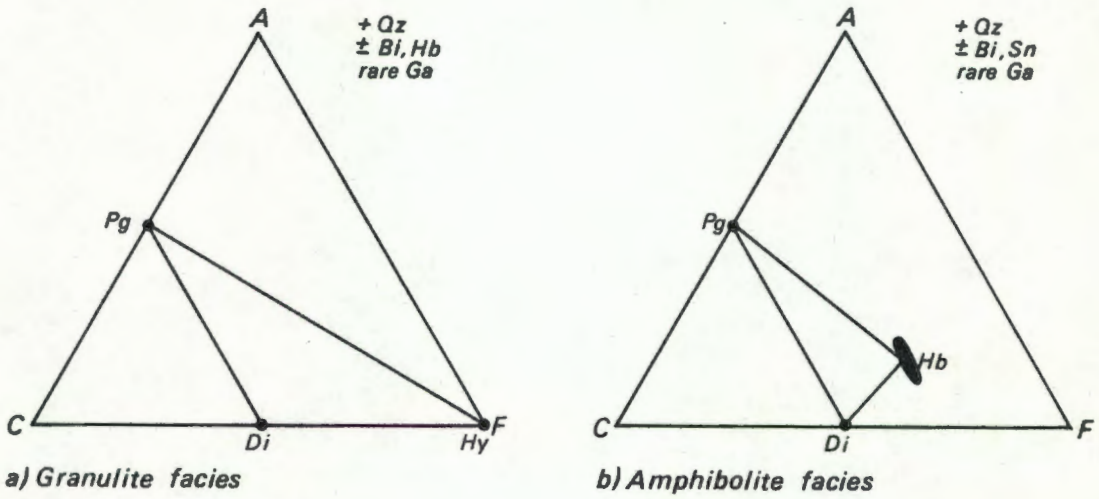


Fig. 7 ACF diagrams showing mineral parageneses in the mafic rocks. Abbreviations as in preface.

These parageneses can be divided broadly into two major groups, one containing orthopyroxene while in the other group this mineral is lacking. The orthopyroxene-bearing parageneses, schematically shown in ACF projection in Fig. 7a characterise the granulite facies terrane (de Waard, 1965b; Turner, 1968; Winkler, 1967) and their host rocks are here referred to as granolites in the sense of Winkler and Sen (1973) and Winkler (1976, p. 258).

These granolites generally contain clinopyroxene in addition to orthopyroxene. In fact, only three of the 38 specimens examined do not contain any clinopyroxene. Hydrous minerals, predominantly hornblende and occasionally biotite are recorded in the majority of the specimens and only nine of the 38 granolite specimens are completely devoid of hydrous phases. Garnet has only been noticed in one of the specimens in association with orthopyroxene and clinopyroxene. Garnet-granolite assemblages are generally regarded to indicate higher pressure conditions (Ringwood and Green, 1966; Green and Ringwood, 1967; de Waard, 1967), however, their scarcity and close spatial association with garnet-free, two-pyroxene assemblages in the study area is considered to indicate that chemistry rather than pressure exerted the dominant control over the formation of garnet. Sphene has never been observed in the granolites suggesting that orthopyroxene and sphene are incompatible.

The mineral parageneses devoid of orthopyroxene are schematically shown in ACF projection in Fig. 7b and according to Turner (*op.cit.*) are characteristic of the amphibolite facies. Hydrous minerals, particularly hornblende and occasionally biotite, dominate these parageneses. Clinopyroxene is frequently recorded and according to Miyashiro (1973a) clinopyroxene-bearing calcite-free amphibolites indicate upper amphibolite facies metamorphic conditions. It is, therefore, not surprising that primary epidote is not encountered in any of the specimens examined. Garnet is very rare and has only been recorded in two of the 42 amphibolite specimens, while sphene is a common accessory phase.

These two contrasting groups of mineral assemblages recorded in the mafic rocks suggest the existence of two distinctly different metamorphic environments involving granulite facies and upper amphibolite facies conditions respectively, and this is now evaluated with reference to the spatial relationships of the mineral parageneses.

Fig. 8 Regional distribution of the mineral assemblages in mafic rocks. All parageneses containing orthopyroxene are shown as solid symbols. Crosses indicate assemblages in clinopyroxene-bearing amphibolites and open symbols represent salite-free amphibolites. The assemblages in brackets at locality I 3 are not plotted in their proper position, but occur approximately 2 km further eastwards off the map (these specimens were collected at the Gal Puts pan). The broken line (map A) indicates the approximate position of the "orthopyroxene isograd". Also note the occurrence of granolite north of this line at I 3. The significance of the broken lines on Map B is discussed in the text. Maps A and B have been placed next to each other for convenience. Each of these maps comprises six 1:50 000 topographic sheets, the reference numbers of which are listed.

MAP A

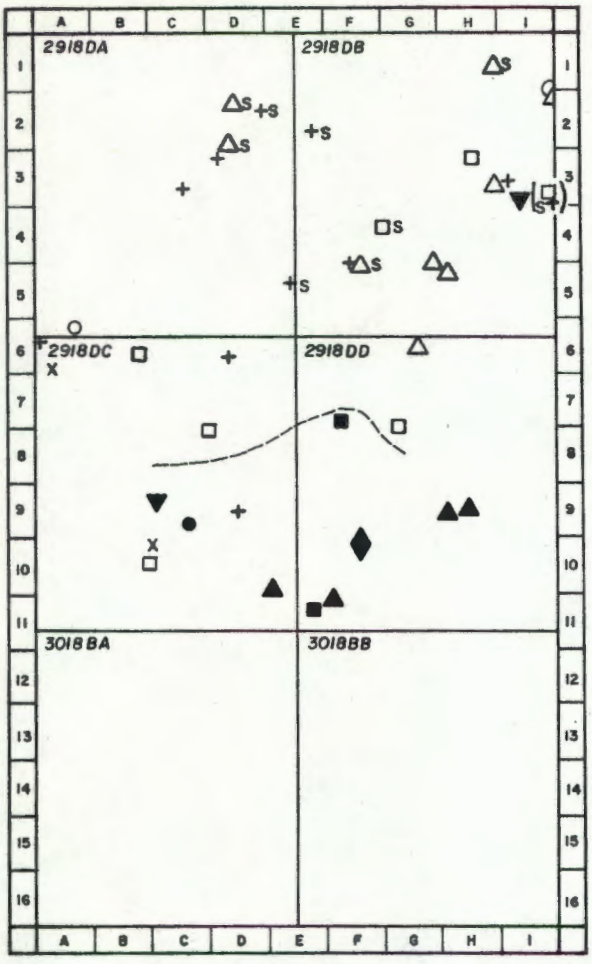


MAP B

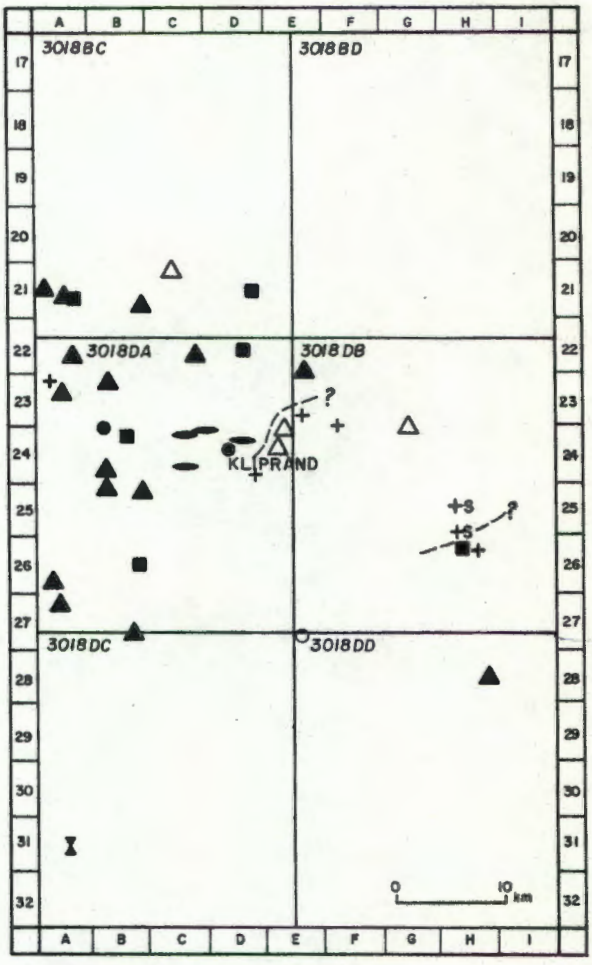


Key:

▲ orthopyroxene + clinopyroxene + hornblende
● orthopyroxene + clinopyroxene + hornblende + biotite
♦ orthopyroxene + clinopyroxene + garnet
⬬ orthopyroxene + clinopyroxene + biotite
⧗ orthopyroxene + biotite
■ orthopyroxene + clinopyroxene
▼ orthopyroxene + hornblende
\+ clinopyroxene + hornblende
× clinopyroxene + hornblende + biotite
○ hornblende + garnet
□ hornblende + biotite
△ hornblende
s sphene

## 2 Regional Distribution of Mineral Parageneses

Previous investigations by several authors indicate a distinct change in mineral assemblages along a north-south section across Namaqualand into Bushmanland. For example, Joubert (1971a) investigating the terrane to the west of the area now studied finds that extensive parts of the Namaqualand Metamorphic Complex are underlain by granulite facies assemblages. Bushmanland, in contrast, appears to have been subjected to lower grades of regional metamorphism, as Moore (1977) investigating the geology of Namiesberg to the northeast of the study area does not observe any orthopyroxene amongst the mafic mineral assemblages, while amphibolite facies parageneses are common. Similarly, Rozendaal (1978) working in the Gamsberg area, notes that the mafic mineral association is typical of the amphibolite facies. He also records some orthopyroxene-bearing assemblages, but these appear to be uncommon (Rozendaal, *op.cit.*). It was, therefore, speculated that the amphibolite-granulite facies transition should be encountered somewhere within the area investigated. Accordingly, a large number of suitable specimens have been collected in order to delineate this boundary.

All mineral parageneses recorded in the mafic rock specimens from the study area are shown in Fig 8, witnessing a regional change in mineral assemblages across the area. The northern part (map A) is dominated by amphibolite facies parageneses, while the southern part is underlain largely by granulite facies assemblages. Accordingly, the granulite-amphibolite facies transition is located somewhere along the top half of sheets 29 18DC and 29 18DD (map A rows 7 and 8, Fig. 8). It is rather unfortunate that this critical area of the transition contains hardly any outcrops as most of this part of Bushmanland is covered by surface limestone and sand. Nevertheless, the regional distribution of mafic parageneses suggests that the orthopyroxene isograd (indicated as a broken line in Fig. 8, map A) follows approximately an east-west trend.

In Fig. 8 it is also demonstrated that amphibolite facies mineral assemblages are not restricted to the northern part of the area. Isolated amphibolites are scattered throughout the granulite facies terrane and they are particularly common in an extensive area to the east of Kliprand where a large patch of amphibolite facies paragenesis is outlined by broken lines (3018DA and 3018DB Fig. 8, map B). Although these amphibolites lack orthopyroxene and are, therefore, not characteristic of the granulite facies, evidence suggesting that these amphibolites have originated under similar physical conditions to the surrounding granolites exists. In contrast to the green colour (indicating lower metamorphic grades) of the hornblendes in the amphibolite facies terrane in the northern part of the study area, the amphiboles in the amphibolites to the east of Kliprand are characterised by brownish-green or brown Z-absorption colours, which also characterise hornblendes in granulite facies basic rocks. Orthopyroxene-K-feldspar assemblages of the charnockite suite are spatially associated with these amphibolites. Geothermometric/barometric determinations do not indicate a significant change in termperature-pressure conditions across the zone containing these

amphibolites. Subsequent fieldwork has confirmed that granolites occur amongst the amphibolites.

The presence of sphene in some of these rocks (Fig. 8 , H 25) could be taken as evidence for a lower metamorphic grade, but amphibolites containing sphene are always found in close spatial association with calc-silicate rocks and it is, therefore, very likely that their different bulk composition permits the stable coexistence of sphene even at very high metamorphic grades. It is emphasised that in contrast to basic lithologies, sphene is stable in calc-silicate rocks throughout the granulite facies terrane. The possibility that sphene represents a retrograde phase in these rocks is excluded on textural grounds.

Attention is also drawn to the occurrence of an isolated small outcrop area of granolites on the farm Gal-Puts (I 3, Fig. 8 ) remote from the granulite-amphibolite facies transition. Clinopyroxene has not been observed in the one specimen studied, while orthopyroxene and hornblende are abundant. The hornblende has a green colour and not brownish green or brown as is characteristic for the granulite facies, and the orthopyroxene is not as pleochroic as elsewhere in the granulite facies terrane. Pelitic gneisses associated with the basic granolites on Gal-Puts are cordierite-hypersthene-anthophyllite rocks with anthophyllite forming coronas around hypersthene porphyroblasts clearly indicating retrogression. Owing to the lack of outcrop it is not possible to establish whether the facies transition swings sharply northwards to join up with the granolites on Gal-Puts or whether the latter are isolated within the amphibolite facies terrane.

The mineral parageneses in the mafic rocks and their regional distribution are cited as evidence for an increasing grade of metamorphism from upper amphibolite facies conditions in the north to granulite facies conditions in the central and southern parts of the area studied. This conclusion is also supported by certain universally observed changes in mineral abundances and optical properties of minerals as well as changes in mineral chemistry.

## 3 Colour Changes in Hornblende

The literature on colour changes in hornblende as a function of metamorphic conditions is voluminous. There seems to be a world-wide consistent trend in hornblende Z-absorption colours ranging from blue-green→green → brownish green→ to brown in response to increasing metamorphic grade (Miyashiro, 1958, 1973; Shido, 1958; Engel and Engel, 1962a,b; Binns, 1965a; Bard, 1970; Jackson, 1976).

In this study hornblende Z-absorption colour was observed under the microscope using a day-light filter. The colours of 67 specimens investigated can be grouped into four catergories.

1. brown (16 specimens)

2. brownish green (24 specimens)
3. green (25 specimens)
4. bluish green (2 specimens)

These colours are plotted in Fig. 9 to show their regional distribution in relation to the "orthopyroxene isograd", and they are seen to define two distinct regions. With minor exceptions, hornblendes within the granulite facies area are characterised by brown to brownish-green Z-absorption colours, whereas amphibolite facies hornblendes are typically green. Blue-green hornblendes have been found in the amphibolite facies, but are rare.

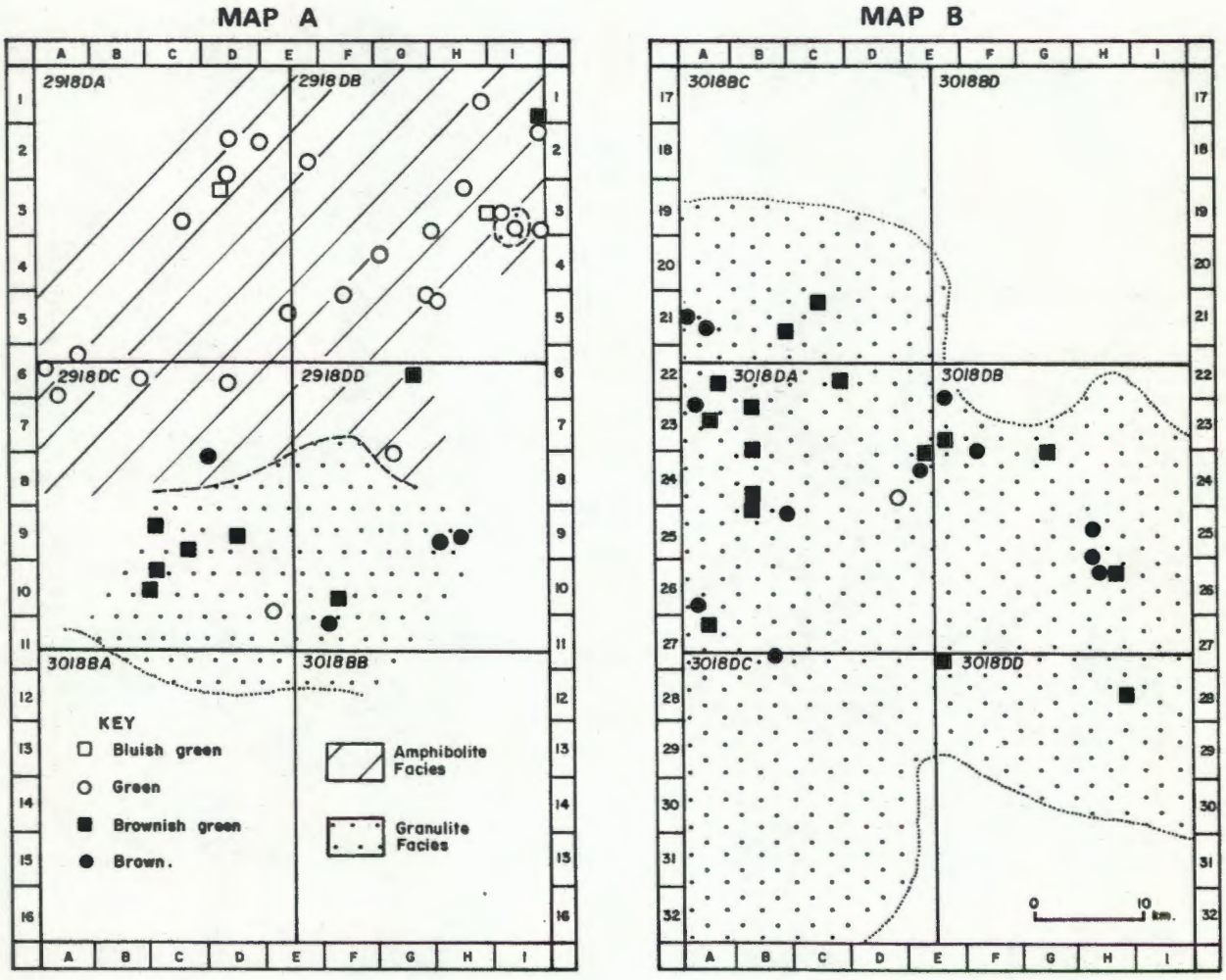


Fig. 9 Sketch map showing the regional distribution of hornblende Z-absorption colours. The broken line on map A indicates the approximate position of the "orthopyroxene isograd". Open symbols are used for green colours while brown or brownish-green colours are shown as solid symbols.

## 4 Changes in the Modal Abundance of Minerals across the Amphibolite-Granulite Facies Boundary

The ralative abundances of minerals in basic rocks change considerably across the transition from the amphibolite facies terrane into the granulite facies terrane. Certain minerals show a trend towards decreasing abundance, while others become increasingly more common across the "orthopyroxene isograd". As this boundary trends approximately east-west, the major changes in mineral abundances are evaluated along a north-south traverse across the area. In order to permit a meaningful comparison of the relative abundance of minerals in the two contrasting metamorphic terranes, differences in bulk chemical composition have to be taken into account. Strictly speaking, only rocks of similar chemistry should be considered in this comparative study. To circumvent the influence of bulk chemistry on the abundance of minerals, modal ratios of certain minerals, rather than their actual modes have been used. The ratios considered here include the following:

$$\frac{\text{plagioclase}}{\text{hornblende + plagioclase}}, \quad \frac{\Sigma \text{ hydrous minerals}}{\Sigma \text{ mafic minerals}}, \quad \frac{\text{hornblende}}{\Sigma \text{ mafic minerals}}, \quad \frac{\text{salite}}{\Sigma \text{ mafic minerals}}$$

and $\frac{\text{hypersthene}}{\Sigma \text{ mafic minerals}}$. These modal ratios, expressed as per cent were evaluated from the modal compositions tabulated in Tables 4,5,6 pages 31,35 and 36 for all the specimens. Mean ratios were then computed for each of the east-west rows numbered 1 to 32 in Fig. 9 and are graphically presented in Fig. 10. Since amphibolites are common in the granulite facies terrane, these have been excluded from the computations of the mean values in the granulite facies area.

The results (Fig. 10) allow the following qualitative conclusions to be drawn regarding the major changes in mineral abundances across the transition from the upper amphibolite facies into the granulite facies.

(a) $\frac{\text{plagioclase} \times 100}{\text{hornblende + plagioclase}}$ ratio (A) increases across the amphibolite-granulite facies boundary. As plagioclase becomes increasingly more abundant relative to hornblende with increasing metamorphic grade, this can be interpreted in terms of reactions involving the gradual destruction of hornblende with the release of the anorthite molecule. The change in the (A) ratio is quite remarkable. In the amphibolite facies terrane the mean ratio has a value of 43,6 $\pm$ 15 per cent compared to a mean of 80,8 $\pm$ 20 per cent for (A) in the granulite facies terrane.

(b) The $\frac{\Sigma \text{ hydrous minerals} \times 100}{\Sigma \text{ mafic minerals}}$ ratio (B) and $\frac{\text{hornblende} \times 100}{\Sigma \text{ mafic minerals}}$ ratio (C) decrease across the facies transition from the amphibolite into the granulite facies, implying that the hydrous minerals gradually become replaced by anhydrous phases with an increasing metamorphic grade. The mean values for ratio (B) are 92,1 $\pm$ 19 per cent and 37,0 $\pm$ 28 per cent and for ratio (C)

86,8 ± 21 per cent and 31,5 ± 30 per cent in the amphibolite and granulite facies terrane respectively. Qualitatively this observation is consistent with the findings of Engel and Engel (1962b) and Jackson (1976).

(c) Clinopyroxene forms at the expense of hornblende in the upper amphibolite facies (textural evidence is presented in Chapter III.B.7). The $\frac{\text{salite} \times 100}{\Sigma \text{ mafic minerals}}$ ratio (D) in Fig. 10 suggests an increase of this ratio across the amphibolite-granulite boundary indicating that salite becomes more abundant with increasing metamorphic grade. The mean value for ratio (D) is 7,9 ± 28 per cent and 21,3 ± 16 per cent in the amphibolite and granulite facies terranes respectively.

(d) By definition hypersthene is absent in the amphibolite facies area. The $\frac{\text{hypersthene} \times 100}{\Sigma \text{ mafic minerals}}$ ratio (E) increases steadily into the granulite facies terrane implying that hypersthene becomes increasingly abundant. The mean value for ratio (E) in the granolites is found to be 41,2 ± 21 per cent.

The observed changes in mineral abundances outlined above are best accounted for by a dehydration reaction of the type:

hornblende I + quartz $\rightleftharpoons$ hornblende II + orthopyroxene + clinopyroxene + plagioclase + $H_2O$ (1)

as suggested by Engel and Engel (*op.cit.*) and Binns (1969,b). This reaction can satisfactorily explain the gradual destruction of hornblende and its progressive replacement by anhydrous minerals (orthopyroxene, clinopyroxene and plagioclase) in response to increasing metamorphic grade. If quartz is consumed as indicated in the above reaction, this mineral is expected to decrease in abundance from the amphibolite to the granulite facies terrane. In the study area 80 per cent of all amphibolite specimens contain quartz, as opposed to 61 per cent of all granolites. The mean modal quartz content of amphibolites and granolites are found to be 7,0 + 8,3 per cent and 5,9 ± 8,8 per cent, respectively. Based on these figures alone it is not possible to judge whether quartz has been consumed during granulite facies metamorphism.

---

Fig. 10 Changes of mineral ratios, expressed as per cent, along a north-south traverse across the amphibolite-granulite facies boundary. Mean ratios have been computed for each east-west segment numbered 1 to 32 corresponding to the grid in Fig. 8. The computations are based on modal analyses of the mafic rocks. The heavy vertical line marks the transition from the granulite to the amphibolite facies terrane.

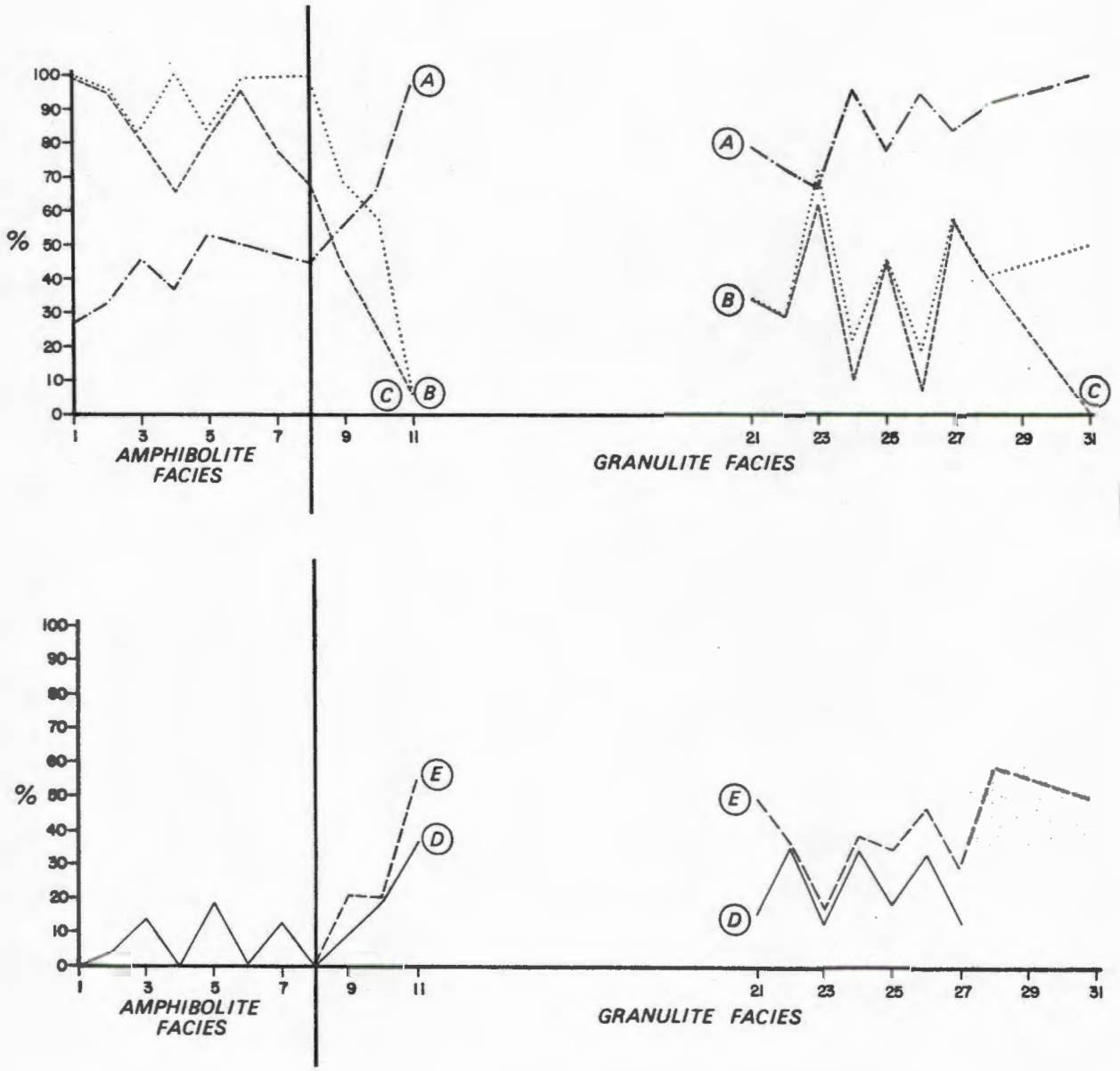


(A) $\frac{\text{PLAGIOCLASE} \times 100}{\text{HORNBLENDE + PLAGIOCLASE}}$

(B) $\frac{\Sigma \text{ hydrous minerals} \times 100}{\Sigma \text{ mafic minerals}}$

(C) $\frac{\text{HORNBLENDE} \times 100}{\Sigma \text{ mafic minerals}}$

(D) $\frac{\text{SALITE} \times 100}{\Sigma \text{ mafic minerals}}$

(E) $\frac{\text{HYPERSTHENE} \times 100}{\Sigma \text{ mafic minerals}}$

In most granulite facies terranes the dehydration reactions have not gone to completion so that hornblende-free pyroxene granolites are rare (De Waard, 1967; Sen, 1970). De Waard (1964) ascribes the co-existence of hornblende-free and hornblende-rich granolites to variations in water pressure, while Sen (*op.cit.*) and Sen and Ray (1971, 1972) argue that besides water pressure, the availability of quartz will determine whether reaction (1) will go to completion or not. They point out that hornblende-rich granolites never contain large amounts of quartz.

## 5 Mineral Chemistry and its Relationship to Metamorphic Grade

In the hornblende dehydration reaction (1) the reactants involve minerals typical for amphibolite facies parageneses, while the products of the reaction are those encountered in specimens from the granulite facies area. The equilibrium, as written, is seen to contain hornblende on the reactant as well as on the product side, but the non-equivalence of the two amphiboles is symbolised by roman cyphers. The first part of this section is devoted to outlining the progressive changes in chemical composition of the hornblende in response to increasing metamorphic grade. These chemical changes are consistent with reaction (1) and support its validity.

### (a) Hornblende

Deer *et al.* (1971) describe the hornblende structure as consisting of double chains of $(Si\ Al)O_4$ tetrahedra of the composition $(Si_4O_{11})_n$ arranged parallel to the C-crystallographic axis. Between the inward pointing apices of these tetrahedra, octahedrally co-ordinated cations occupy the $M_1$, $M_2$ and $M_3$ sites. These units are linked by larger cations situated in the $M_4$ site. In some amphiboles an additional site, the A site, is occupied by larger cations, but since this site does not always contain atoms, it is also referred to as the "vacant" site. Amphiboles are a complicated group of minerals because their structure allows a very wide range of substitutions. Ernst (1968) points out that cations, with radii ranging between 0,4 and 1,4A°, a range which includes most of the major cations of the earth's crust, can substitute into this structure. For this reason he describes amphiboles as "mineralogic wastebaskets". The most important ionic substitutions include $Mg \rightleftharpoons Fe$, $Al \rightleftharpoons Si$, $(Mg\ Fe) \rightleftharpoons Al$, $Na \rightleftharpoons Ca$ and the introduction of Na and K into the A site (Deer *et al.*, *op.cit.*). Except for the first one, which does not require a charge balance, all other substitutions listed can maintain a balance of charge only if more than one substitution takes place simultaneously.

The general amphibole structural formula representing one half of the atoms per unit cell can be expressed as:

$$A_{0-1}^{XII}\ X_2^{VIII}\ Y_5^{VI}\ Z_8^{IV}\ O_{22}\ (OH,O,F)_2$$ (Ernst, 1968; Bard, 1970; Deer *et al.*, *op.cit.*)

A symbolises the 10-to 12-fold co-ordinated cations, particularly Ca, Na and K which cannot be accommodated in the $M_4$ site and must, therefore, be absorbed by the A site. The maximum number of ions per structural formula that can enter into this site is one, but commonly this site is not fully occupied. (Appendix II, Table A2-1).

X stands for 6-to 8-fold co-ordinated cations in the $M_4$ site predominantly Ca, but also Mg and Na.

Y accommodates 6-fold co-ordinated cations ($Al^{VI}$, Ti, Mn, Fe, Mg) in the $M_1$, $M_2$ and $M_3$ sites.

Z contains 4-fold co-ordinated cations (Si, $Al^{IV}$) in the centres of $SiO_4$ tetrahedra.

In this study, hornblendes of 15 specimens were analysed, seven of which are from the amphibolite facies area, including three salite-free amphibolites and four clinopyroxene-bearing amphibolites, while the remaining eight specimens are hypersthene-pyroclase granolites from the granulite facies terrane. Two to five hornblende analyses were done per specimen and mean compositions are tabulated in Appendix II, Table A2-2, while the structural formulae based on these mean compositions are shown in Appendix II, Table A2-1. The analyses were done with the aid of the microprobe analyser omitting OH and F. Borg (1967) suggests that the ionic proportions of amphiboles should be calculated on the basis of 23 oxygens if the hydroxyl ion is ignored. Under these circumstances the amphibole formula is reduced to $A_{0-1}\ X_2\ Y_5\ Z_8\ O_{23}$.

According to Ernst (1968) the amphiboles broadly fall into three groups depending on the type of atom predominantly occupying the $M_4$ site. Iron-magnesium amphiboles have Fe-Mg as dominant x-cation and in calcic amphiboles Ca is the dominant x-cation, while sodic amphiboles are characterised by Na in the $M_4$ site. In this sense the amphiboles considered in this section belong to the calcic category. There appears to be considerable confusion in the literature on amphibole nomenclature. Leake (1968) describes the existing nomenclature as a "jungle of confusion" and proposes a new system based on the three variables: Si, Ca+Na+K and Mg/(Mg+Fe+Mn) for calciferous amphiboles. In order to qualify as a calciferous amphibole the mineral should possess at least 1,50 ions of Ca per half unit cell. Amphiboles containing between 1,00 and 1,50 Ca ions per half unit cell are referred to as sub-calciferous. In this study, the nomenclature proposed by Leake (*op.cit.*) is used (Fig. 11). Examination of Fig. 11 shows that the majority of the hornblendes studied tend to be enriched in Mg relative to Fe, and all amphiboles from hypersthene-pyroclase granolite specimens have Ca+Na+K in excess of 2,5 ions per formula. Seven of the eight analyses plot into the ferroan-pargasitic hornblende field, while only one analysis plots into the edenitic hornblende field. In contrast, the compositions of the hornblendes from amphibolite facies basic rocks are more variable, probably a reflection of variations in bulk chemical compositions of these rocks.

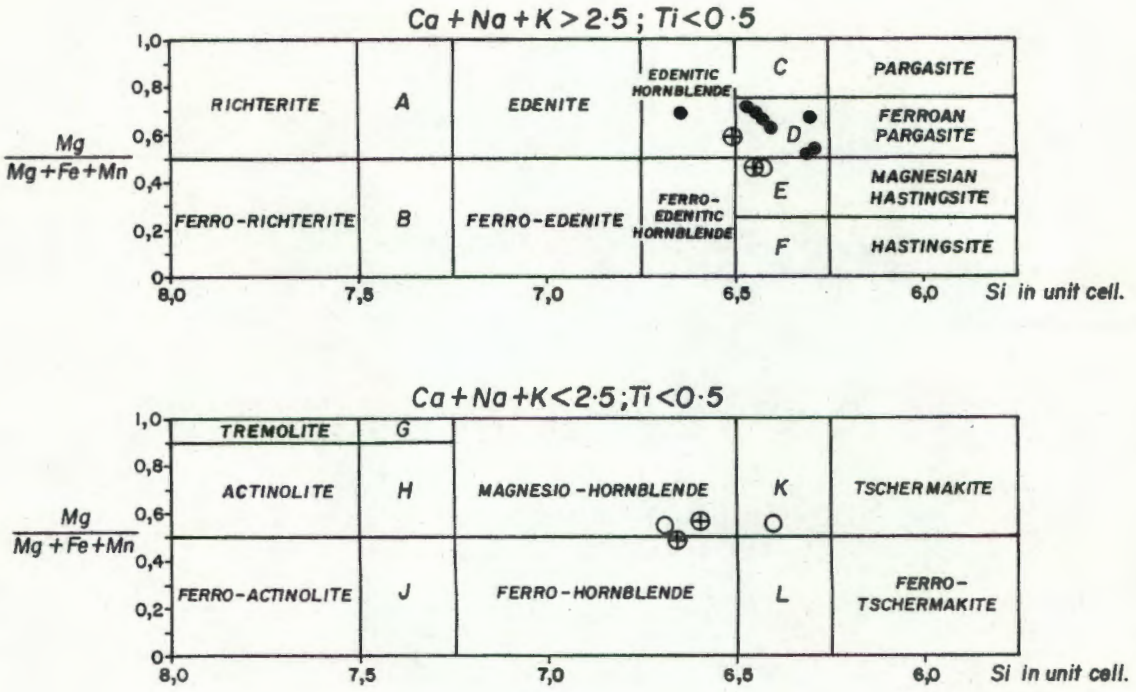


KEY

A RICHTERITIC EDENITE
B FERRO-RICHTERITIC EDENITE
C PARGASITIC HORNBLENDE
D FERROAN PARGASITIC HORNBLENDE
E MAGNESIAN HASTINGSITIC HORNBLENDE
F HASTINGSITIC HORNBLENDE
G TREMOLITIC HORNBLENDE
H ACTINOLITIC HORNBLENDE
J FERRO-ACTINOLITIC HORNBLENDE
K TSCHERMAKITIC HORNBLENDE
L FERRO-TSCHERMAKITIC HORNBLENDE

Fig. 11 Hornblendes plotted in terms of the Leake (1968) nomenclature. Solid symbols (•) represent hornblendes from hypersthene-pyroclase granolites and open symbols are used for hornblendes from the amphibolite facies terrane. ( ⊕ = hornblendes in salite-bearing amphibolite, O = hornblende in clinopyroxene-free amphibolites). Each symbol represents a mean composition based on 2 to 5 analyses per specimen.

Some of the ionic substitutions in hornblende appear to be controlled by the metamorphic environment and certain chemical trends are observed world-wide in response to increasing metamorphic grade. Similar chemical trends are recorded in the study area and are outlined below.

(i) The relationship between Si and Al

The substitution of the type (M) Si $\rightleftharpoons$ Al (M symbolises ions

able to maintain charge balance) is referred to as tschermakitic substitution (Binns, 1969a; Miyashiro, 1973a).

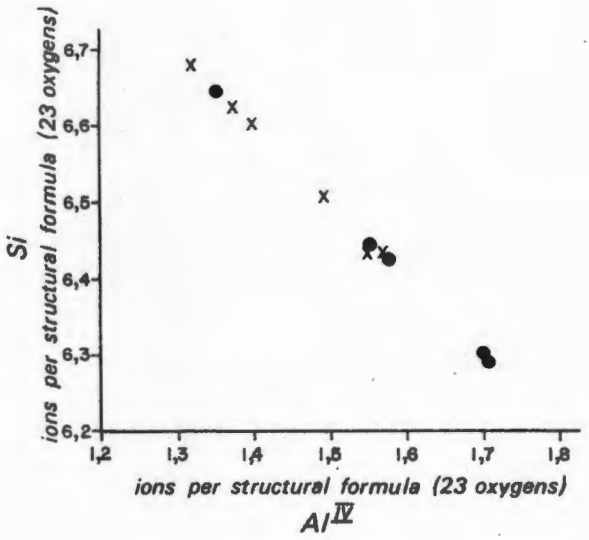


Fig. 12 Relationship between silicon and tetrahedral aluminium in hornblende. Solid dots represent hornblendes from the granulite facies and crosses symbolise amphibolite facies hornblendes.

Fig. 12 is a plot of Si versus tetrahedral Al and it shows that hornblendes from the granulite facies terrane generally contain lower Si contents and consequently higher $Al^{IV}$ compared to hornblendes from the amphibolite facies terrane. All Al in excess of the amount required to fill the Z-site enters the Y-site (see structural formulae Appendix II, Table A2-1), where it is octahedrally co-ordinated. The variation in total Al-concentration is small, the granulite facies hornblendes having a slightly higher Al-content than those from the amphibolite facies area (mean $Al_{total}$ in granulite facies hornblendes = 1,9513 $\pm$ 0,1268, mean $Al_{total}$ in amphibolite facies hornblendes = 1,9302 $\pm$ 0,0731 ions per structural formula).

In Fig. 13 the relationship between $Al^{VI}$ and Si is shown and it is demonstrated that hornblendes from the amphibolite facies area contain higher $Al^{VI}$ concentrations compared to their counterparts in the granulite facies terrane. The two groups plot into distinct fields, the dividing line being approximately 0,4 $Al^{VI}$ ions per structural formula. This observation implies a decrease in tschermakite substitution with increasing metamorphic grade and is in accord with findings of other authors (Leake, 1965, 1971; Binns, 1965a, 1969a; Jackson, 1976). In contrast, Engel and Engel (1962) find no correlation between Si/Al ratio and metamorphic grade. Bard (1970) shows that Si and $Al^{IV-VI}$ of hornblendes depend neither on host-rock composition or on metamorphic grade.

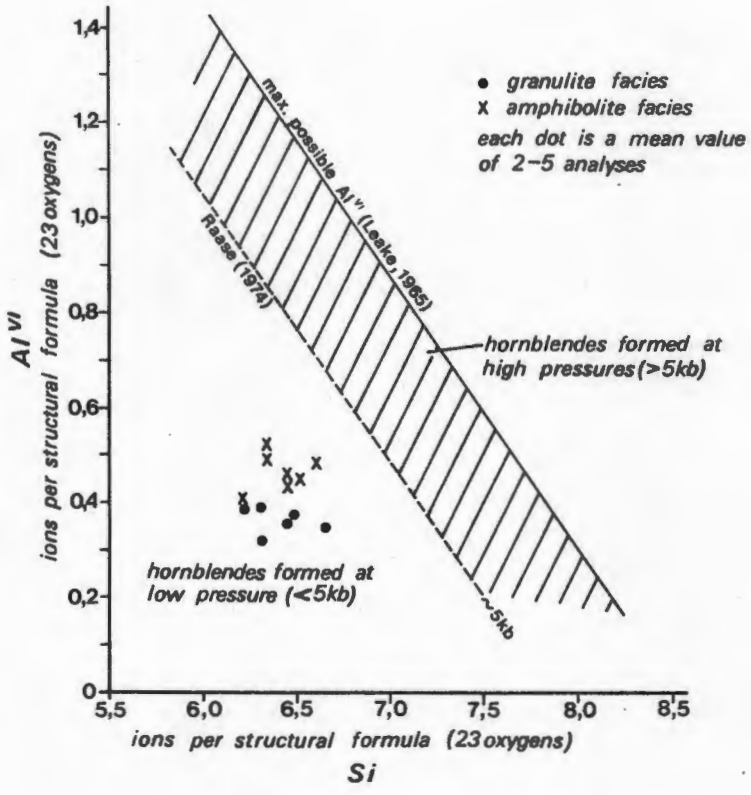


Fig. 13 Relationship between $Al^{VI}$ and Si in hornblendes from the study area. Solid dots represent hornblendes from the granulite facies terrane and crosses symbolise amphibolite facies hornblendes. The lower diagonal line divides the hornblende field into a high and low-pressure environment (after Raase, 1974) with hornblendes formed at low pressure (< 5kb) plotting below the line while those of high pressure terranes plot above this line. The upper diagonal line represents the maximum possible $Al^{VI}$ concentration in hornblende (after Leake, 1965).

Leake (1971) suggests that there is a positive correlation between $Al^{IV}$ and $Al^{VI}$ and concludes that the $Al^{VI}$ content in amphiboles is a function of bulk rock composition, but also pressure with high pressure favouring $Al^{VI}$. Kostyuk and Sobolev (1969) and Leake (1968) conclude that $Al^{VI}$ increases with increasing pressure. Raase (1974) conducts a statistical study of calciferous hornblendes from various petrographically well-known metamorphic terranes and this permits a good distinction between hornblendes of high and low pressure metamorphism (Fig.13). According to Raase (*op.cit.*) low-pressure amphiboles contain low $Al^{VI}$ and Si concentrations while amphiboles of high-pressure origin (in excess of $\pm$ 5kb) are characterised by higher $Al^{VI}$ contents. From Fig. 13 it can be demonstrated that the hornblendes must have

crystallised at relatively low pressure as they plot within the low pressure field defined by Raase (*op.cit.*).

(ii) Alkali enrichment as a function of metamorphic grade

The total alkali content of amphiboles can vary due to the presence of the large A-site ("vacant site") which can accommodate any fraction of ions ranging between zero and one ion per structural formula in order to maintain charge balance. The alkali ions entering into the "vacant site" are also referred to as "edenite alkalis" (Binns, 1969a). It is well known that the alkali concentration increases with prograde metamorphism (Engel and Engel, 1962b; Binns, 1965a,1969a; Leake, 1965,1968; Bard, 1970; Miyashiro, 1973a; Jackson, 1976).

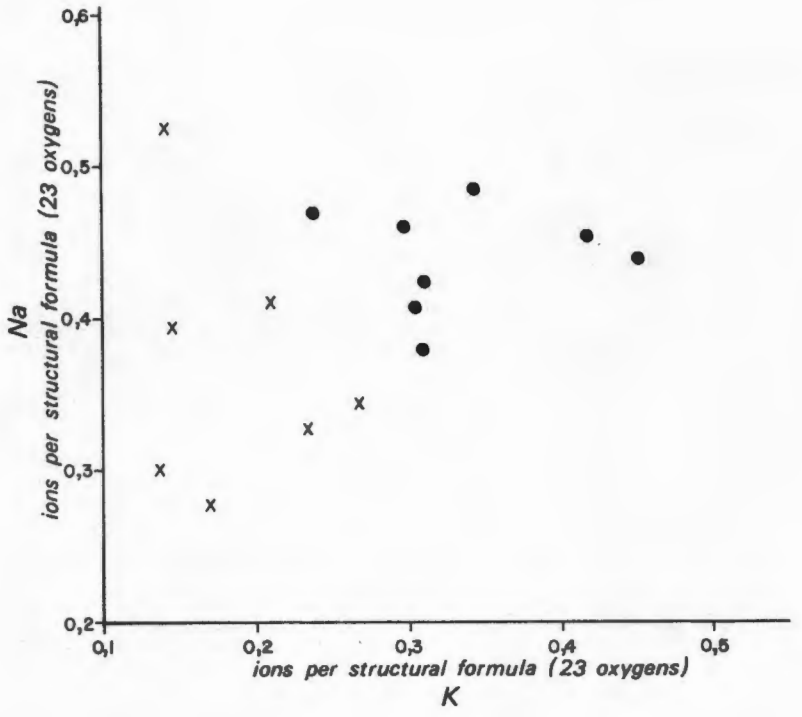


Fig. 14 The relationship between sodium and potassium in hornblende from the study area. Solid dots represent hornblendes from the granulite facies terrane and crosses are used for hornblendes from the amphibolite facies terrane.

In Fig. 14 the relationship between Na and K in hornblende is shown. It is evident that hornblendes from the granulite facies terrane are markedly enriched in K relative to their counterparts in the amphibolite facies area and also tend to have higher Na contents. Binns (1965a, 1969a) points out that the A-site alkalis are grade dependent. In Fig.15 the "edenite alkalis"

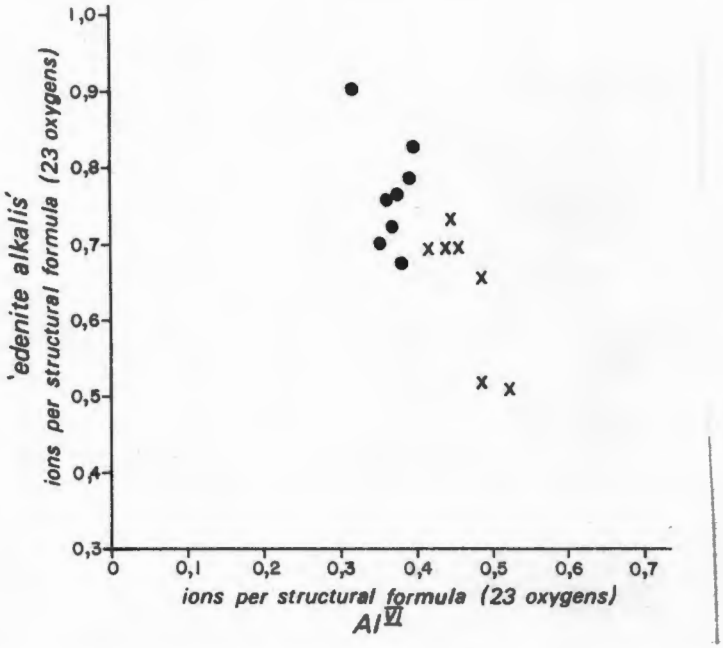


Fig. 15 Plot of "edenite alkalis", i.e. ions occupying the "vacant" or A-site versus octahedral aluminium. Solid dots are from hornblendes in hypersthene-pyroclase granolites and crosses symbolise hornblendes from the amphibolite facies terrane.

have been plotted against $Al^{VI}$ and it is obvious that hornblendes from the granulite facies are more edenitic and less tschermakitic than their ancestors in the amphibolite facies. This is also seen from a graph proposed by Miyashiro (1973a) which is reproduced as Fig. 16 where Si is plotted versus total alkalis (Σ Ca + Na + K). The hornblende analyses plot within the field of green and brown hornblendes in two distinct regions, with hornblendes from the granulite facies closer to the edenite-pargasite join, while those of the amphibolite facies plot nearer the tschermakite composition.

The enrichment in alkalis, particularly K, can be taken as a consequence of hornblende breakdown. As hornblende decreases in abundance from the amphibolite to the granulite facies area and potassium is not readily incorporated into any of the associated minerals (biotite occurs only in a few specimens), it follows that the K-content in hornblende must increase.

The behaviour of Ca also requires discussion. The hornblendes in the granulite facies contain on average less Ca (mean 1,8855 $\pm$ 0,0291 ions per structural formula) than those of the amphibolite facies (mean 1,9046 $\pm$ 0,0642 ions per structural formula). If the clinopyroxene-free and salite-bearing amphibolites are considered separately, the former yield a mean Ca content of 1,8654 $\pm$ 0,0773 ions per formula compared to 1,9341 $\pm$ 0,0396 ions per formula for the latter. This shows that the spread of Ca concentration in the

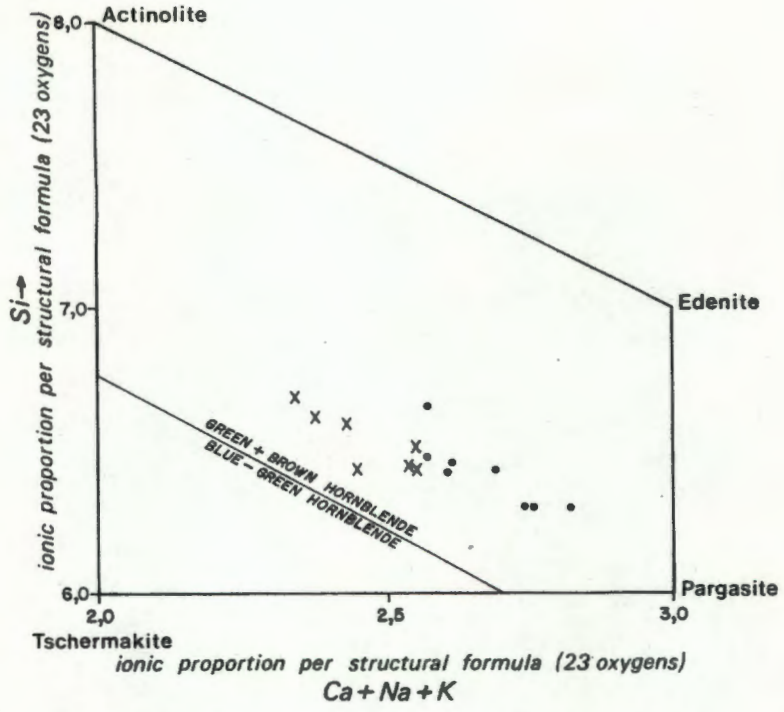


Fig. 16 Hornblende analyses from the study area plotted in terms of the Miyashiro (1973a) classification. Solid symbols represent hornblendes from the granulite facies area and crosses indicate amphibolite facies hornblendes. The lower diagonal line separates the field of blue-green hornblendes from those with a green or brown Z-absorption colour.

amphibolite facies is quite considerable suggesting that Ca is not grade dependent to the extent of the other alkalis. This is consistent with the observations of Engel and Engel (1962b) who note that the Ca content of hornblende remains nearly constant in a traverse from the amphibolite to the granulite facies terrane. Leake (1968) records that the Ca concentration remains more or less constant, while Na and K increase with increasing grade. Bard (1970) also concludes that Ca variations are independent of metamorphic grade and host-rock chemistry.

(iii) The relationship between Ti concentration and metamorphic grade

It is a well-established observation that the Ti concentration (provided that sufficient Ti is available in the host-rock) is a function of metamorphic grade (Shido, 1958; Engel and Engel, 1962b; Binns, 1965a, 1969a; Bard, 1970; Raase, 1974; Jackson, 1976). The Ti concentration is reported to increase from 0,08 to 0,29 ions per formula (ionic proportions on the basis of 23 oxygens) from the greenschist-amphibolite transition to the granulite facies (Raase, *op.cit.*).

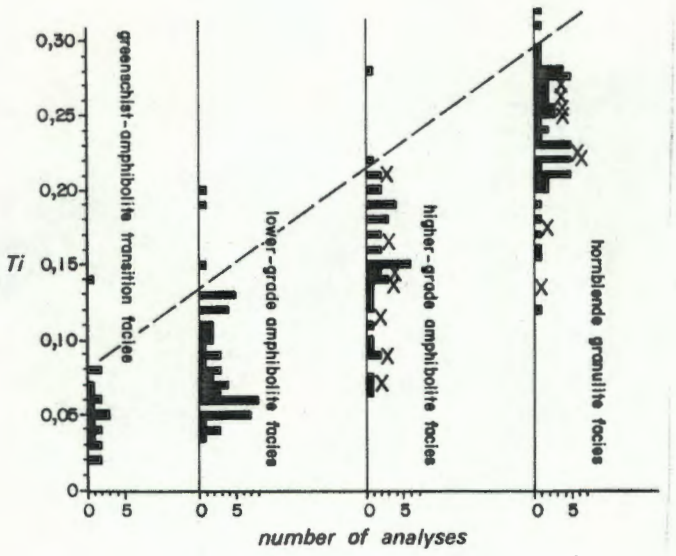


Fig. 17 Histogram of Ti contents of hornblende (based on 23 oxygens) versus metamorphic grade (after Raase, 1974). Note the increase of Ti with increasing metamorphic grade. Solid bars refer to the data compiled by Raase (*op.cit.*) and crosses mark the Ti concentration of hornblende in this study.

The hornblende analyses in the present study contain Ti ionic proportions ranging from 0,07 in the amphibolites to 0,27 in the granolites. Hornblendes in amphibolites have a mean concentration of 0,13 $\pm$ 0,05 ions of Ti per formula, while hornblendes in granolites have considerably higher Ti concentrations with a mean of 0,23 $\pm$ 0,05 ions per 23 oxygens, thus supporting the observations in other areas. In Fig.17 the hornblende analyses of this study (marked as X) are compared to the histogram compiled by Raase (*op.cit.*). The low Ti values can generally be correlated with low ilmenite contents in the host rock suggesting that these samples are not saturated with respect to Ti.

The titanium enrichment in hornblendes with increasing metamorphic grade can be explained as the product of amphibole breakdown reactions. It has already been shown that hornblende decreases in abundance from the amphibolite to the granulite facies terrane, where it is replaced by anhydrous minerals. If it is assumed that the Ti concentration of the host rock remains constant, a decrease in the amount of hornblende combined with the fact that Ti is not readily incorporated into associated minerals such as

pyroxene and plagioclase, necessitates an increase in Ti concentration in the remaining hornblende. Once saturation is achieved, Ti is expelled from the hornblende structure and forms its own minerals such as ilmenite. Sen (1970) and Sen and Ray (1971) argue that the crowding of ilmenite granules along the margins of hornblende crystals (a phenomenon frequently observed in the thin sections of mafic rock specimens studied) is evidence in favour of the prograde nature of the dehydration reaction.

Binns (1969a) suggests that the enrichment in Ti accounts to a large extent for the observed trend of increasing $Al^{IV}$ with increasing grade.

(iv) Mn concentration as a function of metamorphic grade

The Mn content of hornblende has been reported to decrease with increasing metamorphic grade (Engel and Engel, 1962b). From this study it is evident that there is also a good correlation between Mn concentration and metamorphic grade (Fig. 18). Hornblendes in the amphibolites have higher Mn contents (mean 0,0378 ± 0,0051 ions per formula) compared to their counterparts in the granulite facies area (mean 0,0178 ± 0,0038 ions per formula).

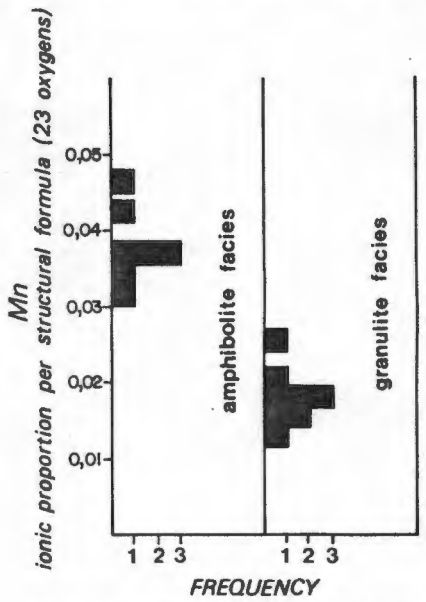


Fig. 18 Histogram showing the Mn concentration in hornblende from the study area. Note the lower Mn content of hornblendes from the granulite facies terrane compared to those of the amphibolite facies.

(v) Correlation between Ti concentration and hornblende colour

Binns (1965a) suggests that the colour changes in hornblende with increasing metamorphic grade can be correlated with increasing Ti and

decreasing $Fe^{+3}$ contents of hornblende.

In Fig. 19, the hornblende Z-absorption colour is plotted versus the Ti content and it is shown that, if specimen HA 926 with Ti <0,14 and brown colour is ignored, there is a good correlation between hornblende colour and Ti concentration. Green hornblendes have the lowest Ti content (mean 0,12 ± 0,04 ions per formula), followed by brownish green (mean 0,20 ± 0,03 ions per formula), while brown hornblende has the highest Ti concentration (mean 0,25 ± 0,02 ions per formula, if HA 926 is ignored). However, the fact that one specimen (HA 926) contains brown hornblende with relatively low Ti concentration (0,1367 ions per formula) suggests that Ti is not the only factor controlling hornblende colour. Bard (1970) demonstrates that the relationship between Ti content, colour and prograde metamorphism is not always systematic since green, lower grade hornblendes can contain as much Ti as higher grade, brown varieties and he suggests that other ions such as $Fe^{+3}$ are also able to enhance the brown colour.

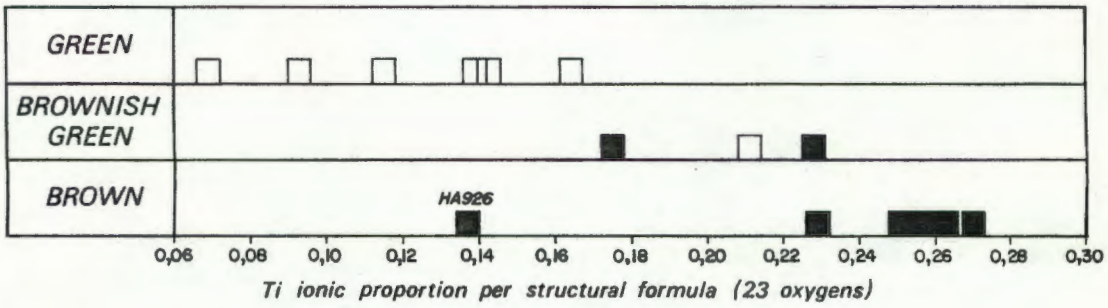


Fig. 19 Hornblende Z-absorption colour versus Ti content. Sodid squares represent hornblendes from the granolite specimens and open squares are used for hornblendes from salite-bearing and clinopyroxene-free amphibolites from the amphibolite facies terrane.

(b) Plagioclase Compositions and Metamorphic Grade

At low metamorphic grades up to the epidote-amphibolite facies the plagioclases are characterised by low An contents and are generally of albitic composition (Miyashiro, 1973a; Winkler, 1976). However, in the upper amphibolite facies and granulite facies more calcic plagioclases, commonly in the range labradorite-bytownite, are encountered. Wenk and Keller (1969) record that in the central Alps the anorthite content of the plagioclases in basic rocks increases with increasing metamorphic grade. They studied plagioclases from 700 amphibolite specimens and conclude that these define four prograde zones: albite amphibolite, oligoclase amphibolite, andesine amphibolite, and labradorite amphibolite. A similar prograde basification of the plagioclase has been described by Jackson (1976) for the Aus area, but he admits that there is considerable compositional overlap between the various metamorphic zones.

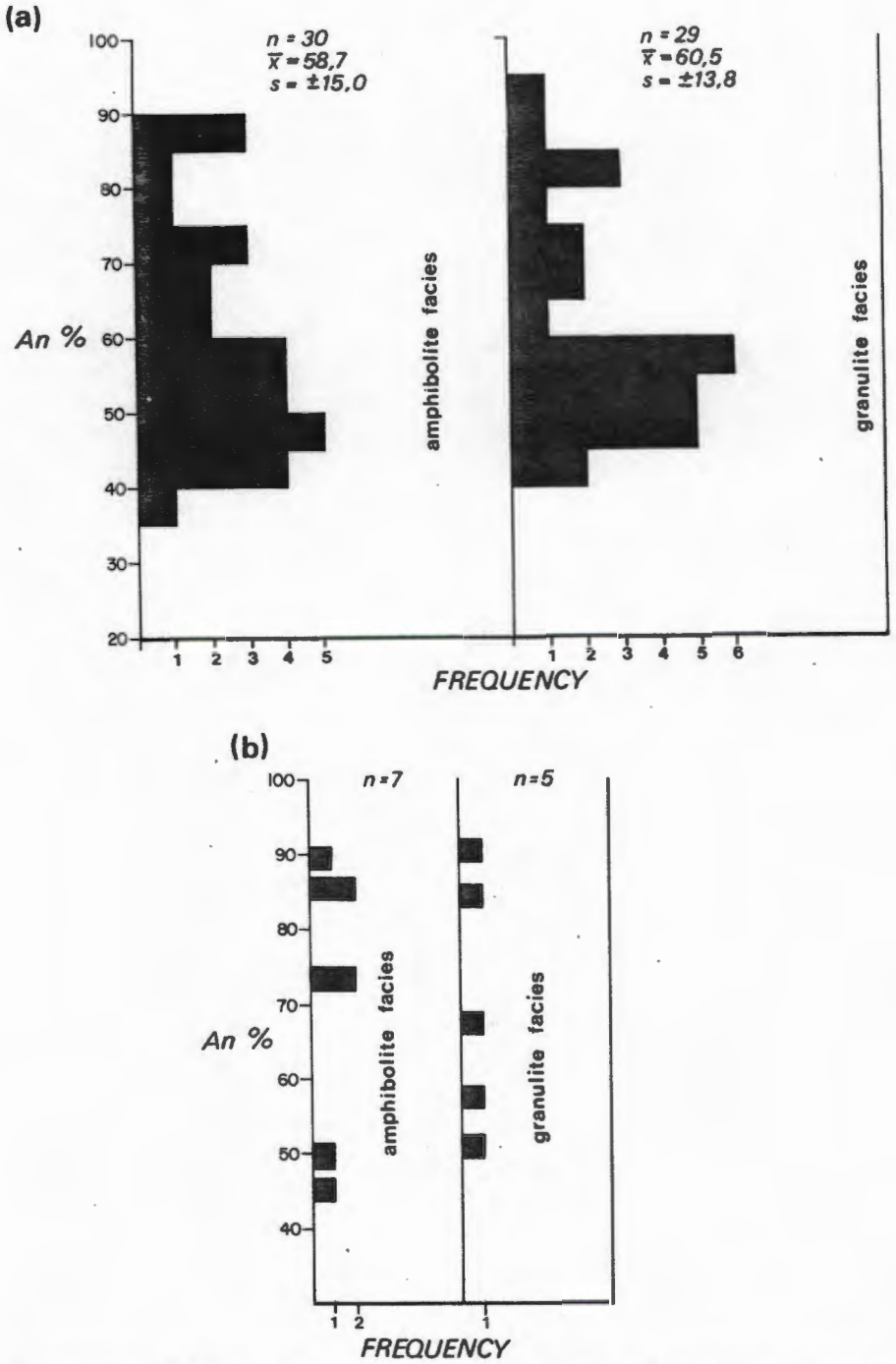


Fig. 20 Frequency histograms showing the range of plagioclase compositions in mafic rocks from the amphibolite and granulite facies terranes of the study area. Compositional determinations (a) based on flat-stage microscope using extinction angles (Deer *et al.*, 1971) (b) microprobe analyses of plagioclases.

(Appendix II, Table A2-3).

In this study plagioclase compositions have been determined optically on the flat-stage microscope using the extinction angle techniques described by Deer *et al.* (1971). These compositions are plotted as a frequency histogram in Fig. 20a, but there appears to be little difference in the histograms of the amphibolite and the granulite facies terranes. The anorthite content of amphibolite facies plagioclases ranges from $An_{38}$-$An_{89}$ with a mean of 58,7 $\pm$ 15,0 mole per cent anorthite. In granulite facies plagioclases the range is $An_{43}$-$An_{90}$ with a mean of 60,5 $\pm$ 13,8. The almost identical means suggest that in the present area there is no significant difference in plagioclase composition between amphibolites and granolites.

In order to check the optical composition determination, plagioclases in twelve specimens were analysed by means of microprobe techniques (Appendix II, Table A2-3). The mean compositions of a number of analyses per specimen are plotted in Fig. 20b which supports the wide compositional spread of plagioclases in the upper amphibolite and granulite facies terranes. Binns (1965b) finds a similar wide range in plagioclase compositions in basic rocks of the amphibolite and granulite facies at Broken Hill. The labradorite composition of the plagioclase in the amphibolites and the lack of primary clinozoisite and chlorite as well as the frequent occurrence of salite, indicate conditions of high grade metamorphism in the sense of Winkler (*op.cit.*).

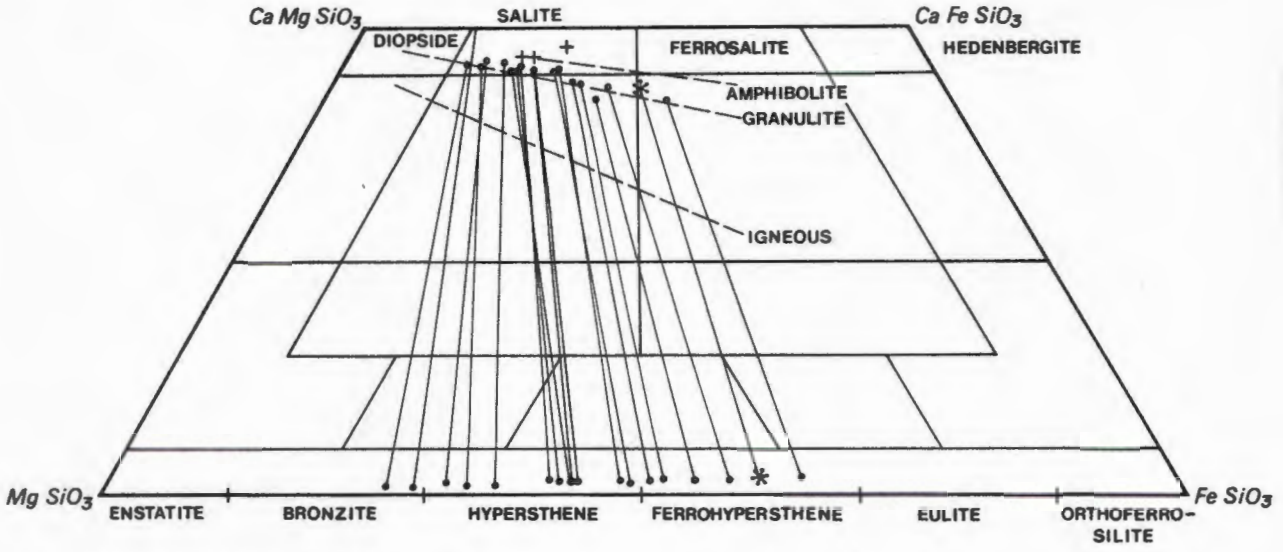


Fig. 21 Coexisting clino-and ortho-pyroxenes plotted with respect to Ca, Mg and Fe + Mn atoms in the nomenclature of Poldervaart and Hess (1951) and Deer *et al.* (1971, 1978). Solid dots represent pyroxenes in hypersthene-pyroclase granolites and crosses indicate the compositions of clinopyroxenes in salite-bearing amphibolites. Each dot is based on the mean composition determined from 2 to 6 spot analyses per specimen. Tie-lines link pairs of coexisting pyroxenes. Diagonal trend lines are taken from Binns (1965b) and represent calcic pyroxene compositions in amphibolites, granulite facies and igneous rocks, respectively. * Represents coexisting pyroxenes in garnet granulite specimen HA 1030.

(c) Coexisting Pyroxenes

Coexisting Ca-rich and Ca-poor pyroxenes in eighteen mafic fock specimens from the granulite facies terrane of the study area have been analysed by microprobe techniques (Appendix II, Tables A2-4 and A2-5). The aim has been to use their compositions in quantitative geothermometry (to be discussed in Chapter IV). The mean compositions of these pyroxenes in the specimens studied are shown in Fig. 21. Coexisting pairs are linked with tie-lines.

(i) Orthopyroxene

The orthopyroxene investigated in this study plot mainly into the hypersthene and ferrohypersthene fields with only two analyses of bronzite composition (Fig. 21). In Fig. 22 some chemical components of the orthopyroxenes are plotted as a function of increasing mole per cent ferrosilite and it is apparent that, as the Fe concentration of the mineral

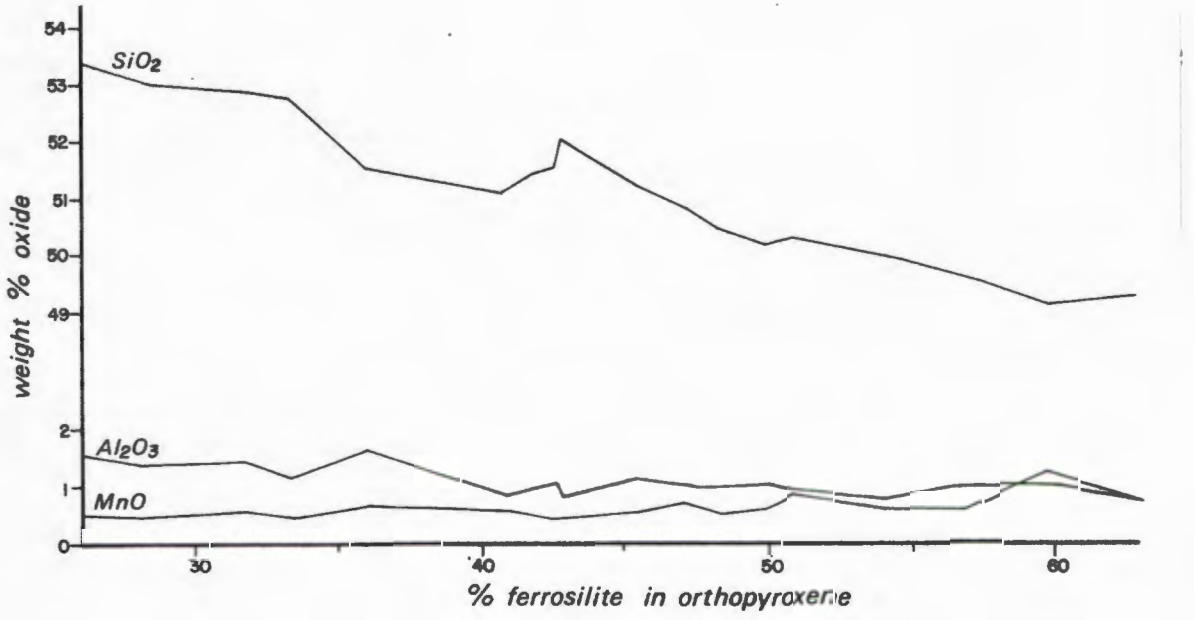


Fig. 22 The variation of $SiO_2$, $Al_2O_3$ and MnO in orthopyroxene with increasing ferrosilite content.

increases, there is a decrease in $SiO_2$ and $Al_2O_3$ while MnO tends to increase, thus supporting the observations of Jan and Howie (1980). Saxena (1968a) points out that for coexisting clinopyroxene and orthopyroxene, the orthopyroxene contains about twice the amount of MnO recorded in the clinopyroxene. The Ca concentration is very low (0,424 to 1,172 weight per cent CaO) and there is a tendency for Ca to increase in Fe-rich compositions (Fig. 21) consistent with the observations of Binns (1965b) and Davidson (1969). The Ca concentration in orthopyroxene is generally regarded to be a function of temperature. Atlas (1952) has experimentally investigated the system $MgSiO_3$ - $CaMgSi_2O_6$ and finds that the maximum number of Ca-atoms in enstatite increases with increasing temperature (at 1100°C - 0,115; at 1000°C - 0,050; at 700°C - 0,030 ions of Ca per 6 oxygens). Binns (1962) also suggests that CaO in orthopyroxene increases with increasing temperature in the Broken Hill area. It is well established by numerous experiments that the miscibility gap between coexisting pyroxenes decreases with increasing temperature. The absence of exsolution lamellae in orthopyroxene in the present area is considered as evidence for their crystallisation at temperatures lower than those at which appreciable solid solution between the ortho and clinopyroxene takes place.

The solubility of $Al_2O_3$ in orthopyroxene is largely considered to be a function of pressure and/or temperature (Green, 1964; Green and Ringwood, 1967; Dobretsov *et al.*, 1973; Anastasiou and Seifert, 1972; Medaris, 1972; Ramaswamy and Murty, 1973; Obata, 1976; Wilson, 1976). The system $MgO$-$Al_2O_3$ - $SiO_2$ ($H_2O$) is experimentally investigated by Anastasiou and Seifert (*op.cit.*) who conclude that the solubility of $Al_2O_3$ in enstatite in the low-pressure environment is essentially a function of temperature (in the range 900 - 1000°C) and is much less dependent on pressure. The $Al_2O_3$ concentrations of the orthopyroxenes analysed in this study are low, ranging from 0,787 - 1,632 weight per cent, but in these basic compositions the orthopyroxenes do not coexist with highly aluminous phases and, therefore, cannot be regarded as being saturated with respect to $Al_2O_3$. For this reason, the experimental results of Anastasiou and Seifert (*op.cit.*) cannot be applied to the pyroxenes in evaluating the temperatures of equilibration.

Ramaswamy and Murty (*op.cit.*) correlate the high $Al_2O_3$ content with high pressure. The orthopyroxenes from the charnockite series in India contain considerably higher $Al_2O_3$ (up to 4,82 weight per cent) compared to those of this study.

From theoretical considerations the substitution of $Al^{VI}$ (0,53A°) for the larger $Fe^{+2}$ (0,77A°) or Mg (0,72A°) implies a decrease in volume and it seems, therefore, reasonable that this substitution takes place with increasing pressure. When Si (0,26A°) is replaced by the larger $Al^{IV}$ (0,39A°), the volume is increased and, therefore, this substitution is expected in response to increasing temperature (discussed by Wilson, 1976).

Other authors suggest that the bulk chemical rock compositions influence the $Al_2O_3$ concentration in orthopyroxene (Howie, 1965; Binns, 1965b; Davidson and Mathison, 1974). In view of the uncertainty in the factors

controlling $Al_2O_3$ contents of orthopyroxene, it is concluded that this parameter should be used with caution for estimating P-T conditions during metamorphism.

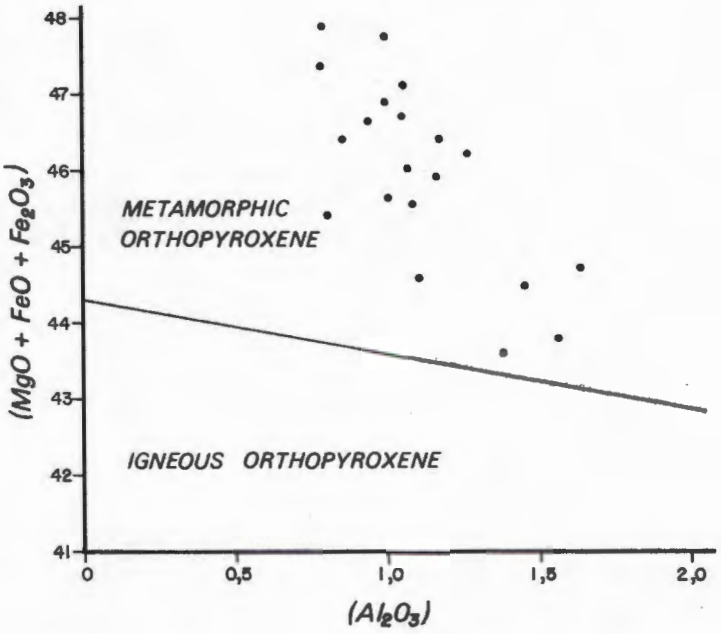


Fig. 23 Compositions of the orthopyroxenes from the study area in terms of (MgO + FeO + $Fe_2O_3$) and ($Al_2O_3$). The diagonal line obeys the equation (MgO + FeO + $Fe_2O_3$) + 0,775 $Al_2O_3$ = 44,304 and separates the igneous from the metamorphic pyroxene field (after Bhattacharyya, 1971).

Bhattacharyya (1971) shows that metamorphic and igneous orthopyroxenes can be distinguished by their chemistry. In a plot of (MgO + FeO + $Fe_2O_3$) versus $Al_2O_3$ metamorphic and igneous orthopyroxenes fall into two separate fields. The demarcation line obeys the equation (MgO + FeO + $Fe_2O_3$) + 0,775 $Al_2O_3$ = 44,304 intersecting the ordinate at 44,3 per cent (MgO + FeO + $Fe_2O_3$) (Bhattacharyya, *op.cit.*). In Fig.23 the orthopyroxenes in granolite specimens from the study area are plotted into Bhattacharyya's diagram, showing that they all fall into the metamorphic orthopyroxene field. This suggests that although most of these rocks have demonstrably been intruded and are thus of igneous origin, the pyroxenes subsequently recrystallised and re-equilibrated during granulite facies metamorphism to lose their igneous identity.

(ii) Clinopyroxene

The mean compositions of clinopyroxenes are plotted in terms of Ca, Mg and Fe + Mn atoms in Fig. 21 and the terminology discussed by Poldervaart

and Hess (1951) and Deer *et al.* (1971, 1978) is used in this study. Clinopyroxenes in specimens of hypersthene-pyroclase granolite plot close to the salite-augite field boundary with only two samples falling into the ferroaugite field. Three clinopyroxenes from amphibolite facies mafic rocks (Appendix II, Table A2-6) are also shown in Fig. 21 and these have higher Ca concentrations than their equivalents in the granulite facies terrane.

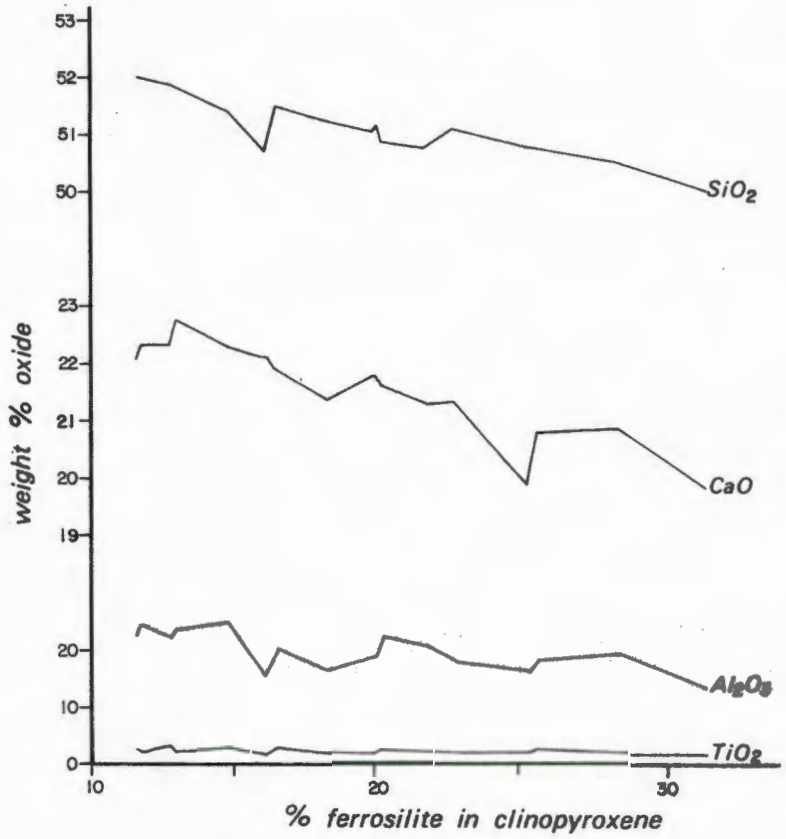


Fig. 24 Compositional variation of clinopyroxenes with increasing concentration of the ferrosilite molecule.

In Fig. 24, compositional variations are shown as a function of increasing ferrosilite component in clinopyroxene. It is evident that as the Fe content of the mineral increases, $SiO_2$, CaO and $Al_2O_3$ tend to decrease and this is consistent with the observations by Jan and Howie (1980).

Binns (1962, 1965b) also points out that for clinopyroxenes in hypersthene-pyroclase granolites the Ca concentration tends to decrease with increasing Fe content and that clinopyroxenes in amphibolites have higher Ca concentrations than those in granolites which in turn are more calcic than those in igneous rocks. This observation is considered to reflect the decreasing

miscibility gap between coexisting pyroxenes with increasing temperature (*ibid.*). The amphibolite, granolite and igneous compositional trends for lime-rich pyroxenes (after Binns, 1965b) are shown in Fig. 21 and are in harmony with the Namaqualand granolites.

A comparison of clinopyroxenes of similar ferrosilite concentration from the amphibolite and granulite facies environments shows that the former contain higher $SiO_2$, CaO, MnO and lower $Al_2O_3$ and $TiO_2$ than the latter while $Na_2O$ remains fairly constant.

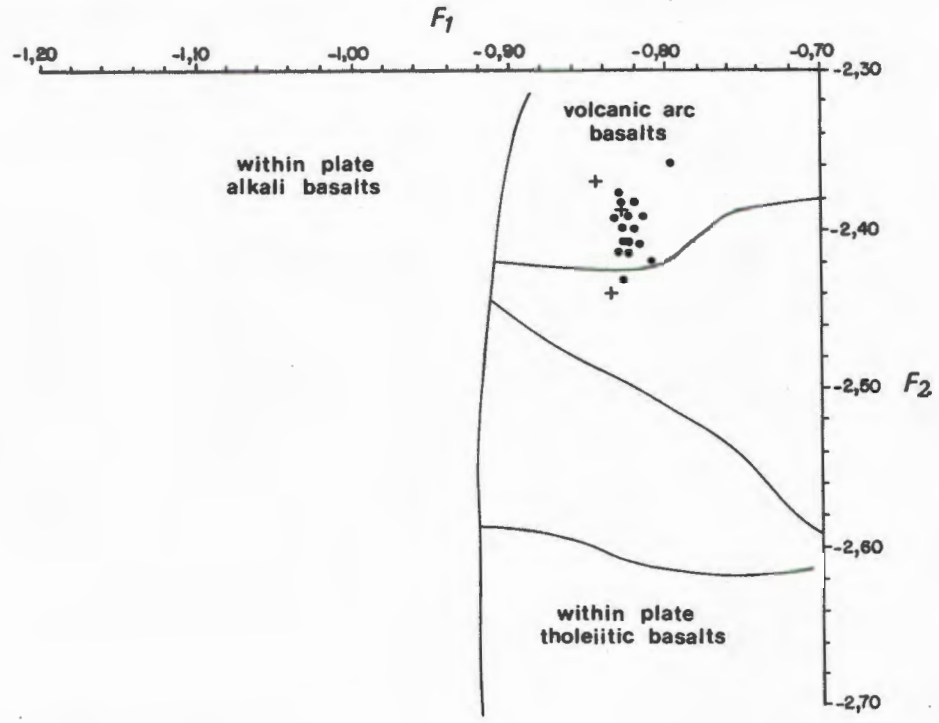


Fig. 25 Discriminant functions $F_1$ and $F_2$ for clinopyroxenes from the study area. Solid dots represent clinopyroxenes in hypersthene-pyroclase granolites and crosses indicate the compositions of clinopyroxenes in amphibolites.

$F_1 = -0,012 \times SiO_2 - 0,0807 \times TiO_2 + 0,0026 \times Al_2O_3 - 0,0012 \times FeO - 0,0026 \times MnO + 0,0087 \times MgO - 0,0128 \times CaO - 0,0419 \times Na_2O.$

$F_2 = -0,0469 \times SiO_2 - 0,0818 \times TiO_2 - 0,0212 \times Al_2O_3 - 0,0041 \times FeO - 0,1435 \times MnO - 0,0029 \times MgO + 0,0085 \times CaO + 0,0160 \times Na_2O$

(after Nisbet and Pearce, 1977).

Nisbet and Pearce (1977) show that the chemical characteristics of

clinopyroxene can often be used to identify the parent magma of the various tectonic environments. They use two discriminant functions ($F_1$ and $F_2$, Fig. 25) and conclude that clinopyroxenes from within plate alkali basalts are most successfully discriminated by these functions, but that there is considerable overlap between pyroxene compositions from volcanic arc basalts, ocean floor basalts and within plate tholeiitic basalts. These discriminatory functions have been calculated for the clinopyroxene analyses of the study area and are plotted in Fig. 25. The greater majority of the clinopyroxene analyses fall into the field of volcanic arc basalts.

(iii) Element distribution between coexisting ortho- and clinopyroxene

The distribution of elements, expressed as weight per cent oxides, between coexisting ortho- and clinopyroxene is summarised in Table 11, showing that clinopyroxene is enriched in $TiO_2$, $Al_2O_3$, $Cr_2O_3$ and $Na_2O$ relative to orthopyroxene. MnO, on the other hand, is concentrated in orthopyroxene. These observations are in agreement with Deer *et al.* (1978), Fleet (1974b) and Jan and Howie (1980). In 11 of the 18 specimens analysed clinopyroxene has the higher $SiO_2$ concentration, while in the remaining seven specimens orthopyroxene is the more siliceous of the two minerals. Fleet (*op.cit.*) and Jan and Howie (*op.cit.*) find that $SiO_2$ tends to prefer the orthopyroxene structure.

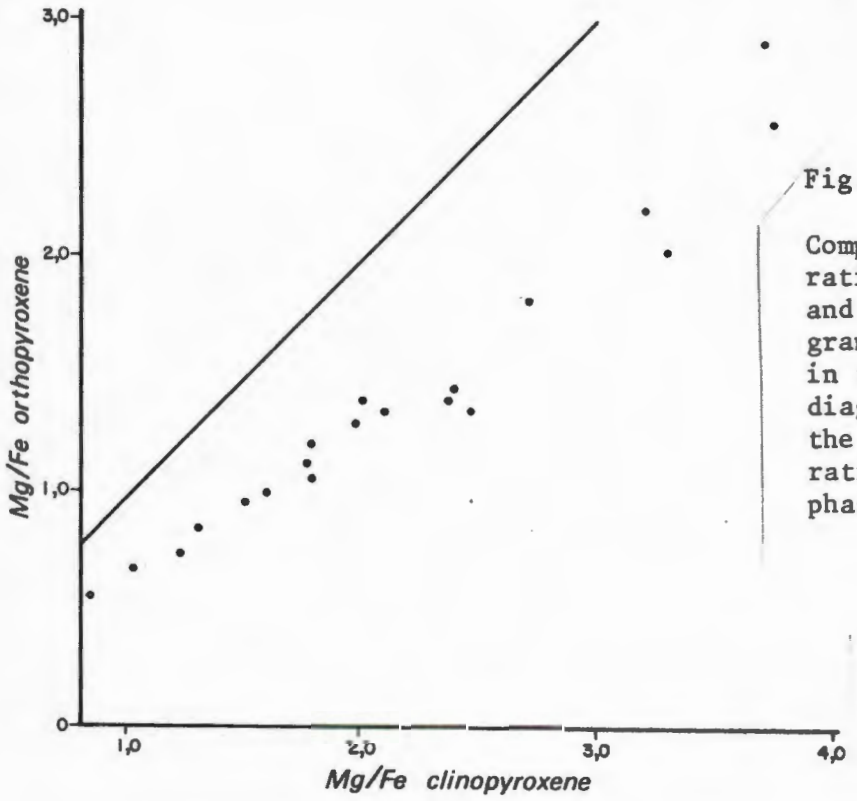


Fig. 26

Comparison of the Mg/Fe ratio of coexisting ortho- and clinopyroxene from the granulite facies mafic rocks in the study area. The diagonal line represents the trend of equal Mg/Fe ratios between the two phases.

Table 11 Comparison of metal-oxide distributions between coexisting ortho- and clinopyroxenes. In parenthesis are mean weight per cent oxide over entire compositional range studied, followed by standard deviation.

| oxide | clinopyroxene | | orthopyroxene |
|---|---|---|---|
| $TiO_2$ | (0,228 ± 0,041) | > | (0,092 ± 0,016) |
| $Al_2O_3$ | (2,007 ± 0,307) | > | (0,105 ± 0,246) |
| $Cr_2O_3$ | (0,055 ± 0,055) | > | (0,035 ± 0,031) |
| $Na_2O$ | (0,347 ± 0,103) | > | (0,013 ± 0,013) |
| MnO | (0,281 ± 0,091) | < | (0,632 ± 0,185) |
| Mg/Fe | Mg/Fe cp | > | Mg/Fe op |
| $SiO_2$ | For 11 specimens $SiO_2$ cp | > | $SiO_2$ op |
| | For 7 specimens $SiO_2$cp | < | $SiO_2$ op |

In Fig. 26, the comparison of the Mg/Fe ratio between coexisting pyroxenes is shown and it is evident that for all specimens clinopyroxene has the higher Mg/Fe ratio and this agrees well with the observations of Jan and Howie (*op.cit.*).

(iv) Pyroxene tie-lines

Coexisting pyroxenes are linked with tie-lines in Fig. 21, some of which are seen to cross each other. According to Hess (1941) coexisting ortho- and clinopyroxenes in igneous rocks have tie-lines intersecting the wollastonite-enstatite join at about $Wo_{75}$. Brown (1961) points out that igneous and metamorphic pyroxene pairs have the same tie-line intersection on the Wo-En join at about $Wo_{82}$ and he concludes that the exact position of intersection has no petrogenetic significance, but is indicative of chemical equilibrium between coexisting pyroxenes. Ramaswamy and Murty (1973) suggest that all tie-lines, regardless of the origin of the pyroxenes (igneous or metamorphic), tend towards $Wo_{75}$, a feature regarded as indicating chemical equilibrium. The same conclusion is reached by Jan and Howie (1980) who consider the close clustering of tie-line intersections between $Wo_{75}$ and $Wo_{85}$ as support for the attainment of equilibrium.

The majority of the tie-lines in the present study (Fig. 21) intersect the En-Wo join in the range $Wo_{76}$-$Wo_{82}$. Only three pyroxene pairs yield tie-line intersections between $Wo_{72}$ and $Wo_{75}$. According to the literature, this narrow interval of tie-line intersections may suggest that the coexisting pyroxenes in the specimens studied are in chemical equilibrium, a pre-requisite for the application of pyroxene geothermometry. Jan and Howie (*op.cit.*) regard values deviating from the range $Wo_{60}$ to $Wo_{90}$ as indicative of disequilibrium.

## 6 The Occurrence of Garnet-Granolite in the Study Area

It has already been pointed out that the assemblage "garnet + clinopyroxene + orthopyroxene" (the garnet being an almandine-rich phase) has only been observed in one specimen, (HA 1030), where these minerals coexist with plagioclase and quartz and that garnet-granolites are regarded to indicate higher pressure conditions.

Coexisting minerals in this specimen were analysed by microprobe techniques (Appendix II, Table A2-7. Four plagioclase analyses indicate that this mineral is anorthite with grain centre compositions ranging between $An_{89,8}$ and $An_{90,4}$. This is the highest anorthite content recorded for plagioclase in specimens containing both clino- and orthopyroxene. Such high Ca contents are more commonly recorded in plagioclases in calc-silicate rocks. In fact, this particular specimen is closely associated with calc-silicate rocks, and this may explain the very calcic nature of the plagioclase.

Seven grains of orthopyroxene were analysed and these are found to have fairly constant core compositions, the mean of which in terms of Fe, Mg, Ca and Mn ions is recorded in Table 12. The $\frac{Fe}{Fe+Mg}$ ratio of this mineral is 0,602 and in the terminology used by Deer *et al.* (1971), the chemical composition plots into the field of ferrohypersthene (see Fig. 21, page 85).

Seven clinopyroxene analyses have yielded the mean composition shown in Table 12. The $\frac{Fe}{Fe+Mg}$ ratio of this mineral is computed as 0,494 and in the terminology used by Deer *et al.* (*op cit.*) its composition is intermediate between augite and ferroaugite and plots close to the salite-ferrosalite compositional fields. The mineral composition plots along the trend of granulite facies clinopyroxenes as defined by Binns (1965b) and shown graphically in Fig. 21, page 85. Both pyroxenes are very similar in chemical composition to their equivalents in other granolites of similar ferrosilite content, but they have slightly higher manganese contents.

Five garnets have been analysed in specimen HA 1030 and the grain centre compositions are found to be fairly uniform, the mean of which, in terms of $Fe^{+2}$, Mg, Ca and Mn atoms is listed in Table 12. The ionic proportions for garnet have been corrected for $Fe^{+3}$ by the method outlined in Appendix ID. Although the garnet is an almandine-rich phase, it contains considerably higher Ca and Mn contents compared to garnets in pelitic gneiss specimens. This garnet contains about 3.0 per cent by weight of MnO and 7,6 weight per cent CaO. Both these components have the effect of increasing the stability field of this mineral. Very similar garnet compositions are recorded in other

Table 12 Compositional data for coexisting garnet-orthopyroxene-clinopyroxene assemblage in specimen HA 1030 in terms of ionic proportions. Garnet has been corrected for $Fe^{+3}$.

| Mineral | Oxygens for ionic proportions | Fe | Mg | Ca | Mn |
|---|---|---|---|---|---|
| garnet | 12 | 1,8699 | 0,2978 | 0,6487 | 0,2020 |
| orthopyroxene | 6 | 1,1610 | 0,7664 | 0,0395 | 0,0416 |
| clinopyroxene | 6 | 0,5395 | 0,5532 | 0,8647 | 0,0192 |

metamorphic terranes (e.g. Binns, *op.cit.*). Recently Dahl (1980) has published garnet compositions coexisting with clinopyroxene and orthopyroxene from the Ruby Range area in southwestern Montana. These garnets are compositionally very similar to the ones analysed in this study. The physical conditions of metamorphism envisaged by Dahl (*op.cit.*) for these garnet granolites are 745 ± 50°C/7,2 ± 1,2 kb and 675 ± 45°C/6,2 ± 1,2 kb, respectively for two small areas investigated by him. The important point is that the assemblage "garnet + orthopyroxene + clinopyroxene" is stable at relatively low pressures of 5-7 kb if the almandine-rich garnet contains appreciable amounts of the grossular and spessartine molecules. Therefore, it is concluded that this occurrence of garnet-granolite in the study area is compatible with a relatively low pressure environment indicated by the common assemblage "orthopyroxene + clinopyroxene + plagioclase" (Green and Ringwood, 1967, 1972).

## 7 Textural Evidence for the Partial Breakdown of Hornblende in the Upper Amphibolite Facies

Salite-bearing amphibolites provide textural evidence for the breakdown reaction of hornblende to clinopyroxene as shown in Fig.27 which is a sketch from a thin section of sample HA 1091. Hornblende is surrounded by a rim of clinopyroxene. The grain boundaries between the two minerals are ragged and the manner in which the clinopyroxene surrounds the hornblende, suggests that the former is developing at the expense of the amphibole. Quartz is not observed in the thin section of this specimen, indicating that this mineral is not involved in the reaction. The general observation of increasing basification and abundance of plagioclase with increasing metamorphic grade (Wenk and Keller, 1969) suggests that plagioclase could be a product phase of this reaction, although this is not clear purely from textural evidence. In simplest terms the observed reaction can be represented as :

$$\text{hornblende} \rightleftharpoons \text{clinopyroxene} + \text{plagioclase} + H_2O \qquad (2)$$

The liberation of water in reaction (2) is a requirement when hydrous minerals are replaced by anhydrous phases.

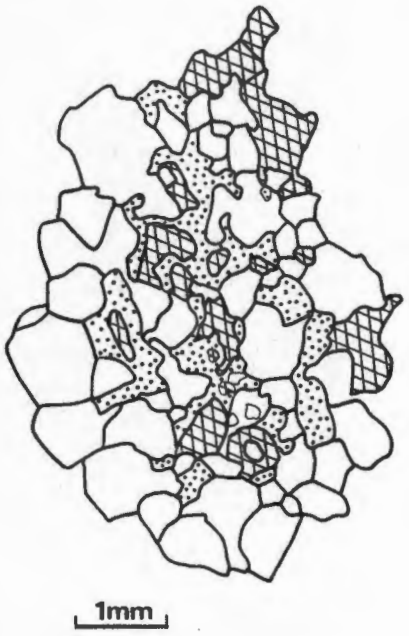


Fig. 27

Textural evidence for the breakdown of hornblende to yield salite in salite-bearing amphibolite specimen HA 1091. Hornblende (hatched) is partially or completely enclosed by salite (stippled). The clear spaces represent plagioclase.

## 8 Discussion on Amphibole Stability

Experimental studies on the stability limits of calcic amphiboles are summarised by Ernst (1968) and the upper temperature stability limit of the magnesian end-member tremolite ($Ca_2Mg_5Si_8O_{22}(OH)_2$) has been determined by Boyd (1959). This mineral breaks down according to the reaction:

$$\text{tremolite} \rightleftharpoons \text{2 diopside + 3 enstatite + quartz + } H_2O \qquad (3)$$

(Tr, Fig. 28) at a temperature of 870°C when $P_{H_2O} = P_{total} = 2$ kb. Under isobaric conditions the upper temperature stability limit of tremolite is displaced towards lower temperature with increasing $X_{CO_2}$ of the gas phase (Greenwood, 1962a). Substitution of $Fe^{+2}$ lowers the stability of the amphibole as is evident from the experimental results of Ernst (1966) on ferrotremolite ($Ca_2Fe_5^{+2}Si_8O_{22}(OH)_2$). (Fe-Tr, Fig. 28). Boyd (*op.cit.*) shows that pargasite $NaCa_2Mg_4Si_6Al_2O_{22}(OH)_2$ is stable up to very high temperatures (1040°C at $P_{fluid}$ = 1 kb), but the substitution of $Fe^{+2}$ for Mg reduces the stability. This is demonstrated by Gilbert (1966) who investigates the upper temperature stability limit of ferropargasite ($NaCa_2Fe_4^{+2}AlSi_6Al_2O_{22}(OH)_2$) under controlled conditions of oxygen fugacity (see reaction boundaries Par and Fe-Par in Fig 28).

Ernst (1968) points out that $f_{O_2}$ becomes an important additional variable in the stability of Fe-bearing amphiboles because Fe can have more than one

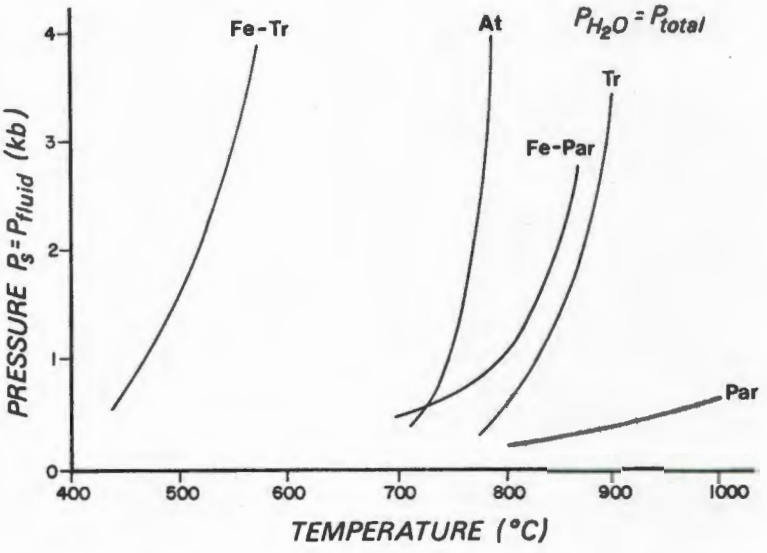


Fig. 28 Experimentally determined upper stability limits of amphibole end-member compositions under the conditions $P_{H_2O} = P_{total}$.

Fe-Tr - upper temperature stability of ferrotremolite (Ernst, 1966)
Tr - upper temperature stability of Mg-tremolite (Boyd, 1959)
Par - upper temperature stability of pargasite (Boyd, 1959)
Fe-Par - upper temperature stability of ferropargasite (Gilbert, 1966)
At - upper temperature stability of anthophyllite (Greenwood, 1963)

oxydation state effecting the stability of the mineral. This is also apparent from the experiments of Gilbert (*op.cit.*). From the literature it appears that calcic amphiboles are stable over a large range of P-T conditions and that the upper stability limits depend on composition (Mg/Fe ratio), $P_{total}$, $P_{H_2O}$ and $f_{O_2}$.

The natural amphiboles of the study area are not pure end-member compositions, but are mixtures of the various end-members and accordingly will have different upper temperature stability limits. Binns (1969b) investigates experimentally the breakdown of hornblende at the amphibolite-granulite facies boundary using natural amphibolite and hypersthene-pyroclase granolite from Broken Hill. The experiments were monitored with the quartz-fayalite-magnetite buffer with excess water ($P_{H_2O} = P_{total}$). The results indicate that, provided $P_{H_2O} = P_{total}$, the amphibolite-granulite facies boundary occurs at 770°C in the pressure range 1-3 kb. However, in the natural environment the condition $P_{H_2O} < P_{total}$ is more likely (Winkler, 1976) and, therefore, the hornblende

breakdown curve determined by Binns (*op.cit.*) will be shifted towards lower temperatures. Depending on the composition of the fluid phase during metamorphism, the amphibolite-granulite facies transition should occur somewhere between 700 and 750°C which roughly corresponds to the breakdown of anthophyllite (Greenwood, 1963) in Fig. 28.

Similar experiments were recently conducted by Spear (1981) on hornblende stability and compositional variability as a function of T, $P_{fluid}$ and $fO_2$ under amphibolite and granulite facies conditions using olivine tholeiite as a starting material and three different buffers to control the oxygen fugacity. His findings support previous experiments and demonstrate that increasing Al, Na, K and Ti in hornblende are related to rising temperature while decreasing Si and rising $Al^{IV}$ and $Al^{VI}$ are recorded in response to rising pressure.

## C Metamorphism of Pelitic Rocks

### 1 Mineral Assemblages in Pelitic Gneisses

Reinhard (1968) stresses the importance of recognising those minerals that occur in equilibrium with each other as these may only form part of the entire mineral assemblage within a metamorphic rock. Such equilibrium assemblages are also referred to as mineral parageneses (Winkler, 1976). The pelitic gneiss specimens investigated in this study contain up to nine mineral phases and from textural relationships it is apparent that not all of them are in equilibrium with each other. This is particularly obvious from the numerous corona textures present in these rocks.

Quartz, K-feldspar, plagioclase, opaque minerals and hercynite-spinel solid solutions occur in most of the 38 specimens examined and can therefore be ignored in the mineral assemblages listed below, arranged in order of decreasing frequency (numbers in brackets indicate the frequency of occurrence of a specific mineral assemblage).

cordierite + garnet + sillimanite (10)
cordierite + garnet + sillimanite + biotite (8)
cordierite + sillimanite (7)
cordierite + biotite + sillimanite (3)
cordierite + biotite (2)
cordierite + garnet + biotite (1)
cordierite + garnet (1)
cordierite (1)
garnet + sillimanite (1)
cordierite + biotite + hypersthene + (anthophyllite) (1)
cordierite + biotite + garnet + (anthophyllite) (1)
cordierite + biotite + hypersthene (1)
garnet + hypersthene (1)

Textural relationships between anthophyllite and the associated minerals suggest a retrograde origin of the orthoamphibole after hypersthene and is therefore parenthesized.

Coexisting garnet, cordierite and biotite in some of the pelitic gneiss specimens from the granulite facies terrane have been analysed by microprobe techniques (Appendix II, Tables A2-8, A2-9 and A2-10). Several grains of each mineral were analysed in their centres and the mean core compositions were then computed and plotted in AFM projection (Thompson, 1957; Reinhard, *op. cit.*) as shown in Fig. 29a.

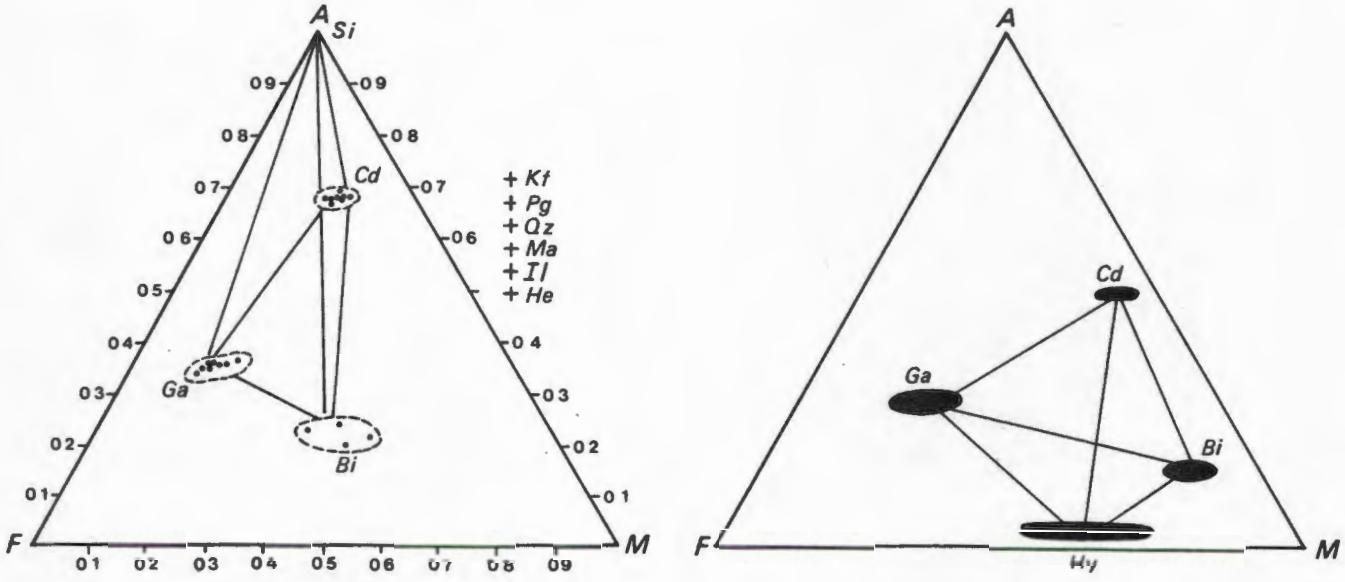


Fig. 29 (a) Coexisting minerals in pelitic gneiss specimens (hypersthene-free) in AFM projection (through K-feldspar) linked by tie-lines. The compositions refer to grain centres of these minerals.

(b) Schematic presentation of mineral assemblages in hypersthene-bearing pelitic gneisses (after Reinhard, 1968).

Abbreviations as in preface

Following Reinhard (*op.cit.*), K-feldspar has been used as the projection-point and the apices of the AFM diagram represent the following oxides:

$A = Al_2O_3 - K_2O - Na_2O - CaO$

$F = FeO + Fe_2O_3 - TiO_2$

$M = MgO$

Strictly speaking $Fe_2O_3$ should be subtracted from the total iron oxide, but as $Fe^{+3}$ and $Fe^{+2}$ are not distinguished by the microprobe it is convenient to ignore $Fe_2O_3$ (if present in small amounts) and plot total iron instead.

From Fig. 29a it is apparent that the garnet-cordierite and sillimanite-biotite tie-lines cross each other. Crossing tie-lines in the AFM diagram indicate discontinuous reactions (Thompson, 1976). Experimental studies on pelitic bulk compositions demonstrate that biotite-sillimanite assemblages are stable at lower temperatures, being replaced by cordierite-garnet assemblages (when quartz is present in excess) in response to increasing temperature (Holdaway and Lee, 1977). The reaction likely to account for the observed change in mineral assemblage involves the breakdown of biotite and sillimanite in the presence of quartz to yield cordierite, garnet and K-feldspar via the equilibrium

biotite + sillimanite + quartz $\rightleftharpoons$ cordierite + garnet + K-feldspar + $H_2O$ (4)

(Holdaway and Lee, *op.cit.*). This reaction in the Fe-end member system has

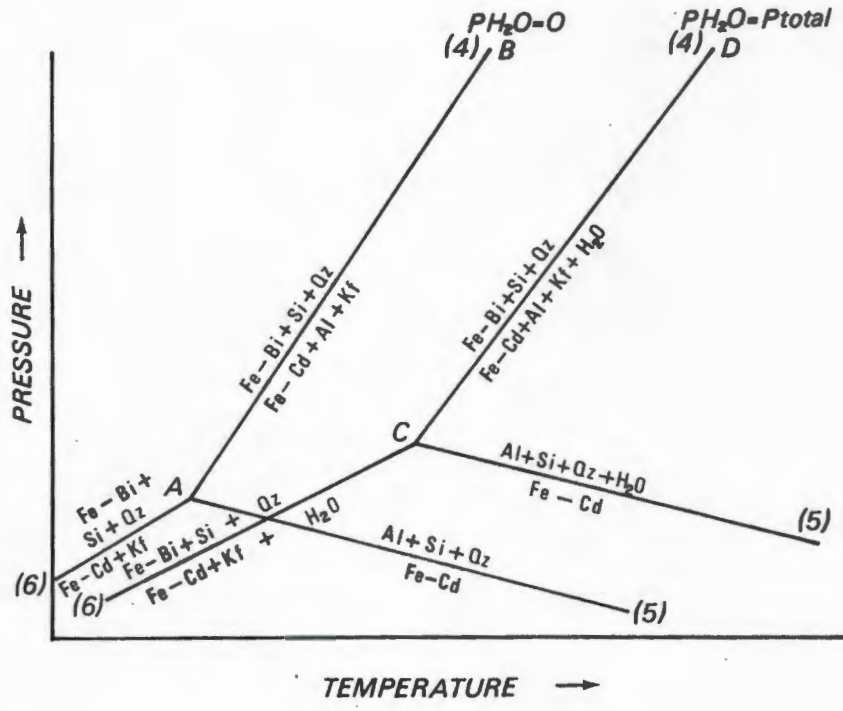


Fig. 30 Schematic presentation of the equilibria

Fe-biotite + sillimanite + quartz $\rightleftharpoons$ Fe cordierite + almandine + K-feldspar + $H_2O$ (4)

Fe-cordierite $\rightleftharpoons$ almandine + sillimanite + quartz + $H_2O$ (5)

Fe-cordierite + K-feldspar + $H_2O \rightleftharpoons$ Fe biotite + sillimanite + quartz (6)

under the conditions $P_{H_2O} = P_{total}$ and $P_{H_2O} = 0$ in P-T space (after Holdaway and Lee, 1977).

been experimentally investigated by Holdaway and Lee (*op.cit.*) and is schematically shown in Fig. 30 for two extreme conditions, namely when $P_{H_2O} = 0$ and $P_{H_2O} = P_{total}$. The fairly steep dP/dT slope and the marked effect of $P_{H_2O}$ on the equilibrium (4) are evident from Fig. 30. In a prograde process at pressures above A and C (Fig. 30) this reaction can proceed until at least one of the reactants has been consumed. If, for example, biotite is the first mineral to be used up by reaction (4), the stable paragenesis will be "cordierite + garnet + sillimanite" (this is a very common assemblage in the pelitic gneisses of the study area). Alternatively, sillimanite may be the first phase to be consumed by reaction (4) leaving the stable mineral assemblage "cordierite + garnet + biotite" (this assemblage is very rare in the area investigated). In either case, the sillimanite-biotite tie-line in the AFM projection is replaced by the garnet-cordierite tie-line in response to prograde metamorphic conditions.

The stable coexistence of all four phases garnet, cordierite, biotite and sillimanite all in equilibrium is only possible along the equilibrium boundary of reaction (4) (A-B and C-D in Fig. 30 depending on the water pressure during metamorphism. Note that in the Fe-Mg system this boundary becomes divariant).

If both biotite and sillimanite in reaction (4) are consumed simultaneously the higher grade "cordierite + garnet" assemblage is formed. The assemblage "cordierite + garnet + sillimanite" can also result from the reaction.

$$\text{cordierite} \rightleftharpoons \text{garnet} + \text{sillimanite} + \text{quartz} \qquad (5)$$

(The Fe-end member reaction is schematically shown in Fig.30 ).

Mineral assemblages observed in the pelitic gneisses of the study area that cannot be accounted for by the two reactions (4) and (5) include "cordierite + sillimanite", "cordierite + biotite + sillimanite" and "cordierite + biotite". According to Holdaway and Lee (*op.cit.*), these assemblages can be formed on the low temperature side of reaction (4) and may be related to the following equilibrium (Fig.30 ).

$$\text{cordierite} + \text{K-feldspar} + H_2O \rightleftharpoons \text{biotite} + \text{sillimanite} + \text{quartz} \qquad (6)$$

The ubiquitous coexistence of garnet and cordierite is indicative of high grades of regional metamorphism. The absence of garnet in many cordierite-bearing gneisses is considered to be a function of host rock chemical composition rather than indicative of lower metamorphic grade (see Fig. 29a) This is particularly evident from banded pelitic gneisses in which garnet-free and garnet-bearing bands alternate and demonstrate the stable coexistence of both types of assemblages.

Coexisting mineral phases in hypersthene-bearing pelitic gneisses have not been analysed chemically and are only shown schematically in Fig. 29b.

(drawn after Reinhard, *op.cit.*). The configuration in the AFM diagram (Fig. 29b) allows two crossing tie-lines to be drawn, namely the garnet-biotite and cordierite-hypersthene tie-lines, suggesting a discontinuous reaction (Thompson, 1976a) of the type

$$\text{garnet} + \text{biotite} \rightleftharpoons \text{cordierite} + \text{hypersthene} \qquad (7)$$

as proposed by Reinhard (*op.cit.*). Two of the specimens studied contain the assemblage "cordierite + biotite + hypersthene" possibly suggesting that the cordierite-hypersthene tie-line is stable in the study area. The likely former coexistence of all four phases involved in reaction (7) is, however, indicated by the assemblage "cordierite + biotite + garnet + anthophyllite" in one of the specimens with anthophyllite being retrograde after hypersthene.

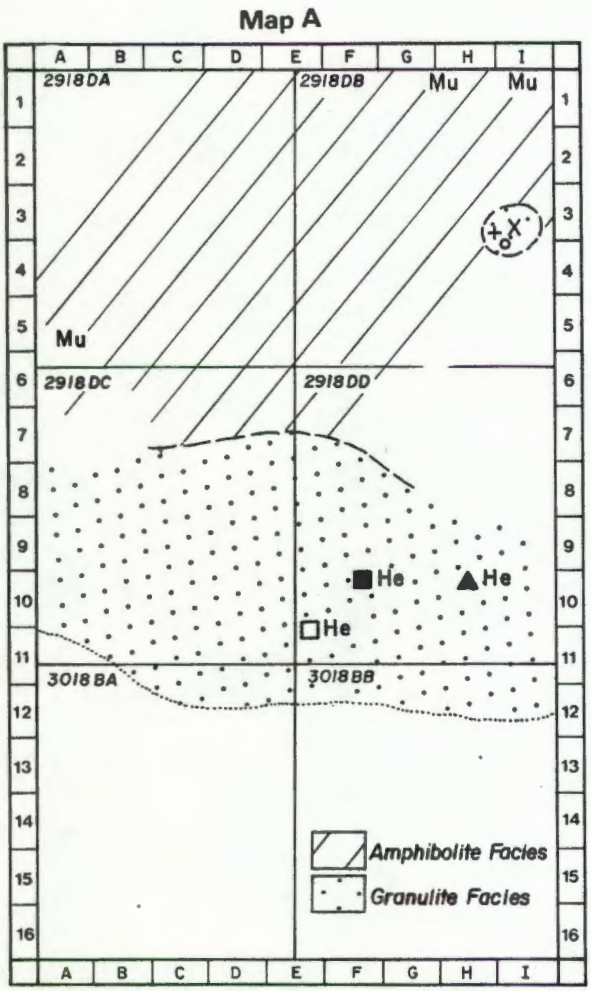


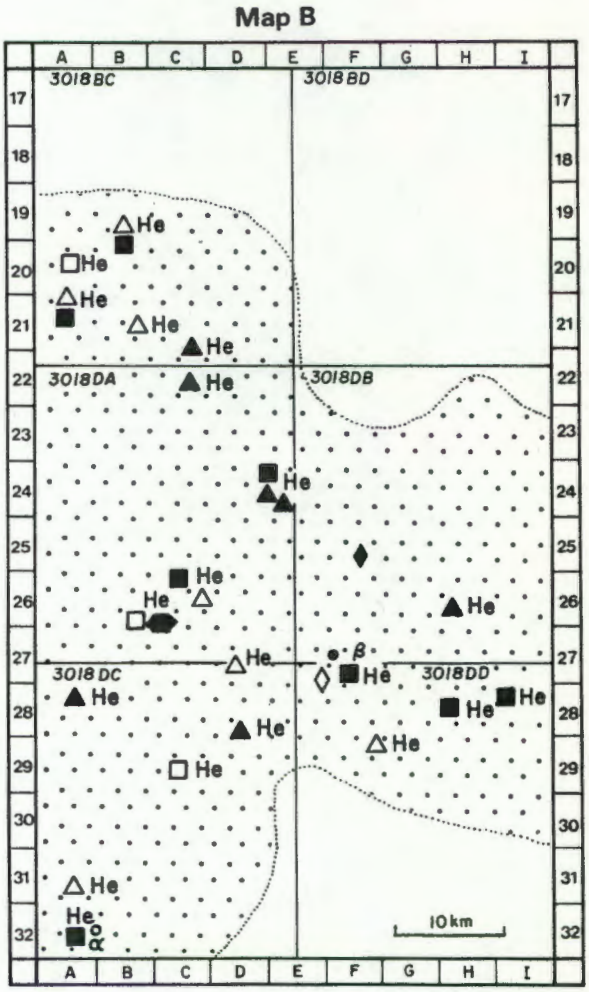

## 2 Distribution and Significance of Mineral Assemblages

The mineral assemblages in gneisses of pelitic composition and their regional distribution are shown in Fig. 31. All specimens have been collected in the granulite facies terrane and, except for some retrograde muscovite-bearing schists, no pelitic rocks were encountered within the amphibolite facies terrane. This is rather unfortunate, because the minerals in pelitic rocks yield valuable information regarding their physical conditions of formation. With only one exception, all solid symbols in Fig. 31 indicate assemblages containing both garnet and cordierite, while open symbols have been used for parageneses lacking garnet. Both types of assemblages are closely associated in space. Garnet and cordierite coexist in half of the number of pelitic gneiss specimens studied. This assemblage is commonly reported from various areas within the Namaqualand Metamorphic Complex (von Backström, 1964; Joubert, 1971a, Beukes, 1973; Blignault *et al.*, 1974; Toogood, 1976; Jackson, 1976; Jack, 1980; van Zyl, 1981). It is also reported from other high grade metamorphic terranes (Wynne-Edwards and Hay, 1963; de Waard, 1966; Reinhard, 1968; Currie, 1971; Hutcheon *et al.*, 1974). Various authors have attempted to outline the P-T conditions of formation of garnet and cordierite, either by experiment or by means of thermochemical considerations (Hirschberg and Winkler, 1968; Hensen and Green, 1971, 1972, 1973; Currie, 1971, 1974; Hutcheon *et al.*, *op.cit;* Thompson, 1976a,b; Holdaway and Lee, 1977).

---

Fig. 31 Regional distribution of mineral assemblages in pelitic gneisses.

Key to symbols:

| | | |
|---|---|---|
| ▲ | cordierite + garnet + sillimanite + biotite | (8) |
| ■ | cordierite + garnet + sillimanite | (10) |
| ⬬ | cordierite + garnet + biotite | (1) |
| • | cordierite + garnet | (1) |
| ⧫ | garnet + sillimanite | (1) |
| □ | cordierite + biotite + sillimanite | (3) |
| △ | cordierite + sillimanite | (7) |
| ○ | cordierite + biotite | (2) |
| ◊ | cordierite | (1) |
| + | cordierite + biotite + hypersthene + (anthophyllite) | (1) |
| x | cordierite + biotite + garnet + (anthophyllite) | (1) |
| α | cordierite + biotite + hypersthene | (1) |
| β | garnet + hypersthene | (1) |
| He | hercynite-spinel solid solution | |
| Mu | muscovite | |

Figures in brackets behind each mineral assemblage indicates its frequency of occurrence.

The experiments of Hensen and Green (*op.cit.*) provide a general phase diagram for pelitic compositions and demonstrate the existence of a large stability field for "garnet + cordierite" assemblages at elevated temperatures. These authors emphasise the importance of bulk chemical composition, particularly the MgO/(MgO + FeO) ratio, which has a major influence on the position and width of the garnet-cordierite stability field (decreasing the Mg/(Mg + Fe) ratio shifts the stability field towards lower pressure). Hensen and Green (*op.cit.*) show that at low pressures both garnet and cordierite are more Fe-rich, becoming increasingly enriched in magnesium with increasing pressure, the Mg/(Mg + Fe) ratio in both coexisting phases varying systematically as a function of pressure and temperature. They also demonstrate that for aluminous compositions at high temperatures the low pressure assemblage "cordierite + sillimanite + quartz" is replaced by the assemblage "garnet + cordierite + sillimanite + quartz" and finally "garnet + sillimanite + quartz" in response to increasing pressure.

Unfortunately other experimental data, for example, Currie (*op.cit.*) are inconsistent with those obtained by Hensen and Green (*op.cit.*). As pointed out by Hensen (1977), the major discrepancy between the experimental results of the two laboratories involves the relationship between temperature and the distribution coefficient ($K_D$) for the Fe - Mg exchange reaction in garnet, cordierite, sillimanite, quartz equilibria ($K_D$ is defined as:

$$K_D = \frac{X_{Cd}\ (1 - X_{Ga})}{X_{Ga}\ (1 - X_{Cd})}$$ where $X = Mg/(Mg + Fe^{+2})$ and Ga and Cd represent the two mineral phases garnet and cordierite respectively). The experiments of Currie (*op.cit.*) indicate that $K_D$ increases with increasing temperature while the data of Hensen and Green (*op.cit.*) suggest the opposite. According to Currie (*op.cit.*) the garnet-cordierite stability field is wedge shaped, becoming wider with increasing temperature. Another point of disagreement is that the results of Currie (*op.cit.*) indicate that the maximum stability field of coexisting garnet and cordierite (sillimanite and quartz being additional phases) is some 2-3 kb lower than suggested by Hensen and Green (*op.cit.*).

Thompson (1976a) has derived schematic isobaric T - X (Mg - Fe) and isothermal (Mg - Fe) relations for reactions in pelitic rocks, which predict the Fe - Mg distribution between coexisting ferromagnesian minerals as functions of pressure and temperature (Thompson, *op.cit.*, Fig. 3, p.419). His plot of ln $K_D$ versus $\frac{1}{T}$ for the Mg - Fe exchange reaction between garnet and cordierite (Thompson, 1976b) is in disagreement with Currie (*op.cit.*) and is consistent with the results of Hensen and Green (*op.cit.*). It is striking, however, that the computations of Thompson (*op.cit.*) support the stability field for coexisting garnet and cordierite to fall some 3 kb below the upper pressure limit suggested by Hensen and Green (*op.cit.*).

Water is known to have a marked effect on the stability of cordierite. Newton (1972) has investigated experimentally the high pressure stability

limits of Mg - cordierite. The results demonstrate that under anhydrous conditions cordierite breaks down at 8,2 kb, while when $P_{H_2O} = P_{total}$ the mineral is stable to higher pressures of 11,2 kb. This supports the idea that cordierite is formed at relatively shallow depths in the earth's crust.

Hypersthene is recorded in some of the assemblages shown in Fig. 31. This mineral is not very common and is encountered in only three of the 38 specimens examined. Experimental studies by Hensen and Green (1971, 1972, 1973) on silica-saturated pelites demonstrates that bulk chemical composition determines whether hypersthene can develop in pelitic lithologies during granulite facies metamorphism. According to them, for bulk compositions with $Al_2O_3/(MgO + FeO) > 1$, hypersthene is only formed at very high pressures above cordierite stability in rocks with a high Mg/Fe ratio. For bulk compositions of $Al_2O_3/(MgO + FeO) < 1$, hypersthene can be expected to form at low and intermediate pressures. At very low pressures cordierite and hypersthene are associated and with increasing pressure this assemblage is replaced by "garnet + hypersthene + cordierite". At very high pressures only garnet remains stable. Hensen and Green (*op.cit.*) have shown that the stability field of coexisting cordierite and hypersthene is very sensitive to the Mg/(Mg + Fe) ratio - an increase of this ratio, increases the stability field towards higher pressure. The implication of the above experiments is that pressures below 10 kb are required to account for the observed coexistence of hypersthene and cordierite in the study area.

On the basis of thermodynamic considerations in conjunction with field observations, Hess (1969) has constructed a petrogenetic grid displaying schematically the P-T stability fields of various cordierite-bearing assemblages. According to him, reactions introducing hypersthene into pelitic rocks occur on the high temperature side of the muscovite breakdown reactions and assemblages bearing cordierite and hypersthene are stable only at temperatures in excess of 750°C and pressures up to 5 kb.

High temperature metamorphism is suggested by the ubiquitous occurrence of a dark green spinel (hercynite-spinel solid solution) in the pelitic gneiss specimens (Fig. 31). Experimental studies under conditions of low $f_{O_2}$ and low $P_{H_2O}$ indicate that cordierite breaks down at very high temperatures to form sapphirine and hercynite-rich spinel in Mg-rich and Fe-rich compositions respectively (Hensen and Green, 1971, 1972, 1973). Under these experimental conditions the assemblage "hercynite + quartz" is formed at temperatures in excess of 900°C. However, these authors point out that increasing $f_{O_2}$ will increase the stability field of hercynite.

Zinc-rich spinels in the ternary system $Mg\ Al_2\ O_4$, $Zn\ Al_2\ O_4$ and $Fe\ Al_2\ O_4$ have been reported from metapelites that have undergone high-grade regional metamorphism (e.g. Reinhard, 1968; Gable and Sims, 1969; Frost, 1973; Wagner and Crawford, 1975; Stoddard, 1976, 1979. Spinels are also common in pelitic gneisses in other parts of the Namaqualand Metamorphic Complex (e.g. Joubert, 1971a, Jackson, 1976; van Bever Donker, 1980, Jack, 1980; van Zyl, 1981).

Stoddard (*op.cit.*) notes that although quartz is commonly present, it does not occur in direct contact with spinel. This observation is also made by Atkin (1978) who finds that the spinels are always surrounded by garnet, cordierite and feldspars. In contrast, Wagner and Crawford (*op.cit.*) consider quartz and spinel to be in equilibrium. Because Zn is also known to partition into staurolite (Albee, 1972; Griffen and Ribbe, 1973) and because of various theoretical arguments it has been suggested that Zn-rich hercynite could form as a result of staurolite breakdown (Loomis, 1972; Stoddard, *op.cit.*; Atkin, *op.cit.*). Stoddard (*op.cit.*) suggests reactions of the type:

staurolite + biotite + quartz $\rightleftharpoons$ sillimanite + K-feldspar + spinel + garnet ± rutile + $H_2O$ (8)

or staurolite + zoisite + quartz $\rightleftharpoons$ spinel + cordierite + anorthite + $H_2O$ (9)

Atkin (*op.cit.*) attributes the formation of Zn-rich hercynite to the reaction

Zn-staurolite $\rightleftharpoons$ Zn-hercynite + cordierite + sillimanite (10)

Richardson (1968) has studied experimentally the magnesium-free system Fe-Al-Si-O-H and notes that the invariant point for the coexistence of almandine + sillimanite + cordierite + hercynite + quartz occurs at 790°C and 2-3 kb; accordingly the lower temperature stability limit of the assemblage hercynite + sillimanite + quartz occurs at 790°C. It must be stressed, however, that this is applicable only to the above system under very specific experimental conditions. The addition of MgO to this system results in the appearance of a divariant band in the P-T field. Other components in hercynite such as ZnO are also likely to influence its stability field. During the experiments the $f_{O_2}$ was controlled by the QFM buffer and the author points out that an increasing $f_{O_2}$ would result in a migration of the invariant point towards higher pressure (*ibid.*).

According to the experimental investigation of Holdaway and Lee (1977) in the abovementioned Mg-free system under conditions of QFM buffer, the invariant point between Fe-cordierite, almandine, hercynite, sillimanite and quartz is located at 2,8 kb, 768°C which represents the lower temperature stability limit of the paragenesis hercynite + sillimanite + quartz under these conditions. The reaction giving way to this paragenesis results in the breakdown of Fe-cordierite according to:

Fe-cordierite $\rightleftharpoons$ hercynite + sillimanite + quartz + vapor (11)

The textural relations in specimens from the study area leave little doubt that the assemblage "hercynite + quartz" or "hercynite + sillimanite + quartz" was stable during the peak P-T conditions attained during granulite facies metamorphism, but hercynite and quartz have, subsequently become incompatible as a result of declining metamorphic conditions and this is

manifested by the ubiquitously developed coronas involving garnet, sillimanite and cordierite which now shield the spinel from the quartz.

In Fig. 31 it is shown that muscovite occurs at three localities within the amphibolite facies terrane. Although muscovite is probably common in the northern part of the study area, muscovite-bearing schists are only rarely encountered in outcrop. Quartz-biotite-muscovite and quartz-muscovite schists are generally associated with metaquartzites. The occurrence of muscovite requires some comment. Microscopic examination has shown that reddish-brown biotite crystals are well orientated in the regional foliation. Muscovite flakes are frequently orientated at high angles to the trend defined by the biotite crystals and on average are of considerably smaller grain size than the associated biotites. The small muscovite flakes often occur in clusters with individual crystals randomly orientated. Biotite, where in contact with muscovite always has ragged grain boundaries with small subhedral muscovites penetrating the biotite. The high angular relationships to the biotite foliation, the random orientation and the contact relationships between biotite and muscovite, indicate that muscovite growth is late and clearly post-dates the regional foliation defined by the biotite. Therefore, from textural relationships it is concluded that the muscovite was not present during the peak conditions of regional metamorphism and its formation must be related to subsequent retrogression. The random orientation is cited in support of muscovite growth outlasting deformation in the area concerned.

## 3 Textures Recorded in Pelitic Gneisses

Reinhard (1968) records that: "Most natural assemblages are masked by minor prograde and retrograde crystallisation so that one must carefully assess which minerals represent the main metamorphic equilibration. This is often a difficult task because a certain reliance must be placed on textural criteria." Optical examination of pelitic gneiss specimens from the study area have revealed that not all the minerals recorded within a single thin section are in textural equilibrium with each other and it is therefore desirable to outline some of the textural relationships between mineral phases.

### (a) Biotite and Cordierite Relations

In specimens containing the phases cordierite, biotite and sillimanite with or without garnet (K-feldspar, plagioclase, quartz, hercynite and opaque minerals are additional phases), there is ubiquitous evidence that biotite and cordierite occur in a "frozen-state" of reaction. This is manifested by the ragged boundaries between the two minerals and their textural relationships suggests that cordierite is forming at the expense of biotite. The potassium released by biotite breakdown is likely to enter K-feldspar which is invariably present in close proximity to cordierite and biotite. Garnet, although often

closely associated with these minerals, is not always in the immediate vicinity of the cordierite-biotite assemblage suggesting that this mineral is not necessarily involved in biotite breakdown. In contrast sillimanite and quartz are generally proximal phases.

All the minerals recorded in the pelitic gneisses, with the exception of plagioclase, can be considered to belong to the system $SiO_2$-$K_2O$-$Al_2O_3$-FeO-MgO-$H_2O$ if minor components are ignored. This "pelitic system" can be simplified to five components by ignoring MgO (it must be kept in mind, however, that MgO is an important component of cordierite, biotite and garnet) and if only the following seven phases: almandine, Fe-biotite, Fe-cordierite, sillimanite, K-feldspar, quartz and $H_2O$ are considered, it is apparent from the phase rule (Turner, 1968) that an invariant situation exists when all seven phases coexist in equilibrium. Some possible invariant reactions are the following:

3 Fe-biotite + 7 sillimanite + 11 quartz $\rightleftharpoons$ 1 almandine + 3 Fe-cordierite + 3 K-feldspar + $H_2O$ (4)

1 K-feldspar + 3 Fe-cordierite $\rightleftharpoons$ 1 almandine + Fe-biotite + 5 sillimanite + 7 quartz + $H_2O$ (12)

Several univariant reactions (labelled by the phase not participating in the reaction) are possible in this system:

(biotite, K-feldspar) 3 Fe-cordierite $\rightleftharpoons$ 2 almandine + 4 sillimanite + 5 quartz + $nH_2O$ (5)

(almandine) 2 Fe-biotite + 6 sillimanite + 9 quartz $\rightleftharpoons$ 2 K-feldspar + 3 Fe-cordierite + $nH_2O$ (6)

(sillimanite) 4 Fe-biotite + 3 Fe-cordierite + 3 quartz $\rightleftharpoons$ 4 K-feldspar + 6 almandine + $nH_2O$ (13)

(Fe-cordierite) 1 Fe-biotite + 2 quartz + 1 sillimanite $\rightleftharpoons$ 1 almandine + 1 K-feldspar + $nH_2O$ (14)

Of the above equilibria reactions (4) and (6) can account for the formation of cordierite at the expense of biotite. In order to appreciate the significance of the above reactions in terms of changing P-T conditions, the univariant equilibria can be placed in relative sequence around the invariant point by the method of Schreinemaker's (Zen, 1966) and orientated in P-T space in a manner that is consistent with experimental studies and field observation. The resulting topology (Fig. 32) is discussed in detail by Thompson (1976a) and demonstrates that the formation of cordierite at the expense of biotite is a prograde process.

So far MgO has been ignored, but as it is an important component, its effect on the above system has also to be considered. If the number of phases are kept constant, the addition of another component increases the variance of the system by one, which means that the invariant point (I, Fig. 32) becomes a univariant line while the invariant equilibria all become divariant. The relative orientation of the equilibria in P-T space is,

however, not affected.

In some of the pelitic gneiss specimens the minerals biotite and sillimanite (quartz is present in excess) occur in apparent textural equilibrium in contact with each other suggesting that the prograde reactions (4) and (6) have not been crossed. With reference to Fig. 30 and Fig. 32 the stable coexistence of biotite + sillimanite + quartz may be interpreted as either reflecting a lower thermal regime or higher $P_{H_2O}$ compared to those garnet-cordierite assemblages in which biotite + sillimanite do not coexist.

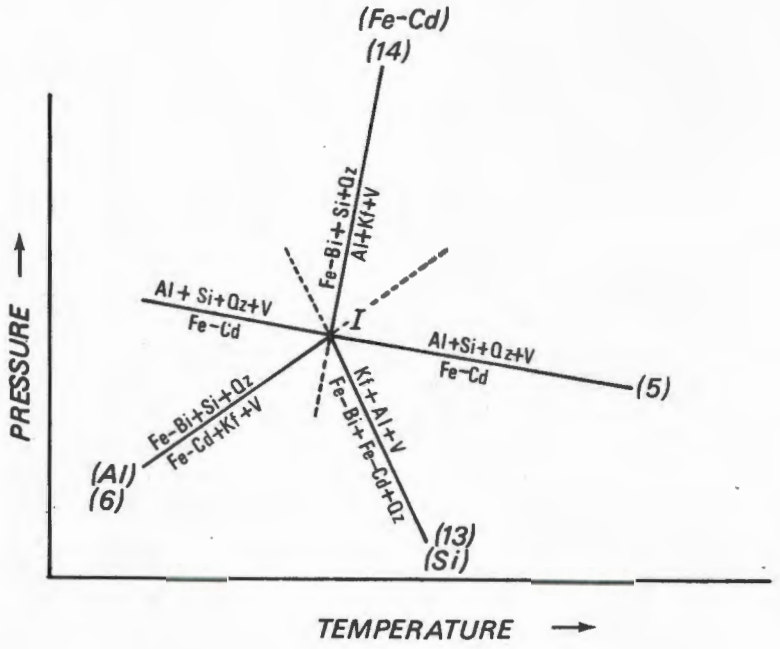


Fig. 32 Invariant equilibria involving the phases Fe-biotite (Fe-Bi), Fe-cordierite (Fe-Cd), almandine (Al), sillimanite (Si), quartz (Qz) and $H_2O$ (V) in the system $SiO_2$ - $K_2O$ - $Al_2O_3$ - FeO - MgO - $H_2O$.

I represents the invariant point and the univariant reactions are placed around I by the method of Schreinemakers (Zen, 1966). The topology is consistent with experimental studies on the above system.

(b) Corona Textures

Corona textures are particularly common in pelitic gneiss specimens and their significance warrants some discussion. A corona is defined as a rim consisting of one or more minerals partially or completely enclosing another mineral (Shand, 1945; Mason, 1967; Spry, 1969). Textural descriptions of coronas, often accompanied by microprobe analyses of corona minerals have been published for a variety of rock types (Shand, *op.cit.*; Brink, 1950; Mason, *op.cit.*; Moore, 1969; Spry, *op.cit.*; Griffin and Heier, 1969, 1971; Griffin, 1971a, b, 1972; Griffin and Raheim, 1973; Whitney and McLelland, 1973; Kwak, 1974). The majority of these publications are concerned with corona textures in basic rocks, but these textures have also been studied in high grade pelitic gneisses (e.g. Moore, *op.cit.*; Kwak, *op.cit.*).

Possible geneses of corona formation are summarised by Spry (*op.cit.*, p. 105). The term "corona" is generally applied in a genetic way in the sense of "reaction rim", implying an origin by reaction between two or more adjoining primary minerals. In this sense coronas are the manifestation of discontinuous reactions giving rise to a new mineral or minerals along the interface of the reactants at the expense of the latter and provide the only direct glimpse at the natural chemical transfer involved. According to Spry (*op.cit.*, p. 107) coronas indicate textural disequilibrium and they can result from prograde as well as retrograde reactions triggered off by changes in environmental conditions.

(i) Hypersthene - Anthophyllite relationships

The coexistence of hypersthene and anthophyllite has been recorded in one specimen (HA 1120) collected on the farm Gal Puts (Fig. 31, I3, page 100. It also contains cordierite, biotite, quartz, plagioclase and opaque minerals.

The thin section of this specimen (Fig. 33) displays the textural relationships between hypersthene, anthophyllite, cordierite and quartz. A hypersthene porphyroblast poikiloblastically encloses cordierite and quartz and is in turn surrounded by a rim of anthophyllite. Note that anthophyllite is generally lacking along the contact between cordierite and hypersthene, suggesting that cordierite is not involved in the anthophyllite-producing reaction, while anthophyllite is invariably developed along the contacts between quartz and hypersthene. The manner in which the anthophyllite rims the pyroxene indicates that it is forming at the expense of hypersthene and the textural relationships between the minerals support a reaction of the type:

$$\text{hypersthene} + \text{quartz} + H_2O \rightarrow \text{anthophyllite} \quad (15)$$

From the experimental studies on this reaction (Greenwood, 1963), it is known that anthophyllite occurs on the low temperature side and that the reaction has a very steep $\frac{dP}{dT}$ slope as schematically shown in Fig. 34. Therefore,

temperature and water pressure are the dominant factors controlling the equilibrium and consequently the observed texture must have developed in response to falling temperature and/or increasing $X_{H_2O}$ of the gas phase.

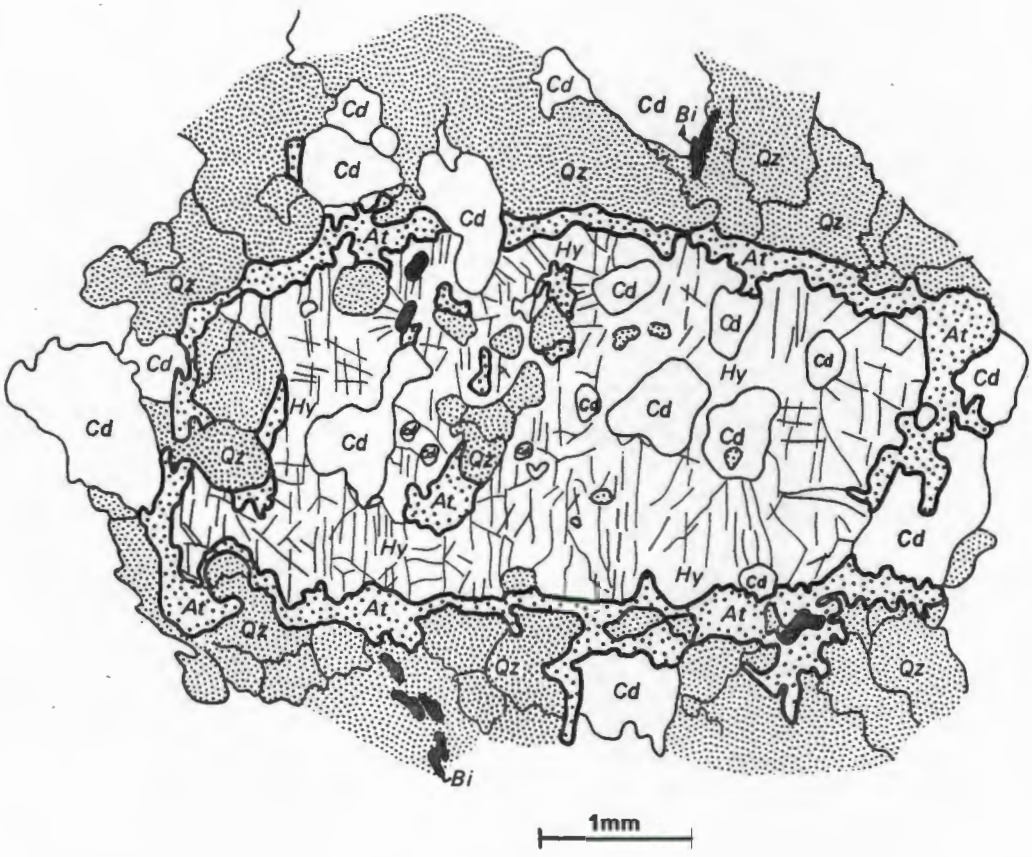


Fig. 33 Textural relationship between hypersthene and anthophyllite recorded in specimen HA 1120. A hypersthene porphyroblast (Hy) poikiloblastically enclosing cordierite (Cd - blank) and quartz (dotted) is rimmed by a corona of anthophyllite (At - dotted). Note that anthophyllite is developed along the contact between quartz and hypersthene, while the interface between cordierite and hypersthene is generally characterised by the absence of anthophyllite, suggesting that cordierite was not involved in the anthophyllite-producing reaction.

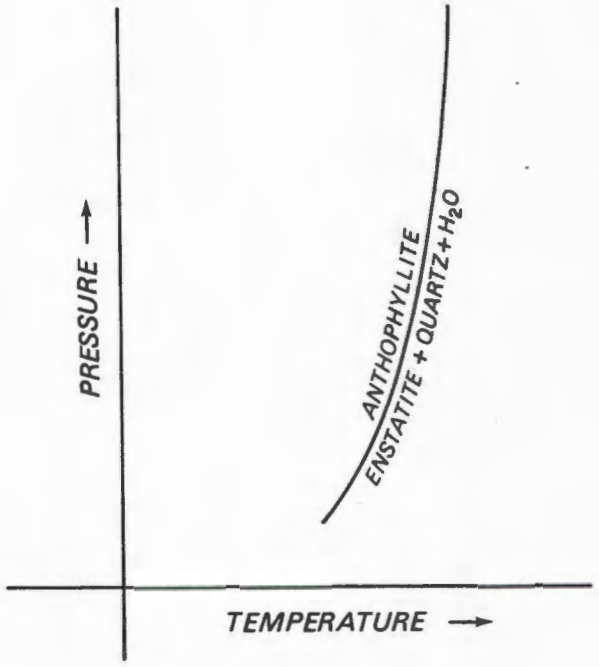


Fig. 34 Schematic P-T plot for the equilibrium anthophyllite → enstatite + quartz + water (after Greenwood, 1963).

Vernon (1972) describes very similar textures of anthophyllite partly replacing hypersthene which he ascribes to the reaction:

hypersthene + water → anthophyllite (16)

Anthophyllite, being an amphibole, requires water (Deer *et al.*, 1971) and derivation from an anhydrous orthopyroxene implies that water must have been introduced into the system. The corona texture shown in Fig. 33 therefore demonstrates that hydration must have occurred subsequent to granulite facies metamorphism.

(ii) Cordierite, Sillimanite and Garnet Coronas

It has already been stated that at very high grades of low pressure regional metamorphism the minerals hercynite and quartz can occur in contact as stable phases and they are formed by reactions involving the breakdown of almandine and cordierite. This is apparent from experimental studies by Richardson (1968), Hensen and Green (1971, 1972, 1973) and Holdaway and Lee (1977).

In the pelitic gneiss specimens studied spinel and quartz do not occur in contact but are generally separated from each other by corona-forming minerals. The most common corona mineral is cordierite and some of the textures encountered are illustrated in Fig. 35. Sillimanite and garnet coronas are also recorded (Fig. 36).

The implication of these corona textures may be interpreted with reference to a simplified experimental system involving the components $Fe - O - Al_2O_3 - SiO_2 - H_2O$. Univariant reactions within this chemical system applicable to high temperature-low pressure metamorphism are illustrated schematically in Fig. 37 and are consistent with experiments (Richardson, *op.cit.*).

The corona textures provide evidence that the following reactions must have occurred:

hercynite + quartz → garnet + sillimanite (18)
hercynite + sillimanite + quartz → cordierite (11)
hercynite + quartz → garnet + cordierite (19)

From an inspection of Fig. 37 it is apparent that in order for these reactions to have proceeded in the way indicated above the temperatures must have decreased from a thermal peak at which spinel and quartz were presumably stable in contact with each other. It is proposed that the coronas were formed in response to cooling of the terrane.

## 4 Colour Changes in Biotite

It is a well established observation that the colour of biotite varies with metamorphic grade (Hyndman, 1972). In low grade metamorphic terranes this mineral has a green colour and in high grade environments the biotite colour is generally deep red (*ibid.*). From the studies by Binns (1969) on biotites in pelitic gneisses it is apparent that the colour changes are related to changes in chemical composition. Binns (*op.cit.*) records a gradual increase in titanium and $Mg/(Mg + Fe^{+2})$ ratio of biotite with increasing metamorphic grade. In pelitic gneisses biotite is the dominant site for titanium. With rising temperature the abundance of biotite decreases as this mineral becomes increasingly involved in various dehydration reactions. The combination of these two factors leads to the observed increase in titanium concentration in the remaining biotite.

In this study the Z-absorption colour of biotite was examined in 91 specimens including a wide range of rock types such as charnockite (31 specimens), metabasites (28 specimens), pelitic and semipelitic gneisses (23 specimens) and quartzo-feldspathic gneisses (9 specimens) in order to establish whether any systematic colour changes can be detected. To allow

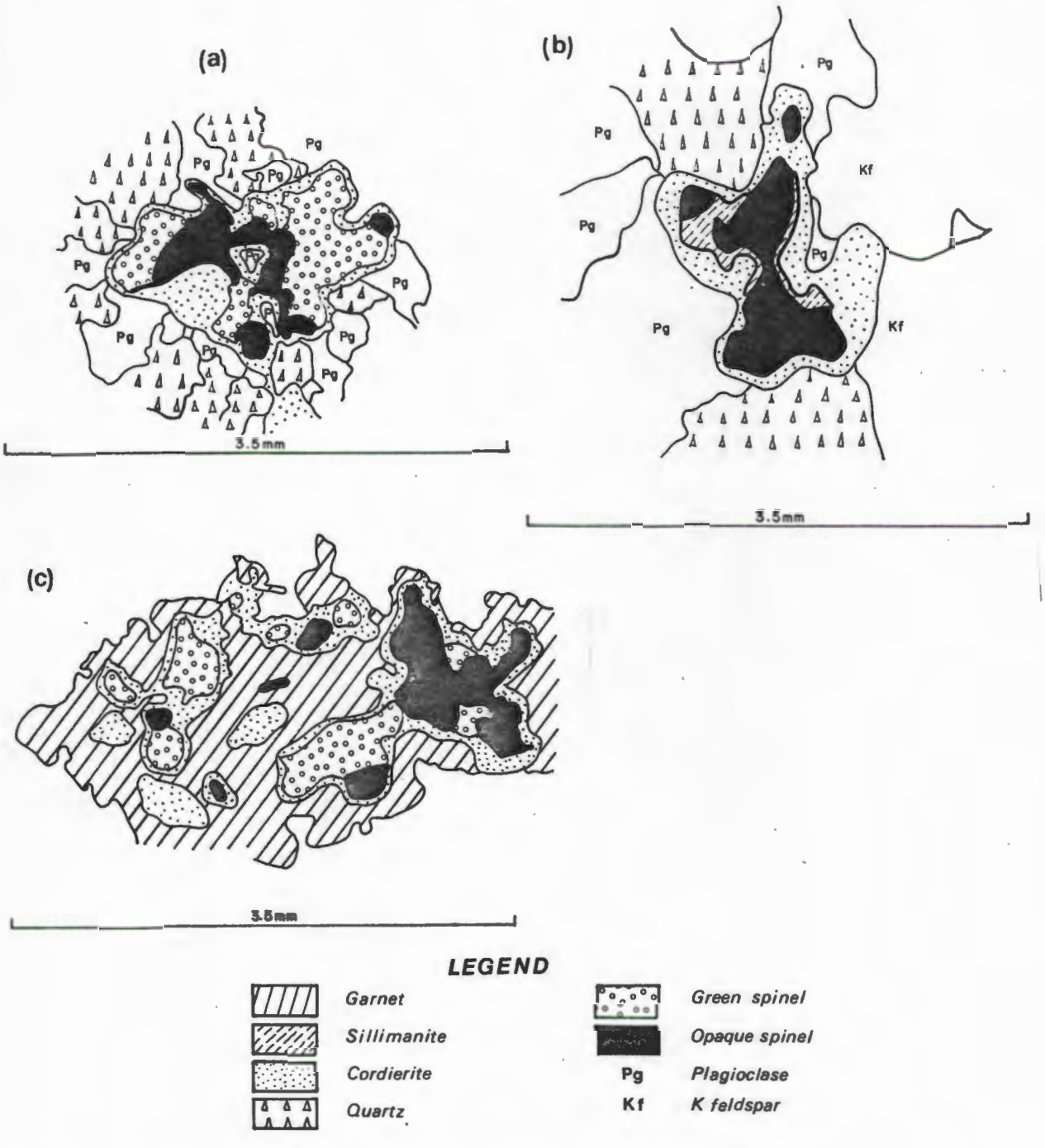


Fig. 35 Cordierite coronas in pelitic gneiss specimens

(a) Corona of cordierite developed along the contact between opaque and green spinel and silicates (quartz and plagioclase).
(b) Cordierite corona surrounding opaque spinel and sillimanite.
(c) Corona of cordierite between garnet and spinel.

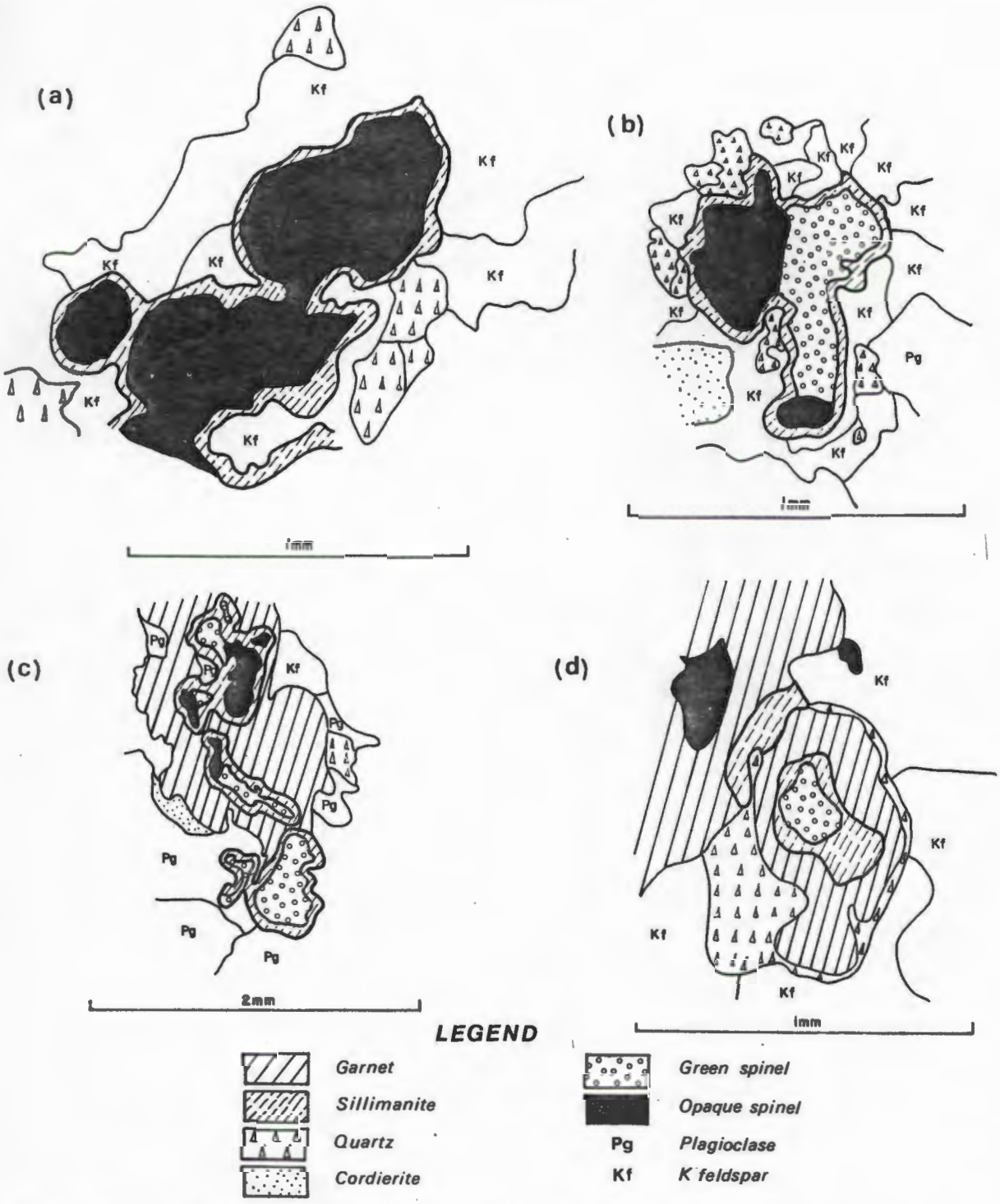


Fig. 36 Sillimanite coronas in pelitic gneiss specimens

(a) + (b) Sillimanite corona around spinel in a feldspar-quartz matrix.
(c) + (d) Sillimanite corona around spinel and enclosed by garnet.

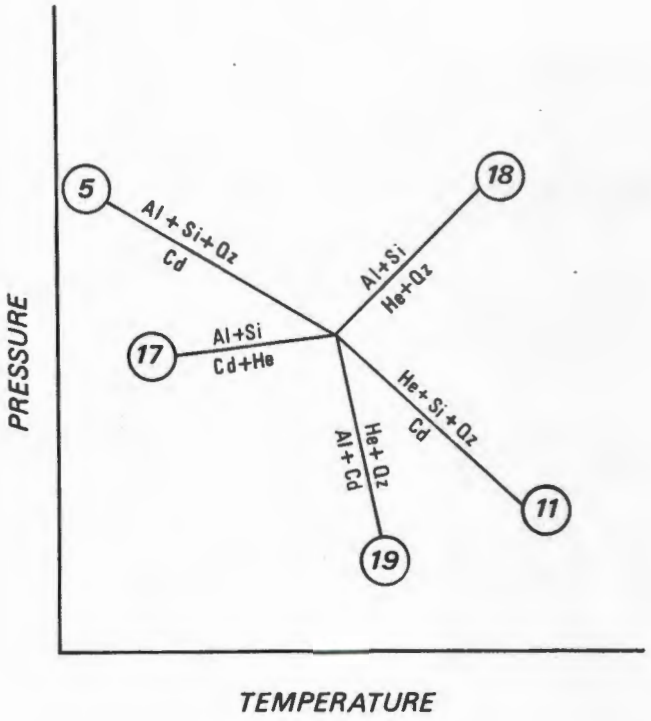


Fig. 37 Schematic pressure-temperature diagram showing univariant reactions involving almandine, cordierite, sillimanite and quartz in the system Fe - O - $Al_2O_3$ - $SiO_2$ - $H_2O$ and applicable to high temperature-low pressure metamorphic conditions. Abbreviations as in preface. The diagram is based on experimental studies by Richardson (1968).

sufficient aerial coverage it was necessary to include all these rock types in this study and it is realised that the bulk composition of the host rock will obviously have an influence on the biotite chemistry and therefore on its colour.

On the basis of their Z-absorption colour the biotites studied can be grouped into two varieties namely red to red-brown and brown which are here referred to as "red" and "brown" respectively. Some of the biotite grains are partially chloritised, but primary green biotites typical of low grade metamorphic terranes are not recorded.

Fig. 38 shows the regional distribution of the biotite colours in relation to the granulite-amphibolite facies transition. Within the granulite facies terrane the biotite colour is, with a few exceptions, of the red variety while biotites in the amphibolite facies terrane tend to be predominantly brown. This change in colour across the area is consistent with the changes recorded by the metamorphic index minerals and this suggests that the biotite

colour is largely related to metamorphic grade in the area studied.

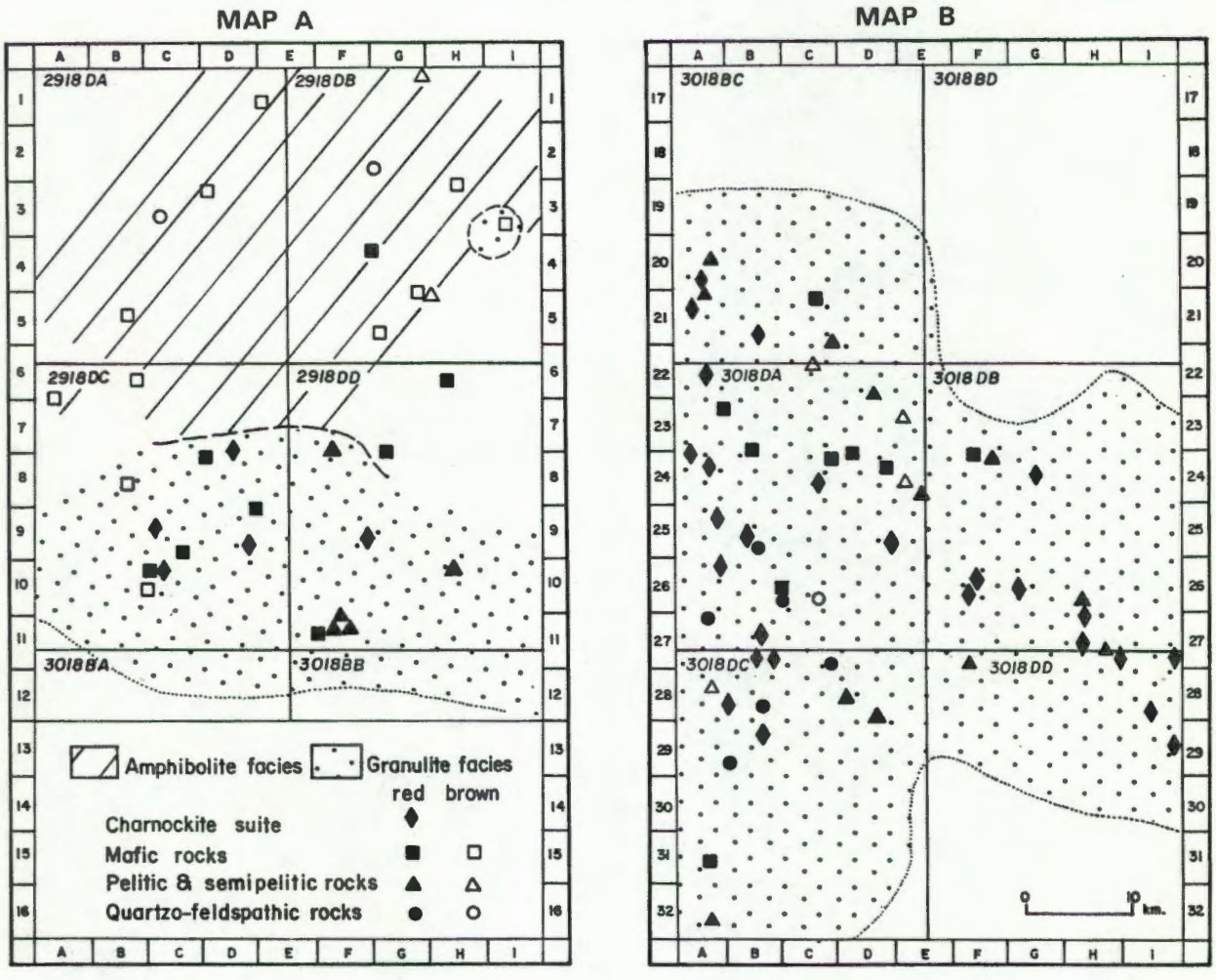


Fig. 38 Geographic distribution of the Z-absorption colour of biotite in charnockites, metabasites, pelitic and semipelitic gneisses and quartzo-feldspathic gneisses.

## 5 Chemical Compositions of Minerals in Pelitic Gneisses

Before proceeding with a quantitative evaluation of the P-T conditions likely to have prevailed during regional metamorphism (Chapter IV) the chemical compositions of the minerals should be examined.

### (a) Garnet

Garnets coexisting with cordierite (with or without sillimanite and/or biotite) were analysed in 14 pelitic gneiss specimens (Appendix II, Table A2-8). In Table 13 their compositions are expressed in terms of the end member molecules and Fig. 39 is a graphic display of the garnet chemistry.

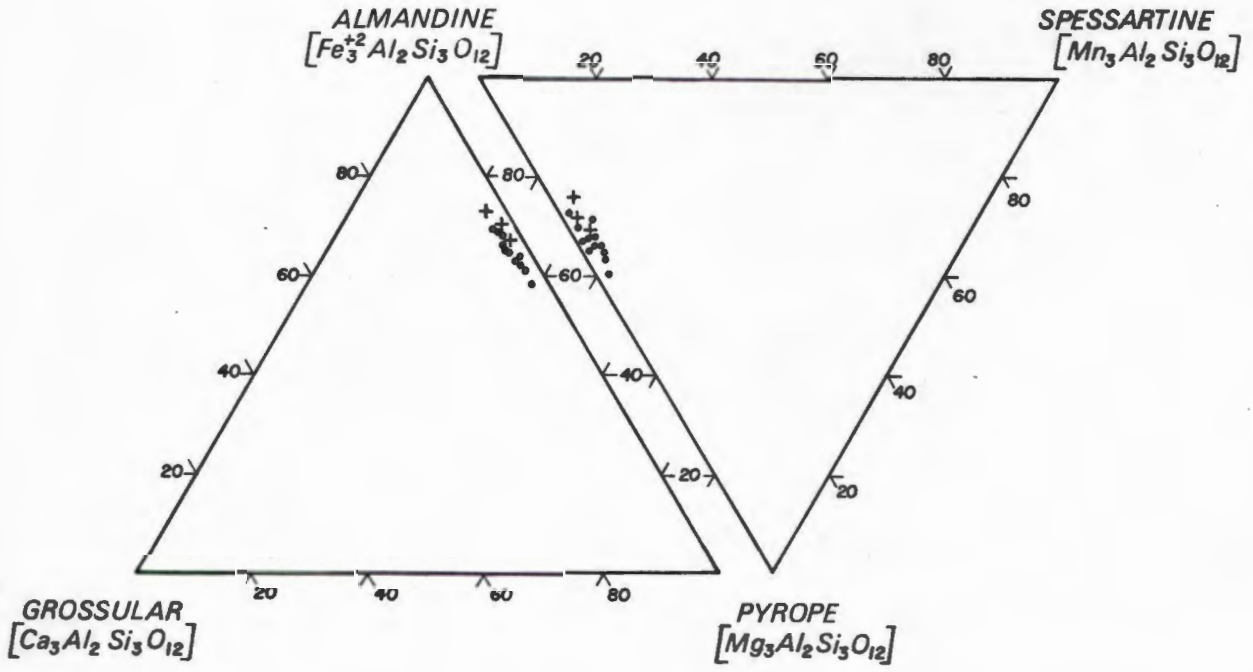


Fig. 39 Chemical compositions of garnet in 14 specimens of aluminous gneiss from the granulite facies terrane plotted in terms of the end member molecules almandine, pyrope, grossular and spessartine. Solid dots represent core compositions and crosses symbolise rim compositions of the grains. Note that the garnets are essentially almandine-pyrope solid solutions with very small amounts of the grossular and spessartine molecules.

Table 13 Garnet compositions in pelitic gneisses. All specimens are from the granulite facies terrane. C and R represent core and rim compositions and the figures in brackets indicate the number of analyses per specimen.

| Specimen No. | Almandine | Pyrope | Grossular | Spessartine |
|---|---|---|---|---|
| HA 1026 - C (5) | 64,32 | 30,73 | 3,68 | 1,26 |
| HA 1036 - C (6) | 63,04 | 29,19 | 4,17 | 3,60 |
| HA 681 - C (5) | 60,27 | 32,97 | 3,17 | 3,59 |
| HA 870 - C (6) | 67,72 | 27,60 | 2,80 | 1,88 |
| HA 708 - C (3) | 65,03 | 29,42 | 3,12 | 2,42 |
| HA 632 - C (6) | 56,86 | 38,43 | 2,82 | 1,89 |
| HA 841 - C (4) | 66,65 | 28,75 | 2,85 | 1,75 |
| HA 841 - C (1) | 68,28 | 27,09 | 2,98 | 1,65 |
| HA 143 - C (6) | 62,75 | 33,28 | 2,56 | 1,40 |
| HA 143 - C (1) | 64,80 | 31,04 | 2,56 | 1,60 |
| HA 982B - C (4) | 61,18 | 32,29 | 3,05 | 3,48 |
| HA 982B - C (2) | 65,33 | 27,55 | 3,04 | 4,08 |
| HA 869B - C (1) | 68,33 | 27,18 | 2,83 | 1,65 |
| HA 869B - C (4) | 66,71 | 28,80 | 2,86 | 1,63 |
| HA 505 - C (3) | 64,77 | 28,24 | 2,82 | 4,17 |
| HA 505 - C (4) | 58,97 | 35,26 | 2,63 | 3,14 |
| HA 505 - R (1) | 59,50 | 34,79 | 2,58 | 3,12 |
| HA 514 - C (7) | 64,15 | 30,74 | 3,06 | 2,05 |
| HA 514 - R (2) | 68,08 | 26,91 | 2,30 | 2,01 |
| HA 329 - C (6) | 62,51 | 32,84 | 2,21 | 2,45 |
| HA 329 - R (1) | 64,96 | 29,94 | 2,26 | 2,82 |
| HA 164 - C (5) | 64,55 | 29,14 | 3,20 | 3,11 |
| HA 164 - R (4) | 70,23 | 22,52 | 3,44 | 3,81 |

From Table 13 and Fig. 39 it is apparent that the garnets are essentially almandine-pyrope solid solutions with an almandine/pyrope ratio of approximately 2:1. The contribution of the grossular and spessartine molecules towards the bulk composition of the garnets is small (the grossular molecule accounts for 2-4 per cent and the spessartine molecule for 1-4 per cent of the bulk composition). Such almandine-rich garnets are characteristic for granulite facies terranes (Mehnert, 1972; Winkler, 1976).

The majority of the garnet grains were analysed in their centres and these grain core compositions fall into the following range:

$\text{Almandine}_{56,9 - 68,3}$ $\text{Pyrope}_{27,1 - 38,4}$ $\text{Grossular}_{2,2 - 4,2}$

$\text{Spessartine}_{1,3 - 4,2}$

The subscripts indicate the contribution of each end member molecule (in per cent) towards the bulk composition of the mineral. In every specimen 3 to 7 grains were analysed in their centres and where these core compositions were found to be fairly homogeneous a mean composition was computed. In some specimens, however, the core compositions of the garnet grains are not sufficiently uniform and a single mean composition computed from all the analyses would not be representative of the garnet population. Frequency histograms of the five specimens in which the garnets have non-uniform core compositions are shown in Fig. 40. For these specimens two mean compositions are recorded in Table 13 and also in Appendix II, Table A2-8 in order to demonstrate the bimodal nature of the garnet core compositions.

This non-uniformity of the core compositions requires some explanation. If all the garnets in a particular specimen belong to the same generation and they have crystallised under conditions of equilibrium, their compositions are expected to be uniform, at least in the central parts of the grains which are more shielded from retrograde effects. The fact that the core compositions in some specimens are non-uniform suggests either disequilibrium or alternatively that not all of the garnets belong to the same generation. Texturally the garnets have variable expressions. Some are elongated and contain numerous small sillimanite inclusions which frequently appear to outline minor folds within the garnet, while others are more rounded and generally lack inclusions. A comparison of the textural appearance with the chemical composition of the garnets failed to show any convincing correlation. Another factor to be considered is the influence of inclusions on the composition of the garnet, for example biotite or magnetite/spinel are frequently recorded within the garnets. During the cooling stage these inclusions re-equilibrate with the garnet and change its composition in the immediate vicinity of the inclusion. Although analyses proximal to these inclusions have been avoided in the two-dimensional sections, it is not known if such inclusions were not present along the dimension at right angles to the sections studied.

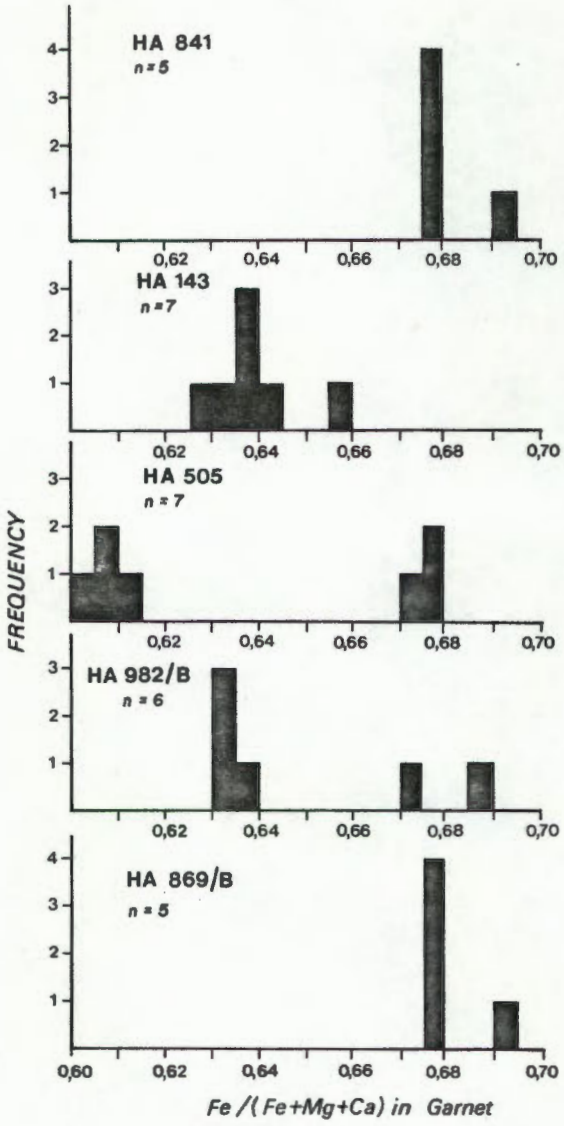


Fig. 40 Frequency histograms showing the variation in chemical composition of garnet (grain centres) in five pelitic gneiss specimens. The number of analyses per specimen is indicated by n.

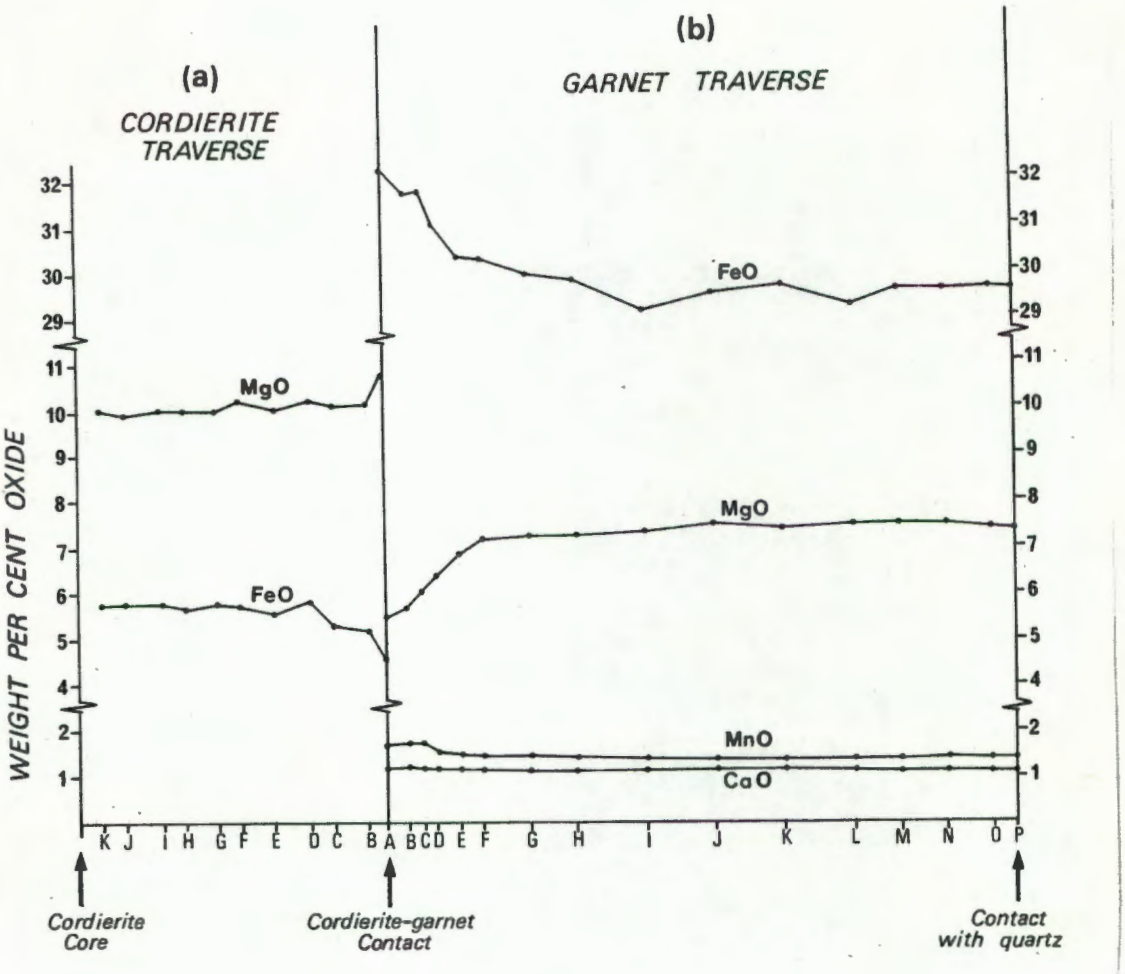


Fig. 41 Chemical zonation pattern of garnet and cordierite in specimen HA 164. A, B, C, D etc. represent spot analyses along a traverse across the grains (the analyses are tabulated in Appendix II, Tables A2-11 and A2-12). Both grains are in mutual contact with each other.

(a) Traverse across a cordierite grain. Analysis A represents the rim composition at the contact with garnet and analysis K has been recorded in the centre of the grain. Note that the MgO concentration in cordierite increases while the FeO concentration decreases simultaneously as the contact with garnet is approached.

(b) Garnet zonation along a traverse across the grain from the cordierite contact (analysis A) to the contact with a quartz grain on the opposite side of the traverse (analysis P). Note the marked increase in the FeO concentration and simultaneous decrease in MgO concentration in the garnet grain as the cordierite contact is approached. The MnO concentration in garnet also increases slightly towards the cordierite contact.

The garnet grains are compositionally zoned and an example of a typical zonation pattern is displayed in Fig.41 (b). The 16 spot analyses (labelled A - P in Fig. 41 (b) and tabulated in AppendixII, Table A2-11) along a traverse across a garnet grain in specimen HA 164, outline the changes in chemical composition. Note that the garnet grain in Fig.41 (b) is in contact with cordierite and quartz, respectively, at both ends of the traverse. It is evident from an inspection of Fig.41 (b) that the FeO concentration in garnet increases and simultaneously the MgO concentration decreases in close proximity to the contact with cordierite. In contrast the garnet composition does not seem to change at the contact with quartz. The CaO and MnO concentrations of the garnet are fairly uniform along the traverse across the grain and MnO increases only slightly at the contact with cordierite). The difference in chemical composition (Mg/(Mg + Fe) ratio) between grain core and rim can vary quite considerably as is evident from Fig. 42. However, in all the specimens the Mg/(Mg + Fe) ratio of the grain cores exceeds the Mg/(Mg + Fe) ratio recorded in the rims of the grains. The observed zonation patterns of the garnets have important implications on the application of thermometry/barometry which will be discussed after a consideration of the zonation pattern recorded in cordierite.

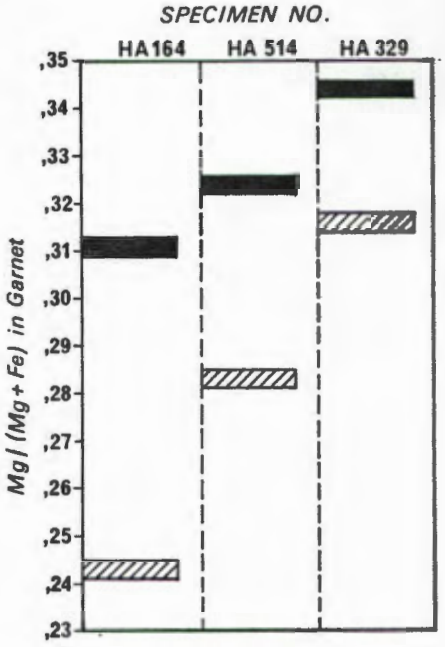


Fig. 42 Compositional difference [Mg/(Mg + Fe)] between garnet grain centres (solid bars) and grain rims (hatched bars) in three pelitic gneiss specimens. Note that the core compositions of garnet porphyroblasts always have a higher Mg/(Mg + Fe) ratio compared to the rims of the grains.

(b) Cordierite

Cordierite grains were analysed in the same 14 specimens that were selected for garnet analyses. Three to six grain centres were analysed per specimen. Only larger porphyroblasts were selected and the core compositions of these were found to be fairly uniform. Mean core compositions were then computed for each specimen using all core analyses and only these mean compositions are recorded in Appendix II, Table A2-9. The cordierite grains coexisting with garent have a fairly restricted Mg/(Mg + Fe) ratio ranging between 0,68 and 0,77 with a mean Mg/(Mg + Fe) ratio of 0,73 ± 0,03 (for grain cores) (Fig. 43). Cordierite like garnet is compositionally zoned and

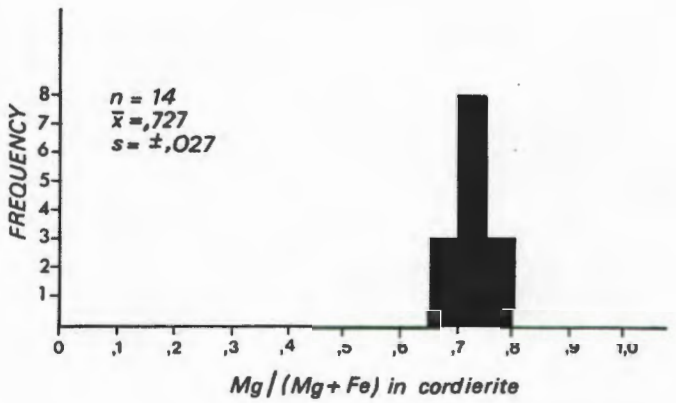


Fig. 43 Frequency histogram showing the Mg/(Mg + Fe) compositional ratio of cordierite (grain centres) in fourteen pelitic gneiss specimens from the granulite facies terrane.

the typical zonation pattern displayed by cordierites in contact with garnet is shown in Fig. 41 (a). Eleven spot analyses (labelled A to K in Fig. 41 (a) and tabulated in Appendix II, Table A2-12) are recorded along a traverse across a cordierite grain in specimen HA 164 from the centre of the grain towards the contact with the garnet described previously. It is evident from Fig. 41 (a) that as the garnet contact is approached along the traverse, the concentration of MgO in cordierite increases, while the FeO concentration decreases simultaneously. This zonation is thus exactly opposite to the one recorded in the

adjacent garnet. The compositional difference [Mg/(Mg + Fe)]ratio between cordierite core and rim can vary quite considerably as is apparent from Fig. 44, but the rims always have the higher Mg/(Mg + Fe) ratio when compared to the grain centres. Small cordierite inclusions have Mg/(Mg + Fe) ratios (in the centres of the inclusions) that are intermediate between the core and rim compositions of the porphyroblasts (Fig.44, specimen HA 708).

It has already been mentioned that the recognition of compositional zonation has important implications for quantitative thermometry and barometry and this is now further substantiated. In the thermodynamic approach of P-T evaluation (Chapter IV) the chemical compositions of coexisting minerals expressed in terms of the distribution coefficient ($K_D$) are shown to bear a definite relationship to temperature and/or pressure prevailing during metamorphism. For the Mg - Fe exchange reaction between garnet (Ga) and

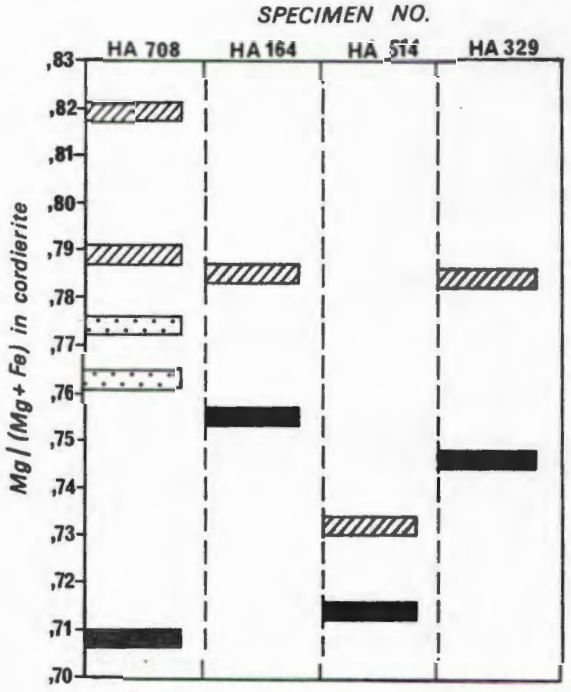


Fig. 44 Comparison of cordierite grain core compositions (solid bars) with rim compositions (hatched bars) in four pelitic gneiss specimens. Note that the core compositions of the cordierite grains always yield a lower Mg/(Mg + Fe) ratio compared to the rims. Small cordierite inclusions within garnet porphyroblasts yield intermediate Mg/(Mg + Fe) ratios (stippled bars - specimen HA 708).

cordierite (Cd) the relationship between $K_D$ ($K_D = \frac{X_{Fe}^{Cd} \cdot X_{Mg}^{Ga}}{X_{Mg}^{Cd} \cdot X_{Fe}^{Ga}}$ where

x = mole fraction) and equilibration temperature has recently been established (Thompson, 1976b, Holdaway and Lee, 1977) and is shown graphically in Fig. 45 With reference to the recorded chemical zonation pattern in garnet and cordierite (Fig. 41) it is apparent that $K_D$ as defined above decreases progressively in numerical value from the core towards the rim compositions of these grains. According to Fig. 45 a decrease in the value of $K_D$ is expected with declining temperature and for this reason we may interpret the observed zonation pattern in garnet and cordierite (Fig. 41) to be the manifestation of retrograde ion exchange subsequent to the thermal peak of the metamorphism and related to falling temperature. As the temperature decreases after the metamorphic peak the two minerals will continue to exchange ions in an attempt to re-equilibrate under the declining thermal regime. This exchange of ions, at least in larger grains, appears to be restricted to the outer rims of the grains presumably because diffusion processes proceed at a slower rate under lower temperature conditions. The important conclusion that can be drawn from the observed zonation pattern in garnet and cordierite in the light of the experimentally determined relationship between ln $K_D$ and the equilibrium temperature is that the core compositions of these minerals should be used in quantitative thermometry/barometry as they are less likely to have been altered by subsequent retrograde ion exchange. Note that the computed temperature difference obtained from $K_D$ of rim compositions compared to $K_D$ based on core compositions within the same specimen can be as much as 130°C.

(c) Plagioclase

Plagioclase compositions in 12 pelitic gneisses were determined with the aid of the electron microprobe analyser. Three to six grains were analysed (in their cores) per specimen and mean compositions were then computed (Appendix II, Table A2-13). The plagioclase compositions of the specimens studied are found to vary between oligoclase ($An_{23}$) and labradorite ($An_{69}$), but the majority (60 per cent) fall into the range $An_{30}$ to $An_{40}$ (Fig. 46).

All plagioclase grains are generally zoned, but the degree of zonation varies quite considerably. In Fig.47 the three extreme types of zonation recorded in the specimens studied are shown. Note that all grains represented in Fig. 47 are in contact with garnet. The plagioclase grains in specimen HA 841 (Fig. 47a) display a very gentle zonation with only small compositional differences between rims and core (the difference between rim and core amounts to at most 2 per cent An). Normal zonation characterised by a decrease in anorthite content from core to rim is encountered in specimen HA 1036 (Fig.47b ). In some grains the compositional difference between rim and core can amount to as much as 17 per cent of the anorthite molecule (grain 5, Fig. 47b). In specimen HA 1026 (Fig.47c) the plagioclase grains have high An-contents at the rim, decreasing rapidly and then increasing again towards the

grain cores. All those zonations are continuous and there is no optical evidence for an aburpt change in the zonation pattern.

(d) Alkali Feldspar

The alkali feldspars in the pelitic gneiss specimens studied are invariably perthitic. Seven grains in seven specimens were analysed by the method outlined in Appendix IC. The microprobe analyses are tabulated in Appendix II, Table A2-17. The concentration of the albite molecule in the feldspars analysed is found to vary quite considerably between 12 and 27 per cent (Fig. 48).

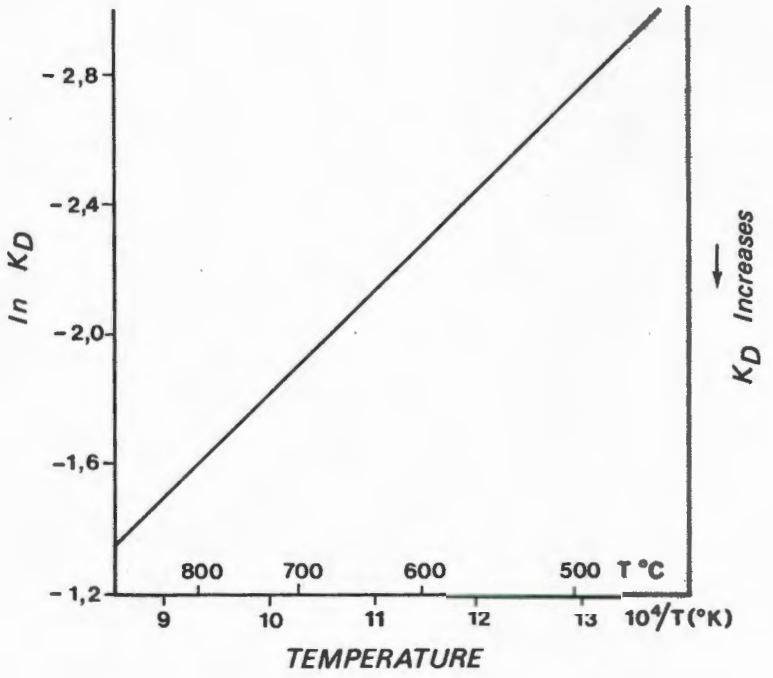


Fig. 45 Schematic relationship between $K_D$ ($K_D = \frac{X_{Fe}^{Cd} \cdot X_{Mg}^{Ga}}{X_{Mg}^{Cd} \cdot X_{Fe}^{Ga}}$) and temperature for the Mg - Fe exchange reaction

$\frac{1}{2}$ Mg - cordierite + $^1/_3$ almandine $\rightleftharpoons$ $\frac{1}{2}$ Fe - cordierite + $^1/_3$ pyrope

(based on Thompson (1976b) and Holdaway and Lee (1977)).

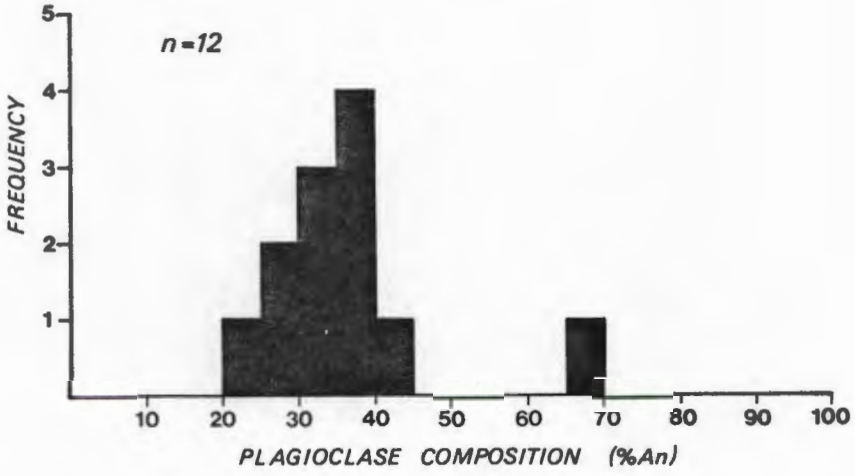


Fig 46 Frequency histogram showing plagioclase compositions (core compositions) in 12 pelitic gneiss specimens from the granulite facies terrane.

(e) Spinel

Dark green spinels in the pelitic gneisses collected in the granulite facies terrane consist predominantly of aluminium, iron and magnesium. In the terminology used by Deer *et al.* (1971) these spinels are solid solutions of the two end members, spinel *sensu stricto* (Mg $Al_2O_4$) and hercynite (Fe $Al_2O_4$) with the hercynite component dominating (Fig.49 ). Eight grains were analysed in four specimens (microprobe analyses are tabulated in Appendix II, Table A2-18) and the Fe/(Fe + Mg) ratio in these minerals is found to vary between 0,57 and 0,81. Within a particular specimen the Fe/(Fe + Mg) ratio can vary considerably. The oxide totals of the mineral analyses (excepting for two analyses) are close to 100 per cent, suggesting that the zinc-rich component (gahnite) does not contribute any significant portion towards the mineral composition. (The low totals obtained for spinels in specimens HA 1036 and HA 841 in Appendix II, Table A2-18 are considered to result from analytical error, as considerable current drift was noted at the time of probing).

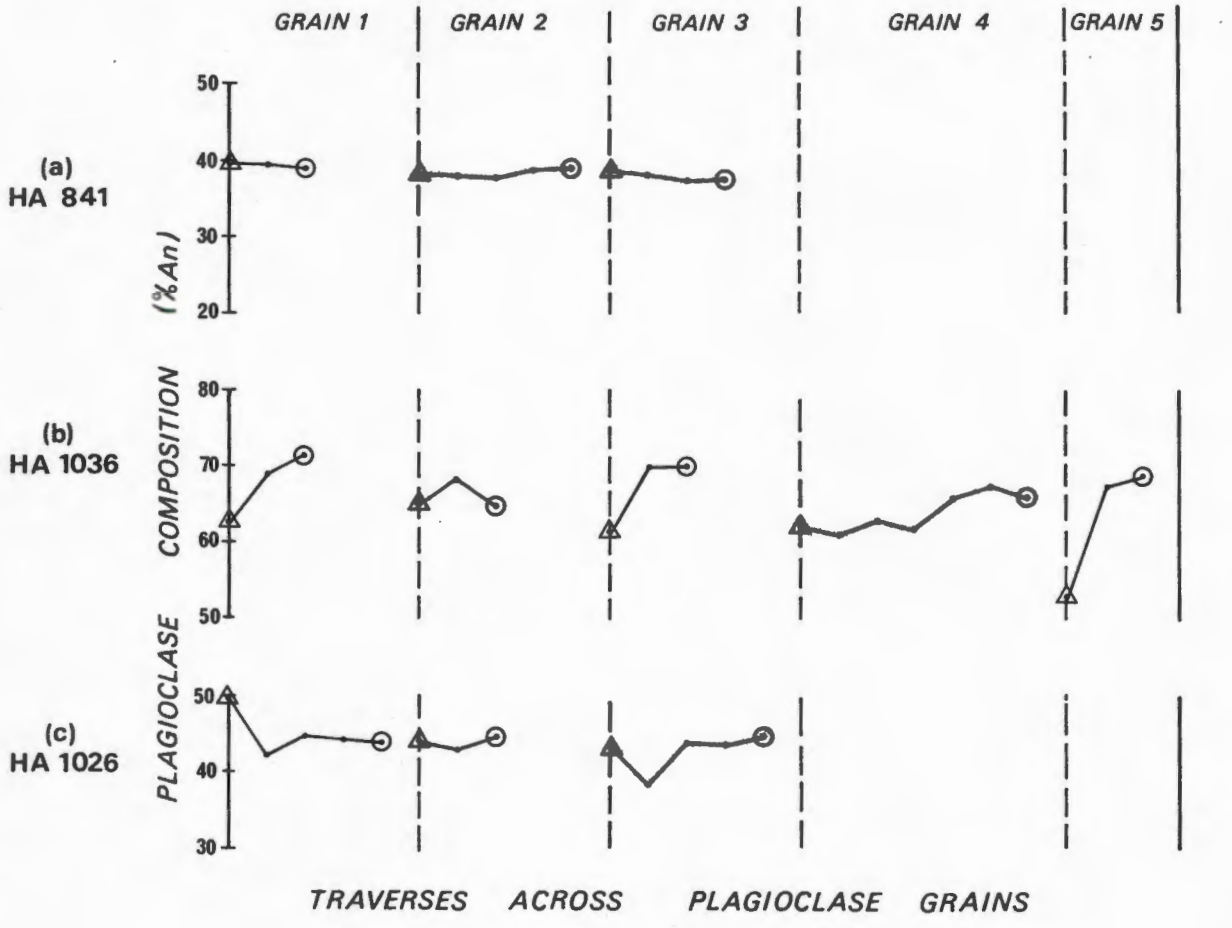


Fig. 47 Chemical zonation of plagioclase grains in three pelitic gneiss specimens along traverses from rim (open triangles) to core (open circles). Mircoprobe spot analyses are tabulated in Appendix II, Tables A2-14, A2-15 and A2-16.

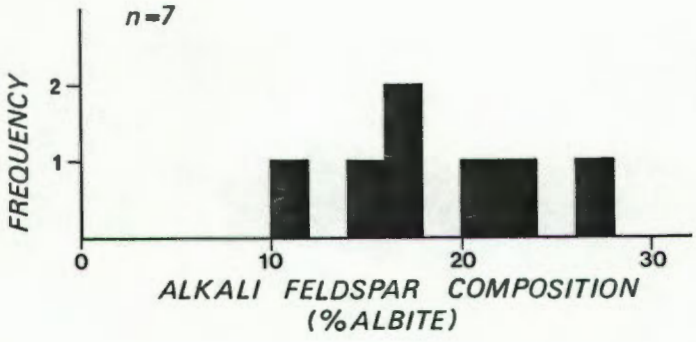


Fig. 48 Frequency histogram showing the compositional range of alkali feldspars in pelitic gneisses from the granulite facies terrane.

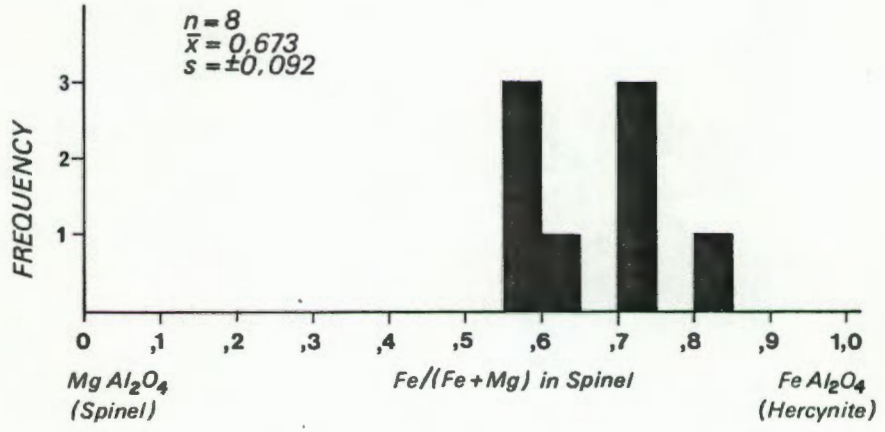


Fig. 49 Frequency histogram showing the compositional range of green spinels in four pelitic gneiss specimens from the granulite facies terrane.

## 6 Physical Conditions Accompanying Regional Metamorphism in the Light of Experimental Petrology

Sillimanite is the only $Al_2SiO_5$ polymorph recorded in rocks of pelitic composition in the study area. The stability fields of the three $Al_2SiO_5$ polymorphs (kyanite, sillimanite, andalusite) have been established experimentally by numerous petrologists (Althaus, 1969) and the determinations of the position of the triple point of the three phase region in pressure - temperature space vary considerably. In the words of Winkler (1976, page 91) " .... the results on the $Al_2SiO_5$ (polymorphs) are almost as variable as the number of laboratories working on the problem". Explanations for the experimental discrepancies are given by Richardson *et al.* (1969), Winkler (*op.cit.*) and Vernon (1976). According to Vernon (*op.cit.*) these polymorphic transformations involve large activation energies as strong Al-O and Si-O bonds have to be broken. The problem of metastability is discussed by Gilbert *et al.* (1969). The experimental results of Richardson *et al.* (1968, 1969) are widely quoted in the literature and their interpretation of the stability fields of the $Al_2SiO_5$ polymorphs is shown in Fig. 50 (curve 20). Fortunately, in the study area the temperatures during metamorphism, as based on other evidence, far exceeded the uncertainty in the position of the $Al_2SiO_5$ triple point. It is significant that both kyanite and andalusite are absent from all parageneses suggesting a high temperature environment of low to intermediate pressure.

Primary muscovite is not encountered in rocks of semipelitic or pelitic composition in the study area, suggesting that this mineral was not stable under the conditions prevailing during regional metamorphism. Winkler (1976) has chosen muscovite breakdown in quartz and plagioclase-bearing assemblages to mark the boundary between medium grade and high grade metamorphism and he points out that muscovite consuming reactions yield mineral parageneses involving K-feldspar and sillimanite. The lack of primary muscovite and the ubiquitous occurrence of K-feldspar and sillimanite in rocks of appropriate chemistry is cited as evidence for conditions of high grade regional metamorphism in the sense of Winkler (*op.cit.*).

With reference to Fig. 51 some of the most significant experimentally investigated reactions involving "muscovite + quartz" stability are briefly outlined. The upper stability limit for coexisting muscovite and quartz in systems with excess $H_2O$ and lacking plagioclase is governed by the reactions:

muscovite + quartz $\rightleftharpoons$ K-feldspar + $Al_2SiO_5$ + $H_2O$ (21) (Althaus *et al.*, 1970)
and muscovite + quartz + $H_2O \rightleftharpoons$ melt + sillimanite (22) (Storre and Karotke, 1972).

When K-feldspar is also available as reactant together with muscovite and quartz, melt can be produced via the reaction:

K-feldspar + quartz + muscovite + $H_2O \rightleftharpoons$ melt (23) (in Winkler, *op.cit.*)

In anhydrous systems lacking plagioclase, the upper stability limit for co-existing muscovite and quartz is controlled by the reaction:

muscovite + quartz $\rightleftharpoons$ melt + K-feldspar + sillimanite (24)(Storre, 1972).

If both plagioclase and quartz are available as reactants, muscovite breaks down at much lower temperatures compared to plagioclase-free reactions (22), (23) and (24) via:

muscovite + quartz + plagioclase + $H_2O \rightleftharpoons$ melt + $Al_2SiO_5$ (Storre and Karotke, 1971)

and muscovite + quartz + plagioclase + K-feldspar + $H_2O \rightleftharpoons$ melt (26) (in Winkler, 1976)

Reaction (26) has the same equilibrium conditions as the minimum melting in the system

albite + K-feldspar + quartz + $H_2O$ (Tuttle and Bowen, 1958; Merrill *et al.*, 1970).

These reactions cause anatexis in the gneisses, and according to Winkler (*op.cit.*) define the beginning of high grade metamorphism if $PH_2O > 3,5$ kb. At lower water pressures reaction (21) marks the beginning of high grade metamorphism. The ubiquitous occurrence of quartzo-feldspathic neosomes in the study area is cited as evidence for anatexis during regional metamorphism, demanding P-T conditions on the high temperature side of reaction (26). The complete absence of *primary* muscovite from all parageneses in the study area requires P-T conditions on the high temperature side of equilibrium (21) and (22) (see Fig. 51).

In summary then, the absence of muscovite indicates conditions of high grade regional metamorphism affecting the entire area. The P-T conditions that were prevailing during metamorphism are expected to fall somewhere into the hatched area shown in Fig. 51. Obviously all equilibria in Fig. 51 involving $H_2O$ are sensitive to the composition of the fluid phase and will be displaced towards lower temperatures with decreasing $X_{H_2O}$ of the fluid.

Experimental studies on the alkali feldspar solvus indicate that at a temperature less than the critical line (curve 27 in Fig. 50) a solid solution of alkali feldspar will unmix to form perthite (Morse, 1970). Thus, the metamorphic temperatures must have exceeded those of the "critical line". Morse (*op.cit.*) points out that an introduction of Ca has a marked effect on the position of this line and that "the addition of anorthite shifts the critical line rapidly towards higher temperatures". Thus, the experimental data on the Ca-free system give minimum temperature estimates, which means that when $P_{H_2O} = P_{total}$, the presence of perthite demands temperatures in excess of 700°C at pressures above 3 kb.

The absence of staurolite in rocks of pelitic composition and the ubiquitously recorded stable association of its breakdown products (garnet + hercynite + sillimanite) indicates temperatures in excess of the reaction

staurolite $\rightleftharpoons$ garnet + hercynite + sillimanite + $H_2O$ (28) (Fig. 50).

The coexistence of orthopyroxene and quartz in some of the pelitic

gneisses suggests that orthoamphibole was unstable in the granulite facies during regional metamorphism. The experimental data of Greenwood (1963) on anthophyllite stability extrapolated to higher pressures indicates that the upper temperature stability limit of anthophyllite under the conditions $P_{H_2O} = P_{total}$ occurs between 780° and 800°C in the pressure range 5-10 Kb. At higher temperatures the orthoamphibole decomposes according to the reaction:

anthophyllite $\rightleftharpoons$ enstatite + quartz + $H_2O$ (15)

The absence of *primary* orthoamphibole and the coexistence of "orthopyroxene + quartz" indicates that the temperatures in the granulite facies during regional metamorphism must have been in excess of curve (15) in Fig. 50. The effect of composition on the stability field of the orthoamphibole is apparent from the experiments of Ravoir and Hinrichsen (1975) who have shown that a decrease in Mg/(Mg + Fe) ratio from 0,8 to 0,6 for synthetic Al-free anthophyllite at 6 Kb water pressure decreases the upper temperature stability of anthophyllite from 775°C to 735°C. These authors have also shown that at the same $P_{H_2O}$ Al-containing natural anthophyllite with an Mg/(Mg + Fe) ratio equal to 0,9 is stable up to 835°C relative to its breakdown products (hypersthene + quartz).

The maximum stability field for coexisting garnet and cordierite in pelitic bulk compositions is outlined experimentally by Hensen and Green (1971, 1972, 1973) and provides an upper temperature limit for the regional metamorphism of the study area (curves 29, Fig. 50).

Pressure constraints are fewer than those for temperature. The ubiquitous occurrence of cordierite in specimens of pelitic gneisses places an upper pressure limit on the regional metamorphism. According to Newton (1972) the decomposition of hydrous cordierite ($P_{H_2O} = P_{total}$) at 830° proceeds at 11,2 Kb by the reaction:

hydrous cordierite $\rightleftharpoons$ enstatite + sillimanite + quartz $\pm$ vapour (30)

The slope of the equilibrium boundary is very shallow in P-T space (curve (30) in Fig. 50). Newton (*op.cit.*) also shows experimentally that anhydrous cordierite is stable up to 8,2 Kb pressure. Since the cordierites involved in reactions (30) and (31) refer to the magnesian end members which are stable at higher pressures than the iron end member cordierites (Holdaway and Lee, 1977), it is concluded that the maximum pressures possible for the regional metamorphism in the study area based on the presence of cordierite alone, could not have exceeded 8-11 Kb. This conclusion is consistent with the absence of kyanite from all parageneses in the pelitic gneisses.

Additional pressure constraints are obtained from the mineral parageneses recorded in mafic rocks. The stable coexistence of orthopyroxene and plagioclase in these rocks indicates that the pressures must have been lower than

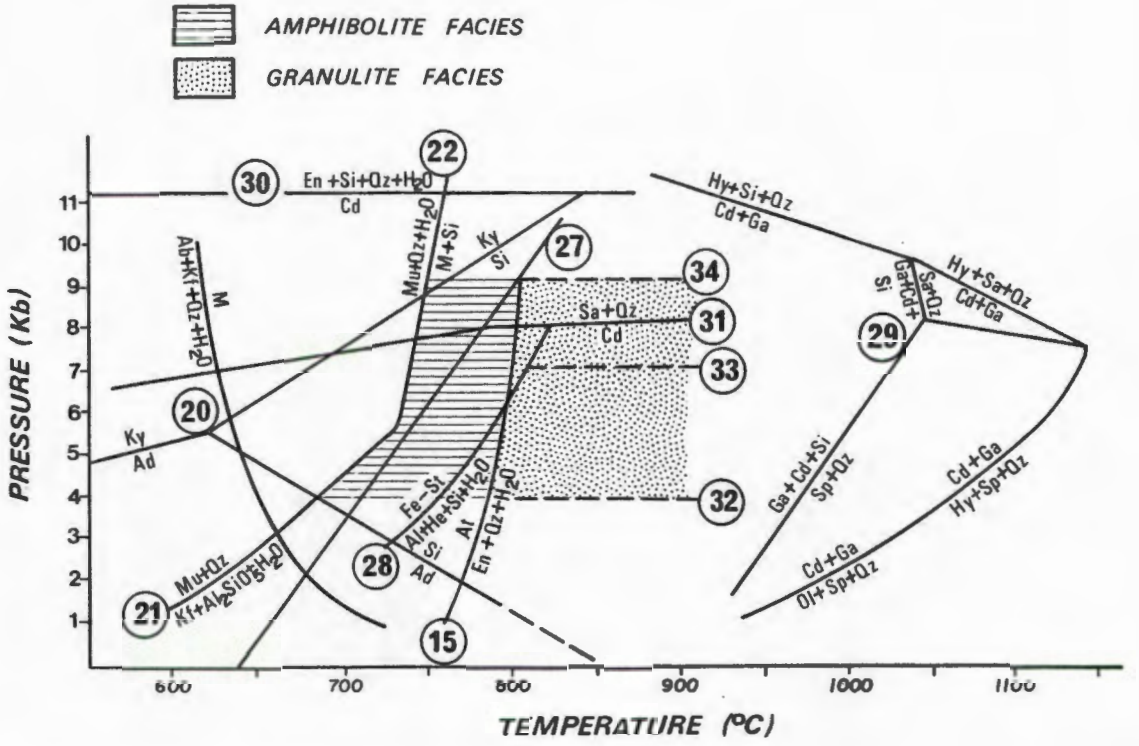


Fig. 50 Experimentally determined equilibria relevant to the metamorphism of pelitic gneisses in the study area. The likely P-T conditions that were prevailing during the regional metamorphism in the upper amphibolite and granulite facies terranes are indicated by the hatched and stippled areas respectively. Abbreviations are explained in the preface.

(15) The reaction: anthophyllite $\rightleftharpoons$ enstatite + quartz + $H_2O$ (Greenwood, 1963).

(20) $Al_2SiO_5$ triple point after Richardson *et al.* (1968, 1969).

(21) Stability limit of muscovite + quartz under low $P_{H_2O}$ conditions (Althaus *et al.*, 1970).

(22) High temperature, high pressure stability limit of muscovite + quartz under hydrous conditions (Storre and Karotke, 1972).

(27) Critical mixing of albite and orthoclase, after Morse (1970).

(28) Schematic equilibrium curve for the reaction Fe-staurolite $\rightleftharpoons$ almandine + hercynite + sillimanite + $H_2O$

($P_{H_2O} = P_{total}$), after Richardson (1968).

(29) Stability limits for coexisting garnet and cordierite (Hensen and Green, 1973).

(30) Upper pressure stability limit of hydrous Mg - cordierite (Newton, 1972).

those required for the formation of almandine-rich garnet and clinopyroxene, a reaction which occurs at pressures in excess of 8 Kb at a temperature of 800°C (Green and Ringwood, 1967). This places the conditions of regional metamorphism into the intermediate pressure range in the sense of Green and Ringwood (*op.cit.*).

Apparently most of the naturally occurring garnet-cordierite granulites are created in the pressure range 4 to 7 Kb (Lee and Holdaway, 1977) or according to Hensen (1977) in the range 4 to 9 Kb. This pressure range is consistent with the observed mineral assemblages in the study area.

The likely P-T conditions attained during regional metamorphism in the study area will be evaluated quantitatively in more detail by the application of thermodynamic principles in Chapter IV, but from the recorded mineral assemblages, in the light of experimental petrology, it is tentatively concluded that the temperatures must have been in excess of 700°C with pressures probably not exceeding 8 Kb. The likely P-T range that can account for the observed mineral assemblages in the amphibolite and granulite facies terranes of the study area are schematically indicated in Fig. 50.

Fig. 50 (continued)

(31) Upper pressure stability limit of anhydrous Mg-cordierite (Newton, 1972).

(32) Lower pressure limit for naturally coexisting garnet and cordierite in granulites (Lee and Holdaway, 1977; Hensen, 1977).

(33) Upper pressure limit for naturally coexisting garnet and cordierite in granulites (Lee and Holdaway, 1977).

(34) Upper pressure limit for naturally coexisting garnet and cordierite in granulites (Hensen, 1977).

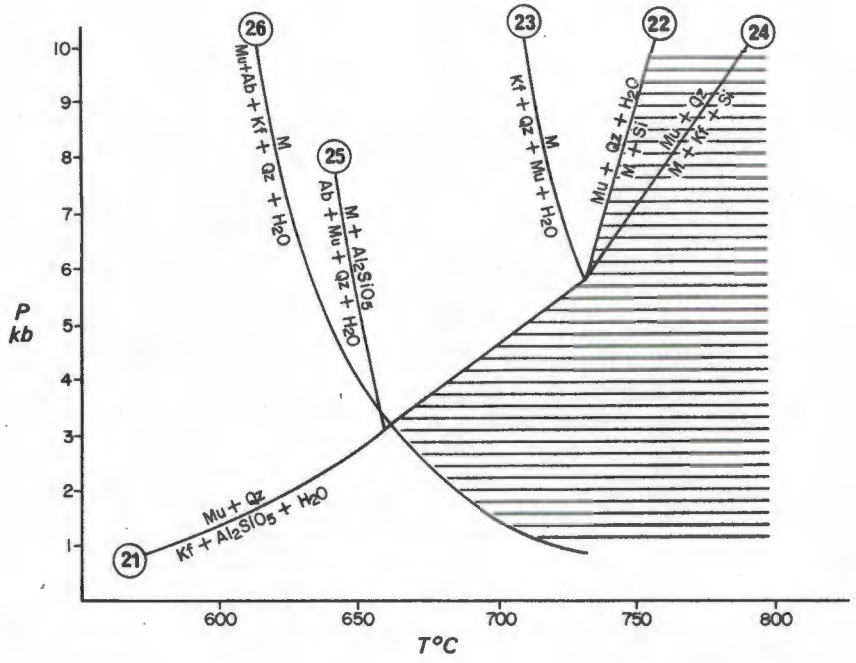


Fig. 51 Experimentally investigated equilibria involving the stability of muscovite and quartz (after Winkler, 1976, p.84). $P_{H_2O} = P_{total}$.

Abbreviations as in preface.

(21) muscovite + quartz $\rightleftharpoons$ K-feldspar + $Al_2SiO_5$ + $H_2O$ (Althaus *et al.*, 1970)

(22) muscovite + quartz + $H_2O$ $\rightleftharpoons$ melt + sillimanite (Storre and Karotke, 1972).

(23) K-feldspar + muscovite + quartz + $H_2O$ $\rightleftharpoons$ melt (in Winkler, *op.cit.*)

(24) muscovite + quartz $\rightleftharpoons$ melt + K-feldspar + sillimanite (Storre, 1972)

(25) muscovite + quartz + plagioclase + $H_2O$ $\rightleftharpoons$ melt + $Al_2SiO_5$ (Storre and Karotke, 1971).

(26) muscovite + quartz + plagioclase + K-feldspar + $H_2O$ $\rightleftharpoons$ melt (in Winkler, *op.cit.*).

Note that all dehydration reactions are sensitive to the composition of the gas phase and when $P_{H_2O}$ is less than $P_{total}$, the dehydration reactions are shifted towards lower temperatures. The hatched area indicates the minimum temperature conditions ($P_{H_2O} = P_{total}$) for the regional metamorphism of the study area.

## D Metamorphism of Calcareous Rocks

The majority of the calc-silicate rocks encountered in the study area are carbonate-free or contain carbonates only in accessory amounts. The calcareous affinity of these rocks is, however, evident from the calcic nature of the constituent minerals. Proper marbles (> 90 per cent carbonate minerals) are extremely rare and during the period of field mapping only one outcrop locality was recorded on the farm Kat Vlei (235)(C9).

### 1 Mineral Parageneses and Their Significance

Although calc-silicate rocks can provide valuable information regarding the progressive changes in physical conditions during metamorphism, the lithologies encountered in the present area are not suited for subdividing the terrane into sectors of contrasting metamorphic grade, as most of the minerals recorded appear to be stable throughout the upper amphibolite and granulite facies. Nevertheless, the mineral parageneses observed in these rocks (Fig. 52) can provide additional information on some of the factors controlling the metamorphism.

Sphene is a very common accessory mineral and forms an additional phase in the majority of the mineral assemblages tabulated (Fig. 52). In the discussion on the metamorphism of mafic rocks it was pointed out that orthopyroxene and sphene are incompatible and that sphene is restricted to the amphibolite facies terrane. This contrasts with the observation that sphene persists as a stable mineral in calc-silicate rocks metamorphosed under granulite facies conditions. According to Dobretsov *et al.* (1973, p.34) sphene is stable in quartz-bearing carbonate rocks over a wide range of P-T conditions in the granulite facies, while rutile replaces sphene in those carbonate rocks which are undersaturated with respect to $SiO_2$.

The stability of sphene has been investigated experimentally by Schuiling and Vink (1967) and Hunt and Kerrick (1977) and these authors have demonstrated that at low temperatures sphene-bearing assemblages can form irrespective of the composition of the gas phase ($X_{CO_2}$). The lower temperature stability of sphene is given by the reaction

$$\text{rutile} + \text{calcite} + \text{quartz} \rightleftharpoons \text{sphene} + CO_2 \qquad (35)$$

the equilibrium boundary of which is shown in Fig. 53 at a fluid pressure of 5 kb. At temperatures above this equilibrium sphene may be replaced by rutile in rocks of low $SiO_2$ content, but rutile has not been observed in any of the specimens studied. Sphene is generally accompanied by plagioclase and this association can be formed by the reaction

$$2 \text{ zoisite} + 1 \text{ rutile} + 1 \text{ quartz} \rightleftharpoons 1 \text{ sphene} + 3 \text{ anorthite} + H_2O \qquad (36)$$

the equilibrium condition of which occurs at a temperature of about 500°C when $P_{fluid}$ = 5 kb (Hunt and Kerrick, *op.cit.*). Thus the coexistence of plagioclase and sphene indicates temperatures in excess of 500°C for the regional metamorphism that affected the area.

Clinopyroxenes of the diopside - hedenbergite series are recorded in the majority of the specimens studied. Their chemical compositions plot closer to the iron-rich side of the solid solution series (Fig. 55 , page 147). The stability fields of various diopside-bearing assemblages in P-T-$X_{CO_2}$ space have been established experimentally in recent years. Probably the most important diopside-forming reaction involves the decomposition of tremolite in the presence of calcite and quartz according to the reaction

$$1 \text{ tremolite} + 3 \text{ calcite} + 2 \text{ quartz} \rightleftharpoons 5 \text{ diopside} + 3\ CO_2 + 1\ H_2O \qquad (37)$$

The conditions of equilibrium for reaction (37) have been determined experimentally by Metz (1970) at fluid pressures of 0,5, 1,3 and 5 kb under variable $X_{CO_2}$ concentrations of the gas phase and is shown as curve (37) in Fig. 53. At $P_{fluid}$ = 1 kb the maximum stability of tremolite in the presence of calcite and quartz occurs at 545°C, while at $P_{fluid}$ = 5 kb this maximum stability limit is displaced to 660°C (Metz, *op.cit.*). The equilibrium for reaction (37) has been computed by Skippen (1971, 1974) who determines a maximum temperature stability limit of tremolite in calcite-quartz assemblages of 500°C at $P_{fluid}$ = 1 kb, i.e. 45°C lower than the equilibrium as obtained by Metz (*op.cit.*). The results of Slaughter *et al.* (1975) indicate even lower temperatures for the same reaction, but at $P_{fluid}$ = 5 kb their results agree well with those of Metz (*op.cit.*).

Over a wide compositional range ($X_{CO_2}$) of the gas phase reaction (37) is the only diopside-forming reaction and only at very high $X_{CO_2}$ are other diopside-forming reactions important, e.g.

$$1 \text{ dolomite} + 2 \text{ quartz} \rightleftharpoons 1 \text{ diopside} + 2\ CO_2 \qquad (38)$$

the conditions of equilibrium of which have been determined by Metz (*op.cit.*), Skippen (*op.cit.*) and Slaughter *et al.* (*op.cit.*) and is shown as curve (38) in Fig. 53. At a fluid pressure of 1 kb reaction (38) takes place at 495°C (Metz, *op.cit.*). The data of Skippen (*op.cit.*) and Slaughter *et al.* (*op.cit.*) on the other hand, suggest lower temperatures of 475°C and 450°C respectively at the same pressure. Although these authors agree on the topology, there are considerable variances in the actual position of this equilibrium boundary in P-T-$X_{CO_2}$ space. At $P_{fluid}$ = 5 kb the equilibrium temperatures determined by Metz (*op.cit.*) and Slaughter *et al.* (*op.cit.*) agree very well at about 625°C. The two reactions (37) and (38) determine the lower temperature stability limit of all diopside-bearing assemblages. The general absence of

tremolite (with one exception - to be discussed in Chapter III D 2 d) and the ubiquitously recorded occurrence of clinopyroxene in the calc-silicate rocks, therefore, suggests that the metamorphic temperatures must have been on the high temperature side of these two equilibria (Curves (37) and (38) in Fig.53.

Andradite-grossular garnets are common in the calc-silicate rocks and the stability fields of various grandite-bearing parageneses requires some discussion. In order to gain some insight into the phase relationships of Ca-rich garnets a pure end-member system ($CaO-Al_2O_3-SiO_2-CO_2-H_2O$) may be investigated as a first approximation. The literature on this simplified system is voluminous. Some of the publications concerning grossularite in particular include Roy and Roy (1957); Pistorius and Kennedy (1960); Newton (1965, 1966); Hays (1967); Liou (1969); Storre (1970); Gordon and Greenwood (1971). These authors have shown that the stability field of grossularite in the absence of quartz is very large. At extreme temperatures (in excess of 1000°C at 5 kb pressure) grossularite decomposes to anorthite + gehlenite + wollastonite (Boettcher, 1970). However, when quartz is present the stability field of grossularite is much reduced and the upper temperature stability limit is then determined by the reaction

$$1 \text{ grossularite} + 1 \text{ quartz} \rightleftharpoons 2 \text{ wollastonite} + 1 \text{ anorthite} \qquad (39)$$

The conditions for equilibrium for reaction (39) have been experimentally determined by Newton (1966), Boettcher (1970) and Storre (1970). At a pressure of 2 kb Newton's (*op.cit.*) experiments yield an equilibrium temperature of 600°C which is consistent with that determined by Boettcher (*op.cit.*). The experiments of Storre (*op.cit.*) on the other hand, indicate a slightly higher equilibrium temperature of 630°C at a pressure of 2 kb, while Gordon and Greenwood (1971) favour 590°C at the same pressure. At higher pressures (5 kb) the equilibrium for reaction (39) is found to be at a temperature of about 720°C (Boettcher, *op.cit.*). It is independent of the composition of the gas phase in the range up to $X_{CO_2} \approx 0,2$. Equilibrium (39) is shown as curve (39) in Fig. 53. Apparently the assemblage 'wollastonite + anorthite' is rare in regionally metamorphosed terranes and Newton (*op.cit.*) concludes on the basis of experimental and field evidence that this paragenesis can only be expected in areas that were subjected to the highest grades of regional metamorphism. In the area presently investigated coexisting wollastonite and plagioclase are recorded in one specimen (HA 1155) in the paragenesis 'wollastonite + diopside - hedenbergite + scapolite + calcite + plagioclase + quartz'. The three minerals plagioclase, calcite and quartz are, however, only present in small amounts (each mineral accounts for less than 1 per cent of the modal composition). Grossularite-rich garnet has not been observed and if it had been present previously, it has probably reacted to yield 'wollastonite + plagioclase' according to reaction (39).

In this particular specimen (HA 1155) calcite and quartz occur in contact with each other. According to Winkler (1976) calcite + quartz are stable even at the highest temperatures reached during regional metamorphism because in such rocks $X_{CO_2}$ is generally very high. Under certain circumstances, how-

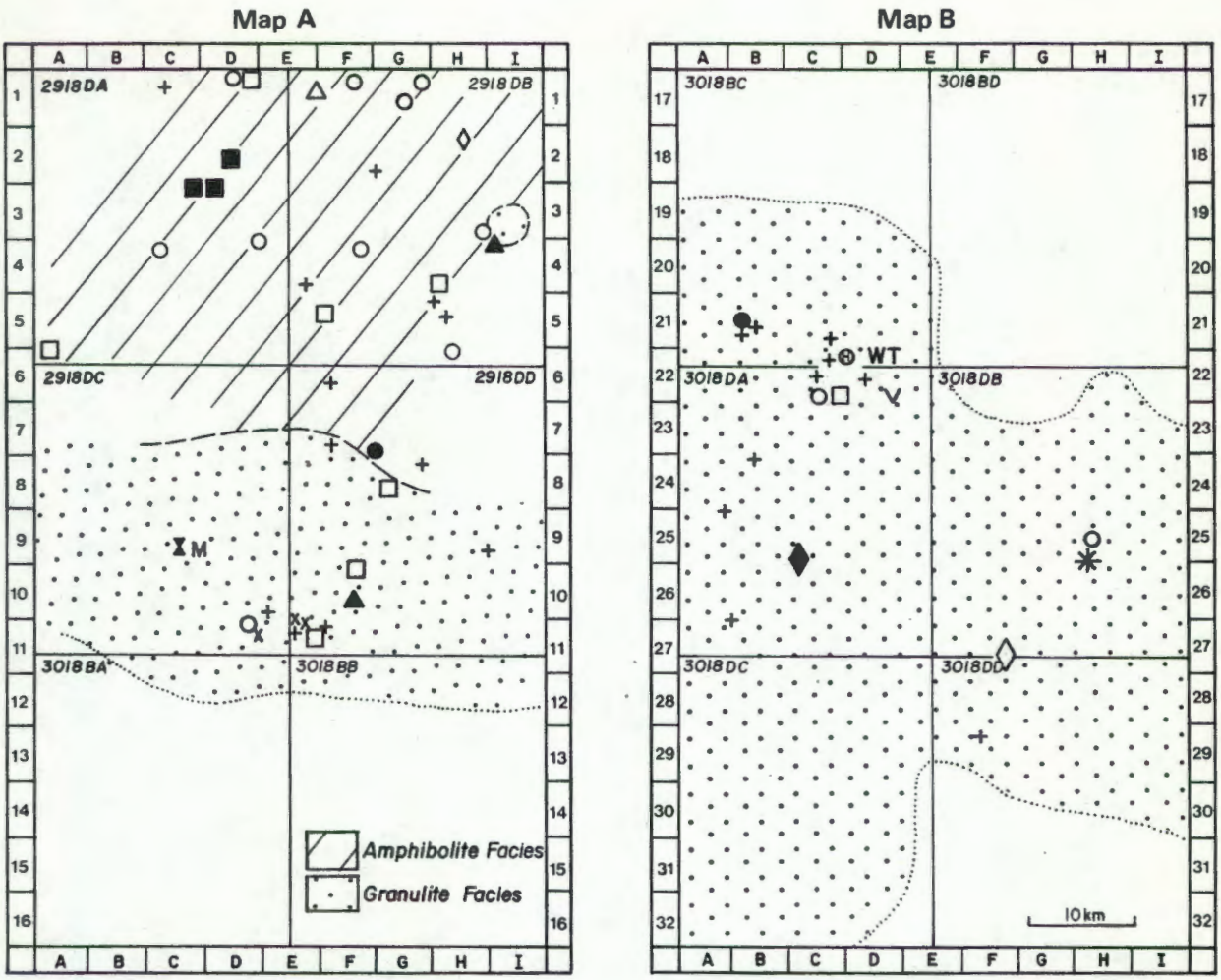


Fig. 52 Geographic distribution of mineral parageneses in calc-silicate rocks and marbles. The frequency of occurrence is indicated in brackets. The metamorphic zonation is based on the parageneses recorded in mafic rock types.

Key:

| | | |
|---|---|---|
| + | diopside - hedenbergite + plagioclase + quartz (± calcite) | (22) |
| ○ | diopside - hedenbergite + plagioclase + grandite (± calcite) | (12) |
| □ | diopside - hedenbergite + plagioclase + grandite + quartz (± calcite) | (8) |
| △ | grandite + plagioclase | (1) |
| ◊ | grandite + plagioclase + quartz | (2) |
| ■ | diopside - hedenbergite + grandite + scapolite + plagioclase + quartz | (3) |
| ▲ | diopside - hedenbergite + grandite + plagioclase + scapolite | (2) |
| ● | diopside - hedenbergite + grandite + scapolite + quartz + calcite | (3) |

| | | |
|---|---|---|
| ⧗ | diopside - hedenbergite + scapolite + calcite | (1) |
| V | diopside - hedenbergite + quartz | (1) |
| x | diopside - hedenbergite + plagioclase | (3) |
| ♦ | diopside - hedenbergite + scapolite + plagioclase + quartz (± calcite) | (1) |
| ✳ | diopside - hedenbergite + scapolite + plagioclase (± calcite) | (1) |
| M | dolomite + calcite + forsterite + clinohumite + spinel ± phlogopite | (1) |
| W | wollastonite + diopside - hedenbergite + scapolite + calcite + plagioclase + quartz | (1) |
| ⊛ | magnesio - hornblende + quartz | (1) |
| T | tremolite + quartz | (1) |

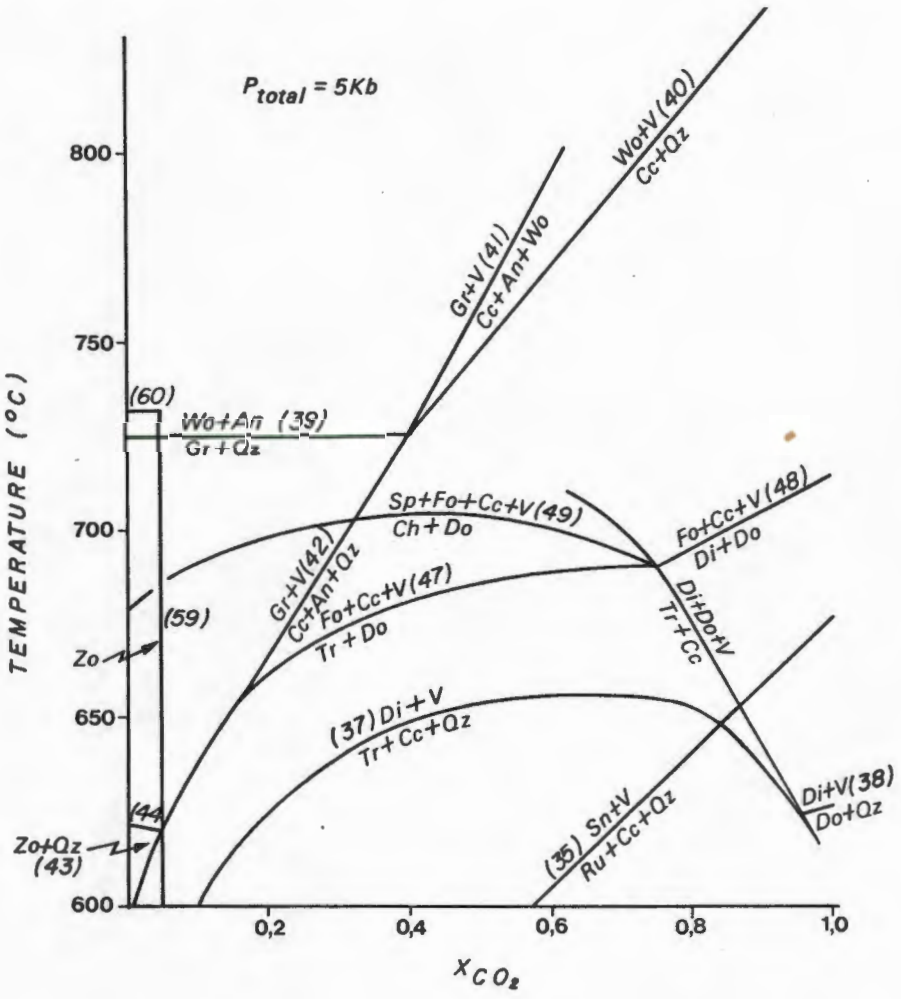


Fig. 53 Reactions in calcareous rocks in an isobaric T-$X_{CO_2}$ diagram at a pressure of 5 kb. Numbers along equilibrium boundaries correspond to the reactions discussed in the text.

ever, the gas phase may be diluted with $H_2O$, particularly when thin carbonate units are interbanded with pelitic rocks and the two minerals may then react to form wollastonite according to the reaction

$$\text{calcite} + \text{quartz} \rightleftharpoons \text{wollastonite} + CO_2 \qquad (40)$$

The physical conditions for chemical equilibrium of reaction (40) have been determined experimentally (Greenwood, 1967) at fluid pressures of 1 kb and 2kb. These experiments have clearly demonstrated that the equilibrium temperature at a fixed fluid pressure increases with increasing $X_{CO_2}$ of the gas phase and at very high $X_{CO_2}$ the equilibrium temperatures at pressures applicable to regional metamorphic terranes are so high that wollastonite cannot be formed by the breakdown of calcite and quartz, unless the fluid phase is considerably diluted. The experimental data on reaction (40) have been extrapolated to $P_{fluid}$ = 5 kb and the equilibrium boundary is shown as curve (40) in Fig. 53. The equilibrium paragenesis 'calcite + wollastonite + quartz' can, according to Fig. 53, coexist over a very large temperature range (650 - 850°C) at $P_{fluid}$ = 5 kb. The coexistence of wollastonite and plagioclase, however, indicates that temperatures in excess of 720°C must have prevailed during regional metamorphism of the area concerned (specimen HA 1150 has been collected in the granulite facies terrane on the farm Dabidas (407)(D22)).

The stability field of grossularite is not only restricted with respect to temperature (reaction 39), but is also restricted with respect to the composition of the fluid phase ($X_{CO_2}$) by the following reactions, arranged in order of decreasing temperature.

$$1 \text{ grossularite} + 1\ CO_2 \rightleftharpoons 1 \text{ calcite} + 1 \text{ anorthite} + 1 \text{ wollastonite} \qquad (41)$$

$$1 \text{ grossularite} + 2\ CO_2 \rightleftharpoons 2 \text{ calcite} + 1 \text{ anorthite} + 1 \text{ quartz} \qquad (42)$$

$$3 \text{ grossularite} + 5\ CO_2 + 1\ H_2O \rightleftharpoons 2 \text{ zoisite} + 5 \text{ calcite} + 3 \text{ quartz} \qquad (43)$$

The equilibrium boundaries for these reactions are shown as curves (41), (42) and (43) respectively in Fig. 53. These reactions have been experimentally investigated by Gordon and Greenwood (1971) at $P_{fluid}$ = 2 kb and they have shown that grossularite-bearing assemblages are possible only when the fluid compositions are characterised by low partial pressures of $CO_2$.

The lower temperature stability limits of grossularite is determined by the reaction

$$4 \text{ zoisite} + 1 \text{ quartz} \rightleftharpoons 1 \text{ grossularite} + 5 \text{ anorthite} + 2\ H_2O \qquad (44)$$

The experimental studies on this reaction (Strens, 1965, 1968; Nitsch and Winkler, 1965; Newton, 1966; Boettcher, 1970; Holdaway, 1972; Liou, 1973) indicate that the equilibrium boundary at $P_{fluid}$ = 5 kb occurs between 620°C 650°C. Reaction (44) is shown as curve (44) in Fig. 53. As primary

zoisite is not observed in any of the specimens studied while 'grandite + plagioclase' assemblages are ubiquitously recorded, it is concluded that the temperatures during regional metamorphism of the entire area must have been in excess of 620°C.

Storre (1970), Boettcher (*op.cit.*) and Gordon and Greenwood (1971) have pointed out that, although individual minerals may have very large stability fields, particular parageneses may be very restricted. For example, reactions (39), (42) and (44) define a field in T-$X_{CO_2}$ space that restricts the parageneses 'grossularite + anorthite + quartz'. In Fig. 53, it is shown that both these assemblages are only possible in the temperature range 620° - 725°C provided that $X_{CO_2}$ of the gas phase is low (< 0,4 when $P_{fluid}$ = 5 kb).

Scapolite is a common mineral in the calc-silicate specimens studied. Scapolites are known to form a solid solution series between the end-members marialite (3Na Al $Si_3$ $O_8$ Na Cl) and meionite (3Ca $Al_2$ $Si_2$ $O_8$ Ca $CO_3$) (Shaw, 1960a, b; Evans *et al.*, 1969; Deer *et al.*, 1971; Goldsmith, 1976). The substitutions possible are complex and of the type Na⇌K, $CO_3$⇌$SO_4$ and particularly Na Si⇌Ca Al (Deer *et al.*, *op.cit.*).

Scapolites are stable over a wide range of metamorphic conditions ranging from the amphibolite facies (Misch, 1964; Turner, 1968 p.318-319) to the granulite facies (Lovering and White, 1964; Turner, 1968 p.321). Some scapolites, particularly in the granulite facies, contain abundant $SO_4$" and according to Lovering and White (*op.cit.*) the sulphur content of scapolite increases with increasing metamorphic grade.

Orville (1975) has experimentally investigated the system Na Al $Si_3$ $O_8$ - Ca $Al_2$ $Si_2$ $O_8$ - Na Cl - Ca $CO_3$ at pressures of 4 kb and 750°C and his data and those presented by Goldsmith (*op.cit.*) suggest a lower temperature stability of 750-800°C for marialite relative to albite + Na Cl in the pressure range zero to 8 kb. (This reaction has a very steep slope in P-T space).

The scapolites encountered in the area under discussion are probably not rich in Cl' because scapolites in the granulite facies are rich in carbonate and sulphate (Lovering and White, *op.cit.*; Orville, *op.cit.*; Goldsmith, *op. cit.*). Accordingly, the carbonate-sulphate system is more applicable. This system has been experimentally investigated by Goldsmith and Newton (1977). The two equilibria studied are:

$$3 \text{ anorthite} + 1 \text{ calcite} \rightleftharpoons 3 \text{ meionite} \qquad (45)$$

$$3 \text{ anorthite} + 1 \text{ Ca } SO_4 \rightleftharpoons 3 \text{ sulphate meionite} \qquad (46)$$

The equilibrium of reaction (45) is independent of pressure and meionite is stable only above 875°C. On the other hand reaction (46) has a negative slope in P-T space and at a pressure of 5 kb sulphate meionite can only occur above 925°C. However, in nature extensive Na substitution can be expected and Orville (*op.cit.*) has shown that such substitution stabilises both scapolites to lower temperature. Goldsmith and Newton (*op.cit.*) have investigated the temperature dependence of Na-Ca partitioning between scapolite and anorthite-rich plagioclase and they have shown that scapolites become more

enriched in Na relative to plagioclase with decreasing temperature.

On the farm Kat Vlei (235)(C9) marbles contain the paragenesis

dolomite + calcite + forsterite + clinohumite + spinel ± phlogopite

These marbles are associated with hypersthene-pyroclase granolites indicating that they have recrystallised under granulite facies metamorphic conditions. Of the two marble specimens studied the one contains one grain of tremolite while the other is completely free of this mineral. Diopside is not observed in association with forsterite and, therefore, all reactions leading to the simultaneous formation of both minerals can be disregarded in this discussion. Experimental studies (Skippen, 1974; Slaughter *et al.*, 1975; Metz, 1976) have shown that the dominant forsterite-producing reaction involves the decomposition of tremolite in the presence of dolomite according to:

$$1 \text{ tremolite} + 11 \text{ dolomite} \rightleftharpoons 8 \text{ forsterite} + 13 \text{ calcite} + 9\ CO_2 + 1\ H_2O \qquad (47)$$

The physical conditions for equilibrium of reaction (47) have been experimentally determined at pressures of 0,5 kb and 1 kb (Metz, 1967) and at pressures of 3 kb and 5 kb (Metz, 1976). At 1 kb pressure the experimental data agree well with the computed reaction boundary (Skippen, *op.cit.*), but at higher pressures there is considerable discrepancy, e.g. at 3 kb the maximum temperature for equilibrium (47) as computed by Skippen (*op.cit.*) occurs at about 40°C below the experimentally determined boundary (Metz, 1976). This discrepancy increases with increasing pressure. Nevertheless, the experiments show that reaction (47) is possible over a wide range of $X_{CO_2}$. The equilibrium boundary of reaction (47) is shown as curve (47) in Fig. 53. At very high $X_{CO_2}$ other forsterite-producing reactions are possible, e.g.:

$$1 \text{ diopside} + 3 \text{ dolomite} \rightleftharpoons 2 \text{ forsterite} + 4 \text{ calcite} + 2\ CO_2 \qquad (48)$$

the conditions for chemical equilibrium of which has been experimentally determined by Käse and Metz (1980). At a pressure of 5 kb the intersection of the equilibrium boundaries (47) and (48) in $T\text{-}X_{CO_2}$ space occurs at $T = 690 \pm 15$°C and $X_{CO_2} = 0,7 - 0,8$ (Käse and Metz, *op.cit.*). The equilibrium boundary for reaction (48) is shown as curve (48) in Fig. 53. Both these reactions are significant because the assemblage 'forsterite + dolomite + calcite' is only possible on the high temperature side of reactions (47) and (48) (see Fig. 53).

Magnesium chlorite, commonly observed in low and medium grade dolomites becomes unstable at higher grade and is replaced by spinel. Rice (1977) has studied progressive contact metamorphism of impure dolomitic limestones around the Boulder Batholith (Montana) and at the highest temperatures, close to the batholith, he records that chlorite has become unstable and he observes the paragenesis 'calcite + dolomite + olivine + spinel ± phlogopite' which is often associated with clinohumite. Rice (*op.cit.*) ascribes the

formation of spinel to the reaction:

$$\text{chlorite} + 2\ \text{dolomite} \rightleftharpoons 3\ \text{forsterite} + 2\ \text{calcite} + \text{spinel} + 2\ CO_2 + 4\ H_2O \qquad (49)$$

The physical conditions for equilibrium of reaction (49) has been experimentally determined by Widmark (1980) at fluid pressures of 1 kb, 2 kb and 3 kb. The equilibrium boundary occurs on the high temperature side of reaction (47) and marks the lower temperature stability limit for the paragenesis 'dolomite + forsterite + calcite + spinel'. The approximate position of the equilibrium boundary of reaction (49) at 5 kb pressure is shown as curve (49) in Fig. 53. A minimum temperature of about 700°C can thus be deduced for the Kat Vlei marbles to account for the observed coexistence of all four minerals 'dolomite + forsterite + calcite + spinel'.

Little is known about the stability fields of the humite group minerals. They can be represented by the general formula

$$n\ Mg_2SiO_4 \ .\ Mg_{1-x}\ Ti_x\ (OH,F)_{2-2x}O_{2x}$$

(where n = 1 for nordbergite, n = 2 for chondrodite, n = 3 for humite and n = 4 for clinohumite) and ionic substitutions of the type $OH \rightleftharpoons F$, $Mg + 2(OH, F) \rightleftharpoons Ti + 2(O)$ and $Mg \rightleftharpoons Fe(Mn, Ca, Zn)$ are possible (Rice, 1980).

The stability field of clinohumite in $P\text{-}T\text{-}X_{fluid}$ $(CO_2\text{-}H_2O\text{-}HF)$ space has been computed by Rice (*op.cit.*). According to Kerrick *et al.*, (1973), Moore and Kerrick (1976) and Rice (1977) clinohumite is observed in nature to form at the expense of forsterite and dolomite by the reaction:

$$4\ \text{forsterite} + \text{dolomite} + H_2O \rightleftharpoons \text{clinohumite} + \text{calcite} + CO_2 \qquad (50)$$

This equilibrium limits the coexistence of clinohumite and calcite with respect to the fluid composition. Rice (1980) points out that fluorine substitution has a major effect on the stability of clinohumite. (The stability field is markedly increased with increasing F-substitution). He has also shown that the stability field for coexisting clinohumite and calcite (at a fixed fluorine content of clinohumite) decreases with increasing pressure. With respect to temperature the clinohumite-calcite stability field is limited by the reaction:

$$\text{tremolite} + 13\ \text{magnesite} + H_2O \rightleftharpoons 2\ \text{clinohumite} + 2\ \text{calcite} + 11\ CO_2 \qquad (51)$$

Another reaction which can produce the paragenesis "dolomite + clinohumite + calcite + spinel" involves the breakdown of chlorite and dolomite according to:

$$4\ \text{chlorite} + 11\ \text{dolomite} \rightleftharpoons 3\ \text{clinohumite} + 4\ \text{spinel} + 11\ \text{calcite} + 13\ H_2O + 11\ CO_2 \qquad (52)$$

which has been observed in nature (Trommsdorff, 1966; Rice, 1973). Humite group minerals also occur in kimberlites (Merrill, 1970; Aoki *et al.*, 1976) indicating that these minerals are stable under high pressure conditions.

It is apparent from the above discussion that the majority of the mineral assemblages recorded in the calcareous rocks of the study area have large stability fields. These rocks are, therefore, not suitable indicators of prograde metamorphism. Relatively high temperatures are suggested by the absence of tremolite and the ubiquitous occurrence of clinopyroxene instead, the absence of primary epidote from all assemblages (except for some primary orthite? as pointed out in Chapter II) and the parageneses 'wollastonite + plagioclase' and 'dolomite + calcite + forsterite + spinel' the latter of which suggest temperatures in excess of 700 - 720°C for granulite facies metamorphism. Tremolite as a major constituent is recorded in one of the specimens (HA 997) and its significance is to be discussed in Chapter III D 2 d).

## 2 Chemical Compositions of some Calc-Silicate Minerals

### (a) Garnet

It has already been pointed out that the calc-silicate rocks investigated in this study frequently contain garnet with a characteristic orange-brown colour. These garnets are particularly common and widespread in the amphibolite facies terrane, but they have also been recorded in specimens collected in the granulite facies terrane. Similar garnets are also known from the south and southeast of Springbok where they coexist with bytownite, quartz, green pleochroic clinopyroxene, sphene and opaque minerals (Joubert, 1971a) which constitutes a mineral assemblage typical of the calc-silicate rocks described in this study.

Chemical analyses of coexisting mineral phases in calc-silicate rocks are generally lacking for the Namaqualand Metamorphic Complex and, therefore, it was decided to provide some analytical information regarding mineral chemistry in this study. Eleven specimens, three of which have been collected in the granulite facies terrane, were selected for garnet analyses (Appendix II, Table A2-19. The initial microprobe analyses were computed on the assumption that the total Fe in the specimen exists as $Fe^{+2}$. These analyses yielded low oxide totals and ionic proportions far in excess of the expected 8 per 12 oxygens. Stoichiometric considerations, however, indicate the presence of considerable $Fe^{+3}$, which necessitated the recalculation of all the garnet analyses to account for $Fe^{+3}$. Those recalculated analyses are presented in Appendix II, Table A2-19. The method of recalculation utilised in this study is outlined in Appendix II. The corrected ionic proportions (allowing for $Fe^{+3}$) come into close agreement with the expected 8 per 12 oxygens and the oxide totals (allowing for $Fe_2O_3$) approach the expected 100 per cent level more closely after recalculation (Appendix II, Table A2-19). The corrected analyses are expressed in terms of molecular per cent end-member molecules in Table 14 and are displayed graphically in Fig. 54.

The data shown in Table 14 and Fig. 54 indicate that the garnets in the calc-silicate rocks are composed essentially of the andradite and grossular molecules with the andradite component generally dominating. The contributions of the almandine and spessartine molecules to the bulk composition is

Table 14 Garnet compositions in calc-silicate rocks expressed as molecular per cent end-member molecules. *indicates specimens collected in the granulite facies terrane. All other specimens are from the upper amphibolite facies terrane.

| Specimen No. | Grain | Andradite | Grossular | Almandine | Spessartine | Pyrope |
|---|---|---|---|---|---|---|
| HA 1101 | 1 | 69,97 | 20,06 | 7,96 | 1,39 | 0,62 |
| HA 1094 | 1 | 56,26 | 39,46 | 2,98 | 0,62 | 0,68 |
| HA 1094 | 2 | 54,68 | 40,82 | 3,31 | 0,64 | 0,56 |
| HA 1097 | 1 | 51,54 | 44,77 | 2,17 | 0,97 | 0,55 |
| HA 1097 | 2 | 45,35 | 51,57 | 1,38 | 0,88 | 0,82 |
| HA 1148 | 1 | 71,22 | 24,47 | 1,00 | 1,81 | 1,50 |
| HA 1087 | 1 | 66,44 | 22,03 | 9,94 | 1,14 | 0,45 |
| HA 1087 | 2 | 65,96 | 22,38 | 10,40 | 0,71 | 0,56 |
| HA 1087 | 3 | 66,44 | 22,34 | 9,45 | 1,28 | 0,48 |
| HA 1093 | 1 | 72,39 | 16,25 | 9,07 | 1,91 | 0,38 |
| HA 1093 | 2 | 67,65 | 20,33 | 9,40 | 2,20 | 0,42 |
| HA 1093 | 3 | 68,02 | 20,39 | 9,14 | 2,04 | 0,42 |
| HA 1140 | 1 | 67,72 | 18,77 | 11,13 | 1,89 | 0,49 |
| HA 1140 | 2 | 68,18 | 19,14 | 10,45 | 1,78 | 0,45 |
| HA 1140 | 3 | 67,58 | 17,79 | 12,23 | 1,93 | 0,47 |
| HA 1132 | 1 | 73,60 | 16,31 | 8,64 | 0,86 | 0,60 |
| HA 1132 | 2 | 75,32 | 15,12 | 8,11 | 0,83 | 0,62 |
| HA 1013* | 1 | 69,36 | 18,17 | 8,06 | 3,98 | 0,44 |
| HA 1013* | 2 | 69,59 | 16,93 | 8,41 | 4,58 | 0,49 |
| HA 1152* | 1 | 50,57 | 42,06 | 5,10 | 1,57 | 0,71 |
| HA 1152* | 2 | 51,12 | 41,88 | 4,87 | 1,39 | 0,74 |
| HA 459* | 1 | 67,71 | 27,60 | 2,47 | 1,34 | 0,78 |
| HA 459* | 2 | 67,79 | 27,05 | 3,00 | 1,38 | 0,78 |

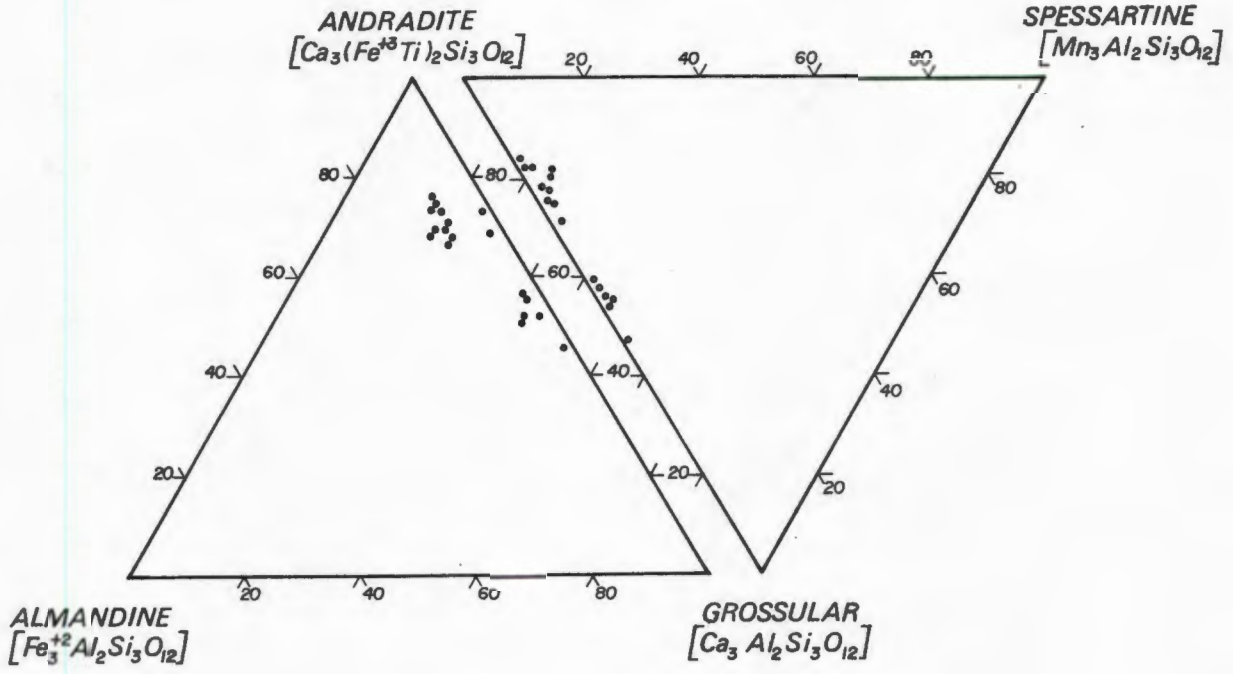


Fig 54 Chemical compositions of garnets in eleven calc-silicate specimens from the granulite and upper amphibolite facies terrane plotted in terms of the end-member molecules andradite, grossular, almandine and spessartine. Note that these garnets are essentially andradite-grossular solid solutions with only small amounts of the almandine and spessartine molecules.

small and almandine is always more abundant than the spessartine molecule. The contribution of pyrope to the bulk composition is negligible. In summary, the range in chemical compositions of the garnets presented in Table 14 can be expressed as follows:

$Andradite_{45-75}$ $Grossular_{15-52}$ $Almandine_{1-12}$ $Spessartine_{0,6-4}$ $Pyrope_{0,4-1,5}$

The subscripts indicate the range of molecular percentages contributed by each end-member molecule to the bulk composition of the garnets.

Garnets consisting essentially of the andradite and grossular molecules

are generally referred to as grandite (Deer *et al.*, 1971). These garnets contain insufficient $TiO_2$ (generally < 1 per cent) to be termed melanite. The andradite molecule can be generated via the reaction

$$3\ CaCO_3 + Fe_2O_3 + 3\ SiO_2 \rightleftharpoons Ca_3Fe_2Si_3O_{12} + 3\ CO_2 \qquad (53)$$

and if FeO is also present in the environment clinopyroxenes can form

$$2\ Fe_2O_3 + 2\ FeO + 5\ SiO_2 + 4\ CaCO_3 \rightleftharpoons Ca_3Fe_2Si_3O_{12} + CaFeSi_2O_6 + Fe_2O_3 + 4\ CO_2 \qquad (54)$$

In fact, clinopyroxenes and magnetite are frequently associated with the grandites in the study area.

(b) Clinopyroxene

The clinopyroxenes recorded in calc-silicate rocks are generally dark green and weakly pleochroic. Microprobe analyses of clinopyroxene grains in 10 specimens (three of which are from the granulite facies terrane) are presented in Appendix II, Table A2-20.

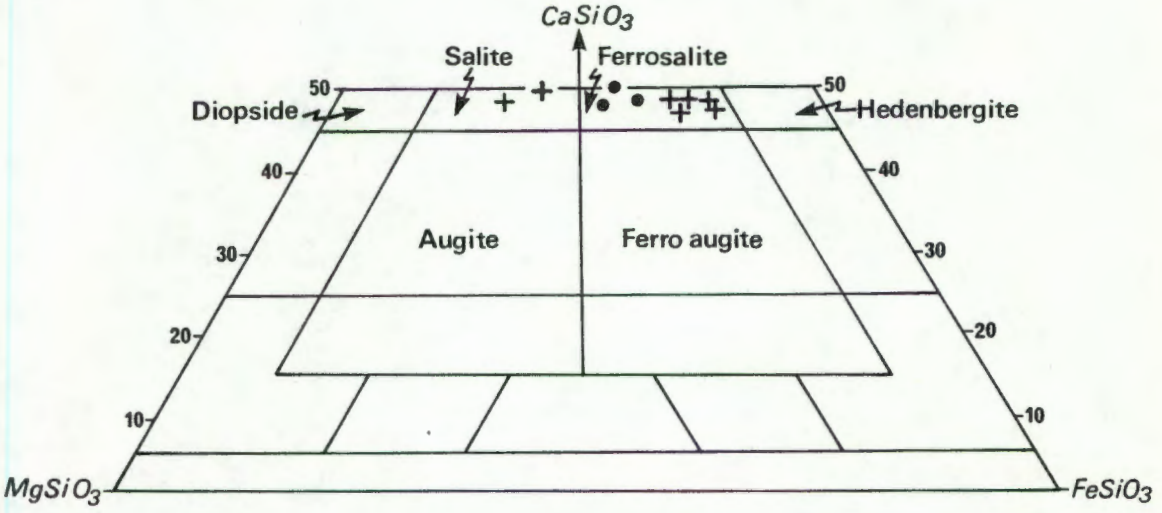


Fig. 55 Clinopyroxenes in calc-silicate rocks plotted in terms of the Poldervaart and Hess (1951) classification. Solid dots are clinopyroxene compositions from specimens collected in the granulite facies terrane and crosses show the range of compositions encountered in the upper amphibolite facies terrane.

The chemical compositions of these clinopyroxenes are plotted in the ternary system $MgSiO_3$, $FeSiO_3$, $CaSiO_3$ (Fig.55 ) and are seen to fall into the compositional range of salite and ferrosalite in the classification for clinopyroxenes proposed by Poldervaart and Hess (1951). The clinopyroxenes, like the grandites are particularly iron-rich, indicating a very ferruginous environment of the host rocks. In contrast to the grandite, however, the pyroxenes contain a fair amount of MgO (4-12%). With reference to reaction (54) this suggests that at least some dolomite must have been present in the carbonate phase. In comparison to the chemistry of the salites in hypersthene -pyroclase granolites the clinopyroxenes in the calc-silicate rocks contain higher CaO, FeO, $Al_2O_3$ and distinctly lower MgO and $SiO_2$. The MnO concentration is low (generally < 0,5 per cent) and only in one specimen does MnO account for 1 per cent.

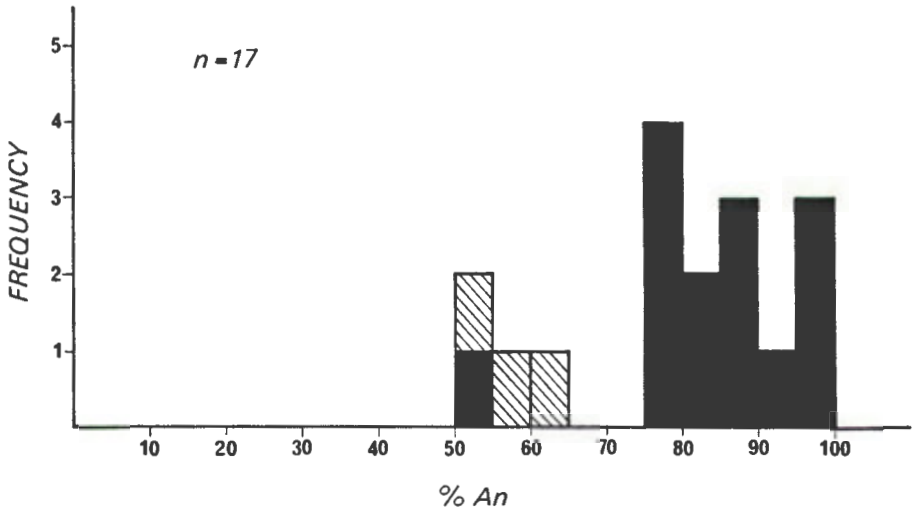


Fig. 56 Core compositions of plagioclase in calc-silicate rocks (determined by microprobe analyses - Appendix II, Table A2-21). Except for one specimen (containing plagioclase of $An_{96}$ composition) which has been collected in the granulite facies terrane, all other specimens are from the upper amphibolite facies terrane (see Appendix III ). Some grains display on microscopic examination an abrupt discontinuous zonation pattern. Core compositions of these grains have lower anorthite contents (hatched) compared to their surrounding rims (black with An > 75) yielding a bimodal distribution of plagioclase compositions. The zoned plagioclase grains are described in detail on page 151. Note the high anorthite contents (>$An_{75}$) for plagioclase in the majority of the specimens.

(c) Plagioclase

Optical examination of plagioclase coexisting with grandite and ferrosalite indicates a very high anorthite content. This is supported by microprobe analyses (Appendix II, Table A2-21). The anorthite contents of some plagioclases (determined by microprobe techniques) are shown as a frequency histogram in Fig. 56 and it is seen that the compositions generally plot into the bytownite and anorthite fields. A few specimens show a bimodal frequency distribution of plagioclase compositions. They contain zoned plagioclase grains, the cores of which are of labradorite composition (shown hatched in Fig. 56) while the surrounding rims are more calcic and of bytownite-anorthite composition (shown black in Fig. 56). These textures will be discussed in more detail (Section III D 3 a).

(d) Amphiboles

Calcic amphiboles are particularly common in mafic rocks and have already been discussed (Chapter III B). There are, however, some other amphiboles with different optical properties to the ones described previously and these are briefly considered now. Their most obvious microscopic feature is a very pale cream colour when viewed microscopically in plane polarised light. The host rocks are rich in calcium and magnesium. The amphiboles in two specimens (HA 997 and HA 1150), both collected in the granulite facies terrane, were analysed by microprobe techniques (Appendix II, Table A2-22) and were determined as tremolite-actinolite and magnesio-hornblende respectively (Fig. 57).

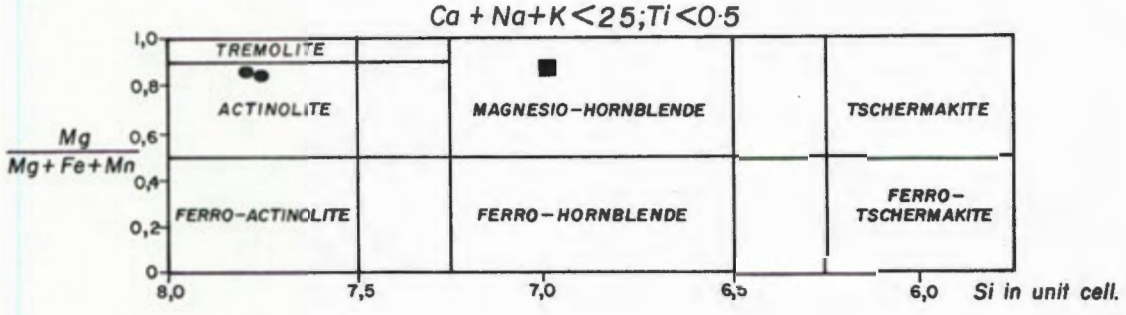


Fig. 57 Amphiboles in calcium-magnesium rich rocks plotted in terms of the Leake (1968) classification. (●) represents the amphibole composition in specimen HA 997 and (■) symbolises the composition of the amphiboles in specimen HA 1150. Both specimens have been collected on the farm Dabidas (407) in the granulite facies terrane.

Tremolite/actinolite-rich rocks (HA 997) occur as small lenses on the farm Dabidas (407) (D22, Fig. 52 ) within migmatitic biotite-garnet gneiss. These rocks contain large (± 2 centimetre), randomly orientated amphibole crystals.

Rather peculiar in hand specimens is the presence of abundant large cavities between the crystals. These cavities are not restricted to the weathered surface, but are also observed in the cores of fresh specimens.

Microscopic examination of one thin section has revealed a virtually monomineralic modal composition with a cream-coloured clinoamphibole accounting for 99 per cent of the mode, while quartz is present as a minor constituent. The presence of tremolite in the granulite facies terrane requires some explanation, because amphiboles of tremolite-actinolite composition are common in greenschist and amphibolite facies terranes (Winkler, 1967), but are not generally found in the granulite facies. Tremolite tends to decompose in carbonate-bearing rocks in response to rising metamorphic grade (Winkler, 1976). The question to consider in this respect is whether the observed tremolite must be interpreted as a retrograde mineral post-dating the main granulite facies metamorphism, or whether it is possible for tremolite to persist stably under the peak P-T conditions prevailing during granulite facies metamorphism.

In high grade rocks individual crystals are generally closely packed giving rise to a granoblastic polygonal texture. Cavities between crystals in high grade rocks can be formed if the minerals that previously occupied these spaces are subsequently leached out, e.g. carbonates removed by solution, or alternatively the cavities represent space previously occupied by a gas phase trapped in the rock. If carbonates (dolomite and/or calcite) once occupied the cavities, the tremolite could not have been stable under the physical conditions in the granulite facies, but is expected to react and yield assemblages containing diopside and forsterite. Some of the predicted reactions are as follows:

$$1\ \text{tremolite} + 3\ \text{calcite} + 2\ \text{quartz} \rightleftharpoons 5\ \text{diopside} + 3\ CO_2 + 1\ H_2O \quad (37)$$

$$1\ \text{tremolite} + 3\ \text{calcite} \rightleftharpoons 4\ \text{diopside} + 1\ \text{dolomite} + 1\ CO_2 + 1\ H_2O \quad (55)$$

$$1\ \text{tremolite} + 11\ \text{dolomite} \rightleftharpoons 8\ \text{forsterite} + 13\ \text{calcite} + 9\ CO_2 + 1\ H_2O \quad (47)$$

$$3\ \text{tremolite} + 5\ \text{calcite} \rightleftharpoons 11\ \text{diopside} + 2\ \text{forsterite} + 5\ CO_2 + 3\ H_2O \quad (56)$$

$$4\ \text{tremolite} + 5\ \text{dolomite} \rightleftharpoons 13\ \text{diopside} + 6\ \text{forsterite} + 10\ CO_2 + 4\ H_2O \quad (57)$$

No trace of either calcite, dolomite or diopside and forsterite has been recorded in the specimen studied. Therefore, it seems very unlikely that any of the above reactions were operative and there is no conclusive evidence in support of a retrograde origin of the tremolite.

If, on the other hand, it is assumed that the observed cavities in the rock were once occupied by a fluid phase we can consider tremolite stability in the presence of fluid (presumably $H_2O$ rich) and quartz under the physical conditions of granulite facies metamorphism. From experimental studies it is known that in the absence of carbonates, tremolite by itself is stable up to very high temperatures. It was pointed out in Chapter III B 8 that the pure end-member decomposes at a temperature of 870°C when $P_{H_2O} = P_{total} = 2$ kb (Boyd, 1959 - see Fig. 28 ) to yield diopside, enstatite and quartz according to the reaction:

$$\text{tremolite} \rightleftharpoons 2 \text{ diopside} + 3 \text{ enstatite} + \text{quartz} + H_2O \qquad (3)$$

The tremolite under discussion contains some iron and, therefore, its upper temperature stability limit will be less than that of the pure Mg-tremolite (Ernst, 1966). Nevertheless, the experimental data demonstrate that tremolite by itself is stable under granulite facies conditions provided that $P_{H_2O}$ is high. Therefore, no retrogression need be invoked to explain the occurrence of tremolite in the granulite facies terrane. High water pressures are, however, atypical for this environment and if tremolite was stable during granulite facies metamorphism, as advocated here, its presence suggests that $H_2O$-rich fluids do at least locally exist within the granulite facies terrane.

The second specimen (HA 1150) also from the farm Dabidas (407)(D22, Fig.52) contains the assemblage magnesio - hornblende + quartz. Secondary retrograde epidote-group minerals are seen to partially replace the amphibole. Like the tremolite this amphibole is characterised by a pale cream colour. Similar amphiboles, but with a much lower $^{Mg}/(Mg + Fe)$, ratio are recorded in common amphibolites.

## 3 Textures in Calc-silicate Rocks

The calc-silicate rocks in the study area generally display a granoblastic polygonal texture, but there are some specimens in which rather peculiar disequilibrium textures are recorded.

### (a) Zoned Plagioclase

Four of the calc-silicate specimens examined contain zoned plagioclase crystals of the type shown in Fig. 58.. Optical studies of the larger plagioclase crystal in the centre of Fig. 58a (grain 1) show that its optical properties are inhomogeneous and that the extinction angle changes abruptly at the interface between rim and core of the grain suggesting a compositional break. This is supported by microprobe analyses indicating a core of more sodic composition compared to the surrounding rim. Grain 1 has been analysed at ten spots (A, B, C, D etc.) along a traverse across the grain and the variation in anorthite content along this traverse is shown in Fig. 58b. These analyses are tabulated in Appendix II,.Table A2-23).Note the gradational continuous zonation in both rim and core and the abrupt change in chemical composition from $An_{74}$ to $An_{62}$ across the boundary between rim and core. Both the rim and core are increasingly enriched in Ca away from the centre of the grain and this type of zonation is generally referred to as reverse zoning (Homma, 1936; Smith, 1974). Virtually identical textures have been described for plagioclase in calc-silicate rocks in the Himalayas (Misch, 1964) and in basic charnockites (Leelanandam, 1968).

Within a specific specimen only some of the plagioclase crystals display this type of zonation. Often the sodic core is not continuous, but consists

of scattered patches in optical continuity and completely surrounded by the more calcic phase. The interface is generally smooth and rounded (resorption ? or due to diffusion ?), but never euhedral (growth zoning) as is common for igneous plagioclase (Smith, *op.cit.*).

Four additional plagioclase grains have been analysed (Appendix II, Table A2-21) in the same specimen at the centres of the crystals. The core compositions of these grains are plotted in Fig. 58c.. Two of the core analyses (grains 2 and 3) are from plagioclases displaying the same optical zonation as shown in Fig. 58a,b while the other two (grains 4 and 5) are from plagioclase grains characterised by a gradual continuous zonation, but lacking an optically detectable abrupt change in zonation. Plagioclase crystals of the type represented by grains 4 and 5 (Fig. 58c ) are dominant in the specimen. In Fig. 58c the bimodal distribution of plagioclase core compositions between the two types of plagioclase crystals within the same specimen (HA 1101) is displayed.

One way of interpreting these textures is that the more sodic cores represent remnants of an older disappearing phase, largely replaced by the more calcic mineral. The plagioclases lacking the abrupt zonation can be interpreted as those in which the replacement has either gone to completion or these grains might have nucleated at a later stage in the metamorphic history. Because the cores and rims have markedly different compositions it seems likely that they have originated under contrasting P-T conditions.

Reactions with plagioclase on the product side at constant pressure and fixed fluid compositions produce an increasing anorthite component in response to increasing temperature. Therefore, the observed zonation could be ex-

---

Fig. 58 (a) Drawing from a thin section of calc-silicate specimen HA 1101 showing discontinuous optical zonation in plagioclase grain 1 (blank). Twin lamellae (broken lines) are continuous across the optical boundary between grain core and rim. Andradite-grossular garnet (in black) occurs in contact with this plagioclase grain. Note that grandite is not always in contact with these zoned plagioclase crystals. Some are completely surrounded by other plagioclase grains.

(b) Compositional variation of the zoned plagioclase grain along a traverse A to J determined by microprobe analytical techniques. ABC etc. represent localities along the traverse and correspond to spot analyses tabulated in Appendix II, Table A2-23.

(c) Core compositions of other plagioclase grains in specimen HA 1101. Grains 2 and 3 display the same type of zonation as shown in (a) and grains 4 and 5 are two plagioclase crystals lacking an optically detectable abrupt change in zonation and display only a smooth continuous zonation.

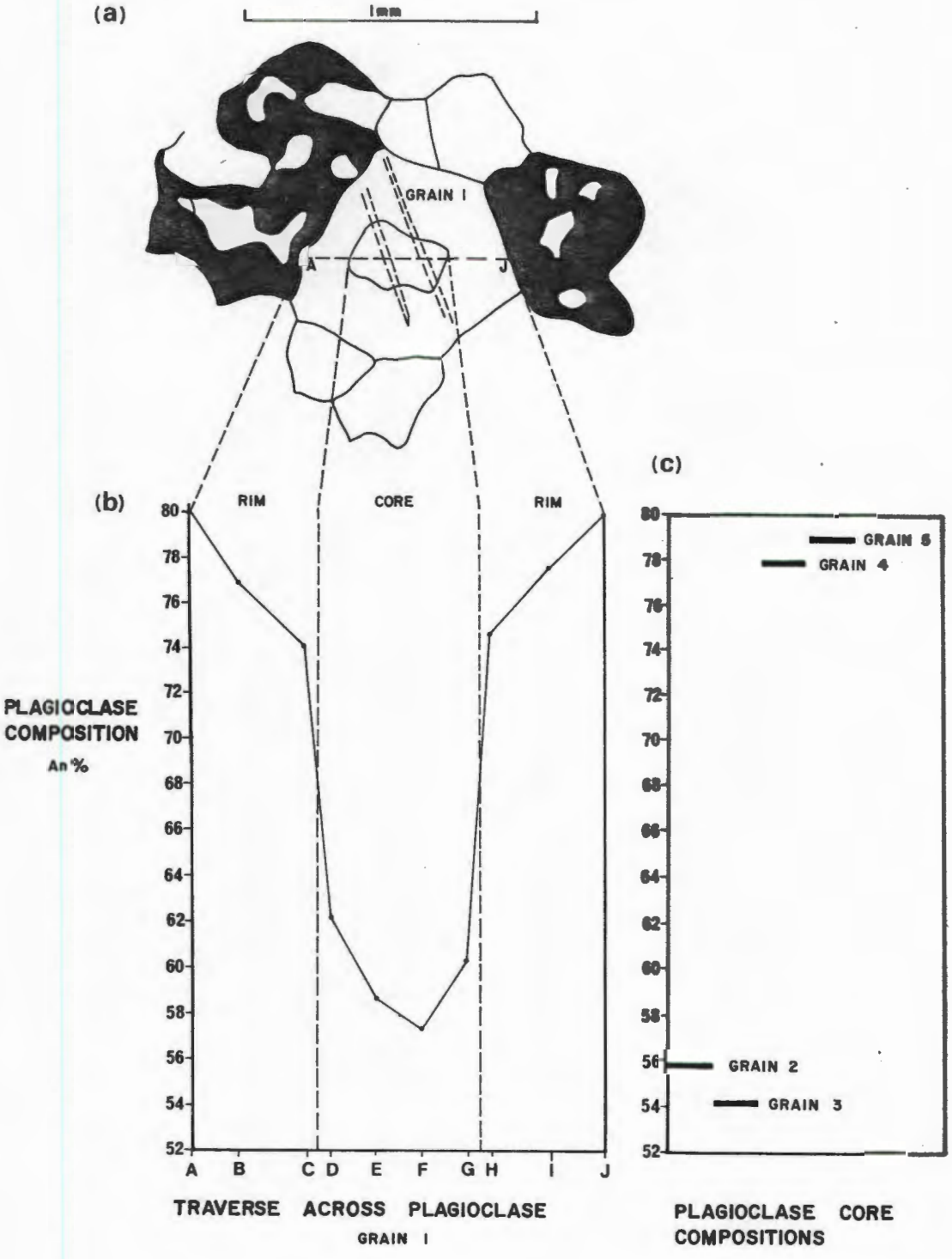
(a)
1mm
GRAIN 1
A
J
(b)
RIM
CORE
RIM
PLAGIOCLASE COMPOSITION
An %
80
78
76
74
72
70
68
66
64
62
60
58
56
54
52
A B C D E F G H I J
TRAVERSE ACROSS PLAGIOCLASE GRAIN 1
(c)
GRAIN 5
GRAIN 4
GRAIN 2
GRAIN 3
PLAGIOCLASE CORE COMPOSITIONS

plained in terms of prograde metamorphism. If, for example, two minerals A and B react to produce plagioclase amongst other phases, the early formed plagioclase will have a lower An content and with increasing temperature the anorthite content in plagioclase increases. If one of the reactants is used up, this plagioclase-producing reaction terminates. With a further increase in temperature another plagioclase-forming reaction may be crossed in P-T space where plagioclase of a much higher anorthite content may be produced. At these elevated temperatures the earlier formed more sodic plagioclase components are no longer in equilibrium with the system and will attempt to re-equilibrate. Complete equilibrium is, however, not attained, otherwise these textures would not have been preserved. Smith (*op.cit.*) has suggested that the early formed plagioclase is difficult to transform due to the high activation energies involved in diffusion of Si and Al.

Alternatively, a drop in pressure at otherwise constant conditions could also cause an increase in the An-content of the plagioclase.

(b) Grandite Coronas

Andradite-grossular garnet is frequently observed to form coronas or partial coronas along the interface between ferrosalite and quartz or ferrosalite and plagioclase (Fig. 59). The manner in which grandite surrounds the clinopyroxene suggests that it forms at the expense of the pyroxene. It is, however, not clear whether to interpret this texture as resulting from prograde metamorphism, i.e. garnet is replacing the ferrosalite in response to increasing metamorphic grade or whether this texture indicates retrogression i.e. garnet forms at the expense of clinopyroxene during uplift and cooling. According to Miyashiro (1973a) Ca-garnet makes its first appearance in the epidote-amphibolite or amphibolite facies and apparently forms at a higher temperature than diopside. This is shown by the prograde sequence observed in the Pyrenees (Bard, 1969). The garnet shown in Fig.59 is particularly rich in the andradite molecule and little is known about the stability of these minerals. In the majority of the specimens studied ferrosalite and grandite coexist in equilibrium (at least texturally) up to the highest grades of regional metamorphism.

(c) Epidote-Zoisite Coronas

Epidote group minerals are frequently observed to form coronas around grandite in specimens of calc-silicate rocks from the amphibolite facies terrane. These coronas are developed along the interface between grandite and plagioclase and consist of two layers. The more prominently developed layer is composed of epidote which always occurs closest to the garnet , while a second less prominent layer consists of zoisite and is always observed along the contact with plagioclase (Fig. 60 ). Microprobe analyses of epidote and zoisite are provided in Appendix II, Table A2-24. The epidote analysis has been recalculated in order to correct for $Fe^{+3}$ by the method outlined in Appendix ID. . The corona texture displayed in Fig.60 indicates that the epidote group minerals have formed at the expense of grandite and plagio-

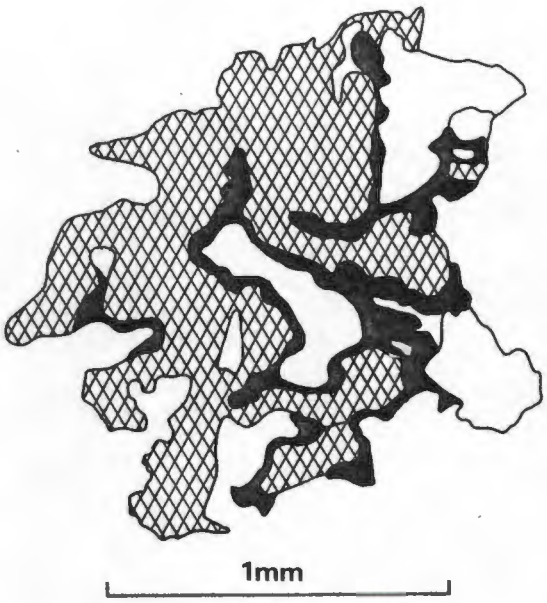


Fig. 59 Partial corona of grandite (black) along the interface between ferrosalite (cross-hatched) and plagioclase (blank)(Specimen HA 1031).

clase and the following reaction is consistent with the observed texture:

$$\text{grandite} + \text{plagioclase} + H_2O \rightleftharpoons \text{epidote} + \text{zoisite} \quad \text{(unbalanced)} \qquad (58)$$

In order to evaluate this reaction in terms of changing physical conditions during metamorphism it is appropriate to review some of the relevant experimental data on reactions involving epidote group minerals.

According to Winkler (1976) zoisite makes its first appearance in low grade metamorphism roughly between 350 and 400°C. Above this temperature zoisite has a large stability field depending primarily on the presence or absence of quartz and the composition of the gas phase. With increasing metamorphic grade the mineral breaks down in the presence of quartz to yield grossularite and anorthite according to the reaction:

$$4 \text{ zoisite} + 1 \text{ quartz} \rightleftharpoons 1 \text{ grossularite} + 5 \text{ anorthite} + 2\ H_2O \qquad (44)$$

This reaction has been experimentally investigated by Strens (1965, 1968), Nitsch and Winkler (1965), Newton (1966), Boettcher (1970), Holdaway (1972) and Liou (1973) and determines the upper temperature stability limits of zoisite in the presence of quartz (it is depicted as curve (44) in Fig.53, p.139). According to Holdaway (*op.cit.*) and Liou (*op.cit.*) at a pressure of $P_{fluid}$ = 5 kb, this reaction takes place at 650°C. The experimental data of Newton (*op. cit.*) and Boettcher (*op.cit.*) on this reaction at $P_{fluid}$ = 5 kb suggest lower

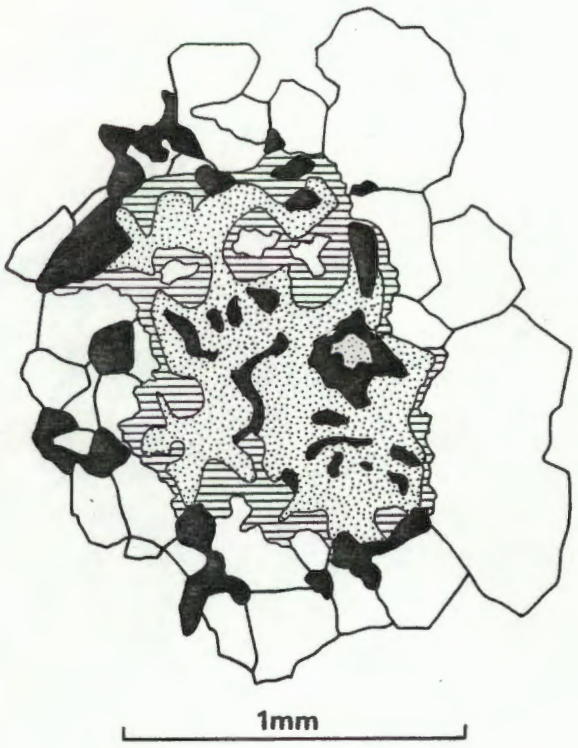


Fig. 60 The development of epidote coronas around grandite in calc-silicate rocks (Specimen HA 1148). Grandite (black) is surrounded by a rim of epidote (stippled), followed by a rim of zoisite (hatched) along the interface with plagioclase (blank). Note that the epidote is always in contact with grandite and zoisite always occurs along the plagioclase contact.

---

temperatures of 620°C and 630°C respectively. Holdaway (*op.cit.*) has investigated experimentally the influence of $fO_2$ on the stability of the epidote group minerals and has concluded that reducing conditions lower the breakdown temperatures of epidote relative to the oxidising environment. At the same time epidote becomes more aluminous and the grandite produced by its breakdown is increasingly enriched in grossularite.

The stability of zoisite is very dependent on the composition of the gas phase. With increasing mole fraction of $CO_2$, zoisite breaks down according to the reaction:

$$2 \text{ zoisite} + 1\ CO_2 \rightleftharpoons 3 \text{ anorthite} + 1 \text{ calcite} + H_2O \qquad (59)$$

experimentally determined at $P_{fluid}$ = 2 kb, 5 kb and 7 kb by Storre and Nitsch (1972) and shown as curve (59) in Fig. 53, p.139. According to them the equilibrium shifts to slightly higher $X_{CO_2}$ concentrations with increasing pressure and to quote some figures:

at $P_{fluid}$ = 2 kb the equilibrium gas phase contains 2 mole per cent $CO_2$ and at $P_{fluid}$ = 5 kb and $P_{fluid}$ = 7 kb, 6 mole per cent and 10 mole per cent respectively (Storre and Nitsch, *op.cit.*) demonstrating that the presence of zoisite demands a very low partial pressure of $CO_2$ in the gas phase. Impurities in zoisite (notably $Fe_2O_3$ substitution for $Al_2O_3$ and substitution of $Na_2O$ for CaO in plagioclase will have opposing effects on the position of this equilibrium (the former will shift the equilibrium of reaction (59) towards higher mole fractions of $CO_2$ while the latter will cause a shift towards the lower $CO_2$ concentration). Thus, even for natural "impure" phases the eipdote group mineral will only be stable at low $X_{CO_2}$.

Reaction (59) determines the stability of zoisite with respect to $X_{CO_2}$ and is applicable whether quartz is absent or not because it is not involved in the reaction.

In the absence of quartz the stability field of zoisite is enlarged and at high grade metamorphism the mineral breaks down according to the reaction:

$$6 \text{ zoisite} \rightleftharpoons 6 \text{ anorthite} + 2 \text{ grossularite} + 1 \text{ corundum} + 3\ H_2O \qquad (60)$$

experimentally investigated by Newton (1965) and Boettcher (*op.cit.*) and depticted as curve (60) in Fig. 53, page 139. This reaction occurs about 100°C above reaction (44) in an isobaric section. However, it is not recognised in the present area because corundum has not been found in any of the assemblages.

The experimental data on reactions involving epidote group minerals support a retrograde origin for the corona textures displayed in Fig. 60 and it is concluded that the epidote group minerals have been formed after the main regional metamorphism in response to uplift and cooling.

## E Mineral Assemblages Recorded in Minor Rock-types

Amongst the less common lithologies are olivine-bearing mafic and ultramafic rocks as well as *manganiferous* rocks and without considering the mineral assemblages recorded in these, this study would be incomplete.

### 1 Mineral Assemblages in Olivine-bearing Mafic and Ultramafic Rocks

Coexisting minerals in one metamorphosed ultramafic specimen (HA 601) from the outcrops on the farm Obees (402)(Fig. 62, H 25) were analysed by microprobe techniques (Appendix II, Table A2-25) and found to contain the following mineral paragenesis (the minerals are arranged in order of

(a)

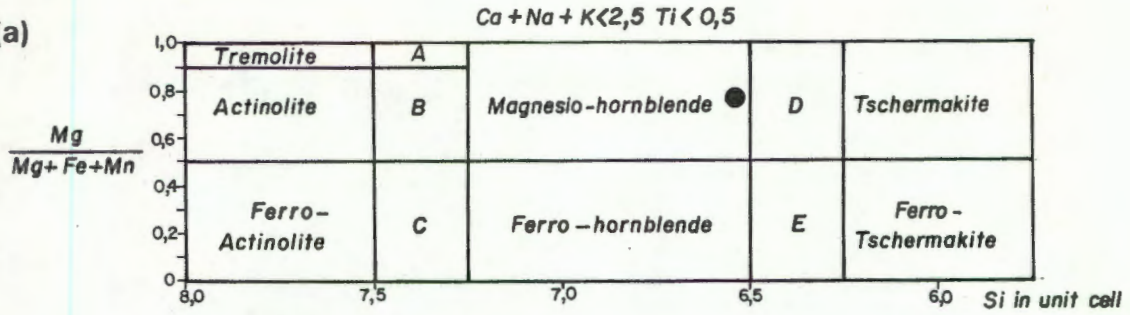


A Tremolitic hornblende
B Actinolitic hornblende
C Ferro-actinolitic hornblende
D Tschermakitic hornblende
E Ferro-tschermakitic hornblende

(b)

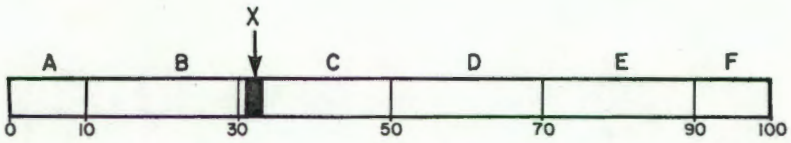


A Forsterite
B Chrysolite
C Hyalosiderite
D Hortonolite
E Ferro-hortonolite
F Fayalite

(c)

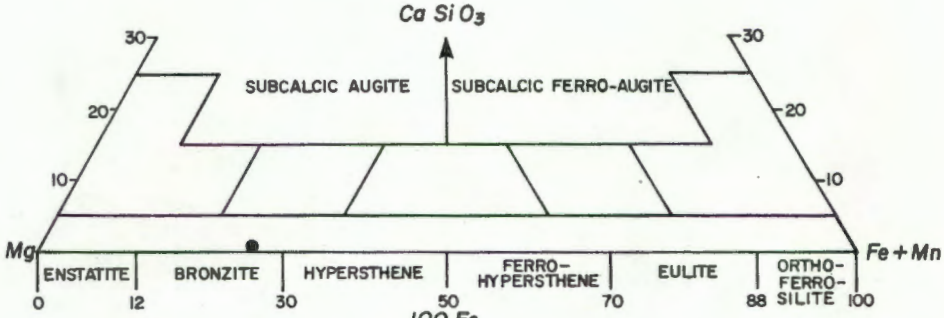


(d)

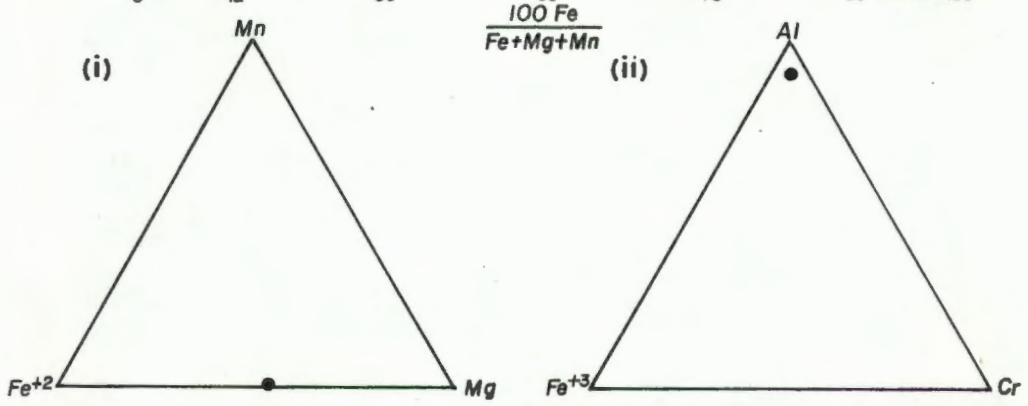

decreasing abundance:

'magnesio-hornblende + hyalosiderite + bronzite + hercynite-spinel solid solution + opaque minerals'.

The amphibole contains Ca-ions in excess of 1,50 per half unit cell and is according to Leake (1968) referred to as calciferous. In the classification of Leake (*op.cit.*) the chemical composition of this mineral plots into the field of magnesio-hornblende (Fig. 61a) with an $^{Mg}/(Mg+Fe+Mn)$ ratio of 0,78.

Core compositions of the three olivine grains analysed are fairly uniform with an $^{Mg}/(Mg+Fe)$ ratio of 0,68. In terms of the nomenclature used in Deer *et al.* (1971) the olivine composition plots into the field of hyalosiderite (Fig. 61b). Olivine in metamorphic rocks has been reported from several localities in the Namaqualand Metamorphic Complex; e.g. Joubert (1971a) records the paragenesis 'pale green hornblende + clinopyroxene + orthopyroxene + olivine' from Bles Krantz and 'brown hornblende + olivine + hypersthene' from the Leliefontein Reserve. Olivine-bearing mafic rocks are also described from the Keimoes area (von Backström, 1964) the Aus area (Jackson, 1976) and the Onseepkans area (Toogood, 1976).

The orthopyroxene in specimen HA 601 has the chemical composition of bronzite ($^{Mg}/(Mg+Fe+Mn)$ = 0,74)(Fig. 61c). This mineral contains 3,0 weight per cent $Al_2O_3$ and as it coexists with spinel, the orthopyroxene can be considered to be saturated with respect to $Al_2O_3$. The Al-content of orthopyroxene is regarded to be a function of temperature (Anastasiou and Seifert, 1972). Considerably higher $Al_2O_3$ contents (5,3 weight per cent $Al_2O_3$) have been reported for bronzite in the paragenesis 'bronzite + plagioclase + tschermakite + hercynite + opaque minerals' (Jack, 1980). Aluminous bronzite has also been reported from the Nababeep District where this mineral is coexisting with sapphirine and cordierite and is reported to contain 7,0 per cent $Al_2O_3$ (Clifford *et al.*, 1975b).

Small amounts of green spinel appear in specimen HA 601. Microprobe analyses for three grains have been corrected for $Fe^{+3}$ by the method outlined in Appendix ID. According to Deer *et al.* (*op.cit.*) the spinel group of minerals can be subdivided into three series depending on the trivalent ion. The spinel series is characterised by $Al^{+3}$, magnetite series by $Fe^{+3}$ and the

---

Fig 61 Compositions of coexisting minerals in ultramafic rock specimen HA 601 from the granulite facies terrane.

(a) Core composition of hornblende (solid dot) plotted in terms of the Leake (1968) classification.
(b) Core composition of olivine (indicated with X) plotted in terms of Deer *et al.* (1971) classification.
(c) Core composition of orthopyroxene (solid dot) plotted in terms of Deer *et al.* (1971) classification.
(d) Spinel core compositions (i) plotted in terms of the divalent ions ($Fe^{+}$, Mg, Mn) (ii) plotted in terms of the trivalent ions (Al, $Fe^{+3}$, Cr.).

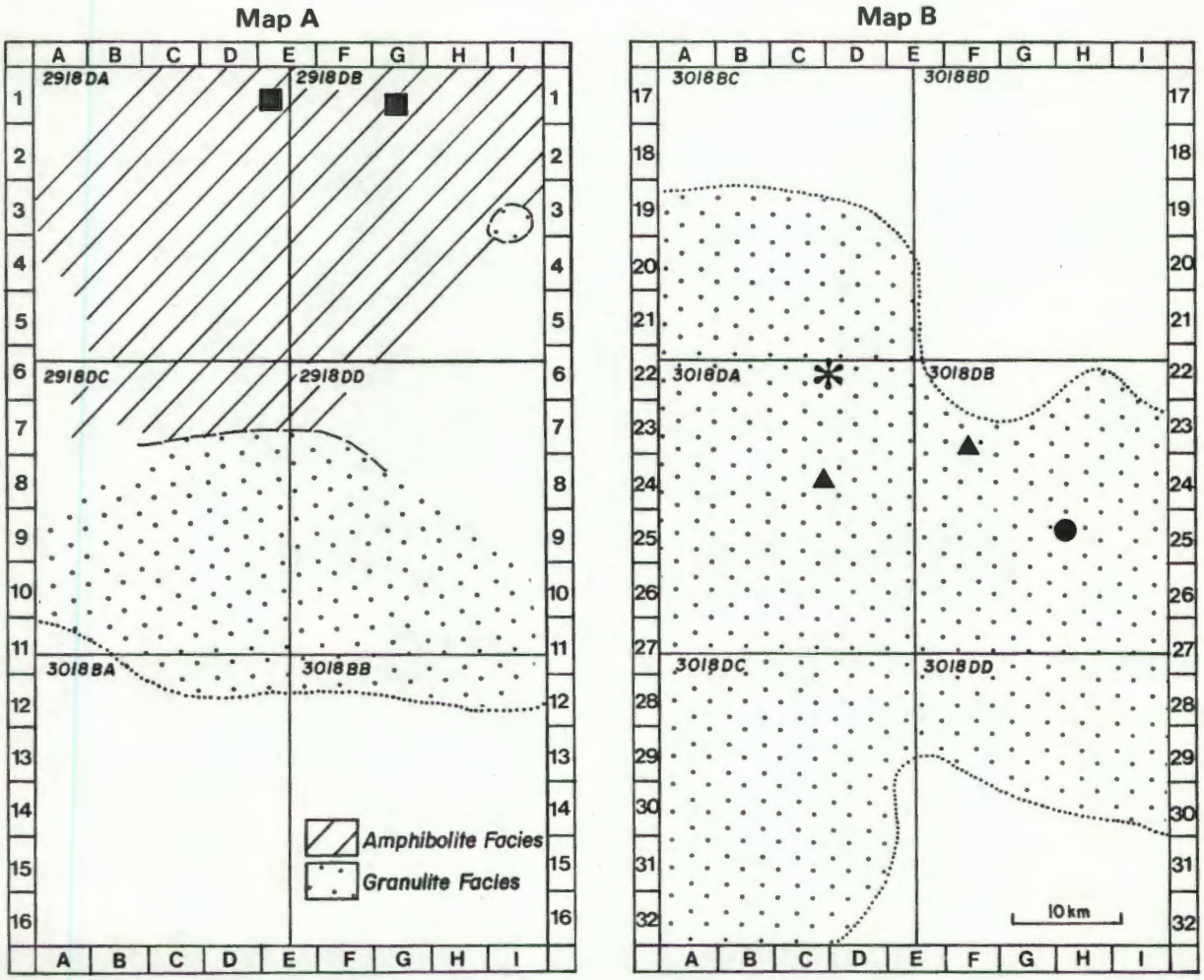


Fig. 62 Geographic distribution of mineral assemblages in minor rock types: Ultramafic and related rocks (solid symbols)

- ● magnesio - hornblende + hyalosiderite + bronzite + hercynite - spinel solid solution + opaque minerals
- ▲ orthopyroxene + plagioclase + amphibole + olivine + green spinel + opaque minerals (± biotite)
- ■ orthopyroxene + plagioclase + olivine + clinopyroxene + amphibole + green spinel + opaque minerals (± biotite) ± zircon

Manganiferous rocks:

- ✱ ferroaugite + quartz + magnetite + spessartine-rich garnet + pyroxmangite

chromite series by $Cr^{+3}$. The chemical compositions of the three spinel grains analysed fall into the category of the spinel series which accounts for 93 per cent of the bulk composition, while the magnetite and chromite series components account for 4 and 3 per cent, respectively. In terms of the end-member molecules the spinel analyses can be expressed as follows (the end-member molecules are arranged in order of decreasing abundance and the contribution of each molecule expressed in molecular per cent is indicated in brackets).

| | | |
|---|---|---|
| spinel $MgAl_2O_4$ | - | (49,13 per cent) |
| hercynite $FeAl_2O_4$ | - | (43,01 per cent) |
| magnesioferrite $MgFe_2^{+3}O_4$ | - | ( 4,06 per cent) |
| chromite $Fe^{+2}Cr_2O_4$ | - | ( 2,96 per cent) |
| galaxite $MnAl_2O_4$ | - | ( 0,42 per cent) |
| ulvöspinel $Fe_2^{+2}TiO_4$ | - | ( 0,26 per cent) |

The chemical compositions of the spinels are plotted in terms of the divalent ions ($Fe^{+2}$, Mg and Mn) in Fig. 61d(i) and in terms of the trivalent ions ($Al^{+3}$, $Fe^{+3}$ and $Cr^{+3}$) in Fig. 61d(ii). In summary then, the spinels in specimen HA 601 are essentially a solid solution between spinel *(senso stricto)* and hercynite. They contain about 2,8 weight per cent $Cr_2O_3$ and 4,4 weight per cent $Fe_2O_3$.

Coexisting minerals in other metamorphosed olivine-bearing mafic rocks have not been analysed. The following mineral assemblages are recorded:

'orthopyroxene + olivine + plagioclase + clinopyroxene + amphibole + green spinel + opaque minerals (± biotite)'

'orthopyroxene + plagioclase + brown amphibole + olivine + green spinel + opaque minerals (± biotite)'.

The geographic localities of these mineral assemblages are shown in Fig. 62 from which it is evident that two of the orthopyroxene-bearing specimens (HA 1112 and HA 1145) occur in a terrane that is otherwise underlain by mafic mineral assemblages lacking orthopyroxene and that are characteristic of the amphibolite facies.

Recently Obata and Thompson (1981) have constructed grids for the model system $CaO+MgO+Al_2O_3+SiO_2+H_2O$ applicable to metamorphism of ultramafic and related rocks. These grids (relevant parts are reproduced in Fig.63 ) are designed with special reference to the role of hydrous minerals and their stability relations in the presence of various anhydrous phases. They demonstrate the modifying effect of these hydrous phases on the anhydrous high temperature gabbro-granulite-eclogite transition.

The presence of orthopyroxene in the specimens from the study area indicate high grade metamorphic conditions (Evans and Trommsdorff, 1970; Winkler, 1976) equivalent to the regional hypersthene zone. Orthopyroxene is intro-

duced by the breakdown of amphibole in reactions of the type:

tremolite $\rightleftharpoons$ diopside + enstatite + quartz + $H_2O$ (3) (Boyd, 1959)

or if olivine is present the amphibole breaks down at lower temperatures

tremolite + forsterite $\rightleftharpoons$ diopside + enstatite + $H_2O$ (61) (Delaney and Helgeson, 1978).

In the presence of $Al_2O_3$ various aluminous minerals can form in addition to pyroxenes. These aluminous phases are good relative barometers, as plagioclase is the stable phase at low pressures, spinel at intermediate pressures and garnet at high pressures (Kushiro and Yoder, 1966; Green and Ringwood, 1967; Emslie, 1970; Frost, 1976; Herzberg, 1976a,b; Jenkins and Newton, 1979; Obata and Thompson, *op.cit.*)

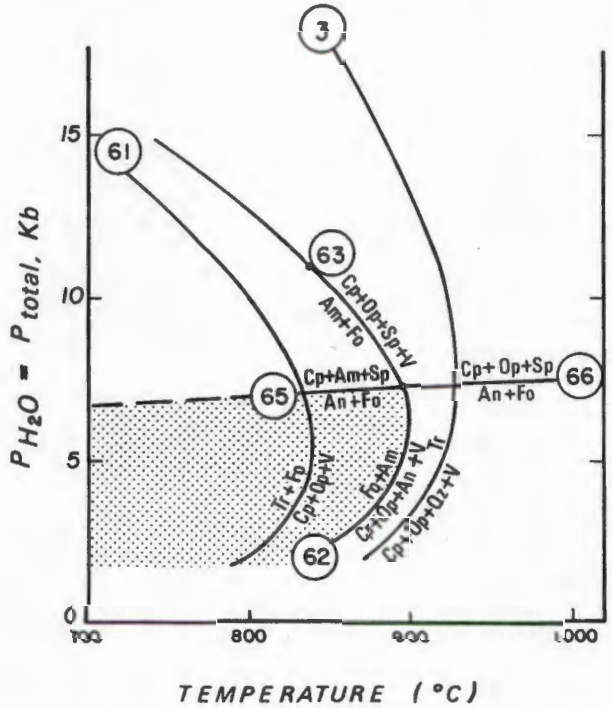


Fig. 63 Estimated P-T positions of some univariant curves in CMASH relevant to the metamorphism of olivine-bearing mafic rocks, reproduced after Obata and Thompson (1981). Circled numbers correspond to reactions mentioned in the text. Abbreviations as in preface. The stippled area indicates the likely P-T conditions during regional metamorphism.

The coexistence of amphibole and olivine in the specimens from the study area places a restriction on the maximum possible temperatures during metamorphism (Fig. 63). Depending on the pressures prevailing during metamorphism coexisting amphibole and olivine decompose at high temperatures via

the following equilibria (see Fig. 63 ):

at low pressures: amphibole + forsterite $\rightleftharpoons$ clinopyroxene + orthopyroxene + anorthite + vapour (62)

at intermediate pressures: amphibole + forsterite $\rightleftharpoons$ clinopyroxene + orthopyroxene + spinel + vapour (63)

at high pressures: amphibole + forsterite $\rightleftharpoons$ clinopyroxene + orthopyroxene + garnet + vapour (64)

The observed coexistence of amphibole and olivine implies temperatures below the amphibole + forsterite breakdown reactions (i.e. < 900°C according to Obata and Thompson, *op.cit.*).

The co-existence of plagioclase and olivine places an upper pressure limit on the regional metamorphism as these two minerals can only coexist stably under low pressure conditions. In response to rising pressure plagioclase and olivine react according to:

anorthite + forsterite + vapour $\rightleftharpoons$ amphibole + clinopyroxene + spinel (65)

and anorthite + forsterite $\rightleftharpoons$ clinopyroxene + orthopyroxene + spinel (66)

In one of the specimens (HA 550) plagioclase and olivine occur in contact, implying pressures less than those required for anorthite and forsterite to react (equilibria 65 and 66). In the other specimens olivine and plagioclase are generally shielded from each other by corona-forming minerals, suggesting that although plagioclase and olivine must have been stable during peak conditions of regional metamorphism, they were subsequently no longer so due to physical changes in the environment.

The upper pressure stability limit for coexisting "olivine and plagioclase" has been determined experimentally (Kushiro and Yoder, 1966; Green and Ringwood, 1967; Irving and Green, 1970; Emslie, 1970). These experiments have shown that equilibria (65) and (66) have a very shallow $\frac{dP}{dT}$ slope (Fig. 63 ) and in the temperature range 700-900°C applicable to the metamorphism of the study area, coexisting olivine and plagioclase-bearing assemblages are only possible at low pressures not exceeding 6 to 8 kb.

## 2 Corona Textures

Two basic types of corona textures are recorded in these rocks:

(a) Olivine - plagioclase coronas
(b) Opaque minerals (± spinel) - plagioclase coronas

The olivine-plagioclase coronas are dominant and are made up of successive concentric shells between olivine and plagioclase (Fig. 64). The olivine is invariably surrounded by an inner shell of orthopyroxene replacing the olivine. This is followed by an intermediate shell of generally inclusion-free

amphibole and an outer shell of an amphibole-spinel symplectite. The pale green to brown amphibole of the middle and outer shells are in optical continuity. Opaque dust is crowded along irregular cracks and grain boundaries of the olivine. The spinel in the symplectite occurs as small worm-shaped rods or vermicules that are generally orientated radially at right angles to the adjacent plagioclase contact. Occasionally the orthopyroxene shell is in direct contact with plagioclase without amphibole and symplectite shells in between.

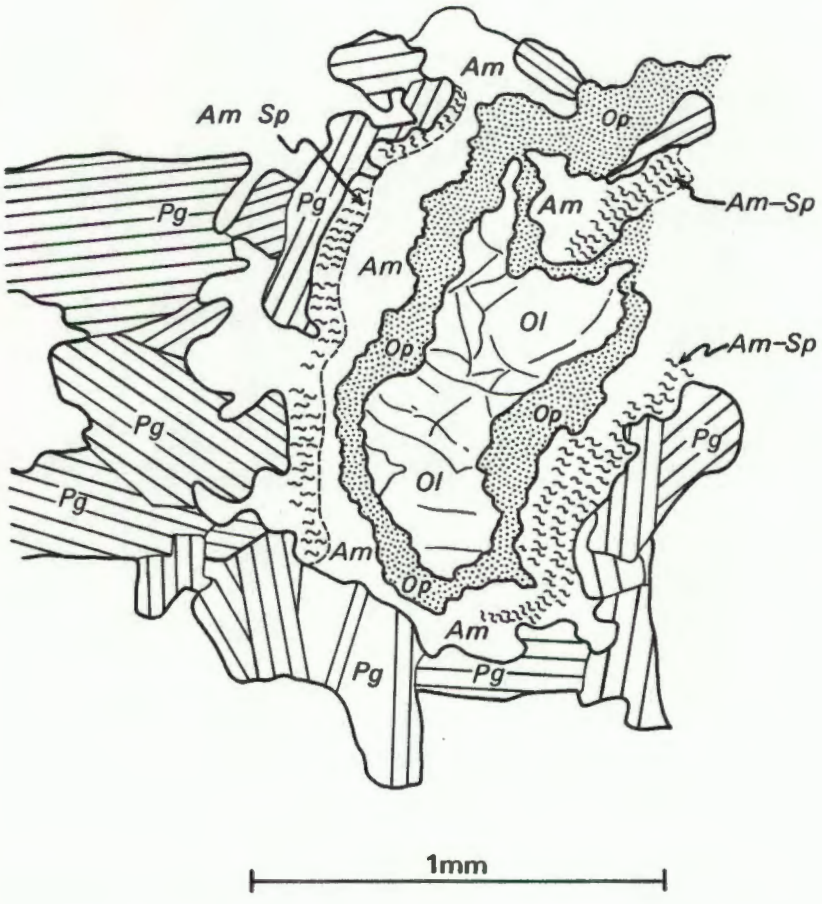


Fig. 64 Corona textures between olivine and plagioclase in olivine-bearing mafic rocks (specimen HA 1145) from the amphibolite facies terrane. Note that an inner shell of orthopyroxene (Op stippled) encloses the grain of olivine (Ol). An outer shell of an amphibole-spinel symplectite (Am-Sp) is situated adjacent to the plagioclase (Pg) contact, with inclusion-free amphibole (Am) in between.

Identical corona textures involving orthopyroxene + amphibole + spinel along the interface between plagioclase and olivine are frequently described

in the literature (Mason, 1967; Frodesen, 1968; Starmer, 1969; England, 1974; Grieve and Gittins, 1975; Sapountzis 1975; Esbensen, 1978; van Lamoen, 1979). Occasionally the replacement of olivine is reported to have gone to completion and orthopyroxene is then present as pseudomorphs (e.g. Frodesen, *op.cit.*). Sometimes garnet is recorded along the interface between amphibole and plagioclase (e.g. Frodesen, *op.cit.*; Starmer, *op.cit.*; Grieve and Gittins, *op.cit.*) and van Lamoen (*op.cit.*) records a thin orthopyroxene - spinel symplectite, separating the amphibole - spinel symplectite from the plagioclase.

Corona textures are generally regarded to provide visible evidence for subsolidus reactions between primary mineral phases in response to changes in physical conditions of their environment (Reynolds and Fredrickson, 1962; Murthy, 1958; Mason, *op.cit.*; Frodesen, *op.cit.*; Starmer, *op.cit.*; Griffin, 1971a,b, 1972; Griffin and Heier, 1969, 1971, 1973; Griffin and Raheim, 1973; England, *op.cit.*; Grieve and Gittins, *op.cit.*; Sapountzis, *op.cit.*; Esbensen, *op.cit.*; van Lamoen, *op.cit.*). Various modes of origin have been suggested for corona formation, including regional metamorphism, thermal metamorphism, metasomatism, retrograde metamorphism and the formation of coronas during cooling of magmatic rocks under constant or increasing pressure.

Most authorities on the subject seem to agree on a sub-solidus mechanism for corona formation involving diffusion of ions via a fluid phase, but the principal discussion is concerned with an open-system reaction involving addition or removal of material versus a closed-system reaction in which diffusion of ions is restricted to those parts of olivine and plagioclase involved in the reaction, but with no additives except for water. Although many authors prefer a closed system reaction model (Mason, *op.cit.*; Frodesen, *op.cit.*; Whitney and McLelland, 1973; England, *op.cit.*; Sapountzis, *op.cit.*; Esbensen, *op.cit.*), van Lamoen (*op.cit.*) has recently argued in favour of an open-system reaction of the type:

$$1{,}0 \text{ olivine} + 1{,}06 \text{ plagioclase} + (0{,}28\ Fe + 0{,}74\ Mg + 0{,}36\ H_2O)\ \text{fluid} \rightleftharpoons$$
$$1{,}36 \text{ orthopyroxene} + 0{,}36 \text{ amphibole} + 0{,}16 \text{ spinel} + (0{,}31\ Na + 0{,}37\ Al)\ \text{fluid} \quad (67)$$

The above reaction is deduced from petrographical and electron microprobe studies (van Lamoen, *op.cit.*) and, as written, requires addition of Fe, Mg and $H_2O$ and the removal of Na and Al from the corona site, thus suggesting an allochemical system.

Equal volume replacement of olivine by orthopyroxene and plagioclase by amphibole and spinel is generally advocated with the present orthopyroxene-amphibole interface believed to correspond to the pre-existing olivine - plagioclase contact (Murthy, *op.cit.*; Mason, *op.cit.*; Frodesen, *op.cit.*; van Lamoen, *op.cit.*) Grieve and Gittins (*op.cit.*), however, conclude that an equal volume model in a closed system leads to excess $Al_2O_3$, CaO and $Na_2O$ and insufficient $SiO_2$, FeO and MgO. To account for the discrepancy, they suggest an alternative model involving the inside migration of the orthopyroxene - hornblende (± spinel) boundary away from the pre-existing olivine - plagioclase

contact towards olivine, implying that the present boundary between the reaction products does no longer correspond with the original contact between the reactants.

Another corona-like texture is recorded between ore minerals and plagioclase (Fig. 65). The ore consists of opaque minerals, presumably ilmenite and titano-magnetite and subordinate green spinel and is generally surrounded by two concentric shells, a thin inner shell consisting of inclusion-free amphibole followed by an outer shell of an amphibole - spinel symplectite. The spinel in the symplectite occurs as worm-shaped rods arranged radially around the ore and at right angles to the amphibole - plagioclase contact.

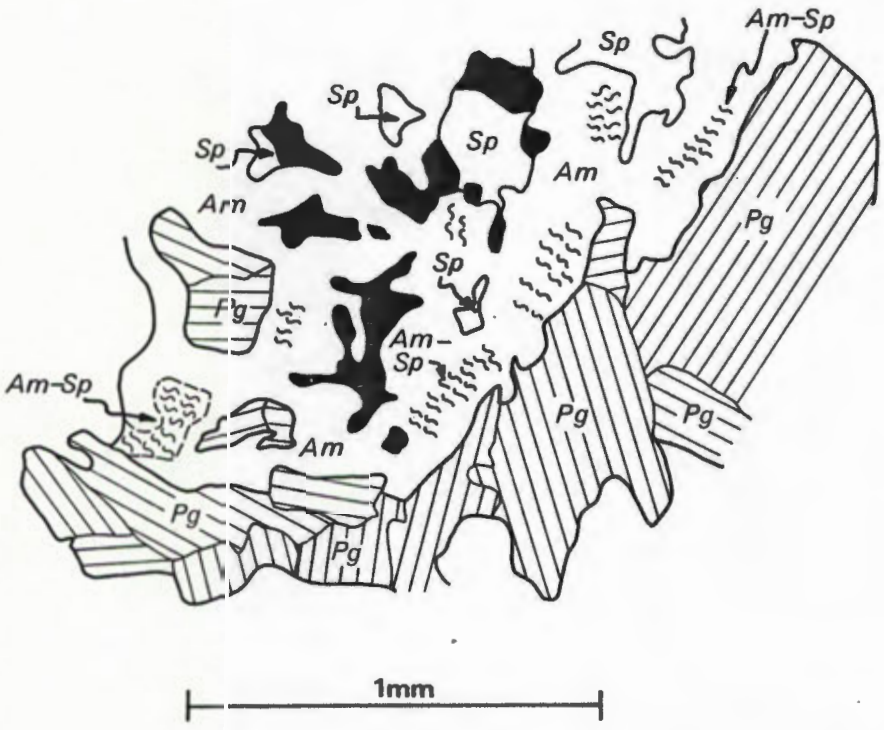


Fig. 65 Corona textures observed between opaque minerals (black) + green spinel (Sp) and plagioclase (Pg) in olivine-bearing mafic rocks (specimen BA 1145) from the amphibolite facies terrane. The ore minerals are surrounded by amphibole (Am) and an amphibole - spinel symplectite (Am-Sp) the latter of which is generally developed in proximity to the plagioclase contact.

Similar textures are described in the literature (e.g. Grieve and Gittins, 1973; Esbensen, 1978; van Lamoen, 1979), sometimes with minor modifications. Grieve and Gittins (*op. cit.*) record an inner rim or red-brown biotite followed by an outer rim of amphibole and spinel and van Lamoen (*op. cit.*) records orthopyroxene amongst the hornblende - spinel symplectite. Based on petrographic

and microprobe studies the latter author proposes a reaction of the type:

$$1{,}0 \text{ plagioclase} + 0{,}34 \text{ magnetite} + (1{,}09\ Mg + 0{,}39\ H_2O)_{fluid} \rightleftharpoons$$

$$0{,}39 \text{ hornblende} + 0{,}15 \text{ spinel} + (0{,}10\ Na + 0{,}30\ Al + 0{,}16\ Fe + 0{,}08\ O_2)_{fluid} \quad (68)$$

From petrographic observations it is concluded here that the observed corona textures provide visible evidence for reaction between primary minerals and that these reactions can be expressed in general terms as follows:

$$\text{olivine} + \text{plagioclase} + H_2O \rightleftharpoons \text{orthopyroxene} + \text{amphibole} + \text{spinel} \quad (69)$$

$$\text{ore minerals} + \text{plagioclase} + H_2O \rightleftharpoons \text{amphibole} + \text{spinel} \quad (70)$$

3 The Occurrence of Orthopyroxene in the Amphibolite Facies Terrane

Two of the olivine-bearing coronite specimens (HA 1145 and HA 1112) have been collected in an area in which other mafic lithologies lack orthopyroxene and contain mineral assemblages characteristic of the amphibolite facies (Fig. 62,p.160). As the presence of orthopyroxene in these specimens indicates environmental conditions equivalent to those in the granulite facies terrane, these two occurrences are anomalous and warrant special mention.

In relatively dry ultramafic rocks under appropriate P-T conditions olivine and plagioclase react to form pyroxenes and spinel (Griffin and Heier, 1973; Obata and Thompson, 1981) via equilibria of the type in reaction (66) (Fig. 63). From experimental studies it is known that reaction (66) has a positive $\frac{dP}{dT}$ slope (Kushiro and Yoder, 1966; Emslie, 1970). This implies that the pyroxene-spinel assemblage is produced from the breakdown of olivine and plagioclase in response to rising pressure and or falling temperature. If water is introduced into this system hydrous phases such as amphibole can be generated by a reaction of the type documented in the corona textures described above (reaction 69). The analogy to the anhydrous reaction suggests that the partially hydrated corona (amphibole + orthopyroxene + spinel) between primary olivine and plagioclase froms in response to declining temperatures and/or rising pressure. The fact that amphibole has formed at the expense of anhydrous minerals documents that water was introduced into the system. It seems unlikely that the confining pressure has increased subsequent to the crystallisation of olivine and plagioclase and it is suggested that the most plausible explanation for the formation of these partially hydrated coronas involves cooling with the introduction of some water. This must have occurred at considerable depth (at least a few Kb) because olivine and plagioclase are stable at shallow crustal levels (Fig. 63).

The presence or absence of orthopyroxene at elevated temperatures is to a large degree a function of the activity of water in the gas phase. In dry rocks orthopyroxene will be stable to lower temperatures compared to equivalent, but more hydrous rocks (Spear, 1981). The fact that orthopyroxene has developed in the coronas suggests that only limited amounts of water were introduced and from the host rock mineralogy it is apparent that these rocks were initially rather dehydrated. This initial dry nature can account for the formation of orthopyroxene within the amphibolite facies environment.

Metamorphosed orthopyroxene-bearing rocks in areas of lower than granulite facies metamorphic grades are not unique to the Namaqualand Metamorphic Complex, but have been described in the literature from other terranes. For example, Frodesen (1968) records the development of orthopyroxene in olivine-plagioclase coronas in lower facies metamorphic terranes (e.g. Bamble and Solör areas, South Norway). Esbensen (1978) points out that the coronas between olivine and plagioclase fall into two categories, namely those involving only anhydrous minerals such as pyroxenes and garnets and commonly recorded in the Adirondack Mountains (e.g. Whitney and McLelland, 1973; McLelland and Whitney, 1980b) as opposed to those that contain hydrous minerals and are of the type described in this study. According to Esbensen (*op.cit.*), the dry corona assemblages are more typical for upper granulite facies terranes, while the coronas containing hydrous minerals (amphibole) originate under medium amphibolite to hornblende-granulite facies conditions. Esbensen (*op.cit.*) has studied hydrous coronas between olivine and plagioclase, which are similar to those described in this study, in rocks with a similar setting to the ones in the Namaqualand Metamorphic Complex involving an upper amphibolite facies terrane. With a thermodynamic model he demonstrates that low water pressures appear to be the dominant control over the formation of orthopyroxene in these coronas and thereby explaining the presence of orthopyroxene in an amphibolite facies terrane. From the literature it appears that occasionally at even lower grades of regional metamorphism the formation of orthopyroxenes is possible. For example, England (1974) has described corona textures between olivine and plagioclase in a metamorphosed dolerite from the Pottoyu Hills, Australia. These coronas consist of magnetite, cummingtonite, hypersthene and pargasitic hornblende and are believed to have originated under upper greenschist to lower amphibolite facies metamorphic conditions.

## 4 Manganiferous Rocks

Dark green to almost black medium to coarse-grained manganiferous rock outcrops are encountered on the farm Dabidas (407) (C22, Fig. 62, p.160) along the Dabidas-Klipfontein road. These rocks are associated with ferruginous quartzite (gossan?) along the contact between pelitic gneisses and pink quartzo-feldspathic rocks. Other lithotypes observed in the immediate vicinity include calc-silicate rocks and grey gneisses, while garnet and magnetite-rich rocks are encountered along strike. The outcrop area of the

ferruginous quartzite is small and lens-shaped and along strike it disappears under sand cover.

One specimen (HA 990) from this locality contains the following mineral paragenesis (the minerals are arranged in order of decreasing abundance):

'ferroaugite + quartz + opaque minerals (predominantly magnetite) + garnet + pyroxmangite'

The chemical compositions of the pyroxene, pyroxenoid and garnet were determined with the aid of the electron microprobe analyser (tabulated in Appendix II, Table A2-26). The pyroxene, when viewed under the microscope, is seen as green, multiple twinned polygonal grains with straight grain boundaries meeting in triple point junctions creating an overall granoblastic polygonal mosaic. The chemical composition of this pyroxene plots into the field of ferroaugite in the Poldervaart and Hess (1951) classification (Fig. 66). The mineral is characterised by low Ti ($TiO_2$ = 0,017 per cent) as opposed to some of the titanaugites that can contain 3-6 per cent $TiO_2$ (Deer *et al.*, 1971). Aluminium is likewise very low ($Al_2O_3$ = 0,64 per cent) and $Na_2O$ and $K_2O$ together account for only 0,2 per cent of the oxides. On the other hand the Mn content of the mineral is very high (MnO = 6,04 per cent).

In contrast to the manganiferous ferroaugite the pyroxenoid is colourless and occurs as long slender laths. Optically the mineral is biaxial positive, has high relief, oblique extinction with angles up to 30° measured on cleavage traces and relatively low birefringence. Chemically its composition can be expressed as $(Fe_{1,05}\ Mn_{0,60}\ Mg_{0,19}\ Ca_{0,16})\ Si_2O_6$ (Appendix II, Table A2-26) which closely approximates the composition of pyroxmangite as described by Deer *et al.* (1971), but has slightly higher FeO content (29,63 per cent FeO). According to Deer *et al.* (*op.cit.*), pyroxmangite is fairly pure (Mn, Fe) $SiO_3$ with FeO varying between nil and 25 per cent.

The garnet has a pink colour and forms coronas around magnetite along the ferroaugite-magnetite contact (Fig. 67) and also occurs interstitially between large pyroxene crystals and edging the clinopyroxene-quartz contacts. Its chemical composition, expressed in terms of end-member molecules is as follows (the end-member molecules are arranged in order of decreasing abundance and the contribution of each molecule towards the bulk composition expressed in molecular per cent is indicated in brackets):

| | | | |
|---|---|---|---|
| spessartine | $Mn_3Al_2Si_3O_{12}$ | - | (39,26 per cent) |
| almandine | $Fe_3^{2}Al_2Si_3O_{12}$ | - | (36,92 per cent) |
| andradite | $Ca_3\ (Fe^{+3},\ Ti)_2\ Si_3O_{12}$ | - | (13,35 per cent) |
| grossular | $Ca_3Al_2Si_3O_{12}$ | - | ( 8,08 per cent) |
| pyrope | $Mg_3Al_2Si_3O_{12}$ | - | ( 2,38 per cent) |

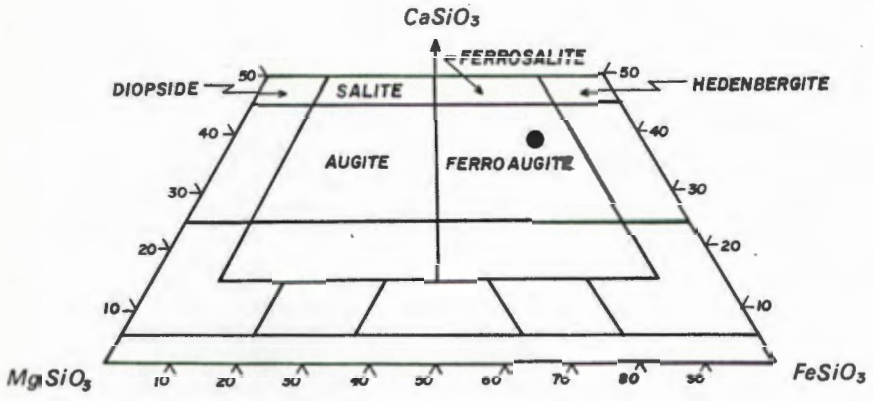


Fig. 66 Core composition of clinopyroxene in specimen HA 990 (solid dot) plotted in terms of the Poldervaart and Hess (1951) classification.

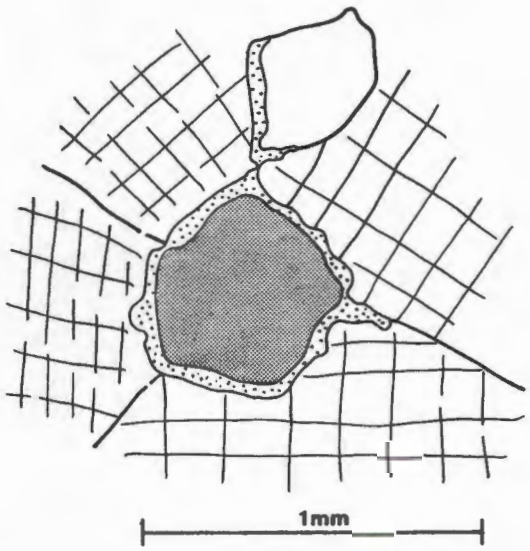


Fig. 67 The development of a garnet corona (stippled) around magnetite (black) along the contact with ferroaugite (cross-hatched). Also note the partial corona of garnet along the contact between quartz (blank) and ferroaugite in the top half of the drawing (Specimen HA 990).

# IV GEOTHERMOMETRY AND GEOBAROMETRY

## A Geothermometry

### 1 Introduction

The mineral assemblages in metamorphic rocks preserve evidence for the P-T conditions during their crystallisation. Experimental petrology has provided invaluable information regarding the equilibrium conditions of important metamorphic reactions in P-T and P-T-X space. These experimental studies have revealed that many mineral assemblages have rather large stability fields in P-T-X space and, therefore, they are only useful in providing a qualitative estimate of the physical conditions that are likely to have prevailed during regional metamorphism. A more sophisticated method exploits the experimentally verified relationships between chemical compositions of coexisting phases and crystallisation conditions and involves thermodynamic models. Although admittedly simplified, these thermodynamic models allow a more precise quantitative evaluation of the physical factors controlling metamorphism provided the chemical composition of the minerals in the natural environment can be accurately determined. It is, therefore, only since the development of the electron microprobe that this technique can be successfully applied. The majority of naturally occurring minerals are "impure" phases, i.e. they are mixtures or solid solutions of various end-member molecules and this is accounted for in the thermodynamic models by activity terms.

An attempt has been made in this study to evaluate the peak P-T conditions that are likely to have prevailed during regional metamorphism by utilising various experimentally calibrated equilibria and empirical equations. The following geothermometers were applied to mafic, semi-pelitic and pelitic rocks :

For mafic rocks :

Coexisting orthopyroxene and clinopyroxene (Wood and Banno, 1973; Wells, 1977)

Coexisting garnet and clinopyroxene (Dahl, 1980)

For semipelitic and pelitic gneisses :

Coexisting garnet and biotite (Ferry and Spear, 1978)

Coexisting garnet and cordierite (Thompson, 1976b; Holdaway and Lee, 1977)

Coexisting alkali-feldspar and plagioclase (Stormer, 1975; Whitney and Stormer, 1977a)

## 2 Pyroxene Geothermometry

Subsequent to the pioneering studies of Ramberg and de Vore(1951) on the partitioning of elements between coexisting mineral phases, the Mg-Fe exchange reaction between orthopyroxene and clinopyroxene received considerable attention, particularly after Kretz (1963) demonstrated that the Mg-Fe distribution coefficient ($K_D$) for igneous and metamorphic pyroxene pairs differ quite remarkably from each other, which he believed to reflect differences in equilibration temperature. The potential of coexisting orthopyroxene and clinopyroxene as geothermometer was well established after the early experimental investigation of the enstatite-diopside miscibility gap, conducted by Boyd and Schairer (1964) and Davis and Boyd (1966). Following a thermodynamic approach, these pioneering experimental results are utilised by Wood and Banno (1973) in an attempt to calibrate the conditions of the equilibrium distribution of the enstatite molecule between orthopyroxene and clinopyroxene. The reaction involved can be written in the following manner :

$$(Mg_2Si_2O_6)_{\text{in op}} \rightleftharpoons (Mg_2Si_2O_6)_{\text{in cp}} \qquad (71)$$

The equilibrium condition for reaction (71) can be expressed as :

$$G^{o}_{P,T} = -RT \ln \frac{a^{cp}_{Mg_2Si_2O_6}}{a^{op}_{Mg_2Si_2O_6}}$$

According to Wood and Banno ( *op.cit.*) the expression

$$T = \frac{-10202}{\ln\left(\frac{a^{cp}_{Mg_2Si_2O_6}}{a^{op}_{Mg_2Si_2O_6}}\right) - 7{,}65\, X^{op}_{Fe} + 3{,}88\left(X^{op}_{Fe}\right)^2 - 4{,}6} \qquad (T1)$$

where $X^{op}_{Fe} = \frac{Fe^{+2}}{Fe^{+2}+Mg^{+2}}$ in orthopyroxene, is consistent with the experimental data of Davis and Boyd (*op.cit.*) at 30 kb and allows the computation of equilibration temperatures of naturally coexisting orthopyroxene and clinopyroxene pairs. Some of the assumptions made by Wood and Banno (*op.cit.*) have been adopted in this study and are, therefore, briefly outlined below:

For the enstatite-diopside solid solution, an ideal two-site solution model has been assumed and since ideal solutions have unit activity coefficients, the activity-composition relationships can be expressed as:

$$a^{\text{clinopyroxene}}_{Mg_2Si_2O_6} = \left(X^{M_2}_{Mg} \cdot X^{M_1}_{Mg}\right)_{\text{clinopyroxene}}$$

$$a^{\text{orthopyroxene}}_{Mg_2Si_2O_6} = \left(X^{M_2}_{Mg} \cdot X^{M_1}_{Mg}\right)_{\text{orthopyroxene}}$$

where $X_{Mg}$ represents the mole fraction of magnesium ions and the superscripts $M_1$ and $M_2$ refer to the two structural sites involved in the Mg-Fe exchange reaction between the two pyroxenes.

In order to determine the concentration of $Mg^{+2}$ and $Fe^{+2}$ in the $M_1$ and $M_2$ sites of the pyroxene structure it is assumed that the larger ions (Ca, Na, K) occupy $M_2$, whereas the smaller ions (Al, Cr, Ti, $Fe^{+3}$) are accommodated in the $M_1$ site. This is in accord with the pyroxene structure as determined by Warren and Bragg (1928) who have shown that these minerals are built up of continuous chains of $SiO_4$ tetrahedra laterally linked by cations in the $M_1$ and $M_2$ positions. The smaller $M_1$ site is located between the apices of these chains, while $M_2$ occurs at the bases of these tetrahedra where more space is available and accordingly will preferentially be occupied by the larger ions. Subtracting the fraction of sites occupied by the ions Ca, Na, K, Al, Cr, Ti, $Fe^{+3}$ from the total number of sites determines the fraction of sites available to accommodate $Fe^{+2}$ and $Mg^{+2}$. Finally it has to be established how the $Fe^{+2}$ and $Mg^{+2}$ ions are distributed amongst the remaining $M_1$ and $M_2$ sites, and Wood and Banno (*op. cit.*) institute the simplest model, namely that of random distribution.

More recently published experimental data on the enstatite-diopside solvus namely Warner and Luth (1974), Nehru and Wyllie (1974), Howells and O'Hara (1975), Lindsley and Dixon (1976) and Mori and Green (1975, 1976) are incon-

sistent at low temperature with the earlier data of Davis and Boyd (*op.cit.*), necessitating the re-evaluation of the earlier Wood and Banno (*op.cit.*) calibration.

Wells (1977) has compiled the available experimental information on the diopside-enstatite miscibility gap and re-formulates the Wood and Banno geothermometer. According to Wells (*op.cit.*) the expression:

$$T = \frac{7341}{3{,}355 + 2{,}44\ X_{Fe}^{op} - \ln K} \qquad (T2)$$

(where $X_{Fe}^{op}$ is the mole fraction of iron in orthopyroxene and K represents the equilibrium constant) successfully reproduces the miscibility gap between diopside and enstatite for the majority of experimental data in the temperature range 800°C to 1700°C.

The Wells (*op.cit.*) geothermometer is based on a larger amount of recently published experimental data and accordingly is expected to yield more accurate temperature estimations compared to the Wood and Banno equation.

(a) Application of the Pyroxene Thermometers

Coexisting orthopyroxene and clinopyroxene grains have been analysed by microprobe techniques in eighteen granolite specimens. Two to seven spot analyses were carried out for each pyroxene type per specimen from which mean compositions were computed (Appendix II, Tables A2-4 and A2-5). The majority of the grains were analysed in proximity to their margins.

Equations (T1) and (T2) were used to calculate the equilibrium temperatures (Table 15). It is evident from Table 15 that the Wood and Banno (*op.cit.*) geothermometer generally tends to yield lower temperatures than the Wells (*op.cit.*) equation. Only for two specimens have both grain rim and grain core compositions been determined and they yield slightly different temperatures. In the case of specimen HA 269 the core compositions yield higher temperatures compared to the temperatures based on rim compositions, while the opposite is suggested by specimen HA 957 where the rim compositions give slightly higher temperature values. All the computed temperatures fall into the range 795°C to 910°C which is regarded as reasonable for granulite facies metamorphism (Turner, 1968).

The geographic distribution of the computed two-pyroxene temperature is shown in Fig. 68, suggesting no significant regional variation in temperature across the entire area underlain by granulite facies mineral assemblages. It is also evident from Fig. 68, that temperatures for closely spaced samples can vary considerably, suggesting either local inhomogeneous temperature distributions during metamorphism (this seems very unlikely) or alternatively that components other than Mg and Fe have an influence on the computed temperatures. Similar observations of sporadic temperature variations are recorded for Adirondack granolites (Bohlen and Essene, 1979).

TABLE 15 : Temperatures computed for coexisting orthopyroxene and clinopyroxene using Wells (1977) and Wood and Banno (1973) geothermometers. The number of analyses used for evaluating the mean composition are indicated in brackets. Calculations are based on the mean compositions and the assumption that $Fe^{+2} = \Sigma$ Fe. R and C refer to rim and core compositions respectively.

| Sample No. | $x^{op}_{Fe}$ | $a^{cp}_{Mg_2Si_2O_6}$ | $a^{op}_{Mg_2Si_2O_6}$ | TEMPERATURE °C WELLS(1977) Equation(T2) | WOOD & BANNO(1973) Equation(T1) | DIFFERENCE |
|---|---|---|---|---|---|---|
| HA 1025(3) C | 0,3318 | 0,0388 | 0,4245 | 847 | 848 | -1 |
| HA 1030(7) C | 0,6024 | 0,0251 | 0,1441 | 844 | 795 | +49 |
| HA 1050(3) C | 0,5125 | 0,0341 | 0,2187 | 863 | 817 | +46 |
| HA 1045(3) C | 0,5025 | 0,0350 | 0,2363 | 858 | 815 | +43 |
| HA 472(6) R | 0,4182 | 0,0397 | 0,3202 | 863 | 835 | +28 |
| HA 980(2) R | 0,3563 | 0,0301 | 0,3902 | 809 | 813 | -4 |
| HA 239(6) R | 0,2808 | 0,0549 | 0,4915 | 905 | 909 | -4 |
| HA 973(5) R | 0,4845 | 0,0332 | 0,2523 | 845 | 810 | +35 |
| HA 269(3) R | 0,4086 | 0,0314 | 0,3333 | 820 | 808 | +12 |
| HA 269(2) C | 0,4194 | 0,0451 | 0,3140 | 889 | 852 | +37 |
| HA 987(5) R | 0,2556 | 0,0384 | 0,5295 | 839 | 870 | -31 |
| HA 957(3) R | 0,4352 | 0,0368 | 0,2989 | 854 | 825 | +29 |
| HA 957(3) C | 0,4546 | 0,0336 | 0,2811 | 841 | 812 | +29 |
| HA 939(4) R | 0,3135 | 0,0290 | 0,4456 | 798 | 818 | -20 |
| HA 306(5) R | 0,4720 | 0,0299 | 0,2590 | 828 | 800 | +28 |
| HA 622(3) R | 0,6442 | 0,0273 | 0,1155 | 880 | 817 | +63 |
| HA 926(6) R | 0,4276 | 0,0452 | 0,3073 | 890 | 851 | +39 |
| HA 888(4) R | 0,5441 | 0,0427 | 0,1958 | 910 | 844 | +66 |
| HA 909(3) R | 0,4278 | 0,0411 | 0,3036 | 874 | 841 | +33 |
| HA 725(3) R | 0,5752 | 0,0303 | 0,1672 | 862 | 810 | +52 |

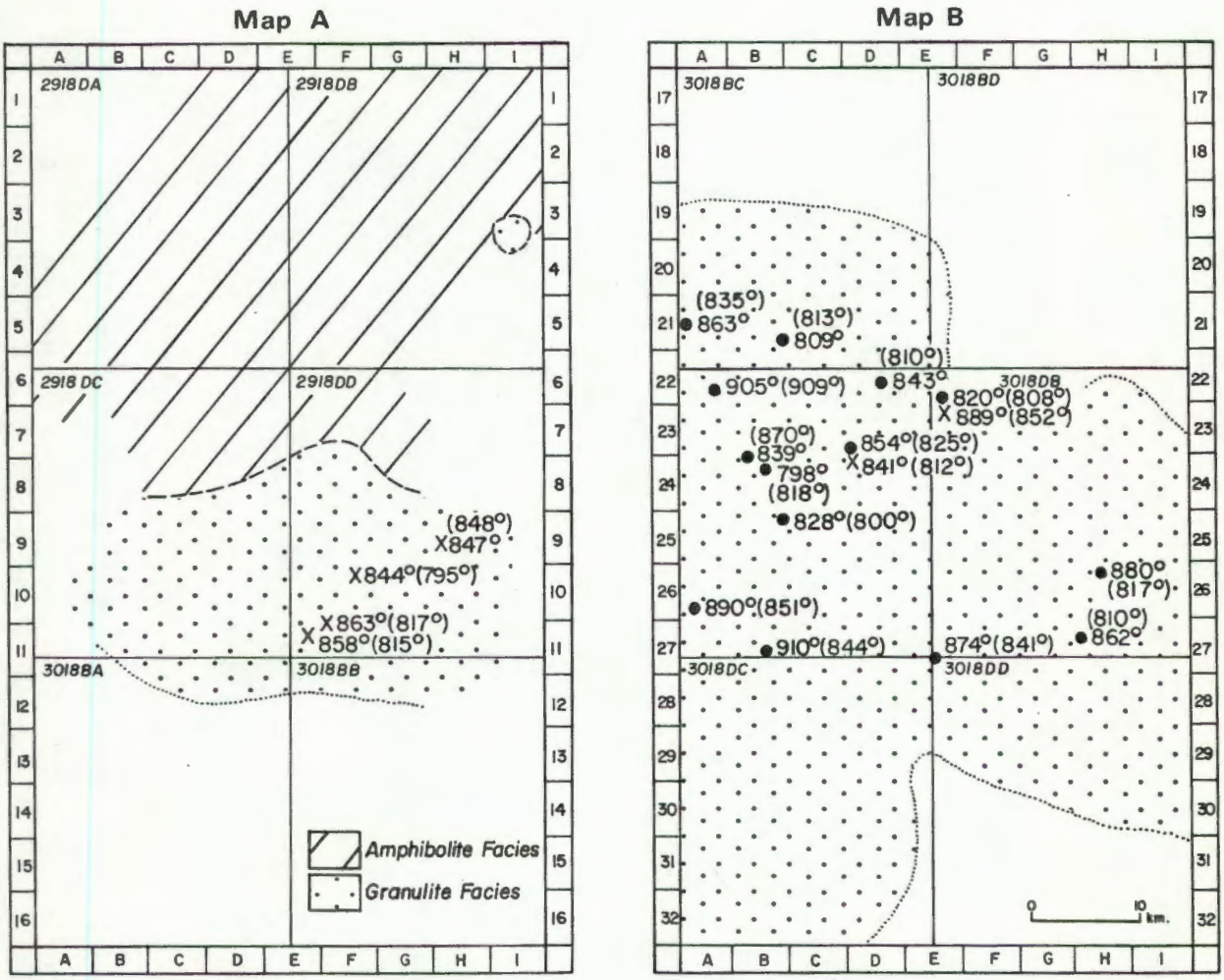


Fig. 68 Geographic distribution of metamorphic temperatures computed for co-existing orthopyroxenes and clinopyroxenes utilising the Wells (1977) and Wood and Banno (1973) geothermometers. The $Fe^{+3}$ content of these minerals is low and it has been assumed that $Fe^{+2} = \Sigma Fe$. The temperatures are based on mean compositions of 2 to 7 analyses per specimen. Calculations based on rim compositions are shown as solid dots while those based on core compositions are indicated by crosses. The temperatures computed by the Wood and Banno (*op.cit.*) method are shown in brackets.

The temperatures computed for the present area are in good agreement with the results obtained by the same techniques in other parts of the Namaqualand Metamorphic Complex (Jack, 1980; Zelt, 1980), suggesting no significant temperature variations across the large granulite facies terrane in western Namaqualand. Identical temperatures are recorded in other granulite facies terranes. For example, Hewins (1975) has determined pyroxene temperatures in the range of 780-860°C for hornblende granolites in various granulite facies terranes including the Adirondacks and terranes in Finland, Australia and in India.

Recently Bohlen and Essene (*op.cit.*) conducted a critical evaluation of two-pyroxene thermometry in Adirondack granolites. These authors compare the temperatures determined by various two-pyroxene thermometers and find large discrepancies. They conclude that the pyroxene thermometers are not useful for quantitative work because they yield inconsistent and scattered temperatures which are frequently too high (by as much as 100-250°C) in comparison with temperatures expected from certain parageneses and those determined from Fe-Ti and two-feldspar geothermometers. They also show that the Wood and Banno and Wells thermometers are dependent to some degree on bulk composition.

There are some indications in the area presently investigated that the temperatures computed for coexisting pyroxenes are probably too high. It is generally suggested that the granulite-amphibolite facies boundary is situated in the vicinity of 750°C (Hietanen, 1967; Winkler, 1967; Turner, 1968; Hyndman, 1972; Miyashiro, 1973; Vernon, 1976). The experiments by Binns (1968, 1969b) on hornblende-pyroxene dehydration reactions suggest that orthopyroxene in naturally occurring amphibolite is formed in the temperature range 760 to 790°C under conditions of $P_{H_2O} = P_{total}$. Recently Spear (1981) experimentally studied hornblende breakdown reactions using different buffers to control the oxygen fugacity and he concludes that the temperatures for the first appearance of orthopyroxene in amphibolites range between 740°C and 800°C under the conditions of $P_{H_2O} = P_{total}$ = 1 to 2 kb. The first appearance of orthopyroxene, according to Spear (*op.cit.*), is dependent on the degree of silica saturation as amphiboles saturated with respect to $SiO_2$ (e.g. tremolite) have a lower upper thermal stability than amphiboles undersaturated with respect to $SiO_2$ (e.g. pargasite).

During granulite facies metamorphism, however, the condition of $P_{H_2O} < P_{total}$ is more likely (Winkler, 1976) and the reaction boundaries for equilibria involving hornblende dehydration as determined by Binns (*op.cit.*) and Spear (*op.cit.*) will drop towards lower temperatures. Therefore, it is concluded that the granulite-amphibolite facies boundary is expected to accur at a temperature of less than 800°C and probably more in the region of 750°C. Contrary to expectation, examination of Fig. 68 shows that in proximity of the granulite-amphibolite facies transition, the computed two-pyroxene temperatures remain high (about 850°C as determined from the Wells geothermometer). This observation casts some doubts on the accuracy of the methods employed in computing the metamorphic temperatures.

Wood (1975) and Wilson (1976) also state that the Wood and Banno (*op.cit.*) geothermometer yields temperatures that are too high and suggest a deduction of 60°C. The mean temperature calculated by the Wood and Banno method in the study area is found to be 830°C which becomes 770°C by deducting 60°C. The mean temperature determined by the Wells (*op.cit.*) method is even higher (856°C) and if it is correct that the Wood and Banno method yields overestimated temperatures of 60°C, it follows that temperatures determined by the Wells method are overestimated by some 90°C. Both authors (Wood and Banno, *op.cit.* and Wells, *op.cit.*) regard their thermometers to be accurate to within 60°C to 70°C. Therefore, it is at present unknown whether the temperatures computed for coexisting pyroxenes are reliable.

(b) Uncertainties in Pyroxene Thermometry

From the brief discussion on pyroxene geothermometry it has become evident that a large number of assumptions have been made in deriving the geothermometers. These assumptions are generally oversimplified, but nevertheless seem to yield results consistent with the experimental data. It is, however, important to realise that the experiments on the enstatite-diopside solvus have been performed largely at high temperatures above the thermal regime expected in the granulite facies. Thus, in order to utilise this experimental data for lower temperature conditions requires extrapolation which can only be reasonably accurate for tight reversal runs of the experiments at lower temperatures. Unfortunately, experimental reversals for temperatures applicable to granulite facies metamorphism are lacking. Bohlen and Essene (1979) point out that the assumption of a straight-line relationship between ln K and $^1/_T$ by Wood and Banno (*op.cit.*) and Wells (*op.cit.*) is not in accord with the data presented by Evans and Trommsdorf (1978, Fig. 4, p. 341) who have shown that this relationship is non-linear and accordingly a straight line assumption yields temperature estimates that are too high.

The assumption that $Fe^{+2}$ and $Mg^{+2}$ are randomly distributed between the two energetically different structural sites $M_1$ and $M_2$ in the pyroxenes is strictly speaking not correct. In orthopyroxene, for example, it has been shown by Mössbauer spectroscopy that $Fe^{+2}$ shows a marked preference for the $M_2$ site (Virgo and Hafner, 1969, 1970; Saxena and Ghose, 1971). The preference of $Fe^{+2}$ for the $M_2$ site implies that the solid solution is non-ideal (Virgo and Hafner, 1970). Only at high temperature does the ion distribution approach an ideal solution model, but with decreasing temperature the deviation from ideality increases (Saxena and Ghose, *op.cit.*). It is also found that the Mg-Fe mixing in the $M_1$ site is less ideal than in the $M_2$ site (Saxena and Ghose, *op.cit.*). Similarly, $Fe^{+2}$ shows a preference for the $M_2$ site in clinopyroxene (Hafner *et al.*, 1971). With this in mind, it is evident that particularly at lower temperatures, the activity coefficient cannot be ignored in the temperature computations.

Both the geothermometers applied in this study are seen to lack a variable involving equilibrium pressure. Some experiments, however, suggest that pressure has at least some influence on the miscibility gap (Mori and Green, 1975, 1976; Lindsley and Dixon, 1976; Nehru, 1976). Neglecting the influence of

pressure, particularly at high temperatures, can cause discrepancies in the temperature estimations according to Nehru (*op.cit.*). Contrary to this, Wood and Banno (*op.cit.*) suggest that the influence of pressure is small and can be neglected. Because of the similar ionic radii of $Fe^{+2}$ and $Mg^{+2}$ it is expected that $\Delta V$, i.e. the volume change of the exchange reaction is small, implying that the influence of pressure on the equilibrium should be small.

Another source of error stems from the inability of the microprobe analyser to discriminate between $Fe^{+2}$ and $Fe^{+3}$. For this reason it is often the practice to assume $Fe^{+2} = \Sigma$ Fe, but if the $Fe^{+3}$ concentration is large a serious error in temperature estimation can result. Edwards (1976) has discussed various methods for estimating $Fe^{+3}$ from microprobe analyses, e.g. the charge balance equation ( Hamm and Vieten, 1971; Papike *et al.*,(1974) formulated as:

$$Fe^{+3} = Na\ (+\ K) + \left[Al^{IV} - (Al^{VI} + Cr + 2Ti)\right]$$

However, these estimates are considered not to be accurate. Temperatures have been recalculated allowing for $Fe^{+3}$ determined from the above charge balance equation for all pyroxene pairs and are found not to be significantly different from those determined from the assumption $Fe^{+2} = \Sigma$ Fe. Weaver *et al.*, (1978) also find that ignoring $Fe^{+3}$ only has minor effects on temperature calculations.

Finally, the influence of chemical composition on the computed temperatures should be mentioned. Numerous recent authors have considered the influence of composition on the distribution coefficient to explain observed variations of $K_D$ within rocks believed to have equilibrated at more or less the same temperature. Maxey and Vogel (1974) point out that $K_D$ can be influenced by mineral composition if one or both pyroxenes deviate markedly from ideal solid solution or if other cations compete with Fe and Mg for the same structural site in which case $K_D$ will vary with the concentration of the competing ions. Saxena (1968a) concludes that, although there is a distinct difference in $K_D$ between igneous and metamorphic pyroxenes, the mineral composition, particularly the Ca-concentration, has some influence on $K_D$. A systematic variation in $K_D$ with increasing Fe + Mn concentrations in the pyroxenes is recorded by Davidson (1969). Some authors, for example Hermes (1970) and Ray and Sen (1970), note a regular variation of $K_D$ with the Ca-concentration of clinopyroxene. Maxey and Vogel (*op.cit.*) show that FeO, MgO and $Al_2O_3$ have an effect on $K_D$, but the variation of $K_D$ with the CaO content of the pyroxenes, according to them, is not systematic. In contrast, Fleet (1974a,b) concludes that the difference in $K_D$ between igneous and metamorphic pyroxene pairs reflects the trend towards Fe-enrichment in clinopyroxene and consequently decreasing Ca-concentration, rather than changes in temperature during crystallisation. Lindh (1975) has statistically studied 117 pyroxene pairs and shows that $K_D$ is influenced by the Mg/Fe ratio, the Ca-content of clinopyroxene and the concentration of tetrahedral Al.

From the literature, it appears that there are numerous chemical factors that could have an influence on $K_D$ and, therefore, also on the temperature calculations. Thus, despite of the great wealth of experimental data, temperatures determined by two-pyroxene geothermometers are subject to considerable uncertainties.

## 3 Garnet-Clinopyroxene Geothermometry

Various authors have attempted to calibrate the Fe-Mg distribution between coexisting clinopyroxene and garnet as a function of temperature (Saxena, 1968b, 1979; Raheim and Green, 1974; Ganguly, 1979; Dahl, 1980). The exchange reaction between the two phases can be written as:

$$CaFeSi_2O_6 + \tfrac{1}{3}Mg_3Al_2Si_3O_{12} \rightleftharpoons CaMgSi_2O_6 + \tfrac{1}{3}Fe_3Al_2Si_3O_{12} \qquad (72)$$

The distribution of $Fe^{+2}$ and Mg between garnet and clinopyroxene is generally expressed in terms of the distribution coefficient, $K_D$, defined as:

$$K_D(\text{Fe-Mg, garnet-clinopyroxene}) = \left(X_{Fe}/X_{Mg}\right)^{\text{garnet}} \Big/ \left(X_{Fe}/X_{Mg}\right)^{\text{clinopyroxene}}$$

where X represents the mole fractions of the ions concerned. Dahl (*op.cit.*) points out that this exchange equilibrium is not only a function of temperature, but also depends on the composition of the minerals particularly as naturally occurring garnets may contain considerable amounts of the grossular and spassartine molecules in solid solution. Thermodynamically, the condition for equilibrium in reaction (72) can be expressed as:

$$RT \ln K_D = -\Delta G - RT \ln \left(\gamma_{Fe}/\gamma_{Mg}\right)^{\text{garnet}} + RT \ln \left(\gamma_{Fe}^{\text{clinopyroxene}} / \gamma_{Mg}^{\text{clinopyroxene}}\right) \qquad (T3)$$

if certain assumptions regarding the solution model and site occupancies are made (Dahl, *op.cit.*). $\gamma$ represents the activity coefficients of the two phases. For garnet, the activity coefficients have been derived by Ganguly and Kennedy (1974) and Ganguly (1979) and are expressed as binary solution interaction parameters which take into account the non-ideality of mixing of the almandine, pyrope, spessartine and grossular components in garnet. Dahl (*op.cit.*) has suggested that the term involving the activity coefficients of clinopyroxene will be very small for clinopyroxenes of low Na contents and can, therefore, be neglected for the pyroxenes concerned in this study.

In an empirical approach Dahl (*op.cit.*) has evaluated $\Delta G$ in equation (T3) for a small area in the Ruby Range (Montana) for which previously the pressure-temperature conditions during metamorphism had been established for other rock types, assuming that the garnet-pyroxene assemblages had equilibrated under similar conditions. Substituting $\Delta G$ derived in this manner and the interaction parameters in garnet solid solutions into equation (T3) yields an empirical geothermometer:

$$T^{o}(K) = \left[2324 + 0{,}022\ P(\text{bars}) + 1509\ (X_{Fe}^{\text{garnet}} - X_{Mg}^{\text{garnet}}) + 2810\ (X_{Ca}^{\text{garnet}}) + 2855\ (X_{Mn}^{\text{garnet}})\right] / (1{,}987 \ln K_D) \quad \text{(Dahl, } op.cit.\text{)} \qquad (T4)$$

Under the known pressure-temperature conditions of the Ruby Range area equation (T4) predicts a $K_D$ which is very close to the actually observed $K_D$, thus supporting its validity (Dahl, *op.cit.*).

Equation (T4) has been applied to two specimens of the study area, HA 1030 and HA 990, for which coexisting garnet and clinopyroxene grains were analysed by microprobe techniques (Table 16 ). The analyses are tabulated in Appendix II, Tables A2-7 and A2-26. In both specimens the ionic proportions of garnet have been recalculated to allow for $Fe^{+3}$ by the method described in Appendix ID.

TABLE 16 : Temperature calculations for coexisting garnet-clinopyroxene assemblages using equation (T4) after Dahl (1980) at 5, 6 and 7 kb.

| Specimen | $K_D$ | $X^{Ga}_{Fe^{+2}}$ | $X^{Ga}_{Mg}$ | $X^{Ga}_{Ca}$ | $X^{Ga}_{Mn}$ | T°C at 5000 bars | T°C at 6000 bars | T°C at 7000 bars |
|---|---|---|---|---|---|---|---|---|
| HA 1030 | 6,4351 | ,6233 | ,0993 | ,2162 | ,0673 | 815 | 821 | 826 |
| HA 990 | 6,7397 | ,3704 | ,0239 | ,2150 | ,3938 | 963 | 969 | 974 |

The temperature computed for specimen HA 990 is considered to be far too high in comparison to the results obtained by the two-pyroxene geothermometers. The discrepancy involves about 100°C and it is, therefore, concluded that equation (T4) is not suitable for garnets of very high spessartine components. The temperature obtained for specimen HA 1030, on the other hand, is somewhat lower than the computed two-pyroxene temperatures, but considering the uncertainties involved, both methods are seen to yield compatible results.

## 4 The Garnet-Biotite Geothermometer

The literature on the partitioning of ions between coexisting garnet and biotite pairs is voluminous and is particularly concerned with the distribution of $Fe^{+2}$ and $Mg^{+2}$ between the two phases. It has long been realised that this partitioning, expressed as the distribution coefficient $K_D$ ($K_D = \frac{Mg/Fe\ garnet}{Mg/Fe\ biotite}$) can be correlated with metamorphic grade. Albee (1965) compiled the earlier literature and demonstrated that $K_D$ increases with increasing metamorphic grade. Many authors have subsequently confirmed this conclusion (Gorbatschev, 1968; Sen and Chakraborty, 1968; Hietanen, 1969; Saxena, 1969; Saxena and Hollander, 1969; Lyons and Morse, 1970; Thompson, 1976; Tracy *et al.*, 1976; Ferry and Spear, 1976, 1978; Goldman and Albee, 1977; Kretz, 1978; Baltatzis, 1979).

Once the temperature dependence of $K_D$ had been recognised some authors, notably Perchuk (1970, 1977), Thompson (*op.cit.*), Goldman and Albee (*op.cit.*) and Ferry and Spear (*op.cit.*) have attempted to calibrate $K_D$ against temperature. Of these, only the geothermometer of Ferry and Spear (*op.cit.*) has been derived experimentally and as it has been used in the present study it will be discussed in more detail. Ferry and Spear (*op.cit.*) experimentally investigated the

Fe-Mg partitioning between pure synthetic annite-phlogopite and almandine-pyrope garnet, the equilibrium of which can be represented as:

$$Fe_3Al_2Si_3O_{12} + KMg_3AlSi_3O_{10}(OH)_2 \rightleftharpoons Mg_3Al_2Si_3O_{12} + KFe_3AlSi_3O_{10}(OH)_2 \quad (73)$$

Thermodynamically the condition of equilibrium is expressed by the relationship

$$\Delta G^o = \Delta H^o - T\Delta S^o + P\Delta V^o + 3\ RT\ \ln K = 0 \quad (T5) \quad \text{(Wood and Fraser, 1977)}$$

Since the reaction involves the exchange of ions of similar size, $\Delta V^o$ is small (+ 0,057 cal/bar) implying that pressure has virtually no effect on the equilibrium. On the assumption that enthalpy and entropy changes are independent of pressure the experiments yield $\Delta S^o$ = 4,662 eu and $\Delta H^o$ = 12 454 cal. It is essential that $\Delta H$ be large so that the thermometer is sufficiently temperature sensitive. The larger $\Delta H$, the faster K changes with temperature (Wood and Fraser, *op.cit.*), K being the equilibrium constant, a term composed of activities. The activities can be expressed as the product of activity coefficient ($\gamma$) and mole fraction (concentration). Only if the solid solution is ideal the activity coefficient can be ignored because by definition for ideal solution $\gamma$ = 1 and activities are then equal to the mole fractions. The term comprising the mole fractions only, is referred to as the distribution coefficient, $K_D$.

Substituting $\Delta H$, $\Delta S$ and $\Delta V$ and R (R is the gas constant = 1,98717) into equation (T5) yields the following relationship:

$$T = \frac{0{,}057P + 12\ 454}{4{,}662 - 5{,}961\ \ln K_D} \quad (T6) \quad \text{(Ferry and Spear, } op.cit.\text{)}$$

where T is the absolute temperature ($^oK$) and P is the pressure in bars.

According to Ferry and Spear (*op.cit.*) the geothermometer should provide temperatures correct to ± 50°C provided the natural garnet-biotite pair approximates closely to the binary Mg-$Fe^{+2}$ system, i.e. for garnet $(Ca + Mn)/(Ca + Mn + Fe + Mg)$ should not exceed 0,2 and $(Al^{VI} + Ti)/(Al^{VI} + Ti + Fe + Mg)$ in biotite should not exceed 0,15. Natural garnet and biotite, however, show rather complex substitutions (Deer, *et al.*, 1971). The natural formulae can be expressed as follows:

garnet - $(Mg,Fe,Mn,Ca)^8_3 \quad (Al,Fe^{+3})^6_2 \quad (Si^4O_4)_3$

biotite - $(K,Na)^{12} \quad (Mg,Fe,Mn)^6_{3-y} \quad (Al,Fe^{+3},Ti)^6_y \quad (AlSi)^4_4\ O_{10} \quad (OH,O,F,Cl)_2$

where the superscripts represent the cation co-ordination numbers.

It is now important to establish whether other substitutions have an influence on $K_D$ and, therefore, on the apparent temperature and what that influence might be. In fact, a number of authors have stressed the influence

of composition on $K_D$. Albee (1965) has shown that $K_D$ is affected by substitution of Ti, Al and $Fe^{+3}$ in biotite and that the distribution coefficient is related to the Mn-content of garnet. Gorbatschev (*op.cit.*) has pointed out that substitution of Mn and Ca in garnet and Ti, Al and $Fe^{+3}$ in biotite have a marked effect on $K_D$. Sen and Chakraborty (*op.cit.*) studied 87 mineral pairs and conclude that $K_D$ is not only a function of metamorphic temperature, but is also influenced by the Ca/Mn ratio in garnet. Saxena (*op.cit.*) also points out the effect of composition on $K_D$. Goldman and Albee (*op.cit.*) have shown that $K_D$ is essentially temperature dependent, but they conclude that there is also a dependence on compositional variation. On the other hand, Baltatzis (*op.cit.*) has not detected an influence of Mn and Ca on $K_D$. Most authors, however, agree that substitutions other than Fe and Mg in garnet and biotite can have a marked effect on $K_D$ and, therefore, on the calculated temperature.

(a) Application of the Garnet-Biotite Geothermometer

This section is devoted to a brief discussion on some of the problems involved in the application of geothermometry to natural systems. An example is presented to demonstrate that meaningful temperature estimates using calibrated equilibria, in this case $Fe^{+2}$-Mg exchange between garnet and biotite, can only be achieved if the chemical zonation of the mineral phases concerned are studied. Coexisting garnet and biotite have been analysed by microprobe techniques and the analyses are tabulated in Appendix II. The first attempt to obtain a metamorphic temperature involved a metapelite specimen (HA 164) from the granulite facies terrane east of Kliprand (E24) and proved to be a complete failure, as the garnet-biotite thermometer yielded very low temperatures. This specimen contains the mineral assemblage cordierite-garnet-biotite-sillimanite, but garnet and biotite, respectively, comprise only about 2 per cent of the modal composition, while cordierite accounts for about 20 per cent of the mode. Small syntectonic biotite flakes (0,3 mm in diameter) are enclosed within large garnets while larger biotite crystals (up to 0,8 mm diameter) occur also outside the garnet boundaries. Both types of biotite and the garnet were analysed at the grain margins in proximity to their respective contacts. These contact compositions (Appendix II, Tables A2-27, A2-28) were used to calculate $K_D$ and the Ferry and Spear (1978) geothermometer (equation T6) was then applied to determine the equilibration temperatures (Table 17).

In Table 17, (i) represents temperatures ($^oC$) calculated for coexisting garnet-biotite pairs with biotite occurring outside the garnet grain boundaries (both minerals are in contact), while (ii) represents temperatures based on contact compositions with biotite completely enclosed by the garnet. The two groups yielded distinctly different temperatures. The mean temperature for garnet-biotite pairs of type (i) varies between 471°C and 476°C in the pressure range 4 to 5,5 kb while garnet-biotite pairs of type (ii) yield higher temperatures with a mean varying between 520°C and 525°C in the same pressure range. These anomalously low temperatures in a rock that has obviously been subjected to granulite facies metamorphism requires some explanation.

The question arises whether the $^{Mg}/_{Fe}$ ratio of garnet and biotite had

TABLE 17 : Garnet-biotite temperatures for specimen HA 164 in the pressure range 4 - 5,5 kb computed by means of the Ferry and Spear (1978) geothermometer.

| Grain | ln $K_D$ | $T^oC$ at 4 kb | $T^oC$ at 4,5 kb | $T^oC$ at 5 kb | $T^oC$ at 5,5 kb |
|---|---|---|---|---|---|
| (i) | | | | | |
| Ga 9-Bi 1 | -2,0161 | 487 | 489 | 491 | 492 |
| Ga 8-Bi 2 | -2,0969 | 466 | 468 | 469 | 471 |
| Ga 7-Bi 3 | -2,0448 | 480 | 481 | 483 | 485 |
| Ga 6-Bi 4 | -2,1507 | 452 | 454 | 456 | 457 |
| (ii) | | | | | |
| Ga 5-Bi 5 | -1,8977 | 521 | 523 | 524 | 526 |
| Ga 4-Bi 6 | -1,8586 | 533 | 534 | 536 | 538 |
| Ga 3-Bi 7 | -1,9047 | 519 | 521 | 522 | 524 |
| Ga 2-Bi 8 | -1,9179 | 515 | 517 | 519 | 520 |
| Ga 1-Bi 9 | -1,9242 | 513 | 515 | 517 | 518 |

changed along their margins in an attempt to re-equilibrate under decreasing temperature in a slowly cooling rock body in which case the observed temperatures could be a function of the cooling history. In a search for an answer to the problem another specimen (HA 1041) of a different modal composition was selected. The specimen has been collected on the farm Zuurwater (242)(F11) in the northern part of the area, but still within the limits of the granulite facies terrane. Orientated syntectonic biotites define the regional foliation. The only ferromagnesian silicates encountered within this rock are garnet and biotite, so that the exchange of $Fe^{+2}$ and Mg is confined to these two minerals. Both minerals are very abundant and conditions for chemical equilibrium between the two phases are very likely. Both minerals are believed to have grown during the main regional metamorphism.

A garnet crystal, approximately 2 mm in diameter has been analysed at 17 spots (Fig. 69(a) A to Q) in a traverse across the grain from the one grain boundary to the other (Appendix II, Table A2-29). The variation of FeO,MgO,MnO and CaO along this traverse is shown in Fig. 69(a). The oxides of Fe and Mg are seen to define a rather smooth, bell-shaped zonation with FeO concentration increasing considerably from the core towards the margin, while MgO shows the opposite relative concentration. MnO is slightly increased at the rims and CaO has its lowest concentration in the grain core slightly increasing symmetrically away from the core and decreasing again slightly at the grain boundary.

On both sides of the garnet traverse, (i.e. at A and Q, Fig. 69(a))biotites occur in contact with the garnet. Spot analyses have been carried out on the biotites along traverses from rim to core and the core compositions of two more biotites in proximity to the garnet have been determined (biotites 1 to 4, Fig. 69(b)) (see Appendix II, Table A2-30). The behaviour of FeO, MgO and $TiO_2$ along the biotite traverses is seen in Fig. 69(b). It is evident that the

biotites do not show nearly as pronounced a zonation as garnet. FeO follows a slight trend of enrichment towards the garnet contact while a zonation with respect to MgO is not as defined, but there is a tendency of higher MgO concentration towards the biotite core.

In order to establish the effect of garnet on the adjacent biotites, a large biotite grain remote from the garnet contact (referred to as matrix biotite) has also been analysed (biotite 5, Fig. 69(b)) along a traverse across the grain. It is remarkable that there is a considerable compositional difference between the two types of biotite (texturally these biotites belong to the same generation). The biotite remote from the garnet contact has a much higher FeO content and correspondingly lower MgO concentration compared to the biotites in contact with garnet.

(b) Interpretation of the Observed Zonation Patterns

Zoned garnets are commonly observed in metamorphic terranes (Atherton and Edmunds, 1966; Hollister, 1966; Harte and Henley, 1966; Linthout and Westra, 1968; Grant and Weiblen, 1971; Kurat and Scharbert, 1972; Anderson and Buckley, 1973; Loomis, 1975; Schmidt and Wood, 1976; Tracy *et al.*, 1976; Olimpio and Anderson, 1978; Selverstone and Hollister, 1980), but it is evident that there are considerable differences in the zonation patterns of garnets that have grown under high grade metamorphic conditions compared to those that have originated in lower grade terranes.

Hollister (*op.cit.*) in studying lower grade garnets, found that Fe and Mg concentrations increase with concomitant decrease in Mn from core to rim in garnet crystals. He has suggested a Raleigh depletion model to explain the bell-shaped pattern in Mn distribution involving a progressive depletion in Mn of the environment surrounding the garnet due to the pronounced partitioning of Mn into the early formed garnet. This explanation is also favoured by Harte and Henley (*op.cit.*).

Grant and Weiblen (*op.cit.*) have studied garnet compositional zoning in high grade pelitic rocks and observe a smooth zonation of elements with lower Fe and Mn concentration and higher Mg in the core relative to the margins. This is identical to the type of zonation observed in this study (Fig. 69(a)). These authors also report that this zoning is not influenced by the type of mineral adjacent to the garnet. The increase of Mn from core to rim is exactly opposite to the zonation expected on the basis of a Raleigh depletion model. Therefore, the authors have suggested alternative explanations involving (i) garnet growth during retrogression or (ii) resorption of garnet with Mn concentrated in the remaining garnet. They illustrate that a decrease in the Mg/(Mg+Fe) ratio in garnet is consistent with garnet resorption and falling temperature during retrograde metamorphism.

Atherton and Edmunds (*op.cit.*) recognise two types of garnet zonation in Dalradian and Moine rocks of Scotland, (i) a symmetrical zonation of maxima and minima of the type described for the study area (Fig. 69(a)) which they regard as a result of continuous growth during a single metamorphism and (ii) a more complex series of maxima and minima resulting from polyphase crystal growth.

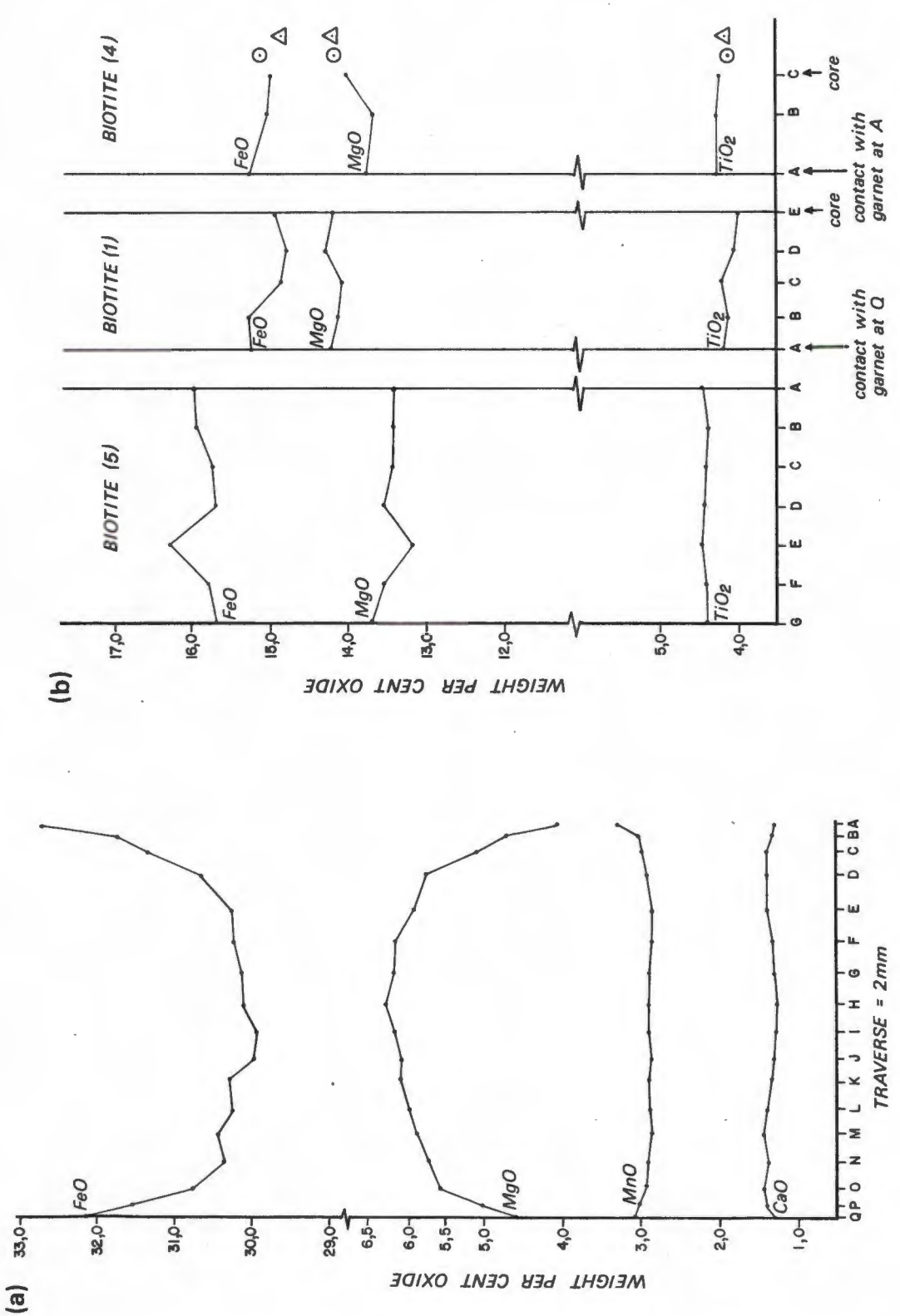
(a)
WEIGHT PER CENT OXIDE
FeO
MgO
MnO
CaO
TRAVERSE = 2mm
(b)
WEIGHT PER CENT OXIDE
BIOTITE (5)
BIOTITE (1)
BIOTITE (4)
FeO
MgO
TiO2
contact with garnet at Q
contact with garnet at A
core

Tracy *et al.* (*op.cit.*) have stressed the importance of understanding the chemical zonation of garnet before geothermometry can be successfully applied to mineral pairs involving this phase. They suggest that garnet zonation of the type shown in Fig. 69 (a) results from retrograde reactions and for high grade rocks, garnet core composition and biotite in the matrix are, therefore, believed to yield the best estimate of prograde temperature (Tracy *et al.*, *op. cit.*). With reference to Fig. 69, it can be appreciated that the calculated distribution coefficient will vary systematically along the garnet profile and likewise will differ for biotites in contact with garnet compared to those remote from the garnet. The compositional difference with respect to FeO and MgO concentration between core and rim in garnet is quite considerable (up to 2,5 per cent FeO or MgO) and this obviously has a marked influence on $K_D$. Thus for the same garnet-biotite generations a wide range of temperatures can be calculated depending on which compositions along the profiles in Fig. 69 have been used to evaluate $K_D$. The aim in this study is to evaluate the equilibrium temperatures that are likely to have prevailed during the thermal peak of regional metamorphism and it now has to be established which of the whole range of compositions in Fig. 69 are most likely to yield this information.

The observed zonation pattern (Fig. 69) can be interpreted with reference to Fig. 70 which graphically displays the experimentally determined relationship between ln $K_D$ and temperature for coexisting garnet and biotite. From the definition of $K_D$ ($K_D = \frac{Mg/Fe\ garnet}{Mg/Fe\ biotite}$) it is apparent that the zonation pattern in Fig.69 (a) yields a decreasing value for $K_D$ along the traverse from garnet core to rim. Likewise $K_D$ decreases with rising MgO concentration and decreasing FeO concentration in biotite. With reference to Fig. 70 a decreasing value for $K_D$ is consistent with falling temperature. Therefore, the observed zonation pattern in coexisting garnet and biotite grains (Fig. 69) is interpreted to result from continued Fe-Mg ion exchange between the two phases in response to decreasing temperature after the thermal peak. It is apparent that this re-equilibration has completely changed the composition of the biotites in contact with the garnet. Biotite grains remote from the

---

Fig. 69 : Zonation of garnet and biotite in specimen HA 1041.
(a) Compositional variation along a 2 mm traverse across a garnet grain. A, B, C, D etc. are spot analyses along the traverse. Both ends of the traverse, i.e. A and Q are rim compositions at the contact with adjacent biotite crystals. Note the smooth bell-shaped zonation pattern defined by MgO and FeO.
(b) Compositional variation in biotites along traverses A, B, C, D etc. Biotites 1 and 4 are in contact with the garnet shown in (a) at localities Q and A of the garnet traverse, respectively. ⊙ and ▲ refer to core compositions of biotites 2 and 3, respectively, both of which occur in close proximity to the garnet contact. Biotite 5 is far removed from any garnet contact. Note the significant compositional difference between this biotite (5) and those in contact with the garnet, i.e. biotites 1,2, 3 and 4.

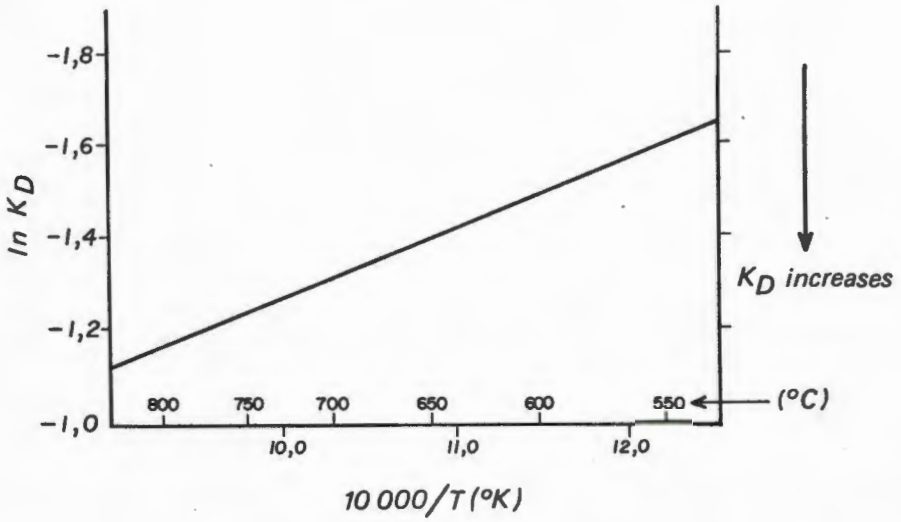


Fig. 70 : Experimentally determined relationship between ln $K_D$ and temperature for the Mg-Fe exchange reaction

$Fe_3Al_2Si_3O_{12} + KMg_3AlSi_3O_{10}(OH)_2 \rightleftharpoons KFe_3AlSi_3O_{10}(OH)_2 + Mg_3Al_2Si_3O_{12}$

(almandine) (phlogopite) (annite) (pyrope)

after Ferry and Spear (1978) $K_D = \frac{(Mg/Fe)\ garnet}{(Mg/Fe)\ biotite}$

Note that the numerical value for $K_D$ increases with increasing temperature.

garnet contact (matrix biotite) are less affected by this re-equilibration, explaining the observed compositional difference (Fig. 69(b)).

The implication of this model is that the compositions of the cores of garnet and matrix biotite (i.e. distal from the garnet-biotite contact) are most likely to approach the equilibrium compositions during the thermal peak. These compositions should be used to evaluate $K_D$. The temperature computed using this $K_D$ must be interpreted as a minimum temperature because it is unknown whether the mineral cores themselves have not re-equilibrated to some extent, particularly in the case of biotite. According to this model, rim compositions are bound to yield low temperatures and this may explain the results obtained for the previous specimen (HA 164) in which rim compositions were used.

In order to demonstrate the range of temperatures that can be obtained, extreme combinations of garnet and biotite compositions of specimen HA 1041 have been used to evaluate $K_D$ (Table 18).

TABLE 18 : Garnet-biotite temperatures for specimen HA 1041 in the pressure range 4-7 kb using the Ferry and Spear (1978) geothermometer (equation T6).

| | ln $K_D$ | T°C at 4 kb | T°C at 5 kb | T°C at 6 kb | T°C at 7 kb |
|---|---|---|---|---|---|
| 1. | -1,9225 | 514 | 517 | 521 | 524 |
| 2. | -1,5209 | 651 | 655 | 659 | 663 |
| 3. | -1,4195 | 693 | 698 | 702 | 706 |

1. Temperatures calculated from rim compositions. These may give some indication of the temperature at which the Fe-Mg exchange between garnet and biotite has slowed down considerably. Alternatively these rims might not be in equilibrium and the computed temperatures may not have any thermodynamic significance.

2. Temperatures calculated from core compositions of garnet and biotite in contact with each other. They are expected to be low due to the re-equilibration of the biotite cores.

3. An indication of the temperatures obtained from core compositions of garnet and matrix biotite. These temperatures are believed to reflect most clearly the peak thermal conditions during regional metamorphism. It is thus concluded that a temperature of approximately 700°C represents a minimum temperature for the area concerned.

This example demonstrates the importance of carefully studying the mineral phases particularly with respect to their zonation before coming to any conclusions regarding the temperature of equilibration.

(c) Additional Results on Garnet-Biotite Thermometry

Core compositions of garnet and matrix biotite (remote from the garnet contact) have been obtained by microprobe techniques (Appendix II, Tables A2-10 and A2-31) for specimens HA 559 and HA 735. In the case of specimen HA 1081 the biotite compositions refer to grains in contact with garnet and with reference to specimen HA 1041 the computed temperatures for this particular specimen are expected to be somewhat on the low side, but contrary to expectation the opposite is observed (Table 19).

These temperatures (Table 19), including specimen HA 1041, are plotted into their correct geographic position in Fig. 71. One of the most striking and contradicting features in Fig. 71 is the very high temperature of 834°C within the area underlain by amphibolite facies rocks. From theoretical considerations it is expected that the garnet-biotite temperatures for amphibolite facies assemblages should be equal to or lower than those computed for granulite facies assemblages, but this is not the case here (Fig. 71). A comparison of the computed temperatures of specimen HA 1041 (granulite facies) and specimen HA 1081 (upper amphibolite facies) suggests an apparent temperature difference of approximately 140°C in favour of the amphibolite facies.

TABLE 19 : Temperatures computed by the Ferry and Spear (1978) equation (T6) for coexisting garnet and biotite in the pressure range 4 to 7 kb. $K_D$ was evaluated from core compositions and $n_{Ga}$ and $n_{Bi}$ represent respectively, the number of garnet and biotite analyses used per specimen to calculate mean ln $K_D$.

| Specimen | $n_{Ga}$ | $n_{Bi}$ | locality | mean ln $K_D$ | T°C at 4 kb | T°C at 5 kb | T°C at 6 kb | T°C at 7 kb |
|---|---|---|---|---|---|---|---|---|
| HA 1081 | 5 | 4 | G5 | -1,1477 | 829 | 834 | 839 | 844 |
| HA 559 | 5 | 6 | F24 | -1,3038 | 747 | 752 | 756 | 761 |
| HA 735 | 4 | 6 | H27 | -1,1138 | 849 | 854 | 859 | 864 |

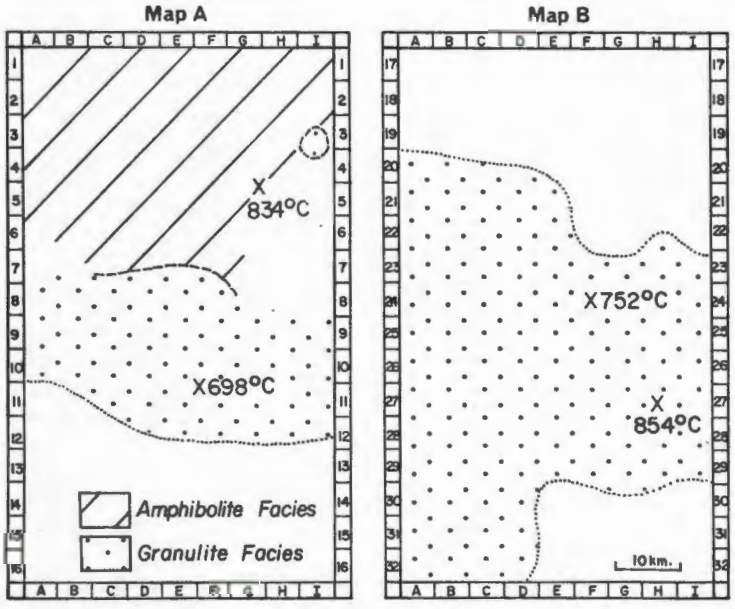


Fig. 71 : Geographic distribution of garnet-biotite temperatures computed by using the Ferry and Spear (1978) geothermometer (Equation T6) assuming an average pressure of 5 kb. The calculations are based on the assumptions that total Fe = $Fe^{+2}$. Only core compositions of garnet and biotite were used to determine $K_D$. In all specimens except for HA 1081 (G5) biotite compositions refer to grains remote from the garnet contact (matrix biotite).

Since this observation is contradicting expectations, some explanations are required.

The zonation pattern of the largest garnet in a thin section from specimen HA 1081 (approximately 3,5 mm in diameter) has been determined from 18 spot analyses (Appendix II, Table A2-32) along a traverse across the grain (Fig. 72 (a)). The pattern of element distribution is in fact very similar to the one discussed previously and can be interpreted as a retrograde zonation. The peak disturbing the smooth bell-shaped zonation (analysis K, Fig. 72 (a) can be accounted for by local ion exchange of the garnet with a small biotite inclusion which occurs in proximity to the spot analyses. Four biotite grains have also been analysed (Appendix II, Table A2-33) and their zonation is shown in Fig. 72 (b). A slight increase of MgO in the biotite towards the contact with garnet is evident, while the zonation with respect to FeO is much more erratic.

(d) Evaluation of Results

It has already been pointed out that various authors have noticed that substitutions other than Mg and $Fe^{+2}$ have a marked effect on $K_D$ and, therefore, the calculated temperature. It is stressed here, that as the microprobe is unable to distinguish between $Fe^{+2}$ and $Fe^{+3}$, total Fe was used in this study to compute $K_D$. If, however, the minerals concerned contain appreciable amounts of $Fe^{+3}$, failure to account for trivalent iron prior to calculating $K_D$ can lead to serious errors in temperature estimates. According to Dallmeyer(1974) an increasing substitution of Ti, $Al^{VI}$ and $Fe^{+3}$ in the octahedral position of biotite would tend to increase $K_D$ at constant P-T conditions. This is the case because Ti, Al and $Fe^{+3}$ have smaller ionic radii compared to $Fe^{+2}$ and $Mg^{+2}$ and, therefore, the octahedral layers would be more compacted while coupled substitution of the larger Al for the smaller Si expands the tetrahedral layer, resulting in an overall structural mismatch which can be restored more readily by the large $Fe^{+2}$ ion rather than the smaller $Mg^{+2}$ ion. Thus in order to achieve a more stable structure, the Fe/Mg ratio of biotite is expected to increase and, therefore, $K_D$ will increase.

On the other hand, the garnet structure is more flexible, and Dallmeyer (*op.cit.*) argues that an increasing substitution of Ca and Mn with their large ionic radii for the small Fe and Mg ions would lead to an expansion of the structure. The large $Fe^{+2}$ cations will preferentially be incorporated into the expanded octahedral sites. Therefore, under constant P-T conditions an increasing substitution of Ca and Mn in garnet is expected to increase the Fe/Mg ratio resulting in a decrease of $K_D$.

The relationship between $K_D$ and the calculated temperature is that the larger the $K_D$ the higher the calculated temperature (Fig. 70). Therefore, increasing substitution of Ti, Al and $Fe^{+3}$ in biotite would tend to increase the apparent (calculated) temperature while increasing Ca and Mn substitution in garnet will result in a decrease in the calculated temperature.

In order to assess the influence of ions other than $Fe^{+2}$ and Mg on the computed temperatures in this study, the specimens have been tabulated in

Fig. 72 Garnet and biotite zonation in a semipelitic biotite-garnet gneiss specimen from the upper amphibolite facies (specimen HA 1081). (a) shows the variation of FeO, MgO, CaO and MnO along a traverse across the garnet. A, B, C, D, etc. represent the individual spot analyses along the traverse. These analyses are tabulated in Appendix II, Table A2-32. The peak disturbing the smoothness of FeO and MgO zonation (K along the traverse) can be related to a biotite inclusion nearby causing local exchange of ions. (b) Variation of FeO, MgO and $TiO_2$ in biotite. Biotite 1 is in contact with the garnet of (a) at R of the garnet traverse and biotites 2 and 3 occur at increasing distance from the garnet, but still in close proximity. Biotite (4) is in contact with the garnet at the A side of the garnet traverse. A,B,C, etc. represent spot analyses along traverses across biotite grains.

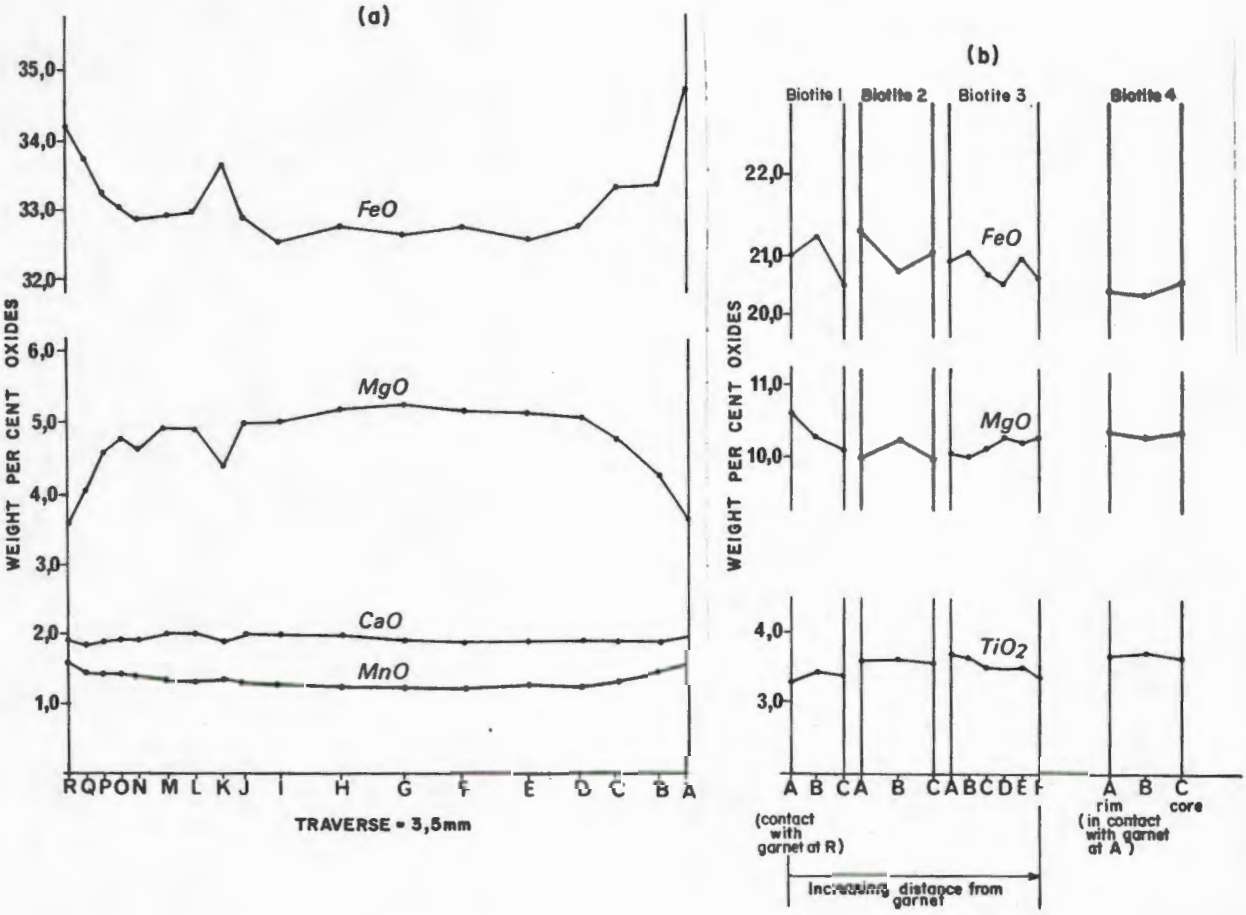

TABLE 20 : Element concentration in biotite and garnet in relation to computed garnet-biotite temperatures. The specimens are arranged in order of increasing computed temperature. Element abundances as ionic proportions.

| Specimen No. | HA 1041 | HA 559 | HA 1081 | HA 735 |
|---|---|---|---|---|
| Calculated Temperature $^{o}C$ | 700 | 752 | 834 | 854 |
| Ti in biotite | 0,2453 | 0,2608 | 0,2049 | 0,3056 |
| $Al^{VI}$ in biotite | 0,1626 | 0,1545 | 0,2253 | 0,0839 |
| Mn in garnet | 0,1940 | 0,0733 | 0,0844 | 0,0208 |
| Ca in garnet | 0,1095 | 0,0978 | 0,1641 | 0,1221 |
| $Al^{VI}$ in garnet | 2,0081 | 2,0038 | 1,9914 | 1,9874 |
| $Fe^{+3}$ in garnet | - | - | small amounts | small amounts |

order of increasing calculated temperature (Table 20). The titanium content in biotite is seen to rise with increasing computed temperature (Table 20) as expected according to Dallmeyer's (*op.cit.*) theory, while $Al^{VI}$, contrary to expectation, decreases. A notable exception is specimen HA 1081, which is characterised by low Ti (as is expected from amphibolite facies biotites), and very high $Al^{VI}$. Mn substitution in garnet is observed to increase with increasing temperature (also conflicting expectations based on Dallmeyer's theory). Specimen HA 1081 is again an exception. The Ca concentration in garnet, according to Table 20, does not seem to bear any systematic relationships to the computed temperature. $Fe^{+3}$ in garnet has been determined from considering the stoichiometry of this mineral. Table 20 shows that garnets yielding the highest temperatures do not contain enough $Al^{VI}$ to completely fill the octahedral sites, suggesting that at least some $Fe^{+3}$ must be present. Unfortunately, $Fe^{+3}$ cannot satisfactorily be computed for biotite and it is very likely that $Fe^{+3}$ could be the dominant factor controlling the observed garnet-biotite temperature pattern. In the light of the uncertainty of $Fe^{+3}$ in biotite the range of garnet-biotite temperatures shown in Fig.71 must not be interpreted as a reflection of the temperature variation across the area. Some of the biotite analyses tabulated in Deer *et al.* (1971) contain very high contents of $Fe^{+3}$ and ignoring the trivalent Fe, as has been done in this study, can lead to a serious overestimation of the temperatures.

It is concluded that unless $Fe^{+3}$ is determined in biotite and accounted for in the temperature calculations using the Ferry and Spear (1978) method, the interpretation of the garnet-biotite temperatures can be misleading.

## 5 Garnet-Cordierite Geothermometry

The garnet-cordierite geothermometer is based on the partitioning of iron and magnesium between the two coexisting mineral phases (Thompson, 1976a,b;

Holdaway and Lee, 1977). Thus, in a binary Fe-Mg system the reaction of interest can be written as:

$$\tfrac{1}{2}\ \text{Mg - cordierite} + \tfrac{1}{3}\ \text{almandine} \rightleftharpoons \tfrac{1}{2}\ \text{Fe - cordierite} + \tfrac{1}{3}\ \text{pyrope} \qquad (74)$$

Because water is not involved in this reaction, the distribution of Fe and Mg between the two phases is expected to be independent of $P_{H_2O}$.

Thermodynamically, the following relationship holds true for reaction (74):

$$\Delta G^{o}_{1,T} = \Delta H^{o}_{1,T} - T\Delta S^{o}_{1,T} + (P-1)\Delta V^{o} + nRT \ln K_D \qquad (T7)$$

where $K_D$ is the distribution coefficient which is defined as

$$K_D = \frac{X^{Cd}_{Fe} \cdot X^{Ga}_{Mg}}{X^{Cd}_{Mg} \cdot X^{Ga}_{Fe}}$$ and $X_{Fe}$ and $X_{Mg}$ are the mole fractions of iron and magnesium in cordierite (Cd) and garnet (Ga).

It is well established from natural assemblages that $K_D$ varies as a function of temperature, increasing steadily with increasing metamorphic grade, but $K_D$ does apparently not change systematically with changing pressure (Holdaway and Lee, *op.cit.*), thus the above equilibrium is a sound geothermometer. The observation that pressure has only a small influence on the exchange reaction can be appreciated from the rather small volume change involved when ions of similar size substitute for each other. According to Thompson (*op.cit.*) the partitioning of Mg and Fe between the coexisting phases is independent of the Fe/Mg bulk composition of the rock.

Considering the condition of equilibrium, i.e. $\Delta G = 0$ and re-arranging equation (T7) yields the expression

$$T = \frac{\Delta H^{o} + (P-1)\ \Delta V^{o}}{\Delta S^{o} - R \ln K_D} \qquad (T8)$$

which can be solved for temperature, provided the thermodynamic parameters $\Delta H$, $\Delta S$, $\Delta V$ and P for the exchange reaction (74) are known. Fortunately, the above reaction has been calibrated experimentally and by using natural assemblages (Thompson, *op.cit*; Holdaway and Lee, *op.cit.*), the following numerical values for $\Delta H$, $\Delta S$ and $\Delta V$ are obtained and listed in Table 21.

TABLE 21 Thermodynamic data for the Mg-Fe exchange reaction between garnet and cordierite.

| Author | $\Delta H^{o}$ (cal) | $\Delta S^{o}$ (cal/deg) | $\Delta V^{o}$ (cal/bar) |
|---|---|---|---|
| Thompson (1976b) | 5415,18 | 1,7806 | 0,0308 |
| Holdaway and Lee (1977) | 6150 | 2,69 | 0,0303 |

Substituting these values into equation (T8) yields the following geothermometers:

$$T = \frac{2724{,}948 + 0{,}0155P}{\ln K_D + 0{,}896} \qquad \text{(T9) - Thompson (1976b)}$$

$$T = \frac{6150 + 0{,}0303P}{2{,}69 - 1{,}98717 \ln K_D} \qquad \text{(T10) - Holdaway and Lee (1977)}$$

It should be pointed out that in these geothermometers $K_D$ in equation (T10) is the same as defined above, while equation (T9) is consistent with the inversed $K_D$, i.e.

$$K_D = \frac{X_{Fe}^{Ga} \cdot X_{Mg}^{Cd}}{X_{Mg}^{Ga} \cdot X_{Fe}^{Cd}}$$

These two geothermometers can be applied to coexisting garnet-cordierite mineral pairs in the natural environment provided their compositions do not deviate markedly from the binary Fe-Mg system.

(a) Application of Garnet-Cordierite Geothermometry

Thirteen metapelite specimens were selected to cover the entire granulite facies terrane of the study area. Coexisting garnet and cordierite grains have been analysed by microprobe techniques. Three to seven spot analyses were carried out per mineral for each specimen and mean compositions were then determined for each mineral (Appendix II, Tables A2-8 and A2-9). In some specimens, the garnets show two distinctly different core compositions in which case mean compositions for each group have been calculated separately. The cordierite grains on the other hand, possess fairly uniform core compositions (Chapter III C5).

Both minerals are zoned (as outlined in Chapter III C5). Cordierite has a distinctly higher Mg/(Mg + Fe) ratio at the rim compared to its core, while garnet cores have a lower Mg/(Mg + Fe) ratio than their corresponding rims. The zonation pattern is smooth and bell-shaped and is interpreted to form as a result of Mg-Fe re-equilibration related to cooling (discussed in Chapter III C5). For this reason only mean core compositions of the coexisting phases have been used in the computation of equilibrium temperatures with the aid of equations (T9) and (T10).

The results obtained with the Holdaway and Lee (*op.cit.*) geothermometer are listed in Table 22 for the pressure range 4-7 kb. The difference in computed temperatures at a pressure of 4 kb compared to the 7 kb results comprises only 16°C. In Table 23, the results obtained with the Thompson (*op. cit.*) calibration (equation T9) are listed. A comparison of the two geothermometers shows that the Thompson calibration invariably yields higher temperatures by as much as 52°C compared with the Holdaway and Lee calibration.

TABLE 22 Temperatures calculated for coexisting garnet and cordierite pairs using the Holdaway and Lee (1977) geothermometer (equation T10). $K_D$ has been evaluated from the mean core compositions. * Indicates specimens with inhomogeneous garnet core compositions.

$K_D = X_{Fe}/X_{Mg}$ cordierite $\cdot$ $X_{Mg}/X_{Fe}$ garnet

| Specimen No. | $K_D$ | ln $K_D$ | T°C at 4 kb | T°C at 5 kb | T°C at 6 kb | T°C at 7 kb |
|---|---|---|---|---|---|---|
| HA 1026 | 0,1897 | -1,6623 | 773 | 778 | 783 | 789 |
| *HA 841 | 0,1962 | -1,6286 | 785 | 790 | 795 | 801 |
| *HA 841 | 0,1805 | -1,7120 | 756 | 761 | 766 | 771 |
| *HA 143 | 0,1827 | -1,6999 | 760 | 765 | 770 | 775 |
| *HA 143 | 0,1651 | -1,8012 | 727 | 732 | 737 | 742 |
| HA 1036 | 0,1704 | -1,7696 | 737 | 742 | 747 | 752 |
| *HA 505 | 0,1473 | -1,9153 | 692 | 697 | 702 | 706 |
| *HA 505 | 0,2021 | -1,5990 | 796 | 801 | 806 | 811 |
| HA 681 | 0,1917 | -1,6518 | 777 | 782 | 787 | 792 |
| HA 870 | 0,1925 | -1,6477 | 778 | 784 | 789 | 794 |
| HA 708 | 0,1863 | -1,6804 | 767 | 772 | 777 | 782 |
| HA 514 | 0,1918 | -1,6513 | 777 | 782 | 787 | 792 |
| HA 329 | 0,1789 | -1,7220 | 753 | 758 | 763 | 768 |
| HA 632 | 0,2068 | -1,5759 | 804 | 809 | 815 | 820 |
| *HA 982/B | 0,1750 | -1,7427 | 746 | 751 | 756 | 761 |
| *HA 982/B | 0,1399 | -1,9670 | 677 | 682 | 687 | 691 |
| *HA 869/B | 0,1775 | -1,7285 | 751 | 756 | 761 | 766 |
| *HA 869/B | 0,1927 | -1,6466 | 779 | 784 | 789 | 794 |
| HA 164 | 0,1466 | -1,9203 | 691 | 696 | 700 | 705 |

TABLE 23 Temperatures calculated for coexisting garnet and cordierite pairs using the Thompson (1976b) calibration (equation T9). $K_D$ has been evaluated from mean core compositions. * Indicates specimens with inhomogeneous garnet core compositions.

$K_D = X_{Fe}/X_{Mg}$ garnet • $X_{Mg}/X_{Fe}$ cordierite

| Specimen No. | $K_D$ | ln $K_D$ | T°C at 4 kb | T°C at 5 kb | T°C at 6 kb | T°C at 7 kb |
|---|---|---|---|---|---|---|
| HA 1026 | 5,2720 | 1,6624 | 816 | 822 | 828 | 835 |
| *HA 841 | 5,0958 | 1,6284 | 831 | 837 | 843 | 849 |
| *HA 841 | 5,5398 | 1,7120 | 796 | 802 | 808 | 813 |
| *HA 143 | 5,4720 | 1,6996 | 801 | 807 | 813 | 819 |
| *HA 143 | 6,0586 | 1,8015 | 760 | 766 | 772 | 777 |
| HA 1036 | 5,8681 | 1,7695 | 773 | 778 | 784 | 790 |
| *HA 505 | 6,7874 | 1,9151 | 718 | 724 | 729 | 735 |
| *HA 505 | 4,9488 | 1,5991 | 844 | 850 | 856 | 863 |
| HA 681 | 5,2157 | 1,6517 | 821 | 827 | 833 | 839 |
| HA 870 | 5,1953 | 1,6477 | 823 | 829 | 835 | 841 |
| HA 708 | 5,3683 | 1,6805 | 809 | 815 | 821 | 827 |
| HA 514 | 5,2127 | 1,6511 | 821 | 827 | 833 | 839 |
| HA 329 | 5,5895 | 1,7209 | 792 | 798 | 804 | 810 |
| HA 632 | 4,835 | 1,5759 | 854 | 861 | 867 | 873 |
| *HA 982/B | 5,7127 | 1,7427 | 783 | 789 | 795 | 801 |
| *HA 892/B | 7,1492 | 1,9670 | 700 | 706 | 711 | 717 |
| *HA 869/B | 5,6323 | 1,7285 | 789 | 795 | 801 | 807 |
| *HA 869/B | 5,1895 | 1,6466 | 823 | 829 | 835 | 841 |

Fig. 73 Geographic distribution of equilibration temperatures (in $^{o}$C) determined for core compositions of coexisting garnet-cordierite pairs in pelitic gneiss specimens. The first figure at each locality represents the temperature calculated by means of the Holdaway and Lee (1977) calibration (equation T10) at an assumed pressure of 5 kb, while the temperatures determined with the Thompson (1976b) geothermometer (equation T9) at 5 kb pressure are shown in brackets. The broken line represents the approximate boundary between the granulite and amphibolite facies terranes.

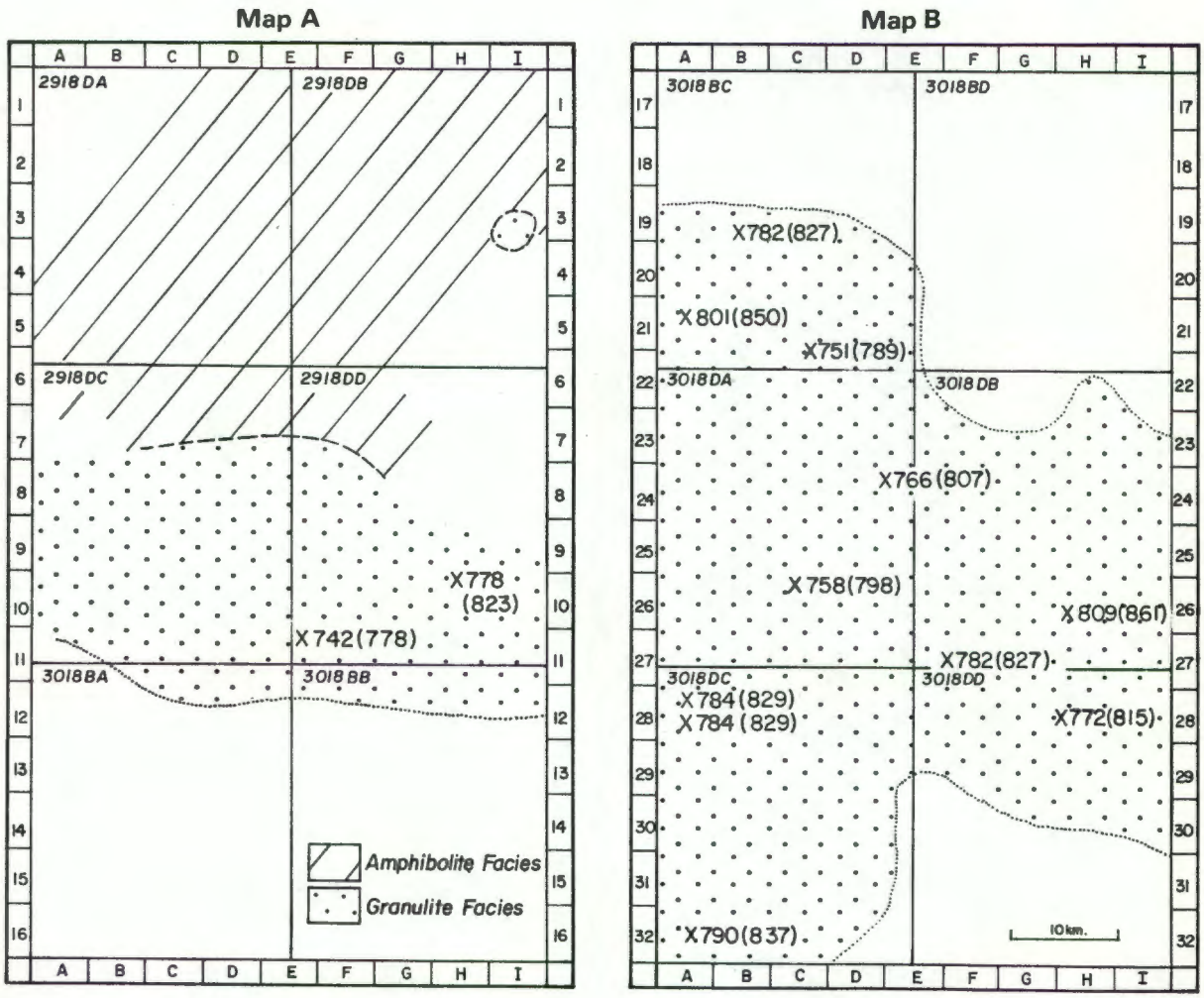

Inspection of Tables 22 and 23 shows that for five specimens (HA 841, HA 143, HA 505, HA 982/B and HA 869/B) two temperatures have been computed. These stem from the inhomogeneous core compositions of the garnet grains as outlined in Chapter III C 5. In each case the higher computed temperature is considered to reflect the thermal peak recorded in the metamorphosed pelitic gneisses. It is also evident from Table 22 that the temperatures computed for specimen HA 164 are somewhat lower compared to all other specimens, but no significance should be assigned to this, because the temperature computations in this specimen are based on the composition of a single small cordierite grain in contact with a larger garnet grain. It is, therefore, very likely that the cordierite grain core was affected by retrograde ion exchange.

The geographic distribution of garnet-cordierite temperatures computed for an assumed pressure of 5 kb is shown in Fig. 73 . Only the maximum temperature estimates are considered as they reflect the peak conditions of metamorphism. The temperatures determined by the Holdaway and Lee (*op.cit.*) method are considered to be more accurate. These fall into the range of 742 - 809°C at 5 kb (disregarding HA 164) with a mean temperature of 778°C ± 19°C. The small standard deviation and inspection of Fig. 73 indicates that the garnet-cordierite temperatures do not suggest any significant regional variation in temperature across the granulite facies area investigated.

## 6 Two-Feldspar Geothermometry

A semi-empirical two-feldspar geothermometer was originally proposed by Barth (1934, 1951, 1956, 1962) and is based on the distribution of the $NaAlSi_3O_8$ molecule between coexisting plagioclase and alkali feldspar, the equilibrium of which can be expressed as:

$$NaAlSi_3O_8\ (Kf) \rightleftharpoons NaAlSi_3O_8\ (Pg) \qquad (75)$$

where Kf and Pg represent, respectively, alkali feldspar and plagioclase feldspar. More recently, several authors have attempted to improve the original formulation of the Barth geothermometer by using a firmer theoretical basis and by exploiting the accumulated knowledge on the experimentally calibrated feldspar solvus (Stormer, 1975; Powell and Powell, 1977; Whitney and Stormer, 1977a; Brown and Parsons, 1981).

The structural state of alkali feldspar has an influence on the thermodynamic parameters of this mineral and becomes a significant factor to be considered when estimating temperatures of equilibration (Whitney and Stormer, *op. cit.*). The two-feldspar geothermometer as formulated by Stormer (*op.cit.*) is based on the thermodynamic parameters for high temperature sanidine solution series and yields the following temperature–composition relationships:

$$T = \frac{\{6326{,}7 - 9963{,}2X_{Kf} + 943{,}3X_{Kf}^2 + 2690{,}2X_{Kf}^3 + (0{,}0925 - 0{,}1458X_{Kf} + 0{,}0141X_{Kf}^2 + 0{,}0392X_{Kf}^3)P\}}{\{-1{,}9872 ln\left(\frac{X_{Kf}}{X_{Pg}}\right) + 4{,}6321 - 10{,}815X_{Kf} + 7{,}7345X_{Kf}^2 - 1{,}5512X_{Kf}^3\}} \qquad (T11)$$

where $X_{Kf}$ and $X_{Pg}$ represent, respectively, the mole fractions of albite in alkali feldspar and plagioclase and P takes into account the pressure of equilibration. A number of assumptions regarding the solution model have been made by Stormer (*op.cit.*). It is assumed that the K component has no effect on the plagioclase and the Ca component has no effect on K feldspar. Brown and Parsons (*op.cit.*), however, have pointed out that this assumption is only justified at near infinite dilution of these components. Based on the data of Orville (1972), unit activity is envisaged for albite solution in plagioclase, while the activity coefficients for albite-alkali feldspar solutions is based on Thompson and Waldbaum (1969) and Waldbaum and Thompson (1969).

This geothermometer is subsequently reformulated by Whitney and Stormer (*op.cit.*) in an attempt to evaluate the effects of ordering in alkali feldspar using the thermodynamic parameters for microcline-low albite solid solutions which yields the following expression:

$$T(K^{o}) = \frac{\{7973,1-16910,6X_{Kf}+ 9901,9X^{2}_{Kf} + (0,11-0,22X_{Kf}+ 0,11X^{2}_{Kf})P\}}{\{-1,987ln\ \frac{X_{Kf}}{X_{Pg}} + 6,48-21,58X_{Kf} + 23,72X^{2}_{Kf} - 8,62X^{3}_{Kf}\}} \quad (T12)$$

Both these equations (T11 and T12) are strictly speaking not applicable to granulite facies mineral assemblages because, although the alkali feldspars are generally microcline microperthite, it is likely that the microcline has inverted from orthoclase (Howie, 1955). If orthoclase was the stable alkali feldspar during the peak conditions of regional metamorphism in the study area, a thermometer involving the thermodynamic parameters of orthoclase is more applicable. Such an equation has not been derived and Whitney and Stormer (*op.cit.*) suggest that the mean temperature computed for equation (T11) and (T12) gives reasonably accurate results for the orthoclase structural state.

The temperature-composition relationships in equations (T11) and (T12) have been utilised in this study. The major problem involved in their application is concerned with the analytical uncertainty in alkali feldspar analyses. The alkali feldspars are invariably perthitic increasing the danger of not obtaining homogeneous bulk compositions by microprobe techniques. This potential danger has been reduced, however, by a method described in Appendix Ic.

Coexisting plagioclase and alkali feldspar have been analysed in seven pelitic gneiss specimens (Appendix II, Tables A2-13 and A2-17). These analyses were used to evaluate $X_{Kf}$ and $X_{Pg}$, and the equilibrium temperatures were then determined with the aid of equations (T11) and (T12) (Table 24). From the results in Table 24 mean temperatures were computed as suggested by Whitney and Stormer (*op.cit.*) (Table 25).

TABLE 24 Temperature (°C) calculated from equations (T11) and (T12) for coexisting alkali feldspar and plagioclase in pelitic gneiss specimens at pressures of 5 to 7 kb.

| Specimen | $X_{Ab}^{Kf}$ | $X_{Ab}^{Pg}$ | TEMPERATURE (°C) Equation (T11) at 5 kb | at 6 kb | at 7 kb | Equation (T12) at 5 kb | at 6 kb | at 7 kb |
|---|---|---|---|---|---|---|---|---|
| HA 1026 | ,118 | ,547 | 579 | 591 | 602 | 624 | 635 | 647 |
| HA 505 | ,265 | ,700 | 696 | 709 | 723 | 795 | 810 | 824 |
| HA 143 | ,205 | ,724 | 618 | 630 | 643 | 688 | 700 | 713 |
| HA 164 | ,162 | ,642 | 604 | 616 | 628 | 659 | 672 | 684 |
| HA 632 | ,232 | ,660 | 684 | 697 | 710 | 767 | 780 | 794 |
| HA 681 | ,171 | ,634 | 620 | 632 | 644 | 678 | 691 | 703 |
| HA 841 | ,154 | ,595 | 615 | 627 | 639 | 668 | 680 | 693 |

TABLE 25 Mean temperatures (°C) computed for coexisting alkali feldspar and plagioclase in seven pelitic gneiss specimens from the granulite facies terrane. These temperatures are based on the mean values computed in equations (T11) and (T12) at the indicated pressure.

| Specimen No. | T at 5 kb | T at 6 kb | T at 7 kb |
|---|---|---|---|
| HA 1026 | 602 | 613 | 625 |
| HA 505 | 746 | 760 | 774 |
| HA 143 | 653 | 665 | 678 |
| HA 164 | 632 | 644 | 656 |
| HA 632 | 726 | 739 | 752 |
| HA 681 | 649 | 662 | 674 |
| HA 841 | 642 | 654 | 666 |

Inspection of Table 25 shows that with the exception of specimens HA 505 and HA 632 all other specimens have yielded rather low temperatures and the question arises whether temperatures below 700°C are realistic for the study area (granulite facies terrane) in the light of the results obtained by the other thermometers. The accuracy of the two-feldspar thermometers are considered to be ± 50°C (Bohlen and Essene, 1977). Both thermometers have been tested in volcanic and granitic rocks (Whitney and Stormer, 1976, 1977b) yielding good results. They have also been applied with success to high grade metamorphic rocks. For example, Stormer and Whitney (1977) compute temperatures ranging between 750-800°C for quartzo-feldspathic granulites in Brazil and Bohlen and Essene (*op.cit.*) record metamorphic temperatures in the range 650 ± 50°C to 750 ± 50°C for coexisting feldspars in the Adirondack Highlands using the same technique.

One possible explanation for the low temperatures computed here involves

a consideration of geometry. The exsolution lamellae in the alkali feldspar show preferred orientation and accordingly the composition of the surface analysed will be influenced by the orientation of the feldspar crystal. According to Hurlbut and Klein (1977), the exsolution lamellae in perthitic alkali feldspar occur roughly parallel to {100}. It should be noted that the high temperatures (HA 505, HA 632) were obtained from the compositions of alkali feldspar surfaces displaying abundant exsolution lamellae while all low temperatures correlate with crystal surfaces not showing much microscopically visible exsolution. It must also be pointed out that these temperature calculations are based only on a single alkali feldspar analysis per specimen because of difficulties experienced with the microprobe when the measurements were being conducted.

It is tentatively concluded that the temperature variations determined for coexisting feldspars in this study could be a reflection of the geometric orientation of the alkali feldspar relative to the electron beam implying that the compositions determined do not represent homogeneous bulk analyses. Therefore, the temperature computations represent absolute minimum temperatures.

## B Geobarometry

### 1 Introduction

It has already been pointed out that the presence of cordierite in pelitic gneisses of the study area can be cited as evidence for pressure conditions of less than 8 to 11 kb during the regional metamorphism (Chapter III C 6). Additional pressure constraints stem from the observed mineral assemblages in mafic rocks. The aluminous phases encountered in mafic rocks are good pressure indicators. Garnet is stable at high pressures, spinel at intermediate pressures and plagioclase at low pressures (Kushiro and Yoder, 1966; Green and Ringwood, 1967; Emslie, 1970; Frost, 1976; Herzberg, 1976a,b; Jenkins and Newton, 1979; Obata and Thompson, 1981).

De Waard (1964, 1965a,b, 1967) subdivides the granulite facies in the Adirondacks into a lower pressure hornblende-orthopyroxene-plagioclase subfacies and a higher pressure hornblende-clinopyroxene-almandine subfacies. The reaction responsible for the formation of garnet is considered to be:

$$\text{orthopyroxene} + \text{anorthite} \rightleftharpoons \text{clinopyroxene} + \text{garnet} + \text{quartz} \qquad (76)$$

The formation of garnet at the expense of orthopyroxene and anorthite has been experimentally investigated by Ringwood and Green (1964, 1966) and Green and Ringwood (1967, 1972) on a range of basaltic compositions at pressures up to 30 kb in the temperature range 1000 - 1250°C. These experiments have shown that for quartz tholeiite, the mineral assemblage pyroxene + plagioclase is replaced by garnet + pyroxene + plagioclase and finally garnet + clinopyroxene + quartz with increasing pressure. The first garnet to form is almandine-rich and with increasing pressure the mineral becomes increasingly enriched in the pyrope molecule. Depending on the mineralogy Green and Ringwood (*op.cit.*)

divide the granulite facies into three pressure zones:

(i) Low-pressure granulites - olivine and plagioclase are associated in basic rocks.

(ii) Intermediate-pressure granulites - olivine is incompatible with plagioclase and is replaced by the association orthopyroxene + plagioclase.

(iii) High-pressure granulite - hypersthene and plagioclase are incompatible while the assemblage garnet + clinopyroxene + quartz typical of eclogites, is stable.

The experimental data presented by Green and Ringwood (*op.cit.*) on the upper stability limit of olivine + plagioclase in basaltic rocks and the lower stability limit of garnet in quartz tholeiite have been extrapolated to lower temperatures and are respectively shown as curves (a) and (b) in Fig. 74.

Kushiro and Yoder (1966) have studied mafic compositions at somewhat lower temperatures and they find that within the temperature range of the granulite facies, garnet is stable in mafic rocks at lower pressures than indicated by the extrapolation of Green and Ringwood (*op.cit.*). The lower stability limit of garnet in mafic rocks as determined by Kushiro and Yoder (*op.cit.*) is shown as curve (c) in Fig. 74. Green and Ringwood (1972), however, point out that the first appearance of garnet in basaltic rocks is dependent on the bulk composition particularly with respect to silica saturation, the Ab/(Ab+An) ratio of the plagioclase and the bulk rock Mg/(Mg+Fe) ratio.

The ubiquitous occurrence of orthopyroxene + plagioclase assemblages in textural equilibrium in the majority of mafic rock specimens from the granulite facies terrane in the study area is cited as evidence for the stable coexistence of the two minerals, suggesting that the granolites must be regarded as intermediate-pressure granulites in the sense of Green and Ringwood (*op. cit.*). Accordingly, the pressures that are likely to have prevailed during granulite facies metamorphism are expected to fall somewhere into the cross-hatched area in Fig. 74. On the other hand, as outlined in chapter III E, some of the mafic rocks contain olivine and plagioclase, suggesting low pressure conditions. The close spatial association of the olivine-bearing and olivine-free metabasites suggests that the presence of olivine is, at least to some extent, controlled by bulk composition.

Experimental studies on the upper pressure stability limit of coexisting olivine and plagioclase (Kushiro and Yoder, *op.cit.;* Green and Ringwood, *op. cit.;* Irving and Green, 1970; Emslie, *op.cit.*) have revealed that in the temperature range 700 to 900°C the coexistence of these two minerals is only possible at low pressures not exceeding 6 to 8 kb.

In order to evaluate the pressures accompanying regional metamorphism in a quantitative manner, some reasonably well-defined, pressure sensitive mineral equilibria in chemical end-member systems have been utilised as geobarometers. Pressures are evaluated from equilibria with relatively shallow $\frac{dP}{dT}$ slopes. The following barometers have been utilised:

Coexisting garnet, plagioclase, sillimanite and quartz (Ghent, 1976)
Coexisting garnet, cordierite, sillimanite and quartz (derived in this study)
Coexisting plagioclase, clinopyroxene and quartz

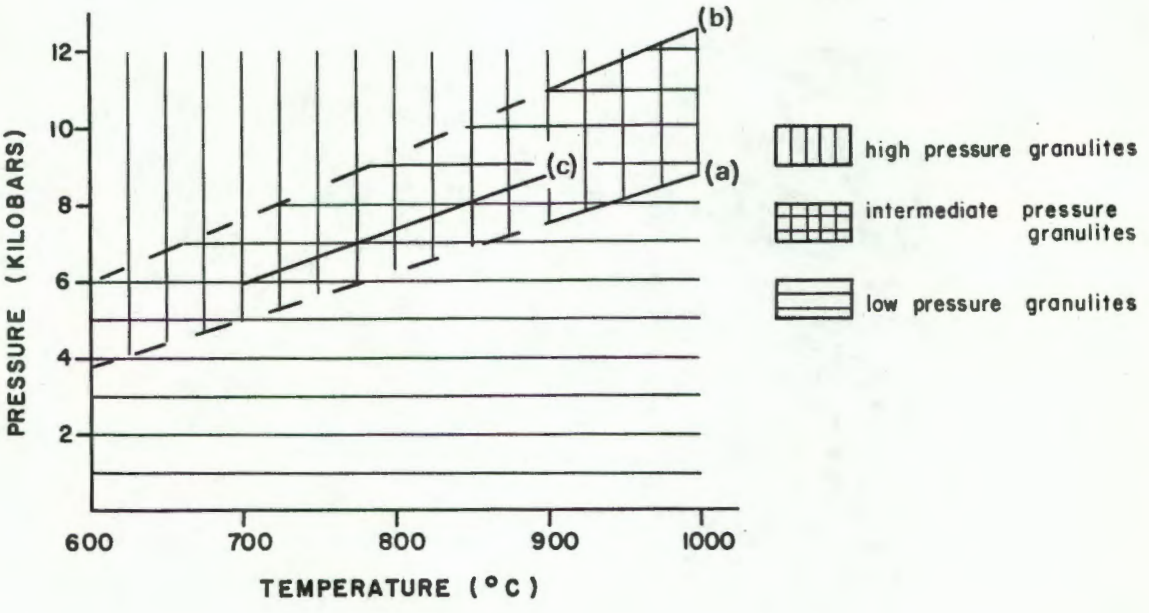


Fig. 74 Schematic subdivision of the granulite facies into low-pressure, intermediate-pressure and high-pressure granulites after Green and Ringwood (1967, 1972).

(a) upper stability limit of olivine + plagioclase in basaltic rocks (Green and Ringwood, 1967).
(b) lower stability limit of garnet in quartz tholeiite (Green and Ringwood, 1967).
(c) lower stability limit of garnet in mafic rocks (Kushiro and Yoder, 1966).

The pressure estimates derived in this study are based mainly on the two equilibria involving garnet - plagioclase - sillimanite - quartz and garnet - cordierite - sillimanite - quartz. Unfortunately, no pelitic gneiss outcrops are encountered in the amphibolite facies terrane of the study area and, therefore, the garnet - sillimanite - quartz equilibria could not be utilised for quantitative pressure estimates in the lower grade part of the area investigated. In order to establish the likely pressure conditions recorded in the amphibolite facies terrane a relative geobarometer involving the equilibrium between Ca-Tschermak's molecule, anorthite and quartz has been applied in this study.

A knowledge of the thermodynamic parameters of enthalpy, entropy and volume changes in end-member reactions can be utilised to evaluate the equilibrium pressures in equivalent natural systems, provided the chemical compositions of the mineral phases and a reasonable solution model can be established. The chemical compositions of coexisting minerals that were used for the evaluation of the pressure conditions are tabulated in Appendix II.

2 Garnet-Plagioclase-Sillimanite-Quartz Equilibria as Geobarometer

According to Ghent (1976), the equilibrium between anorthite, grossular, sillimanite and quartz provides a potential geobarometer. These phases can be related by the reaction:

$$3\ CaAl_2Si_2O_8 \rightleftharpoons Ca_3Al_2Si_3O_{12} + 2\ Al_2SiO_5 + SiO_2 \qquad (76)$$

(anorthite) (Grossular) (sillimanite) (quartz)

At equilibrium, the pure phases in the above reaction obey the expression

$$0 = 7{,}1711 - \frac{2551{,}4}{T} - \frac{0{,}2842\ (P-1)}{T} \quad (T13)\ (\text{Ghent, } op.cit.)$$

which can be solved for the equilibrium pressure (P) at the temperature (T) of interest. This relationship can be applied to the natural system, provided allowance is made for the fact that naturally occurring garnet and plagioclase are mixtures of various end members. The amount of the grossular component in garnet and the anorthite component in plagioclase can be expressed in terms of their respective activities and these activity terms can then be added to the above expression. The activity of grossular in garnet is given by

$a^{garnet}_{grossular} = X^{3\,garnet}_{grossular} \cdot \gamma^{3\,garnet}_{grossular}$ (Wood and Fraser, 1977), where

X is the mole fraction of grossular in garnet and $\gamma$ represents the activity coefficient.

For coupled substitution of the type $CaAl \rightleftharpoons NaSi$ the activity-composition relationship for plagioclase is given by: $a^{plagioclase}_{anorthite} = X^{plagioclase}_{anorthite} \cdot \gamma^{plagioclase}_{anorthite}$. The mole fractions (X) of the two phases are obtained from microprobe analyses of the natural minerals and if the activity coefficients are known and the temperature can be estimated, the equilibration pressure during metamorphism can be calculated by solving the expression

$$P = \frac{7{,}1711 - 2551{,}4 + T\left[\log X^{3Ga}_{Gr} \cdot \gamma^{3Ga}_{Gr} - 3 \log X^{Pg}_{An} \cdot \gamma^{Pg}_{An}\right]}{0{,}2842} + 1 \quad (T14)$$

provided sillimanite and quartz are pure phases (Ghent, *op.cit.*). The activity coefficients of anorthite in plagioclase ($\gamma_{An}$) are not well established. Orville (1972) has calculated $\gamma_{An}$ for the entire range of plagioclase compositions from $X_{An} = 0$ to $X_{An} = 1$ at intervals of 0,1 $X_{An}$ at a temperature of 700°C and pressure of 2 kb. His results indicate a positive deviation from ideality in plagioclases of low and intermediate anorthite content, but with increasing anorthite content the mineral behaves increasingly ideal. The data of Orville (*op.cit.*) have been applied to the present study and a value for $\gamma_{An} = 1,276$ has been used in the pressure calculations.

The mixing properties of garnets have also been investigated experimentally. Cressey *et al.* (1978) have studied almandine-grossular garnet solid solutions in the temperature range, 850-1100°C. They have shown that at low mole fractions of grossular ($X_{grossular} < 0,2$) the activity coefficient $\gamma_{grossular}$ is very close to 1,0. There is only a very slight negative deviation of $\gamma$ from ideality in this range at high pressures. With increasing $X^{garnet}_{grossular}$ (> 0,2) $\gamma_{grossular}$ shows a positive deviation from ideality which again approaches 1,0 at very high grossular contents. The negative deviation at the low $X_{grossular}$ side of the almandine-grossular join increases with decreasing pressure and at 1 bar $\gamma^{garnet}_{grossular}$ reaches the lowest value of approximately 0,8 (Cressey, *et al.*,*op.cit.*). As the garnets in the pelites of the study area have a very low mole fraction of grossular and a very high mole fraction of almandine, it is concluded that $\gamma^{garnet}_{grossular}$ will have a slight negative deviation from ideality. The addition of the pyrope molecule to this garnet has the opposite effect on $\gamma$. The activity coefficients for grossular in pyrope-grossular garnets have been determined by Hensen *et al.* (1975). They have found that at high pressures (16-21 kb) there is a positive deviation from ideality ($\gamma > 1$) for the composition range $X^{garnet}_{grossular}$ = 0,10-0,22. This deviation from ideality increases with decreasing temperature in the temperature range 1000-1300°C. According to Newton *et al.* (1977), the maximum non-ideality on the pyrope-grossular join occurs on the pyrope-rich end, while grossular-rich garnets are more nearly ideal. This positive deviation to some extent cancels the negative deviation on the almandine-grossular join, so that in effect the natural garnet concerned in this study will approach ideality. For this reason $\gamma^{garnet}_{grossular}$ is assumed unity in the pressure calculations.

In order to utilise equation (T14) core compositions of coexisting garnet and plagioclase in pelitic gneisses also containing sillimanite and quartz were determined by electron microprobe techniques. The mean core compositions of the minerals analysed are tabulated in Appendix II, Tables A2-8 and A2-13.

Equilibration pressures were computed using these core compositions and the temperatures previously determined for coexisting garnet and cordierite in equation (T10). Sillimanite and quartz are assumed to be pure phases of unit activity. The results are shown in Table 26 and Fig. 75.

Table 26 Pressures (in bars) computed from the compositions of coexisting garnet and plagioclase in equilibrium with sillimanite and quartz, using the Ghent (1976) geobarometer (equation T14). Only core compositions were used. The assumed equilibrium temperature is based on the computations involving garnet-cordierite equilibria (equation T10). $n_{Ga}$ and $n_{Pg}$ represent the number of garnet and plagioclase analyses respectively which have been used to evaluate the mean core compositions of the two minerals for each specimen.

| Specimen No. | LOCALITY | $n_{Ga}$ | $n_{Pg}$ | $X^{Ga}_{Ca}$ | $X^{Pg}_{An}$ | $X^{Ga}_{Gr}$ | assumed $T^oC$ | pressure (bars) |
|---|---|---|---|---|---|---|---|---|
| HA 870 | A28 | 6 | 4 | 0,0849 | 0,331 | 0,028 | 784 | 4595 |
| HA 329 | C26 | 6 | 1 | 0,0666 | 0,231 | 0,022 | 758 | 4814 |
| HA 632 | H26 | 6 | 4 | 0,0846 | 0,330 | 0,028 | 809 | 4914 |
| HA 505 | A21 | 4 | 3 | 0,0787 | 0,289 | 0,026 | 801 | 5109 |

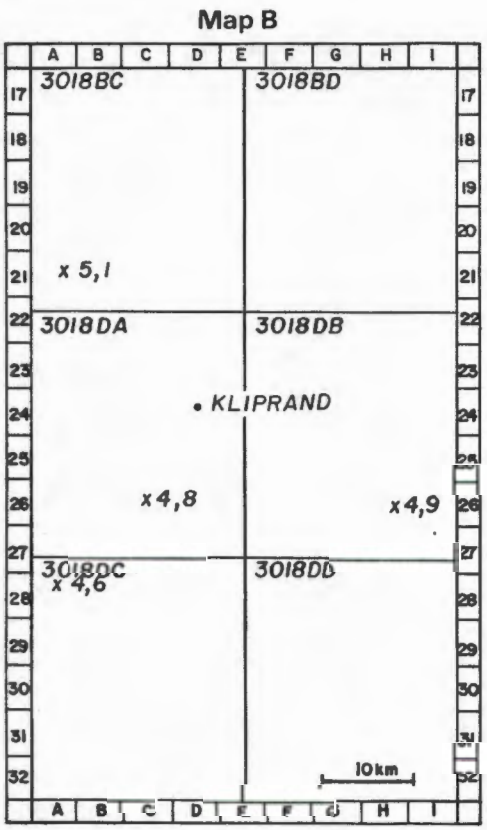


Fig. 75 Pressures in kilobars computed for garnet, plagioclase, sillimanite, quartz equilibria using the Ghent (1976) geobarometer. The calculations are based on mean compositions determined from up to 6 microprobe analyses per mineral per specimen.

The garnet and plagioclase grains that were analysed in the four specimens listed in Table 26 are believed to have crystallised during the main thermal event. Therefore, the above results (Table 26) ) suggest that the pressures that are likely to have prevailed during granulite facies metamorphism in the Kliprand area (MAP B) must have been of the order of 4,6 to 5,1 kb.

### 3 The Garnet-Cordierite Geobarometer

Experimental petrology has revealed that the compositions of coexisting garnet and cordierite in the presence of sillimanite and quartz are very sensitive to changing pressure and thus provide a good geobarometer (Thompson 1976a,b; Holdaway and Lee, 1977). These four phases may be related to each other by the continuous reaction:

$$3\ \text{Fe-Mg-cordierite} \rightleftharpoons 2\ \text{Fe-Mg-garnet} + 4\ \text{sillimanite} + 5\ \text{quartz} \qquad (77)$$

which is bivariant in the system $SiO_2$-$Al_2O_3$-MgO-FeO.

Reaction (77) can be considered as a combination of the following two end member reactions:

$$3\ \text{Mg-cordierite} \rightleftharpoons 2\ \text{pyrope} + 4\ \text{sillimanite} + 5\ \text{quartz} \qquad (78)$$

$$3\ \text{Fe-cordierite} \rightleftharpoons 2\ \text{almandine} + 4\ \text{sillimanite} + 5\ \text{quartz} \qquad (79)$$

Cordierite is known to accommodate water molecules in its channel structure (Schreyer and Yoder, 1964; Newton, 1972). In the presence of water, therefore, the above equilibria become dehydration reactions of the type:

$$3\ \text{Fe-Mg-cordierite} \cdot n\ H_2O \rightleftharpoons 2\ \text{Fe-Mg-garnet} + 4\ \text{sillimanite} + 5\ \text{quartz} + 3n\ H_2O \qquad (80)$$

According to Holdaway and Lee (*op.cit.*), the amount of water in cordierite is a function of $fH_2O$ and temperature. The variable water content in cordierite increases the variance of the system and, therefore, at constant temperature for a garnet-cordierite pair of fixed composition (Mg/(Mg+Fe) ratio) the equilibrium pressure depends on the hydration state of cordierite. If the hydration state of cordierite can be established it is possible to evaluate the equilibrium pressure provided the equilibrium temperature and chemical composition of the phases are known.

The experimentally determined and calculated end member curves for reactions (78) and (79) and their hydrous equivalents are known to have a shallow $\frac{dP}{dT}$ slope with cordierite on the low pressure side. Unfortunately, however, the literature is full of conflicting representations of the univariant end member curves. Some authors prefer a negative $\frac{dP}{dT}$ slope for both reactions (Hensen and Green, 1971; Thompson, *op.cit.*; Holdaway and Lee,

*op.cit.*) while others prefer a positive $\frac{dP}{dT}$ slope for both reactions (Hutcheon, *et al.*, 1974; Martignole and Sisi, 1981). In this study, the derivation of the garnet-cordierite geobarometer is based on the assumption that the Fe-end member reaction has a negative $\frac{dP}{dT}$ slope.

The Fe-end member reaction involving the breakdown of Fe-cordierite to almandine + sillimanite + quartz + water, has been experimentally studied by Richardson (1968) and Holdaway and Lee (*op.cit.*) under the conditions where $P_{H_2O} = P_{total}$. Their experimental results may be used to extract the thermodynamic parameters $\Delta H$ and $\Delta S$, provided the hydration state of cordierite is known. Unfortunately, very little is known about the hydration behaviour of Fe-cordierite, but the hydration of Mg-cordierite has been investigated experimentally (Mirwald and Schreyer, 1977). Newton and Wood (1979) have demonstrated that the molecular water content of cordierite has a large influence on cordierite-breakdown equilibria. These authors have treated Mg-cordierite as an ideal solution between an anhydrous and a fully hydrated end member related by the reaction:

$$Mg_2Al_4Si_5O_{18} + m\ H_2O \rightleftharpoons Mg_2Al_4Si_5O_{18} \cdot m\ H_2O \qquad (81)$$

where m represents the number of moles of $H_2O$ in the hydrated end member. If this reaction is ideal ($\gamma = 1$), the activities are equal to the mole fractions and at chemical equilibrium we have the thermodynamic relationship

$$\Delta H^{o}_{81} - T\Delta S^{o}_{81} + mRT \ln \frac{X}{(1-X)\ f_{H_2O}} + \int_1^P \Delta V_s^{81}\ dP = 0 \qquad (T15)$$

where X represents the mole fraction of the hydrous end member, $\Delta H^o$ and $\Delta S^o$ are respectively, the molar changes in enthalpy and entropy of reaction (81) and $\Delta V_s$ is the volume change of the solids. ($\Delta V_s$ is zero in reaction (81)). The superscript 81 indicates that the thermodynamic parameters refer to reaction (81).

Newton and Wood (*op.cit.*) have fitted their thermodynamic model to the hydration experiments of Mirwald and Schreyer (*op.cit.*) and find that a value of m = 1,2 is most consistent with these experiments which yield the thermodynamic parameters $\Delta V$ =-12300 cal and $\Delta S$ = -32,87 cal/K$^o$ at 1 bar for reaction (81). Thus, one mole of fully hydrated Mg-cordierite contains 1,2 moles of water. As m varies as a function of $P_{H_2O}$ and temperature, however, it is essential to establish how much water cordierite can absorb under given $P_{H_2O}$-temperature conditions. The above data on cordierite hydration allow the calculation of m as a function of pressure and temperature. Rearranging equation (T15) yields

$$\ln f_{H_2O} = \ln X - \frac{\Delta S^{o}_{81} - \frac{\Delta H^{o}_{81}}{T}}{mR} - \ln (1-X) \qquad (T16)$$

which can be solved for $fH_2O$ for a certain value of m and a fixed temperature. The corresponding $P_{H_2O}$ at that temperature can then be determined from the tabulation of Burnham, *et al.* (1969). Equilibrium pressures at fixed temperatures have been calculated for m at intervals of m = 0,1 using the Newton and Wood (*op.cit.*) model. The results of these calculations are tabulated (Table 27 ) and the variation of m as a function of pressure and temperature is shown graphically in Fig. 76.

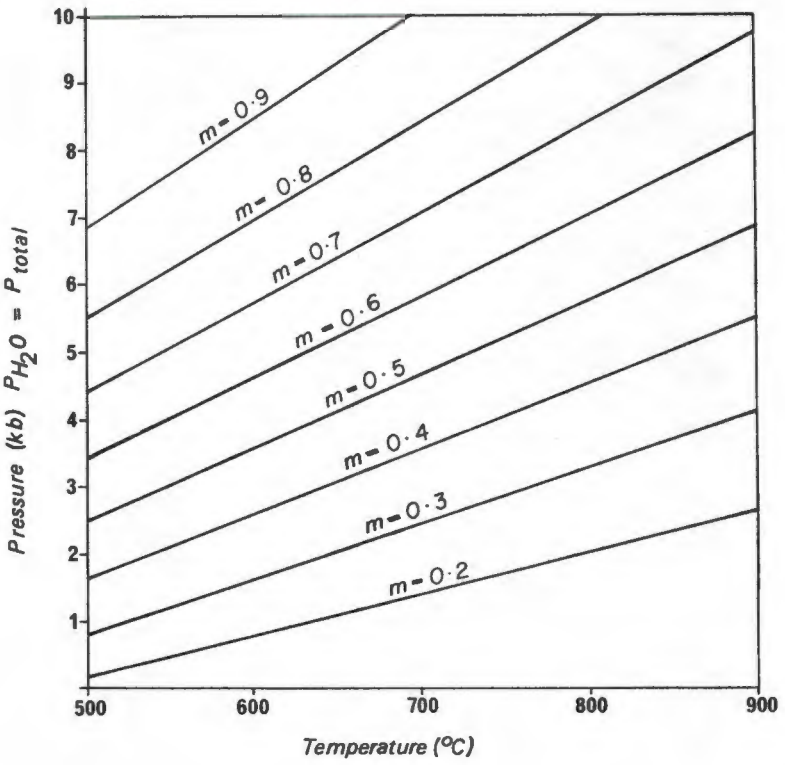


Fig. 76 : The hydration state of Mg-cordierite as a function of $P_{H_2O}$ and temperature. m represents the number of moles of water per mole of cordierite under given $P_{H_2O}$-temperature conditions. The results are based on the thermodynamic model on cordierite hydration of Newton and Wood (1979).

According to Newton and Wood (*op.cit.*) their hydration theory may now be used to recalculate cordierite equilibria determined under the experimental conditions $P_{H_2O} = P_{total}$ onto a $H_2O$-free basis. Thus if the Fe-end member system is considered, the equilibrium of cordierite, garnet, sillimanite and quartz may be represented by the equations:

Table 27 The hydration state of Mg-cordierite as a function of temperature and pressure.

| m | X | ln X | ln (1-X) | $f_{H_2O}$ at 800°K | P bars at 800°K | $f_{H_2O}$ at 900°K | P bars at 900°K | $f_{H_2O}$ at 1100°K | P bars at 1100°K |
|---|---|---|---|---|---|---|---|---|---|
| 0,1 | 0,0833 | -2,4853 | -0,0870 | | | | | 810 | 939 |
| 0,2 | 0,1667 | -1,7916 | -0,1824 | 307 | 360 | | | 1783 | 2212 |
| 0,3 | 0,2500 | -1,3863 | -0,2877 | 512 | 1021 | | | 2971 | 3542 |
| 0,4 | 0,3333 | -1,0987 | -0,4054 | 768 | 1890 | | | 4455 | 4832 |
| 0,5 | 0,4167 | -0,8754 | -0,5391 | 1097 | 2800 | | | 6366 | 6105 |
| 0,6 | 0,5000 | -0,6931 | -0,6931 | 1535 | 3752 | | | 8912 | 7404 |
| 0,7 | 0,5833 | -0,5391 | -0,8754 | 2149 | 4770 | | | 12474 | 8787 |
| 0,8 | 0,6667 | -0,4054 | -1,0987 | 3071 | 5908 | 6287 | 7347 | | |
| 0,9 | 0,7500 | -0,2877 | -1,3863 | 4606 | 7263 | 9430 | 8863 | | |

$$3\ \text{Fe-cordierite}_{(\text{anhydrous})} \rightleftharpoons 2\ \text{Fe-garnet} + 4\ \text{sillimanite} + 5\ \text{quartz} \qquad (79)$$

$$n\ \left[\text{Fe-cordierite} \quad 1.2\ H_2O \rightleftharpoons \text{Fe-cordierite}_{(\text{anhydrous})} + 1.2\ H_2O\right] \qquad (82)$$

However, in order to apply the Newton and Wood (*op.cit.*) thermodynamic data to the Fe-system, it must be assumed that the hydration of cordierite is independent of its Mg/Fe ratio and, in the calculations that follow, it has been assumed the Fe-cordierite has the same hydration behaviour as Mg-cordierite. Furthermore, ideal solution is assumed and sillimanite and quartz are treated as pure substances with unit activity. Under these conditions the Fe-end member system at chemical equilibrium should obey the expression:

$$\Delta H^{o\ 79}_{1,T} - T\Delta S^{o\ 79}_{1,T} + (P-1)\ \Delta VS^{o\ 79}_{s} - n\ RT\ \ln a^{\text{cordierite}}_{\text{anhydrous cordierite}} = 0 \qquad (T17)$$

where $a^{\text{cordierite}}_{\text{anhydrous cordierite}}$ represents the activity of anhydrous cordierite in cordierite and the superscript (79) indicates that the thermodynamic parameters refer to reaction (79). If X represents the mole fraction of hydrous cordierite, by definition, it follows that the mole fraction of anhydrous cordierite is equal to (1-X) and since $\gamma$ is assumed to be unity, the mole fraction is equal to the activity. Substitution and rearranging of equation (T17) yields:

$$(P-1)\ \Delta V_s^{79} - 3\ RT\ \ln\ (1-X) = T\ \Delta S^{o79} - \Delta H^{o79} \qquad (T18)$$

but from equation (T16) we know that

$$\ln\ (1-X) = \ln X - \ln fH_2O - \frac{\Delta S^{o\ 81} - \frac{\Delta H^{o\ 81}}{T}}{mR} \qquad (T19)$$

Substitution of equation (T19) into equation (T18) yields the equilibrium expression for the breakdown of anhydrous Fe-cordierite:

$$(P-1)\ \Delta V_s^{79} - 3\ RT\left[\ln X - \ln fH_2O - \frac{\Delta S^{o\ 81} - \frac{\Delta H^{o\ 81}}{T}}{mR}\right] = T\ \Delta S^{o\ 79} - \Delta H^{o\ 79} \qquad (T20)$$

Equation (T20) has the form of a straight line and plotting the expression on the left-hand side versus temperature yields $\Delta S^{o\ 79}$ as slope and $-\Delta H^{o\ 79}$ as intercept at $T = 0^oK$. In order to extract $\Delta S^{o\ 79}$ and $\Delta H^{o\ 79}$ for the anhydrous reaction (79) the experimental data of Holdaway and Lee (*op.cit.*) and three runs of Richardson (*op.cit.*) have been corrected for $H_2O$ in cordierite using equation (T20). A value of $\Delta V_s^{79} = -4{,}0061$ cal/bar (Holdaway and Lee, *op.cit.*) has been used in the calculations. The experimental runs concerned and the evaluation of the expression on the left-hand side of equation (T20) are tabulated (Table 28). Fig. 77 is a graphical representation of the anhydrous reaction (79) and shows a plot of the expression on the left-hand side of

Table 28 Experimental runs on the equilibrium pressure-temperature boundary for the reaction

3 Fe-cordierite $\rightleftharpoons$ 2 almandine + 4 sillimanite + 5 quartz

after Holdaway and Lee (1977) and Richardson (1968). * indicates almandine + sillimanite stable otherwise cordierite stable. $\Delta V_s$ = -4,0061 cal/bar (Holdaway and Lee, *op.cit.*).

| | X | T(°K) | Pressure (bars) | $f_{H_2O}$ (bars) | (P-1)ΔV | 3RT ln(1-X) | (P-1)ΔV-3RT ln(1-X) |
|---|---|---|---|---|---|---|---|
| (Holdaway and Lee, 1977) | | | | | | | |
| * | ,4119 | 898 | 3800 | 2174 | -15219 | -2842 | -12377 |
| * | ,3968 | 897 | 3600 | 2028 | -14418 | -2703 | -11715 |
| | ,3788 | 899 | 3400 | 1905 | -13617 | -2552 | -11065 |
| | ,3813 | 896 | 3400 | 1888 | -13617 | -2565 | -11052 |
| | ,3643 | 897 | 3200 | 1767 | -12816 | -2423 | -10393 |
| | ,3471 | 898 | 3000 | 1650 | -12014 | -2282 | - 9732 |
| * | ,3701 | 948 | 3800 | 2469 | -15219 | -2612 | -12607 |
| | ,3248 | 947 | 3200 | 2010 | -12816 | -2217 | -10599 |
| | ,3086 | 948 | 3000 | 1875 | -12014 | -2086 | - 9928 |
| | ,2932 | 948 | 2800 | 1743 | -11213 | -1961 | - 9252 |
| * | ,3170 | 999 | 3600 | 2575 | -14418 | -2288 | -12130 |
| * | ,3032 | 998 | 3400 | 2401 | -13617 | -2148 | -11469 |
| * | ,2894 | 997 | 3200 | 2236 | -12816 | -2031 | -10785 |
| | ,2736 | 999 | 3000 | 2089 | -12014 | -1904 | -10110 |
| | ,2748 | 997 | 3000 | 2081 | -12014 | -1910 | -10104 |
| | ,2604 | 997 | 2800 | 1933 | -11213 | -1793 | - 9420 |
| (Richardson, 1963) | | | | | | | |
| * | ,2437 | 1048 | 3000 | 2276 | -12041 | -1745 | -10269 |
| * | ,3284 | 973 | 3500 | 2363 | -14017 | -2309 | -11708 |
| | ,2909 | 973 | 3000 | 1982 | -12014 | -1994 | -10020 |

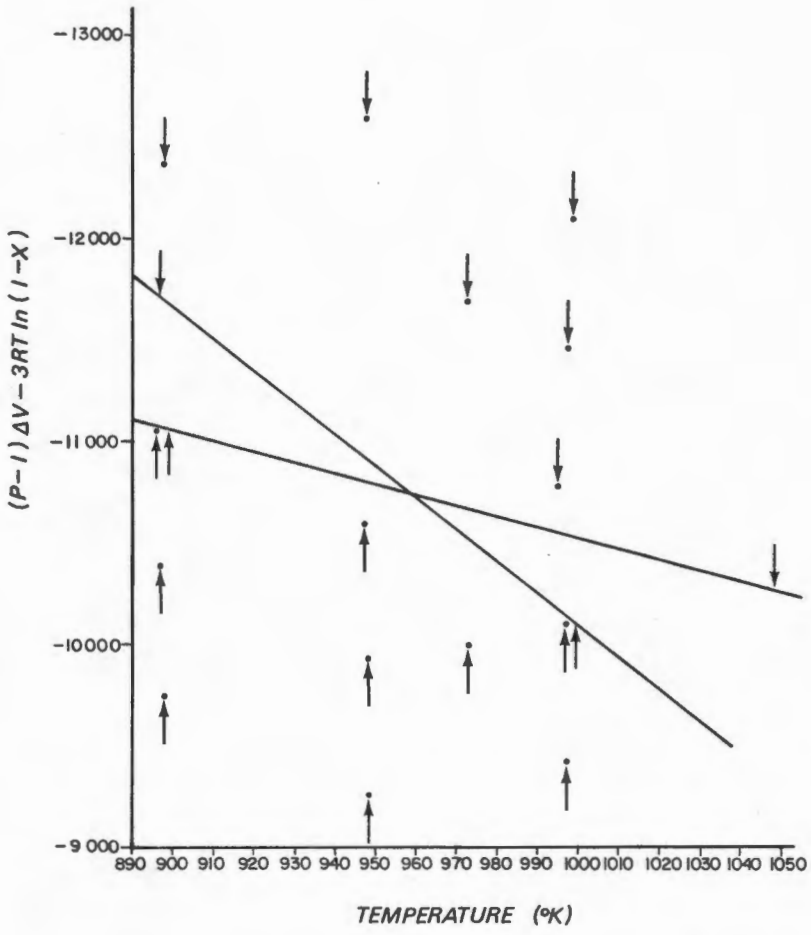


Fig. 77 : Extraction of the thermodynamic parameters $\Delta H$ and $\Delta S$ for the anhydrous cordierite breakdown reaction

3 Fe-cordierite $\rightleftharpoons$ 2 almandine + 4 sillimanite + 5 quartz

using the Holdaway and Lee (1977) and Richardson (1968) experimental results on the above reaction. The two extreme slopes that can be fitted to all the data represent, respectively, $\Delta S_1$ and $\Delta S_2$ which yield a mean $\Delta S$ for the reaction $\left(\frac{\Delta S_1 + \Delta S_2}{2}\right)$ of 10,55 ± 5,27 cal/$^{o}$K while $\Delta H$ for this mean $\Delta S$ is found to be 20857,45 cal..

equation (T20) against temperature from which $\Delta S^{o}_{79}$ and $\Delta H^{o}_{79}$ can be evaluated. If only the experimental runs of Holdaway and Lee (*op.cit.*) are used the two extreme slopes that can be fitted to the data are:

$$\Delta S_1 = 15,82 \text{ cal/K}^{o}$$
$$\Delta S_2 = 2,91 \text{ cal/K}^{o}$$

which yield a mean value for $\Delta S^{o}_{79}$

$$\Delta S^{79}_{mean} = 9,37 \pm 6,45 \text{ cal/K}^{o}$$

Using this mean $\Delta S$ the enthalpy change for reaction (79) is found to be:

$$\Delta H^{79} = 19793,39 \text{ cal}$$

If, however, Richardson's (*op.cit.*) data are included $\Delta S_2$ changes to

$$\Delta S_2 = 5,27 \text{ cal/K}^{o}$$

yielding a mean entropy change $\Delta S^{79}_{mean} = 10,55 \pm 5,27 \text{ cal/K}^{o}$

Using this mean $\Delta S^{79}$ value the enthalpy change for reaction (79) becomes

$$\Delta H^{79} = 20857,45 \text{ cal}$$

For all pressure calculations on the coexisting garnet-cordierite pairs from the study strip containing the assemblages of reaction (79) a value of 10,55 cal/K$^{o}$ has been used for $\Delta S$ and 20857,45 cal for $\Delta H$.

It has already been pointed out that the decomposition of cordierite in reaction (80) liberates water on the high-pressure side of the equilibrium. For any dehydration reaction the equilibrium is very sensitive to changes in $P_{H_2O}$. According to Newton (*op.cit.*) all equilibria with water on the high-pressure side of a reaction shift towards lower pressure with decreasing $P_{H_2O}$. For the reaction concerned, this implies that for a fixed cordierite composition under the conditions $P_{H_2O} = P_{total}$, the mineral is stable to higher pressures than when $P_{H_2O} < P_{total}$, at the same temperature. This demonstrates the necessity of knowledge on $P_{H_2O}$ during metamorphism. If $P_{H_2O}$ is an unknown variable the equilibrium pressures for the two extreme conditions can be calculated, namely when $P_{H_2O} = 0$ (yielding the lower pressure limit) and when $P_{H_2O} = P_{total}$ (which will give the upper pressure limit). The actual pressure must be somewhere in between these two extremes depending on the water pressure.

In the natural system the phases are generally impure so that solid solution has to be taken into account in the equation of state. The most

important deviation of the natural system from the end-member reaction (79) is the substitution of Mg for Fe. An increase in the Mg/(Mg + Fe) ratio will increase the stability field of cordierite relative to its breakdown products (Thompson, *op.cit.*). This can be appreciated from the observed Mg/(Mg+Fe) ratio in naturally coexisting garnet and cordierite pairs where cordierite is always observed to be the more Mg-rich phase of the two. The cordierite analyses of the study area show that this mineral is a fairly pure Mg-Fe phase with only negligible amounts of other impurity ions. Garnet, on the other hand contains, besides the almandine-pyrope components, small amounts of grossular and spessartine in solid solution which tend to stabilise the garnet relative to cordierite, thus shifting the equilibrium towards lower pressures. Ignoring the grossular and spessartine components in garnet will lead to an overestimation of the equilibrium pressures. However, if the compositions of coexisting garnet and cordierite are accurately known, the activity of almandine and Fe-cordierite components in garnet and cordierite respectively, can be determined and can then be incorporated into the equation of state.

With the Newton and Wood (*op.cit.*) model on cordierite hydration and the extracted values of $\Delta H$ and $\Delta S$ for the breakdown reaction of anhydrous cordierite, the condition of chemical equilibrium for any naturally coexisting garnet-cordierite pair that is in equilibrium with sillimanite and quartz can be expressed. Under anhydrous conditions, i.e., when $P_{H_2O}$ is zero, reaction (77) may be formulated as:

$$3(\text{Fe-Mg})\ \text{cordierite}_{\text{anhydrous}} \rightleftharpoons 2(\text{Fe-Mg-Mn-Ca})\ \text{garnet} + 4\ \text{sillimanite} + 5\ \text{quartz} \qquad (83)$$

At equilibrium, assuming sillimanite and quartz pure and $\gamma = 1$, the equation of state has the form:

$$\Delta G^{o} = \Delta H^{o} - T\Delta S^{o} + (P-1)\,\Delta V + 6RT \ln \frac{X^{\text{garnet}}_{\text{almandine}}}{X^{\text{cordierite}}_{\text{Fe-cordierite}}} = 0 \qquad (T21)$$

which can be rearranged to yield an expression for the equilibrium pressure

$$P = \frac{T\Delta S - \Delta H - 6RT \ln \dfrac{X^{\text{garnet}}_{\text{almandine}}}{X^{\text{cordierite}}_{\text{Fe-cordierite}}}}{\Delta V} + 1 \qquad (T22)$$

Substituting the numerical values for the thermodynamic parameters yields

$$P = 5206{,}423 + 2{,}976T \ln \frac{X^{\text{garnet}}_{\text{almandine}}}{X^{\text{cordierite}}_{\text{Fe-cordierite}}} - 2{,}6335T \qquad (T23)$$

Equation (T23) allows the equilibrium pressures to be calculated under the conditions $P_{H_2O} = 0$.

When $P_{H_2O} = P_{total}$ the equation of state for reaction (80) at equilibrium has the form:

$$\Delta G^{o} = 0 = \Delta H^{o} - T\Delta S + (P-1)\Delta V + 6RT \ln \frac{a^{garnet}_{almandine}}{a^{cordierite}_{Fe\text{-}cordierite}} - 3RT \ln a^{cordierite}_{anhyd.\ cordierite} \qquad (T24)$$

where the activity of anhydrous cordierite in cordierite = 1-X

From equation (T19) it can readily be shown that

$$\ln (1-X) = -\ln \left[ e^{\left(\frac{5185,09}{T} - 13,7843\right)} \cdot f_{H_2O} + 1 \right] \qquad (T25)$$

Substitution of equation (T25) into (T24) and rearranging and substituting the thermodynamic parameters by their numerical values yields an expression for $f_{H_2O}$:

$$f_{H_2O} = \frac{e^{\left[ -\left(\frac{20857,45 - 10,55T - 4,0061\ (P-1)}{5,9615T}\right) - 2 \ln \frac{X^{garnet}_{almandine}}{X^{cordierite}_{Fe\text{-}cordierite}} \right]} - 1}{e^{\left(\frac{5185,09}{T} - 13,7843\right)}} \qquad (T26)$$

which can be solved for $f_{H_2O}$ under various $P_{total}$ conditions. Furthermore, from the relationship

$$\frac{f_{H_2O}\ \text{calculated (equation T26)}}{f_{H_2O}\ \text{pure (from tables)}} = X^{fluid}_{H_2O} = 1 \text{ for } P_{H_2O} = P_{total} \qquad (T27)$$

by trial and error a pressure can be found in equation (T26) which yields an $f_{H_2O}$ value that satisfies equation (T27). The pressure so determined must be the equilibrium pressure under the conditions $P_{H_2O} = P_{total}$. Equations (T23), (T26) and (T27) have been used to calculate the equilibrium pressures for the garnet, cordierite, sillimanite, quartz equilibria in the dry and wet systems respectively. The temperature values used in these equations are the ones determined by means of the garnet-cordierite geothermometer discussed in the previous section.

The results of the computations are presented in Table 29 and the geographic distribution of equilibration pressures within the granulite facies terrane of the study area are displayed in Fig. 78.

Table 29 Equilibrium pressures determined for garnet, cordierite, sillimanite, quartz equilibria under the conditions $P_{H_2O} = 0$ and $P_{H_2O} = P_{total}$ using equations (T23), (T26) and (T27) respectively.

| Specimen No. | Temperature °C | Temperature °K | $X_{Al}^{Ga}$ | $X_{Fe}^{Cd}$ | Pressure (bars) at $P_{H_2O} = 0$ | Pressure (bars) at $P_{H_2O}=P_{total}$ |
|---|---|---|---|---|---|---|
| HA 514 | 787 | 1060 | ,643 | ,281 | 5030 | 5952 |
| HA 143 | 770 | 1043 | ,631 | ,256 | 5262 | 6270 |
| HA 1036 | 747 | 1020 | ,631 | ,267 | 5136 | 6154 |
| HA 632 | 815 | 1088 | ,569 | ,230 | 5282 | 6216 |
| HA 841 | 795 | 1068 | ,677 | ,304 | 4938 | 5825 |
| HA 329 | 763 | 1036 | ,628 | ,250 | 5324 | 6361 |
| HA 870 | 789 | 1062 | ,685 | ,316 | 4854 | 5731 |
| HA 982 | 756 | 1029 | ,619 | ,245 | 5340 | 6400 |

In Fig. 78 the highest pressures are suggested for the area around Kliprand, apparently decreasing slightly towards the south and towards the north. However, the regional pattern could merely be a reflection of changes in $P_{H_2O}$ across the area. When $P_{H_2O}$ is assumed to be zero the calculated pressures range from 4,9 - 5,3 kb while, when $P_{H_2O}$ is assumed to equal $P_{total}$, the pressure range is found to be 5,7 - 6,4 kb. The widespread occurrence of K-feldspar + orthopyroxene assemblages in the charnockitic suite and the decrease in abundance of hydrous minerals relative to their anhydrous equivalents, as well as the ubiquitous observed garnetiferous neosomes, suggest that $P_{H_2O}$ must have been less than $P_{total}$.

From the results on garnet-cordierite geobarometry it is concluded that the peak pressures that are likely to have prevailed during regional metamorphism are of the order of 5 to 6 kb.

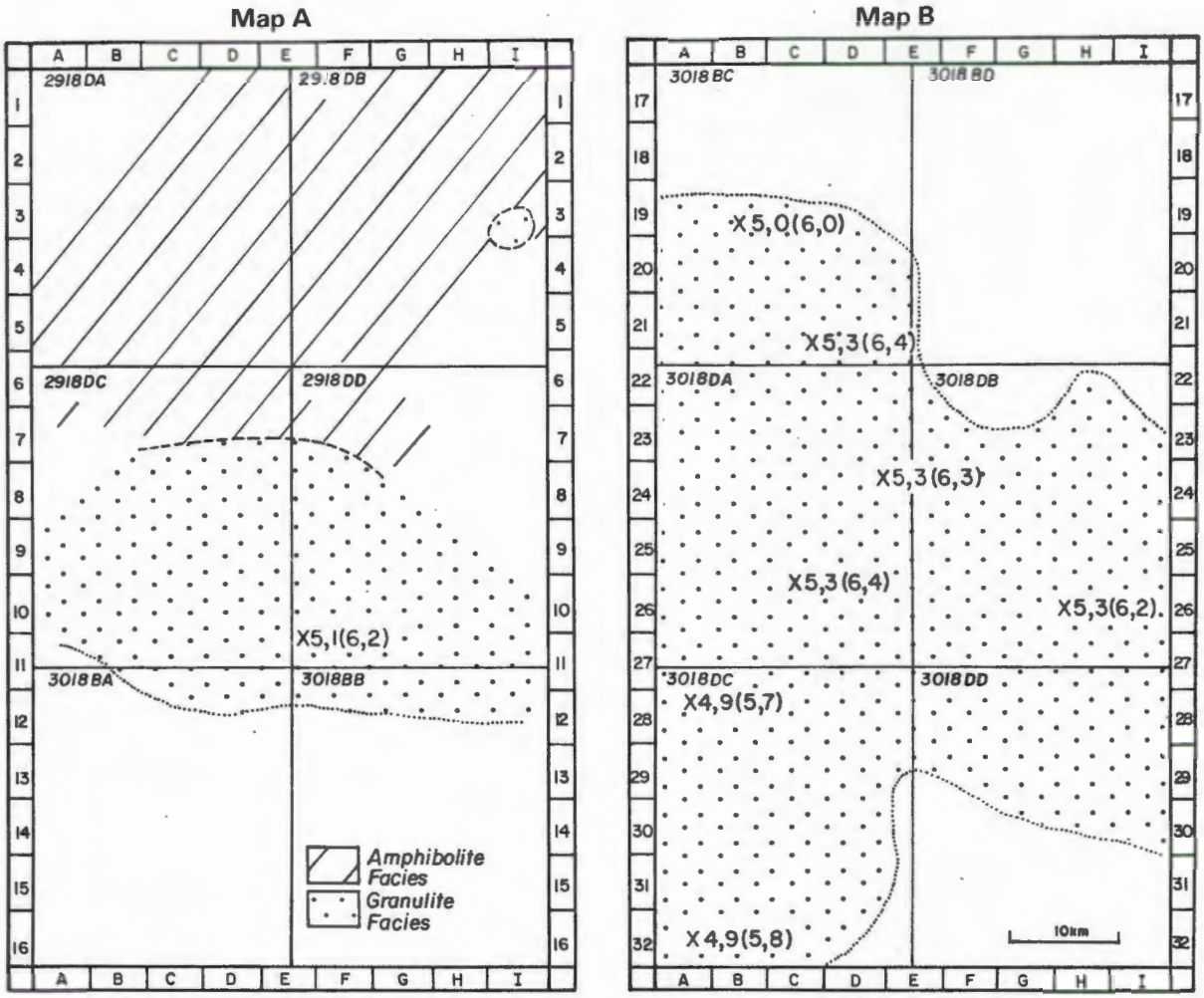


Fig. 78 Geographic distribution of equilibrium pressures (in kb) determined from core compositions of garnet and cordierite coexisting with sillimanite and quartz in granulite facies metapelites. The first figure at each locality represents the computed pressures under the conditions $P_{H_2O} = 0$ and the figures in brackets refer to the corresponding pressure when $P_{H_2O}$ is assumed equal to $P_{total}$. The stipled line represent the approximate boundary between the granulite and amphibolite facies terranes.

## 4 The Reaction Anorthite $\rightleftharpoons$ Ca-Tschermak's Molecule + Quartz as Potential Geobarometer

Experimental studies on the pure end member reaction

$$\text{Anorthite} \rightleftharpoons \text{Ca-Tschermak's molecule} + \text{quartz} \qquad (84)$$

have shown that this reaction has a shallow $\frac{dP}{dT}$slope (Hariya and Kennedy, 1968), making this equilibrium a potential geobarometer. If the reaction involves standard states of the pure phases the condition for chemical equilibrium can be expressed as

$$-RT \ln K = \Delta H^{o}_{1\ bar,T} - T\Delta S^{o}_{T} + \int_{1}^{P} \Delta V^{o}\ dP \quad \text{(T28)} \quad \text{(Wood and Fraser, 1977)}$$

where $\Delta H^{o}_{1\ bar,t}$, $\Delta S^{o}_{T}$ and $\Delta V^{o}$ refer, respectively, to enthalpy (at 1 bar), entropy and volume change of the reaction at the temperature (T) of interest. If $\Delta H$, $\Delta S$ and $\Delta V$ for reaction (84) are known, the equilibrium pressure at any temperature of interest can be determined for impure natural assemblages involving the above equilibrium, provided the mixing properties of the phases involved are known. The equilibrium constant (K) for reaction (84) is defined as

$$K = \frac{{}^{\text{clinopyroxene}}a_{CaAl_2SiO_6} \cdot {}^{\text{quartz}}a_{SiO_2}}{{}^{\text{plagioclase}}a_{CaAl_2Si_2O_8}} \quad \text{(T29)} \quad \text{(Wood, 1977)}$$

A knowledge of the mixing properties of the phases is required since the activities (a) in the equilibrium constant involve the product of mole fraction (X), obtained from the chemical analyses of the minerals, and the activity co-efficient ($\gamma$) which has to be determined experimentally. The general relationship between activity and composition is expressed as $a = (X \cdot \gamma)^{n}$ where n represents the number of sites per formula unit (Wood and Fraser, *op. cit.*).

Wood (1976) has determined the relationship between activity ($a_{CaAl_2SiO_6}$) and mole fraction ($X_{CaAl_2SiO_6}$) of Ca-Tschermak's component in clinopyroxene. The experiments were performed in the pressure range 10 - 25 kb and temperature range 900 - 1300°C yielding the following results:

(a) In $CaAl_2SiO_6$-$CaMgSi_2O_6$ solid solutions $\gamma^{cp}_{CaAl_2SiO_6}$ is slightly greater than 1,0.

(b) In $CaAl_2SiO_6$-$CaFeSi_2O_6$ solid solutions $\gamma^{cp}_{CaAl_2SiO_6}$ is slightly less than 1,0.

(c) In $CaAl_2SiO_6$-clinopyroxene with Mg/(Mg + Fe) = 0,6, $\gamma^{cp}_{CaAl_2SiO_6}$ is approximately 1,0 (Wood, 1976; 1977),

Similar conclusions are reached by Newton *et al.*, (1977). These experiments demonstrate that unless the clinopyroxene is of intermediate composition with respect of the Mg/(Mg+Fe) ratio ideal solution can strictly speaking not be assumed. The activity coefficients for plagioclase solid solutions can be obtained from the experimental work of Orville (1972).

$\Delta V$, $\Delta H$ and $\Delta S$ for reaction (84) have been computed from the tabulation in Robie *et al.*, (1978) and allows the determination of the pressure-temperature conditions for chemical equilibrium for the pure end members (K = 1). This calculated equilibrium curve in P-T space for the pure end member reaction is shown in Fig. 79. Also shown in Fig. 79 is the equilibrium boundary for reaction (84) as deduced by Wood from phase relationships in the system $CaO-Al_2O_3-SiO_2$ (Wood, 1978) and the experimental reversal on reaction (84) as determined by Hariya and Kennedy (*op.cit.*). A comparison of these data reveals a considerable discrepancy with respect to equilibrium pressure (see Fig. 79) According to Hariya and Kennedy (*op.cit.*) the equilibrium boundary for reaction (84) occurs somewhere between 30 and 31,5 kb when the temperature is 1400°C. The data of Wood (*op.cit.*) indicate somewhat higher equilibrium pressures at the same temperature, and Wood (*op.cit.*) ascribes this discrepancy to the non-stoicheiometry of clinopyroxene.

Wood (1977) uses the entropy and volume data from Robie and Waldbaum (1968) and estimates $\Delta H$ from the experiments of Hariya and Kennedy (*op.cit.*) by assuming the attainment of equilibrium at a pressure of 30,8 kb and 1400°C. Wood (*op.cit.*) then extrapolates the equilibrium for K = 1 to lower temperatures and pressures using the high temperature entropy data of Robie and Waldbaum (*op.cit.*) and based on this, constructed equilibrium curves for a range of equilibrium constants in impure systems shown in Fig. 80. This diagram can, however, only serve in a qualitative manner due to the uncertainties in the thermodynamic parameters. Other problems involve the evaluation of the activity of calcium Tschermk's molecule in clinopyroxene and in current literature there is much debate on the formulation of the activity-composition relations (Wood, 1976, 1977, 1979). In the light of these uncertainties equilibrium (84) is only used as a relative geobarometer in this study.

The equilibrium constant (K) has been computed from microprobe analyses of coexisting plagioclase, clinopyroxene and quartz assemblages in four mafic rock specimens from the study area and the results are shown in Table 30.

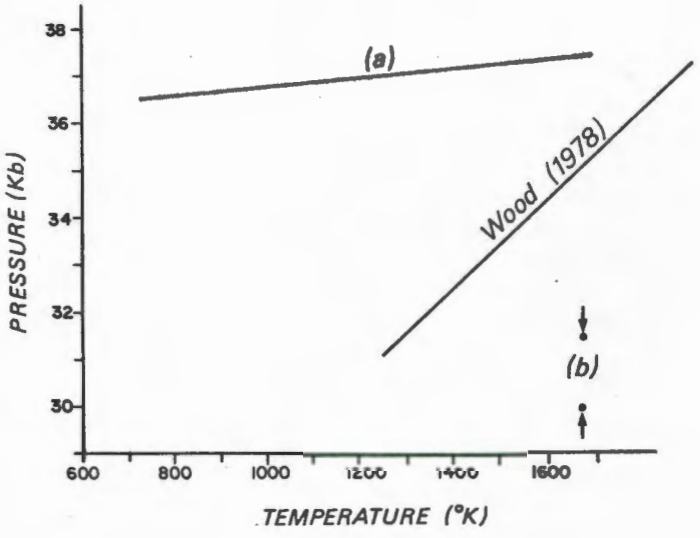


Fig. 79 : Comparison of the equilibrium boundary for the reaction

Anorthite $\rightleftharpoons$ Ca-Tschermak's molecule + quartz

(a) Equilibrium boundary computed for the pure phases from tabulations in Robie, *et al.*, (1978).

(b) Experimental reversals on reaction (84) as determined by Hariya and Kennedy (1968).

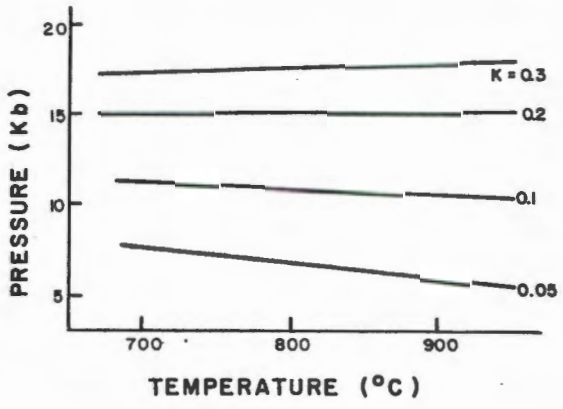


Fig. 80 : The equilibrium constant $K = \dfrac{a^{\text{clinopyroxene}}_{CaAl_2SiO_6} \cdot a^{\text{quartz}}_{SiO_2}}{a^{\text{plagioclase}}_{CaAl_2Si_2O_8}}$

as a function of pressure and temperature after Wood (1977).

Table 30 : Equilibrium constants $K = \frac{a^{\text{clinopyroxene}}_{CaAl_2SiO_6}}{a^{\text{plagioclase}}_{CaAl_2Si_2O_8}}$ for equilibria involving coexisting clinopyroxene, plagioclase and quartz. The specimens are arranged in sequence from the north to the south of the study area.

| Specimen No. | Rock type | K | Locality |
|---|---|---|---|
| HA 1110 | salite-bearing amphibolite | 0,014 | E2 |
| HA 1030 | garnet granolite | 0,014 | F10 |
| HA 1045 | hypersthene-pyroclase granolite | 0,018 | E11 |
| HA 306 | hypersthene-pyroclase granolite | 0,023 | B25 |

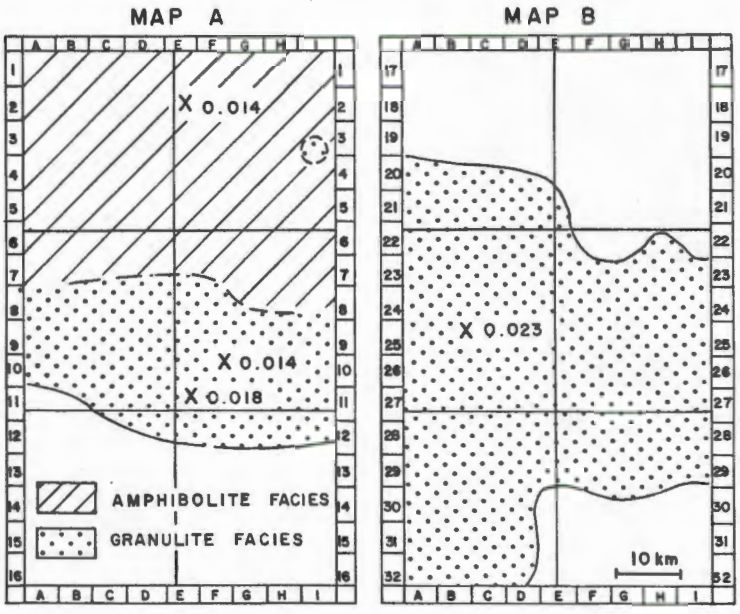


Fig. 81 : Sketch map showing the regional distribution of equilibrium constants $K = \frac{a^{\text{clinopyroxene}}_{CaAl_2SiO_6}}{a^{\text{plagioclase}}_{CaAl_2Si_2O_8}}$ for equilibria involving clinopyroxene, plagioclase and quartz.

Quartz is assumed to be pure (unit activity) and was accordingly ignored in the evaluation of the equilibrium constants. The four specimens are widely separated from each other and cover the entire area including the northern region of the amphibolite facies. The computed equilibrium constants in Table 30 are plotted in a sketch map in Fig. 81, from which it is evident that K increases slightly from the north to the south. With reference to Fig. 81, an increase in the value of the equilibrium constant is related to rising pressure, suggesting that the amphibolite facies was subjected to slightly lower pressures compared to the granulite facies. However, the variation of the equilibrium constant across the area is so small that significant pressure variations cannot be involved. The very low values obtained for the equilibrium constants (Table 30) is indicative for low equilibrium pressures. According to the computations by Wood (1977) as displayed in Fig. 80, the likely pressures to account for the computed equilibrium constants are of the order of 5 kb in the temperature range of 700 - 900°C. At these low pressures the equilibrium boundary for reaction (84) has a small $\frac{dP}{dT}$ slope (Wood, *op.cit.*), so that a drop in temperature at constant pressure is also expected to shift the equilibrium constant towards lower values. Thus, the observed trend of decreasing K from the granulite to the amphibolite facies could also result from a drop in temperature.

In summary, then, it is concluded that although no reliable quantitative pressure estimates are made by using this geobarometer two important qualitative conclusions can be drawn, namely, that the low values for the equilibrium constants are indicative of low equilibrium pressures of the order of 5 kb, and that the similarity of the K values excludes the possible existence of significant regional pressure changes across the study area.

## C Summary of the Peak P-T Conditions during Prograde Regional Metamorphism

Phase compositions in pelitic, semipelitic and mafic gneisses place tight constraints on pressure and to a lesser extent on temperature during prograde regional metamorphism in the Namaqualand Metamorphic Complex. The P-T estimates presented in this study are heavily biased towards the granulite facies terrane as suitable outcrops of pelitic and semipelitic gneisses were not encountered in the area underlain by amphibolite facies assemblages.

The temperatures computed in the various geothermometers utilised in this study are summarised as frequency histograms in Fig. 82. Taking all results into consideration, the computed temperatures are seen to cover a wide temperature range from 600°C to over 900°C (Fig. 82). This temperature range does not reflect changes in metamorphic grade, as the phase compositions used in each geothermometer are obtained from specimens covering the same area as those used in the other geothermometers. As all the temperature estimates refer to the same area and the same metamorphic event, it is concluded that the geothermometers used in this study yield inconsistent results. These inconsistencies can partly be accounted for by the uncertainties in mineral

composition, for example the amount of $Fe^{+3}$ in biotite (failure to account for $Fe^{+3}$ in biotite leads to an overestimation of the temperature) and the problem of obtaining homogeneous bulk compositions of K-feldspar which show considerable exsolution. For this reason not much reliance is placed on the results obtained by the two-feldspar geothermometers and some of the results obtained by the garnet-biotite geothermometer are considered to be too high (for example specimen HA 1081). If the temperatures based on compositions of coexisting feldspars are ignored, and this is justifiable, it is evident from an inspection of Fig. 82 that the thermal peak during progressive regional metamorphism must have reached temperatures of 700 to 900°C in the granulite facies terrane.

One interesting feature shown in Fig. 82 and worth commenting on is that the computed temperatures based on phase compositions in mafic rocks are higher than those derived from mineral compositions in pelitic gneiss specimens. This is evident from a comparison of the histograms shown in (a) and (b) in Fig. 82 for coexisting pyroxenes in mafic rocks with those for coexisting garnet and cordierite in pelitic rocks (c) and (d) in Fig. 82 . If for both rock types the mean temperatures ($\bar{x}$) obtained by the more recent calibrations (Wells, 1977 and Holdaway and Lee, 1977) are considered the recorded temperature difference is enhanced; 860°C for mafic rocks as opposed to 780°C for pelitic rocks. This observation can be interpreted in several ways. It has previously been argued that the temperatures derived in the two-pyroxene geothermometers tend to be somewhat on the high side. This would imply that some of the assumptions made in the derivation of the geothermometers are invalid and that the equations, although successfully applied to the miscibility gap at high temperatures, fail to accurately describe the temperature-composition relationships at lower temperatures applicable to granulite facies metamorphism. Alternatively, the recorded temperature differences may reflect real differences in crystallisation temperature and the different mineral assemblages may have closed at different P-T conditions, thus reflecting a time sequence in a polychronic metamorphic event as suggested recently by Rollinson, *et al.*, (1981). A detailed chronological study of the minerals involved would be required to verify this model.

If the two-pyroxene geothermometers are regarded as reliable and the uncertainty involves ± 70°C as claimed by Wood and Banno (1973) and Wells (1977) the results obtained in this study indicate a mean temperature of 830 to 860°C (± 70°C) for mafic rocks and, depending on which of the garnet-cordierite geothermometers is considered to be more accurate, a mean temperature of 780 to 820 (± 60°C) for pelitic rocks. The garnet-biotite and garnet-clinopyroxene geothermometers yield similar results, but the temperatures obtained by the two-feldspar geothermometers are inconsistent with those obtained by the other methods.

Phase compositions utilised for the estimation of pressures support previous conclusions based on mineral assemblages and are cited as evidence for low-pressure metamorphism. The computed pressures recorded in specimens from the granulite facies terrane range between 4,6 to 5,1 kb for garnet-plagioclase-sillimanite-quartz equilibria and slightly higher pressure esti-

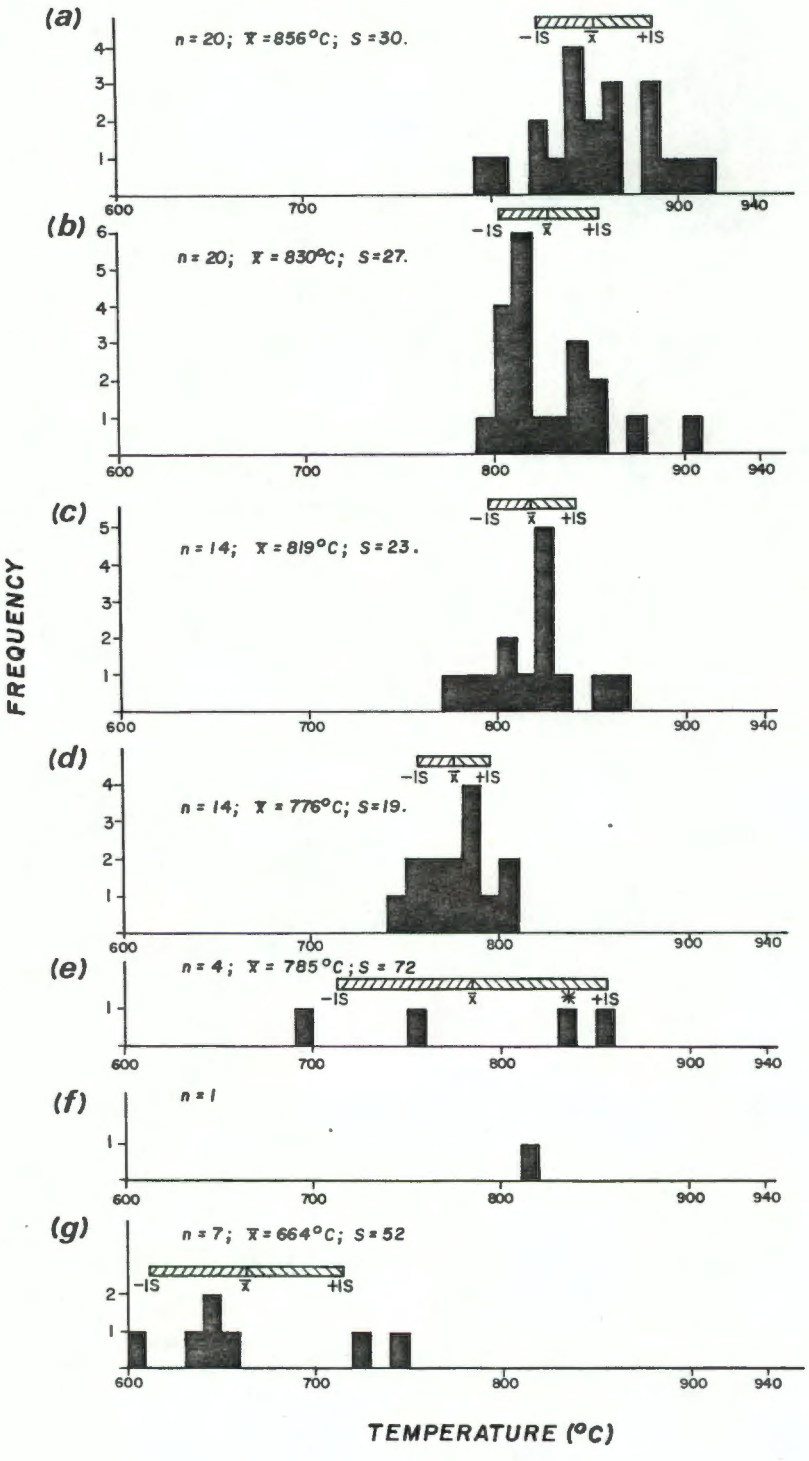
(a)
n = 20; x̄ = 856°C; S = 30.
−1S x̄ +1S
(b)
n = 20; x̄ = 830°C; S = 27.
(c)
n = 14; x̄ = 819°C; S = 23.
(d)
n = 14; x̄ = 776°C; S = 19.
(e)
n = 4; x̄ = 785°C; S = 72
(f)
n = 1
(g)
n = 7; x̄ = 664°C; S = 52
FREQUENCY
TEMPERATURE (°C)
600
700
800
900
940

mates are based on garnet-cordierite-sillimanite-quartz equilibria, the latter of which yields pressures ranging between 4,9 and 5,3 kb assuming $P_{H_2O}$ = zero and 5,7 to 6,4 kb when $P_{H_2O}$ is assumed equal to $P_{total}$. Allowing for experimental and analytical errors, this leads to the conclusion that pressures of the order of 5 to 6 kb (± 1 kb) must have accompanied regional metamorphism of the granulite facies terrane in the study area.

Unfortunately, suitable outcrops of pelitic rocks were not encountered in the amphibolite facies terrane and accordingly these two geobarometers could not be applied to the northern part of the area. In order to extend the studies to include the amphibolite facies terrane $K_D$ is evaluated for equilibria involving plagioclase, Ca-Tschermak's molecule in clinopyroxene and quartz and is observed to decrease slightly from the south to the north across the granulite-amphibolite facies transition. This may indicate that the granulite terrane was subjected to slightly higher pressures compared to the amphibolite facies terrane. The low values obtained for $K_D$ in mafic rocks are consistent with the low pressures recorded in the pelitic rocks.

---

Fig. 82 : Frequency histograms showing the metamorphic temperatures computed for calibrated mineral equilibria from compositions of coexisting minerals determined by microprobe techniques. All the specimens are from the granulite facies terrane excepting the one indicated with an asterisk (*) in (e) which refers to coexisting garnet and biotite in the upper amphibolite facies terrane.

(a) Temperatures computed for coexisting ortho-and clinopyroxenes in mafic granolites using the Wells (1977) geothermometer - equation (T2).

(b) Temperatures computed for coexisting ortho-and clinopyroxenes in mafic granolites using the Wood and Banno (1973) geothermometer - equation (T1).

(c) Temperatures obtained for coexisting almandine and cordierite in pelitic gneisses using the Thompson (1976b) calibration (equation T9) and assuming a pressure of 5 kb.

(d) Temperatures obtained for coexisting almandine and cordierite in pelitic gneisses using the Holdaway and Lee (1977) calibration (equation T10) and assuming a pressure of 5 kb.

(e) Temperatures derived from coexisting almandine and biotite in semipelitic migmatites using the Ferry and Spear (1978) calibration (equation T6) and assuming a pressure of 5 kb.

(f) Temperatures derived for coexisting garnet and clinopyroxene in garnet granulite specimen HA 1030 using the empirical equation of Dahl (1980) (equation T4) and assuming a pressure of 5 kb.

(g) Temperatures based on compositions of coexisting alkali feldspar and plagioclase in pelitic gneiss specimens using the mean values obtained by the Stormer (1975) and Whitney and Stormer (1977a) calibrations (equations T11 and T12).

# V MIGMATITES

## A Introduction

According to Mehnert (1968) the term migmatite refers to a "megascopically composite rock consisting of two or more petrographically different parts, one of which is the country rock generally in a more or less metamorphic stage, the other is of pegmatitic, aplitic, granitic or generally plutonic appearance". These mixed rocks form an integral part of the geology of the study area and are most spectacularly developed in the southern granulite facies terrane (map B). Megascopic evidence for migmatisation diminishes considerably in the northern part of the area. Rock types most severely affected by migmatisation include pelitic gneisses, semipelitic biotite-garnet-bearing gneisses as well as various biotite-bearing quartzo-feldspathic gneisses, the latter collectively referred to as migmatitic gneisses.

The profound effect the process of migmatisation had on the pre-existing gneisses necessitates a brief discussion on the likely causes of migmatisation in the study area.

## B The Transition from Metamorphism to Melting and the Origin of Migmatites

Winkler (1976) points out that migmatites are generally spatially associated with areas preserving evidence for highest grades of regional metamorphism which suggests a genetic relationship between the high thermal environment and the origin of migmatites. The genesis of migmatites, however, is a very controversial subject. Discussions concerning their mode of origin revolve around four major processes which involve, respectively, anatexis, igneous injection, metamorphic differentiation and metasomatism (Mehnert *op.cit.*; Hyndman, 1972). Plausible arguments in favour of each of these processes have been presented in the literature suggesting that one or more may be involved. These unlike processes are expected to lead to different responses and it should be possible to find criteria by which each of these four mechanisms can be recognised. Summaries of such useful criteria are presented by various authors notably Mehnert (*op.cit.*), Hyndman (*op.cit.*) and Yardley (1978). Before deciding on the most likely mode of origin of the migmatites in the study area, it is desirable to review some of the criteria that may be used for distinguishing between the various mechanisms leading to migmatisation. The terminology used by Mehnert (*op.cit.*) for describing migmatites will be adhered to: thus the term *paleosome* refers to the parent rock, i.e. the country rock gneiss, while *neosome* refers to the newly formed rock portion which generally comprises two types, a *leucosome* consisting pre-

dominantly of quartz, alkali feldspar, plagioclase and subordinate garnet and a *melanosome* which occurs immediately adjacent to the leucosome and contains abundant mafic minerals, particularly biotite.

## 1 *In Situ* Differential Anatexis of the Gneisses during High Grade Regional Metamorphism

An anatectic model must be in harmony with the following criteria:

(a) The bulk composition of the migmatised rock is not changed by anatexis, i.e. the resultant chemistry of the leucosome and adjacent melanosome should be equal to that of the paleosome provided the melt remained *in situ*.

(b) The composition of the leucosome must be consistent with predictions based on partial melt experiments. In detail the leucosome composition is a function of P, T, $P_{H_2O}$ as well as the bulk composition of the paleosome (e.g. Whitney, 1975; Winkler *op.cit.*; Wyllie, 1977). One essential requirement is that K-feldspar occurs in the leucosome, because melting studies on a wide range of rock compositions has revealed that K-feldspar crystallises from the early melt (Tuttle and Bowen, 1958) even if no K-feldspar occurs in the original rock and muscovite and/or biotite are the only potassic minerals present (von Platen, 1965; von Platen and Höller, 1966; Hoschek, 1976; Winkler *op.cit.*)

(c) During partial melting the fusible components, i.e. those with the lowest melting points, will enter the liquid phase (leucosome) leaving behind a residual of the higher melting point minerals (melanosome)(Brown and Fyfe, 1970; Fyfe, 1973; Green, 1976). Thus the complementary leucosome - melanosome pair is a requirement.

(d) Experiments on plagioclase-bearing systems coexisting with melt indicate that the albite molecule preferentially fractionates into the melt (Steuhl, 1962; Winkler *et al.*, 1975; Drake, 1976; Winkler, 1976) which implies that the plagioclase crystallising from the melt is expected to be enriched in the albite molecule compared to the more An-rich restite plagioclase. Therefore, the plagioclase in the leucosome should be more albitic compared to its equivalent in the melanosome. This will, however, only hold true provided the system did not respond to complete subsolidus re-equilibration during cooling.

(e) When melting affects large volumes of rock simultaneously the vast amounts of liquid (if it remains *in situ*) is likely to mechanically weaken the rocks. This results in the formation of agmatites (migmatites with breccia-like structure) and allows rotation of the gneiss fragments.

(f) Leucosome formation should be restricted to those rock types with abundant low melting point minerals. Rocks that are expected to remain solid under the P-T conditions of high grade regional metamorphism include amphibolites, granolites, calc-silicate rocks, marbles and pure quartzites (Winkler, 1976).

(g) The P-T conditions of the environment must be of such a nature that anatexis is possible, i.e. upper amphibolite to granulite facies terranes.

## 2 Injection of Magma to form Granitoid Veins

Injection migmatisation can give rise to a very broad spectrum of igneous rock types which can be injected into any type of country rock. Magmatic injection can be recognised by the following criteria:

(a) The bulk composition of the migmatised rock is likely to change, because the compositions of the injected igneous rocks could be quite different.

(b) The composition of the leucosomes can vary considerably as a wide range of igneous compositions are possible, but the mineralogy and texture must be consistent with an igneous source.

(c) The plagioclase composition in the leucosome may vary and, depending on the type of magma injected, can even be more An-rich than its equivalent in the host rock.

(d) The morphology of the leucosomes may display a strongly anisotropic pattern with individual veins frequently occurring at an angle to the foliation of the metamorphic rock. Individual leucocratic bands need not all have been molten at the same time and, therefore, rotation of the enclosed host rock is not necessarily expected, but may occur.

(e) The complementary development of a leucosome - melanosome pair is not expected, but may occur as illustrated by Jackson (1976).

(f) Leucosomes may be encountered in any type of host rock including carbonate rocks, ultramafic rocks and other rocks of extreme composition (i.e. independent of the melting point of the host rock).

(g) Chilled margins and contact metamorphic phenomena are possible depending on the thermal state of the environment.

## 3 Metamorphic Segregation (Differentiation)

Differentiation involves the formation of bands of contrasting bulk compositions in originally unbanded rocks and is generally regarded to require some form of diffusion. Robin (1979) has outlined a simplified model for metamorphic segregation accompanying deformation involving processes such as pressure solution and diffusion creep by which certain chemical components, notably silica, are transported more rapidly than others, e.g. micas in response to stress induced pressure gradients. Some recent studies on migmatites favour metamorphic segregation as the most plausible mode of origin (Hedge, 1972; Amit and Eyal, 1976; Yardley, 1978, Fediukova and Suk, 1979). The following criteria apply:

(a) The bulk composition of the migmatised rock is not changed, i.e. the resultant composition of the leucosome and melanosome are equal to that of the paleosome.

(b) The leucosomes may have variable composition, but the minerals in the leucosome and melanosome are expected to have compositions similar to the equivalent minerals in the paleosome. The plagioclase compositions in the leucosomes and melanosomes are expected to be similar.

(c) Complementary formation of leucosome and melanosome is expected.

(d) The morphology of the leucosomes must reflect the small amount of fluid present at any one time and accordingly extensive closely spaced leucosomes are possible without rotation of the enclosed host rock.

(e) The leucosomes are probably preferentially developed along planes of weakness.

(f) The P-T conditions reflected by the mineralogy in the leucosomes must be consistent with those reflected by the host rock.

## 4 Metasomatism

Metasomatism involves the introduction and/or removal of elements to allow the formation of granitic leucosomes. The source for the introduced elements such as Na and K is generally considered to occur outside the immediate vicinity of the migmatites. The following criteria apply to the process of metasomatism:

(a) The bulk composition of the migmatised rock is changed by the introduction of new material.

(b) The mineral phases in the leucosome are not related to the mineralogy in the host rock and both types may be incompatible with each other.

(c) The plagioclase composition in the leucosome is not defined.

(d) The morphology of the leucosomes must reflect the small amount of fluid present at any moment in time and accordingly closely spaced leucosomes are possible without rotation of the enclosed host rock, i.e. the paleosome is not disturbed during the formation of the leucosomes.

(e) The leucosomes may develop in rocks of any bulk composition, but is likely to be preferentially developed along fracture zones.

(f) The P-T conditions recorded in the leucosome mineralogy may deviate considerably from those in the host rock.

(g) The replacement of pre-existing minerals may be evident from relict textures.

## 5 Origin of the Migmatites in the Study Area

No single mechanism can account for all the observed features displayed by the migmatites and it seems likely that all four mechanisms listed above were involved in some degree in their formation. There is, however, strong evidence that anatexis of the gneisses during high grade regional metamorphism played the dominant role in migmatite genesis. This statement is verified by the following observations:

(a) The genesis of migmatites is characterised by selectivity as witnessed by the restriction of the leucosomes to rock types (generally biotite-bearing) with abundant low melting point minerals.

(b) Large garnet porphyroblasts are surrounded by leucocratic quartzo-feldspathic "diffusion haloes" in biotite-rich gneisses (Plate 2). These are interpreted to indicate the initiation of migmatisation and they lend strong support for the *in situ* formation of the leucosomes. In fact, garnet porphyroblasts feature prominently in the majority of the leucosomes throughout the migmatite terrane (Plates 6 and 7).

(c) The leucosomes are generally bordered by a narrow, dark-coloured melanosome which is distinguished from the adjacent paleosome, into which it grades, by the higher concentration of ferromagnesian minerals (predominantly biotite). The neosome-paleosome relationship is illustrated in Fig. 83.

(d) A typical representative migmatite specimen (HA 875) from the farm Tafelberg (64) (A29) has been selected to illustrate the major changes in mineralogy and mineral abundance that is encountered across the melanosome-leucosome contact (Table 31).

Table 31 : Modal compositions (in volume per cent) of the leucosome and adjacent melanosome recorded in specimen HA 875. Abbreviations as in preface (m = < 1 per cent)

| | Quartz | K-feldspar | Plagioclase | Garnet | Biotite | Others |
|---|---|---|---|---|---|---|
| leucosome | 40 | 38 | 14 | 8 | m | Ap., Om., Zc |
| melanosome | 40 | 16 | 27 | m | 16 | Ap., Om., Zc |

With reference to Table 31 the following observations are significant: Biotite forms an abundant phase in the melanosome while garnet features prominently in the leucosome (frequently in the central parts). It is worth noting that garnet in this particular specimen is not recorded amongst the mineral phases encountered in the paleosome and it occurs only in trace amounts within the melanosome in proximity to the melanosome - leucosome contact where it is occasionally seen to form a narrow rim around biotite.

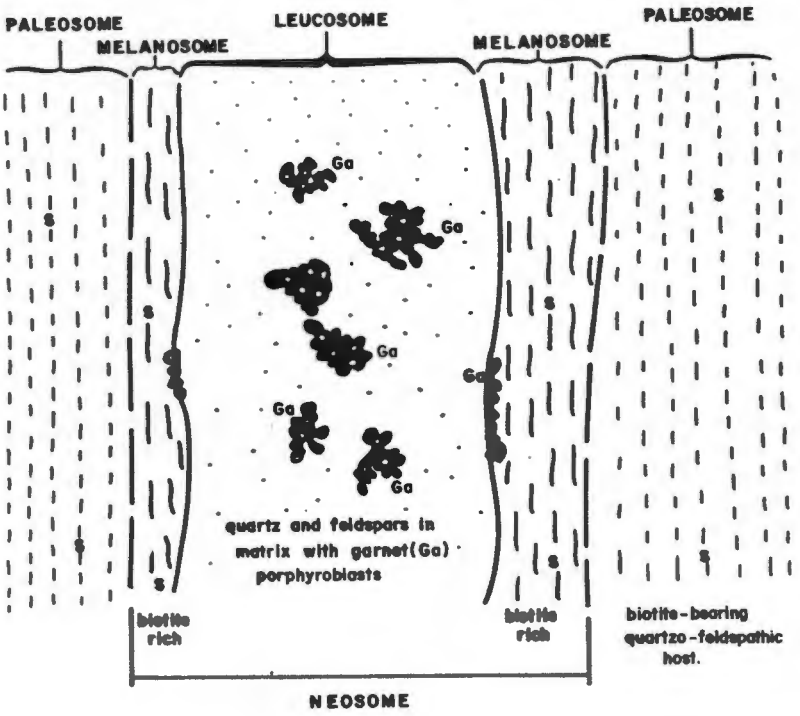


Fig. 83 : Schematic neosome - paleosome relationships in migmatitic gneisses on the farm Tafelberg (64). The leucosome has a granitic composition with low biotite content, but numerous garnet poikiloblasts (Ga) generally encountered along the central parts of the leucosome. Narrow biotite-rich melanosomes border the leucosome on both sides; these are characterised by a much higher mafic mineral content (mainly biotite, possibly minor amphibole) than the adjacent paleosome and has a much higher plagioclase/alkali feldspar ratio than the leucosome. The regional planar fabric (S) is well defined in the melanosome by the preferred orientation of biotite, but due to the virtual absence of biotite, the leucosome has an igneous appearance.

These corona textures suggest that the formation of garnet is accomplished by the breakdown of biotite, an indication of the *in situ* nature of the migmatites.

Alkali feldspar (microcline microperthite) is encountered in both parts of the neosome, but is much more abundant (by a factor of 2) in the leuco-

some. The increase in alkali feldspar concentration is interpreted to be a direct consequence of the breakdown of biotite which releases the potassic molecule.

In contrast to alkali feldspar, plagioclase is much more abundant in the melanosome (by a factor of 2) relative to the leucosome. This points towards a more refractory nature of the melanosome. Optically the plagioclase in the melanosome appears to be only slightly more An-rich than its equivalent in the leucosome.

In terms of the quartz, alkali feldspar, plagioclase ratios (Table 31) the leucosome has a granitic composition while the melanosome is distinctly more basic.

(e) High temperatures of formation are suggested by the mineralogy of the neosomes. Temperatures computed from coexisting garnet and biotite are consistent with those expected in granulite facies metamorphic terranes.

(f) In certain areas (e.g. on the farm Tafelberg 64) migmatisation has yielded agmatites (Plate 6). These demonstrate unequivocally that the leucosomes (at least the quartzo-feldspathic components) must have been liquid at some stage. The outcrop shown in Plate 6 displays angular blocks of country rock gneiss surrounded by garnetiferous leucosomes. Adjacent fragments of gneiss separated by a leucosome frequently display matching outlines and continuity of structures. Some of the angular blocks, however, show signs of slight rotation, indicating that the leucosomes were once a melt which mechanically weakened the gneisses.

The evidence presented above is consistent with an anatectic model and it is concluded that the bulk of the migmatisation of the gneisses in the study area can be ascribed to the process of *in situ* anatexis which is believed to be a direct consequence of the high grade regional metamorphism.

## C Crustal Anatexis in the Light of Experimental Petrology

It has been experimentally verified that migmatites can be generated by partial melting of a wide range of crustal rocks under the P-T conditions believed to have prevailed in areas of high grade regional metamorphism. The areas of *in situ* migmatisation provide a glimpse into the melting region of the lower crust. Ever since the pioneering experiments of Tuttle and Bowen (1958), the process of anatexis has been recognised as a potential mechanism for producing granitic liquids, which on migration and concentration could yield large intrusions of batholithic dimensions (Wyllie, 1977).

The experimental studies on the process of anatexis is focused on the determination of phase relationships of minerals in simple synthetic and natural rock systems in $P\text{-}T\text{-}X_{H_2O}$ space. Excellent reviews on the subject of anatexis have been published recently (e.g. Luth, 1976; Winkler, 1976; Wyllie *op.cit.*). Three basic types of melting, relating to the availability of water, are distinguished by experimental petrologists namely, melting of

dry rocks; melting in the presence of excess water, i.e. $H_2O$-saturated systems and melting in water deficient systems, i.e. all water is locked up in hydrous minerals.

The simple granite system involving the minerals albite, orthoclase and quartz in the presence of excess water has been extensively studied under a wide range of P-T conditions (e.g. Tuttle and Bowen *op.cit.*; Luth *et al.*, 1964; Boettcher and Wyllie, 1968; Lambert *et al.*, 1969; Merrill *et al.*, 1970; Steiner *et al.*, 1975; Huang and Wyllie, 1975) and may serve as a starting point in a discussion on the process of anatexis. From these experimental runs it has become evident that partial melting generates granitic liquids at surprisingly modest temperatures provided water is present in excess. The early formed liquid composition is a function of the prevailing pressure. At low pressures this liquid has a granitic bulk composition which becomes increasingly enriched in the albite component and concomitantly more depleted in $SiO_2$ (i.e. more granodioritic) in response to rising pressure. The implication is that liquids approaching granite composition can only be generated by partial melting at relatively shallow crustal levels.

Phase relationships in this simple "granite" system can, however, not serve as a basis for granite petrogenesis by anatexis because the anorthite component in plagioclase has a marked effect on the melting behaviour of natural rocks. Winkler *et al.* (1975) and Winkler (1976) have demonstrated experimentally that the "melting path" followed by the system depends on the An/Ab ratio of the plagioclase. The presence of anorthite increases the Or/Ab ratio of the early formed melts relative to the anorthite-free system (*ibid.*). In response to rising temperature and rising pressure, increasing amounts of the anorthite component can dissolve in the melt, but as long as quartz, anorthite, albite, orthoclase and vapor coexist with this melt, the anorthite concentration of the liquid will remain low and the melts will be of granite to granodiorite composition (*ibid.*).

The temperatures required to initiate anatexis in water-saturated quartzo-feldspathic systems at fixed pressure is largely dependent on the anorthite content of the plagioclase. The higher the anorthite content of the plagioclase, the higher the temperature for the initial melt (*ibid.*). This is also evident from the experiments of Hoschek (1976) who finds that initial melting in biotite-albite-quartz assemblages at $P_{H_2O}$ = 4 kb commences at 650 ± 25°C as opposed to 725 ± 25°C for the same system involving anorthite instead of albite. Whitney (1975) records that with increasing anorthite content of the system the liquidus is shifted towards higher temperature and the melting interval increases.

The water content has a considerable influence on the melting behaviour of natural rocks. Wyllie (1977) has stressed that the phase relationships determined for $H_2O$-saturated experimental systems must be regarded as a limiting case as most natural magmas are water-undersaturated. This applies particularly to anatexis in the granulite facies terranes. The presence of garnet in the leucosomes rather than a hydrous phase, suggests low water contents (Fyfe, 1971) during anatexis and accordingly water-

saturated experiments cannot be applicable to migmatite genesis in this granulite facies terrane. In fact, Winkler (1976) has argued that the limited availability of water in migmatite terranes may be one of the "effective obstacles to complete melting". Experiments performed under variable water pressures demonstrate that, under otherwise constant conditions, the temperature for the beginning of anatexis increases with decreasing water content and concomitantly the melting interval increases considerably (Huang and Wyllie, 1973; Whitney, 1975; Wyllie, 1977). In the dry system alkali feldspar, plagioclase and quartz are stable to much higher temperatures compared to the water-saturated system (Huang and Wyllie, *op.cit.*). For a fixed bulk composition at constant P-T conditions in the melting region, the amount of water available determines the amount of melt (Büsch *et al.*, 1974; Huang and Wyllie, *op.cit.*; Whitney, *op.cit.*; Wyllie, *op.cit.*). Completely dry systems require extremely high temperatures for melting (> 1000°C) and as these temperatures were certainly not reached during granulite facies metamorphism in the area studied, it is concluded that at least some water must have been present to initiate anatexis.

The formation of garnet at the expense of biotite in the migmatites studied provides a clue on the important role of hydrous minerals in the process of anatexis in relatively "dry" terranes and suggests that at least some of the water required to generate granitic melts under geologically reasonable P-T conditions in granulite facies terranes is released by the dehydration of hydrous minerals. This is not a new concept (Brown and Fyfe, 1970, 1972; Fyfe, 1971, 1973). The common hydrous phases encountered in high grade metamorphic terranes include micas and amphiboles. In experimental systems lacking free water but containing hydrous minerals, anatexis commences with the breakdown of the hydrates at higher temperatures than in a water-saturated system (Wyllie, 1977). The breakdown of muscovite, biotite and hornblende requires progressively higher temperatures (Brown and Fyfe *op.cit.*; Wyllie *op.cit.*) and the amount of melt produced under certain physical conditions, is a function of the amount of hydrate that has decomposed and also depends on the type of hydrate involved because micas generally contain higher water contents than amphiboles (Deer *et al.*, 1971).

The availability of water during anatexis in the study area is an unknown factor and because water has such a dramatic influence on the melting behaviour of rocks, it is desirable to establish whether anatexis of appropriate bulk compositions is possible if no free water is available, the only source of water being the hydrous phases. Fig. 84a outlines the approximate P-T conditions for granulite facies metamorphism derived at in this study in relation to various experimentally determined melting curves. Three of the curves at lower temperature refer to the beginning of melting of granite, tonalite and amphibolite (gabbro) under water-saturated conditions while the remaining three curves at progressively higher temperatures represent the vapor-absent melting curves for metamorphic rocks containing, respectively, muscovite, biotite and amphibole. It is evident from Fig. 84a that the temperatures recorded in the gneisses of the Namaqualand Metamorphic Complex are well in excess of those required for water-saturated

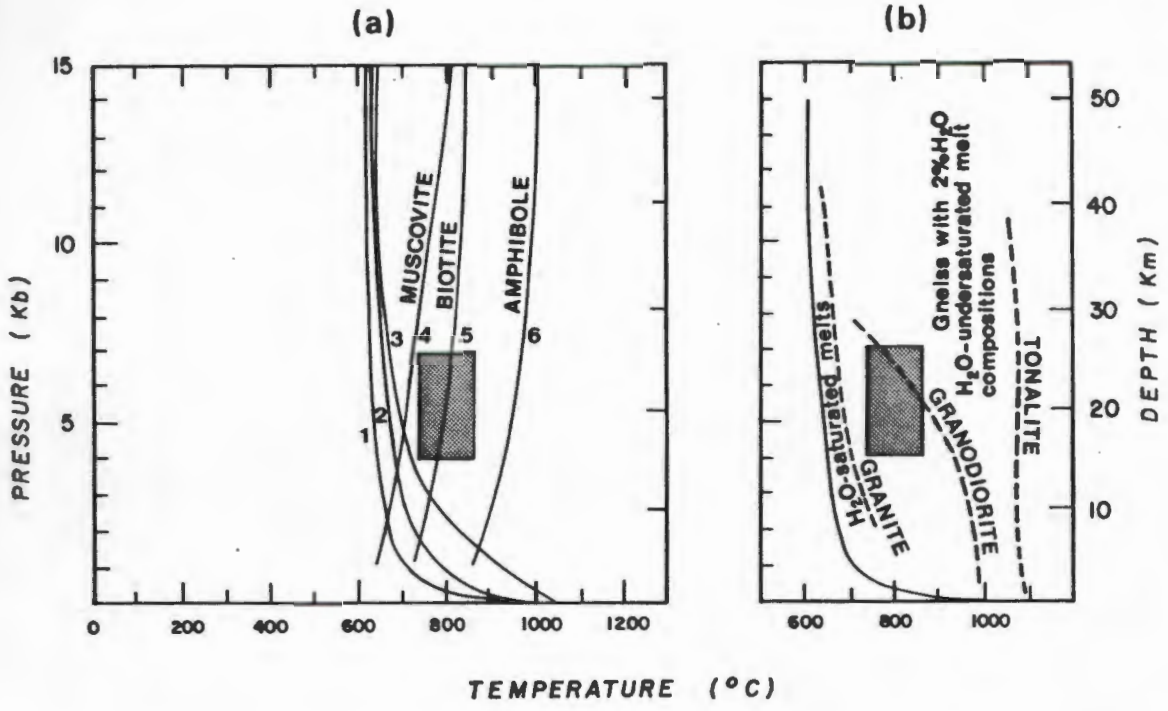


Fig. 84 : Experimentally determined fusion curves for a wide range of bulk compositions in relation to the estimated P-T conditions during granulite facies metamorphism in the study area (stippled rectangle).

(a) Curves 1,2 and 3 represent, respectively, the minimum temperature for the beginning of melting of granite, tonalite and amphibolite bulk compositions that are saturated with respect to water ($P_{H_2O} = P_{total}$). Curves 4,5 and 6 are largely schematic and represent, respectively, the initiation of vapor-absent melting in muscovite, biotite and amphibole-bearing crustal rocks. (Sources of information are largely from Wyllie (1977) and other references cited therein).

(b) The types of liquids that can be generated by anatexis from a wide range of bulk compositions of crustal rocks containing 2 per cent water. Melting for such diverse bulk compositions as gabbro, tonalite, granite, greywacke and shales commences with a narrow temperature interval labelled "$H_2O$-saturated melts". Under the P-T conditions for granulite facies metamorphism estimated in this study (stippled rectangle) anatexis of crustal gneisses containing 2 per cent water are expected to yield $H_2O$-undersaturated granitic liquids. (This diagram is based on Wyllie (1977)).

melting of a wide range of bulk compositions. The temperatures have also exceeded the vapor-absent muscovite melting curve and the complete absence of muscovite from all granulite facies mineral assemblages indicates that this

mineral was no longer stable under the prevailing P-T conditions and probably contributed considerably towards the formation of melts. It is also clear from Fig. 84a that the estimated thermal peak during metamorphism was high enough to initiate melting in vapor-absent biotite-bearing assemblages, but was not high enough to cause melting of amphibole-bearing assemblages in the absence of a pore fluid. Fig. 84a confirms that anatexis in the granulite facies terrane is possible in quartzo-feldspathic gneisses containing biotite as the sole source for water. The amount of water released by the partial breakdown of biotite will be small so that only limited amounts of melt can be generated. Some gneisses, however, have reached an advanced stage of migmatisation (Plate 7) and, therefore, it is suggested that at least some free water must have been present.

The present water contents of pelitic and semipelitic gneisses in the Namaqualand Metamorphic Complex generally do not exceed 2 per cent by weight (J.M. Moore, pers.comm., 1981). Fig. 84b illustrates the type of liquids that could be formed by anatexis from gneisses covering a wide compositional range for a generous allowance of 2 per cent water, and it is evident that under the estimated P-T conditions of the area concerned, the liquids are $H_2O$-undersaturated granites. It has been pointed out by Wyllie (1977) that tonalitic and dioritic melts require very high temperatures (see Fig. 84b) and cannot be generated by anatexis during high grade regional metamorphism.

Numerous experimental studies have verified that many minerals only show a limited solubility in quartzo-feldspathic liquids near solidus temperatures. These include biotite, amphibole, clinopyroxene, orthopyroxene, anorthite-rich plagioclase, sillimanite, cordierite and garnet. They coexist with granitic liquids over a wide temperature interval and tend to form a refractory crystalline residuum (restite) should the liquid migrate out of the melting zone (Fyfe, 1973; Green, 1976). The *in situ* formation of restites may be equated with the melanosomes observed in the migmatites.

## D Mesoscopic Field Appearance of the Migmatites

The style of migmatisation is a complex function of the physical and chemical properties of the host rocks which determines how they respond to their tectono-thermal environment. In general, however, the diatectic styles which refer to complete or nearly complete melting (i.e. schlieric, nebulitic and homophaneous rocks) characterise the central parts of anatectic massifs and these are generally surrounded by migmatites displaying metatectic styles, a term referring to incipient partial melting where molten and unmolten portions are still discernible, i.e. blastic, stromatic and phlebitic migmatites (Mehnert, 1968).

Ophthalmic (augen) structures are extremely common in the study area and are generally observed as large ovoid feldspar crystals. The mode of origin of these feldspar augen is not always obvious. Some of these, no doubt, have formed by blastesis especially when occurring as isolated augens that are not restricted by lithological boundaries. The majority of these feldspar augen (e.g. in augen gneisses) are, however, more likely to re-

present deformed phenocrysts of porphyritic intrusive rocks. Very similar features of "augen"-shaped quartzo-feldspathic segregations are sometimes recorded in biotite-bearing quartzo-feldspathic gneisses (Plate 1). These "augen" differ from those consisting of a single feldspar crystal in being composed of more than one mineral which generally involves numerous quartz and feldspar grains that tend to be coarser grained in the central parts of the "augen". A narrow rim of ferromagnesian minerals (largely biotite) is generally apparent along the margin of the quartzo-feldspathic segregation. The long axes of these augen-structures conform with the regional foliation.

Spectacular garnet-blastesis is commonly displayed by semipelitic biotite-garnet-bearing gneisses (Plate 2). Note that the large euhedral garnet porphyroblasts (black spots) are surrounded by leucocratic quartzo-feldspathic haloes in the biotite-rich host-rock. These textures provide convincing evidence for the *in situ* nature of migmatisation.

Stromatic (layered) migmatites and phlebitic (vein) migmatites are the most common migmatite styles encountered in the area studied. A typical example of stromatic migmatites is illustrated in Plate 3 which shows alternating leucocratic and melanocratic layers developed parallel to the regional foliation. Although individual leucosomes can frequently be traced over long distances they tend to lens out along strike and they generally have rather irregular outlines characterised by thickening and thinning in a boudinage-like manner. A narrow selvedge of mafic minerals (melanosome) generally borders the leucosomes.

Some of the leucosomes are bent into tight isoclinal folds which have apparently not affected adjacent leucosomes (Plate 4, above pencil). Such structures are indicative of polymigmatisation. In fact, folding is a very common phenomenon in these migmatites frequently resulting in rather complicated ptygmatic structures which apparently bear no relationship to the associated macroscopic folds. The styles and orientation of these minor folds shows a considerable variation even in a very restricted area of a single outcrop.

The polymigmatitic nature of the terrane is apparent from cross-cutting relationships between various generations of leucosomes as illustrated in Plate 5 and at least three generations of leucosomes are shown, two of which are likely to have formed by magmatic injection rather than *in situ* anatexis.

Agmatites (migmatites with a breccia-type structure) are commonly observed in the extreme southern part of the area where spectacular outcrops are encountered on the farm Tafelberg 64 (Plate 6). These consist of angular blocks of country rock gneiss separated from each other by garnetiferous leucosomes. Some of their characteristic features, notably the rotation of the angular fragments has been cited as evidence supporting the once molten state of the leucosomes.

In a large area centred around Kliprand the above-mentioned migmatite styles are observed to grade into schlieric and nebulitic migmatites. A typical example of a schlieric migmatite is illustrated in Plate 7.

In some outcrops the paleosome and neosome are no longer discernible and hand specimens have a magmatic appearance. "Ghost structures" of pre-existing gneisses can, however, still be recognised in outcrop and the rocks are best described as nebulites. Excellent examples of nebulitic migmatites occur on the farm Kamaboos (22) and the surrounding territory. In fact, in this particular part of the study area the extent of leucosome formation in the migmatitic gneisses is observed to increase steadily along strike as the nebulitic migmatites are approached and illustrates how progressive migmatisation converts pre-existing gneisses into rocks of magmatic appearance. According to Mehnert (*op.cit.*) nebulites develop in the central parts of migmatite massifs and are considered to represent the link between migmatite *sensu stricto* and truely magmatic rocks.

Various types of biotite, garnet and amphibole-bearing granitoids of demonstrably intrusive origin occur as large bodies throughout the granulite facies terrane. The refractory minerals are likely to represent relict source material (Green, 1976; White and Chappell, 1977) suggesting that some of these granitoids could well be of the S-type derived from partial melting of pelitic and semipelitic gneisses at a crustal depth below the present level of exposure.

# VI ORIGIN OF GRANULITES AND THE NATURE OF ASSOCIATED CHARNOCKITES

## A Introduction

The most outstanding feature of the gneisses in the granulite facies terrane is their overall "dry" mineralogy consisting largely of anhydrous phases. This is in marked contrast to the adjacent amphibolite facies terrane in which hydrous minerals feature prominently. One of the fundamental questions concerns the factors controlling the formation of these contrasting environments. From experimental studies it is apparent that several alternatives could account for the recorded distribution of minerals and mineral assemblages in the study area, but at the present state of knowledge it is not possible to decide on that applicable to the Namaqualand Metamorphic Complex. In spite of this, the most important factors likely to be involved in the generation of the granulite facies rocks are briefly outlined.

Charnockites feature prominently in the granulite facies terrane studied and their relationship to the metamorphic environment requires discussion.

## B Generation of Granulites by Partial Melting

From the brief review of experimental studies relevant to the formation of migmatites outlined in the previous chapter it is evident that partial melting is likely under conditions of high grade regional metamorphism. That this process was in fact operative in large parts of the Namaqualand Metamorphic Complex is witnessed by the ubiquitous occurrence of garnetiferous migmatites and related granitoids. If the anatectic melts are removed from their source region, the composition of the remaining material will change to a crystalline residuum of refractory minerals which, according to some authors (e.g. Brown and Fyfe, 1970, 1972; Fyfe, 1973; McCarthy, 1976; White and Chappel, 1977), accounts for the mineral assemblages recorded in granulite facies terranes. Accordingly, granulites can be generated from amphibolite facies rocks simply by the formation of granitic liquids. Due to the high solubility of water in granitic melts (Brown, 1973) considerable amounts of water can be transported to higher crustal levels leaving behind relatively "dry" granulites. According to Fyfe (*op.cit.*) "the most efficient high-temperature dehydration process involves the partial formation of a silicate melt where water is effectively diluted and removed in solution by a silicate fluid".

This model has been successfully tested recently for New Quebec and Adirondack granulites in North America (Nesbitt, 1980) by utilising the concept that if partial melting is solely responsible for the difference

between hydrous amphibolite facies rocks and their genetically related dehydrated granulite facies equivalents, then the difference in bulk composition between the two rock types should be that of a granitic melt composition. The studies conducted by Nesbitt (*op.cit.*) confirm that in certain areas the compositional difference between amphibolite and equivalent granulite can be explained by anatexis of the amphibolite facies gneiss to yield a granulite residue and a granitic melt. Granulites formed in this manner are also referred to as *fusion granulites* (*ibid.*).

Whether partial melting did in fact play an important role in the generation of granulites in the Namaqualand Metamorphic Complex is controversial. This model is favoured by McCarthy (*op.cit.*) and Clifford *et al.*, (1981), the latter author suggesting that the cordierite-orthopyroxene rocks in the Nababeep District represent restites of argillites from which considerable amounts of granitic liquid have been extracted. Contrary to this, Moore (pers.comm., 1982) concludes from a geochemical study of metapelites that the granitic melt fraction seen in the leucosomes have remained *in situ*.

If partial melting did play a dominant role in the generation of this granulite facies terrane, a major migmatite complex would be expected to have formed along the amphibolite-granulite facies transition. There is, however, no evidence for this in the area studied. Although migmatites are common they are best developed in the southern part of the area removed from the granulite-amphibolite facies transition.

### C The Generation of Granulites by Dehydration Metamorphism

It has been pointed out by Nesbitt (*op.cit.*) that some granulites involve partial melting while others are considered to have formed merely as a result of dehydration reactions liberating $H_2O$ and thereby yielding anhydrous mineral assemblages, also referred to as *dehydration granulites* (*ibid*). These dehydration reactions can be activated by either increasing the temperature beyond the stability limit of the hydrous phase (e.g. Binns, 1969b; Spear, 1981), or alternatively, by reducing the activity of water in the gas phase at elevated temperatures (Althaus, 1968; Spear *op.cit.*). If $P_{H_2O}$ is lowered relative to $P_{total}$ the upper temperature stability limit of hydrous minerals (such as, for example, amphiboles) decreases and accordingly the partial pressure of water in the gas phase plays an important role in the granulite-amphibolite facies transition. The significance of water during metamorphism is increasingly recognised in recent literature(Janardhan *et al.*, 1979; Phillips, 1980; Glassley and Sørensen, 1980).

Phillips (*op.cit.*) has attempted to evaluate the changes in water activity across the amphibolite-granulite facies transition in the Willyama Complex, Broken Hill (S.E. Australia) by thermodynamically modelling mineral equilibria in pelitic and mafic gneisses in conjunction with partial melting data. He records a decrease in $a_{H_2O}$ as well as a concomitant rise in

temperature indicating that both factors were operative in producing the contrasting mineralogies across the transition (*ibid.*).

The important role played by the gaseous components in phase transformations is also demonstrated by Glassley and Sørenson (*op.cit.*) who have studied metamorphically zoned dolerite dykes in West Greenland. The entire transition from upper amphibolite facies through pyroxene granulite to garnet granulite facies is preserved within a single dyke which is believed to have been subjected to essentially isobaric and isothermal conditions during the formation of the metamorphic zonation. $X_{H_2O}$ in the gas phase is considered to have exerted the dominant control over the entire transition (*ibid.*).

Only future detailed studies will reveal the mode of origin of the granulite facies assemblages in the Namaqualand Metamorphic Complex. It is suggested that promising fields of additional investigations concern thermodynamic models aimed at evaluating $a_{H_2O}$-changes across the granulite-amphibolite facies transition as well as geochemical studies concerning changes in bulk composition of equivalent rock types in the contrasting facies which could clarify the involvement of anatexis in the generation of the granulites. As the P-T conditions in this study are focused on the granulite facies terrane future studies should concentrate on thermodynamically evaluating these parameters for the adjacent amphibolite facies terrane in order to establish the role played by temperature in the transition.

## D Fluids Accompanying Granulite facies Metamorphism

The "anhydrous" conditions reflected by granulite facies mineral assemblages may be the result of a lowering in water pressure relative to the load pressure. Such a reduction in water pressure can be achieved either by metamorphism of fairly "dry" rocks involving high temperature magmatic intrusives/extrusives or metamorphites produced by repeated high grade metamorphism of pre-existing water-saturated sediments or alternatively, by diluting the fluid phase with other gaseous components causing a reduction of the partial pressure of water even though the fluid pressure remains high.

Considerable progress has been made in recent years in gaining some insight into the composition of the gas phase accompanying regional metamorphism. Such information stems mainly from tiny fluid inclusions trapped in minerals (particularly quartz) during crystallisation. Studies of these inclusions in granulite facies rocks (including charnockites) have revealed the presence of a carbonic fluid consisting predominantly of $CO_2$, $CH_4$ and other hydrocarbons and NaCl (Touret, 1971, 1972, 1974, 1977; Berglund and Touret, 1976; Hoefs and Touret, 1976; Hollister and Burruss, 1976; Ormaasen, 1977). $CO_2$ and $H_2O$ are also present in fluid inclusions from amphibolite facies rocks, but according to Touret (1972) water is much more abundant in this environment and the fluids are predominantly hydrous. These fluid inclusions provide evidence supporting high $X_{CO_2}$ contents of the fluid phase emanating from or passing through terranes undergoing granulite

facies metamorphism which in itself implies a reduction in $X_{H_2O}$ because the fluid pressure cannot exceed the total load pressure (Heier, 1973). Unfortunately, nothing is known about the composition of fluid inclusions in the study area, but there is some indication from the Aus environment in SWA/Namibia that granulites in the Namaqualand Metamorphic Complex are also characterised by carbonic fluids (Jackson, 1976).

The contrasting compositions of the fluids accompanying regional metamorphism in the amphibolite (mainly hydrous) and granulite facies (mainly carbonic) has major implications for the stability of hydrous minerals. The difference in mineralogy between the two facies is largely the result of dehydration reactions by which hydrous minerals are replaced by anhydrous phases with the liberation of water (e.g. orthopyroxene forming at the expense of hornblende). Such reactions are very sensitive to the concentration of water in the accompanying fluid and at otherwise constant conditions will proceed at progressively lower temperatures as the partial pressure of water decreases (i.e. the partial pressure of $CO_2$ increases). Consequently, at appropriate elevated temperatures amphibolite facies assemblages can be converted into granulites under isothermal and isobaric conditions by merely diluting the hydrous fluid by $CO_2$. The fact that both metamorphic facies are characterised by very different fluid compositions points to the strong possibility that other gaseous components and in particular $CO_2$ may play a major role in the observed metamorphic zonation of the study area.

Although the temperature conditions in the upper amphibolite facies terrane of the study area have not been established quantitatively, the results obtained from coexisting garnet and cordierite and coexisting pyroxenes do not indicate a gradual drop in temperature as the transition between the two facies is approached. This suggests that factors other than temperature (presumably fluid composition) may well be largely responsible for the observed change in mineralogy, but this can only be confirmed once the temperature conditions for the upper amphibolite facies have been evaluated quantitatively.

If the carbonic fluids play a major role in the genesis of granulite facies assemblages, where do they come from? $CO_2$ is released in numerous reactions involving carbonate and calc-silicate minerals. Therefore, if rocks containing these minerals were important contributors of $CO_2$ in the granulite facies terrane studied, they would be expected to be very abundant, but as this is not the case, they can be excluded as a major source of $CO_2$.

In the recent literature a primitive upper mantle source for $CO_2$ is increasingly involved in the process leading to the conversion of the crust into granulite facies assemblages (Touret, 1971; Tarney and Windley, 1977; Collerson and Fryer, 1978; Janardhan *et al.*, 1979). According to several authors $CO_2$ may form an important constituent of the upper mantle (Green and Radcliffe, 1975; Mysen *et al.*, 1975, 1976; Wyllie and Huang, 1975; Eggler, 1976; Eggler and Mysen, 1977). Much of the mantle-derived $CO_2$ could be locked up in plagioclase in the form of scapolite, considered a major constituent of deep crustal levels (Newton and Goldsmith, 1975; Goldsmith, 1976; Goldsmith and Newton, 1977) and, therefore, a potential source of $CO_2$.

## E Charnockites and the Granulite Facies Terrane

In current literature considerable debate is focused on the relationship between charnockites and their metamorphic environment, the prime concern being the question of whether the charnockites are the products or the causes of granulite facies metamorphism.

Charnockites and related rock types are very common in the southern part of the area (Fig. 85) and isolated outcrops have also been encountered further north (map A).

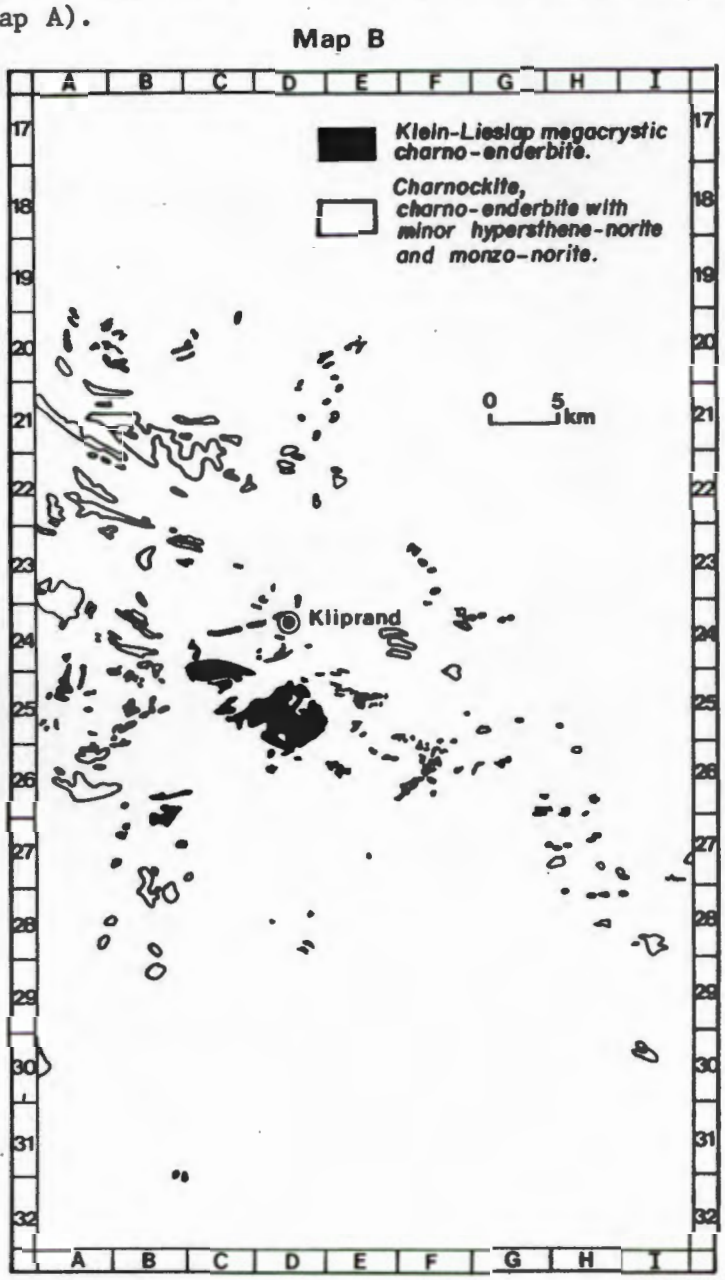


Fig. 85 : Sketch map showing the regional distribution of charnockites and related rocks in the Kliprand area.

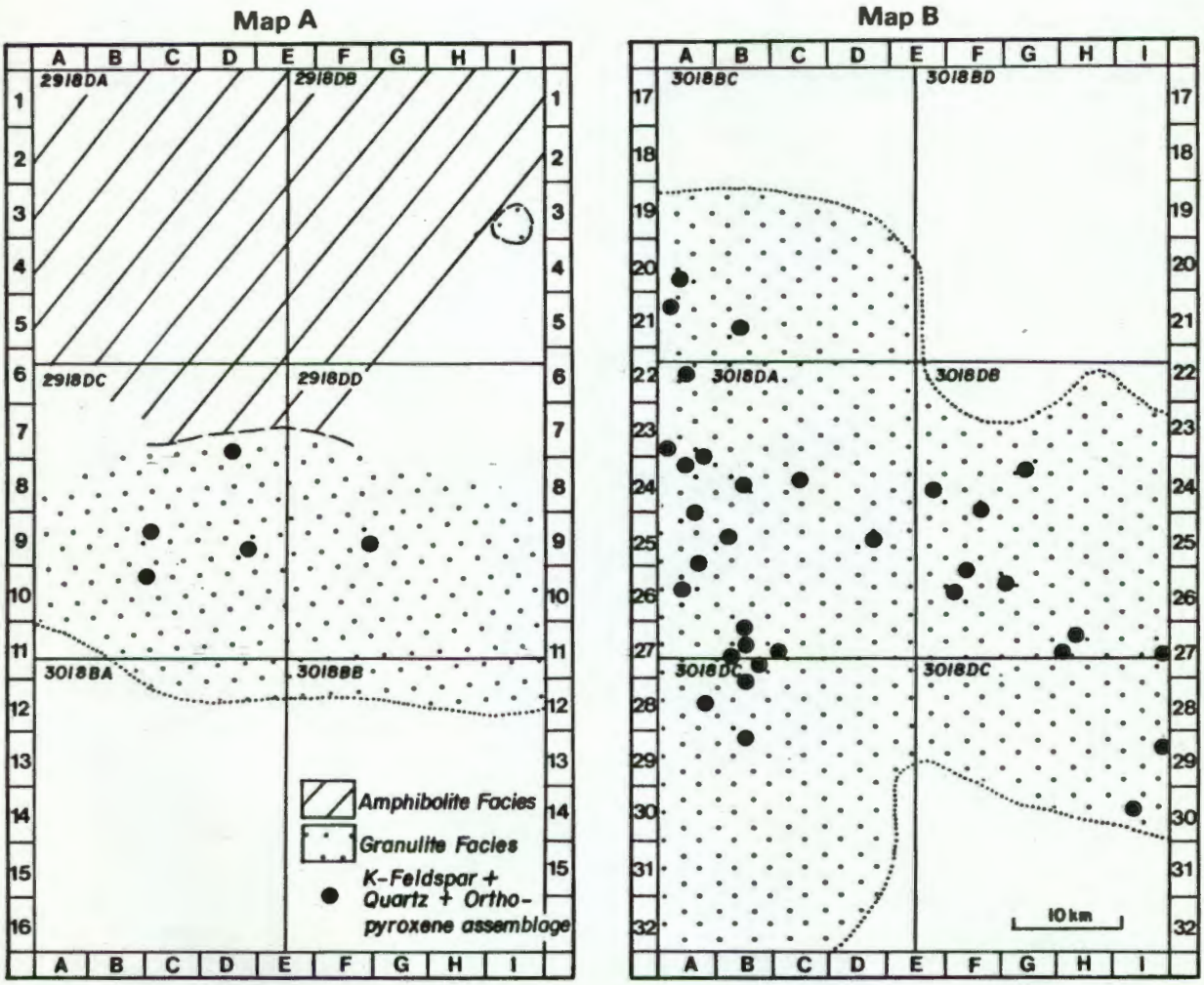


Fig. 86: Geographic distribution of the mineral assemblage "K-feldspar + quartz + orthopyroxene", in charnockites and related rock types. Note that this assemblage is spatially restricted to the granulite facies environment.

All the known occurrences of charnockites and related rocks in the study area are spatially restricted to the granulite facies terrane (Fig. 86). The mineral assemblage "K-feldspar + orthopyroxene + quartz" although searched for, has not been found anywhere in the amphibolite facies terrane, suggesting that in the area studied, charnockite genesis was restricted to the granulite facies environment.

The close spatial association of charnockites with the granulite facies terrane in the Namaqualand Metamorphic Complex has previously been stressed by Jackson (1976, 1979) and it appears also to be true for other high grade meta-

morphic terranes (Pichamuthu, 1953; Howie, 1955, 1964; Ramaswamy and Murty, 1973; Malm and Ormaasen, 1978; Martignole, 1979; Janardhan *et al.*, 1979), but charnockites are not entirely restricted to this environment (Pichamuthu *op.cit.*; de Waard, 1969). Nevertheless, in the current literature it is indicated that charnockite occurrences in areas not underlain by granulite facies mineral assemblages are rare.

Outside the borders of the study area charnockite-type rocks have been reported from extensive areas within the Namaqualand Metamorphic Complex. Along the Natal coast Namaqua-type gneisses are exposed north of Port Edward with an increasing metamorphic grade towards the south and away from the Kaapvaal craton and ranging from greenschist facies to middle amphibolite facies in the vicinity of Durban (Cain, 1975), while granulite facies assemblages are recorded in the region between "Marble Delta" (Simpson and Tregidga, 1956) and Port Edward. Associated with this granulite facies environment are numerous charnockites and related rocks described by Gevers and Dunne (1942) and McIver (1966) and these are considered to be of intrusive origin (McIver, *op.cit.*).

There appears to be a considerable similarity between the setting of the Natal charnockites and those observed in the study area, both terranes being characterised by an increase in metamorphic grade from the north to the south. It seems likely that both charnockite provinces form part of a continuous belt of charnockite-granulite assemblages, now largely covered by sediments of the Karoo Sequence. This belt most certainly continues westwards into the area investigated by Joubert (1971a). Although Joubert (*op.cit.*) does not mention the occurrence of charnockites as such, he describes pyroxene granulites containing potash feldspar, large quartz grains and antiperthitic plagioclase and generally lacking clinopyroxene which clearly indicates the presence of these rock types. Likewise Jack (1980) has not recorded any charnockite-type rocks from western Namaqualand and it is, therefore, uncertain how far westwards this belt extends.

Another charnockite-granolite province within the Namaqualand Metamorphic Complex occurs within a northwest-trending belt extending from the Upington-Kakamas area in the northern Cape Province to Aus in Namibia. This province has been extensively described in the literature (von Backström, 1964; Blignault *et al.*, 1974; van Bever Donker, 1980; Stowe, 1981).

From the experimental studies of Luth (1967) on the chemical system $KAlSiO_4$-$Mg_2SiO_4$-$SiO_2$-$H_2O$ it is apparent that the coexistence of orthopyroxene and K-feldspar requires low water pressures. It has been verified that in the above system orthoclase and enstatite coexist in the temperature range 700 - 1150°C provided that the water pressures do not exceed 0,7 kb (*ibid.*). Thus it is concluded that charnockites can only develop under relatively dry conditions which is consistent with the low concentration of hydrous phases recorded in these rocks. In fact, it is this "dry" nature that both charnockites and their surrounding environment have in common. Some of the mechanisms leading to dehydration have already been outlined and in particular the composition of the fluid phase accompanying regional metamorphism appears to play a significant role in the genesis of granolites and charnockites. Some authors speculate that intrusive charnockites may be the

transporting medium of $CO_2$-rich volatiles presumably from a source in the upper mantle or lower crust.

In the Aus area (Namibia), for example, Jackson (1976) has suggested that charnockites have intruded as magmas into a hot environment, carrying with them $CO_2$-rich volatiles which, in response to decreasing pressure during upward movement are liberated and dilute the gas phase in the country rock and thereby promoting dehydration reactions to proceed at lower temperatures yielding granulite facies assemblages. This is a very plausible mechanism, but would imply that fluid inclusions nearest to the centres of charnockite intrusion should be most carbonic while those progressively further away should become progressively less $CO_2$-rich. Only future detailed studies are likely to throw some light on this hypothesis.

Although the charnockitic rocks in the study area in their present state are characterised by metamorphic textures, there is indisputable field evidence that their early history was one of magmatic intrusion as witnessed by the ubiquitously recorded xenoliths of country rock and their cross-cutting contact relationships with the host gneisses. The absence of chilled margins along the country rock contacts is taken as evidence that these magmas intruded into a previously heated environment. This implies that metamorphism had already commenced prior to charnockite intrusion, but the grade prevailing at that time is unknown. The abundant xenoliths of granolite within the charnockites, however, may suggest that granulite facies metamorphism already prevailed when the charnockites intruded and their fabrics indicate that granulite facies metamorphism continued while these rocks crystallised. Although it is possible that charnockites may have played an important role as a transporting medium of carbonic fluids and heat to higher crustal levels and thereby may have contributed towards the formation of granulite facies conditions in their surrounding environment (i.e. low $P_{H_2O}$ and high temperature), the available evidence suggests that both granulite facies metamorphism and charnockite genesis are caused by the same process, considered to involve a deep-seated heat source.

That charnockite magmas must have been very hot can be concluded from their mineralogy and "dry" nature. The presence of orthopyroxene and perthitic K-feldspar are both consistent with a high temperature environment (Spear, 1981; Morse, 1970). It has been pointed out that dry melts require much higher temperatures than water-saturated melts (Chapter V) and because the charnockite mineralogy suggests that these rocks are relatively "dry", their high temperature character is apparent.

Speculation on the ultimate source of these charnockitic magmas is beyond the scope of this study. Some authors consider the frequently recorded spatial association of charnockites with anorthosites to indicate petrogenetic consanguinity (Hyndman, 1972; de Waard *et al.*, 1974). In the area studied no anorthosites have been encountered and this can either mean that in the present situation there is no genetic relationship between charnockites and anorthosites or alternatively, the anorthosites occur at a deeper crustal level (not exposed) where they may be associated with garnet granulites which are likely to occur at deeper levels than the presently ex-

posed pyroxene granulites.

Malm and Ormaasen (1978) suggest that the mangerite-charnockite intrusives in the Lofoten-Vesterålen area (Northern Norway) represent products of fractional crystallisation derived from a deep-seated gabbroic magma source at the base of the crust, considered to be generated by partial fusion of the underlying mantle. This gabbroic source is also regarded as a likely precursor for anorthosites in granulite facies terranes (*ibid.*). A similar source is envisaged by Petersen (1980) who concludes, from a geochemical study involving REE distributions in highly differentiated charnockitic rocks from Norway, that charnockite and rapakivi granites are genetically related and appear to have formed as a result of fractional crystallisation of a magma derived from a basic source.

# VII STRUCTURE

## A Introduction

The polyphase deformational nature of the Namaqualand Metamorphic Complex is well documented (Joubert, 1971a, 1974c; Stowe, 1980) and in this respect the area studied is no exception. Several episodes of superimposed folding created a fascinating interference pattern. The presence of sinistral and dextral ductile shear zones and brittle fault zones is also recorded in the study area.

As the prime object of the fieldwork was geared at mapping the regional geology of an extensive, previously unmapped area in the shortest possible time, it was obviously impossible to investigate all the aspects of the geology in depth. The bias in this thesis towards metamorphism reflects the author's preference. In a complex polydeformational terrane metamorphism can, however, not be studied in isolation from regional tectonism as recrystallisation and deformation are frequently intricately related processes. A basic structural investigation was therefore indispensable and the major structural elements are briefly outlined here.

The succession of fold generations was established by the criteria described by Tobisch (1966) and Joubert (1971a). These include the following:

(a) Refolding - involves the concept that if the axial plane or fold axis of a fold A is folded by a fold B the latter must be the younger. This is generally regarded to be the most reliable method of deciphering the chronological order of folds.

(b) Correlation by fold style - This criterion must be used with caution as Hobbs *et al.* (1976) point out that style varies with lithology and that structures with identical style need not belong to the same fold generation.

(c) Metamorphic grade associated with folding and the absence or presence of an axial-planar foliation.

(d) Fold orientation - This criterion is only of limited value as folds of the same generation can have variable orientation (Hobbs *et al.*, *op.cit.*).

Tectonically produced planar fabrics are commonly described as foliation, cleavage and schistosity. In this study, following Turner and Weiss (1963) and Whitten (1966), the term "foliation" is applied in a general way to cover all types of mesoscopically recognisable secondary planar fabrics of metamorphic origin. The term "lineation" according to Turner and Weiss (*op.cit.*) is used in a restricted sense for those linear structures that are penetrative in hand specimens (e.g. mineral lineation, axes of small folds and intersections of S-surfaces).

The symbolism utilised for the structural elements are as follows: successive episodes of deformation are designated $D_1$, $D_2$ *etc.*, associated folds $F_1$, $F_2$ *etc.*, planar structures and lineations which were generated during these deformational episodes are referred to as $S_1$, $S_2$ and $l_1$, $l_2$ etc., respectively, and $f_1$, $f_2$ *etc.* are applied to foldaxes of successive generations. The $D_1$, $D_2$, $D_3$ *etc.* episodes are correlated with the $F_1$, $F_2$, $F_3$ *etc.* episodes of Joubert (1971a) unless otherwise stated.

The structural elements are plotted on equal area lower hemisphere stereographic projections (Schmidt net) and the contouring of the data is accomplished by utilising a contouring net of the type illustrated by Kröner (1968, p. 26, Fig. 6). For contoured projections the contour intervals are indicated as per cent of points per unit area. Planar fabrics are plotted as $\pi$-diagrams (Ramsay, 1967). True north is indicated on the margin of all projections. The number of measurements plotted in each projection is indicated by N.

## B The First Episode of Deformation ($D_1$?)

The metasediments and metavolcanics generally display a gneissic banding which is folded by, and therefore pre-dates, the $D_2$ fold generation. This banding is expressed by alternating leucocratic and melanocratic layers and is here designated $S_1$. In the paragneisses this surface can either be interpreted as an inherited pre-existing bedding ($S_0$) or alternatively as a tectonically produced surface. At some localities small intrafolial folds ($F_1$?) with axial planes parallel to the banding have been recorded. As these structures are commonly regarded to be indicative for transposition of S-surfaces (Turner and Weiss, 1963), it is very likely that the gneissic banding represents a tectonic fabric. The presence of intrafolial folds in itself does, however, not imply an earlier deformation as these structures can also form during a single progressive deformation (Ramsay, 1967, p. 119-120). Thus, unless these intrafolial folds are refolded by the succeeding $D_2$ structures there is no justification to regard them as being of an older generation. These tight folds are not very common and the $D_1$ - $D_2$ refolding relationships have not been established with certainty in this study so that the existence of a $D_1$ episode of deformation is uncertain.

According to Joubert (1971a) the lithological layering was formed as a result of translative movements accompanying a pre-$D_2$ episode of deformation ($F_1$ in the sense of Joubert, *op.cit.*). Many geologists working in the area fail to recognise the early $F_1$ folds, but Joubert (1974c) reconfirms their existence and also states that they pre-date the $F_2$ folds as they are refolded by the latter.

## C The Second Episode of Deformation ($D_2$)

Minor folds of the $D_2$ generation are ubiquitously recorded in the supracrustal gneisses of the study area. These are generally, but not always isoclinal with round to sharp hinge zones and long limbs lying more or less parallel to the gneissic banding. Rather open folding is developed in places reflecting the variability in style of these structures. The minor folds are symmetrical and possess a penetrative axial-planar foliation, here referred to as $S_2$. Owing to the isoclinal nature of the folding the $S_2$ fabric is essentially co-planar with the gneissic banding along the limbs of the $F_2$ folds and the discordance between the two fabrics is most obvious in the $F_2$ hinge zones. The present orientation of the axial planes of the $F_2$ folds varies considerably and their vergence is commonly southwesterly, southerly and southeasterly.

Joubert (1971a) remarks that the mineral lineation which is prominently developed in the Namaqualand gneisses always plunges parallel to the axes of $F_2$ minor folds with the understanding that this applies only to areas outside structures which are obviously related to later deformation such as shear zones. This conclusion is in agreement with observations made in the present study. A prominently developed mineral lineation occurs as a b-fabric in minor folds belonging to the $D_2$ generation. This mineral lineation, which is here referred to as $l_2$, is recognised throughout the study area and is expressed by the alignment of the high grade metamorphic minerals. The interpretation of this regionally developed mineral lineation is, however, often not straightforward owing to the fact that minor folds belonging to the $D_2$ and $D_3$ generations are frequently co-axial or very nearly so and accordingly share the same mineral lineation (Fig. 87). This co-axial nature hampers the decision as to whether the mineral lineation is genetically related to the $F_2$ or $F_3$ structure. It is quite possible that the regionally developed linear fabric comprises an $l_2$ as well as an $l_3$ element. In some of the macroscopic $F_3$ folds it has been convincingly established that the mineral lineation is deformed and for this reason must be a pre-$D_3$ fabric i.e. $l_2$. This is illustrated by way of two examples in Fig.88. On the farm Obeeb(8) the change in trend of the mineral lineation across the $S_3$ axial plane is quite considerable (Fig. 88a). In the limb to the north of the $S_3$ axial plane the $l_2$ trends are west-northwesterly which contrasts markedly with the west-southwesterly trends of the same fabric in the limb south of the hinge zone. A similar but less dramatic change in trend of the mineral lineation across the axial plane of an $F_3$ fold is documented in an antiform on the farms Roode Kloof (14) and Groot Klip (16) where $l_2$ on the northern limb are west-trending as opposed to the west-southwesterly trend recorded in the southern limb and fold closure (Fig. 88b). From observations like these it is concluded that the mineral lineation although it commonly plunges parallel to the $f_3$ fold axes pre-dates the $F_3$ folds and its parallelism with $f_2$ suggests that it represents an $l_2$ fabric.

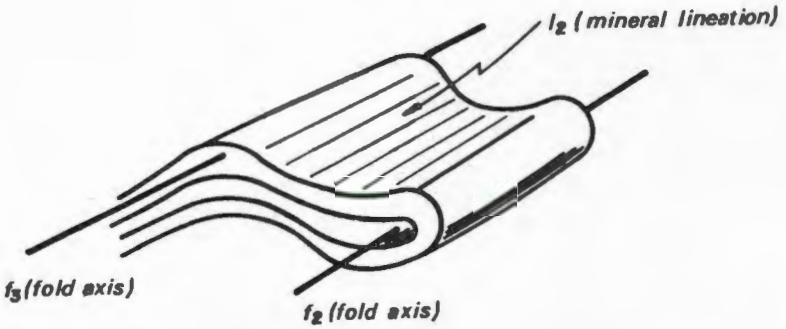


Fig. 87 Sketch showing an $F_2/F_3$ interference structure. The axes of the two fold generations ($f_2$ and $f_3$) are parallel to each other and share a common orientation with the $l_2$ mineral lineation.

The variability in orientation of the mineral lineation and for that matter of $f_2$ in the study area is apparent from Fig. 89. Re-orientation of this fabric no doubt, was accomplished by post-$D_2$ deformation and has created a fascinating regional pattern shown in Fig.90 and Annexure 3. The systematics reflected by this mineral lineation allows the subdivision of the region into several areas numbered I to VII (Fig.91) in each of which the lineation assumes a trend or trends markedly different from the adjacent area (s). Most of these areas may be referred to as domains in the sense that they show homogeneity (statistically speaking) in at least one of the fabric elements (Turner and Weiss, 1963).

*Domain I* comprises the northernmost part of the study area between latitudes 29° 48'S and 29° 30'S (Fig.91). Strictly speaking this area should be further subdivided, but owing to very poor exposure the number of measurements are too few to allow further meaningful subdivision. From the available data it is apparent that the trends of $l_2$ range between 0 and 120 degrees (Fig.92a) while only three of the 41 mineral lineations measured trend slightly north of west.

*Domain II* adjoins onto the southern part of Domain I (Fig. 91) and is also characterised by poor exposure. Nevertheless, the preponderence of east-southeasterly to east-northeasterly plunge directions of $l_2$ is shown in Fig. 92b.

*Domain III* comprises the eastern closure of a basin-shaped interference structure (Fig.91) where the $l_2$ fabric plunges mainly westerly to west-southwesterly (Fig.92c). This trend is similar to the one established in Domain II, but with opposite plunge direction. The reversal in plunge of $l_2$ arises as a consequence of fold interference creating the basin-shaped structure.

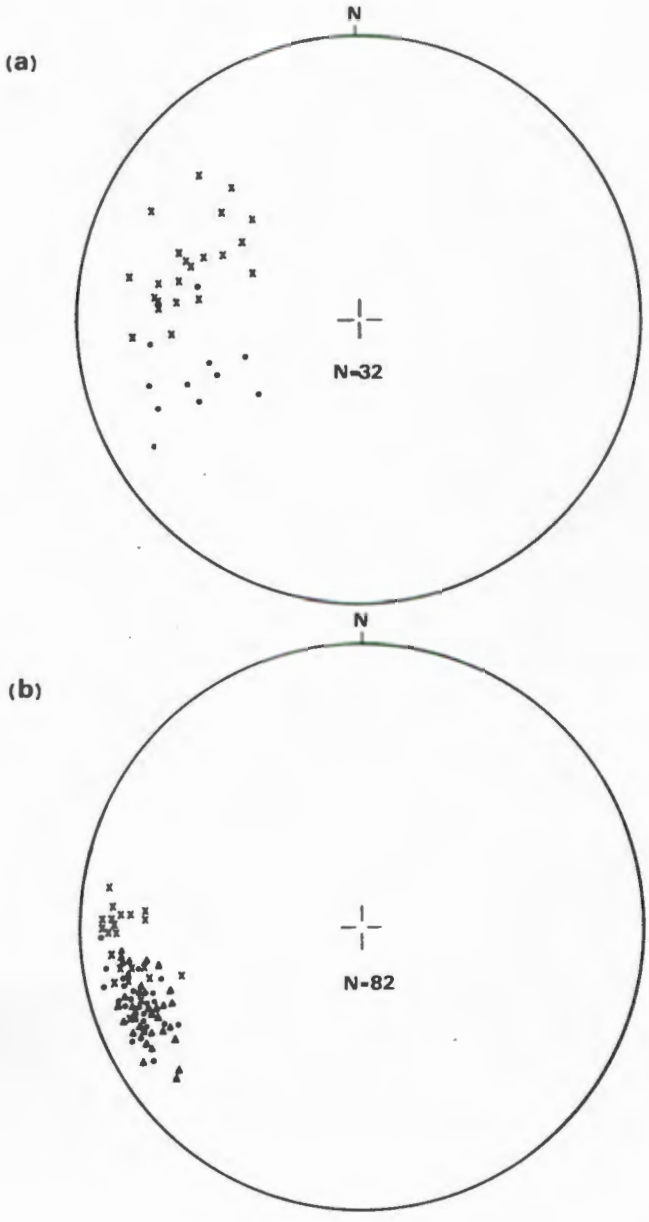


Fig. 88 (a) Equal area projection of $l_2$ mineral lineations measured around the closure of an $F_3$ fold on the farm Obeeb (8). Crosses represent lineations from the northern limb and dots are their equivalents from the southern limb. Note the variation in $l_2$ -trend around the fold closure.

(b) Equal area projection of $l_2$ mineral lineations measured in an $F_3$ antiform on the farms Roode Kloof (14) and Groot Klip (16). Lineations along the northern limb are shown as crosses and those from the hinge zone and southern limb are indicated by triangles and dots respectively.

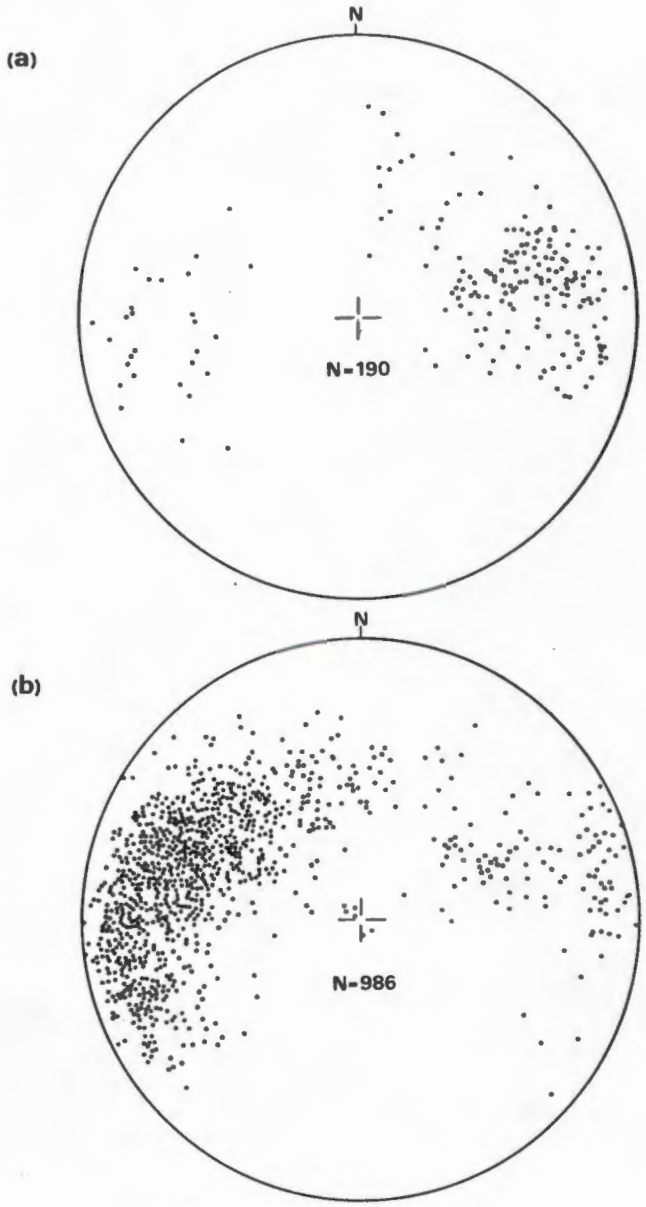


Fig 89 (a) Synoptic equal area projection of $1_2$ mineral lineations from the northern part of the study area (Map A).

(b) Synoptic equal area projection of $1_2$ mineral lineations from the southern part of the study area (Map B). N = number of measurements.

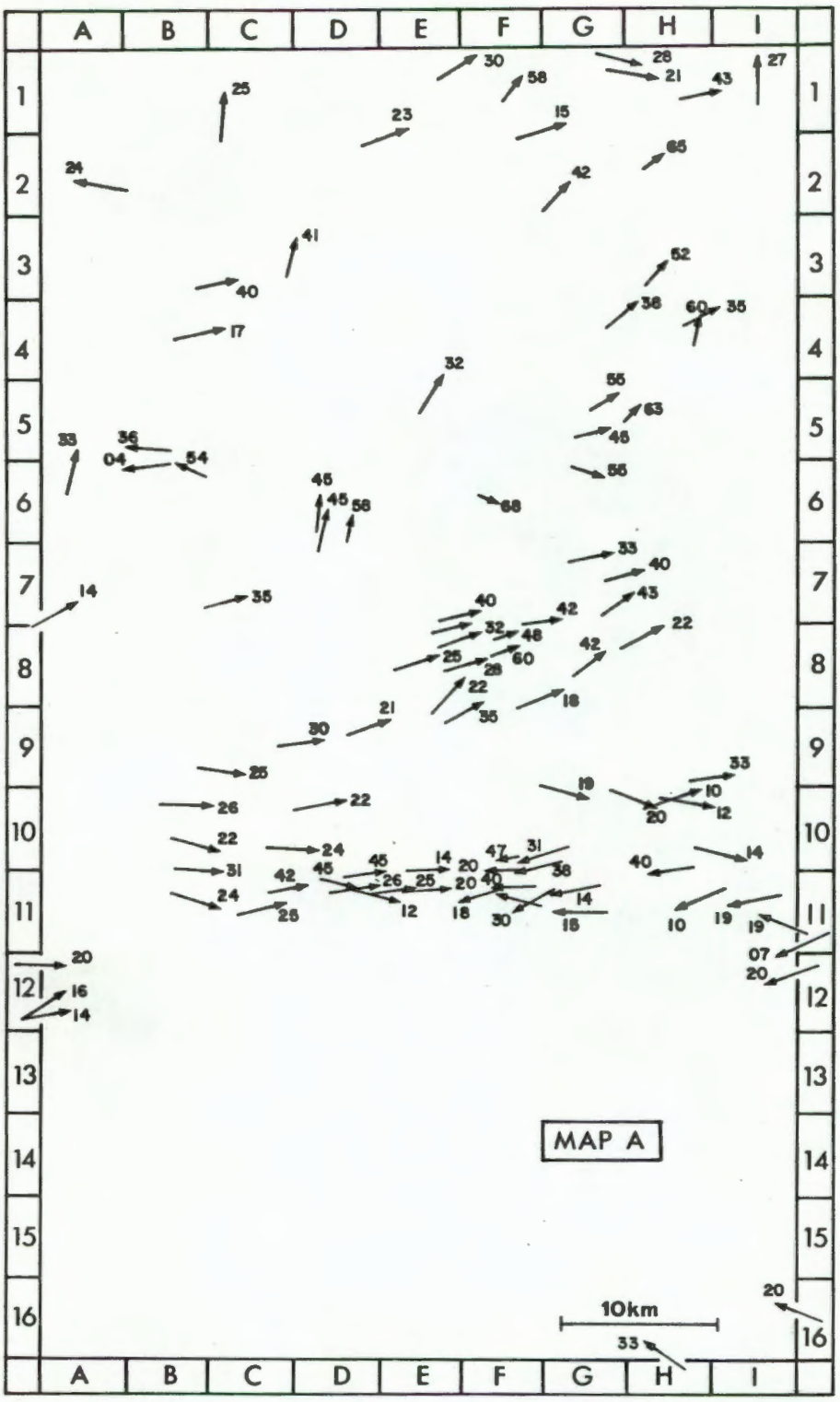


Fig. 90 Variation in trend and plunge of $l_2$ mineral lineations in the northern part of the study area. See also Annexure 3 for trends of $l_2$ on Map B (southern part of study area).

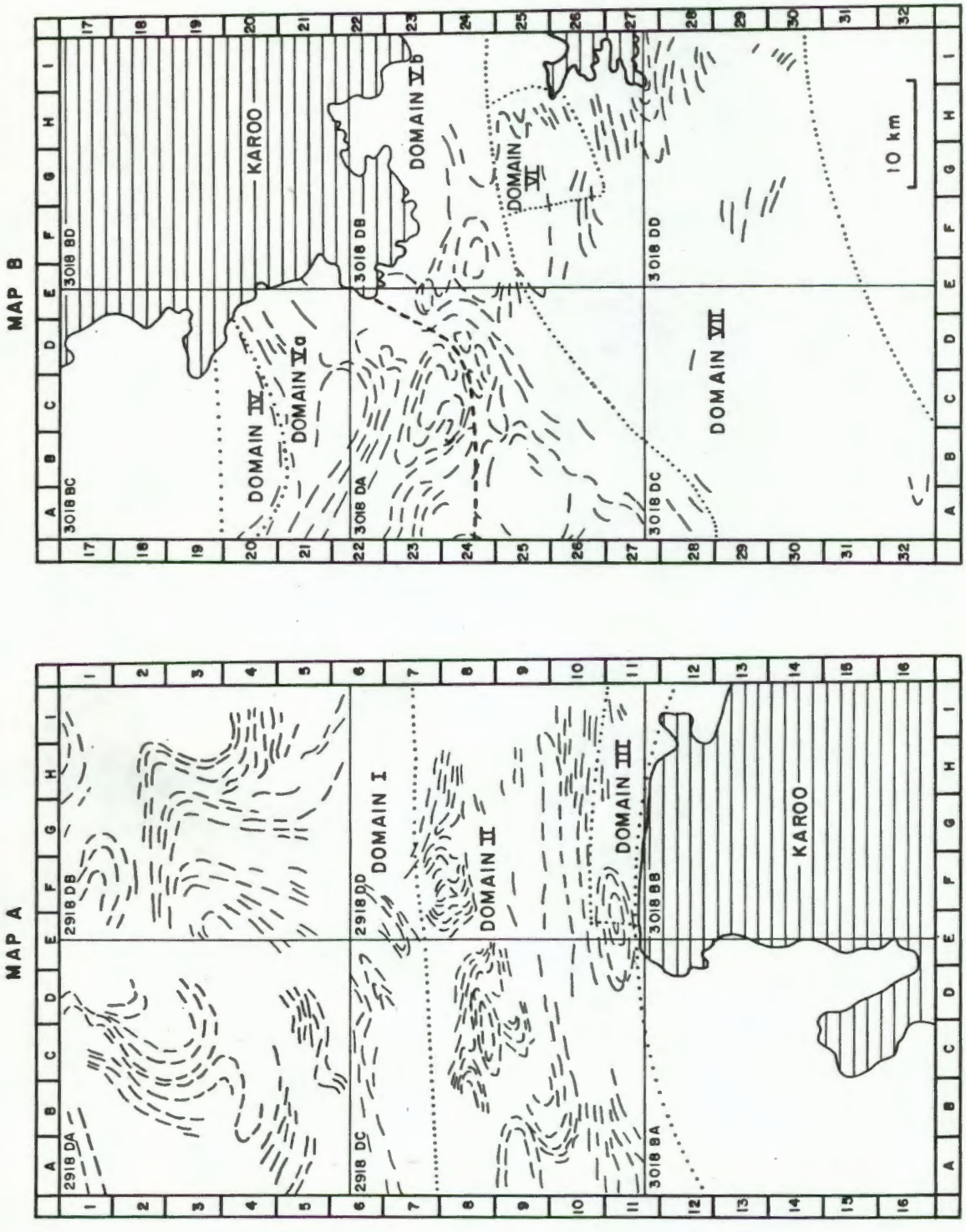


Fig. 91 Subdivision of the area into structural domains

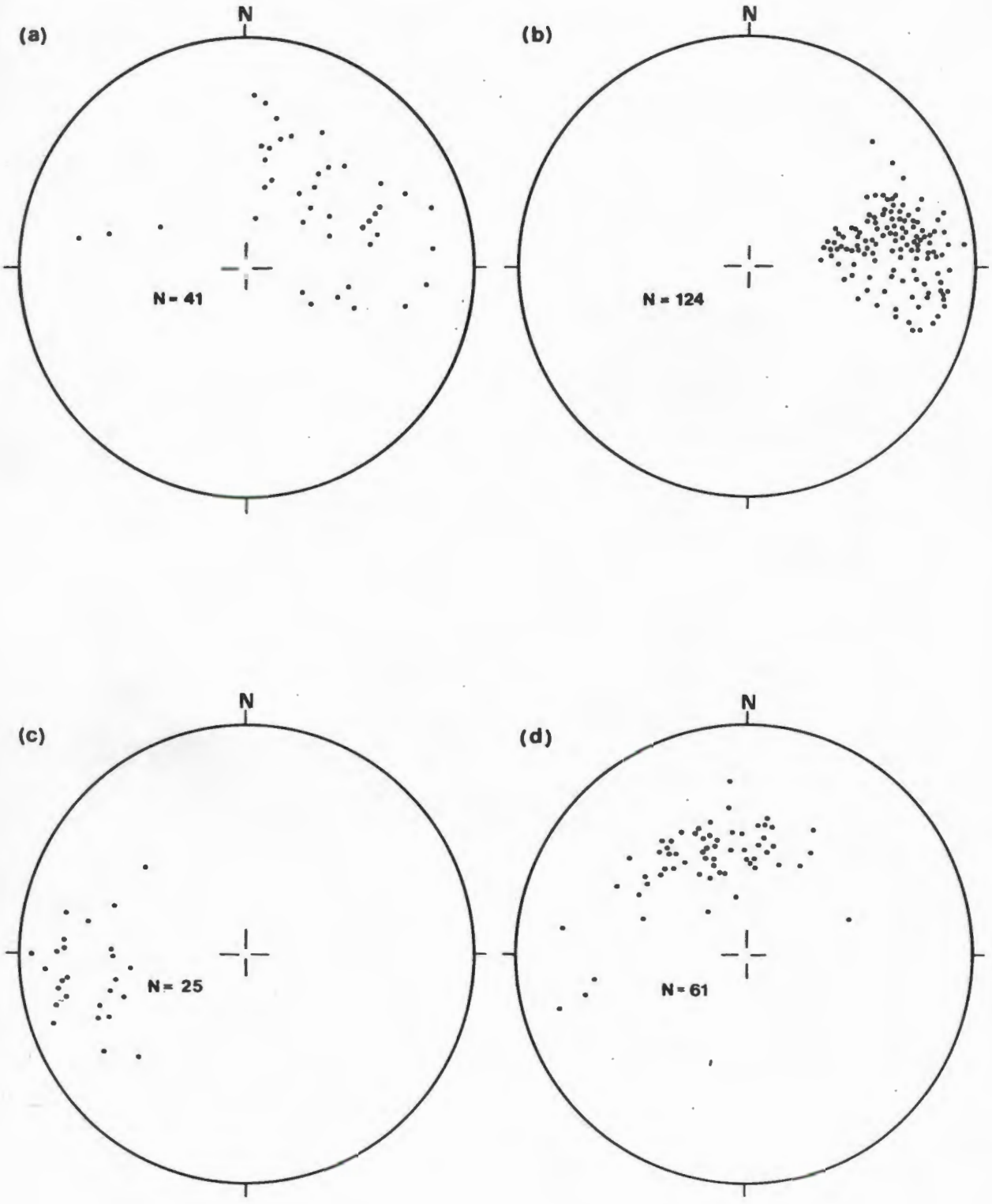
(a)
N
N = 41
(b)
N
N = 124
(c)
N
N = 25
(d)
N
N = 61

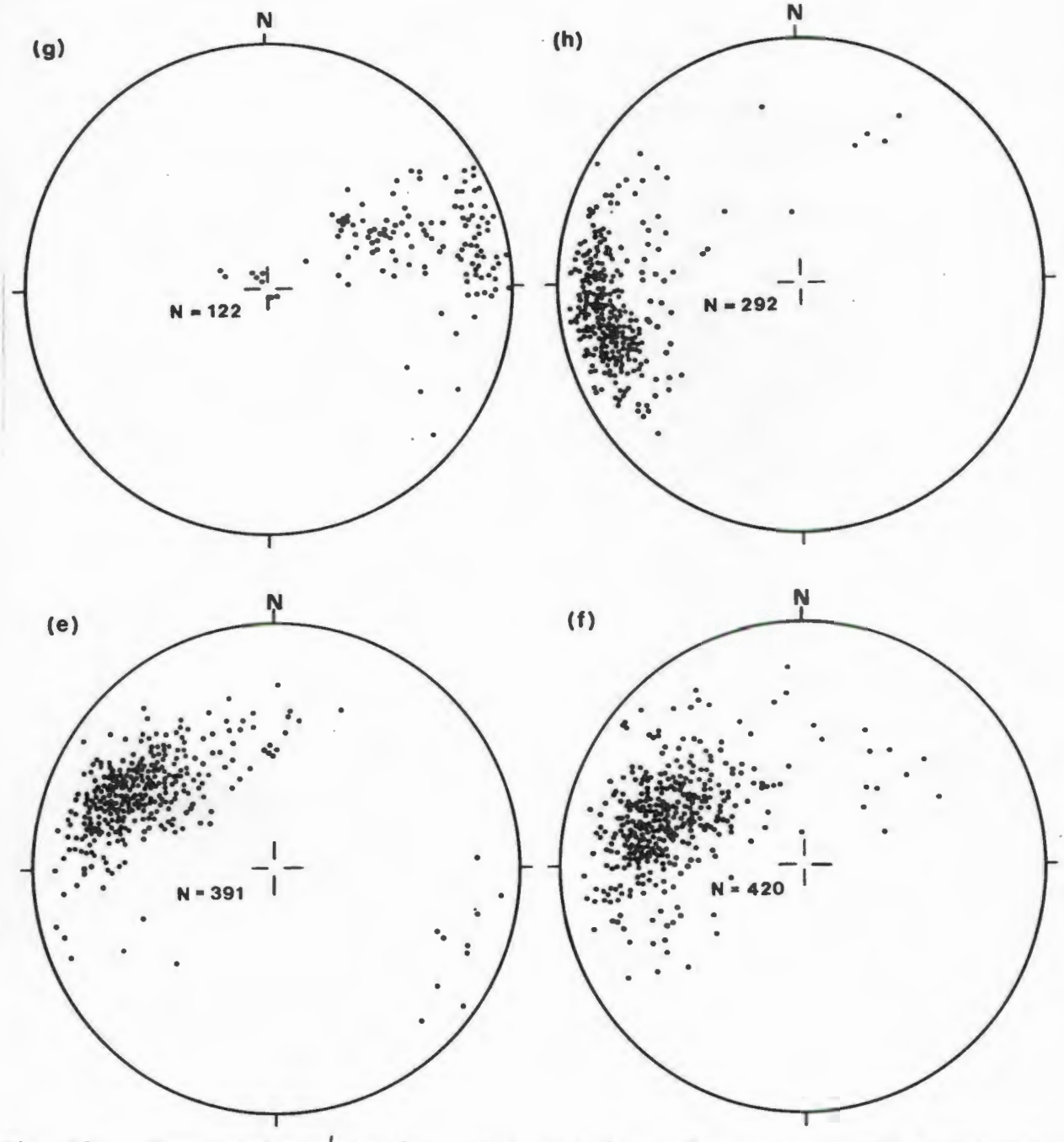


Fig. 92 Equal area projections of $l_2$ fabrics. N represents the number of measurements plotted within each domain.

(a) Domain I (b) Domain II (c) Domain III (d) Domain IV
(e) Domain Va (f) Domain Vb (g) Domain VI (h) Domain VII

*Domain IV* is separated from domains II and III by a wide terrane which is essentially covered by sand and Karoo sediments (Fig. 91). Isolated outcrops within this concealed zone indicate that the $l_2$ fabric assumes a northwesterly trend (Fig. 90 and Annexure 3). Within Domain IV the $l_2$ fabric displays considerable variation but northerly to northwesterly trends are dominant (Fig. 92d).

*Domain V* comprises by far the best exposed part of the study area and involves a large terrane around Kliprand (Fig.91). Owing to the high density of collected data this area has been split up into two terranes labelled Va and Vb (Fig. 91) and the corresponding $l_2$ fabrics are plotted as Fig. 92e and Fig. 92f respectively. From an inspection of these plots a dominantly west-northwest to northwest trend for $l_2$ is apparent.

*Domain VI* consists of a small area covering parts of the farms Obees (402), Daauws (404), Koker Boom Kraal (13) and Aasvogel Kop (403). The $l_2$ fabrics here plunge dominantly east-northeast (Fig.92g) closely resembling the trends recorded in domain II.

*Domain VII* involves the southernmost part of the study area (Fig. 91). The $l_2$ mineral lineation trends dominantly to the west-southwest, but west-northwesterly trends are also common (Fig. 92h).

This illustrates that the orientation of the mineral lineation ($l_2$) appears to change in a systematic manner across the area. Microscopic examination has revealed that the linear fabric and $S_2$ foliation accommodate the high grade metamorphic minerals suggesting that the peak of regional metamorphism accompanied the $D_2$ episode of folding.

## D The Third Episode of Deformation ($D_3$)

Folds of the $D_3$ generation ($F_3$) are the most obvious structural feature of the study area. The majority of the macroscopic open folds are $F_3$ structures. Minor folds are generally asymmetric and display a variable style which is largely controlled by the lithology involved in the deformation. Flexural slip type deformation (Plate 8) is common, but similar and chevron folds are also recorded. In contrast to the $F_2$ folds a prominent axial-planar foliation is not recognised in the fold closures. Refoliation in $F_3$ folds does, however, occur and comprises two geometric variaties (Fig. 93).

Intense shearing documented along the steeper dipping limbs of the asymmetric minor folds created an $S_3$ fabric discordantly cutting across the pre-existing $S_2$ fabric and the geometry is consistent with a left-lateral shear couple operating during $F_3$ folding in the southern part of the study area (Fig.93a). The second type of refoliation involved concordant shearing along the pre-existing foliation with the new fabric ($S_3$) developed

essentially parallel to the older $S_2$ fabric (Fig.93b ). This concordant refoliation is most obviously recognised where the coarse-grained gneissic banding has been replaced by narrow zones of mylonite. A prominent mineral lineation ($l_3$) is recognised within the $S_3$ fabric and it plunges parallel to the axes of $F_3$ minor folds ($f_3$).

According to Joubert (1971a, 1974c) the $F_3$ folds in Namaqualand have axial-planar trends very close to east-west and in places are trending east-northeast with generally near vertical axial planes and fold axes plunging either slightly south of west or north of east. This also applies to parts of the study area, notably domains II, III, VI and VII (Fig.95). In the vicinity of Kliprand (domain V), however, the open folds change their axial-planar trend and plunge direction drastically from a west-southwest-trend to a west-northwest-trend. Initially (Albat,1979) it was believed that these two trends are related to two separate episodes of deformation which were referred to as $F_3$ and $F_4$, respectively. Based on additional fieldwork, however, it is now believed that both the west-northwest and west-southwest trending open folds belong to the same generation ($D_3$) and that the change in trend of these folds was accomplished by subsequent deformation.

The orientation of $F_3$ minor folds in domain V (Fig.91) is depicted in Fig.94 where it is shown that the axial planes of these structures vary in strike between 240 and 310 degrees dipping north-northwesterly to north-easterly at angles generally in excess of 50 degrees (Fig.94a). The corresponding $f_3$ fold axes plunge west-southwest to west-northwest at angles of 20 to 60 degrees (Fig. 94b).

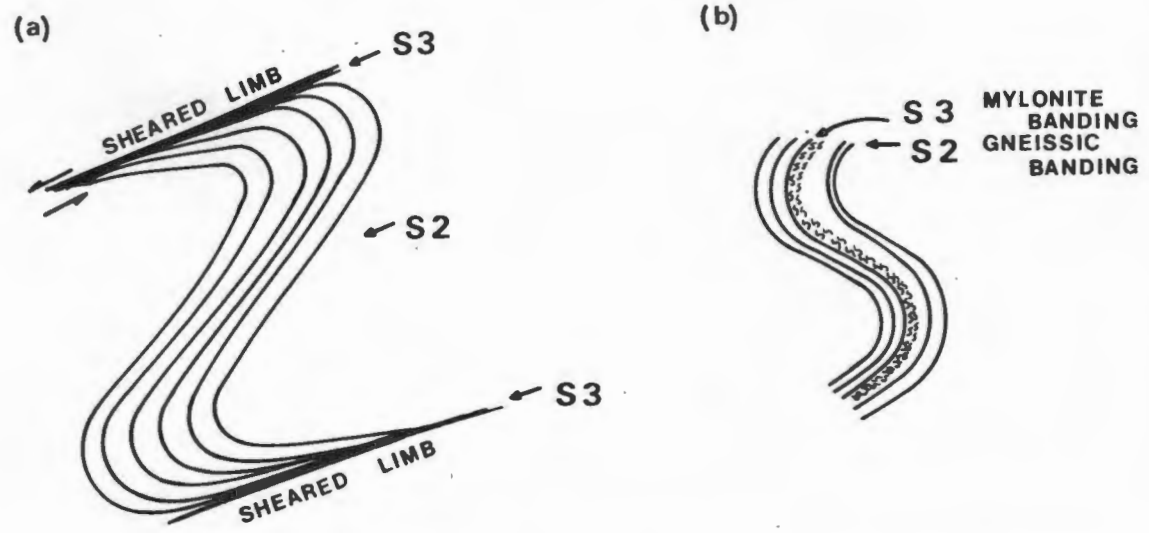


Fig.93 (a) Sketch showing the development of the $S_3$ fabric along the steeply dipping limb of an $F_3$ fold (farm Kamas 405). Note the inferred left lateral shear couple.

(b) Sketch showing the development of an $S_3$ mylonite fabric parallel to the $S_1/S_2$ fabric in an $F_3$ fold (farm Obeeb 8).

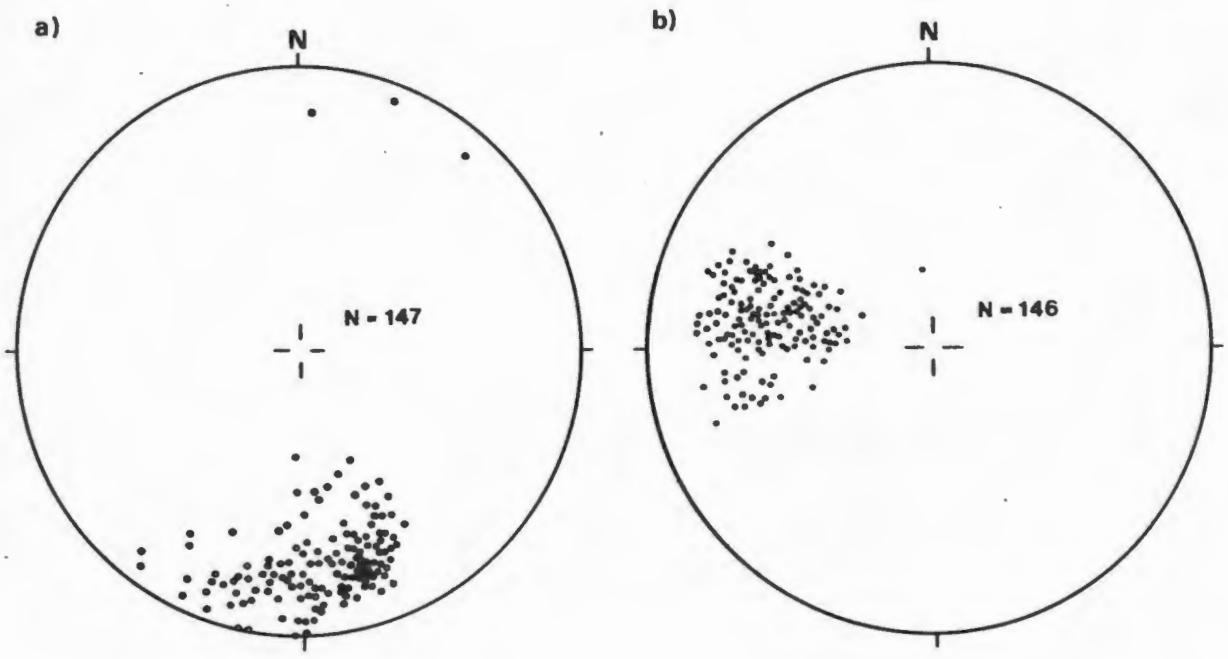


Fig. 94 Fabric orientation data for $F_3$ folds in Area V.
(a) 147 poles to axial planes of $F_3$ minor folds.
(b) 146 fold axes of $F_3$ minor folds ($f_3$).

## E The Fourth Episode of Deformation ($D_4$)

Evidence for the existence of $F_4$ folds is witnessed by the reorientation of the pre-existing $S_3$ fabric (Fig.96). In the southern part of the study area the axial planes of the $F_3$ folds have been folded about an axis plunging 66 degrees in the direction 326 degrees (Fig. 96). Minor folds deforming $D_3$ structures have axial planes striking northeasterly with steep northwesterly dips and these are here referred to as $D_4$ folds.

In the Aggeneys area Lipson (1978) describes the third episode of deformation as comprising two types of structures referred to as $F_{3a}$ and $F_{3b}$ folds; $F_{3a}$ being the east-west-trending open folds (axial-planar trend N 075 degrees to 080 degrees E) while the $F_{3b}$ folds have axial-planar orientations of N35 degrees to 55 degrees E. By way of their similar trends and overall style the $D_4$ structures in the study area are correlated with the $F_{3b}$ folds of Lipson (*op.cit.*) and the $F_4$ structures in the Namiesberg (Moore, 1977). The $D_4$ folds are not considered to be the equivalent of the $F_4$ folds of Joubert (1971a, b; 1974c).

The axial planes of the $F_3$ folds outline a sigmoidal pattern in the southern part of the study area and this geometry can best be explained as having arisen from dextral shearing accompanying $D_4$ folding. Reorientation of the $l_2$ fabric was mainly accomplished by this deformational episode. Discordant shears occupied by pegmatite veins are commonly developed parallel to the axial planes of $F_4$ folds.

Superimposition of the $D_2$, $D_3$ and $D_4$ fold generations has created a rather complex interference pattern in which basin-and-dome type structures feature prominently. These are particularly common in domain V and resemble the structures described by Tobisch (1966). The geometry of these basin-and-dome structures is unusual as they generally assume the shape of flattened cylinders plunging to the west-northwest like sheath folds. Opposing closures in the periclinal structures have antiformal and synformal geometries whose plunges are essentially parallel to each other (Fig. 97) a feature which arises from the superimposition of two fairly tight vergent folds.

## F Shear Zones

Structures generally referred to as shear zones (Ramsay and Graham, 1970) occur on various scales throughout the Namaqualand Metamorphic Complex (Joubert, 1971a; Blignault *et al.*, 1974; Stowe, 1980) and by far the most prominent of these is a west-northwest-trending zone of dextral transcurrent shearing which is known as the Pofadder Lineament (Joubert, 1974b). Similar structures, but differing somewhat in geometry are of considerable economic significance in the Okiep Copper District where they are referred to as "steep structures" (Benedict *et al.*, 1964; van Zyl, 1967; Lombaard and Schreuder, 1978; Hälbich, 1978).

Shear zones characterised by intense refoliation and generally mylonitisation of the gneisses with concomitant reconstitution of mineral assemblages are ubiquitously documented in the study area. By way of their overall geometry and relationships to folds these zones of shearing conform a two-fold classification into what is frequently described as tectonic slides (Fleuty, 1964; Joubert, 1971a; Hutton, 1979) on the one hand as opposed to discrete shear zones displaying identical geometric features to the examples illustrated by Ramsay and Graham (*op.cit.*).

The tectonic slides occur as concordant or discordant high strain zones associated with post-$D_2$ open folds with which they appear to have formed contemporaneously. Concordant slides are located parallel to the regionally developed banding in the gneisses and feature prominently along the limbs of the open folds. Despite this parallelism the tectonic slides are readily recognised where the widely spaced gneissic banding has been obliterated and replaced by a much finer planar fabric that is most distinctive in concordant mylonite zones. Discordant slides differ in their geometric relationship to the associated fold in that they cut across the fold limb along a plane more

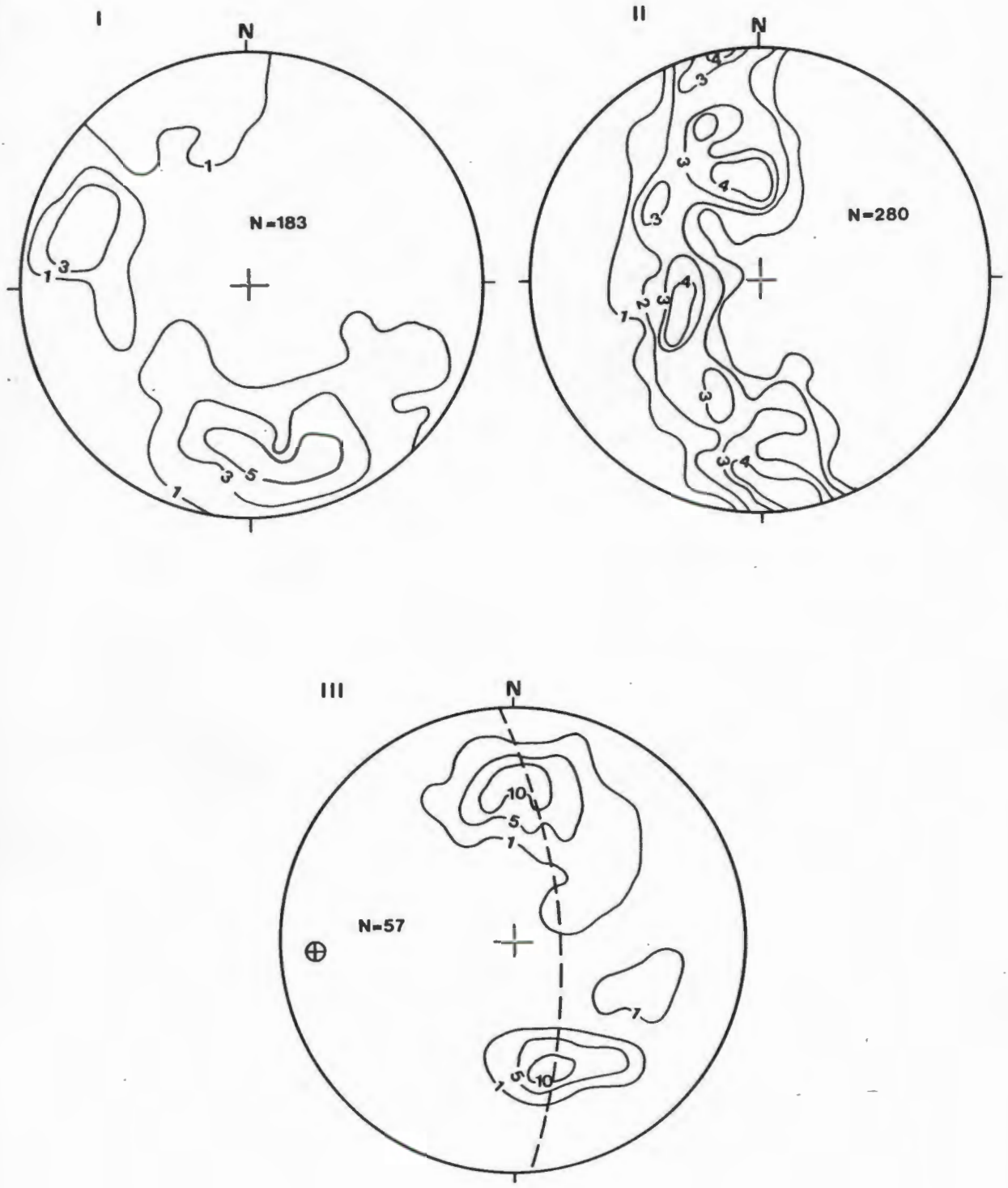
I
N
N=183
1
3
1
3
5
1
II
N
N=280
4
3
3
4
3
4
1
2
3
3
3
4
III
N
N=57
10
5
1
1
1
5
10

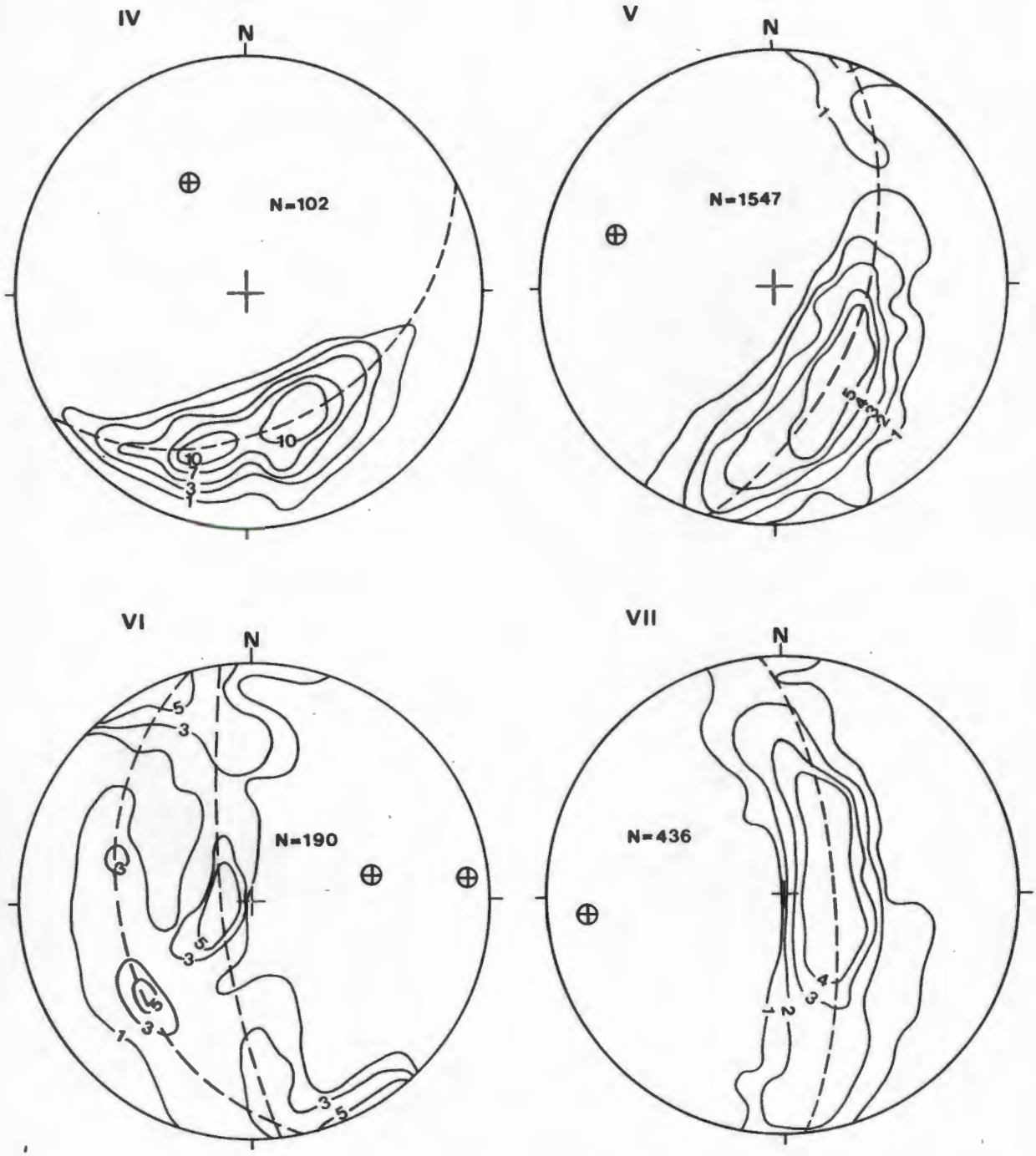


Fig. 95 Equal area projections of poles to the $S_2$ fabric (regional foliation) for domains I to VII as defined in Fig. 91. Diagrams II, III, V, VI and VII specify $F_3$ fold axes as π-poles; diagram IV defines an $F_4$ fold axis while the pattern in I appears to reflect both $F_3$ and $F_4$ folding.

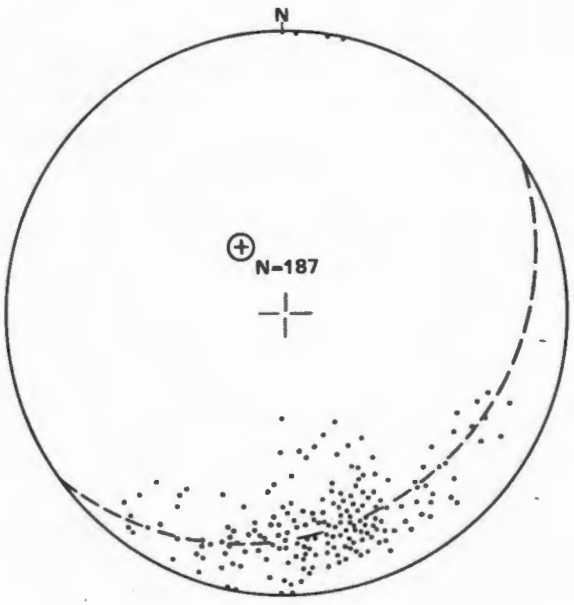


Fig. 96 Equal area projection of poles to axial planes of $F_3$ minor folds from the southern part of the study area (Map B). The $\pi$-axis plunges 66 degrees in the direction 326 degrees.

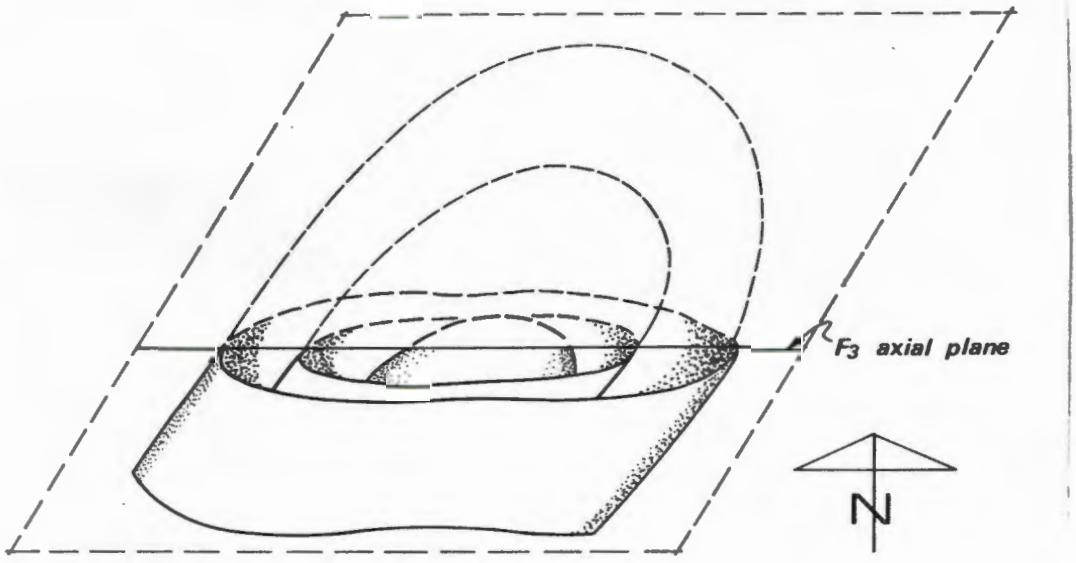


Fig. 97 Three dimensional sketch of a domal interference structure resembling a flattened cylinder. Note the parallel-plunge of opposing closures of the antiformal and synformal geometries. The structure shown occurs on the farm Obeeb (8).

or less parallel to the axial plane (Hutton, *op.cit.*). Both types of tectonic slides occur on various scales in the area studied and the newly developed planar fabric within these structures invariably contains a prominent linear fabric (mineral lineation) which plunges parallel to the axis of the associated fold. It is not uncommon to record orientated sillimanite needles within the slide plain.

The presence of tectonic slides illustrates two significant features:

(a) Extensive shear deformation must have accompanied the generation of the open folds. It is recalled here that Joubert (1974b) has previously proposed that the open folds in Namaqualand and Bushmanland have formed in response to wrench-fault tectonics.

(b) The mylonites within the tectonic slides represent high strain zones and this illustrates that the strain distribution during folding was heterogeneous with much of the strain concentrated in rather narrow zones, a feature which is particularly relevant to strain analysis.

From the geometry of discrete shear zones in the study area both sinistral as well as dextral shear couples can be deduced. Orientation measurements on these structures indicate that the dextral shear zones assume west-northwest or east-northeast strike directions while their sinistral equivalents strike east, northeast and occasionally north-northwest to north. The age relationship between these structures is uncertain and it is possible that at least some of them occur as conjugate sets. Shear zones crossing each other were only recorded at two localities. From the cross-cutting relationships on the farms Roode Kloof (14) and Obees (402) it has, respectively, been deduced that the west-northwest (dextral) shear zones post-date the east-northeast (dextral) ones and that the sinistral east-trending shear zones are younger than the west-northwest-trending dextral zones.

The planar fabric (shear foliation) within the discrete shear zones is generally steeply dipping and often close to vertical. At one locality, however, on the farm Obees (402) the mylonite zone has a rather shallow southwest-dipping (approximately 25 degrees) foliation.

Many discrete shear zones have acted as convenient access routes for a variety of magma types as testified by the diversity of dykes and pegmatite bodies commonly located within these structures. Quartz veins are also frequently recorded within the shear zones. Many of the dykes are themselves foliated along trends approximately parallel to the shear direction and pegmatite bodies are frequently partially mylonitised. These magmatic rocks are likely to have intruded after the initial formation of the shear zones and were subsequently involved in renewed shear deformation. This suggests a complex history of repetitive movements along the same zone of weakness. Re-activation of existing shears can also be deduced from the observation that some of these structures accommodate mineral assemblages belonging to contrasting metamorphic facies.

The metamorphic conditions recorded in tectonic slides and discrete shear zones, judging by the associated mineral assemblages, cover a wide pressure-temperature range and the metamorphic history of these structures is often complex; particularly where they have been involved in repetitive re-activation. Granulite facies metamorphic conditions prevailed during the formation of the older shear zones and hypersthene and other high grade minerals feature prominently in specimens collected from these structures. Examples of east-northeast-trending granulite facies-grade shear zones have been recorded on the farm Aasvogel Kop (403). The features aiding in their recognition include the flaggy appearance of calc-silicate gneisses and amphibolites, the steeply dipping almost vertical foliation, the steeply plunging (close to vertical) penetrative mineral lineation and the diversity and complex entanglement of lithologies including quartzose, quartzo-feldspathic, mafic, semipelitic and calc-silicate rocks in rather restricted zones. Pronounced migmatitic banding is a common phenomenon in the semi-pelitic rocks encountered within these zones. Somewhat similar structures occur on the farms Dood Drink (406) and Roode Kloof (14).

In several mylonite specimens from other zones of shearing the mineral assemblage "K-feldspar + sillimanite" is indicative of high grade metamorphic conditions (Winkler, 1976). Some of the sheared mafic rocks studied contain minerals such as chlorite, green hornblende and epidote clearly indicating lower grade conditions. Pre-existing granoblastic textures are frequently still partly preserved and remnants of pre-existing orthopyroxene, clinopyroxene, brown hornblende and calcic plagioclase are often still discernible in a chloritised matrix.

The relationship between shear zones and faults has received considerable attention in recent literature. Bak, Sørensen *et al.*, (1975) illustrate that major Precambrian shear zones in Greenland are wedge shaped, narrowing upwards towards higher crustal levels and they propose that these ductile shear zones represent the roots at depth of major transcurrent faults (e.g. San Andreas fracture system) at surface. This view is shared by Sibson (1977) who models a major shear zone-fault system comprising a near-surface regime of incohesive gouge and fault breccia followed with increasing depth by an "elastico-frictional" domain of random fabric calaclasite series, while at even greater depth ductile deformation generates mylonite. The relationship between deep-level ductile shear zones and high-level brittle zones has also been outlined by Ramsay (1980).

Mylonite, in various stages of development, is commonly recorded in discrete shear zones and tectonic slides in the Kliprand area. The term "mylonite" is generally reserved for rock types displaying a very characteristic texture ("fluxion structure", Higgins, 1971). A large number of mylonite specimens have been studied microscopically and their component grains display a variety of strain features including undulatory extinction, deformation bands and lamellae and provide also evidence for recrystallisation accompanying mylonitisation. The significance of this is to be discussed in the light of the most recent literature on the subject. The finely banded nature of

mylonite comprises discontinuous monomineralic layers of variable thickness. Quartz and feldspar lamina alternate with each other in a compositional layering which according to Vernon (1974) forms as a consequence of extensive flattening deformation and recrystallisation of larger crystals to yield layers of smaller crystals in the ductile environment. The mylonites are always considerably finer grained than their host rocks illustrating that the process of mylonitisation involves a reduction in grain size. From the microscopic studies it has become apparent that the various minerals of the host rock have responded quite differently to the deformation. Biotite is generally reduced to extremely fine grain size with concomitant exsolution of an opaque phase. More resistant augen-shaped grains have proved on microscopic examination to invariably consist of feldspar while quartz is always much reduced in size witnessing its lower resistence to mylonitisation.

The feldspar augen are always arranged in such a manner that their longest axes lie within the banding while their shortest axes occur perpendicular to the layering. This is generally regarded as evidence for flattening perpendicular to the banding which is considered to represent the XY plane of the finite strain ellipsoid (Johnson, 1967; Ramsay and Graham, 1970).

The genesis of mylonites is a rather controversial matter and is presently debated in the literature. Earlier ideas were based on the premise that the grain size reduction accompanying mylonitisation has been brought about by the mechanical granulation of larger crystals. This is apparent from terms such as "cataclastic", "crushing" and "milling" which are extensively used even in the more recent literature (e.g. Higgins, 1971). Transmission electron microscopic studies and detailed optical studies on experimentally and naturally deformed quartz (McLaren and Retchford, 1969; McLaren *et al.*, 1970; White, 1971, 1973, 1975, 1976; McLaren and Hobbs, 1972; Ardell *et al.*, 1973; Bell and Etheridge, 1973; Tullis *et al.*, 1973; White and Treagus, 1975) have, however, provided insight into the question of mylonite genesis and it is now generally agreed that the textures previously interpreted as evidence for brittle deformation (e.g. larger clasts surrounded by finer grained material) are in fact formed as a result of dynamic recrystallisation during ductile deformation. The major new discoveries that have elucidated natural rock deformation involve the recognition of crystal defects and the significant role these defects play during deformation (Hobbs *et al.*, 1976).

Laboratory experiments have shown that undulatory extinction in quartz, deformation bands, deformation lamellae and subgrain formation are strain effects (White, 1971) which can be correlated with specific dislocation substructures (White, 1973, 1975, 1976; White and Treagus, 1975). Continuous deformation increases the dislocation density in the grains and thereby increases the crystal energy which can be released by the two processes generally referred to as recovery and recrystallisation. Recovery involves a process by which the strained crystal attempts to return to its unstrained state prior to deformation (Bell and Etheridge, 1973; White, 1977). Recovery leads to polygonisation i.e. the formation of subgrains (*ibid.*). When new

strain-free grains are developed the term primary recrystallisation is applied to describe this process (Bell and Etheridge, *op.cit.*). If deformation continues after recrystallisation, the whole sequence from the build up of dislocations to recrystallisation is repeated and according to White (1976) such a repeated process leads to the steady state flow of the material. Recrystallisation commences in areas of highest strain, i.e. areas with the highest dislocation density (Bell and Etheridge, 1976; White, *op.cit.*) such as deformation band boundaries. One of the features stressed in the literature is that a very important consequence of dynamic recrystallisation in ductile materials is the reduction in grain size (Bell and Etheridge, 1973, 1976; White, 1973, 1976, 1977; Etheridge, 1975) and consequently there is no need to involve a mechanical crushing process to account for the fine grain size in mylonites. There appears to be an equilibrium grain size, however, that is stable throughout any further deformation (Hobbs, 1966; Bell and Etheridge, 1973; White, 1976; Etheridge and Wilkie, 1979).

The relationship between deformation mechanism, the intracrystalline dislocation structures and the associated optical strain features have been established by White (1975) who has shown that continuous undulatory extinction in quartz grains is the first manifestation of strain. Increasing strain results in discontinuous undulatory extinction, deformation bands and lamellae, formation of subgrains and finally development of equidimensional subgrains - in that order (White, *op.cit.*).

## G FAULTS

North-south and north-northwesterly-trending faults are common in the area, but only the major fractures are shown on the accompanying geological map. On outcrops these are generally expressed as breccia zones frequently with quartz veining. Where a three-dimensional view was possible the fault plane was generally observed to be near vertical. From observations made in the extreme southern part of the study area, it is concluded that at least some of these faults post-date the deposition of the Nama sediments and that the downthrow side was to the east.

# VIII DISCUSSION OF REGIONAL ASPECTS

## A Age of the Supracrustal Volcano-Sedimentary Sequence

Conventional radiometric age determinations on various rock types from extensive parts of the Namaqualand Metamorphic Complex fall into the Kibaran (Clifford, 1970) range of 1100 ± 200 Ma (Nicolaysen and Burger, 1965; Burger and Coertze, 1973; Clifford *et al.*, 1975a, 1981). It is now generally accepted that these isotopic ages reflect a major tectono-thermal and plutonic event, while the true age of deposition of the supracrustal rocks may be much older. At the present state of knowledge it is not known whether all the supracrustal gneisses in the Namaqualand Metamorphic Complex can be regarded as chronostratigraphic equivalents or whether more than one metavolcano-sedimentary sequence of contrasting age does exist.

In the past the supracrustal gneisses of the Namaqualand Metamorphic Complex were correlated with the Kheis sequence, originally divided into the Marydale, Kaaien and Wilgenhoutsdrif "beds" (Gevers *et al.*, 1937; Coetzee, 1942b; von Backström, 1964; Joubert, 1971a, 1976; von Backström and de Villiers, 1972; Vajner 1974; Botha *et al.*, 1976). Vajner (*op.cit.*) considers the supracrustal gneisses to be of Archaean age, a conclusion based on his interpretation that the Marydale Group is intruded by the Draghoender/ Skalkseput granites dated at 2900 and 2500 Ma respectively (Burger and Coertze, *op.cit.*). The antiquity of the Kheis sequence is subsequently questioned (Cornell, 1975; van der Westhuizen, 1977; Linström, 1977; Smit, 1977) while Botha *et al.* (*op.cit.*) consider the Draghoender and Skalkseput granites to form the basement to the supracrustal formations. According to Cornell (*op.cit.*) the age of the Marydale Group is 1900 Ma, but subsequently Cornell and Barton (1979) obtained a 3000 Ma Pb-Pb isochron age for the Modderfontein iron formation and they now consider this to be the minimum age of the Marydale Group thereby lending support to Vajner's view concerning the intrusive relationship between the Archaean granitoids and the Marydale Group. It is now known that the Kaaien and Wilgenhoutsdrif Groups are considerably younger than the Marydale Group and consequently the name Kheis has been dropped. The Dagbreek Formation of the Kaaien Group is regarded as having a maximum age of 2400 Ma (SACS, 1980). The Groblershoop Formation has been dated at 1750 Ma (Burger and Coertze, 1973) while the Wilgenhoutsdrif Formation has yielded an age of 1360 Ma (Burger and Walraven, 1978). The correlation of the rocks in the Kheis Province (i.e. the area between the Brakbosch fault and the Kaapvaal craton) with the Namaqualand gneisses is complicated by extensive dextral shearing and intense plutonism in the transitional zone (Stowe, in press). Despite this it has been proposed that certain lithologies in the Namaqua Foreland (Vajner, 1974) can be correlated with gneisses in the Namaqua Province (Stowe, *op.cit.*) suggesting that at least parts of the Namaqualand Metamorphic Complex consists of reworked older rocks of the Kheis Province. This implies that the supracrustal Namaqualand gneisses could be as old as

2400 Ma. Botha *et al.* (1976) conclude that the Wilgenhoutsdrif Group represents a facies equivalent of the Groblershoop Schist Formation and they equate these with certain formations forming part of the Korannaland Sequence. The equivalence of the Wilgenhoutsdrif Group and Groblershoop Schist Formations is, however, questioned on the basis of their different radiometric ages.

Apart from the older age of 1700 Ma obtained from rocks of the Okiep area (Clifford *et al.*, 1981) the antiquity of the Namaqualand supracrustal gneisses is further supported by the correlation of certain gneisses with rocks in the Richtersveld Province. It has been suggested that some of the gneisses represent reconstituted Orange River Group rocks (Bertrand, 1975; Blignault, 1977). The Goudom and Hom Subgroups of the Bushmanland Group may be regarded as the lateral equivalents of the Orange River Group with sediments becoming gradually more abundant eastwards away from the volcanic centre (Bertrand, *op.cit.*). As the Haib Subgroup of the Orange River Group has been dated at 1996 Ma (Reid, 1979a) this correlation implies that at least some of the supracrustal gneisses within the Namaqualand Metamorphic Complex must have been deposited about 2000 Ma ago and this is consistent with the 1900 - 2000 Ma Sm - Nd ages determined by Reid (1981) on supracrustal rocks from Bushmanland.

Some authors, notably Cornell (1975, 1978) and Köppel (1978, 1980), however, question this antique age and point out that isotopic studies of ore bodies indicate (provided that they are syngenetic with their host rocks) that the Aggeneys Subgroup of the Bushmanland Group and the Jannelsepan Formation of the Korannaland Sequence cannot be older than 1200 - 1500 Ma.

This dispute illustrates that the true age of deposition of the supracrustal Bushmanland/Namaqualand gneisses is still to be established.

Regional maps showing the distribution of rocks and localities mentioned in this section have been compiled for convenience of the reader unfamiliar with South African geology (Appendix IV and V).

## B Basement/Cover Problem

One of the major problems in Namaqualand geology concerns the presence of a basement to the volcano-sedimentary sequence(s). The nature of these supracrustal gneisses indicates that they have been largely deposited in a continental shelf-type environment and it is therefore speculated that they should be underlain by some type of sialic basement. The recognition of this basement has been a very controversial matter. Joubert (1971a) proposes that the Nababeep-type gneisses (Benedict, *et al.*, 1964) represent the platform onto which the paragneisses have been deposited. Based on evidence from the Pofadder area, however, Joubert (1974c) indicates that the porphyroblastic gneisses, which he calls the Aroams gneiss, can also be interpreted as a

batholith intruded during the main deformation ($F_2$) or alternatively as a remobilised basement on account of its intrusive relationship to the supracrustal gneisses. It appears that the Aroams gneiss of the Pofadder-Aggeneys area can be correlated with the Nababeep-type gneiss as both these rock types have very similar chemistries (Lipson and McCarthy, 1977). Paizes (1975) and Moore (1977) regard equivalents of the Aroams gneiss to represent the basement to the Bushmanland Group. Moore (*op.cit.*) recognises at least one other episode of deformation in the banded grey gneisses associated with the Aroams gneiss absent from the overlying supracrustal sequence and by this structural evidence argues in favour of an ancient deformed basement.

Lipson (1978, 1980) does not consider the Aroams-type gneiss as basement, but finds evidence for an igneous origin and suggests that it may represent a rapakivi-type intrusive (intensely deformed with the pre-existing rapakivi-texture destroyed) forming part of an anorthosite,charnockite, rapakivi-type suite as known from other high grade metamorphic terranes.

Certain grey gneisses have also been cited as possible basement candidates (e.g. Blignault, 1977). Theart (1980) describes a finely laminated biotite gneiss (Vaalheuwel type) as occurring at the base of the metasedimentary succession in the Steinkopf area and according to Bertrand (1975), grey gneisses in the Goodhouse-Henkries area have been deformed and metamorphosed prior to the intrusion of the Vioolsdrif batholith. He therefore regards these as representing an old basement onto which the Bushmanland Group of metasediments and metavolcanics have been deposited.

Within the confines of the present study area criteria to prove the existence of an older basement beyond doubt have not been recognised. Augen-type gneisses, almost certainly to be correlated with the Nababeep and Aroams gneisses, occur throughout the area, but their relationship to the supracrustal gneisses yield conflicting evidence. In some localities the augen gneisses are undoubtedly intrusive and this is witnessed by abundant paragneiss inclusions interpreted as xenoliths as well as cross-cutting contact relationships, but elsewhere they are in apparent conformity with the volcano-sedimentary succession and either have sharp or gradational contacts. It is possible that more than one type of augen gneiss exists. Other likely candidates for a basement in the study area are certain grey quartzo-feldspathic gneisses or some of the biotite-bearing pink gneisses, but this is purely speculative and the true nature of the basement (if it is exposed) remains uncertain.

### C Timing of Regional Metamorphism

In the area presently investigated field and textural evidence indicates that the regional metamorphic event ($M_1$) and associated anatexis accompanied and outlasted the main episode of deformation ($D_2$). Many previous investi-

gators in adjacent areas of western Namaqualand have come to tne same conclusion (e.g. Joubert, 1971a, 1974c, 1981; Clifford *et al.*, 1975a, 1981; Moore, 1977; Jack, 1980), but there is no consensus regarding the actual age of this metamorphic event.

Clifford *et al.* (*op.cit.*) consider the Rb - Sr whole rock isochron age of 1187 ± 22 Ma, which they have derived for the Nababeep gneiss and associated granulites to represent the age of the thermal peak of the dominant regional metamorphism and associated recumbent folding ($F_2$) around Nababeep. This metamorphic event is believed to pre-date the open folding ($F_3$) recorded in the "Springbok Dome" and "Ratelpoort Synform" (*ibid.*). In this respect, it is interesting to note that the monazite at Steenkampskraal in the extreme south of the study area is situated in a post-$D_2$ structure and yields a U-Pb age of 1180 ± 40 Ma (Nicolaysen and Burger, 1965) which is not in harmony with the results of Clifford *et al.* (*op. cit.*) as the $D_2$ structures of the study area are most certainly equivalents of the $F_2$ recumbent folds at Nababeep. Although previously no subsequent thermal high following onto the main regional metamorphism has been considered by Clifford *et al.* (*op.cit.*), Professor Clifford (pers. comm., 1982) does not exclude the possibility that a second thermal peak also of granulite facies grade may well have followed after the main regional metamorphism during the emplacement of the Okiep noritoid suite some 1100 Ma ago.

In marked contrast to the conclusions reached by Clifford *et al.* (*op.cit.*) Joubert (1976, 1981) argues in favour of two separate metamorphic events and suggests that the 1100 ± 200 Ma ages which are ubiquitously recorded in the Namaqualand Metamorphic Complex (Nicolaysen and Burger, 1965; Burger and Coertze, 1973; Clifford *et al.*, *op.cit.*) are related to a major thermal event associated with the intrusion of abundant Concordia-type granitoids considered to have been emplaced more or less during $F_3$ deformation. This thermal event is thought to have been preceded by the main regional metamorphism (Joubert, *op.cit.*) believed to be responsible for the metamorphic zonation in western Namaqualand (Joubert, 1971a) and regarded to pre-date the emplacement of the 1700 - 1900 Ma old (Reid, 1979b) Vioolsdrif batholith (Joubert, 1975, 1976). On the other hand Ward (1974) and Blignault (1977) propose that the main tectono-thermal imprint in Namaqualand occurred more or less synchronously with the emplacement of the Vioolsdrif batholith. In this respect, it is interesting to note that the U-Pb zircon age of 1500 - 1700 Ma yielded by orthopyroxene-cordierite gneisses from the Nababeep area have been interpreted as the inherited age of the provenance rocks (Clifford *et al.*, 1981).

Indisputable evidence for the existence of two separate metamorphic events as proposed by Joubert (1976, 1981) has not been found during the present study.

## D Metamorphism - Time Relationships

During the entire life span of a metamorphic belt one or several major periods of regional metamorphism may occur and during each such period several phases of recrystallisation are possible. According to Sutton (1965) these major periods are referred to as *metamorphic events* and each such event may comprise several *episodes* of metamorphism. The individual event is characterised by a thermal "high", separated from the previous event by a thermal "trough". This means that successive events represent successive periods of renewed metamorphism.

In the past several authors (e.g. Joubert, 1971a; Moore, 1977), in describing the metamorphism of the Namaqualand Metamorphic Complex, have used the connotation $M_1$, $M_2$, $M_3$ etc., when referring to successive growth periods of metamorphic minerals and for these they have used the term "event". In the definition outlined above this connotation is confusing, because it implies a situation where successive events labeled $M_1$, $M_2$, $M_3$ represent distinct thermal peaks (Fig. 98a). These authors have, however, not presented evidence for the existence of thermal "troughs" between their postulated successive "events" and therefore the question arises whether regional metamorphism in the Namaqualand Metamorphic Complex was in fact intermittent as implied by the schematic model shown in Fig.98a or whether it can be regarded as a continuous process as depicted in Fig.98b. Model A involves fluctuations in the thermal regime, while in Model B the rocks are heated to a climax after which they gradually cool off.

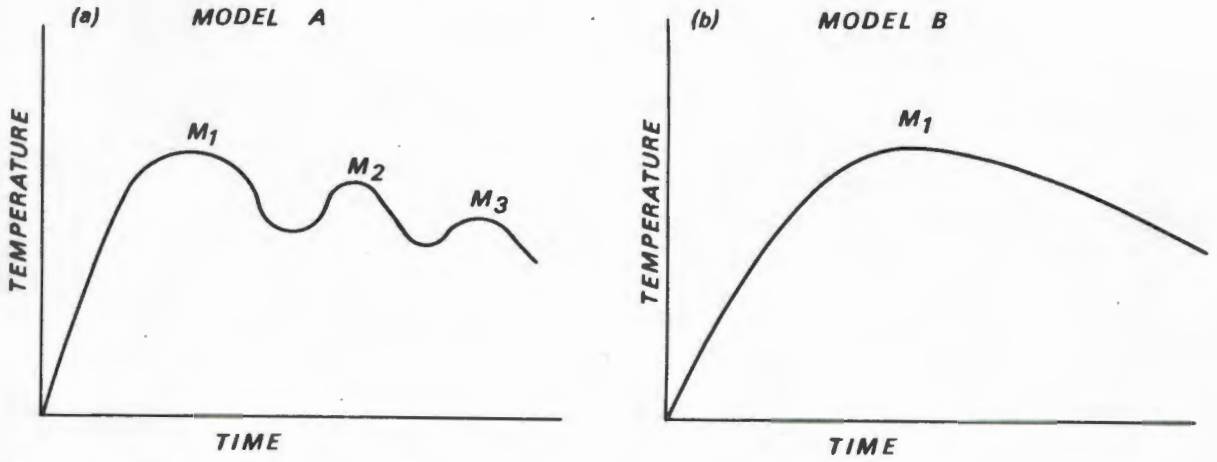


Fig.98 Two schematic models of thermal changes with time.

(a) Successive metamorphic events labeled $M_1$, $M_2$ and $M_3$ are separated by thermal "troughs" illustrating fluctuations in the thermal regime through time.

(b) A single continuous metamorphic event reaching a thermal climax ($M_1$) after which the metamorphic belt gradually cools off.

The present study has not revealed any conclusive evidence for the existence of more than one major regional metamorphic event and it is therefore suggested that Model B is applicable to the study area. This conclusion is supported by the zonation patterns of certain minerals studied and is consistent with the microtextural and field evidence.

If the Mg - Fe exchange reactions between certain minerals such as garnet and biotite or garnet and cordierite are temperature sensitive, as suggested by Holdaway and Lee (1977) and Ferry and Spear (1978), it is expected that thermal fluctuations would be recorded in these minerals in the form of distinct zonation patterns. Therefore, the metamorphic history should be documented within the high grade minerals themselves. The continuous symmetrical zonation patterns around a single maximum or minimum recorded in the garnets and cordierite studied (Fig.41 page 120 and Fig.69 page 186) consistent with a model involving continuous growth during a single metamorphism characterised by progressively lower temperatures (i.e. Model B). Polyphase mineral growth, in contrast, is considered to yield a more complex series of maxima and minima in the zonation patterns (Atherton and Edmunds, 1966).

This major thermal event (in the sense of Sutton *op.cit.*) culminated during $D_2$ ($F_2$ *sensu* Joubert 1971a) and the thermal peak is here referred to as $M_1$. The possible existence of an older metamorphic event (pre-$M_1$) cannot, however, be ruled out entirely, but the evidence has been destroyed by the subsequent high grade regional metamorphism ($M_1$).

Several episodes of largely retrograde recrystallisation can be recognised subsequent to the metamorphism characteristic of the thermal peak, but it is stressed here that this in itself cannot be taken as evidence in favour of Model A (Fig.98a). The post-peak episodes of recrystallisation have a more restricted distribution and are closely related to areas of higher strain imposed on the rock body by post $D_2$ deformations. This suggests that the deformation has acted like a catalyst in locally promoting renewed metamorphic reactions. These episodes of recrystallisation are here regarded to be related to the cooling stages of the same regional metamorphism which, during the thermal climax, gave rise to the high grade mineral assemblages and according to Model B (Fig. 98b) progressively younger structures would be expected to have associated with them progressively lower grade minerals; a feature which in general terms appears to be applicable to the Namaqualand Metamorphic Complex.

In contrast to the model proposed here, Joubert (1981) suggests that the metamorphic evolution of western Namaqualand involves at least two distinct thermal events in the sense outlined above with a thermal "trough" believed to be situated somewhere between $F_2$ and $F_3$ fold episodes.

## E Metamorphic Zonation Pattern of Namaqualand

The pioneer presentation of a model delineating the regional metamorphic zonation pattern of Namaqualand (Joubert, 1971a) depicts a prograde zonation with the lower grade zones along the west coast and a high grade core of "garnet granulites" in the area between Springbok and Gamoep. This model requires some revision in the light of the present and other recent studies. Joubert (*op.cit.*) proposes that zone E (comprising "garnet granulites" consisting of bytownite, quartz, yellow to blue-green pleochroic clinopyroxene, orange-pink garnet and abundant sphene), relative to the other zones, appears to have been subjected to the highest grade of metamorphism in Namaqualand, but remarks that the presence of sphene in these rocks poses a problem and speculates that sphene is a retrograde mineral. This view is not shared here because rocks with an identical mineralogy and texture to the "garnet granulites" described by Joubert (*op.cit.*) referred to here as calc-silicate gneiss, feature prominently in the amphibolite facies terrane and where encountered within the area affected by granulite grade metamorphism, these rocks are closely associated with mafic gneisses in which both orthopyroxene and plagioclase occur in stable coexistence, while garnet is notably lacking from the metabasites. This observation militates against Joubert's (*op.cit.*) conclusion that the garnet-clinopyroxene-plagioclase assemblage in these calc-silicate rocks is indicative of a higher pressure/temperature zone within the granulite facies terrane.

According to Winkler (1976) the mineral assemblage clinopyroxene + garnet + quartz + either plagioclase or hypersthene characteristic of the higher pressure clinopyroxene-almandine-quartz granolite subzone of the regional hypersthene zone results from the instability of coexisting orthopyroxene and plagioclase in response to rising pressure. Joubert (*op.cit.*) indicates that his "garnet granulites" coexist with orthopyroxene + clinopyroxene + plagioclase-bearing metabasites and accordingly orthopyroxene and plagioclase occur as a stable assemblage within zone E.

The present study has revealed that the orange-pink garnet in the calc-silicate gneisses consists essentially of the andradite and grossular molecules and the green clinopyroxene is ferrosalite or salite (Chapter III.D.2.). The bulk composition of these calc-silicate gneisses is not likely to allow the formation of orthopyroxene in the first place and the assemblage andradite/grossular garnet + ferrosalite/salite + quartz + plagioclase characteristic of Joubert's (*op.cit.*) zone E does not form as a result of the breakdown of the hypersthene-plagioclase assemblage, but is due to other reactions.

In the light of the above, the proposal that zone E comprises mineral assemblages indicative for the highest pressure/temperature conditions attained during metamorphism seems unfounded as there is no mineralogical justification for the existence of such a metamorphic zone. This view is shared by Zelt (1980) who, in addition questions the justification for

separating zones C and D (Joubert, *op.cit.*) as two-pyroxene-bearing metabasites apparently also occur within the area occupied by zone C (*ibid*).

An east-west-trending metamorphic zonation has been established for the area between Springbok and Vioolsdrif (van Aswegen, 1981) with the grade of metamorphism increasing from north to south (*ibid*). This is supported by the conclusions reached by Theart (1980) in the adjacent area to the west. An essentially east-west striking metamorphic zonation has also emerged from the present study. This trend contrasts with the northwest zonation established for the Aus/Upington area (Blignault *et al.*, 1974; Linström, 1977; Smit, 1977; Botha and Grobler, 1979; van Zyl, 1981) which is now generally regarded to relate to the late stage activation of the Namaqua Front (Vajner, 1974), a zone of dextral transcurrent shearing, magma intrusion and differential uplift. (Stowe, in press).

The granulite-amphibolite facies boundary in the area now studied occurs almost forty kilometres south of its location to the north of Springbok. The location of this boundary between the two areas is at present unknown owing to the lack of published information there, but it is apparent that the granulite facies boundary outlines a major warp around the Springbok area resulting in the southward swing of the boundary to meet up with that in the presently investigated area. These warps appear to be largely structurally controlled and most certainly dictated by the later open folds and associated high strain zones post-dating the main metamorphism.

Considerable confusion is documented in the current literature regarding the metamorphic history and metamorphic zonation of the area adjoining the west coast. According to the model proposed by Joubert (1971a) most of the metamorphic minerals encountered along the coastal strip (including kyanite) are regarded to be related to the Namaqua Event with the grade of metamorphism decreasing westwards and metamorphic zones trending more or less sub-parallel to the coast line. Subsequent studies by Jack (1979, 1980) apparently support this model. The staurolite and kyanite-bearing schists previously described by Joubert (*op.cit.*) from the area northwest and west of Nababeep are also encountered by Jack (*op.cit.*) and both authors propose that these lower grade assemblages along the west coast are related to the Namaqua Event.

This conclusion has been challenged by Zelt (1979, 1980) who regards the amphibolite facies zone in the coastal region as a later retrogressive metamorphism and not a prograde Namaqua metamorphism as envisaged by Joubert (*op. cit.*) and Jack (*op.cit.*). Theart (1980 page 91-92) concludes that "the fabric imprint on the rocks exposed along the coast south of Kleinsee resulted from thrusting after the deposition of the Stinkfontein quartzites when both the basement and cover rocks were deformed. The mineral assemblages of these rocks (south of Kleinsee) correspond to a higher pressure metamorphic event than expected at similar temperature conditions during the Namaqualand metamorphic events. Evidence of the older Namaqualand deformation and metamorphism in the coastal rocks was almost totally obliterated by the influence of the subsequent Pan-African Orogenesis".

Jack (1980) and Zelt (1980) consider the "Zoutpan schists" to form part of the supracrustal Namaqualand gneisses, but these are now correlated with the post-Namaqualand gneiss formations and the growth of staurolite, kyanite and related minerals are now regarded to post-date the Namaqua Event (Joubert and Waters, 1980). According to Waters (pers. comm.,1983) it is now almost certainly established that the coastal amphibolite facies assemblages, at least over major parts of the coastal area, are not related to the Namaqua Event, but were formed during younger events. Waters (pers. comm., 1983) regards the metamorphic history in the coastal area as complex involving more than one post-Namaqua event.

The metamorphic zonation models of Joubert (1971a) and Jack (*op.cit.*) fail to account for the superimposition of metamorphic events along the west coast and accordingly yield the wrong impression regarding the zonation pattern related to the Namaqua Event. There are some indications that the metamorphic zonation related to the Namaqua cycle is more or less east-west (probably modified by post Namaqua deformation along the coast) as opposed to the north to north-northwest trend proposed previously (Joubert, *op.cit.*; Jack, *op.cit.*). Much of the coastal area south of Hondeklip Bay must have been of granulite facies grade prior to subsequent overprinting by post Namaqua events as remnant granulites and granolites have been traced all the way to the coast (Jack, 1979, 1980; Moore, pers. comm., 1983; Waters, pers. comm., 1983).

Interesting is also the recent discovery that the metamorphic grade declines from granulite to amphibolite facies conditions to the south of Bitterfontein (Moore, *op.cit.*; Waters, *op.cit.*) and it does appear that this lower grade zone has an approximate east-west orientation.

## F Geotectonic Models

### 1 Plate Tectonic Model

There is general consensus among geologists that crustal evolution involves plate tectonic processes and that Phanerozoic orogenic belts are generated by the interaction of lithospheric plates during an ocean opening and closing cycle which is generally referred to as the Wilson cycle (Dewey and Burke, 1974). During the convergence phase of this cycle juvenile crust is generated in island-arc systems and crustal material becomes intensely deformed and metamorphosed leading to the formation of linear mountain belts.

The new global theory has been extremely successful in modelling Phanerozoic orogens and has become an acceptable paradigm, but attempts to apply the plate tectonic concepts to the Precambrian have not been very encouraging. Opinions are now divided on the issue as to when the Wilson cycle commenced to operate on earth and whether Proterozoic and Archaean fold belts can in fact be accommodated in a plate tectonic framework (Dewey and Spall, 1975; Burke, *et al.*, 1976, 1977). Some geologists are guided by uniformitarian principles and explain all crustal evolution through time in terms of the currently operating plate tectonics (e.g. Dewey and Burke, 1973; Burke, *et al.*, 1977; Windley, 1977, 1981), while others stress the considerable diferences recorded in Precambrian mobile belts compared to Phanerozoic orogens (Sutton and Watson, 1974; Watson, 1976; Baer, 1977) and question the world wide operation of the Wilson cycle in the Precambrian (Baer, *op.cit.*; Lambert, 1976) and propose modified ensialic models (Wynne-Edwards, 1976; Martin and Porada, 1977; Kröner, 1977, 1979, 1981a,b; Dimroth, 1981).

It is now widely presumed that plate motion is a consequence of thermally driven convection cells in the interior of the earth (Froidevaux and Nataf, 1981). Plate motion is well documented by palaeomagnetic evidence for much of the Precambrian (Burke *et al.*, 1976; McWilliams, 1981). Owing to the exponential decay rate of radioactive isotopes, heat flow and consequently heat convection is regarded to have been more vigorous in the past than at present (Windley, 1981; Hargraves, 1981) and uniformitarianists argue that if the intensity of plate motion can be equated with the rate of heat generation and dissipation (Burke *et al.*, 1977), the convection constraints proposed for the past militates against the denial of plate tectonic activity during the Precambrian. It appears that processes associated with plate tectonics provide the dominant mechanism of dispelling the heat generated within the earth and it has been proposed that Precambrian heat generation and convection has demanded a plate system operating faster than the present one (Burke *et al.*, 1976). From the geological record, however, it appears that subduction signatures only become common about 900 Ma ago (Kröner, 1977; Baer, 1977, 1981a). It has been pointed out in the literature that the higher heat flow in the past could have caused all early lithosphere to be positively buoyant and this would prohibit subduction (Baer, 1981a). The negative buoyancy of cold oceanic lithosphere is at present recognised as one of the major forces initiating subduction (Hargraves, 1981) and once the oceanic plate has reached a certain depth along the Benioff zone, subduction is enhanced by the basalt to eclogite conversion (Ringwood, 1975). According to Hargraves (*op.cit.*), buoyancy-powered subduction might only have commenced once the lithosphere was sufficiently thick and cool.

If the heat flux of the earth has decreased considerably through time as suggested in the literature, one can hardly escape the conclusion that this must have been accompanied by gradual changes of the physical properties (rigidity) of the crust. Therefore, even if the same plate driving mechanism envisaged for the present (mantle convection) was operative throughout the earth's history, the lithosphere (owing to changes in its mechanical properties) might have responded differently to convection and early plate tectonic

processes may have yielded signatures quite different from those recorded in the Phanerozoic. The lack of Phanerozoic plate tectonic signatures in Precambrian mobile belts has often been cited as evidence against the operation of plate tectonics throughout the entire earth's history, but the evolutionary nature of the crust is then ignored and it would be desirable to render the new global theory more flexible in order to accommodate the less rigid regimes of the past.

The prime concern here is to establish from the available evidence to what extent, if at all, the evolution of the Namaqualand Metamorphic Complex can be modelled in terms of the new global theory. In the past several attempts (some of local significance only) have been made to fit the Namaqualand Metamorphic Complex into a plate tectonic framework and these models are briefly reviewed below.

(a) Matthews (1972) regards the Natal thrust belt, which comprises a series of north-directed overthrusts along the margin between the Kaapvaal Craton and the Namaqua-Natal Mobile Belt, as an obduction zone and considers the Mfongosi Formation and the extensively migmatised Tugela Complex as part of a highly metamorphosed ophiolite nappe marking the suture along the southward subducting northern plate of the Kaapvaal craton. Subsequently Matthews (1981b) proposes a modified two-stage obduction process.

(b) A northward directed subduction zone in the vicinity of the present day Kaaien Hills has been proposed for the northeastern part of the Namaqualand Metamorphic Complex (Botha and Grobler, 1979). Their model comprises an arc system (Jannelsepan Formation) which separates a back-arc miogeosynclinal basin (Kheis domain) from the eugeosynclinal basin (Namaqualand gneisses). The evidence presented in favour of this model includes a large body of basic rocks south of Copperton which is regarded as a metamorphosed ophiolite complex, a narrow kyanite-bearing zone which could be equated with a high pressure belt and the calc-alkaline character of the proposed volcanic arc system (Botha and Grobler, *op.cit.*).

(c) Moen (1980) proposes a plate tectonic model for northeastern Namaqualand and this comprises a "Griqualand West Plate" subducted beneath a "Korannaland Plate". The Olifantshoek Sequence, Groblershoop Schist Formation and Sultanaoord Formation have been regarded to represent a continental margin sedimentary prism and the Wilgenhoutsdrif Group is considered to have oceanic crustal affinities and has been obducted during collision. The problem regarding the abundance of voluminous felsic volcanics in the Wilgenhoutsdrif Group is realised and accounted for by an obduction-subduction process during which oceanic crust is obducted onto sialic crust and some sialic crust is subducted yielding a partial melt that accounts for the silicic volcanics. A repetitive process of this type is envisaged. The Jannelsepan Formation is considered to represent a fossil volcanic arc in this model.

(d) Stowe (1980) and van Zyl (1981) propose that the zone with distinct geophysical expression under the Karoo cover to the south of Namaqualand (De Beer, 1978) represents a suture zone. The $F_2/F_3$ structural grain is regarded to indicate underthrusting of a southern plate with a north-directed compressive stress. The high grade Namaqualand terrane represents a crustal wedge overlying the subduction zone with the Cordilleran-type infrastructure now exposed due to regional uplift. Van Zyl (*op.cit.*) postulates that a triple junction rift related to early spreading gave rise to a north-trending failed arm (aulacogen) and an east-west elongated ocean with the deposition of continental and shallow marine sediments on an extensive shelf along the newly developed continental margin. In contrast Stowe (in press) considers the northwest trending belt in SWA/Namibia as an ensialic late dextral shear system related to the convergence of the plates.

(e) From a geochemical study of the volcanics of the Sinclair Sequence in SWA/Namibia Watters (1974) proposes the existence of a fossil volcanic arc ("Rehoboth Magmatic Arc") along the margin of the Kalahari plate above a southeasterly dipping subduction zone. Radiometric age determinations (Watters, *op.cit.*; SACS, 1980) fall into the Kibaran range and suggest that the volcanic activity along the Rehoboth Magmatic Arc was coeval with the Namaqua tectogenesis.

Whether or not a Wilson cycle was operative during the evolution of the Namaqualand Metamorphic Complex can only be judged from the available geological evidence preserved in the rock record. Characteristic criteria defining Phanerozoic plate tectonic regimes are extensively outlined in the literature (e.g. Dickinson, 1972; Oxburgh, 1975; Condie, 1976; Baer, 1981b). The Wilson cycle commences with rupture of the continent which leads to the production of an Atlantic-type continental margin characterised by a distinctive stratigraphic prism (Dewey and Bird, 1970). The most obvious signatures, however, are those related to the convergence phase of the Wilson cycle (Dewey and Burke, 1974) which in Phanerozoic orogenic belts, yields very characteristic rock types such as glaucophane schists, ophiolites and island arc andesites and the question arises how the Namaqualand Metamorphic Complex satisfies these Phanerozoic plate tectonic criteria.

There is general consensus that the majority of the pre-tectonic gneisses (quartzite, feldspathic quartzite, aluminous gneiss and schist, dolomitic marble, calc-silicate gneiss and iron formation) in the Namaqualand Metamorphic Complex are metasedimentary in origin (Coetzee, 1942b; Brink, 1950; von Backström, 1964; Frick and Coetzee, 1974; Paizes, 1975; Jackson, 1976; Moore, 1977, 1980; Colliston, 1979).

By analogy to modern continental shelf sedimentation which is now well documented (Ginsburg and James, 1974; Mayhew, 1974; Renard and Mascle, 1974; Sheridan, 1974; Siesser, *et al.*, 1974; Swift, 1974; Urien and Ewing, 1974; Dickinson and Seely, 1979) the supracrustal sequence in Bushmanland and Namaqualand can best be modelled as having been largely deposited in a continental shelf type environment. Whether the basal pink quartzo-

feldspathic gneisses should be interpreted as meta-arkose (Kröner, 1968; Moore, 1977) and possible equivalents of continental red beds (Moore, 1980) or whether they represent acid volcanics or a mixture of both is at present not clear.

The regional distribution of the metasediments is commonly regarded to represent original sedimentary facies variation (Paizes, *op.cit.*; Jackson, *op.cit.*; Moore, *op.cit.*). Moore (1980) recognises the following broad sedimentary facies in Bushmanland and Namaqualand :

(a) A northern continental/shallow marine facies dominated by red beds (pink quartzo-feldspathic gneiss), aluminous pelitic rocks and pure quartzites with intercalations of iron formation, baritic beds and highly aluminous sediments (sillimanite-corundum rocks).

(b) A central marine facies dominated by finer marine sediments (biotite schists and gneisses) and impure and pure carbonate rocks (calc-silicate rocks and dolomitic marbles).

(c) A southern shallow marine (?) facies dominated by feldspathic sandstones and poorly sorted pelitic rocks (cordierite gneisses).

It appears thus that these metasediments are essentially of shallow water to continental type, a feature previously suggested by Colliston (1979) and Malherbe (1979). It is striking that the eugeosynclinal stratigraphic prism which characterises Phanerozoic belts is not recognised in Namaqualand. Great sediment thickness in exposed orogenic belts are generally attributed to deposition in trenches, but the sedimentary fill in present trenches shows considerable variation in thickness. The north Pacific trenches generally contain several kilometres of sediment, while other trenches in the circum-Pacific region have only little sediment (Hayes, 1974; Scholl, 1974). Trench sediments consist essentially of turbidite successions overlying pelagic sediments (Hayes, *op.cit.*; von Huene, 1974; Scholl, *op.cit.*).

From a geochemical study of the supracrustal Namaqualand gneisses Moore (1980) concludes that immature sediments such as greywackes are not recognised, implying that deep-sea trench deposits have apparently not been recognised.

The metamorphism related to Phanerozoic plate tectonic activity yields a very characteristic signature. The duality of many metamorphic belts has long been recognised (Zwart, 1967). In the circum-Pacific region contemporaneous metamorphic belts are paired (Miyashiro, 1973a,b) and comprise a broad region of high temperature-low pressure recrystallisation spatially associated with the volcanic front and characerised by abundant granites and migmatites and juxtaposed to a low temperature-high pressure belt (jadeite-glaucophane) with abundant ophiolites. These paired metamorphic belts can be explained in terms of the plate tectonic theory and an understanding of the behaviour of isotherms along a convergent continental margin (Ernst, 1974).

The isotherms, which can as a first approximation, be regarded to be more or less parallel to the earth's surface in tectonically stable crust, are considerably disturbed along a convergent, plate margin (Turcotte and Oxburgh, 1972; Toksöz and Bird, 1977). Where the relatively cool subducted slab descends into the hotter asthenosphere, the isotherms are deflected downwards (Fig. 99 ) creating the necessary conditions for high pressure-low temperature metamorphism. Extensive plutonism and volcanism in the adjacent continental margin overlying the Benioff Zone, on the other hand, result in the upward deflection of the isotherms giving rise to a borad area of high temperature-low pressure metamorphism accompanied by migmatisation and the generation of granites by partial melting (Fig. 99 ). The approximate spatial distribution of metamorphic facies to be expected in the crust along an active convergent plate junction have been outlined by Ernst (*op.cit.*) as illustrated in Fig. 100.

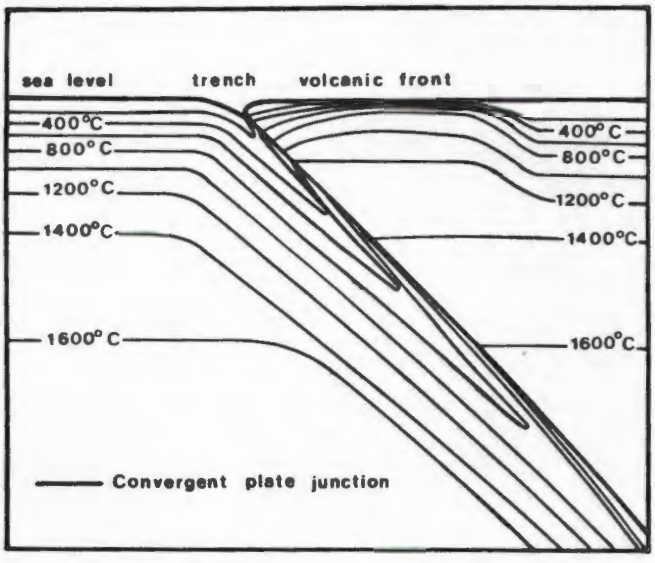


Fig. 99 Schematic model illustrating the isotherm pattern along an active convergent plate margin, simplified after Turcotte and Oxburgh (1972).

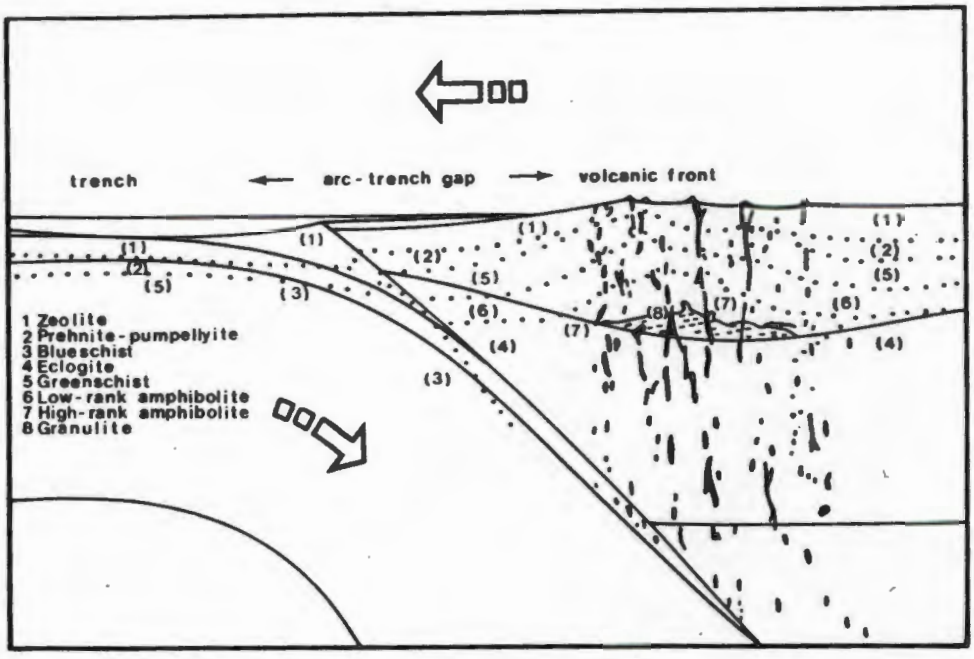


Fig.100 Schematic illustration of the distribution of metamorphic facies in crustal rocks near an active convergent plate junction after Ernst (1974).

If the metamorphic pattern documented in the Namaqualand gneisses is compared with the model shown in Fig.100, it is apparent that the low temperature-high pressure belt is lacking. From the present and previous studies it is well established that the regional metamorphism of the Namaqualand Metamorphic Complex is of the low pressure-high temperature type only (Joubert, 1971a; Clifford, *et. al.*, 1975a; Jackson, 1976; Toogood, 1976; Blignault, 1977; Linström, 1977; Moore, 1977; Smit, 1977; Botha and Grobler, 1979; Botha, *et.al.*, 1979b; Jack, 1980; Theart, 1980; van Bever Donker, 1980; Zelt, 1980; van Aswegen, 1981).

Several authors have documented the presence of kyanite within the area occupied by the Namaqualand Metamorphic Complex. It has already been discussed that the occurrences of kyanite along the west coast appear to be related to overprinting of the Namaqua metamorphic cycle by younger post-Namaqua events (Joubert and Waters, 1980). Kyanite-bearing rocks are also recorded from an area bounding the Kheis and Namaqua domains (Smit, 1977; Botha *et.al.*, 1979b) and have been cited as evidence for a possible high pressure belt related to convergent plate tectonic activity (Botha and Grobler, 1979). The validity of equating a narrow kyanite-bearing zone with a high pressure belt related to the Namaqua tectogenesis is questioned since according to Stowe (in press) the kyanite-bearing fabric appears to pre-date the main ($F_2$) Namaqua tectogenesis.

Whether or not, and to what extent, the high pressure-low temperature environment is developed in a convergent Pacific-type margin depends essentially on the extent of downwarping of the isotherms which is a function of the thickness and thermal state of the subducting plate as well as the angle of descent and the rate of convergence, and may also be related to the extent of decoupling between the interfering plates (Turcotte and Schubert, 1973; Ernst, 1974). For a hot and/or thin downgoing plate descending slowly the isotherms may be depressed only slightly prohibiting the formation of the characteristic high pressure belt (Ernst, 1974). Therefore, the absence of blue schists or related high pressure assemblages should in itself not be weighed too heavily as evidence against plate tectonics. It may be recalled here that England and Richardson (1977) propose that thermal relaxation during uplift may be an important mechanism through which deeper crustal levels lose their high pressure-low temperature metamorphic record. Evidence for considerable uplift is recorded in the high grade minerals. If the pressures derived from this study represent hydrostatic pressures, we cannot escape the conclusion that the granulites now exposed in Namaqualand must have originated at a depth of at least 20 km and consequently a thick pile of gneisses must have been eroded away to expose the infrastructure. This requires considerable uplift and if the driving mechanism involves buoyancy adjustment it implies that the Namaqualand Metamorphic Complex must have been underlain by a thickened sialic crust.

The most conclusive evidence for the existence of an ocean prior to the formation of a fold belt is documented in collisional sutures decorated with a fully developed ophiolite sequence (Burke *et.al.*, 1977). The anatomy of ophiolites is now well established (Church and Stevens, 1971; Coleman and Irwin, 1974; Hawkins, 1974) and the term is restricted to a distinctive assemblage of mafic and ultramafic rocks which, in a fully developed sequence from bottom to top, include the following rock types: ultramafic phases, gabbroic rocks, mafic sheeted dykes, mafic volcanics (pillow lavas) and associated pelagic sediments. By analogy to oceanic crust, ophiolites are generally regarded to represent either ocean floor generated at the mid-oceanic ridges (Moores and Vine, 1971; Coleman and Irwin, *op.cit.*) or alternatively they may represent floor to marginal rear-arc or inter-arc basins (Dewey and Bird, 1971; Dalziel, 1974; Dewey, 1974; Hawkins, *op.cit.*) of the Japan Sea type.

Mafic and ultramafic rocks of various ages occur throughout the Namaqualand Metamorphic Complex, generally as small bodies (Benedict *et.al.*, 1964; von Backström, 1964; Joubert, 1971a, 1974c; Beukes, 1973; Vajner, 1974; Cornell, 1975; Zelt, 1975; Jackson, 1976; Stumpfl *et.al.*, 1976; Toogood, 1976; Moore, 1977; Reid, 1977; Lombaard and Schreuder, 1978; Geringer, 1979; Kartun, 1979; Theart, 1980; Jack, 1980; van Bever Donker, 1980; van Zyl, 1981). No unambiguous fully developed ophiolites have, however, been recognised as yet. One possible candidate, the Wilgenhoutsdrif Group, contains characteristic features such as serpentinite, tholeiitic basic lavas with pillow structures and chert (Moen, 1980), but on account of the presence of vast amounts of acid volcanics, it is considered unlikely that these rocks

could represent obducted oceanic crust as proposed by Moen (*op.cit.*).

Coleman and Irwin (1974) point out that ophiolites are generally tectonically emplaced (obducted) and during this process individual rock units may become dismembered and when also extensively metamorphosed it might be difficult if not impossible to decide without the aid of geochemistry, whether these highly modified rocks do in fact represent parts of oceanic lithosphere.

In the absence of ophiolites sutures may be extremely difficult to recognise (Dewey and Burke, 1973; Dewey, 1977) particularly in deeper crustal levels and Dewey (*op.cit.*) remarks that "the effect of intense suturing may transport the signatures to high structural levels above a downward tapering suture zone at deep levels across which intense convergence may reduce the zone to a very narrow high strain zone a cryptic suture".

The intensely fractured and sheared boundary between the Namaqua Province on the one side and the Kheis Province and the Kaapvaal craton on the other (Namaqua Front/Namaqua Foreland of Vajner, 1974) is not likely to represent such a cryptic suture zone as the Kheis sequence has been correlated with certain Namaqualand-type gneisses across the boundary (Joubert, 1971a; Vajner, 1974; Botha *et.al.*, 1976; Stowe, 1980). Provided this correlation across the Namaqua Front is correct, it implies that these tectonic units could not have been separated from each other at least since the deposition of the Kheis Province sequences. Stowe (*op.cit.*) observes, however, that lithostratigraphic correlations across this zone are rendered more difficult owing to considerable lateral and vertical displacements, plutonism and folding. According to Pretorius (1979) a gravity survey across this boundary zone suggests that the Kaapvaal craton and the Namaqualand Metamorphic Complex formed a cohesive crustal unit during the Proterozoic. This observation is further supported by a magnetometer array study (de Beer, 1978) which failed to detect a deep seated tectonic boundary with traces of oceanic floor that could be equated with a cryptic suture.

Joubert (1974c) describes two main east-west trending belts of mafic gneisses. One occurs to the south of Gamoep and extends into the present area as a high strain zone of the $D_3$ generation. In the study area this zone contains hypersthene-pyroclase granolite of which the Bosluis basic body is the largest single outcropping mass. The second belt of mafic gneisses runs to the north of the Okiep mining area between northeast of Kleinsee and Nouzees/Pofadder. According to Joubert (*op.cit.*) mafic bodies occur mainly associated with these belts and several large bodies of olivine norite and gabbro are known from Nouzees.

A decision whether these mafic belts represent modified oceanic crust of rear-arc, inter-arc or open ocean type must await future geochemical studies. Geochemical studies indicate that many amphibolites and hypersthene-pyroclase granolites in Namaqualand and Bushmanland may represent metamorphic equivalents of continental basalts (Zelt, 1975; Moore, 1977; Geringer, 1979).

The lack of evidence for an obvious suture zone within the outcrop limits of the Namaqualand gneisses (with the possible exception of the Natal sector) has stimulated speculations that the high grade granulites and associated intrusives may represent a Cordilleran-type infrastructure above the Benioff-zone with a geophysically expressed suture to the south and at present concealed by younger sediments (Stowe, 1980, in press; van Zyl, 1981). In this connection it is recalled that the very prominent Beattie Ridge magnetic anomaly (de Beer *et al.*, 1974) runs parallel and to the north of the Cape Fold Belt in an east-west direction for a distance of about 900 km. According to de Beer (1978), deep Schlumberger soundings indicate that this anomaly is an expression of a deep-seated structure. Magnetometer array studies (*ibid.*) support the presence of an east-west conductor underlying the deep Karoo trough and Cape Fold Belt to the south of Beaufort West and more or less coinciding with the Beattie Ridge. De Beer (*op.cit.*) proposes that serpentinised ophiolites could account for the observed anomaly pattern. If a linear belt of oceanic lithosphere underlies the Cape and Karoo sediments in the southern Cape Province, it would serve as a strong argument in support of plate tectonics as proposed by Stowe (1980, in press) and van Zyl (1981). The question still to be answered, however, is whether this postulated ophiolite forms part of the post-Namaqua, pre-Cape Malmesbury Geosynclinal Belt and/or Cape Fold Belt as suggested by de Beer (*op.cit.*) and de Beer *et al.*, (1974), or whether it occupies the southern edge of the Namaqualand Metamorphic Complex and marks the subduction suture related to the Kibaran tectono-thermal Namaqua Event. If the latter is correct the apparent lack of signatures such as sediments characterising the subduction complex, high pressure-low temperature matamorphism and obvious ophiolites within the outcrop area of the Namaqualand gneisses becomes understandable.

The recognition of fossil volcanic arcs can also aid in the identification of ancient convergent plate margins. It is now well established that subduction zones are the sites where the calc-alkaline series of magmas are generated (Condie, 1976; Dickinson and Seely, 1979). Along modern continental margins overlying a subduction zone, the calc-alkaline series of volcanic rocks feature prominently. These volcanic rocks and their plutonic equivalents at depth (composite batholiths) display a distinct compositional polarity (Hatherton and Dickinson, 1969; Dickinson, 1970; Jakes and White, 1972) which appears to be related to the depth of the Benioff zone (Hatherton and Dickinson, *op.cit.*; Dickinson, *op.cit.*) and also to crustal thickness (Condie, 1973). Whether or not such a polarity is documented within the intrusive rocks of the Namaqualand Metamorphic Complex is at present not known and will only become apparent from future geochemical studies.

In the southern Andes the andesitic volcanic chain appears to be rooted in a major batholith (Dalziel, 1974; Dalziel *et al.*, 1974). An analogous situation is encountered in the Richtersveld Province (Reid, 1974, 1977; Blignault, 1977; Ritter, 1980) and the calc-alkaline trend of these igneous rocks (Reid, *op.cit.*) supports a continental margin type comparison. Taking the radiometric ages of these rocks into consideration the igneous activity in the Richtersveld Province by analogy to modern convergent plate margins,

points towards the operation of plate tectonics in the time 1700 - 2000 Ma (Reid, 1979a,b).

If we believe that the 1187 ± 22 Ma age derived by Clifford *et al.* (1981) for the thermal peak of regional metamorphism and accompanying recumbent ($F_2$) folding in the Nababeep area is correct, it is hard to escape the conclusion that the Richtersveld igneous activity is not likely to be linked with active convergence and subduction that might have caused the tectono-thermal imprint in Namaqualand. Purely on geochronological evidence, it appears that the suggested fossil arc in the Richtersveld Province could have been generated in a pre-Namaqua tectono-thermal event, probably related to the pre-Namaqua east-directed convergent event documented in the 2100 - 1750 Ma old sequences in the Kheis Province (Stowe, in press). It is interesting in this respect to note that Reid (1982, in press) has been able to detect an isotopic resetting in the core of the Richtersveld Province and this provides further evidence that the Kibaran Namaqua Event overprinted these older rocks.

From a geochemical study Geringer (1979) concludes that amphibolites in the Jannelsepan Formation, exposed south of Upington, have affinities with calc-alkaline rocks of active continental margins. Rocks dated at Copperton yield ages in the range of 1200 - 1500 Ma which has been regarded to represent the age of deposition (Cornell, 1975, 1978; Köppel 1978) and consequently it is possible that these rocks have evolved in an arc-like setting related to the early stages of the Kibaran Namaqua Event.

The Wilson cycle involves the opening and closing of an ocean which under favourable conditions may be detected by palaeomagnetic studies. The basic assumption is that the Earth's magnetic field in the past has always approximated a dipole and that the natural remnant magnetism recorded in rocks represents a mean orientation of this dipole at the time when the rocks were formed. Changes in the palaeomagnetic field of crustal rocks as manifested by apparent polar wander paths, or apparent polar wander swathes some 10 to 15 degrees in width, provide a quantitative method of detecting relative movements of crustal plates through time (Piper *et al.*, 1973; Piper, 1974, 1976; Briden, 1976). The uncertainties and limitations of Precambrian palaeomagnetic data have recently been reviewed by McWilliams (1981) who suggests that evidence for the operation of the Wilson cycle during the Precambrian can only be detected if the apparent polar motion of the cratons on either side of the mobile belts exceeds the limits of the apparent polar wander swathe. It has been proposed by Piper *et al.* (*op.cit.*) that all continents moved as a single cohesive unit, a large "Proterozoic Supercontinent", at least for a considerable time period during the Precambrian. The existence of such a long-lived supercontinent has subsequently been challenged by McWilliams (*op.cit.*) who observes that east and west Gondwana are characterised by distinctly different polar wander paths until these continents collided along the Pan-African Mozambique belt and formed a short-lived single unit (Gondwanaland) until its final break-up in the Mesozoic. This conclusion illustrates that independent plate motion must have been operative in the Proterozoic. According to McWilliams (*op.cit.*), however,

the palaeomagnetic data for Africa, within limits of uncertainty, indicate that the older cratons within the continent have retained their present configuration during much of the Precambrian. This observation can be interpreted to indicate negative evidence for the operation of the Wilson cycle during the formation of the African Proterozoic mobile belts, but a plate tectonic model cannot be dismissed solely on palaeomagnetic evidence because of the uncertainties and limitations of Precambrian palaeomagnetic data (*ibid.*) which are not sufficiently complete to justify definite conclusions (Dewey and Spall, 1975).

From the above discussion it appears that the Namaqualand Metamorphic Complex does not convincingly satisfy Phanerozoic plate tectonic criteria as the most distinctive signatures particularly those defining the subduction complex (Dickinson and Seely, 1979) are not recognised within the outcrop area. Despite this, there is no justification at the present state of knowledge to argue against a plate tectonic model. Only a very small portion of the entire mobile belt is exposed and to date even this has not been studied in any great detail. Nothing is known about the geology of the vast areas likely to be covered by younger sediments to the south of the outcrop limits. Existing models (Stowe, 1980, in press; van Zyl, 1981) propose that the subduction complex is concealed by Karoo and Cape sediments, possibly explaining the lack of criteria in existing outcrops.

Most of the geological aspects of the study area can quite adequately be explained in terms of the plate tectonic model proposed for the Namaqualand Metamorphic Complex by Stowe (in press).

Briefly, in this model it is suggested that the study area forms part of the deeply eroded high temperature-low pressure belt occurring above a northerly dipping subduction zone. The major weakness of this model, however, is that it is based largely on speculation which, owing to the inaccessibility of the subduction complex, is impossible to substantiate at present.

## 2 Ensialic Model

Plate tectonic concepts imply a model of crustal evolution involving continental accretion and progressive growth of smaller primitive cratons by the marginal welding of younger orogenic belts onto an older nucleus in the manner proposed by Clifford (1970) for the evolution of the African continent. An alternative model involving plate destruction as opposed to accretion is proposed by Kröner (1976, 1977) who argues in favour of a large Southern African continental plate believed to have existed since early Proterozoic times and subsequently progressively destroyed during repeated crustal reworkings within ensialic belts. According to this model the Namaqualand Metamorphic Complex has gone through a non-Wilson cycle intra-plate evolution and was underlain by sialic crust during the entire period of its development

(Kröner, 1979, 1981a,b). This view is supported by Shackleton (1973a,b) who notes that in some Precambrian terranes older structures can be traced from the craton into the mobile belt and sometimes through to another craton, implying that the adjacent cratons were not separated by an ocean and explaining the apparent lack of criteria pointing towards seafloor spreading and Benioff subduction from many Proterozoic mobile belts (Kröner, 1979, 1981a,b).

Models involving ensialic orogeny and basement reactivation become increasingly popular in explaining the evolution of many Precambrian mobile belts (Wynne-Edwards, 1976; Baer 1977, 1981b; Kröner, 1977, 1979, 1981a,b; Martin and Porada, 1977) and one of the best studied examples of ensialic orogeny is documented in the Labrador Trough (Dimroth, 1981).

In view of the somewhat speculative nature of the plate tectonic model that has been proposed for Namaqualand (Stowe, in press; van Zyl, 1981), it is desirable to consider ensialic orogeny as an alternative. Ensialic models proposed to date involve essentially the upwelling and cessation of a thermal plume and some of these models applicable to the Namaqualand Metamorphic Complex are briefly reviewed :

(a) The millipede model of Wynne-Edwards (1976) involves ductile spreading of the heated sialic crust above an upwelling mantle plume. This causes attenuation of the crust above the thermal rise leading to the formation of a shallow intracontinental sea in which typical platform-type sediments are deposited on the sialic basement. Metamorphism and igneous activity are considered to be a consequence of higher heatflow related to plume activity, while deformation commences as the ductile crust moves unilaterally off the spreading system and enters a compressional regime adjacent to cooler crust. During this process the basement and cover rocks become intensely deformed obscuring the basement-cover relations and isotopic systems are reset in the basement. Differential spreading may lead to major transformal shear zones (e.g. Pofadder Lineament).

(b) A model involving the progressive development from rifting through aulacogene formation to mobile belt has been envisaged by Botha and Grobler (1979) for the evolution of northeastern Namaqualand. This model involves repeated activation of a mantle plume set up along the edge of the present Kaapvaal craton causing a repetition of doming and rifting of the crust. Initial rifting yields two basins (Kheis and Namaqua grabens) on either side of a prominent horst ("Marydale High"). Sediments and volcanics accumulated and filled the grabens which eventually merged into a single large basin some 1800 - 2100 Ma ago. Cessation of mantle upwelling caused subcrustal contraction giving rise to compressive folding, regional metamorphism, anatexis and the emplacement of granitoids during the time interval 950 - 1400 Ma. Subsequent reactivation of the mantle plume caused renewed rifting and graben formation where the Koras volcanics and sediments accumulated.

(c) A very generalised model for Proterozoic ensialic orogenesis has been proposed by Kröner (1979, 1981a,b). The basic assumption underlying this model is that the asthenosphere is hotter and therefore less dense than the immediately overlying "chilled" subcontinental lithosphere rendering it gravitationally unstable. Any mechanism that allows the lower lithosphere to be detached from the overlying crust would cause it to sink into the asthenosphere. Apparently this subcrustal detachment has recently been recognised as an important mechanism in the mountains of Zagros (Bird, 1978a), Himalaya (Bird, 1978b) and in the Colorado Plateau (Bird, 1979) and is generally referred to as continental delamination (Bird, 1978a,b, 1979). In brief Kröner's (*op.cit.*) model comprises the following :

A convection roll starts in the asthenosphere along the Kaapvaal craton causing a broad linear region of rising isotherms within the subcontinental lithosphere above the vertical upwelling section of the convection roll rendering this belt more ductile. The sub-lithospheric horizontal currents related to this convection cell causes the ductile crust to stretch and fissure, but provided these forces are not strong enough to cause complete rupture, the linear zone of weakness will evolve into (a) shallow basin(s), graben systems or aulacogenes (Hoffmann, 1973; Hoffmann *et al.*, 1974). Terrigenous sediments and volcanics (bimodal) will provide the initial filling in the depressions and with continuous subsidence stable shelf-type sediments may be deposited (e.g. Bushmanland Group).

The less dense and less viscous asthenospheric material may gain access to higher crustal levels along the deep ruptures in the lithosphere and may eventually spread laterally along the continental crust-mantle boundary and thereby detaching and replacing the subcontinental lithosphere. Once the hot asthenospheric material reaches the lower continental crust, it heats up the latter considerably causing regional metamorphism and anatexis as the isotherms progressively move upwards. Large bodies of S-type granitoids may be generated and intrude overlying rocks. A considerable pressure drop experienced by the rapidly rising asthenosphere may lead to the liberation of $CO_2$-rich fluids which may invade the overlying sediments, diluting the essentially aqueous fluids and thereby promoting dehydration reactions. Partial melting of asthenospheric material is also promoted by the pressure drop and a wide range of differentiated magmas may invade the crust.

Once the asthenosphere has sufficiently weakened the crust-mantle boundary, the delaminated subcrustal lithosphere sinks into the asthenosphere in an attempt to balance densities. The tensional regime then reverses to compression which causes orogenesis. Van Zyl (1981) points out that the geometry of the resulting folds will depend on the geometry of the delaminated mantle and as this geometry may change through time, this model could account for the variation in structural orientation documented in the successive episodes of deformation. During orogenesis the crust is thickened by folding, the addition of syntectonic magmas and possibly by limited A-subduction (Bird, 1978a,b; Molnar and Gray, 1979; Kröner, 1981b). Thrusts and shear zones are likely to develop along the cooler edge of the delaminated

region (Bird, 1978b) where the stress difference is greatest. As compression ceased, the thickened crust rises rapidly to readjust its buoyancy.

A model of this type can adequately explain the various geological features recorded within the study area.

# IX SUMMARY AND CONCLUSIONS

1. The basement rocks of the study area form part of an extensive Proterozoic migmatite-gneiss terrane referred to as the Namaqualand Metamorphic Complex (SACS, 1980). A supracrustal sequence of metavolcanics and metasediments comprising calcareous, pelitic, semipelitic, quartzose, quartzo-feldspathic, ferrugenous and mafic units constitute the oldest rocks. Presumably these were deposited on some sort of pre-existing sialic basement, the nature of which is speculative. The transformation of the sediments and volcanic rocks into gneisses and migmatites was accomplished by intense regional metamorphism. A variety of magmas of differing ages and ranging in composition from ultramafic to granitic intruded the supracrustal sequence on a grand scale. In the extreme south of the area the Proterozoic gneisses are unconformably overlain by Late-Precambrian sediments of the Nama Group and sediments comprising the basal Karoo Sequence (underlying the Whitehill Shale Formation) form an extensive cover in the central parts of the area. Igneous activity of Phanerozoic age occurs as Karoo dolerite, plugs of olivine mililitites and kimberlite pipes.

2. Regional metamorphism reached granulite facies grade over the major part of the study area, but in the extreme north upper amphibolite facies conditions prevailed. The decline in metamorphic grade towards the north is seen in the change in mineral assemblages recorded in metamorphosed mafic rocks with two pyroxene-bearing granolites giving way to clinopyroxene and/or sphene-bearing amphibolites, and in the Z-absorption colour of hornblende from brown/brownish-green to green which appears to be largely controlled by the Ti concentration, the changing chemistry of hornblende (amphiboles in granolite specimens are characterised by higher Mg/(Mg + Fe + Mn) ratio, higher $Al^{IV}$, edenite alkalies and Ti but lower Si, $Al^{VI}$ and Mn concentrations compared to the amphiboles in amphibolites) and in the change in Z-absorption colour of biotite from red/red-brown to brown. The amphibolite-granulite facies boundary is concealed by superficial cover, but from the available evidence gathered in isolated outcrops, it appears that the transition occurs in an east-west-trending zone approximately along latitude 29° 49'S.

3. Retrograde Mg/Fe compositional zoning characterises the metamorphic minerals particularly garnet and cordierite. This has major implications for quantitative geothermometry/geobarometry involving these minerals. Only grain centres are likely to preserve equilibrium compositions attained during the peak P-T conditions of metamorphism.

4. Quantitative geothermometry on specimens from the granulite facies terrane yielded the following results (assuming a pressure of 5 Kb):

| Method | T-range (°C) | mean T (°C) |
|---|---|---|
| two pyroxenes (Wood and Bonno, 1973) | 795-909 | 830 (±27) |
| two pyroxenes (Wells, 1977) | 798-905 | 856 (±30) |
| garnet-clinopyroxene (Dahl, 1980) | 815-969 | |
| garnet-biotite (Ferry and Spear, 1978) | 798-854 | 785 (±72) |
| garnet-cordierite (Holdaway and Lee, 1977) | 696-809 | 776 (±19) |
| garnet-cordierite (Thompson, 1976b) | 706-861 | 819 (±23) |
| two feldspars (Stormer, 1975; Whitney and Stormer, 1977a) | 602-746 | 664 (±52) |

Considering all the evidence, it must be concluded that the temperatures based on the two feldspar method are too low. The other thermometers indicate a thermal peak in the temperature range 700-900°C for granulite facies metamorphism. The temperatures based on phase compositions in mafic rocks are higher than those derived from mineral compositions in pelitic gneisses. From theoretical arguments it appears that the two pyroxene thermometers are not very sensitive under granulite facies conditions and that they yield temperatures that are too high. The garnet-cordierite geothermometer of Holdaway and Lee (1977) is regarded to yield the best results.

5. Pressures accompanying regional metamorphism were relatively low. This conclusion is supported by the stable coexistence of "orthopyroxene + plagioclase" in metamorphosed basic rocks, the abundance of cordierite in pelitic gneisses, the chemistry of metamorphic minerals (amphibole, garnet) and quantitative geobarometry. The garnet-plagioclase geobarometer (Ghent, 1976) yielded pressures in the range 4,6 - 5,1 Kb. Slightly higher pressures are indicated by the garnet-cordierite geobarometer (derived in this study): 4,9 - 5,3 Kb ($P_{H_2O} = 0$) and 5,7 - 6,4 Kb ($P_{H_2O} = P_{total}$) from which it is concluded that pressures of the order of 5-6 Kb prevailed during granulite facies metamorphism.

6. Migmatites with abundant garnetiferous leucosomes feature prominently in the granulite facies terrane and provide a glimpse into the melting region of the crust. Their genesis is largely ascribed to the process of *in situ* anatexis of the gneisses presumably in response to higher heatflow during metamorphism. Hydrous minerals are considered to play an important role in this process as they may provide the dominant source of water in the granulite facies environment. It is quite conceivable that at least some of the intrusive granitoids are the products of anatexis.

7. The most distinctive feature of the granulite facies terrane is the relatively "dry" mineralogy comprising a large proportion of anhydrous minerals. Dehydration is achieved either by partial melting and removal of the anatectic melts from the source region or by dehydration metamorphism.

Charnockite and charno-enderbite are common rock types and these are spatially restricted to the granulite facies terrane. They appear to have reached their present position as magmas.

8. Polyphase deformation has affected the area. At least three episodes of folding ($D_2$ - $D_4$) deform the gneissic banding which itself may be of tectonic origin ($D_1$?). The $D_2$ structures are tight isoclinal folds frequently with a penetrative axial-plane foliation and prominent b-mineral lineation ($l_2$). $D_3$ folds are the most prominent structures varying in orientation from east-northeast-trending with near vertical axial planes and fold axes plunging either south of west or north of east, to west-northwest with axial planes dipping north-northwesterly to northeasterly and fold axes plunging west-southwest to west-northwest in the Kliprand area. $D_4$ structures are open folds trending northeasterly. The folding was accompanied and followed by shearing. Discrete dextral shear zones strike west-northwest and east-northeast and their sinistral equivalents strike east, northeast and occasionally north-northwest to north. Shear zones are frequently offset by faults striking north to north-northwest. Some of these faults are of post-Nama age.

9. Regional metamorphism in the study area is modelled as a continuous process involving one major prograde event comprising several episodes of recrystallisation, the younger being retrograde.

10. The metamorphic zonation created by the Namaqua Event in western Namaqualand comprises essentially east-west-trending zones, modified in detail, with the grade decreasing northwards and southwards (?) from an extensive granulite facies core. Post-Namaqua metamorphic and structural events are superimposed on the Namaqua Event in a north-south-trending zone along the west coast.

11. The Namaqualand Metamorphic Complex does not convincingly satisfy Phanerozoic plate-tectonic criteria as the most distinctive signatures defining a subduction complex (trench sediments, ophiolites and high pressure-low temperature metamorphism) are not recognised within the outcrop area. At the present state of knowledge, however, there is no justification to argue against a plate-tectonic model in view of the fact that only a small portion of the mobile belt is exposed and the subduction complex may be concealed by younger strata (Cape and Karoo sediments), a feature which has some support from geophysical studies and is also consistent with the east-west metamorphic zonation in the Namaqualand Metamorphic Complex.

## REFERENCES


Adamson, R.S. (1931). Note on some petrified wood from Banke, Namaqualand. *Trans. R. Soc. S. Afr.*, 19, 255-258.

Albat, H.M. (1979). Preliminary report on the geology of the Kliprand area in Namaqualand. *Ann. Rep. Precambr. Res. Unit, Univ. Cape Town*, 16, 47-57.

Albee, A.L. (1965). Distribution of Fe, Mg and Mn between garnet and biotite in natural mineral assemblages. *J. Geol.*, 73, 155-164.

_____ (1972). Metamorphism of pelitic rocks : reaction relations of chloritoid and staurolite. *Bull. geol. Soc. Am.*, 83, 3249-3268.

Allsopp, H.L., Köstlin, E.O., Welke, H., Burger, A.J., Kröner, A. and Blignault, H.J. (1979). Rb-Sr and U-Pb geochronology of Late Precambrian - Early Palaeozoic igneous activity in the Richtersveld (South Africa) and southern South West Africa. *Trans. geol. Soc. S. Afr.*, 82, 185-204.

Althaus, E. (1968). Der Einfluss des Wassers auf metamorphe Mineralreaktionen. *Neues Jb. Miner. Mh.* 9, 289-306.

_____ (1969). Das System $Al_2O_3$ - $SiO_2$ - $H_2O$. Experimentelle Untersuchungen und Folgerungen für die Petrogenese der metamorphen Gesteine. Teil II, III. *Neues. Jb. Miner. Abh.*, 111 (2), 111-161.

_____, Karotke, E., Nitsch, K.H. and Winkler, H.G.F. (1970). An experimental re-examination of the upper stability limit of muscovite plus quartz. *Neues Jb. Miner. Mh.*, 7, 325-336.

Amit, O. and Eyal, Y. (1976). The genesis of Wadi Magrish migmatites (N-E Sinai). *Contr. Miner. Petrol.*, 59, 95-110.

Anastasiou, P. and Seifert, F. (1972). Solid solubility of $Al_2O_3$ in enstatite at high temperatures and 1 - 5 Kb. water pressure. *Contr. Miner. Petrol.*, 34, 272-284.

Anderson, D.E. and Buckley, G.R. (1973). Zoning in garnets; diffusion models. *Contr. Miner. Petrol.*, 40, 87-104.

Anderson, J.M. (1977). The biostratigraphy of the Permian and Triassic. *3 : Mem. Bot. Surv. S. Afr.*, 41, 1-67.

Anhaeusser, C.R., Mason, R. Viljoen, M.J. and Viljoen, R.P. (1968). A reappraisal of some aspects of Precambrian shield geology. *Bull. geol. Soc. Am.*, 80, 2175-2200.

Aoki, A., Fujino, K. and Akaogi, M. (1976). Titanochondrodite and Titanoclinohumite from the upper mantle in the Buell Park Kimberlite, Arizona. *Contr. Miner. Petrol.*, 56, 243-253.

Ardell, A.J., Christie, J.M. and Tullis, J.A. (1973). Dislocation substructures in deformed quartz rocks. *Crystal Lattice Defects*, 4, 275-285.

Atherton, M.P. and Edmunds, W.M. (1966). An electron microprobe study of some zoned garnets from metamorphic rocks. *Earth Planet. Sci. Lett.*, 6, 185-193.

Atkin, B.P. (1978). Hercynite as a breakdown product of staurolite from within the aureole of the Ardora Pluton, Co. Donegal, Eire. *Mineralog. Mag.*, 42, 237-239.

Atlas, L. (1952). The polymorphism of Mg Si $O_3$ and solid state equilibria in the system Mg Si $O_3$ - Ca Mg $Si_2$ $O_6$. *J. Geol.*, 60, 125-147.

Baer, A.J. (1977). Speculations on the evolution of the lithosphere. *Precambrian Res.* 5, 249-260.

_____ (1981a). Geotherms, evolution of the lithosphere and plate tectonics. *Tectonophysics*, 72, 203-227.

_____ (1981b). A Grenvillian model of Proterozoic plate tectonics, 353-385. *In :* Krӧner, A. (Ed.). Developments in Precambrian geology, Vol. 4. *(Precambrian plate tectonics).* Elsevier Scientific Publishing Company, Amsterdam, 781p.

Bailey, E.H. and Stevens, R.E. (1960). Selective staining of K-feldspar and plagioclase on rock slabs and thin sections. *Am.Miner.* 45, 1020-1023.

Bak, J., Kôrstgard, J. and Sørensen, K. (1975). A major shear zone within the Nagssuqtoqidian of West Greenland. *Tectonophysics*, 27, 191-209.

_____, Sørensen, K., Grocott, J., Kôrstgard,J.A.,Nash, D. and Watterson, I. (1975). Tectonic implications of Precambrian shear belts in western Greenland. *Nature*, 254, 566-569.

Baltatzis, E. (1979). Distribution of Fe and Mg between garnet and biotite in Scottish Barrovian metamorphic zones. *Mineralog. Mag.* 43, 155-157.

Bard, J.P. (1969). *Le metamorphisme regional progressif des Sierras d'Aracena en andalousie occidentale (Espagne).* Univ. Montpellier, unpubl.

_____ (1970). Composition of hornblendes formed during the Hercynian progressive metamorphism of the Aracena metamorphic belt (S.W. Spain). *Contr. Miner. Petrol.*, 28, 117-134.

Barth, T.F.W. (1934). Temperaturen i lava og magmamasser, sam et nylt geologisk termometer. *Naturen*, 6, 187-192.

_____ (1951). The feldspar geological thermometers. *Neues Jb. Miner.* 82, 143-154.

_____ (1956). Studies in gneiss and granite. *Norsk Vidensk Acad. Oslo, l Mat - Natura Klasse*, 1, 263-274.

_____ (1962). The feldspar geologic thermometer. *Norsk Geol. Tidsskr.*, 42, 330-339.

Barton, E.S., Harmer, R.E. and Burger, A.J. (1981). Isotopic studies in the Namaqua- Natal Mobile Belt. *Abstracts 19th Congress geol. Soc. S. Afr.*, 12-13.

Bell, T.H. and Etheridge, M.A. (1973). Microstructures of mylonites and their descriptive terminology. *Lithos*, 6, 337-348.

_____ and Etheridge, M.A. (1976). The deformation and recrystallisation of quartz in a mylonite zone, central Australia. *Tectonophysics*, 32, 235-267.

Benedict, P.C., Wiid, D. de N., Cornelissen, A.K. and Staff (1964). Progress report on the geology of the O'okiep Copper District, 238-318. *In* : Haughton, S.H. (Ed.). *The geology of some ore deposits in Southern Africa.* *Geol. Soc. S. Afr.*, 2, 739p.

Berglund, L. and Touret, J. (1976). Garnet - biotite gneiss in "Systeme du Graphite" (Madagascar) : Petrology and fluid inclusions. *Lithos*, 9, 139-148.

Bertrand, J.M. (1975). Granitoids and deformation sequence in the Goodhouse-Henkries area. A new interpretation between rocks in the Vioolsdrif-Goodhouse area and the Namaqualand and Bushmanland gneisses. *Ann. Rep. Precambr. Res. Unit, Univ. Cape Town*, 13, 61-70.

Beukes, G.J. (1973). *'n Geologiese ondersoek van die gebied suid van Warmbad Suidwes-Afrika, met spesiale verwysing na die metamorf-magmatiese assosiasies van die Voorkambriese gesteentes.* Unpubl. D. Sc. thesis, Univ. Orange Free State, 333p.

Bhattacharyya, C. (1971). An evaluation of the chemical distinctions between igneous and metamorphic orthopyroxenes. *Am. Miner.* 56, 499-506.

_____ (1972). Granitisation in relation to the evolution of charnockite series from the Eastern Ghat hills, Strikakulam district Andra Pradesh, India. *Neues Jb. Miner. Mh.* 5, 220-240.

Binns, R.A. (1962). Metamorphic pyroxenes from the Broken Hill district, New South Wales. *Mineralog. Mag.*, 33, 320-338.

_____ (1965a). The mineralogy of metamorphosed basic rocks from the Willyama Complex, Broken Hill district, New South Wales, Part I - Hornblendes. *Mineralog. Mag.*, 35, 306-326.

_____ (1965b). The mineralogy of metamorphosed basic rocks from the Willyama Complex, Broken Hill district, New South Wales, Part II - Pyroxenes, garnets, plagioclases and opaque oxides. *Mineralog. Mag.*, 35, 561-587.

_____ (1968). Experimental studies of metamorphism at Broken Hill. *In :* Radmonovich, M. and Woodcock, J.T. (Eds.). *'Broken Hills Mines.' Monograph 3 Aust. Inst. Mining and Metallurgy,* 199-204.

_____ (1969a). Ferromagnesian minerals in high-grade metamorphic rocks. *Spec. Publication geol. Soc. Aust.*, 2, 323-332.

_____ (1969b). Hydrothermal investigations of the amphibolite-granulite facies boundary. *Spec. Publication geol. Soc. Aust.*, 2, 341-344.

Bird, P. (1978a). Finite element modeling of lithosphere deformation : The Zagros collision orogeny. *Tectonophysics*, 50, 307-336.

_____ (1978b). Initiation of intracontinental subduction in the Himilaya. *J. Geophys. Res.*, 83, 4975-4987.

_____ (1979). Continental delamination and the Colorado Plateau. *J. Geophys. Res.*, 84, 7561-7571.

Blignault, H.J. (1974a). The tectonic zonation of part of the Namaqua Province in the lower Fish River/Narubis cross-section. *Ann. Rep. Precambr. Res. Unit, Univ. Cape Town,* 10-11, 43-45.

_____ (1947b). Aspects of the Richtersveld Province. *In :* Krüner, A. (Ed.). *Contributions to the Precambrian geology of Southern Africa,* 49-56. *Bull. Precambr. Res. Unit. Univ. Cape Town,* 15, 213p.

_____ (1977). Structural-metamorphic imprint on part of the Namaqua mobile belt in South West Africa. *Bull. Precambr. Res. Unit, Univ. Cape Town,* 23, 197p.

_____, Jackson, M.P.A., Beukes, G.J. and Toogood, D.J. (1974). The Namaqua Tectonic Province in South West Africa. *In :* Krüner, A. (Ed.). *Contributions to the Precambrian geology of Southern Africa,* 29-47. *Bull. Precambr. Res. Unit, Univ. Cape Town,* 15, 213p.

Boettcher, A.L. (1970). The system $CaO-Al_2O_3 - SiO_2 - H_2O$ at high pressures and temperatures. *J. Petrology,* 11, 337-379.

_____ and Wyllie, P.J. (1968). Melting of granite with excess water to 30 Kilobars pressure. *J. Geol.,* 76, 235-244.

Bohlen, S.R. and Essene, E.J. (1977). Feldspar and oxide thermometry of granulites in the Adirondack Highlands. *Contr. Miner. Petrol.,* 62, 153-169.

_____ and Essene, E.J. (1979). A critical evaluation of two-pyroxene thermometry in Adirondack granulites. *Lithos,* 12, 335-345.

Borg, I.Y. (1967). On conventional calculations of amphibole formulae from chemical analyses with inaccurate $H_2O$ (+) and F determinations. *Mineralog. Mag.,* 36, 583-590.

Botha, B.J.V., Grobler, N.J., Linström, W. and Smit, C.A. (1976). Stratigraphic correlation between Kheis and Matsap formations and their relation to the Namaqualand Metamorphic Complex. *Trans. geol. Soc. S.Afr.,* 79, 304-311.

_____, Grobler, N.J., Linström, W. and Smit, C.A. (1977). Major structural features of the area between the Langeberg Range and Kenhardt, Northern Cape Province. *Trans. geol. Soc. S. Afr.,* 80, 101-109.

Botha, B.J.V. and Grobler, N.J. (1979). Models for the geotectonic evolution of the Middle to Late Precambrian Namaqua Mobile Belt in eastern Namaqualand, South Africa. *Precambrian Res.* 10, 21-41.

_____, Grobler, N.J. and Burger, A.J. (1979a). New U-Pb age measurements on the Koras Group, Cape Province and its significance as a time reference horizon in eastern Namaqualand. *Trans. geol. Soc. S. Afr.*, 82, 1-5.

_____, Smit, C.A., Linström, W. and Grobler, N.J. (1979b). Metamorphic zonation in the Matsap, Kheis and Namaqua domains east and west of the Kaaien Hills, Northern Cape Province. *Trans. geol. Soc. S. Afr.*, 82, 55-66.

Boyd, F.R. (1959). Hydrothermal investigations of amphiboles, 377-397. *In :* Abelson, P.H. (Ed.). *Researches in geochemistry.* Wiley, New York.

_____ and Schairer, J.F. (1964). The system Mg Si $O_3$ - Ca Mg $Si_2O_6$. *J. Petrology* , 5, 275-309.

_____, Finger, L.W. and Chayes, F. (1968). Computer reduction of electron probe data. *Carnegie Inst. Wash. Yearbook*, 67, 210-215.

Braun, E. and Müller, G. (1975). Zur chemischen, Variabilität regional-metamorph gebildeter Plagioklase, Epidote und Granate. *Contr. Miner. Petrol.*, 52, 193-211.

Briden, J.C. (1976). Application of palaeomagnetism to Proterozoic tectonics. *Phil. Trans. R. Soc. Lond.*, A280, 405-416.

Brink, W.C. (1950). The geology, structure and petrology of the Nuwerus area, Cape Province. *Ann.Univ.Stellenbosch*, 26, 97-221.

Brown, G.C. (1973). Evolution of granite magmas at destructive plate margins. *Nature*, 241, 26-28.

_____ and Fyfe, W.S. (1970). The production of granitic melts during ultra-metamorphism. *Contr. Miner. Petrol.*, 28, 310-318.

_____ and Fyfe, W.S. (1972). The transition from metamorphism to melting : status of the granulite and eclogite facies. *24th Int. geol. Congress*, Section 2, 27-34.

Brown, G.M. (1961). Co-existing pyroxenes in igneous assemblages : A re-evaluation of the existing data on tie-line orientations. *Geol. Mag.*, 98, 333-343.

Brown, W.L. and Parsons, I. (1981). Towards a more practical two-feldspar geothermometer. *Contr. Miner. Petrol.*, 76, 369-377.

Burger, A.J. and Coertze, F.J. (1973). Radiometric age measurements on rocks from Southern Africa to the end of 1971. *Bull. geol. Surv. S. Afr.*, 58, 46p.

_____ and Walraven, F. (1978). Summary of age determinations : April 1976 - March 1979. *Ann. geol. Surv. S. Afr.*, 12, 199-218.

Burke, K., Dewey, J.F. and Kidd, W.S.F. (1976). Precambrian palaeomagnetic results compatible with contemporary operation of the Wilson cycle. *Tectonophysics*, 33, 287-299.

_____Dewey, J.F. and Kidd, W.S.F. (1977). World distribution of sutures - the sites of former oceans. *Tectonophysics*, 40, 69-99.

Burnham, C.W., Holloway, J.R. and Davis, N.F. (1969). Thermodynamic properties of water to 1000°C and 10 000 bars. *Spec. Paper geol. Soc. Am.*, 132, 96p.

Büsch, W., Schneider, G. and Mehnert, K.R. (1974). Initial melting at grain boundaries. Part II. Melting in rocks of granodioritic, quartzdioritic and tonalitic composition. *Neues Jb. Miner. Mh.*, 8, 345-370.

_____, Matthes, S., Mehnert, K.R. and Schubert, W. (1980). Zur genetischen Deutung der Kinzigite im Schwarzwald und Odenwald. *Neues Jb. Miner. Abh.*, 137(3), 223-256.

Cahen, L. and Snelling, N.J. (1966). *The geochronology of equatorial Africa.* North-Holland Publishing Company, Amsterdam, 195p.

Cain, A.C. (1975). A preliminary review of the stratigraphic relationships and distribution of metamorphism in the northern part of the Natal-Namaquarides, South Africa. *Geol. Rdsch.*, 64, 192-216.

Church, W.R. and Stevens, R.K. (1971). Early Paleozoic ophiolite complexes of the Newfoundland Appalachians as mantle-oceanic crust sequences. *J. Geophys. Res.*, 76, 1460-1466.

Clifford, T.N. (1970). The structural framework of Africa. *In :* Clifford, T.N. and Gass, I.G. (Eds.). *African magmatism and tectonics,* 1-26. Oliver and Boyd, Edinburgh, 461p.

_____, Gronow, J., Rex, O.C. and Burger, A.J. (1975a). Geochronological and petrogenetic studies of high grade metamorphic rocks and intrusives in Namaqualand, South Africa. *J. Petrology,* 16(1), 154-188.

_____, Stumpfl, E.F. and McIver, J.R. (1975b). A sapphirine - cordierite - bronzite - phlogopite paragenesis from Namaqualand, South Africa. *Mineralog. Mag.,* 40, 347-356.

_____, Stumpfl, E.F. and Burger, A.J. (1978). Mineralogical and isotopic studies of the crystalline rocks of the Okiep-Nababeep district, Namaqualand, 345-347. *In :* Verwoerd, W.J. (Ed.). *Mineralization in metamorphic terranes. Spec. Publication geol. Soc. S. Afr.,* 4, 552p.

_____, Stumpfl, E.F., Burger, A.J., McCarthy, T.S. and Rex, D.C.(1981). Mineral-chemical and isotopic studies of Namaqualand granulites, South Africa : A Grenville Analogue. *Contr. Miner. Petrol.,* 77, 225-250.

Coetzee, C.B. (1940). Sillimanite-corundum rock : A metamorphosed bauxite in Namaqualand. *Trans. R. Soc. S. Afr.,*28, 199-205.

_____ (1942a). The petrology of the Goodhouse - Pella area, Namaqualand, South Africa. *Trans. geol. Soc. S. Afr.,* 44, 167-206.

_____ (1942b). Metamorphosed sediments from the Goodhouse - Pella area, Namaqualand, South Africa. *Trans R. Soc. S. Afr.,* 29, 91-112.

_____ (1958). Manganiferous iron ore, haematite, barite and sillimanite on Gams (Portion 1), Namaqualand. *Bull. geol. Surv. S. Afr.,* 28, 29p.

Coleman, R.G. and Irwin, W.P. (1974). Ophiolites and ancient continental margins, 921-931. *In :* Burk, C.A. and Drake, C.L. (Eds.). *The geology of continental margins.* Springer - Verlag, Berlin, 1009p.

Collerson, K.D. and Fryer, B.J. (1978). The role of fluids in the formation and subsequent development of early continental crust. *Contr. Miner. Petrol.,* 67, 151-167.

Colliston, W.P. (1979). The stratigraphy of the Namaqualand Metamorphic Complex in Bushmanland. *Abstracts 18th Congress geol. Soc. S. Afr.*, 85-105.

Condie, K.C. (1973). Archaean magmatism and crustal thickening. *Bull. geol. Soc. Am.*, 84, 2981-2992.

_____ (1976). *Plate tectonics and crustal evolution.* Pergamon Press, New York, 288 p.

Cooray, P.G. (1969). Charnockites as metamorphic rocks. *Am. J. Sci.*, 267, 969-982.

Cornelissen, A.K. and Verwoerd, W.J. (1973). The Bushmanland kimberlites. *In :* Ahrens, L.H. et al. (Eds.). *Int. conference on kimberlites, Univ. Cape Town (1973).*

_____ and Verwoerd, W.J. (1975). The Bushmanland kimberlites and related rocks, 71-80. *In* : Ahrens, L.H. et al. (Eds.). *Physics and chemistry of the Earth*, Vol. 9, Pergamon Press, Oxford.

Cornell, D.H. (1975). *Petrology of the Marydale metabasites.* Unpubl. Ph.D. thesis, Univ. Cambridge, 216 p.

_____ (1978). Age and metamorphism of the Copperton Formation, Prieska district. *In :* Verwoerd, W.J. (Ed.). *Mineralization in metamorphic terranes. Spec. Publication geol. Soc. S. Afr.*, 4, 223-234.

_____ and Barton, E.S. (1979). Age of the Marydale Group banded iron formation by the Pb-Pb method. *Abstracts 18th Congress geol. Soc. S. Afr.*, 111-114.

Cressey, G., Schmid, R. and Wood, B.J. (1978). Thermodynamic properties of almandine - grossular garnet solid solutions. *Contr. Miner. Petrol.*, 67, 397-404.

Crowell, J.C. and Frakes, L.A. (1972). Late Paleozoic glaciation; Part V, Karoo Basin, South Africa. *Bull. geol. Soc. Am.*, 83, 2887-2912.

Currie, K.L. (1971). The reaction : 3 cordierite = 2 garnet + 4 sillimanite + 5 quartz as a geological thermometer in the Opinicon Lake region, Ontario. *Contr. Miner. Petrol.*, 33, 215-226.

_____ (1974). A note on the calibration of the garnet - cordierite geothermometer and geobarometer. *Contr. Miner. Petrol.*, 44, 35-44.

Dahl, P.S. (1980). The thermal-compositional dependence of $Fe^{+2}$-Mg distributions between coexisting garnet and pyroxene : applications to geothermometry. *Am. Miner.*, 65, 852-866.

Dallmeyer, R.D. (1974). The role of crystal structure in controlling the partitioning of Mg and Fe between coexisting garnet and biotite. *Am. Miner.*, 59, 201-203.

Dalziel, I.W.D. (1974). Evolution of the margins of the Scotia Sea, 567-579. *In :* Burk, C.A. and Drake C.L. (Eds.). *The geology of continental margins.* Springer-Verlag, Berlin,1009p.

_____, de Wit, M.J. and Palmer, K.F. (1974). Fossil marginal basin in the southern Andes. *Nature*, 250, 291-294.

Davidson, L.R. (1969). $Fe^{++}$ - $Mg^{++}$ distribution in coexisting metamorphic pyroxenes. *Spec. Publication geol. Soc. Aust.*, 2, 333-339.

_____ and Mathison, C.I. (1974). Aluminous orthopyroxenes and associated cordierites, garnets and biotites from granulites of the Quairading district, Western Australia. *Neues Jb. Miner. Mh.*, 6, 272-287.

Davis, B.T.C. and Boyd, F.R. (1966). The join $Mg_2 Si_2 O_6$ - $Ca Mg Si_2 O_6$ at 30 Kilobars pressure and its applications to pyroxenes from kimberlites. *J. Geophys. Res.*, 71, 3567-3576.

de Beer, J.H. (1978). The relationship between the deep electrical resistivity structure and tectonic provinces in Southern Africa. Part 2. Results obtained by magnetometer array studies. *Trans. geol. Soc. S. Afr.*, 81, 143-154.

_____, Van Zijl, J.S.V. and Bahnemann, F.K. (1974). Plate tectonic origin for the Cape Fold Belt? *Nature*, 252, 675-676.

De Beer, J.H. and Gough, D.I. (1980). Conductive structures in southernmost Africa : A magnetometer array study. *Geophys. J.R. astr. Soc.*, 63, 479-495.

Deer, W.A., Howie, R.A. and Zussman, J. (1971). *An introduction to the rockforming minerals.* Longman, London, 528p.

_____, Howie, R.A. and Zussman, J. (1978). *Rock-forming minerals, Vol2A. Single-chain silicates.* Longman, London, 668p.

De Jager, D.H. (1963). Sillimanite in Namaqualand : review of reserves and report on some low-grade deposits. *Bull. geol. Surv. S. Afr.*, 40, 42p.

De Jager, D.H. and von Backström, J.W. (1961). The sillimanite deposits in Namaqualand near Pofadder. *Bull. geol. Surv. S. Afr.*, 33, 49p.

_____ and Simpson, N. (1962). Wollastonite near Garies, Namaqualand. *Ann. geol. Surv. Dep. Min. S. Afr.*, 1, 127-135.

Delaney, J.M. and Helgeson, H.C. (1978). Calculation of the thermodynamic consequences of dehydration in subduct: Oceanic crust 100 Kb and 800°C. *Am. J. Sci.*, 278, 638-686.

De Villiers, J. and Söhnge, P.G. (1959). The geology of the Richtersveld. *Mem. geol. Surv. S. Afr.*, 48, 266p.

De Waard, D. (1964). Metamorphism and magmatism in the charnockite terrane of the Adirondack highlands. *U.S.A. Int. geol. Congress 22nd New Delhi 1964 Proc.*

_____ (1965a). The occurrence of garnet in the granulite facies terrane of the Adirondack highlands. *J. Petrology*, 6(1), 165-191.

_____ (1965b) A proposed subdivision of the granulite facies. *Am. J. Sci.*, 263, 455-461.

_____ (1966). On water-vapor pressure in zones of regional metamorphism and the nature of the hornblende-granulite facies. *Proc. K. Ned. Akad. Wet. Amsterdam*, 69, 453-458.

_____ (1967). Absolute P-T conditions of granulite-facies metamorphism in the Adirondacks. *Proc. K. Ned. Akad. Wet. Amsterdam*, 70, 400-410.

_____ (1969). The occurrence of charnockite in the Adirondacks : A note on the origin and definition of charnockite. *Am. J. Sci.*, 267, 983-987.

_____, Duchesne, J.C. and Michot, J. (1974). Anorthosites and their environment. *Cent. Soc. Geol. Belgique*, 1974, 323-346.

Dewey, J.F. (1974). Continental margins and ophiolite obduction : Appalachian - Caledonian system, 933-950. *In :* Burk, C.A. and Drake, C.L. (Eds.). *The geology of continental margins.* Springer-Verlag, Berlin, 1009p.

_____ (1977). Suture zone complexities : a review. *Tectonophysics*, 40, 53-67.

_____ and Bird, J.M. (1970). Mountain belts and the new global tectonics. *J. Geophys. Res.*, 75(14), 2625-2647.

Dewey, J.F. and Bird, J.M. (1971). Origin and emplacement of the ophiolite suite : Appalachian ophiolites in Newfoundland. *J. Geophys. Res.*, 76(14), 3179-3206.

_____ and Burke, K.C.A. (1973). Tibetan, Variscan and Precambrian basement reactivation : products of continental collision. *J. Geol.*, 81, 683-692.

_____ and Burke, K.C.A. (1974). Hot spots and continental breakup : implications for collisional orogeny. *Geology*, 2, 57-60.

_____ and Spall, H. (1975). Pre-Mesozoic plate tectonics. *Geology*, 3, 422-424.

Dickinson, W.R. (1970). Relations of andesites, granites, and derivative sandstones to arc-trench tectonics. *Rev. Geophys. Space Phys.*, 8, 813-860.

_____ (1972). Evidence for plate tectonic regimes in the rock record. *Am. J. Sci.*, 272, 551-576.

_____ and Seely, D.R. (1979). Structure and stratigraphy of forearc regions. *Bull. Am. Ass. Petrol. Geol.*, 63, 2-31.

Dimroth, E. (1981). Labrador geosyncline : type example of early Proterozoic cratonic reactivation, 331-352. *In :* Kröner, A. (Ed.). Developments in Precambrian geology, Vol. 4 *(Precambrian plate tectonics)*. Elsevier Scientific Publishing Company, Amsterdam, 781 p.

Dobretsov, N.L., Khlestov, V.V. and Sobolev, V.S. (1973). *The facies of regional metamorphism at moderate pressures.* (Translated from russian by D.A. Brown). Aust. National University Canbera, 299p.

Drake, M.J. (1976). Plagioclase-melt equilibria. *Geochim.* cosmochim. *Acta* , 40, 457-466.

Edwards, A.C. (1976). A comparison of the methods for calculating $Fe^{+3}$ contents of clinopyroxenes from microprobe analysis. *Neues Jb. Miner. Mh.*, 11, 508-512.

Eggler, D.H. (1976). Does $CO_2$ cause partial melting in the low velocity layer of the mantle? *Geology*, 4, 69-72.

_____ and Mysen, B.O. (1977). The solubility of CO in silicate melts at high pressures. *Abstracts Prog. geol. Soc. Am.*, 9, 964.

Emslie, R.F. (1970). Upper P-T stability of a natural olivine - plagiaclase assemblage. *Carnegie Inst. Wash. Yearbook*, 69, 154-155.

Engel, A.E.J. and Engel, C.G. (1962a). Progressive metamorphism of amphibolites, northwest Adirondack mountains, New York. *Geol. Soc. Am.*, Buddington Vol., 37-82.

_____ and Engel, C.G. (1962b). Hornblendes formed during progressive metamorphism of amphibolites, northwest Adirondack mountains, New York. *Bull. geol. Soc. Am.*, 73, 1499-1514.

England, R.N. (1974). Corona structures formed by near-isochemical reaction between olivine and plagioclase in a metamorphosed dolerite. *Mineralog. Mag.*, 39, 816-818.

England, P.C. and Richardson, S.W. (1977). The influence of erosion upon the mineral facies of rocks from different metamorphic environments. *J. geol. Soc. Lond.*, 134, 201-213.

Ernst, W.G. (1966). Synthesis and stability relations of ferrotremolite. *Am. J. Sci.*, 264, 37-65.

_____ (1968). *Amphiboles : Crystal chemistry, phase relations and occurrence.* Springer-Verlag, New York, 115p.

_____ (1974). Metamorphism and ancient continental margins, 907-919. *In :* Burke, C.A. and Drake, C.L. (Eds.). *The geology of continental margins.* Springer-Verlag, Berlin, 1009p.

Esbensen, K.H. (1978). Coronites from the Fongen gabbro complex, Trondheim Region, Norway : role of water in the olivine-plagioclase reaction. Neues Jb.Miner.Abh., 132(2), 113-135.

Etheridge, M.A. (1975). Deformation and recrystallization of orthopyroxene from the Giles Complex, central Australia. *Tectonophysics*, 25, 87-114.

_____ and Wilkie, J.C. (1979). Grainsize reduction, grain boundary sliding and the flow strength of mylonites. *Tectonophysics*, 58, 159-178.

Evans, B.W., Shaw, D.M. and Haughton, D.R. (1969). Scapolite stoichiometry. *Contr. Miner. Petrol.*, 24, 293-305.

Evans, B.W. and Trommsdorff, V. (1970). Regional metamorphism of ultramafic rocks in the central Alps. Parageneses in the system CaO-MgO-$SiO_2$-$H_2O$. *Schweiz. miner. petrogr. Mitt.*, 50, 481-492.

_____ and Trommsdorff, V. (1978). Petrogenesis of garnet lherzolite, Cima Di Gagnone, Lepontine Alp. *Earth Planet. Sci. Lett.*, 40, 333-348.

Fediukova, E. and Suk, M. (1979). An example of migmatite origin by dehydrating metamorphism. *Bull. geol. Soc. Finl.*, 51, 1-9.

Ferry, J.M. and Spear, F.S. (1976). Experimental calibration of the partitioning of Fe and Mg between biotite and garnet. *Carnegie Inst. Wash. Yearbook*, 76, 579-581.

_____ and Spear, F.S. (1978). Experimental calibration of the partitioning of Fe and Mg between biotite and garnet. *Contr. Miner. Petrol.*, 66, 113-117.

Fisher, D.E. (1976). Rare gas clues to the origin of the terrestrial atmosphere. *In :* Windley B.F. (Ed.). *The early history of the Earth*, 547-556. John Wiley & Sons, London, 618p.

Fleet, M.E. (1974a). Partition of Mg and $Fe^{+2}$ in coexisting pyroxenes. *Contr. Miner. Petrol.*, 44, 251-257.

_____ (1974b). Partition of major and minor elements and equilibration in coexisting pyroxenes. *Contr. Miner. Petrol.*, 44, 259-274.

Fleuty, M.J. (1964). Tectonic slides. *Geol. Mag.*, 101, 452-456.

Frick, C. and Coetzee, C.B. (1974). The mineralogy and petrology of the sillimanite deposits west of Pofadder, Namaqualand. *Trans. geol. Soc. S. Afr.*, 77 (2), 169-184.

Frodesen, S. (1968). Coronas around olivine in a small gabbro intrusion, Bamble area, South Norway. *Norsk geol. Tidsskr.*, 48, 201-206.

Froidevaux, C. and Nataf, H.C. (1981). Continental drift : What driving mechanism? *Geol. Rdsch.*, 70(1), 166-176.

Frost, B.R. (1973). Ferroan gahnite from quartz - biotite - almandine schist, Wind River Mountains, Wyoming. *Am. Miner.*, 58, 831-834.

Frost, B.R. (1976). Limits of the assemblage forsterite-anorthite as inferred from peridotite hornfelses, Icicle Creek, Washington. *Am. Miner.*, 61, 732-750.

Fyfe, W.S. (1971). Some thoughts on granitic magmas, 201-216. *In :* Newall, G. and Rast, N. (Eds.). *Mechanisms of igneous intrusions.* Geol. J. Spec. Issue 2, Gallery Press, Liverpool.

_____ (1973). The granulite facies, partial melting and the Archaean crust. *Phil. Trans. R. Soc. Lond.*, A273, 457-461.

Gable, D.J. and Sims, P.K. (1969). Geology and regional metamorphism of some high-grade cordierite gneisses, Front Range, Colorado. *Spec. Pap. geol. Soc. Am.*, 128.

Ganguly, J. (1979). Garnet and clinopyroxene solid solutions, and geothermometry based on Fe-Mg distribution coefficient. *Geochim. cosmochim. Acta* , 43, 1021-1029.

_____ and Kennedy, G.C. (1974). The energetics of natural garnet solid solution. 1. Mixing of the aluminosilicate end-members. *Contr. Miner. Petrol.*, 48, 137-148.

Geringer, G.J. (1973). *Die geologie van die Argeiese gesteentes en jongere formasies in die gebied wes van Upington met spesiale verwysing na die verskillende granietvoorkomstes.* Unpubl. Ph.D. thesis, Univ. Orange Free State, 203p.

_____ (1979). The origin and tectonic setting of amphibolites in part of the Namaqua Metamorphic Belt, South Africa. *Trans. geol. Soc. S. Afr.*, 82, 287-303.

_____ and Botha, B.J.V. (1977). Anatektiese graniete in die mobiele gordel Namaqualand, wes van Upington. *Bull. geol. Surv. S. Afr.*, 61, 36p.

Germs, G.J.B. (1972). The stratigraphy and paleontology of the lower Nama Group, South West Africa. *Bull Precambr. Res. Unit, Univ. Cape Town*, 12, 250p.

_____ (1974). The Nama Group in South West Africa and its relationship to the Pan-African Geosyncline. *J. Geol.*, 82(3), 301-317.

Gevers, T.W., Partridge, F.C. and Joubert, G.K. (1937). The pegmatite area south of the Orange River in Namaqualand. *Mem. geol. Surv. S. Afr.*, 31, 180p.

Gevers, T.W. and Dunne, J.C. (1942). Charnockite rocks near Port Edward in Alfred County, Natal. *Trans. geol. Soc. S. Afr.*, 45, 183-213.

Ghent, E.D. (1976). Plagioclase - garnet - $Al_2 SiO_5$ - quartz : a potential geobarometer-geothermometer. *Am. Miner.*, 61, 710-714.

Gilbert, M.C. (1966). Synthesis and stability relations of the hornblende ferropargasite. *Am. J. Sci.*, 264, 698-742.

_____, Bell, P.M. and Richardson, S.W. (1969). The andalusite - sillimanite transition and the aluminium silicate triple point. *Ann.Rep. Dir. Geophys. Lab.*, 1967-1968, 135-137.

Ginsburg, R.N. and James, N.P. (1974). Holocene carbonate sediments of continental shelves, 137-155. *In :* Burk, C.A. and Drake, C.L. (Eds.). *The geology of continental margins.* Springer-Verlag, Berlin, 1009p.

Giraud, P. (1964). Essai de classification modale des roches a caractere charnockitique. *Bull. Bur. Rech. geol. min.*, 4, 1-17.

Glassley, W.E. and Sørensen, K. (1980). Constant $P_s$ - T amphibolite to granulite facies transition in Agto (West Greenland) metadolerites : Implication and application. *J. Petrology*, 21(1), 69-105.

Goldman, D.S. and Albee, A.L. (1977). Correlation of Mg/Fe partitioning between garnet and biotite with $O^{18}/O^{16}$ partitioning between quartz and magnetite. *Am. J. Sci.*, 277, 750-767.

Goldsmith, J.R. (1976). Scapolites, granulites and volatiles in the lower crust. *Bull. geol. Soc. Am.*, 87, 161-168.

_____ and Newton, R.C. (1977). Scapolite-plagioclase stability relations at high pressures and temperatures in the system $Na\ Al\ Si_3\ O_8$ - $Ca\ Al_2\ Si_2\ O_8$ - $Ca\ CO_3$ - $Ca\ SO_4$. *Am. Miner.*, 62, 1063-1081.

Gorbatschev, R. (1968). Distribution of elements between cordierite, biotite and garnet. *Neues Jb. Miner. Abh.*, 110, 57-80.

Gordon, T.M. and Greenwood, H.J. (1971). The stability of grossularite in $H_2O$ - $CO_2$ mixtures. *Am. Miner.*, 56, 1674-1688.

Grant, J.A. and Weiblen, P.W. (1971). Retrograde zoning in garnet near the second sillimanite isograd. *Am. J. Sci.*, 270, 281-296.

Green, D.H. (1964). The petrogenesis of high-temperature peridotite intrusion in the Lizard area, Cornwall. *J. Petrology*, 5, 134-188.

_____ and Ringwood, A.E. (1967). An experimental investigation of the gabbro to eclogite transformation and its petrological implications. *Geochim. cosmochim. Acta*, 31, 767-833.

_____ and Ringwood, A.E. (1972). A comparison of recent experimental data on the gabbro-garnet granulite - eclogite transition. *J. Geol.*, 80, 277-288.

Green, H.W.H. and Radcliffe, S.V. (1975). Fluid precipitates in rocks from the Earth's mantle. *Bull. geol. Soc. Am.*, 86, 846-852.

Green, T.H. (1976). Experimental generation of cordierite - or garnet - bearing granitic liquids from a pelitic composition. *Geology*, 4, 85-88.

Greenwood, H.J. (1962). Metamorphic reactions involving two volatile components. *Carnegie Inst. Wash. Yearbook*, 61, 82-85.

_____ (1963). The systhesis and stability of anthophyllite. *J. Petrology*, 4, 317-351.

_____ (1967). Wollastonite : stability in $H_2O$ - $CO_2$ mixtures and occurrence in a contact-metamorphic aureole near Salmo, British Columbia, Canada. *Am. Miner.*, 52, 1669-1680.

Grieve, R.A.F. and Gittins, J. (1975). Composition and formation of coronas in the Hadlington gabbro, Ontario, Canada. *Can. J. Earth Sci.*, 12, 289-299.

Griffen, D.T. and Ribbe, P.H. (1973). The crystal chemistry of staurolite. *Am. J. Sci.*, Cooper Vol. 273-A, 479-495.

Griffin, W.L. (1971a). Genesis of coronas in anorthosites of the Upper Jotun Nappe, Indre Sogn, Norway. *J. Petrology*, 12, 219-243.

_____ (1971b). Mineral reactions at a peridotite-gneiss contact, Jotunheimen, Norway. *Mineralog. Mag.*, 38, 435-445.

_____ (1972). Formation of eclogites and the coronas in anorthosite, Bergen Arcs, Norway. *Mem. geol. Soc. Am.*, 135, 37-63.

_____ and Heier, K.S. (1969). Parageneses of garnet in granulite-facies rocks, Lofoten-Vesteraalen, Norway. *Contr. Miner. Petrol.*, 23, 89-116.

Griffin, W.L. and Heier, K.S. (1971). The occurrence of olivine hyperite at Ødegaardens Verk, Bamble, South Norway, by M. Gloveris. *Norsk geol. Tidsskr.*, 51, 89-91.

_____ and Heier, K.S. (1973). Petrological implications of some corona structures. *Lithos*, 6, 315-335.

_____ and Råheim, A. (1973). Convergent metamorphism of eclogites and dolerites, Kristiansund area, Norway. *Lithos*, 6, 21-40.

Grobler, N.J., Botha, B.J.V. and Smit, C.A. (1977). The tectonic setting of the Koras Group. *Trans. geol. Soc. S. Afr.*, 80(3), 167-176.

Hafner, S.S., Virgo, D.and Warburton, D. (1971). Cation distributions and cooling history of clinopyroxenes from Oceanus Procellarum. *Geochim. cosmochim. Acta (Suppl. 2., Proc. 2nd Lunar Sci. Conf.)*, 1, 91-108.

Hälbich, I.W. (1962). On the morphology of the Dwyka Series in the vicinity of Loeriesfontein, Cape Province. *Ann. Univ. Stellenbosch*, 37 (A2).

_____ (1978). Minor structures in gneiss and the origin of steep structures in the Okiep Copper District, 297-322. *In :* Verwoerd, W.J. (Ed.). *Mineralization in metamorphic terranes. Spec. Publication geol. Soc. S. Afr.*, 4, 552p.

Hamm, H.M. and Vieten, K. (1971). Zur Berechnung der kristallchemischen Formel und des $Fe^{+3}$ - Gehaltes von Klinopyroxen aus Elektronenstrahl-Mikroanalysen. *Neues Jb. Miner. Mh.*, 1971, 310-314.

Hargraves, R.B. (1981). Precambrian tectonic style : a liberal uniformitarian interpretation, 21-56. *In :* Kröner, A. (Ed.). Developments in Precambrian geology, Vol. 4. *(Precambrian plate tectonics).* Elsevier Scientific Publishing Company, Amsterdam, 781p.

Hariya, Y. and Kennedy, G.C. (1968). Equilibrium study of anorthite under high pressure and high temperature. *Am. J. Sci.*, 266, 193-203.

Harte, B. and Henley, K.J. (1966). Occurrence of compositionally zoned garnets in regionally metamorphosed rocks. *Nature*, 210, 689-692.

Hatherton, T. and Dickinson, W.R. (1969). The relationship between andesitic volcanism and seismicity in Indonesia, the Lesser Antilles and other island arcs. *J. Geophys. Res.*, 74, 5301-5310.

Haughton, S.H. (1931). On a collection of fossil frogs from the clays at Banke. *Trans. R. Soc. S. Afr.*, 19, 233-249.

_____ (1969). *Geological history of Southern Africa.* Cape and Transvaal Printers Ltd., 535p.

Hawkins, J.W. (1974). Geology of the Lau Basin, a marginal sea behind the Tonga Arc, 505-520. *In :* Burk, C.A. and Drake, C.L. (Eds.). *The geology of continental margins.* Springer-Verlag, Berlin, 1009p.

Hayes, D.E. (1974). Continental margin of western South America, 581-590. *In :* Burk, C.A. and Drake, C.L. (Eds.). *The geology of continental margins.* Springer-Verlag, Berlin, 1009p.

Hays, J.F. (1967). Lime - alumina - silica. *Carnegie Inst. Wash. Yearbook*, 65, 234-239.

Hedge, C.E. (1972). Source of leucosomes of migmatites in the Front Range, Colorado. *Mem. geol. Soc. Am.*, 135, 65-72.

Heier, K.S. (1973). Geochemistry of granulite facies rocks and problems of their origin. *Phil. Trans. R. Soc. Lond.*, A273, 429-442.

Hensen, B.J. (1977). Cordierite - garnet - bearing assemblages as geothermometers and barometers in granulite facies terranes. *Tectonophysics*, 43, 73-88.

_____ and Green, D.H. (1971). Experimental study of the stability of cordierite and garnet in pelitic compositions at high pressures and temperatures. I. Compositions with excess alumina-silicate. *Contr. Miner. Petrol.*, 33, 309-330.

_____ and Green, D.H. (1972). Experimental study of the stability of cordierite and garnet in pelitic compositions at high pressures and temperatures. II. Compositions without excess alumina-silicate. *Contr. Miner. Petrol.*, 35, 331-354.

_____ and Green, D.H. (1973). Experimental study of cordierite and garnet in pelitic compositions at high pressures and temperatures. III. Synthesis of experimental data and geological applications. *Contr. Miner. Petrol.*, 38, 151-166.

Hensen, B.J., Schmid, R. and Wood, B.J. (1975). Activity - composition relations for pyrope - grossular garnet. *Contr. Miner. Petrol.*, 51, 161-166.

Hermes, O.D. (1970). Petrochemistry of coexistent mafic silicates from Mecklenburg gabbro - metagabbro complex, North Carolina. *Bull. geol. Soc. Am.*, 81, 137-164.

Herzberg, C.T. (1976a). The plagioclase/spinel-lherzolite facies boundary : its bearing on corona structure formation and tectonic history of the Norwegian Caledonides, 233-235. *In : Progress in experimental petrology.* Nat. Environment Res. Coun. Publications, London.

_____ (1976b). The lowest pressure pyralspite garnet-bearing reaction in CaO- MgO - $Al_2O_3$ - $SiO_2$; the Seiland/Ariegite subfacies boundary in simple spinel lherzolite; 235-237. *In : Progress in experimental petrology.* Nat. Environment Res. Coun. Publications, London.

Hess, H.H. (1941). Pyroxenes of common mafic magmas, part 2. *Am. Miner.*, 26, 573-594.

Hess, P.C. (1969). The metamorphic paragenesis of cordierite in pelitic rocks. *Contr. Miner. Petrol.*, 24, 191-207.

Hewins, R.H. (1975). Pyroxene geothermometry of some granulite facies rocks. *Contr. Miner. Petrol.*, 50, 205-209.

Hietanen, A. (1967). On the facies series in various types of metamorphism. *J. Geol.*, 75, 187-214.

_____ (1969). Distribution of Fe and Mg between garnet, staurolite, and biotite in aluminium-rich schist in various metamorphic zones north of the Idaho batholith. *Am. J. Sci.*, 267, 422-456.

Higgins, M.W. (1971). Cataclastic Rocks. *Prof. Pap. U.S. geol. Surv.*, 687, 97p.

Hirschberg, A. and Winkler, H.G.F. (1968). Stabilitätsbeziehungen zwischen chlorit, cordierit und Almandine bei der Metamorphose. *Contr. Miner. Petrol.*, 18, 17-42.

Hobbs, B.E. (1966). Microfabrics of tectonites from the Wyangala Dam area, New South Wales, Australia. *Bull. geol. Soc. Am.*, 77, 685-706.

Hobbs, B.E., Means, W.D. and Williams, P.F. (1976). *An outline of structural geology.* John Wiley & Sons, New York, 571p.

Hødal, J. (1945). Rocks of the anorthosite kindred in Vossestrand (Norway). *Norsk geol. Tidsskr.*, 24, 129-243.

Hoefs, J. and Touret, J. (1976). Fluid inclusions and carbon isotope study from Bamble granulites (South Norway). *Contr. Miner. Petrol.*, 52, 165-174.

Hoffmann, P. (1973). Evolution of an early Proterozoic continental margin : the Coronation geosyncline and associated aulacogens of the northwestern Canadian shield. *Phil. Trans. R. Soc. Lond.*, A 273, 547-581.

_____, Dewey, J.F. and Burke, K. (1974). Aulacogens and their genetic relation to geosynclines, with a Proterozoic example from Great Slave Lake, Canada. *In :* Dott, R.H. and Shaver, R.H. (Eds.). *Modern and ancient geosynclinal sedimentation, 38-55. Spec. Publ. Soc. Econ. Palaeont. Min.* 19.

Holdaway, M.J. (1972). Thermal stability of Al-Fe epidote as a function of $fO_2$ and Fe content. *Contr. Miner. Petrol.*, 37, 307-340.

_____ and Lee, S.M. (1977). Fe-Mg cordierite stability in high-grade pelitic rocks based on experimental, theoretical and natural observations. *Contr. Miner. Petrol.*, 63, 175-198.

Holland, D.H. (1976). The evolution of seawater. *In :* Windley B.F. (Ed.). *The early history of the Earth,* 559-567. John Wiley & Sons, London, 618p.

Hollister, L.S. (1966). Garnet zoning : an interpretation based on the Rayleigh fractionation model. *Science,* 154, 1647-1651.

_____ and Burruss, R.C. (1976). Phase equilibria in fluid inclusions from the Khtada Lake metamorphic complex. *Geochim.* cosmochim. *Acta,* 40, 163-175.

Homma, F. (1936). Classification of the zonal structure of plagioclase. *Mem. College of Science, Kyoto Imp. Univ.*, B11, 135-155.

Hoschek, G. (1976). Melting relationships of biotite + plagioclase + quartz. *Neues Jb. Miner. Mh.*, 2, 79-83.

Howells, S. and O'Hara, M.J. (1975). Palaeogeotherms and the diopside - enstatite solvus. *Nature,* 254, 406-408.

Howie, R.A. (1955). The geochemistry of the charnockite series of Madras, India. *Trans. R. Soc. Edinb.*, 62, 725-768.

_____ (1964). Charnockites. *Sci. Prog.*, 52, 628-644.

_____ (1965). The pyroxenes of metamorphic rocks. *In :* Pitcher, W.S. and Flinn, G.W. (Eds.). *Controls of metamorphism*, 319-326. Oliver & Boyd, Edinburgh, 368p.

Huang, W.L. and Wyllie, P.J. (1973). Melting relations of muscovite-granite to 35Kbar as a model for fusion of metamorphosed subducted oceanic sediments. *Contr. Miner. Petrol.*, 42, 1-14.

_____ and Wyllie, P.J. (1975). Melting reactions in the system $NaAlSi_3O_3$ - $KAlSi_3O_8$ - $SiO_2$ to 35 Kilobars, dry and with excess water. *J. Geol.*, 83, 737-748.

Hugo, P.J. (1969). The pegmatites of the Kenhardt and Gordonia Districts, Cape Province. *Mem. geol. Surv. S. Afr.*, 58, 94p.

Hunt, J.A. and Kerrick, D.M. (1977). The stability of sphene : experimental redetermination and geologic implications. *Geochim. cosmochim. Acta* , 41, 279-288.

Hurlbut, C.S. and Klein, C. (1977). *Manual of Mineralogy (19th Ed.).* John Wiley & Sons, New York, 532p.

Hutcheon, I., Froese, E. and Gordon, T.M. (1974). The assemblage quartz - sillimanite - garnet - cordierite as an indicator of metamorphic conditions in the Daly Bay Complex N.W.T. *Contr. Miner. Petrol.*, 44, 29-34.

Hutton, D.H.W. (1979). Tectonic slides : a review and reappraisal. *Earth - sci. Rev.*, 15(2), 152-172.

Hyndman, D.W. (1972). *Petrology of igneous and metamorphic rocks.* McGraw-Hill Book Company, New York, 533p.

Irving, A.J. and Green, D.H. (1970). Experimental duplication of mineral assemblages in basic inclusions of the Delegate breccia pipes. *Phys. Earth Planet. Interiors*, 3, 385-389.

I U G S Subcommission (1973). Classification and nomenclature of plutonic rocks. Recommendations. *Neues Jb. Miner. Mh.*, 1973, 149-164.

Jack, A.M. (1979). Metamorphic variations across western Namaqualand. *Ann. Rep. Precambr. Res. Unit, Univ. Cape Town*, 16, 35-46.

Jack, A.M. (1980). The geology of western Namaqualand. *Bull. Precambr. Res. Unit, Univ. Cape Town*, 29, 173p.

Jackson, M.P.A. (1976). High grade metamorphism and migmatization of the Namaqua Metamorphic Complex around Aus in the southern Namib Desert, South West Africa. *Bull. Precambr. Res. Unit, Univ. Cape Town*, 18, 299p.

_____ (1979). A major charnockite-granolite province in South-Western Africa. *Geology*, 7, 22-26.

Jakes, P. and White, A.J.R. (1972). Major and trace element abundances in volcanic rocks of orogenic areas. *Bull. geol. Soc. Am.*, 83, 29-40.

Jan, M.G. and Howie, R.A. (1980). Ortho - and clinopyroxenes from the pyroxene granulites of Swat Kohistan, northern Pakistan. *Mineralog. Mag.*, 43, 715-726.

Janardhan, A.S., Newton, R.C. and Smith, J.V. (1979). Ancient crustal metamorphism at low $P_{H_2O}$ : charnockite formation at Kabbaldurga, south India. *Nature*, 278, 511-514.

Jansen, H. (1960). The geology of the Bitterfontein area, Cape Province. *Geol. Surv. S. Afr., Expl. of sheet 253 (Bitterfontein)*.

Jenkins, D.M. and Newton, R.C. (1979). Experimental determination of the spinel peridotite to garnet peridotite inversion at 900°C and 1000°C in the system CaO - MgO - $Al_2O_3$ - $SiO_2$, and at 900°C with natural garnet and olivine. *Contr. Miner. Petrol.*, 68, 407-419.

Johnson, M.R.W. (1967). Mylonite zones and mylonite banding. *Nature*, 213, 246-247.

Joubert, P. (1971a). The regional tectonism of the gneisses of part of Namaqualand. *Bull. Precambr. Res. Unit, Univ. Cape Town*, 10, 220p.

_____ (1971b). Geological survey of part of Namaqualand and Bushmanland. *Ann. Rep. Precambr. Res. Unit, Univ. Cape Town*, 7-9, 4 - 11.

_____ (1973). The development of the gneisses of part of Namaqualand. *Spec. Publication geol. Soc. S. Afr.*, 3, 289-305.

_____ (1974a). Geological survey of Namaqualand and Bushmanland. *Ann. Rep. Precambr. Res. Unit, Univ. Cape Town*, 10-11, 24-30.

Joubert, P. (1974b). Wrench-fault tectonics in the Namaqualand Metamorphic Complex. *Bull. Precambr. Res. Unit, Univ. Cape Town*, 15, 17-23.

_____ (1974c). The gneisses of Namaqualand and their deformation. *Trans. geol. Soc. S. Afr.*, 77, 339-345.

_____ (1975). Geological map released by the Precambrian Research Unit at Geocongress '75.

_____ (1976). The relationship between the Namaqualand Metamorphic Complex and the Kheis Group. *S. Afr. J. Sci.*, 72, 312-313.

_____ (1978). The fault pattern south of Kakamas - an example of convergent wrench fault tectonics, 215-222. *In :* Verwoerd, W.J. (Ed.). *Mineralization in metamorphic terranes. Spec. Publication geol. Soc. S. Afr.*, 4, 552p.

_____ (1981). The Namaqualand Metamorphic Complex, 671-705. *In :* Hunter, D.R. (Ed.). Developments in Precambrian geology, Vol. 2. *(Precambrian of the southern hemisphere).* Elsevier Scientific Publishing Company, Amsterdam, 882p.

_____ and Kröner, A. (1972). The Stinkfontein Formation south of the Richtersveld. *Trans. geol. Soc. S. Afr.*, 75, 47-54.

_____ and Waters, D. (1980). The occurrence of kyanite at Zoutpan and metamorphism in western Namaqualand. *Ann. Rep. Precambr. Res. Unit, Univ. Cape Town*, 17, 74-87.

Kartun, K.G. (1979). *The geology of the Tantalite Valley Mafic-Ultramafic Complex and the Kum-Kum Metamorphic-Igneous Massif near Warmbad, South West Africa (Namibia).* Unpubl. Ph.D. Thesis, Univ. Cape Town, 461p.

Käse, H.R. and Metz, P. (1980). Experimental investigation of the metamorphism of siliceous dolomites. IV. Equilibrium data for the reaction : 1 diopside + 3 dolomite = 2 forsterite + 4 calcite + 2 $CO_2$. *Contr. Miner. Petrol.*, 73, 151-159.

Kerrick, D.M., Crawford, K.E. and Randazzo, A.F. (1973). Metamorphism of calcareous rocks in three roof pendants in the Sierra Nevada, California. *J. Petrology*, 14, 303-325.

Köppel, V. (1978). Lead isotope studies of stratiform ore deposits of Namaqualand northwest Cape Province, South Africa and their implications on the age of the Bushmanland Supergroup, 223-226. *In :* Zartman, R.E. (Ed.). *Short papers of the fourth International Conference on geochronology, cosmochronology, isotope geology, 1978. U.S. geol. Surv. Open File Report,* 78-701.

_____ (1980). Lead isotope studies of stratiform ore deposits of Namaqualand, N W Cape Province, South Africa, and their implications on the age of the Bushmanland Sequence. *Proc. 5th I A G O D Symp.*, 1, 195-207.

Kostyuk, E.A. and Sobolev, V.S. (1969). Paragenetic types of calciferous amphiboles of metamorphic rocks. *Lithos*, 2, 67-82.

Kretz, R. (1963). Distribution of magnesium and iron between orthopyroxene and calcic pyroxenes in natural mineral assemblages. *J. Geol.*, 71, 773-784.

_____ (1978). Distribution of Mg, Fe and Mn in some calcic pyroxene-hornblende - biotite - garnet gneisses and amphibolites from the Grenville Province. *J. Geol.*, 86(5), 599-619.

Kröner, A. (1968). The gneiss-sediment relationships northwest of Vanrhynsdorp, Cape Province. *Bull. Precambr. Res. Unit, Univ. Cape Town*, 3, 233p.

_____ (1974). The Gariep Group. Part 1. Late Precambrian formations in the western Richtersveld, Northern Cape Province. *Bull. Precambr. Res. Unit, Univ. Cape Town.*, 13, 115p.

_____ (1975). Geochronology. *Ann. Rep. Precambr. Res. Unit, Univ. Cape Town*, 13, 139-143.

_____ (1976). Proterozoic crustal evolution in parts of Southern Africa and evidence for extensive sialic crust since the end of the Archaean. *Phil. Trans. R. Soc. London*, A280, 541-553.

_____ (1977). The Precambrian geotectonic evolution of Africa. Plate accretion versus plate destruction. *Precambrian Res.*, 4, 163-213.

_____ (1979). Precambrian crustal evolution in the light of plate tectonics and the undation theory. *Geologie Mijnb.*, 58, 231-240.

Krӧner, A. (1981a). Precambrian plate tectonics, 57-90. *In :* Krӧner, A. (Ed.). Developments in Precambrian geology, Vol. 4. *(Precambrian plate tectonics).* Elsevier Scientific Publishing Company, Amsterdam, 781p.

_____ (1981b). Precambrian crustal evolution and continental drift. *Geol. Rdsch.*, 70(2), 412-428.

_____, Anhaeusser, C.R. and Vajner, V. (1973). Neue Ergebnisse zur Evolution der präkambrischen Kruste im südlichen Afrika. *Geol. Rdsch.*, 62, 281-309.

_____ and Blignault, H.J. (1976). Towards a definition of some tectonic and igneous provinces in western South Africa and southern South West Africa. *Trans. geol. Soc. S. Afr.*, 79, 232-238.

_____, Vajner, V. and Burger, A.J. (1977). Geotectonic significance of radiometric age data from the late Proterozoic Koras Group, northern Cape Province, South Africa. *9th Colloquium on African Geology, Univ. Göttingen.*

Kurat, G. and Scharbert, H.G. (1972). Compositional zoning in garnets from granulite facies rocks of the Moldanubian Zone, Bohemian Massif of lower Austria. *Earth Planet. Sci. Lett.*, 16(3), 379-387.

Kushiro, I. and Yoder, H.S. (1966). Anorthite - forsterite and anorthite - enstatite reactions and their bearing on the basalt-eclogite transformation. *J. Petrology*, 7, 337-362.

Kwak, T.A.P. (1974). Natural staurolite breakdown reactions at moderate to high pressures. *Contr. Miner. Petrol.*, 44, 57-80.

Lambert, I.B., Robertson, J.K. and Wyllie, P.J. (1969). Melting reactions in the system $KAlSi_3O_8$ - $SiO_2$ - $H_2O$ to 18.5 Kbar. *Am. J. Sci.*, 267, 609-626.

Lambert, R.S.J. (1976). Archaean thermal regimes, crustal and upper mantle temperatures and a progressive evolutionary model for the Earth, 363-376. *In :* Windley, B.F. (Ed.). *The early history of the Earth.* John Wiley & Sons, London, 618p.

Leake, B.E. (1965). The relationship between composition of calciferous amphibole and grade of metamorphism, 299-317. *In :* Pitcher, W.S. and Flinn, G.W. (Eds.). *Controls of metamorphism.* Oliver & Boyd, Edinburgh, 368p.

Leake, B.E. (1968). A catalog of analysed calciferous and sub-calciferous amphiboles together with their nomenclature and associated minerals. *Spec. Pap. geol. Soc. Am.*, 98, 210p.

_____ (1971). On aluminous and edenitic hornblendes. *Mineralog. Mag.*, 38, 389-407.

Lee, S.M. and Holdaway, M.J. (1977). Significance of Fe-Mg cordierite stability relations on temperature, pressure and water pressure in cordierite granulites, 79-94. *In :* Heacock, J.G. (Ed.). *The Earth's crust : its nature and physical properties. Am. Geophys. Union Monogr.*, 20.

Leelanandam, C. (1968). Paired pyroxenes from Kondapalli. *J. Indian geosci. Ass.*, 8, 89-92.

Lindh, A. (1975). Coexisting pyroxenes - a multivariate statistical approach. *Lithos*, 8, 151-161.

Lindsley, D.H. and Dixon, S.S. (1976). Diopside - enstatite equilibria at 850° - 1400°C, 5-35 Kb. *Am.J. Sci.*, 276, 1285-1301.

Linström, W. (1977). *Die geologie tussen Kenhardt en Marydale met spesiale verwysing na die verband tussen die Kheis - gesteentes en die Namaqualandse Mobiele Gordel.* Unpubl. D. Sc. thesis, Univ. Orange Free State.

Linthout, K. and Westra, L. (1968). Compositional zoning in almandine - rich garnets and its relation to the metamorphic history of their host rocks. *Proc. K. Ned. Akad. Wet. Amsterdam*, 71B, 297-312.

Liou, J.G. (1969). Synthesis and stability relations of prehnite. *Geol. Soc. Am. Meet. Abstr. Progr.* 135.

_____ (1973). Synthesis and stability relations of epidote, $Ca_2 Al_2 Fe Si_3 O_{12} (OH)$. *J. Petrology*, 14, 381-414.

Lipson, R.D. (1978). *Some aspects of the geology of part of the Aggeneysberge and surrounding gneisses, Namaqualand.* Unpubl. M. Sc. thesis, Univ. Witwatersrand, 100p.

_____ (1980). The granitic rocks surrounding the Aggeneysberge- a metamorphosed rapakivi suite. *Trans. geol. Soc. S. Afr.*, 83, 179-192.

Lipson, R.D. and McCarthy, T.S. (1977). Geochemical correlation between some rock-types of the Namaqualand granite-gneiss complex. *Trans. geol. Soc. S. Afr.*, 80, 177-181.

Lombaard, A.F. and Schreuder, F.J.G. (1978). Distribution pattern and general geological features of steep structures, magabreccias and basic rocks in the Okiep Copper District, 269-296. *In :* Verwoerd W.J. (Ed.). *Mineralization in metamorphic terranes. Spec. Publication geol. Soc. S. Afr.*, 4, 552p.

Loomis, T.P. (1972). Contact metamorphism of pelitic rocks by Ronda ultramafic intrusion, southern Spain. *Bull. geol. Soc. Am.*, 83, 2449-2473.

_____ (1975). Reaction zoning of garnet. *Contr. Miner. Petrol.*, 52, 285-305.

Lovering, J.F. and White, A.J.R. (1964). The significance of primary scapolite in granulitic inclusions from deep-seated pipes. *J. Petrology*, 5, 195-218.

Luth, W.C. (1967). Studies in the system KAl $SiO_4$ - $Mg_2$ $SiO_4$ - $SiO_2$ - $H_2O$. I. Inferred phase relations and petrologic applications. *J. Petrology*, 8, 372-416.

_____ (1976). Granitic rocks, 335-417. *In :* Bailey, D.K. and Macdonald, R. (Eds.). *The evolution of the crystalline rocks.* Academic Press, New York, 482p.

_____ , Jahns, R.H. and Tuttle, O.F. (1964). The granite system at pressures of 4 to 10 Kilobars. *J. Geophys. Res.*, 69, 759-773.

Lyons, J.B. and Morse, S.A. (1970). Mg/Fe partitioning in garnet and biotite from some granitic, pelitic and calcic rocks. *Am. Miner.* 55, 231-245.

Mabbutt, J.H. (1955). Erosion surfaces in Namaqualand and the ages of surface deposits in the south-western Kalahari. *Trans. geol. Soc. S. Afr.*, 58, 13-30.

Malherbe, S.J. (1979). *'n Duisend miljoen jaar in Noord-Kaapland.* Abstracts 18th Congress geol. Soc. S. Afr., 271-274.

Malm, O.A. and Ormaasen, D.E. (1978). Mangerite-charnockite intrusives in the Lofoten-Vesterålen Area, north Norway : petrography, chemistry and petrology. *Norges geol. Unders.*, 338, 83-114.

Marais, J.A.H., Packham, B. de V. and Schreuder, F.J.G. (1975). Regional geology of the O'okiep Copper District. *Abstracts 16th Congress geol. Soc. S. Afr.*, 88-89.

Martignole, J. (1979). Charnockite genesis and the Proterozoic crust. *Precambrian Res.*, 9, 303-310.

_____ and Sisi, J.C. (1981). Cordierite - garnet - $H_2O$ equilibrium, geological thermometer, barometer and water fugacity indicator. *Contr. Miner. Petrol.*, 77, 38-46.

Martin, H. (1965). *The Precambrian geology of South West Africa and Namaqualand.* Precambrian Res. Unit, Univ. Cape Town. Rustica Press (Pty) Ltd., Wynberg, 159p.

_____ and Porada, H. (1977). The intracratonic branch of the Damara Orogen in South West Africa. I. Discussion of geodynamic models. II. Discussion of relationships with the Pan-African Mobile Belt system. *Precambrian Res.*, 5,311-357.

Mason, R. (1967). Electron-probe microanalysis of coronas in a troctolite from Sulitjelma, Norway. *Mineralog. Mag.*, 36, 504-514.

Mathias, M. (1940). The occurrence of barite in an iron ore deposit in Namaqualand. *Trans. R. Soc. S. Afr.*, 28, 207-217.

Matthews, P.E. (1972). Possible Precambrian obduction and plate-tectonics in southeastern Africa. *Nature*, 240, 37-39.

_____ (1981a). Eastern or Natal sector of the Namaqua-Natal Mobile Belt in Southern Africa, 705-715. *In :* Hunter, D.R. (Ed.). Developments in Precambrian geology, Vol. 2. *(Precambrian of the southern hemisphere).* Elsevier Scientific Publishing Company, Amsterdam, 882p.

_____ (1981b). A new tectonic model for the northern region of the Namaqua-Natal belt in Natal. *Abstracts 19th Congress geol. Soc. S. Afr.*, 150-151.

Maxey, L.R. and Vogel, T.A. (1974). Compositional dependence of the coexisting pyroxene iron-magnesium distribution coefficient. *Contr. Miner. Petrol.*, 43, 295-306.

Mayhew, M.A. (1974). Geophysics of Atlantic North America, 409-427. *In :* Burk, C.A. and Drake, C.L. (Eds.). *The geology of continental margins.* Springer-Verlag, Berlin, 1009p.

McCarthy, T.S. (1976). Chemical interrelationships in a low-pressure granulite terrain in Namaqualand, South Africa, and their bearing on granite genesis and the composition of the lower crust. *Geochim. cosmochim. Acta* , 40, 1057-1068.

_____ (1978). A geochemical study of the gneisses of the Nababeep district, Namaqualand. *Spec. Publication geol. Soc. S. Afr.*, 4, 351-354.

McDaid, J.A. (1975). Preliminary report on the geology of the northern part of Diamond Area No. 1, South West Africa. *Ann. Rep. Precambr. Res. Unit, Univ. Cape Town*, 13, 89-96.

_____ (1978). The geology of the norhtern part of Diamond Area No. 1., South West Africa. *Ann. Rep. Precambr. Res. Unit, Univ., Cape Town*, 14-15, 124-140.

McIver, J.R. (1966). Orthopyroxene-bearing granitic rocks from southern Natal. *Trans. geol. Soc. S. Afr.*, 69, 99-117.

McLaren, A.C. and Retchford, J.A. (1969). Transmission electron microscope study of the dislocations in plastically deformed synthetic quartz. *Phys. Status Solidi*, 33, 657-668.

_____, Turner, P.G., Boland, J.N. and Hobbs, B.E. (1970). Dislocation structure of deformation lamellae in synthetic quartz. *Contr. Miner. Petrol.*, 29, 104-115.

_____ and Hobbs, B.E. (1972). Transmission electron microscope investigation of some naturally deformed quartzites. *Geophys. Monogr.*, 16, 55-66.

McLelland, J.M. and Whitney, P.R. (1980a). A generalized garnet-forming reaction for metaigneous rocks in the Adirondacks. *Contr. Miner. Petrol.*, 72, 111-122.

_____ and Whitney, P.R. (1980b). Compositional controls on spinel clouding and garnet formation in plagioclase of olivine metagabbros, Adirondack Mountains, New York. *Contr. Miner. Petrol.*, 73, 243-251.

McWilliams, M.O. (1981). Palaeomagnetism and Precambrian tectonic evolution of Gondwana, 649-687. *In :* Kröner, A. (Ed.). Developments in Precambrian geology, Vol. 4. *(Precambrian plate tectonics).* Elsevier Scientific Publishing Company, Amsterdam, 781p.

Medaris, L.G. (1972). High pressure peridotite in southwestern Oregon. *Bull. geol. Soc. Am.*, 83, 41-58.

Mehnert, K.R. (1968). *Migmatites and the origin of granitic rocks.* Elsevier Scientific Publishing Company, Amsterdam, 405p.

_____ (1972). (Compiler). Granulites : results of a discussion,II. *Neues Jb. Miner. Mh.*, 4, 139-150.

Merrill, R.B. (1970). Stability of titanoclinohumite and the role of water in the upper mantle. *Geol. Soc. Am. Abstr. Progr.*, 2, 620-621.

_____, Robertson, J.K. and Wyllie, P.J. (1970). Melting reactions in the system Na Al $Si_3$ $O_8$ - $KAlSi_3$ $O_8$ - $SiO_2$ - $H_2O$ to 20 Kilobars compared with results for other feldspar - quartz - $H_2O$ and rock - $H_2O$ systems. *J. Geol.*, 78, 558-569.

Metz, P. (1967). Experimentelle Bildung von Forsterit und Calcit aus Tremolit und Dolomit. *Geochim. cosmochim. Acta* ,31, 1517-1532.

_____ (1970). Experimentelle Untersuchung der Metamorphose von kieselig dolomitischen Sedimenten. II. Die Bildungsbedingungen des Diopsids. *Contr. Miner. Petrol.*, 28, 221-250.

_____ (1976). Experimental investigation of the metamorphism of siliceous dolomites. III. Equilibrium data for the reaction : 1 tremolite + 11 dolomite = 8 forsterite + 13 calcite + 9 $CO_2$ + 1 $H_2O$ for the total pressures of 3000 and 5000 bars. *Contr. Miner. Petrol.*, 58, 137-148.

Meyer, R. (1981). Geophysical characteristics of the boundaries of the Namaqua - Natal Belt. *Abstracts 19th Congress geol. Soc. S. Afr.*, 154-155.

_____ and Duvenhage, A.W.A. (1981). A regional gravity survey of part of the northwestern Cape Province. *Trans. geol. Soc. S. Afr.*, 84, 85.

Middleton, R.C. (1976). The geology of Prieska Copper Mines Limited. *Econ. Geol.*, 71, 328-350.

Mirwald, P.W. and Schreyer, W. (1977). Die stabile und metastabile Abbaureaktion von Mg-cordierit in Talk, Disthen und Quartz und ihre Abhangigkeit vom Gleichgewichtswassergehalt des Cordierits. *Fortschr.Miner.*, 55, 95-97

Misch, P. (1964). Stable association wollastonite-anorthite and other calc-silicate assemblages in amphibolite facies crystalline schists of Nanga Parbat, northwest Himalayas. *Beitr. Miner. Petrogr.*, 10, 315-356.

Miyashiro, A. (1958). Regional metamorphism of the Gosaisyo-Takanuki district in the central Abukuma Plateau. *Tokyo Univ. Fac. Sci. J.*, Sect. 2, 11, 219-272.

_____ (1973a). *Metamorphism and metamorphic belts.* George, Allen & Unwin, London, 492p.

_____ (1973b). Paired and unpaired metamorphic belts. *Tectonophysics*, 17, 241-254.

Moen, H.G.F. (1980). *Petrology and geological setting of the Wilgenhoutsdrif Formation, northern Cape Province.* Unpubl. M.Sc. thesis, Univ. Orange Free State, 287p.

Molnar, P. and Gray, D. (1979). Subduction of continental lithosphere : some constraints and uncertainties. *Geology*, 7, 58-62.

Moore, A.C. (1969). Corona textures in granulites from the Tomkinson Ranges, central Australia. *Spec. Publication geol. Soc. Aust.*, 2, 361-366.

Moore, A.E. (1979). *The geochemistry of olivine melilitites and related rocks of Namaqualand - Bushmanland, South Africa.* Unpubl. Ph. D. thesis, Univ. Cape Town, 199p.

Moore, J.M. (1977). The geology of Namiesberg, Northern Cape. *Bull. Precambr. Res. Unit, Univ. Cape Town*, 20, 69p.

_____ (1980). A study of certain paragneiss associations and their metallogenic characteristics in Namaqualand and Bushmanland. *Ann. Rep. Precambr. Res. Unit, Univ. Cape Town*, 17, 65-73.

Moore, J.N. and Kerrick, D.M. (1976). Equilibria in siliceous dolomites of the Alta aureole, Utah. *Am. J. Sci.*, 276, 502-524.

Moores, E.M. and Vine, F.J. (1971). The Troodos massif, Cyprus and other ophiolites as oceanic crust, evaluation and implications. *Phil. Trans. R. Soc. London*, A268, 443.

Mori, T. and Green, D.H. (1975). Pyroxenes in the system $Mg_2 Si_2 O_6$ - Ca $Mg Si_2 O_6$ at high pressure. *Earth. Planet.Sci. Lett.*, 26, 277-286.

Mori, T. and Green, D.H. (1976). Subsolidus equilibria between pyroxenes in the CaO-MgO-$SiO_2$system at high pressures and temperatures. *Am. Miner.*, 61, 616-626.

Morse, S.A. (1970). Alkali feldspars with water at 5 Kb. *J. Petrology*, 11, 221-251.

Murthy, M.V.N. (1958). Coronites from India and their bearing on the origin of coronas. *Bull. geol. Soc. Am.*, 69, 23-38.

Mysen, B.O., Arculus, R.J.V. and Eggler, D.H. (1975). Solubility of carbon dioxide in melts of andesite, tholeiite and olivine nephelinite composition to 30 Kbar pressure. *Contr. Miner. Petrol.*, 53, 227-239.

_____, Eggler, D.H., Seitz, M.G. and Holloway, J.R. (1976). Carbon dioxide in silicate melts and crystals. Part I - Solubility measurements. *Am. J.Sci.*, 276, 455-479.

Nehru, C.E. (1976). Pressure dependence of the enstatite limb of the enstatite-diopside solvus. *Am. Miner.* 61, 578-581.

_____ and Wyllie, P.J. (1974). Electron microprobe measurement of pyroxenes coexisting with $H_2O$ - undersaturated liquid in the join Ca Mg $Si_2$ $O_6$ - $Mg_2$ $Si_2$ $O_6$ - $H_2O$ at 30 Kilobars, with applications to geothermometry. *Contr. Miner. Petrol.*, 48, 221-228.

Nesbitt, H.W. (1980). Genesis of the New Quebec and Adirondack granulites : evidence for their production by partial melting. *Contr. Miner. Petrol.*, 72, 303-310.

Newton, R.C. (1965). The thermal stability of zoisite. *J. Geol.*, 73, 431-441.

_____ (1966). Some calc-silicate equilibrium relations. *Am. J. Sci.*, 264, 204-222.

_____ (1972). An experimental determination of the high pressure stability limits of magnesian cordierite under wet and dry conditions. *J. Geol.*, 80, 398-420.

_____ and Goldsmith, J.R. (1975). Stability of the scapolite meionite (Ca $Al_2$ $Si_2$ $O_8$ · Ca $CO_3$) at high pressures and storage of $CO_2$ in the deep crust. *Contr. Miner. Petrol.*, 49, 49-62.

Newton, R.C., Charlu, T.V. and Kleppa, O.J. (1977). Thermochemistry of high pressure garnets and clinopyroxenes in the system CaO - MgO - $Al_2O_3$ - $SiO_2$. *Geochim. cosmochim. Acta*, 41, 369-377.

_____ and Wood, B.J. (1979). Thermodynamics of water in cordierite and some petrologic consequences of cordierite as a hydrous phase. *Contr. Miner. Petrol.*, 68 (4), 391-405.

Nicolaysen, L.O. (1962). Stratigraphic interpretations of age measurements in Southern Africa. *Geol. Soc. Am.*, Buddington Vol.,569-598.

_____ and Burger, A.J. (1965). Note on an extensive zone of 1000 million-year old metamorphic and igneous rocks in Southern Africa. *Sci. de la Terre.*, 10, 497-518.

Nisbet, C.E. and Pearce, J.A. (1977). Clinopyroxene composition in mafic lavas from different tectonic settings. *Contr. Miner. Petrol.*, 63, 149-160.

Nitsch, K.H. and Winkler, H.G.F. (1965). Bildungsbedingungen von Epidot und Orthozoisit. *Beitr. Miner. Petrogr.*, 11, 470-486.

Obata, M. (1976). The solubility of $Al_2O_3$ in orthopyroxenes in spinel and plagioclase peridotites and spinel pyroxenite. *Am. Miner.*, 61, 804-816.

_____ and Thompson, A.B. (1981). Amphibole and chlorite in mafic and ultramafic rocks in the lower crust and upper mantle. A theoretical approach. *Contr. Miner. Petrol.*, 77, 74-81.

Olimpio, J.C. and Anderson, D.E. (1978). The relationship between chemical and textural (optical) zoning in metamorphic garnets, South Morar, Scotland. *Am. Miner.*, 63, 677-689.

Oliver, R.L. and Schultz, P.K. (1968). Colour in charnockites. *Mineralog. Mag.*, 36, 1135-1138.

Ormaasen, D.E. (1977). Petrology of the Hopen mangerite-charnockite intrusion, Lofoten, north Norway. *Lithos*, 10, 291-310.

Orville, P.M. (1972). Plagioclase cation exchange equilibria with aqueous chloride solution : results at 700°C and 2000 bars in the presence of quartz. *Am. J. Sci.*, 272, 234-272.

_____ (1975). Stability of scapolite in the system Ab - An - Na Cl - $CaCO_3$ at 4 Kb and 750°C. *Geochim. cosmochim. Acta*, 39, 1091-1105.

Oxburgh, E.R. (1975). Plate collisions,41-45. *In : Geodynamics today. A review of the Earth's dynamic processes. R.Soc. Lond.*,197p.

Paizes, P.E. (1975). *The geology of an area between Vaalkop and Aggeneys, in the vicinity of Pofadder, north-western Cape Province.* Unpubl. M.Sc. thesis, Univ. Witwatersrand, 220p.

Papike, J.J., Cameron, K.L. and Baldwin, K. (1974). Amphiboles and pyroxenes : characterization of other than quadrilateral components and estimates of ferric iron from microprobe data. *Geol. Soc. Am. Abstr. Progr.*, 6, 1053-1054.

Parras, K. (1958). On the charnockites in the light of highly metamorphic rock complex in southwestern Finland. *Bull. Comm. geol. Finl.*, 181, 137p.

Perchuk, L.L. (1970). Equilibrium of biotite with garnet in metamorphic rocks. *Geochemistry Int.*, 7, 157-179.

_____ (1977). Thermodynamic control of metamorphic processes, 285-352. *In :* Saxena, S.K. and Bhattacharji, S. (Eds.). *Energetics of geological processes.* Springer-Verlag, New York.

Petersen, J.S. (1980). Rare-earth element fractionation and petrogenetic modelling in charnockitic rocks, S.W. Norway. *Contr. Miner. Petrol.*, 73, 161-172.

Phillips, G.N. (1980). Water activity changes across an amphibolite-granulite facies transition, Broken Hill, Australia. *Contr. Miner. Petrol.*, 75, 377-386.

Pichamuthu, C.S. (1953). The charnockite problem. *Mysore Geologists' Association, Bangalore,* 178p.

Pike, D.R. (1959). *The monazite deposits of the Vanrhynsdorp Division, Cape Province.* Unpubl. M. Sc. thesis, Univ. Pretoria.

Piper, J.D.A. (1974). Proterozoic crustal distribution, mobile belts and apparent polar movement. *Nature,* 251, 381-384.

_____ (1976). Palaeomagnetic evidence for a Proterozoic super-continent. *Phil. Trans. R. Soc. Lond.*, A280, 469-490.

_____, Briden, J.C. and Lomax, K. (1973). Precambrian Africa and South America as a single continent. *Nature,* 245, 244-248.

Pistorius, C.W.F.T. and Kennedy, G.C. (1960). Stability relations of grossularite and hydrogrossularite at high temperatures and pressures. *Am. J. Sci.*, 258, 247-257.

Poldervaart, A. and von Backström, J.W. (1949). A study of an area at Kakamas (Cape Province). *Trans. geol. Soc. S. Africa.*, 52, 433-495.

_____ and Hess, H.H. (1951). Pyroxenes in the crystallization of basaltic magmas. *J. Geol.*, 59, 472-489.

Powell, M. and Powell, R. (1977). Plagioclase - alkali feldspar geothermometry revisited. *Mineralog. Mag.*, 41, 253-256.

Pretorius, D.A. (1974). The structural boundary between the Kaapvaal and Sonama crustal provinces. *Inf. Circ. Econ. geol. Res. Unit, Univ. Witwatersrand*, 88, 27p.

_____ (1979). The crustal architecture of southern Africa. Alex L. du Toit Mem. Lect., 13. *Geol. Soc. S. Afr.*, Annex. to Vol. 76, 60p.

Raase, P. (1974). Al and Ti contents of hornblende, indicators of pressure and temperature of regional metamorphism. *Contr. Miner. Petrol.*, 45, 231-236.

Råheim, A. and Green, D.H. (1974). Experimental determination of the temperature and pressure dependence of the Fe-Mg partition coefficient for coexisting garnet and clinopyroxene. *Contr. Miner. Petrol.*, 48, 179-202.

Ramaswamy, A. and Murty, M.S. (1973). Ortho- and clinopyroxenes from the charnockite series of Amaravathi, Andhra Pradesh, South India. *Mineralog. Mag.*, 39, 74-77.

Ramberg, H. and de Vore, G. (1951). The distribution of $Fe^{+2}$ and $Mg^{+2}$ in co-existing olivines and pyroxenes. *J. Geol.*, 59, 193-210.

Ramsay, J.G. (1967). *Folding and fracturing of rocks.* McGraw-Hill Book Company, New York, 568p.

_____ (1980). Shear zone geometry : a review. *J. Struct. Geol.*, 2 (1/2), 83-99.

_____ and Graham, R.H. (1970). Strain variation in shear belts. *Can. J. Earth-sci.*, 7, 786-813.

Ravoir, E. and Hinrichsen, T. (1975). Upper stability of synthetic anthophyllite mixed crystals. *Neues Jb. Miner. Mh.*, 4, 162-166.

Ray, S. and Sen, S.K. (1970). Partitioning of major exchangeable cations among orthopyroxene, calcic pyroxene and hornblende in basic granulites from Madras. *Neues Jb. Miner. Abh.*, 114, 61-88.

Reid, D.L. (1974). Preliminary report on the petrologic studies of volcanic and intrusive rocks in the Vioolsdrif region, lower Orange River, 57-68. *In :* Kröner, A. (Ed.). *Contributions to the Precambrian geology of Southern Africa. Bull. Precambr. Res. Unit, Univ., Cape Town,* 15, 213p.

_____ (1977). Geochemistry of Precambrian igneous rocks in the lower Orange River region. *Bull Precambr. Res. Unit, Univ., Cape Town,* 23, 397p.

_____ (1979a). Total rock Rb - Sr and U - Th - Pb isotopic study of Precambrian metavolcanic rocks in the lower Orange River region, Southern Africa. *Earth Planet. Sci. Lett.*, 42, 368-378.

_____ (1979b). Age relationships within the Mid-Proterozoic Vioolsdrif Batholith, lower Orange River region. *Trans. geol. Soc. S. Afr.*, 82, 305-311.

_____ (1981). Sm - Nd ages from the Namaqua and Richtersveld Provinces. *Abstracts 19th Congress geol. Soc. S. Afr.*,173-174.

_____ (1982 in press). Age relationships within the Vioolsdrif Batholith lower Orange River region. II. A two stage emplacement history and the extent of Kibaran overprinting. Submitted to *Trans. geol. Soc. S. Afr.*

_____ and Barton, E.S. (1982 in press). Geochemical characterization of granitoids in the Namaqualand Geotraverse. Submitted to *N G P, Namaqualand Volume.*

Reinhard, E.W. (1968). Phase relations in cordierite - bearing gneisses from the Gananoque area, Ontario. *Can. J. Earth Sci.*, 5, 455-482.

Renard, V. and Mascle, J. (1974). Eastern Atlantic continental margins : various structural and morphological types, 285-291. *In :* Burk, C.A. and Drake, C.L. (Eds.). *The geology of continental margins.* Springer-Verlag, Berlin, 1009p.

Rennie, J.V.L. (1931). Note on fossil leaves from the Banke clays. *Trans. R. Soc. S. Afr.*, 19, 251-253.

Reuning, E. (1931). Contribution to the geology and palaeontology of the Bushmanland Plateau. *Trans. R. Soc. S. Afr.*, 19, 215-232.

Reynolds, R.C. and Fredrickson, A.F. (1962). Corona development in Norwegian hyperites and its bearing on the metamorphic facies concept. *Bull. geol. Soc. Am.*, 73, 59-71.

Rice, J.M. (1973). Phase equilibria and chemistry of metamorphosed impure dolomite, Ross Lake, Washington. *Geol. Soc. Am. Abstr. Progr.*, 5, 96.

_____ (1977). Contact metamorphism of impure dolomitic limestone in the Boulder aureole, Montana. *Contr. Miner. Petrol.*, 59, 237-259.

_____ (1980). Phase equlibria involving humite minerals in impure dolomitic limestones. Part I. Calculated stability of clinohumite. *Contr. Miner. Petrol.*, 71, 219-235.

Richardson, S.W. (1968). Staurolite stability in a part of the system Fe - Al - Si - O - H. *J. Petrology*, 9(3), 467-488.

_____, Bell, P.M. and Gilbert, M.C. (1968). Kyanite - sillimanite equilibrium between 700° and 1500°C. *Am. J. Sci.*, 266, 513-541.

_____, Gilbert, M.C. and Bell, P.M. (1969). Experimental determination of kyanite - andalusite and andalusite - sillimanite equilibria; the aluminium silicate triple point. *Am. J. Sci.*, 267, 259-272.

Ringwood, A.E. (1975). *Composition and petrology of the Earth's mantle.* McGraw-Hill, New York, 618p.

_____ and Green, D.H. (1964). Experimental investigations bearing on the nature of the Mahorovicic discontinuity. *Nature*, 201, 566-567.

_____ and Green, D.H. (1966). An experimental investigation of the gabbro-eclogite transformation and some geophysical implications. *Tectonophysics*, 3 (5), 383-427.

Ritter, U. (1980). The Precambrian evolution of the eastern Richtersveld. *Bull. Precambr. Res. Unit, Univ., Cape Town*, 26, 276p.

Robie, R.A. and Waldbaum, D.R. (1968). Thermodynamic properties of minerals and related substances at 298. 15°K (25.0°C) and one atmosphere (1.013 bars) pressure and at higher temperatures. *U.S. geol. Surv. Bull.*, 1259, 256p.

_____, Hemmingway, B.S. and Fischer, J.R. (1978). Thermodynamic properties of minerals and related substances at 298.15K and 1 bar ($10^5$ Pascals) pressure and at higher temperatures. *U.S. geol. Surv. Bull.*, 1452.

Robin, P.Y.F. (1979). Theory of metamorphic segregation and related processes. *Geochim. cosmochim. Acta* , 43, 1587-1600.

Rogers, A.W. (1911). The Kheis Series. *Trans. geol. Soc. S. Afr.*, 13 (1910), 93-104.

_____ (1912). Report on the geological survey of parts of the Divisions of Van Rhyn's Dorp and Namaqualand. *Ann. Rep. geol. Comm. Cape Good Hope*, 16 (1911), 7 - 85.

_____ (1913). The Nama System in the Cape Province. *Trans. geol. Soc. S. Afr.*, 15, 31-50.

_____ (1916). The nature of the copper deposits of Little Namaqualand. *Proc. geol. Soc. S. Afr.*, 19, XXI - XXXV.

_____ and Schwarz, E.H.L. (1900). Geology of the Orange River Valley in the Hope Town and Prieska Districts. *Ann. Rep. geol. Comm. Cape Good Hope*, 4, 67-97.

_____ and du Toit, A.L. (1910). Report on the geology of parts of Kenhardt, Prieska, Victoria West and Carnarvon. *Ann. Rep. geol. Comm. Cape Good Hope*, 14, 8-108.

Rollinson, H.R., Windley, B.F. and Ramakrishnan, M. (1981). Contrasting high and intermediate pressures of metamorphism in the Archaean Sargur Schists of Southern India. *Contr. Miner. Petrol.*, 76, 420-429.

Roy, D.M. and Roy, R. (1957). System CaO - $Al_2O_3$ - $SiO_2$ - $H_2O$. The grossularite - 3 CaO - $Al_2O_3$ - 6 $H_2O$ join. *Bull. geol. Soc. Am.*, 68, 1788 - 1789.

Rozendaal, A. (1978). The Gamsberg zinc deposit, Namaqualand. *In :* Verwoerd, W.J. (Ed.) *Mineralization in metamorphic terranes. Spec. Publication geol. Soc. S. Afr.*, 4, 235-265.

S A C S (1980). South African Committee for Stratigraphy (S A C S), 1980. Stratigraphy of South Africa. Part 1 (Comp. L.E. Kent). Lithostratigraphy of the Republic of South Africa, South West Africa/Namibia, and the Republics of Bophuthatswana, Transkei and Venda. *Handb. geol. Surv. S. Afr.*, 8.

Sapountzis, E.S. (1975). Coronas from the Thessaloniki gabbro (North Greece). *Contr. Miner. Petrol.*, 51. 197 - 203.

Saxena, S.K. (1968a). Crystal-chemical aspects of distribution of elements among certain coexisting rockforming silicates. *Neues Jb. Miner. Abh.*, 108, 292-323.

_____ (1968b). Distribution of iron and magnesium between co-existing garnet and clinopyroxene in rocks of varying metamorphic grade. *Am. Miner.*, 53, 2018-2024.

_____ (1969). Silicate solid solution and geothermometry : III. Distribution of Fe and Mg between coexisting garnet and biotite. *Contr. Miner. Petrol.*, 22, 259-267.

_____ (1979). Garnet-clinopyroxene geothermometer. *Contr. Miner. Petrol.*, 70, 229-235.

_____ and Hollander, N.B. (1969). Distribution of iron and magnesium among coexisting biotite, garnet and cordierite. *Am. J. Sci.*, 267, 210-216.

_____ and Ghose, S. (1971). $Mg^{+2}$ - $Fe^{+2}$ order - disorder and the thermodynamics of the orthopyroxene- crystalline solution. *Am. Miner.*, 56, 532-559.

Schmid, R. and Wood, B.J. (1976). Phase relationships in granulite metapelites from the Ivrea-Verbano zone (Northern Italy). *Contr. Miner. Petrol.*, 54, 255-279.

Scholl, D.W. (1974). Sedimentary sequences in the North Pacific trenches, 493-504. *In* : Burk, C.A. and Drake, C.L. (Eds.). *The geology of continental margins.* Springer-Verlag, Berlin, 1009p.

Schreyer, W. and Yoder, H.S. (1964). The system Mg - cordierite - $H_2O$ and related rocks. *Neues Jb. Miner. Abh.*, 101, 271 - 342.

Schuiling, R.P. and Vink, B.W. (1967). Stability relations of some titanium minerals (sphene, perovskite, rutile and anatase). *Geochim. cosmochim. Acta* , 31, 2399-2411.

Selverstone, J. and Hollister, L.S. (1980). Cordierite-bearing granulites from the coast ranges British Columbia : P - T conditions of metamorphism. *Can. Miner.*, 18, 119-129.

Sen, S.K. (1970). Magnesium-iron compositional variance in hornblende-pyroxene granulites. *Contr. Miner. Petrol.*, 29, 76-88.

_____ and Chakraborty, K.R. (1968). Magnesium-iron exchange in garnet-biotite and metamorphic grade. *Neues Jb. Miner. Abh.*, 108,181-207.

_____ and Ray, S. (1971). Breakdown reactions for natural hornblendes in granulite facies. *Neues Jb. Miner. Abh.*, 114(3), 301-319.

_____ and Ray, S. (1972). Hornblende - pyroxene granulites versus pyroxene granulites : a study from the type charnockite area. *Neues Jb. Miner. Abh.*, 115, 291-314.

Shackleton, R.M. (1973a). Problems of the evolution of the continental crust. *Phil. Trans. R. Soc. Lond.*, A273, 317-320.

_____ (1973b). Correlation of structures across Precambrian orogenic belts in Africa, 1011-1033. *In :* Tarling, D.H. and Runcorn S.K. (Eds.). *Implications of continental drift to the earth sciences.* Academic Press, New York, 1184p.

Shand, S.J. (1945). Coronas and coronites. *Bull. geol. Soc. Am.*, 56, 247-266.

Shaw, D.M. (1960a). The geochemistry of scapolite. Part I. Previous work and general mineralogy. *J. Petrology*, 1, 218-260.

_____ (1960b). The geochemistry of scapolite. Part II. Trace elements, petrology and general geochemistry. *J. Petrology*, 1, 261-285.

Sheridan, R.E. (1974). Atlantic continental margin of North America,391-407, *In:*Burk, C.A. and Drake, C.L. (Eds.). *The geology of continental margins.* Springer-Verlag, Berlin, 1009p.

Shido, F. (1958). Plutonic and metamorphic rocks of the Nakoso and Iritono districts in the central Abukuma Plateau. *Tokyo Univ. Fac. Sci. J.*, Sect. 2, 11, 131-217.

Sibson, R.H. (1977). Fault rocks and fault mechanisms. *J. geol. Soc. London*, 133, 191-213.

Siesser, W.G., Scrutton, R.A. and Simpson, E.S.W. (1974). Atlantic and Indian Ocean margins of Southern Africa, 641-654. *In :* Burk, C.A. and Drake, C.L. (Eds.). *The geology of continental margins.* Springer-Verlag, Berlin, 1009p.

Simpson, E.S.W. and Tregidga, J.A. (1956). The Archaean rocks of the Marble Delta district, Natal. *Trans. geol. Soc. S. Afr.*, 59, 237-258.

Skippen, G.B. (1971). Experimental data for reactions in siliceous marbles. *J. Geol.*, 79, 457-481.

_____ (1974). An experimental model for low pressure metamorphism of siliceous dolomitic marble. *Am. J. Sci.*, 274, 487-509.

Slaughter, J., Kerrick, D.M. and Wall, V.J. (1975). Experimental and thermodynamic study of equilibria in the system Ca O - MgO - Si $O_2$ - $H_2$ O - $CO_2$. *Am. J. Sci.*, 275, 143-162.

Smit, C.A. (1977). *Die geologie rondom Groblershoop, met spesiale verwysing na die verband tussen die Namakwalandse Mobiele Gordel en Matsap-Kheisgesteentes.* Unpubl. Ph.D. thesis, Univ., Orange Free State.

Smith, J.V. (1974). *Feldspar minerals Vol. 1, 2 and 3.* Springer-Verlag, Berlin.

Söhnge, P.G. (1950). The tungsten mine near Nababeep, South Africa. *Am. Miner.*, 35, 931-940.

Spear, F.S. (1981). An experimental study of hornblende stability and compositional variability in amphibole. *Am. J. Sci.*, 281, 697-734.

Spry, A.H. (1969). *Metamorphic textures.* Pergamon Press, London, 350p.

Starmer, I.C. (1969). Basic plutonic intrusions of the Risør-Sondeled area, South Norway. The original lithologies and their metamorphism. *Norsk geol. Tidsskr.*, 49, 403-431.

Steiner, J.C., Jahns, R.H. and Luth, W.C. (1975). Crystallization of alkali feldspar and quartz in the haplogranite system Na Al $Si_3$ $O_8$ - KA1 $Si_3$ $O_8$ - $SiO_2$ - $H_2$ O at 4 Kbar. *Bull. geol. Soc. Am.*, 86, 83 - 98.

Steuhl, H.H. (1962). Die experimentelle Metamorphose und Anatexis eines Parabiotitgneisses aus dem Schwarzwald. *Chem. Erde.*, 21, 413-449.

Stoddard, E.F. (1976). Sillimanite - spinel segregations in granulite facies metapelites and a possible breakdown reaction of staurolite. *Geol. Soc. Am. Abstr. Progr.*, 8, 1125.

_____ (1979). Zinc-rich hercynite in high-grade metamorphic rocks : a product of the dehydration of staurolite. *Am. Miner.*, 64, 736 - 741.

Stormer, J.C. (1975). A practical two-feldspar geothermometer. *Am. Miner.*, 60, 667-674.

_____ and Whitney, J.A. (1977). Two-feldspar geothermometry in granulite facies metamorphic rocks. *Contr. Miner. Petrol.*, 65, 123-133.

Storre, B. (1970). Stabilitätsbeziehungen Grossular-führender Paragenesen im System Ca O - $Al_2O_3$ - $SiO_2$ - $CO_2$ - $H_2O$. *Contr. Miner. Petrol.*, 29, 145-162.

_____ (1972). Dry melting of muscovite + quartz in the range $P_s$ = 7 Kb. to $P_s$ = 20 Kb. *Contr. Miner. Petrol.*, 37, 87-89.

_____ and Karotke, E. (1971). An experimental determination of the upper stability limit of muscovite + quartz in the range 7 - 20Kb. water pressure. *Neues Jb. Miner. Mh.*, 1971, 237-240.

_____ and Karotke, E. (1972). Experimental data on melting reactions of muscovite + quartz in the system $K_2O$ - $Al_2O_3$ - $SiO_2$ - $H_2O$ to 20 Kb water pressure. *Contr. Miner. Petrol.*, 36(4), 343-345.

Stowe, C.W. (1979). The Upington Geotraverse National Geodynamics Project - 1979. Progress report and outline of macrostructure. *Ann. Rep. Precambr. Res. Unit, Univ., Cape Town*, 16, 20-34.

_____ (1980). Preliminary report on geodynamics in the Upington Geotraverse. *Ann. Rep. Precambr. Res. Unit, Univ., Cape Town*, 17, 24-48.

_____ (1981). The Upington Geotraverse and its implications for craton margin tectonics. *Abstracts 19th Congress geol. Soc. S. Afr.*, 208-209.

Stowe, C.W. (1982 - in press). Early Proterozoic terranes in Southern Africa. *Ann. Rep. Precambr. Res. Unit, Univ., Cape Town.*

Stowe, C.W. (in press). The Upington Geotraverse and its implications for craton margin tectonics. *Namaqualand Volume, National Geodynamics Project, Spec. Publ. geol Soc. S. Afr.*

Streckeisen, A.L. (1976). To each plutonic rock its proper name. *Earth-sci. Rev.*, 12, 1-33.

Strens, R.G.J. (1965). Stability and relations of the Al-Fe epidotes. *Mineralog. Mag.*, 35, 464-475.

_____ (1968). Reconnaissance of the prehnite stability field. *Mineral. Mag.*, 36, 864-867.

Stumpfl, E.F., Clifford, T.N., Burger, A.J. and van Zyl, P. (1976). The copper deposits of the O'okiep District, South Africa. New data and concepts. *Miner. Deposita* , 11, 46-70.

Sutton, J. (1965). Some recent advances in our understanding of the controls of metamorphism, 22-45. *In:*Pitcher, W.S. and Flinn, G.W. (Ed.). *Controls of metamorphism.* Oliver & Boyd, Edinburgh, 368p.

_____ and Watson, J.V. (1974). Tectonic evolution of continents in early Proterozoic times. *Nature*, 247, 433-435.

Swift, D.J.P. (1974). Continental shelf sedimentation, 117-135. *In :* Burk, C.A. and Drake, C.L. (Eds.). *The geology of continental margins.* Springer-Verlag, Berlin, 1009p.

Taljaard, M.S. (1937). South African melilite basalts and their relations. *Trans. geol. Soc. S. Afr.*, 39 (1936), 281-316.

Tarney, J. and Windley, B.F. (1977). Chemistry, thermal gradients and evolution of the lower continental crust. *J. geol. Soc. Lond.*, 134, 153-172.

Theart, H.F.J. (1980). The geology of the Precambrian terrane in parts of Western Namaqualand. *Bull. Precambr. Res. Unit, Univ., Cape Town*, 30, 103p.

Theron, J.N. and Blignault, H.J. (1975). A model for the sedimentation of the Dwyka glacials in the Southwestern Cape. *In :* Campbell, K.S.W. (Ed.). *Gondwana Geology : papers from the 3rd Gondwana Symposium*, 347-356. Aust. Nat. Univ. Press.

Thompson, A.B. (1976a). Mineral reactions in pelitic rocks. I. Prediction of P - T - X (Fe - Mg) phase relations. *Am. J. Sci.*, 276, 401-424.

_____ (1976b). Mineral reactions in pelitic rocks. II. Calculation of some P - T - X (Fe - Mg) phase relations. *Am. J. Sci.*, 276, 425-454.

Thompson, J.B. (1957). The graphical analysis of mineral assemblages in pelitic schists. *Am. Miner.*, 42, 842-858.

_____ and Waldbaum, D.R. (1969). Mixing properties of sanidine crystalline solutions. III. Calculations based on two phase data. *Am. Miner.*, 54, 811-838.

Tobi, A.C. (1971). The nomenclature of the charnockitic rock suite. *Neues Jb. Miner. Mh.*, 1971, 193-205.

_____ (1972). The nomenclature of the charnockitic rock suite : reply to a discussion. *Neues Jb. Miner. Mh.*, 2, 78-79.

Tobisch, O.T. (1966). Large-scale basin-and-dome pattern resulting from the interference of major folds. *Bull. geol. Soc. Am.*, 77, 393-408.

Toksöz, M.N. and Bird, P. (1977). Modelling of temperatures in continental convergence zones. *Tectonophysics*, 41, 181-193.

Toogood, D.J. (1976). Structural and metamorphic evolution of a gneiss terrain in the Namaqua Belt near Onseepkans, South West Africa. *Bull. Precambr. Res. Unit, Univ., Cape Town*, 19, 189p.

Torske, T. (1972). The nomenclature of the charnockitic rock suite : a discussion. *Neues Jb. Miner. Mh.*, 2, 74-77.

Touret, J. (1971). Le facies granulite en Norvege meridionale : II Les inclusions fluides. *Lithos*, 4, 423-436.

_____ (1972). Le facies granulite en Norvege meridionale et les inclusions fluide : paragneiss et quartzites. *Sci. Terre Nancy*, 17 (1/2), 179-193.

_____ (1974). Facies granulite et fluides carboniques. *Ann. Soc. geol. Belgique.*, Vol. P. Michot., 267-287.

_____ (1977). The significance of fluid inclusions in metamorphic rocks. *In :* Fraser D.G. (Ed.). *Thermodynamics in geology*, 203-227. D. Reidel Publishing Company, Dortrecht.

Tracy, R.J., Robinson, P. and Thompson, A.B. (1976). Garnet composition and zoning in the determination of temperature and pressure of metamorphism, central Massachussetts. *Am. Miner.*, 61, 762-775.

Trommsdorff, V. (1966). Beobachtungen zur Paragenese Forsterit (Klinohumit, Kondrodit) - Klinochlor in metamorphen Dolomitgesteinen des Lepontins. *Schweiz. miner. petrogr. Mitt.*, 46, 421-429.

Truswell, J.F. (1977). *The geological evolution of South Africa.* Purnell & Sons (Pty) Ltd., 218p.

Tullis, J., Christie, J.M. and Griggs, D.T. (1973). Microstructures and preferred orientations of experimentally deformed quartzites. *Bull. geol. Soc. Am.*, 84, 297-314.

Turcotte, D.L. and Oxburgh, E.R. (1972). Mantle convection and the new global tectonics. *Ann. Rev. Fluid Mech.*, 4, 33-68.

_____ and Schubert, G. (1973). Frictional heating of the descending lithosphere. *J. Geophys. Res.*, 78, 5876-5886.

Turner, F.J. (1968). *Metamorphic petrology, mineralogical and field aspects.* McGraw-Hill Book Company, New York, 403p.

_____ and Weiss, L.E. (1963). *Structural analysis of metamorphic tectonites.* McGraw-Hill Book Company, New York, 545p.

Tuttle, O.F. and Bowen, N.L. (1958). Origin of granite in the light of experimental studies in the system Na Al $Si_3 O_8$ - K Al $Si_3 O_8$ - Si $O_2$ - $H_2O$. *Mem. geol. Soc. Am.*, 74, 153p.

Urien, C.M. and Ewing, M. (1974). Recent sediments and environment of southern Brazil, Uruguay, Buenos Aires and Rio Negro continental shelf, 157-177. *In:* Burke, C.A. and Drake, C.L. (Eds.). *The geology of continental margins.* Springer-Verlag, Berlin, 1009p.

Vajner, V. (1974). The tectonic development of the Namaqua Mobile Belt and its Foreland in parts of the Northern Cape. *Bull. Precambr. Res. Unit, Univ. Cape Town*, 14, 201p.

Van Aswegen, G. (1981). The metamorphic development within the Namaqualand Geotraverse. *Abstracts 19th Congress geol. Soc. S. Afr.*, 211-212.

Van Bever Donker, J.M. (1980). Structural and metamorphic evolution of an area around Kakamas and Keimoes, Cape Province, South Africa. *Bull. Precambr. Res. Unit, Univ. Cape Town*, 28, 165p.

Van der Westhuizen, W.A. (1977). *Die geologie van die gebied Poortjie 3022B in die distrikte Britstown, Carnarvon, Prieska en Victoria-Wes, Noord-Kaapland.* Unpubl. M. Sc. thesis, Univ. Orange Free State.

Van Lamoen, H. (1979). Coronas in olivine gabbros and iron ores from Susimäki and Ruittamaa, Finland. *Contr. Miner. Petrol.*, 68, 259-268.

Van Niekerk, C.B. and Burger, A.J. (1967). Radiometric dating of the Koras Formation. *Ann. geol. Surv. S.Afr.*, 6, 77-82.

Van Zijl, J.S.V. (1978). The relationship between the deep electrical resistivity structure and tectonic provinces in Southern Africa. Part 1. Results obtained by Schlumberger soundings. *Trans. geol. Soc. S. Afr.*, 81, 129-142.

Van Zyl, C.Z. (1981). Structural and metamorphic evolution in the transitional zone between craton and mobile belt, Upington Geotraverse. *Bull. Precambr. Res. Unit, Univ. Cape Town*, 31, 243p.

Van Zyl, D. (1967). The geology of the O'okiep Copper Mine, Namaqualand. *Ann. Univ. Stellenbosch, Ser. A.*, 42(1), 1-68.

Vernon, R.H. (1972). Reactions involving hydration of cordierite and hypersthene. *Contr. Miner. Petrol.*, 35, 125-137.

_____ (1974). Controls of mylonite compositional layering during non-cataclastic ductile deformation. *Geol. Mag.*, 111, 121-123.

_____ (1976). *Metamorphic processes, reactions and microstructure development.* George Allen & Unwin Ltd., London, 247p.

Virgo, D. and Hafner, S. (1969). $Fe^{+2}$, Mg order-disorder in heated orthopyroxenes. *Spec. Pap. Miner. Soc. Am.*, 2, 67-81.

_____ and Hafner, S. (1970). $Fe^{+2}$, Mg order-disorder in natural orthopyroxenes. *Am. Miner.*, 55, 201-223.

Von Backström, J.W. (1950). Notes on a tungsten-tin deposit near Upington, Gordonia District. *Trans. geol. Soc. S. Afr.*, 53, 35-51.

Von Backström, J.W. (1962). The geology along the lower reaches of the Molopo River and a note on the Riemvasmaak thermal spring, Gordonia District, Cape Province. *Ann. geol. Surv. S. Afr.*, 1, 57-66.

_____ (1964). The geology of an area around Keimoes, Cape Province, with special reference to phacoliths of charnockitic adamellite - porphyry. *Mem. geol. Surv. S. Afr.*, 53, 218p.

_____ (1967). The geology and mineral deposits of the Riemvasmaak area, northwest Cape Province. *Ann. geol. Surv. S. Afr.*, 6, 43-51.

_____ (1973). Pegmatite deposits in the Republic of South Africa. *S. Afr. Atomic Energy Board Pel.*, 227.

_____ and de Villiers, J. (1972). The geology along the Orange River valley between Onseepkans and the Richtersveld. Explan. Sheets 2817D (Vioolsdrif), 2818C and D (Goodhouse) and 2819C (Onseepkans). *Geol. Surv. Dep. Min. S. Afr.*, 101p.

Von Huene, R. (1974). Modern trench sediments, 207-211. *In:* Burk, C.A. and Drake, C.L. (Eds.). *The geology of continental margins.* Springer-Verlag, Berlin, 1009p.

Von Platen, H. (1965). Experimental anatexis and genesis of migmatites, 203-218. *In:* Pitcher, W.S. and Flinn, G.W. (Eds.). *Controls of metamorphism.* Oliver and Boyd, Edinburgh, 368p.

_____ and Höller, N. (1966). Experimentelle Anatexis des Stainzer Plattengneises von der Koralpe, Steiermark, bei 2, 4, 7 und 10 Kb $H_2O$ - Druck. *Neues Jb. Miner. Abh.*, 106, 106-130.

Wagner, M.E. and Crawford, M.L. (1975). Polymetamorphism of the Precambrian Baltimore gneiss in southeastern Pennsylvania. *Am. J.Sci.*, 275, 653-682.

Waldbaum, D.R. and Thompson, J.B. (1969). Mixing properties of sanidine crystalline solutions. IV. Phase diagrams from equations of state. *Am. Miner.*, 54, 1274-1298.

Walker, F. and Poldervaart, A. (1941). The Karroo dolerites of the Calvinia District. *Trans. geol. Soc. S. Afr.*, 44, 127-148.

Ward, J.H.W. (1973). The Vioolsdrif batholith. *Abstracts 15th Congress geol. Soc. S.Afr.*, 195-197.

_____ (1974). The Vioolsdrif pegmatite belt. *Ann. Rep. Precambr. Res. Unit, Univ. Cape Town*, 10-11, 38-42.

_____ (1977). *The geology of an area south of Vioolsdrif, Cape Province.* Unpubl. Rep. Precambr. Res. Unit, Univ. Cape Town, 75p.

Warner, R.D. and Luth, W.C. (1974). The diopside-orthoenstatite two-phase region in the system Ca Mg $Si_2 O_6$ - $Mg_2 Si_2 O_6$. *Am. Miner.*, 59, 98-109.

Warren, B.E. and Bragg, W.L. (1928). The structure of diopside Ca Mg $(Si O_3)_2$. *Z. Krist.*, 69, 168-193.

Watson, J.V. (1976). Vertical movements in Proterozoic structural provinces. *Phil. Trans. R. Soc. Lond.*, A280, 629-640.

Watters, B.R. (1974). Stratigraphy, igneous petrology and evolution of the Sinclair Group in southern South West Africa. *Bull. Precambr. Res. Unit, Univ. Cape Town*, 16, 234p.

Weaver, B.L., Tarney, J., Windley, B.F., Sugavanam, E.B. and Venkata Rao, V. (1978). Madras granulites : geochemistry and P - T conditions of crystallization, 177-204. *In :* Windley, B.F. and Naqvi, S.M. (Eds.). Developments in Precambrian geology Vol. 1 *(Archaean geochemistry).* Elsevier Scientific Publishing Company, Amsterdam, 406p.

Wells, R.A. (1977). Pyroxene thermometry in simple and complex systems. *Contr. Miner. Petrol.*, 62, 129-139.

Wenk, E. and Keller, F. (1969). Isograde in Amphibolitserien der Zentralalpen. *Schweis. miner. petrogr. Mitt.*, 49, 157-198.

White, A.J.R. and Chappell, B.W. (1977). Ultrametamorphism and granitoid genesis. *Tectonophysics*, 43, 7-22.

White, S.H. (1971). Natural creep of quartzites. *Nature*, 234, 175-177.

_____ (1973). Syntectonic recrystallization and texture development in quartz. *Nature*, 244, 276-278.

_____ (1975). The effects of polyphase deformation on the intra-crystalline defect structures of quartz. II. Origin of the defect structures. *Neues Jb. Miner. Abh.*, 123, 237-252.

White, S.H. (1976). The effects of strain on the microstructures, fabrics, and deformation mechanisms in quartzite. *Phil. Trans. R. Soc. Lond.*, A283, 69-86.

_____ (1977). Geological significance of recovery and recrystallization processes in quartz. *Tectonophysics*, 39, 143-170.

_____ and Treagus, J.E. (1975). The effects of polyphase deformation on the intracrystalline defect structures of quartz. I. The defect structures. *Neues Jb. Miner. Abh.*, 123, 219-236.

Whitney, J.A. (1975). The effects of pressure, temperature and $X_{H_2O}$ on phase assemblage in four synthetic rock compositions. *J. Geol.*, 83(1), 1-31.

_____ and Stormer, J.C. (1976). Geothermometry and geobarometry in epizonal granitic intrusions : a comparison of iron - titanium oxides and coexisting feldspars. *Am. Miner.*, 61, 751-761.

_____ and Stormer, J.C. (1977a). The distribution of $NaAlSi_3O_8$ between coexisting microcline and plagioclase and its effect on geothermometric calculations. *Am. Miner.* 62, 687-691.

_____ and Stormer, J.C. (1977b). Two-feldspar geothermometry, geobarometry in mesozonal granitic intrusions: three examples from the piedmont of Georgia. *Contr. Miner. Petrol.*, 63, 51-69.

Whitney, P.R. (1972). Spinel inclusions in plagioclase of metagabbros from the Adirondack Highlands. *Am. Miner.*, 57, 1429-1439.

_____ and McLelland, J.M. (1973). Origin of coronas in metagabbros of the Adirondack Mts. N.Y. *Contr. Miner. Petrol.*, 39, 81-98.

Whitten, E.H.T. (1966). *Structural geology of folded rocks.* Rand Mc Nally & Company, Chicago, 678p.

Widmark, E.T. (1980). The reaction chlorite + dolomite = spinel + forsterite + calcite + $CO_2$ + water. *Contr. Miner. Petrol.*, 72, 175-179.

Wilson, A.F. (1960). The charnockite granites and associated granites of central Australia. *Trans. R. Soc. S. Austr.*, 83, 37-75.

Wilson, A.F. (1976). Aluminium in coexisting pyroxenes as a sensitive indicator of changes in metamorphic grade within the mafic granulite terrane of the Fraser Range Western Australia. *Contr. Miner. Petrol.*, 56, 255-277.

Wilson, J.D. (1981). The geology of the Broken Hill deposit, Aggeneys, northwest Cape. *Abstracts 19th Congress geol. Soc. S. Afr.*, 231-233.

Windley, B.F. (1977). *The evolving continents.* John Wiley & Sons, London, 385p.

_____ (1981). Precambrian rocks in the light of the plate tectonic concept, 1-20. *In:* Kröner, A. (Ed.). Developments in Precambrian geology, Vol. 4 *(Precambrian plate tectonics).* Elsevier Scientific Publishing Company, Amsterdam, 781p.

Winkler, H.G.F. (1967). *Petrogenesis of metamorphic rocks.* Springer-Verlag, Berlin, 237p.

_____ (1976). *Petrogenesis of metamorphic rocks.* Springer-Verlag, Berlin, 334p.

_____ and Sen, S.K. (1973). Nomenclature of granulites and other high grade metamorphic rocks. *Neues Jb. Miner. Mh.*, 9, 393-402.

_____, Boese, M. and Marcopoulos, T. (1975). Low-temperature granitic melts. *Neues Jb. Miner. Mh.*, 6, 245-268.

Wood, B.J. (1975). Influence of pressure, temperature and bulk composition on the appearance of garnet in orthogneiss : an example from South Harris, Scotland. *Earth Planet. Sci. Lett.*, 26, 299-311.

_____ (1976). Mixing properties of tschermakitic clinopyroxenes. *Am. Miner.*, 61, 599-602.

_____ (1977). The activities of components in clinopyroxene and garnet solid solutions and their application to rocks. *Phil. Trans. R. Soc. Lond.*, A286, 331-342.

_____ (1978). Reactions involving anorthite and $Ca\ Al_2\ Si\ O_6$ pyroxene at high pressures and temperatures. *Am. J. Sci.*, 278, 930-942.

Wood, B.J. (1979). Activity-composition relationships in Ca (Mg Fe) $Si_2 O_6$ - Ca $Al_2$ Si $O_6$ clinopyroxene solid solutions. *Am. J. Sci.*, 279, 854-875.

_____ and Banno, S. (1973). Garnet-orthopyroxene and orthopyroxene - clinopyroxene relationships in simple and complex systems. *Contr. Miner. Petrol.*, 42, 109-124.

_____ and Fraser, D.G. (1977). *Elementary thermodynamics for geologists.* Oxford University Press, 303p.

Wyllie, P.J. (1977). Crustal anatexis : An experimental Review. *Tectonophysics*, 43, 41-71.

_____ and Huang, W.L. (1975). Influence of mantle $CO_2$ in the generation of carbonatites and kimberlites. *Nature*, 257, 297-299.

Wynne-Edwards, H.R. (1972). The Grenville Province, 263-334. *In :* Price, R.A. and Douglas, R.J.W. (Eds.). *Variations in tectonic styles in Canada. Spec. Pap. geol. Ass. Canada*, 11, 688p.

_____ (1976). Proterozoic ensialic orogenesis : the millipede model of ductile plate tectonics. *Am. J. Sci.*, 276, 927-953.

_____ and Hay, P.W. (1963). Coexisting cordierite and garnet in regionally metamorphosed rocks from the Westport area, Ontario. *Can. Miner.*, 7, 453-478.

Yardley, B.W.D. (1978). Genesis of the Skagit gneiss migmatites, Washington, and the distinction between possible mechanisms of migmatization. *Bull. geol. Soc. Am.*, 89, 941-951.

Zelt, G.A.D. (1975). Preliminary report on the petrochemistry of high-grade metamorphic rocks in Western Namaqualand. *Ann. Rep. Precambr. Res. Unit, Univ. Cape Town*, 13, 83-88.

_____ (1978). Mafic populations and high-grade metamorphic zoning in western Namaqualand. *Ann. Rep. Precambr. Res. Unit, Univ. Cape Town*, 14-15, 103-113.

_____ (1979). Granulite facies metamorphism in Namaqualand, South Africa. *Abstracts 18th Congress geol. Soc. S. Afr.*, 461-462.

Zelt, G.A.D. (1980). Granulite-facies metamorphism in Namaqualand, South Africa. *Precambr. Res.*, 13, 253-274.

Zen, E-an (1966). Construction of pressure-temperature diagrams for multicomponent systems after the method of Schreinemakers - a geometric approach. *Bull. U.S. geol. Surv.*, 1225, 56p.

Zwart, H.J. (1967). The duality of orogenic belts. *Geologie Mijnb.*, 46, 283-309.

# Appendix I

## DETERMINATIVE MINERALOGY AND ANALYTICAL TECHNIQUES

### A Selective Staining of K-feldspar in Thin Sections by the Cobaltinitrite Method

Thin sections of various granitoids including the charnockite suite were stained in a concentrated solution of sodium cobaltinitrite by a method outlined by Bailey and Stevens (1960), in order to allow quick identification of the feldspars and aid in estimating their relative abundance microscopically.

A concentrated solution of sodium cobaltinitrite was prepared by dissolving approximately 60 grams of this chemical in 100 millilitres of distilled water. Concentrated hydrofluoric acid was poured into a plastic vessel until the bottom of the container was covered. The thin sections were placed over the acid vapor face downwards, and etched for a period of approximately 1 to 2 minutes. Subsequently the specimens were dried in air and immersed face upwards in the saturated solution of cobaltinitrite for about 2 minutes. After the short period of staining, the specimens were immediately removed and the excess cobaltinitrite solution removed from the thin sections under gently flowing cold water. The specimens were then allowed to dry at room temperature.

This treatment results in staining of the potassium feldspar to a bright lemon-yellow colour, plagioclase turns chalky-white while quartz is unaffected. The hydrofluoric acid vapor removes the silica as a volatile fluoride and the residual potassium from the K-feldspar yields a yellow-coloured potassium cobaltinitrite.

### B Analytical Techniques

The chemical compositions of minerals were determined with the aid of the Cambridge 5 electron microprobe analyser of the Geochemistry Department, University of Cape Town. Rock specimens were mounted as polished thin sections, previously coated with finely divided carbon whose function is to serve as a conducting medium for the electrons. Operating conditions were as follows:

Accelerating Voltage: 15 KV

Beam Current: $0,15 \times 10^{-6}$A

Analysing crystals: RAP (Si, Al, Mg, Na)
Quartz (Fe, Mn, Cr, Ca, Ti, K)

Detection: Flow counters with $Ar/CO_2$ gas mixtures

Beam Focus: A finely focused beam (1-2μ diameter) was generally used for all the elements, but in the case of plagioclase analyses a defocused beam (5-10μ diameter) was used and K-feldspars were analysed by scanning an approximate 90 $\mu^2$ area.

Calibration was achieved with natural and synthetic standards which were previously independently analysed. The counts were corrected for dead time and background and all the data were computer-processed by the ABFAN programme (Boyd *et al.*, 1968).

## C Microprobe Analyses of Alkali Feldspar

The alkali feldspar in the specimens from the study area is invariably perthitic and in order to determine the homogeneous bulk composition of the mineral prior to exsolution, a special analytical technique is required. In this study the Cambridge 5 electron microprobe analyser has been used, but instead of a finely focused beam, a 90μ stationary electron line was set up and the specimen was then scanned at right angles to this "line" by moving it at a constant speed of 30μ per minute with a mechanised driving system while allowing a detection period of three minutes. In this manner a 90 x 90μ area was analysed. The resulting analyses yielded excellent totals (Appendix II, Table A2-17).

## D Computation of Weight Per Cent $Fe_2O_3$ for Microprobe Analyses

The computer linked to the electron microprobe analyser is programmed in such a way that the total weight per cent Fe is computed as FeO regardless of its actual state of oxidation. This is justified for minerals lacking $Fe^{+3}$ or containing trivalent iron only in trace amounts, but serious errors are introduced in the computation of ionic proportions when minerals contain appreciable amounts of $Fe_2O_3$. The effect of the presence of $Fe^{+3}$ is to reduce the oxide totals and to increase the calculated ionic proportions relative to the ideal expected values, thus necessitating the recalculation of the analyses to correct for the trivalent iron. The method of recalculation used here involves the assumption of exact stoicheiometry which allows the computation of $Fe^{+3}$ ionic proportions needed to satisfy stoicheiometric requirements.

If the real weight per cent FeO is defined as (a) and the real weight per cent $Fe_2O_3$ as (b), the relationship between the weight per cent FeO computed in the original analysis (ignoring $Fe^{+3}$), here referred to as FeO*, and (a) and (b) is as follows:

$$FeO^* = (a) + 0{,}8998 \cdot (b) \qquad (1)$$

where $0{,}8998 = \dfrac{\text{FeO molecular weight} \times 2}{Fe_2O_3 \text{ molecular weight}}$

Therefore: (a) (real weight per cent FeO) = $FeO^* - 0{,}8998 \cdot (b)$ (2)

As the ratio of $\dfrac{Fe^{+3}}{Fe^{+2}}$ (ionic proportions) is known, the ratio by weight of $Fe_2O_3/FeO$ can be calculated from the relationship:

$$\frac{Fe_2O_3 \text{ (by weight)}}{FeO \text{ (by weight)}} = \frac{Fe^{+3}/2 \cdot 159{,}7}{Fe^{+2} \cdot 71{,}85} = \frac{(b)}{(a)} \qquad (3)$$

Let $\dfrac{Fe^{+3}/2 \cdot 159{,}7}{Fe^{+2} \cdot 71{,}85} = X$

and therefore $(b) = X(a)$ (4)

Substitution of equation (4) into equation (2) yields

$$(a) = FeO^* - 0{,}8998 \cdot X(a) \qquad (5)$$

which can be rearranged to yield

$$(a) = FeO^*/(0{,}8998 \cdot X + 1) \qquad (6)$$

= real weight per cent FeO

and therefore

$$(b) = X \text{ (from equation 3)} \cdot (a) \text{ (from equation 6)} \qquad (7)$$

= real weight per cent $Fe_2O_3$

# Appendix II

## TABLES OF MINERAL ANALYSES

Structural formulae of hornblendes in metabasites are given in Table A2-1. Tables A2-2 to A2-33 contain chemical analyses of all the minerals analysed. Dashes indicate elements not analysed for. In some of the Tables mean mineral compositions are given and the number of analyses on which these means are based are indicated in parentheses below the specimen number.

Table A2-1: Structural formulae of hornblendes (23 oxygens) based on averages of 2-5 analyses per specimen, Am = amphibolite, D Am = clinopyroxene-bearing amphibolite, G = granolite

| Sample Number | $A^{(XII-X)}$ | | | | $X^{(VIII-VI)}$ | | | $Y^{(VI)}$ | | | | | $Z^{(IV)}$ | |
|---|---|---|---|---|---|---|---|---|---|---|---|---|---|---|
| | K | Na | Ca | ΣA | Na | Ca | Mg | Mg | Fe | Mn | Ti | Al | Al | Si |
| HA 1125(Am) | 0,2110 | 0,4120 | 0,0723 | 0,6953 | - | 1,8434 | 0,1566 | 1,9078 | 2,4293 | 0,0424 | 0,1642 | 0,4563 | 1,5537 | 6,4463 |
| HA 1111(DAm) | 0,1703 | 0,2798 | 0,0625 | 0,5126 | - | 1,8613 | 0,1387 | 1,9865 | 2,3155 | 0,0374 | 0,1395 | 0,5211 | 1,3759 | 6,6241 |
| HA 1110(DAm) | 0,2345 | 0,3285 | 0,1337 | 0,6967 | - | 1,8527 | 0,1473 | 1,9317 | 2,4537 | 0,0336 | 0,1423 | 0,4387 | 1,5546 | 6,4454 |
| HA 1095(Am) | 0,1370 | 0,2997 | 0,0825 | 0,5192 | - | 1,8216 | 0,1784 | 2,3236 | 2,0380 | 0,0363 | 0,1154 | 0,4867 | 1,3200 | 6,6800 |
| HA 1129(DAm) | 0,1455 | 0,3958 | 0,1176 | 0,6589 | - | 1,7733 | 0,2267 | 2,3285 | 2,0871 | 0,0317 | 0,0689 | 0,4838 | 1,3987 | 6,6013 |
| HA 1091(DAm) | 0,2689 | 0,3456 | 0,1201 | 0,7346 | - | 1,8151 | 0,1849 | 2,4142 | 1,9990 | 0,0464 | 0,0939 | 0,4465 | 1,4900 | 6,5100 |
| HA 1084(Am) | 0,1418 | 0,5269 | 0,0300 | 0,6987 | - | 1,7464 | 0,2536 | 2,2701 | 2,0654 | 0,0368 | 0,2112 | 0,4165 | 1,5688 | 6,4312 |
| HA 1025(G) | 0,2370 | 0,4389 | - | 0,6759 | 0,0287 | 1,9036 | 0,0677 | 2,8399 | 1,4945 | 0,0177 | 0,2697 | 0,3782 | 1,5647 | 6,4353 |
| HA 1050(G) | 0,4506 | 0,4371 | 0,0213 | 0,9090 | - | 1,9127 | 0,0873 | 2,2389 | 2,1865 | 0,0257 | 0,2294 | 0,3195 | 1,7092 | 6,2908 |
| HA 472(G) | 0,3429 | 0,4192 | - | 0,7621 | 0,0644 | 1,8588 | 0,0768 | 2,7265 | 1,6418 | 0,0146 | 0,2559 | 0,3612 | 1,5705 | 6,4293 |
| HA 239(G) | 0,3050 | 0,4078 | 0,0092 | 0,7220 | - | 1,8894 | 0,1106 | 3,0370 | 1,3548 | 0,0160 | 0,2278 | 0,3644 | 1,5524 | 6,4476 |
| HA 269(G) | 0,2984 | 0,4600 | 0,0290 | 0,7874 | - | 1,8572 | 0,1428 | 2,3208 | 2,0224 | 0,0184 | 0,2505 | 0,3879 | 1,7064 | 6,2936 |
| HA 987(G) | 0,3115 | 0,4218 | 0,0337 | 0,7670 | - | 1,8032 | 0,1968 | 3,1006 | 1,3338 | 0,0172 | 0,1755 | 0,3729 | 1,5251 | 6,4749 |
| HA 306(G) | 0,4183 | 0,4096 | - | 0,8279 | 0,0438 | 1,8834 | 0,0729 | 2,2990 | 2,0266 | 0,0198 | 0,2620 | 0,3926 | 1,7015 | 6,2985 |
| HA 926(G) | 0,3088 | 0,3792 | 0,0171 | 0,7051 | - | 1,8655 | 0,1345 | 3,0836 | 1,4127 | 0,0132 | 0,1367 | 0,3538 | 1,3500 | 6,6500 |

TABLE A2-2: Mean microprobe analyses of hornblende in mafic rocks. Ionic proportions on the basis of 23 oxygens. The number of grains analysed are indicated in parentheses. G = hypersthene-pyroclase granolite, DAm = clinopyroxene-bearing amphibolite Am = amphibolite.

| Sample No. | HA1025 | HA1050 | HA472 | HA239 | HA269 | HA987 | HA306 | HA926 |
|---|---|---|---|---|---|---|---|---|
| Rock Type | G(4) | G(2) | G(5) | G(3) | G(5) | G(2) | G(3) | G(2) |
| $SiO_2$ | 43,732 | 40,825 | 43,174 | 43,805 | 41,888 | 43,953 | 41,469 | 45,753 |
| $TiO_2$ | 2,437 | 1,980 | 2,285 | 2,057 | 2,217 | 1,585 | 2,294 | 1,250 |
| $Al_2O_3$ | 11,199 | 11,167 | 11,003 | 11,046 | 11,822 | 10,928 | 11,694 | 9,942 |
| $FeO,Fe_2O_3$ | 12,144 | 16,966 | 13,182 | 11,006 | 16,093 | 10,826 | 15,956 | 11,621 |
| MnO | 0,142 | 0,197 | 0,116 | 0,128 | 0,144 | 0,138 | 0,154 | 0,107 |
| MgO | 13,259 | 10,129 | 12,632 | 14,349 | 11,001 | 15,019 | 10,478 | 14,857 |
| CaO | 12,073 | 11,713 | 11,650 | 12,038 | 11,715 | 11,637 | 11,572 | 12,088 |
| $Na_2O$ | 1,638 | 1,463 | 1,675 | 1,428 | 1,579 | 1,476 | 1,540 | 1,346 |
| $K_2O$ | 1,262 | 2,292 | 1,804 | 1,624 | 1,556 | 1,657 | 2,158 | 1,665 |
| TOTAL | 97,89 | 96,73 | 97,52 | 97,48 | 98,01 | 97,22 | 97,32 | 98,63 |
| Si | 6,4353 | 6,2908 | 6,4293 | 6,4476 | 6,2936 | 6,4749 | 6,2985 | 6,6500 |
| Ti | 0,2697 | 0,2294 | 0,2559 | 0,2278 | 0,2505 | 0,1755 | 0,2620 | 0,1367 |
| Al | 1,9429 | 2,0287 | 1,9317 | 1,9168 | 2,0943 | 1,8980 | 2,0941 | 1,7038 |
| Fe | 1,4945 | 2,1865 | 1,6418 | 1,3548 | 2,0224 | 1,3338 | 2,0266 | 1,4127 |
| Mn | 0,0177 | 0,0257 | 0,0146 | 0,0160 | 0,0184 | 0,0172 | 0,0198 | 0,0132 |
| Mg | 2,9076 | 2,3262 | 2,8033 | 3,1476 | 2,4636 | 3,2974 | 2,3719 | 3,2181 |
| Ca | 1,9036 | 1,9340 | 1,8588 | 1,8903 | 1,8862 | 1,8369 | 1,8834 | 1,8826 |
| Na | 0,4676 | 0,4371 | 0,4836 | 0,4078 | 0,4600 | 0,4218 | 0,4534 | 0,3792 |
| K | 0,2370 | 0,4506 | 0,3429 | 0,3050 | 0,2984 | 0,3115 | 0,4183 | 0,3088 |
| TOTAL | 15,6859 | 15,9090 | 15,7619 | 15,7137 | 15,7870 | 15,7670 | 15,8280 | 15.7051 |

| Sample No. | HA1125 | HA1111 | HA1110 | HA1095 | HA1129 | HA1091 | HA1084 |
|---|---|---|---|---|---|---|---|
| Rock Type | Am(3) | DAm(3) | DAm(3) | Am(3) | DAm(3) | DAm(3) | Am(3) |
| $SiO_2$ | 42,284 | 44,027 | 42,262 | 44,676 | 43,849 | 43,492 | 43,388 |
| $TiO_2$ | 1,432 | 1,233 | 1,241 | 1,026 | 0,609 | 0,833 | 1,894 |
| $Al_2O_3$ | 11,183 | 10,695 | 11,086 | 10,249 | 10,606 | 10,973 | 11,361 |
| $FeO,Fe_2O_3$ | 19,054 | 18,402 | 19,237 | 16,297 | 16,577 | 15,968 | 16,662 |
| MnO | 0,328 | 0,293 | 0,260 | 0,286 | 0,248 | 0,366 | 0,293 |
| MgO | 9,086 | 9,478 | 9,147 | 11,228 | 11,388 | 11,652 | 11,424 |
| CaO | 11,727 | 11,933 | 12,156 | 11,885 | 11,722 | 12,066 | 11,185 |
| $Na_2O$ | 1,393 | 0,959 | 1,111 | 1,033 | 1,356 | 1,190 | 1,833 |
| $K_2O$ | 1,085 | 0,887 | 1,205 | 0,718 | 0,757 | 1,408 | 0,750 |
| TOTAL | 97,57 | 97,90 | 97,71 | 97,39 | 97,11 | 97,95 | 98,79 |
| Si | 6,4463 | 6,6241 | 6,4454 | 6,6800 | 6,6013 | 6,5100 | 6,4312 |
| Ti | 0,1642 | 0,1395 | 0,1423 | 0,1154 | 0,0689 | 0,0939 | 0,2112 |
| Al | 2,0100 | 1,8970 | 1,9933 | 1,8067 | 1,8825 | 1,9365 | 1,9853 |
| Fe | 2,4293 | 2,3155 | 2,4537 | 2,0380 | 2,0871 | 1,9990 | 2,0654 |
| Mn | 0,0424 | 0,0374 | 0,0336 | 0,0363 | 0,0317 | 0,0464 | 0,0368 |
| Mg | 2,0644 | 2,1252 | 2,0790 | 2,5020 | 2,5552 | 2,5991 | 2,5237 |
| Ca | 1,9157 | 1,9238 | 1,9864 | 1,9041 | 1,8909 | 1,9352 | 1,7764 |
| Na | 0,4120 | 0,2798 | 0,3285 | 0,2997 | 0,3958 | 0,3456 | 0,5269 |
| K | 0,2110 | 0,1703 | 0,2345 | 0,1370 | 0,1455 | 0,2689 | 0,1418 |
| TOTAL | 15,6843 | 15,5126 | 15,6967 | 15,5192 | 15,6589 | 15,7346 | 15,6987 |

TABLE A2-3: Mean microprobe analyses of plagioclase in mafic rocks. Ionic proportions on the basis of 8 oxygens. The number of grains analysed are indicated in parentheses. G = hypersthene-pyroclase granolite, DAm = clinopyroxene-bearing amphibolite, Am = amphibolite.

| Sample No. | HA1125 | HA1084 | HA1095 | HA1111 | HA1110 | HA1091 | HA1129 | HA1025 |
|---|---|---|---|---|---|---|---|---|
| Rock Type | Am(3) | Am(3) | Am(3) | DAm(2) | DAm(1) | DAm(3) | DAm(2) | G(3) |
| $SiO_2$ | 55,791 | 56,403 | 46,609 | 46,034 | 46,142 | 49,438 | 48,772 | 51,285 |
| $TiO_2$ | – | – | – | – | – | – | – | – |
| $Al_2O_3$ | 27,700 | 26,913 | 33,306 | 33,706 | 33,160 | 32,235 | 32,204 | 30,409 |
| $FeO,Fe_2O_3$ | 0,044 | 0,098 | 0,145 | 0,118 | 0,186 | 0,178 | 0,151 | 0,099 |
| MnO | 0,024 | 0,000 | 0,010 | 0,000 | – | 0,005 | 0,002 | 0,000 |
| MgO | 0,006 | 0,000 | 0,015 | 0,004 | – | 0,005 | 0,000 | 0,000 |
| CaO | 10,211 | 9,511 | 17,525 | 18,094 | 17,584 | 15,423 | 15,619 | 13,890 |
| $Na_2O$ | 5,568 | 6,326 | 1,619 | 1,239 | 1,543 | 3,117 | 3,005 | 3,622 |
| $K_2O$ | 0,215 | 0,187 | 0,016 | 0,030 | 0,044 | 0,118 | 0,084 | 0,117 |
| TOTAL | 99,56 | 99,44 | 99,25 | 99,23 | 98,66 | 100,52 | 99,84 | 99,42 |
| Si | 2,5203 | 2,5503 | 2,1602 | 2,1363 | 2,1530 | 2,2514 | 2,2381 | 2,3458 |
| Ti | – | – | – | – | – | – | – | – |
| Al | 1,4751 | 1,4346 | 1,8198 | 1,8441 | 1,8241 | 1,7307 | 1,7423 | 1,6397 |
| Fe | 0,0016 | 0,0036 | 0,0056 | 0,0046 | 0,0072 | 0,0068 | 0,0058 | 0,0037 |
| Mn | 0,0009 | 0,0000 | 0,0003 | 0,0000 | – | 0,0002 | 0,0000 | 0,0000 |
| Mg | 0,0004 | 0,0000 | 0,0011 | 0,0003 | – | 0,0004 | 0,0000 | 0,0000 |
| Ca | 0,4942 | 0,4607 | 0,8703 | 0,8997 | 0,8791 | 0,7526 | 0,7680 | 0,6807 |
| Na | 0,4877 | 0,5546 | 0,1455 | 0,1114 | 0,1396 | 0,2752 | 0,2673 | 0,3213 |
| K | 0,0123 | 0,0108 | 0,0009 | 0,0018 | 0,0026 | 0,0069 | 0,0049 | 0,0068 |
| TOTAL | 4,9925 | 5,0146 | 5,0037 | 4,9982 | 5,0060 | 5,0242 | 5,0264 | 4,9980 |

| Sample No. | HA1050 | HA1045 | HA1030 | HA306 |
|---|---|---|---|---|
| Rock Type | G(2) | G(2) | G(4) | G(1) |
| $SiO_2$ | 56,718 | 47,208 | 45,615 | 53,407 |
| $TiO_2$ | – | – | – | – |
| $Al_2O_3$ | 27,702 | 33,004 | 34,403 | 30,797 |
| $FeO,Fe_2O_3$ | 0,135 | 0,241 | 0,262 | 0,095 |
| MnO | 0,000 | – | 0,006 | – |
| MgO | 0,000 | – | 0,005 | – |
| CaO | 10,391 | 17,307 | 18,430 | 11,921 |
| $Na_2O$ | 5,184 | 1,673 | 1,089 | 4,694 |
| $K_2O$ | 0,478 | 0,079 | 0,044 | 0,252 |
| TOTAL | 100,61 | 99,51 | 99,85 | 101,17 |
| Si | 2,5348 | 2,1804 | 2,1077 | 2,3890 |
| Ti | – | – | – | – |
| Al | 1,4596 | 1,7972 | 1,8741 | 1,6241 |
| Fe | 0,0050 | 0,0093 | 0,0101 | 0,0035 |
| Mn | 0,0000 | – | 0,0002 | – |
| Mg | 0,0000 | – | 0,0003 | – |
| Ca | 0,4976 | 0,8566 | 0,9125 | 0,5713 |
| Na | 0,4492 | 0,1498 | 0,0976 | 0,4071 |
| K | 0,0272 | 0,0047 | 0,0025 | 0,0144 |
| TOTAL | 4,9734 | 4,9980 | 5,0050 | 5,0097 |

TABLE A2-4: Mean Microprobe analyses of orthopyroxene in hypersthene - pyroclase granolites. Ionic proportions on the basis of 6 oxygens. R and C refer, respectively, to rim and core compositions. Number of grains analysed are indicated in parentheses.

| Sample No. | HA926 R(6) | HA939 R(4) | HA306 R(5) | HA472 R(6) | HA269 R(3) | HA269 C(2) | HA957 R(3) | HA957 C(3) | HA622 R(3) | HA909 R(3) |
|---|---|---|---|---|---|---|---|---|---|---|
| $SiO_2$ | 51.581 | 52.904 | 50.903 | 51.435 | 51.143 | 50.844 | 51.273 | 50.449 | 49.340 | 52.080 |
| $TiO_2$ | 0.078 | 0.084 | 0.091 | 0.116 | 0.074 | 0.112 | 0.071 | 0.091 | 0.110 | 0.099 |
| $Al_2O_3$ | 1.074 | 1.450 | 1.062 | 1.003 | 0.854 | 1.261 | 1.167 | 1.173 | 0.787 | 0.799 |
| $Cr_2O_3$ | 0.075 | 0.059 | 0.023 | 0.015 | 0.024 | 0.025 | 0.015 | 0.022 | 0.009 | 0.023 |
| $FeO,Fe_2O_3$ | 25.967 | 19.980 | 28.243 | 25.586 | 25.590 | 25.998 | 26.531 | 27.754 | 36.603 | 25.917 |
| MnO | 0.464 | 0.579 | 0.717 | 0.494 | 0.549 | 0.530 | 0.569 | 0.618 | 0.794 | 0.757 |
| MgO | 19.509 | 24.550 | 17.732 | 19.974 | 20.785 | 20.193 | 19.320 | 18.683 | 11.344 | 19.457 |
| CaO | 0.610 | 0.536 | 0.703 | 0.627 | 0.651 | 1.172 | 0.608 | 0.701 | 0.848 | 0.716 |
| $Na_2O$ | 0.000 | 0.007 | 0.011 | 0.002 | - | - | 0.043 | 0.035 | 0.029 | 0.012 |
| $K_2O$ | 0.000 | 0.011 | 0.007 | 0.004 | - | - | 0.040 | 0.006 | 0.019 | 0.008 |
| TOTAL | 99.36 | 100.16 | 99.49 | 99.26 | 99.67 | 100.13 | 99.64 | 99.53 | 99.88 | 99.87 |
| Si | 1.9697 | 1.9481 | 1.9669 | 1.9643 | 1.9484 | 1.9349 | 1.9604 | 1.9464 | 1.9810 | 1.9797 |
| Ti | 0.0022 | 0.0023 | 0.0026 | 0.0033 | 0.0021 | 0.0031 | 0.0020 | 0.0026 | 0.0033 | 0.0028 |
| Al | 0.0489 | 0.0629 | 0.0484 | 0.0451 | 0.0384 | 0.0566 | 0.0526 | 0.0533 | 0.0372 | 0.0358 |
| Cr | 0.0022 | 0.0017 | 0.0006 | 0.0003 | 0.0007 | 0.0007 | 0.0005 | 0.0006 | 0.0003 | 0.0007 |
| Fe | 0.8295 | 0.6153 | 0.9127 | 0.8171 | 0.8154 | 0.8274 | 0.8482 | 0.8955 | 1.2294 | 0.8240 |
| Mn | 0.0150 | 0.0180 | 0.0234 | 0.0159 | 0.0177 | 0.0171 | 0.0184 | 0.0201 | 0.0270 | 0.0243 |
| Mg | 1.1103 | 1.3474 | 1.0211 | 1.1369 | 1.1801 | 1.1452 | 1.1008 | 1.0742 | 0.6790 | 1.1022 |
| Ca | 0.0250 | 0.0211 | 0.0290 | 0.0256 | 0.0265 | 0.0478 | 0.0248 | 0.0290 | 0.0364 | 0.0291 |
| Na | 0.000 | 0.0005 | 0.0008 | 0.0001 | - | - | 0.0032 | 0.0026 | 0.0022 | 0.0009 |
| K | 0.000 | 0.0005 | 0.0003 | 0.0002 | - | - | 0.0019 | 0.0003 | 0.0010 | 0.0004 |
| TOTAL | 4.0028 | 4.0178 | 4.0058 | 4.0088 | 4.0293 | 4.0328 | 4.0128 | 4.0246 | 3.9973 | 3.9999 |

| Sample No. | HA980 (R-2) | HA725 (R-3) | HA239 (R-5) | HA888 (R-4) | HA973 (R-5) | HA987 (R-5) | HA1050 (C-3) | HA1045 (C-3) | HA1025 (C-3) |
|---|---|---|---|---|---|---|---|---|---|
| $SiO_2$ | 51.571 | 49.624 | 53.045 | 50.014 | 50.498 | 53.381 | 50.332 | 50.269 | 52.776 |
| $TiO_2$ | 0.099 | 0.111 | 0.100 | 0.092 | 0.096 | 0.057 | 0.094 | 0.106 | 0.083 |
| $Al_2O_3$ | 1.632 | 1.051 | 1.384 | 0.788 | 0.989 | 1.559 | 0.939 | 1.040 | 1.107 |
| $Cr_2O_3$ | 0.029 | 0.008 | 0.120 | 0.009 | 0.032 | 0.069 | - | - | - |
| $FeO,Fe_2O_3$ | 22.219 | 32.323 | 17.883 | 32.269 | 29.389 | 16.638 | 30.406 | 29.996 | 20.946 |
| MnO | 0.677 | 0.635 | 0.445 | 0.602 | 0.491 | 0.527 | 0.885 | 0.603 | 0.461 |
| MgO | 22.528 | 13.810 | 25.696 | 15.175 | 17.551 | 27.201 | 16.232 | 16.668 | 23.665 |
| CaO | 0.522 | 0.679 | 0.452 | 0.721 | 0.646 | 0.424 | 1.046 | 0.821 | 0.539 |
| $Na_2O$ | 0.013 | 0.000 | 0.014 | 0.000 | 0.026 | 0.024 | 0.000 | 0.000 | 0.006 |
| $K_2O$ | 0.000 | 0.009 | 0.006 | 0.006 | 0.000 | 0.000 | 0.009 | 0.003 | 0.024 |
| TOTAL | 99.29 | 99.25 | 99.16 | 99.68 | 99.72 | 99.88 | 99.94 | 99.51 | 99.60 |
| Si | 1.9398 | 1.9217 | 1.9515 | 1.9682 | 1.9572 | 1.9402 | 1.9613 | 1.9603 | 1.9616 |
| Ti | 0.0028 | 0.0033 | 0.0027 | 0.0027 | 0.0027 | 0.0015 | 0.0027 | 0.0031 | 0.0023 |
| Al | 0.0723 | 0.0492 | 0.0600 | 0.0366 | 0.0452 | 0.0668 | 0.0431 | 0.0478 | 0.0484 |
| Cr | 0.0008 | 0.0002 | 0.0033 | 0.0003 | 0.0009 | 0.0019 | - | - | - |
| Fe | 0.6989 | 1.1073 | 0.5502 | 1.0621 | 0.5059 | 0.5059 | 0.9910 | 0.9782 | 0.6511 |
| Mn | 0.0215 | 0.0213 | 0.0138 | 0.0200 | 0.0162 | 0.0162 | 0.0292 | 0.0199 | 0.0144 |
| Mg | 1.2628 | 0.8177 | 1.4089 | 0.8899 | 1.4732 | 1.4732 | 0.9426 | 0.9686 | 1.4110 |
| Ca | 0.0210 | 0.0288 | 0.0178 | 0.0304 | 0.0165 | 0.0165 | 0.0436 | 0.0343 | 0.0215 |
| Na | 0.0009 | 0.0000 | 0.0009 | 0.0000 | 0.0017 | 0.0017 | 0.0000 | 0.0000 | 0.0004 |
| K | 0.0000 | 0.0003 | 0.0003 | 0.0003 | 0.0000 | 0.0000 | 0.0004 | 0.0001 | 0.0011 |
| TOTAL | 4.0208 | 3.9998 | 4.0094 | 4.0105 | 4.0171 | 4.0239 | 4.0139 | 4.0123 | 4.0118 |

TABLE A2-5: Mean Microprobe analyses of clinopyroxene in hypersthene - pyroclase granolites. Ionic proportions on the basis of 6 oxygens. R and C refer, respectively, to rim and core compositions. Number of grains analysed are indicated in parentheses.

| Sample No. | HA926 (R-6) | HA939 (R-4) | HA306 (R-5) | HA472 (R-6) | HA269 (R-3) | HA269 (C-2) | HA957 (R-5) | HA957 (C-3) | HA622 (R-3) | HA909 (R-3) |
|---|---|---|---|---|---|---|---|---|---|---|
| $SiO_2$ | 52.032 | 51.879 | 51.188 | 51.507 | 50.738 | 50.130 | 51.257 | 50.895 | 50.336 | 52.173 |
| $TiO_2$ | 0.198 | 0.219 | 0.207 | 0.288 | 0.235 | 0.285 | 0.204 | 0.229 | 0.174 | 0.192 |
| $Al_2O_3$ | 1.570 | 2.328 | 1.938 | 2.010 | 2.008 | 2.434 | 1.980 | 2.231 | 1.357 | 1.669 |
| $Cr_2O_3$ | 0.113 | 0.067 | 0.026 | 0.025 | 0.054 | 0.045 | 0.039 | 0.056 | 0.008 | 0.009 |
| $FeO,Fe_2O_3$ | 9.862 | 7.895 | 11.994 | 10.001 | 10.087 | 11.717 | 11.464 | 12.384 | 18.481 | 11.023 |
| MnO | 0.194 | 0.244 | 0.321 | 0.216 | 0.237 | 0.255 | 0.243 | 0.265 | 0.329 | 0.323 |
| MgO | 13.568 | 14.185 | 11.884 | 13.259 | 13.567 | 13.202 | 12.740 | 12.415 | 8.762 | 12.979 |
| CaO | 22.128 | 22.770 | 21.821 | 21.906 | 22.964 | 22.212 | 21.742 | 21.635 | 19.839 | 21.391 |
| $Na_2O$ | 0.135 | 0.425 | 0.334 | 0.365 | - | - | 0.334 | 0.432 | 0.330 | 0.493 |
| $K_2O$ | 0.000 | 0.014 | 0.000 | 0.004 | - | - | 0.000 | 0.000 | 0.000 | 0.010 |
| TOTAL | 99.80 | 100.03 | 99.71 | 99.58 | 99.89 | 100.28 | 100.00 | 100.54 | 99.62 | 100.26 |
| Si | 1.9556 | 1.9327 | 1.9455 | 1.9415 | 1.9157 | 1.8972 | 1.9333 | 1.9225 | 1.9646 | 1.9584 |
| Ti | 0.0055 | 0.0061 | 0.0059 | 0.0081 | 0.0066 | 0.0081 | 0.0058 | 0.0065 | 0.0051 | 0.0054 |
| Al | 0.0695 | 0.1022 | 0.0868 | 0.0893 | 0.0894 | 0.1086 | 0.0884 | 0.0993 | 0.0624 | 0.0738 |
| Cr | 0.0033 | 0.0019 | 0.0007 | 0.0007 | 0.0016 | 0.0013 | 0.0011 | 0.0016 | 0.0002 | 0.0003 |
| Fe | 0.3100 | 0.2459 | 0.3813 | 0.3152 | 0.3185 | 0.3707 | 0.3630 | 0.3912 | 0.6034 | 0.3460 |
| Mn | 0.0062 | 0.0076 | 0.0103 | 0.0069 | 0.0075 | 0.0081 | 0.0077 | 0.0085 | 0.0108 | 0.0102 |
| Mg | 0.7599 | 0.7876 | 0.6731 | 0.7448 | 0.7634 | 0.7446 | 0.7189 | 0.6989 | 0.5096 | 0.7260 |
| Ca | 0.8911 | 0.9089 | 0.8887 | 0.8825 | 0.9290 | 0.9007 | 0.8821 | 0.8757 | 0.8296 | 0.8603 |
| Na | 0.0099 | 0.0307 | 0.0246 | 0.0267 | - | - | 0.0245 | 0.0316 | 0.0249 | 0.0359 |
| K | 0.0000 | 0.0007 | 0.0000 | 0.0001 | - | - | 0.0000 | 0.0000 | 0.0000 | 0.0004 |
| TOTAL | 4.0110 | 4.0243 | 4.0169 | 4.0158 | 4.0317 | 4.0393 | 4.0248 | 4.0358 | 4.0106 | 4.0167 |

| Sample No. | HA980 (R-2) | HA725 (R-3) | HA239 (R-6) | HA888 (R-4) | HA973 (R-5) | HA987 (R-5) | HA1050 (C-3) | HA1045 (C-3) | HA1025 (C-3) |
|---|---|---|---|---|---|---|---|---|---|
| $SiO_2$ | 51.427 | 50.543 | 52.112 | 50.794 | 51.045 | 52.003 | 51.112 | 50.790 | 51.915 |
| $TiO_2$ | 0.285 | 0.232 | 0.259 | 0.205 | 0.239 | 0.191 | 0.194 | 0.214 | 0.327 |
| $Al_2O_3$ | 2.492 | 1.823 | 2.240 | 1.656 | 1.893 | 2.426 | 1.827 | 2.088 | 2.218 |
| $Cr_2O_3$ | 0.012 | 0.013 | 0.216 | 0.024 | 0.054 | 0.124 | - | - | - |
| $FeO,Fe_2O_3$ | 8.866 | 15.245 | 7.013 | 14.960 | 12.136 | 7.135 | 13.647 | 13.085 | 7.717 |
| MnO | 0.302 | 0.339 | 0.197 | 0.264 | 0.217 | 0.210 | 0.399 | 0.280 | 0.200 |
| MgO | 13.522 | 10.466 | 14.748 | 10.946 | 12.149 | 14.878 | 11.517 | 11.669 | 14.326 |
| CaO | 22.300 | 20.833 | 22.154 | 19.899 | 21.807 | 22.375 | 21.356 | 21.335 | 22.346 |
| $Na_2O$ | 0.427 | 0.357 | 0.200 | 0.410 | 0.301 | 0.531 | 0.269 | 0.308 | 0.394 |
| $K_2O$ | 0.004 | 0.000 | 0.002 | 0.000 | 0.000 | 0.000 | 0.000 | 0.002 | 0.032 |
| TOTAL | 99.64 | 99.85 | 99.14 | 99.16 | 99.84 | 99.87 | 100.32 | 99.77 | 99.48 |
| Si | 1.9265 | 1.9441 | 1.9447 | 1.9583 | 1.9388 | 1.9314 | 1.9432 | 1.9369 | 1.9399 |
| Ti | 0.0080 | 0.0066 | 0.0072 | 0.0059 | 0.0068 | 0.0053 | 0.0055 | 0.0061 | 0.0091 |
| Al | 0.1107 | 0.0826 | 0.0985 | 0.0753 | 0.0847 | 0.1062 | 0.0818 | 0.0938 | 0.0977 |
| Cr | 0.0003 | 0.0003 | 0.0063 | 0.0007 | 0.0016 | 0.0036 | - | - | - |
| Fe | 0.2793 | 0.4904 | 0.2189 | 0.4825 | 0.3855 | 0.2216 | 0.4339 | 0.4173 | 0.2411 |
| Mn | 0.0096 | 0.0110 | 0.0062 | 0.0086 | 0.0069 | 0.0066 | 0.0128 | 0.0090 | 0.0063 |
| Mg | 0.7591 | 0.5999 | 0.8202 | 0.6289 | 0.6877 | 0.8235 | 0.6525 | 0.6632 | 0.7978 |
| Ca | 0.9002 | 0.8587 | 0.8858 | 0.8218 | 0.8874 | 0.8904 | 0.8700 | 0.8717 | 0.8947 |
| Na | 0.0311 | 0.0266 | 0.0145 | 0.0307 | 0.0222 | 0.0382 | 0.0198 | 0.0227 | 0.0285 |
| K | 0.0001 | 0.0000 | 0.0001 | 0.0000 | 0.0000 | 0.0000 | 0.0000 | 0.0001 | 0.0015 |
| TOTAL | 4.0249 | 4.0202 | 4.0024 | 4.0127 | 4.0216 | 4.0268 | 4.0195 | 4.0208 | 4.0166 |

TABLE A2-6: Mean microprobe analyses of clinopyroxene in salite-bearing amphibolite specimens. The number of grains analysed are indicated in parentheses. Ionic proportions on the basis of 6 oxygens.

| Sample No. | HA1091 (3) | HA1129 (2) | HA1110 (2) |
|---|---|---|---|
| $SiO_2$ | 52,179 | 51,599 | 50,801 |
| $TiO_2$ | 0,072 | 0,066 | 0,172 |
| $Al_2O_3$ | 1,545 | 1,589 | 1,912 |
| $FeO,Fe_2O_3$ | 9,525 | 10,051 | 11,868 |
| MnO | 0,550 | 0,347 | 0,360 |
| MgO | 13,086 | 12,555 | 11,198 |
| CaO | 23,110 | 22,792 | 23,137 |
| $Na_2O$ | 0,361 | 0,433 | 0,329 |
| $K_2O$ | 0,007 | 0,003 | 0,001 |
| TOTAL | 100,44 | 99,44 | 99,78 |
| Si | 1,9535 | 1,9553 | 1,9380 |
| Ti | 0,0020 | 0,0013 | 0,0049 |
| Al | 0,0681 | 0,0709 | 0,0860 |
| Fe | 0,2982 | 0,3185 | 0,3786 |
| Mn | 0,0174 | 0,0111 | 0,0116 |
| Mg | 0,7301 | 0,7090 | 0,6367 |
| Ca | 0,9271 | 0,9254 | 0,9458 |
| Na | 0,0261 | 0,0318 | 0,0243 |
| K | 0,0003 | 0,0002 | 0,0000 |
| TOTAL | 4,0228 | 4,0235 | 4,0259 |

Table A2-7: Mean microprobe analyses of coexisting minerals in garnet granulite specimen HA1030. The number of grains analysed of each mineral are indicated in parentheses. All grains were analysed in their centres. Ionic proportions were computed on the following basis: garnet - 12 oxygens, orthopyroxene - 6 oxygens, clinopyroxene - 6 oxygens, plagioclase - 8 oxygens. In case of the garnet analyses (a) and (b) represent respectively the uncorrected and $Fe_2O_3$ corrected compositions. Corrections were done by the method outlined in Appendix I D.

| Mineral | GARNET(a) (5) | GARNET(b) (5) | ORTHOPYROXENE (7) | CLINOPYROXENE (7) | PLAGIOCLASE (4) |
|---|---|---|---|---|---|
| $SiO_2$ | 37,191 | 37,191 | 49,191 | 50,056 | 45,615 |
| $TiO_2$ | 0,065 | 0,065 | 0,067 | 0,185 | - |
| $Al_2O_3$ | 20,989 | 20,989 | 0,990 | 1,953 | 34,403 |
| FeO | 29,217 | 28,122 | 34,868 | 16,646 | 0,262 |
| $Fe_2O_3$ | - | 1,216 | - | - | - |
| MnO | 3,000 | 3,000 | 1,235 | 0,588 | 0,006 |
| MgO | 2,513 | 2,513 | 12,916 | 9,550 | 0,005 |
| CaO | 7,615 | 7,615 | 0,927 | 20,890 | 18,430 |
| $Na_2O$ | 0,012 | 0,012 | 0,004 | 0,203 | 1,089 |
| $K_2O$ | 0,000 | 0,000 | 0,011 | 0,003 | 0,044 |
| TOTAL | 100,59 | 100,72 | 100,21 | 100,07 | 99,85 |
| Si | 2,9657 | 2,9567 | 1,9585 | 1,9357 | 2,1077 |
| Ti | 0,0038 | 0,0039 | 0,0020 | 0,0053 | - |
| Al | 1,9732 | 1,9668 | 0,0465 | 0,0887 | 1,8741 |
| $Fe^{+2}$ | 1,9485 | 1,8699 | 0,1610 | 0,5395 | 0,0101 |
| $Fe^{+3}$ | - | 0,0728 | - | - | - |
| Mn | 0,2026 | 0,2020 | 0,0416 | 0,0192 | 0,0002 |
| Mg | 0,2986 | 0,2978 | 0,7664 | 0,5532 | 0,0003 |
| Ca | 0,6506 | 0,6487 | 0,0395 | 0,8647 | 0,9125 |
| Na | 0,0018 | 0,0018 | 0,0003 | 0,0151 | 0,0976 |
| K | 0,0000 | 0,0000 | 0,0005 | 0,0001 | 0,0025 |
| TOTAL | 8,0448 | 8,0204 | 4,0163 | 4,0215 | 5,0050 |

TABLE A2-8: Mean microprobe analyses of garnet in pelitic gneiss specimens from the granulite facies. Ionic proportions on the basis of 12 oxygens. R and C refer, respectively, to rim and core compositions. Number of grains analysed are indicated in parentheses.

| Sample No. | HA1026 C(5) | HA841 C(4) | HA841 C(1) | HA143 C(6) | HA143 C(1) | HA1036 C(6) | HA505 C(3) | HA505 C(4) |
|---|---|---|---|---|---|---|---|---|
| $SiO_2$ | 38,259 | 38,082 | 38,133 | 38,245 | 38,158 | 37,999 | 37,852 | 38,396 |
| $TiO_2$ | 0,018 | 0,042 | 0,047 | - | - | - | 0,017 | - |
| $Al_2O_3$ | 22,290 | 21,823 | 21,871 | 22,049 | 22,007 | 21,934 | 22,112 | 22,333 |
| $Cr_2O_3$ | - | - | - | - | - | - | 0,010 | - |
| $FeO,Fe_2O_3$ | 29,879 | 31,135 | 31,795 | 29,120 | 30,154 | 28.907 | 29,499 | 27,179 |
| MnO | 0,580 | 0,809 | 0,760 | 0,642 | 0,736 | 1,631 | 1,873 | 1,432 |
| MgO | 8,011 | 7,538 | 7,080 | 8,667 | 8,105 | 7,511 | 7,217 | 9,120 |
| CaO | 1,334 | 1,038 | 1,083 | 0,929 | 0,931 | 1,494 | 1,005 | 0,948 |
| $Na_2O$ | - | 0,000 | - | - | - | - | 0,000 | - |
| $K_2O$ | - | 0,001 | - | - | - | - | 0,000 | - |
| TOTAL | 100,37 | 100,47 | 100,77 | 99,65 | 100,09 | 99,48 | 99,59 | 99,41 |
| Si | 2,9655 | 2,9695 | 1,9721 | 2,9745 | 2,9704 | 2,9776 | 2,9705 | 2,9757 |
| Ti | 0,0011 | 0,0024 | 0,0027 | - | - | - | 0,0009 | - |
| Al | 2,0368 | 2,0061 | 2,0096 | 2,0216 | 2,0196 | 2,0263 | 2,0457 | 2,0404 |
| Cr | - | - | - | - | - | - | 0,0006 | - |
| Fe | 1,9369 | 2,0304 | 2,0725 | 1,8941 | 1,9631 | 1,8943 | 1,9360 | 1,7616 |
| Mn | 0,0381 | 0,0534 | 0,0502 | 0,0423 | 0,0485 | 0,1082 | 0,1245 | 0,0939 |
| Mg | 0,9254 | 0,8759 | 0,8224 | 1,0045 | 0,9403 | 0,8771 | 0,8440 | 1,0533 |
| Ca | 0,1108 | 0,0867 | 0,0904 | 0,0774 | 0,0776 | 0,1254 | 0,0845 | 0,0787 |
| Na | - | 0,0000 | - | - | - | - | 0,0000 | - |
| K | - | 0,0001 | - | - | - | - | 0,0000 | - |
| TOTAL | 8,0146 | 8,0245 | 8,0202 | 8,0144 | 8,0199 | 8,0089 | 8,0067 | 8,0036 |

| Sample No. | HA505 R(1) | HA681 C(5) | HA514 C(7) | HA514 R(2) | HA329 C(6) | HA329 R(1) | HA870 C(6) | HA708 C(3) |
|---|---|---|---|---|---|---|---|---|
| $SiO_2$ | 38,723 | 38,732 | 38,200 | 38,220 | 38,315 | 38,149 | 37,828 | 38,139 |
| $TiO_2$ | - | 0,019 | 0,037 | 0,038 | 0,025 | 0,109 | 0,032 | 0,036 |
| $Al_2O_3$ | 22,451 | 22,280 | 22,193 | 22,138 | 22,260 | 22,261 | 21,732 | 22,039 |
| $Cr_2O_3$ | - | - | - | - | - | - | - | - |
| $FeO,Fe_2O_3$ | 27,401 | 27,674 | 29,690 | 31,339 | 29,117 | 30,080 | 31,292 | 30,301 |
| MnO | 1,420 | 1,626 | 0,936 | 0,915 | 1,128 | 1,291 | 0,859 | 1,114 |
| MgO | 8,991 | 8,494 | 7,984 | 6,951 | 8,584 | 7,779 | 7,156 | 7,691 |
| CaO | 0,928 | 1,136 | 1,105 | 1,079 | 0,803 | 0,815 | 1,009 | 1,137 |
| $Na_2O$ | - | - | 0,000 | - | - | - | - | 0,006 |
| $K_2O$ | - | - | 0,018 | - | - | - | - | 0,000 |
| TOTAL | 99,91 | 99,96 | 100,16 | 100,68 | 100,23 | 100,48 | 99,91 | 100,46 |
| Si | 2,9851 | 2,9934 | 2,9687 | 2,9754 | 2,9665 | 2,9621 | 2,9712 | 2,9726 |
| Ti | - | 0,0011 | 0,0021 | 0,0022 | 0,0014 | 0,0063 | 0,0018 | 0,0021 |
| Al | 2,0404 | 2,0300 | 2,0333 | 2,0317 | 2,0317 | 2,0377 | 2,0123 | 2,0250 |
| Cr | - | - | - | - | - | - | - | - |
| Fe | 1,7665 | 1,7886 | 1,9295 | 2,0404 | 1,8853 | 1,9533 | 2,0554 | 1,9751 |
| Mn | 0,0927 | 0,1064 | 0,0616 | 0,0603 | 0,0739 | 0,0849 | 0,0571 | 0,0736 |
| Mg | 1,0330 | 0,9784 | 0,9247 | 0,8065 | 0,9904 | 0,9002 | 0,8376 | 0,8934 |
| Ca | 0,0767 | 0,0941 | 0,0920 | 0,0899 | 0,0666 | 0,0678 | 0,0849 | 0,0950 |
| Na | - | - | 0,0000 | - | - | - | - | 0,0009 |
| K | - | - | 0,0018 | - | - | - | - | 0,0000 |
| TOTAL | 7,9946 | 7,9920 | 8,0137 | 8,0064 | 8,0158 | 8,0125 | 8,0203 | 8,0374 |

TABLE A2-8: (continued)

| Sample No. | HA632 C(6) | HA982B C(4) | HA982B C(2) | HA869B C(1) | HA869B C(4) | HA164 R(4) | HA164 C(5) |
|---|---|---|---|---|---|---|---|
| $SiO_2$ | 38,810 | 37,796 | 37,419 | 37,706 | 37,738 | 37,778 | 38,001 |
| $TiO_2$ | - | - | - | - | - | - | - |
| $Al_2O_3$ | 22,481 | 22,249 | 21,961 | 22,049 | 22,176 | 21,932 | 22,407 |
| $Cr_2O_3$ | - | - | - | - | - | - | - |
| $FeO,Fe_2O_3$ | 26,640 | 28,474 | 30,045 | 31,492 | 30,772 | 31,693 | 29,515 |
| MnO | 0,877 | 1,597 | 1,852 | 0,751 | 0,744 | 1,699 | 1,405 |
| MgO | 10,106 | 8,433 | 7,111 | 7,031 | 7,455 | 5,703 | 7,475 |
| CaO | 1,030 | 1,109 | 1,092 | 1,020 | 1,030 | 1,210 | 1,142 |
| $Na_2O$ | - | - | - | - | - | - | - |
| $K_2O$ | - | - | - | - | - | - | - |
| TOTAL | 99,94 | 99,66 | 99,48 | 100,05 | 99,92 | 100,02 | 99,95 |
| Si | 2,9745 | 2,9478 | 2,9514 | 2,9584 | 2,9546 | 2,9809 | 2,9636 |
| Ti | - | - | - | - | - | - | - |
| Al | 2,0313 | 2,0457 | 2,0421 | 2,0394 | 2,0468 | 2,0402 | 2,0601 |
| Cr | - | - | - | - | - | - | - |
| Fe | 1,7077 | 1,8573 | 1,9819 | 2,0663 | 2,0148 | 2,0915 | 1,9250 |
| Mn | 0,0569 | 0,1055 | 0,1238 | 0,0499 | 0,0493 | 0,1136 | 0,0928 |
| Mg | 1,1543 | 0,9802 | 0,8358 | 0,8220 | 0,8699 | 0,6705 | 0,8689 |
| Ca | 0,0846 | 0,0926 | 0,0923 | 0,0857 | 0,0864 | 0,1023 | 0,0954 |
| Na | - | - | - | - | - | - | - |
| K | - | - | - | - | - | - | - |
| TOTAL | 8,0093 | 8,0291 | 8,0273 | 8,0220 | 8,0218 | 7,9990 | 8,0058 |

TABLE A2-9: Mean microprobe analyses of cordierite in pelitic gneiss specimens from the granulite facies. Ionic proportions on the basis of 18 oxygens. R and C refer, respectively, to rim and core compositions. Number of grains analysed are indicated in parentheses. * cordierite coronas around spinel and opaque minerals, + cordierite inclusions in garnet.

| Sample No. | HA1026 C(5) | HA841 C(6) | HA143 C(5) | HA1036 C(6) | HA505 C(6) | HA681 C(4) | HA514 C(4) | HA514 R(1) |
|---|---|---|---|---|---|---|---|---|
| $SiO_2$ | 48,882 | 48,650 | 48,189 | 48,667 | 49,129 | 49,408 | 48,370 | 48,438 |
| $TiO_2$ | 0,000 | 0,001 | 0,000 | - | 0,006 | 0,002 | 0,018 | 0,042 |
| $Al_2O_3$ | 33,926 | 33,384 | 33,307 | 33,617 | 33,577 | 33,811 | 33,401 | 33,315 |
| $Cr_2O_3$ | - | - | - | - | - | - | - | - |
| $FeO,Fe_2O_3$ | 6,534 | 7,098 | 5,947 | 6,255 | 5,810 | 5,883 | 6,534 | 6,141 |
| MnO | 0,019 | 0,035 | 0,037 | 0,097 | 0,114 | 0,142 | 0,054 | 0,060 |
| MgO | 9,235 | 8,754 | 9,684 | 9,536 | 9,646 | 9,419 | 9,160 | 9,397 |
| CaO | 0,015 | 0,007 | 0,013 | 0,008 | 0,016 | 0,020 | - | - |
| $Na_2O$ | 0,048 | 0,304 | 0,075 | 0,094 | 0,038 | 0,110 | 0,114 | 0,084 |
| $K_2O$ | 0,000 | 0,000 | 0,006 | 0,006 | 0,000 | 0,005 | 0,000 | 0,000 |
| TOTAL | 98,66 | 98,23 | 97,26 | 98,28 | 98,34 | 98,80 | 97,65 | 97,48 |
| Si | 4,9695 | 4,9855 | 4,9619 | 4,9656 | 5,0036 | 5,0253 | 4,9721 | 4,9785 |
| Ti | 0,0000 | 0,0001 | 0,0000 | - | 0,0005 | 0,0002 | 0,0014 | 0,0032 |
| Al | 4,0661 | 4,0333 | 4,0432 | 4,0437 | 4,0260 | 4,0392 | 4,0477 | 4,0367 |
| Cr | - | - | - | - | - | - | - | - |
| Fe | 0,5555 | 0,6082 | 0,5121 | 0,5337 | 0,4948 | 0,5004 | 0,5617 | 0,5279 |
| Mn | 0,0016 | 0,0030 | 0,0032 | 0,0083 | 0,0098 | 0,0123 | 0,0047 | 0,0052 |
| Mg | 1,3992 | 1,3370 | 1,4861 | 1,4501 | 1,4641 | 1,4277 | 1,4032 | 1,4394 |
| Ca | 0,0016 | 0,0007 | 0,0014 | 0,0010 | 0,0017 | 0,0022 | - | - |
| Na | 0,0095 | 0,0605 | 0,0150 | 0,0186 | 0,0076 | 0,0218 | 0,0228 | 0,0169 |
| K | 0,0000 | 0,0000 | 0,0000 | 0,0007 | 0,0000 | 0,0006 | 0,0000 | 0,0000 |
| TOTAL | 11,0030 | 11,0283 | 11,0237 | 11,0217 | 11,0081 | 11,0297 | 11,0136 | 11,0082 |

TABLE A2-9: (continued)

| Sample No. | HA514 R(1) | HA329 C(6) | HA329 C(1) | HA329 R(1) | HA870 C(5) | HA708 C(3) | *HA708 R(1) | *HA708 R(1) |
|---|---|---|---|---|---|---|---|---|
| $SiO_2$ | 48,441 | 48,696 | 48,249 | 48,474 | 48,084 | 48,054 | 48,756 | 48,355 |
| $TiO_2$ | 0,009 | 0,010 | 0,013 | 0,103 | 0,003 | 0,005 | 0,000 | 0,026 |
| $Al_2O_3$ | 33,329 | 33,715 | 33,547 | 33,968 | 33,387 | 33,463 | 34,089 | 33,809 |
| $Cr_2O_3$ | - | - | - | - | - | - | - | - |
| $FeO,Fe_2O_3$ | 6,465 | 5,856 | 6,063 | 5,094 | 7,331 | 6,731 | 4,217 | 4,961 |
| MnO | 0,066 | 0,080 | 0,087 | 0,070 | 0,074 | 0,089 | 0,055 | 0,047 |
| MgO | 9,162 | 9,650 | 9,568 | 10,373 | 8,710 | 9,172 | 10,715 | 10,412 |
| CaO | - | 0,002 | - | - | - | - | - | - |
| $Na_2O$ | 0,108 | 0,122 | 0,151 | 0,103 | 0,058 | 0,095 | 0,030 | 0,036 |
| $K_2O$ | 0,008 | 0,000 | 0,000 | 0,014 | 0,012 | 0,010 | 0,011 | 0,006 |
| TOTAL | 97,59 | 98,13 | 97,68 | 98,20 | 97,66 | 97,62 | 97,87 | 97,65 |
| Si | 4,9806 | 4,9662 | 4,9515 | 4,9278 | 4,9612 | 4,9492 | 4,9477 | 4,9374 |
| Ti | 0,0006 | 0,0007 | 0,0010 | 0,0078 | 0,0002 | 0,0003 | 0,0000 | 0,0020 |
| Al | 4,0401 | 4,0537 | 4,0587 | 4,0710 | 4,0612 | 4,0632 | 4,0782 | 4,0697 |
| Cr | - | - | - | - | - | - | - | - |
| Fe | 0,5559 | 0,4995 | 0,5204 | 0,4331 | 0,6326 | 0,5798 | 0,3579 | 0,4236 |
| Mn | 0,0058 | 0,0068 | 0,0076 | 0,0060 | 0,0065 | 0,0078 | 0,0047 | 0,0041 |
| Mg | 1,4039 | 1,4667 | 1,4635 | 1,5715 | 1,3393 | 1,4079 | 1,6205 | 1,5845 |
| Ca | - | 0,0003 | - | - | - | - | - | - |
| Na | 0,0216 | 0,0242 | 0,0301 | 0,0204 | 0,0116 | 0,0190 | 0,0059 | 0,0072 |
| K | 0,0010 | 0,0000 | 0,0000 | 0,0018 | 0,0016 | 0,0013 | 0,0014 | 0,0008 |
| TOTAL | 11,0098 | 11,0181 | 11,0330 | 11,0399 | 11,0142 | 11,0285 | 11,0167 | 11,0297 |

| Sample No. | +HA708 C(1) | +HA708 C(1) | HA632 C(5) | HA982B C(5) | HA869B C(5) | HA164 R(5) | HA164 C(5) |
|---|---|---|---|---|---|---|---|
| $SiO_2$ | 48,185 | 48,286 | 48,698 | 48,914 | 48,512 | 48,862 | 48,893 |
| $TiO_2$ | 0,000 | 0,000 | 0,004 | 0,003 | 0,003 | 0,008 | 0,012 |
| $Al_2O_3$ | 33,634 | 33,694 | 33,561 | 33,696 | 33,437 | 33,086 | 32,992 |
| $Cr_2O_3$ | - | - | - | - | - | - | - |
| $FeO,Fe_2O_3$ | 5,507 | 5,218 | 5,370 | 5,752 | 7,107 | 5,086 | 5,791 |
| MnO | 0,054 | 0,054 | 0,043 | 0,109 | 0,050 | 0,058 | 0,079 |
| MgO | 9,947 | 10,000 | 9,847 | 9,731 | 8,935 | 10,406 | 10,007 |
| CaO | - | - | - | - | - | - | - |
| $Na_2O$ | 0,076 | 0,131 | 0,034 | 0,090 | 0,104 | 0,058 | 0,066 |
| $K_2O$ | 0,020 | 0,028 | 0,006 | 0,007 | 0,019 | 0,033 | 0,028 |
| TOTAL | 97,42 | 97,41 | 97,56 | 98,30 | 98,17 | 97,60 | 97,87 |
| Si | 4,9445 | 4,9491 | 4,9809 | 4,9764 | 4,9733 | 4,9934 | 4,9988 |
| Ti | 0,0000 | 0,000 | 0,0003 | 0,0003 | 0,0002 | 0,0006 | 0,0009 |
| Al | 4,0688 | 4,0714 | 4,0468 | 4,0416 | 4,0413 | 3,9860 | 3,9766 |
| Cr | - | - | - | - | - | - | - |
| Fe | 0,4726 | 0,4473 | 0,4593 | 0,4894 | 0,6093 | 0,4347 | 0,4951 |
| Mn | 0,0047 | 0,0046 | 0,0037 | 0,0094 | 0,0043 | 0,0051 | 0,0068 |
| Mg | 1,5212 | 1,5275 | 1,5011 | 1,4755 | 1,3652 | 1,5848 | 1,5248 |
| Ca | - | - | - | - | - | - | - |
| Na | 0,0152 | 0,0261 | 0,0068 | 0,0178 | 0,0208 | 0,0115 | 0,0132 |
| K | 0,0026 | 0,0036 | 0,0008 | 0,0010 | 0,0025 | 0,0044 | 0,0036 |
| TOTAL | 11,0299 | 11,0300 | 10,9997 | 11,0114 | 11,0169 | 11,0205 | 11,0198 |

TABLE A2-10: Mean microprobe analyses of biotite in aluminous gneiss (*) and semipelitic biotite-garnet gneiss (▲). Compositions refer to grain centres. The number of analyses per specimen are indicated in parenthesis. Ionic proportions on the basis of 11 oxygens.

| Sample No. | HA632* (3) | HA869/B* (5) | HA1026* (4) | HA982/B* (6) | HA559▲ (6) | HA735▲ (6) | HA1041▲ (4) | HA1081▲ (4) |
|---|---|---|---|---|---|---|---|---|
| $SiO_2$ | 35,581 | 36,536 | 35,777 | 36,275 | 36,215 | 36,842 | 36,331 | 35,085 |
| $TiO_2$ | 4,997 | 4,725 | 5,066 | 4,134 | 4,614 | 5,474 | 4,406 | 3,592 |
| $Al_2O_3$ | 15,823 | 15,678 | 16,529 | 17,010 | 16,155 | 15,416 | 16,869 | 17,501 |
| $FeO,Fe_2O_3$ | 14,253 | 15,692 | 17,670 | 15,316 | 16,744 | 16,293 | 15,795 | 20,476 |
| MnO | 0,018 | - | - | 0,062 | 0,023 | 0,002 | - | 0,036 |
| MgO | 13,991 | 13,325 | 11,211 | 13,188 | 12,193 | 12,865 | 13,475 | 10,218 |
| CaO | 0,002 | 0,021 | 0,038 | 0,006 | 0,023 | 0,024 | 0,016 | 0,010 |
| $Na_2O$ | 0,106 | 0,143 | 0,055 | 0,101 | 0,112 | 0,112 | 0,142 | 0,084 |
| $K_2O$ | 9,529 | 9,441 | 9,488 | 9,392 | 9,478 | 9,509 | 9,394 | 9,479 |
| TOTAL | 94,30 | 95,56 | 95,83 | 95,48 | 95,56 | 96,54 | 96,43 | 96,48 |
| Si | 2,6875 | 2,7326 | 2,6948 | 2,7060 | 2,7227 | 2,7348 | 2,6901 | 2,6607 |
| Ti | 0,2838 | 0,2658 | 0,2869 | 0,2320 | 0,2608 | 0,3056 | 0,2453 | 0,2049 |
| Al | 1,4090 | 1,3824 | 1,4677 | 1,4959 | 1,4318 | 1,3491 | 1,4725 | 1,5646 |
| Fe | 0,9003 | 0,9815 | 1,1131 | 0,9556 | 1,0528 | 1,0116 | 0,9780 | 1,2987 |
| Mn | 0,0011 | - | - | 0,0039 | 0,0015 | 0,0001 | - | 0,0023 |
| Mg | 1,5749 | 1,4850 | 1,2585 | 1,4663 | 1,3661 | 1,4231 | 1,4870 | 1,1549 |
| Ca | 0,0002 | 0,0017 | 0,0031 | 0,0005 | 0,0019 | 0,0019 | 0,0013 | 0,0008 |
| Na | 0,0156 | 0,0208 | 0,0081 | 0,0146 | 0,0164 | 0,0162 | 0,0203 | 0,0124 |
| K | 0,9182 | 0,9009 | 0,9118 | 0,8938 | 0,9090 | 0,9006 | 0,8874 | 0,9171 |
| TOTAL | 7,7906 | 7,7707 | 7,7440 | 7,7686 | 7,7630 | 7,7430 | 7,7819 | 7,8164 |

TABLE A2-11: Microprobe analyses along a traverse across a garnet grain in specimen HA 164. Analysis A represents the composition of the garnet rim at the contact with cordierite and analysis P is the rim composition of the garnet at the contact with quartz. Ionic proportions on the basis of 12 oxygens.

| Analysis | A | B | C | D | E | F | G | H |
|---|---|---|---|---|---|---|---|---|
| $SiO_2$ | 37,722 | 37,759 | 37,778 | 37,773 | 38,129 | 38,031 | 37,830 | 37,703 |
| $Al_2O_3$ | 21,832 | 21,822 | 21,810 | 22,102 | 22,392 | 22,262 | 22,229 | 22,191 |
| FeO | 32,072 | 31,726 | 31,732 | 31,050 | 30,346 | 30,292 | 29,943 | 29,762 |
| MnO | 1,768 | 1,795 | 1,740 | 1,538 | 1,435 | 1,468 | 1,412 | 1,362 |
| MgO | 5,515 | 5,649 | 6,011 | 6,345 | 6,822 | 7,132 | 7,205 | 7,259 |
| CaO | 1,205 | 1,261 | 1,143 | 1,154 | 1,130 | 1,153 | 1,131 | 1,108 |
| TOTAL | 100,11 | 100,01 | 100,21 | 99,96 | 100,25 | 100,34 | 99,75 | 99,38 |
| Si | 2,9803 | 2,9825 | 2,9761 | 2,9704 | 2,9743 | 2,9658 | 2,9640 | 2,9629 |
| Al | 2,0335 | 2,0319 | 2,0256 | 2,0490 | 2,0593 | 2,0467 | 2,0532 | 2,0559 |
| Fe | 2,1191 | 2,0956 | 2,0907 | 2,0420 | 1,9797 | 1,9757 | 1,9620 | 1,9560 |
| Mn | 0,1183 | 0,1201 | 0,1161 | 0,1024 | 0,0948 | 0,0969 | 0,0937 | 0,0906 |
| Mg | 0,6494 | 0,6649 | 0,7058 | 0,7436 | 0,7931 | 0,8289 | 0,8413 | 0,8502 |
| Ca | 0,1020 | 0,1067 | 0,0964 | 0,0972 | 0,0945 | 0,0964 | 0,0950 | 0,0933 |
| TOTAL | 8,0028 | 8,0019 | 8,0109 | 8,0050 | 7,9959 | 8,0107 | 8,0095 | 8,0092 |

| Analysis | I | J | K | L | M | N | O | P |
|---|---|---|---|---|---|---|---|---|
| $SiO_2$ | 37,812 | 37,940 | 38,032 | 38,019 | 37,949 | 38,065 | 38,135 | 38,306 |
| $Al_2O_3$ | 22,917 | 22,342 | 22,316 | 22,728 | 22,343 | 22,307 | 22,262 | 22,221 |
| FeO | 29,105 | 29,542 | 29,699 | 29,171 | 29,617 | 29,545 | 29,593 | 29,570 |
| MnO | 1,351 | 1,376 | 1,409 | 1,389 | 1,417 | 1,434 | 1,426 | 1,437 |
| MgO | 7,337 | 7,492 | 7,459 | 7,467 | 7,508 | 7,451 | 7,434 | 7,350 |
| CaO | 1,134 | 1,161 | 1,172 | 1,114 | 1,163 | 1,101 | 1,149 | 1,140 |
| TOTAL | 99,65 | 99,85 | 100,08 | 99,89 | 99,99 | 99,90 | 100,00 | 100,02 |
| Si | 2,9504 | 2,9626 | 2,9648 | 2,9600 | 2,9606 | 2,9701 | 2,9733 | 2,9842 |
| Al | 2,1082 | 2,0567 | 2,0509 | 2,0861 | 2,0549 | 2,0520 | 2,0463 | 2,0408 |
| Fe | 1,8993 | 1,9292 | 1,9362 | 1,8994 | 1,9324 | 1,9280 | 1,9296 | 1,9266 |
| Mn | 0,0892 | 0,0910 | 0,0930 | 0,0916 | 0,0936 | 0,0948 | 0,0942 | 0,0948 |
| Mg | 0,8531 | 0,8719 | 0,8666 | 0,8664 | 0,8730 | 0,8664 | 0,8638 | 0,8533 |
| Ca | 0,0948 | 0,0972 | 0,0979 | 0,0929 | 0,0972 | 0,0920 | 0,0960 | 0,0951 |
| TOTAL | 7,9953 | 8,0089 | 8,0096 | 7,9968 | 8,0119 | 8,0037 | 8,0034 | 7,9952 |

TABLE A2-12: Microprobe analyses along a traverse across a cordierite grain in specimen HA 164. Analysis 1A represents the composition of cordierite at the contact with garnet and analysis 1K was recorded in the core of the grain. Ionic proportions on the basis of 18 oxygens.

| Analysis | A | B | B | C | D | E | F | G |
|---|---|---|---|---|---|---|---|---|
| $SiO_2$ | 48,922 | 48,555 | 48,622 | 48,983 | 49,168 | 49,001 | 48,740 | 48,954 |
| $TiO_2$ | 0,017 | 0,013 | 0,017 | 0,011 | 0,020 | 0,009 | 0,015 | 0,019 |
| $Al_2O_3$ | 33,672 | 32,588 | 32,594 | 33,178 | 33,121 | 33,010 | 33,009 | 33,080 |
| FeO | 4,518 | 5,289 | 5,357 | 5,612 | 5,884 | 5,553 | 5,743 | 5,805 |
| MnO | 0,047 | 0,060 | 0,051 | 0,068 | 0,078 | 0,059 | 0,069 | 0,082 |
| MgO | 10,641 | 10,109 | 10,094 | 10,207 | 10,079 | 10,185 | 10,019 | 10,073 |
| CaO | 0,000 | — | — | — | — | — | — | — |
| $Na_2O$ | 0,039 | 0,071 | 0,053 | 0,058 | 0,039 | 0,078 | 0,029 | 0,079 |
| $K_2O$ | 0,026 | 0,013 | 0,019 | 0,017 | 0,043 | 0,020 | 0,080 | 0,057 |
| TOTAL | 97,88 | 96,70 | 96,81 | 98,13 | 98,43 | 97,91 | 97,70 | 98,15 |
| Si | 4,9709 | 5,0119 | 5,0141 | 4,9900 | 4,9997 | 5,0014 | 4,9918 | 4,9928 |
| Ti | 0,0013 | 0,0010 | 0,0013 | 0,0008 | 0,0015 | 0,0007 | 0,0011 | 0,0014 |
| Al | 4,0336 | 3,9657 | 3,9627 | 3,9848 | 3,9706 | 3,9721 | 3,9855 | 3,9775 |
| Fe | 0,3839 | 0,4566 | 0,4621 | 0,4781 | 0,5004 | 0,4740 | 0,4919 | 0,4951 |
| Mn | 0,0041 | 0,0052 | 0,0045 | 0,0058 | 0,0067 | 0,0051 | 0,0059 | 0,0071 |
| Mg | 1,6113 | 1,5552 | 1,5514 | 1,5498 | 1,5274 | 1,5492 | 1,5293 | 1,5311 |
| Ca | 0,0000 | — | — | — | — | — | — | — |
| Na | 0,0077 | 0,0143 | 0,0107 | 0,0115 | 0,0076 | 0,0154 | 0,0058 | 0,0156 |
| K | 0,0034 | 0,0018 | 0,0025 | 0,0022 | 0,0056 | 0,0026 | 0,0105 | 0,0075 |
| TOTAL | 11,0165 | 11,0121 | 11,0097 | 11,0235 | 11,0200 | 11,0208 | 11,0223 | 11,0285 |

| Analysis | H | I | J | K |
|---|---|---|---|---|
| $SiO_2$ | 49,113 | 48,819 | 49,027 | 48,550 |
| $TiO_2$ | 0,009 | 0,007 | 0,010 | 0,017 |
| $Al_2O_3$ | 33,073 | 32,920 | 33,169 | 32,719 |
| FeO | 5,723 | 5,843 | 5,821 | 5,761 |
| MnO | 0,078 | 0,078 | 0,071 | 0,086 |
| MgO | 10,094 | 9,900 | 10,067 | 9,900 |
| CaO | — | — | — | — |
| $Na_2O$ | 0,060 | 0,033 | 0,062 | 0,097 |
| $K_2O$ | 0,030 | 0,015 | 0,020 | 0,017 |
| TOTAL | 98,18 | 97,61 | 98,25 | 97,15 |
| Si | 5,0029 | 5,0037 | 4,9933 | 5,0011 |
| Ti | 0,0007 | 0,0005 | 0,0007 | 0,0013 |
| Al | 3,9718 | 3,9778 | 3,9826 | 3,9734 |
| Fe | 0,4875 | 0,5009 | 0,4958 | 0,4963 |
| Mn | 0,0067 | 0,0068 | 0,0061 | 0,0075 |
| Mg | 1,5324 | 1,5123 | 1,5281 | 1,5199 |
| Ca | — | — | — | — |
| Na | 0,0120 | 0,0066 | 0,0122 | 0,0195 |
| K | 0,0039 | 0,0019 | 0,0026 | 0,0022 |
| TOTAL | 11,0184 | 11,0110 | 11,0219 | 11,0216 |

TABLE A2-13: Mean microprobe analyses of plagioclase (core compositions) in pelitic gneiss specimens from the granulite facies terrane. The number of grains analysed per specimen is indicated in brackets. Ionic proportions on the basis of 8 oxygens.

| Sample | HA681 | HA505 | HA1026 | HA841 | HA708 | HA870 |
|---|---|---|---|---|---|---|
| No. | (4) | (3) | (3) | (3) | (5) | (4) |
| $SiO_2$ | 59,588 | 60,716 | 56,879 | 57,819 | 59,628 | 60,068 |
| $Al_2O_3$ | 26,023 | 25,030 | 27,315 | 26,528 | 25,608 | 25,116 |
| FeO | 0,053 | 0,059 | 0,031 | 0,049 | 0,008 | 0,000 |
| CaO | 7,562 | 6,181 | 9,341 | 8,506 | 7,514 | 6,911 |
| $Na_2O$ | 7,501 | 8,269 | 6,358 | 7,091 | 7,214 | 7,569 |
| $K_2O$ | 0,219 | 0,187 | 0,172 | 0,208 | 0,238 | 0,195 |
| TOTAL | 100,95 | 100,44 | 100,10 | 100,20 | 100,21 | 99,86 |
| Si | 2,6372 | 2,6897 | 2,5509 | 2,5882 | 2,6538 | 2,6782 |
| Al | 1,3578 | 1,3073 | 1,4439 | 1,4000 | 1,3437 | 1,3202 |
| Fe | 0,0016 | 0,0021 | 0,0015 | 0,0018 | 0,0003 | 0,0000 |
| Ca | 0,3586 | 0,2933 | 0,4489 | 0,4079 | 0,3583 | 0,3302 |
| Na | 0,6437 | 0,7102 | 0,5529 | 0,6154 | 0,6226 | 0,6544 |
| K | 0,0124 | 0,0105 | 0,0099 | 0,0119 | 0,0135 | 0,0111 |
| TOTAL | 5,0113 | 5,0131 | 5,0080 | 5,0252 | 4,9922 | 4,9941 |

| Sample | HA329 | HA869/B | HA632 | HA164 | HA1036 | HA143 |
|---|---|---|---|---|---|---|
| No. | (1) | (4) | (4) | (6) | (4) | (4) |
| $SiO_2$ | 63,279 | 60,009 | 60,150 | 58,865 | 50,477 | 61,464 |
| $Al_2O_3$ | 23,501 | 25,216 | 25,130 | 25,628 | 31,376 | 21,696 |
| FeO | 0,000 | 0,000 | 0,007 | 0,440 | 0,112 | 0,000 |
| CaO | 4,933 | 6,943 | 6,858 | 7,449 | 14,451 | 5,566 |
| $Na_2O$ | 8,831 | 7,259 | 7,581 | 7,556 | 3,486 | 8,377 |
| $K_2O$ | 0,316 | 0,227 | 0,167 | 0,147 | 0,117 | 0,184 |
| TOTAL | 100,86 | 99,65 | 99,89 | 100,09 | 100,02 | 97,29 |
| Si | 2,7789 | 2,6784 | 2,6799 | 2,6334 | 2,3010 | 2,8017 |
| Al | 1,2167 | 1,3268 | 1,3200 | 1,3516 | 1,6863 | 1,1659 |
| Fe | 0,0000 | 0,0000 | 0,0003 | 0,0165 | 0,0041 | 0,0000 |
| Ca | 0,2321 | 0,3320 | 0,3274 | 0,3570 | 0,7059 | 0,2718 |
| Na | 0,7520 | 0,6283 | 0,6549 | 0,6554 | 0,3080 | 0,7404 |
| K | 0,0177 | 0,0129 | 0,0095 | 0,0084 | 0,0068 | 0,0107 |
| TOTAL | 4,9975 | 4,9784 | 4,9920 | 5,0223 | 5,0121 | 4,9908 |

TABLE A2-14 : Microprobe analyses of zoned plagioclase grains in pelitic gneiss specimen HA841. All grains are in contact with garnet. Analyses A represent rim compositions while 1C, 2E and 3D are core compositions of grains 1,2 and 3 respectively. A,B,C,D etc. are spot analyses along a traverse from rim to core. Ionic proportions on the basis of 8 oxygens.

| Grain | 1A | 1B | 1C | 2A | 2B | 2C |
|---|---|---|---|---|---|---|
| $SiO_2$ | 57,184 | 56,893 | 57,733 | 58,225 | 57,797 | 57,830 |
| $Al_2O_3$ | 25,866 | 26,022 | 25,800 | 25,979 | 26,002 | 25,793 |
| FeO | 0,173 | 0,283 | 0,000 | 0,007 | 0,000 | 0,000 |
| MnO | 0,005 | 0,003 | – | – | – | – |
| MgO | 0,026 | 0,109 | – | – | – | – |
| CaO | 8,583 | 8,508 | 8,380 | 8,349 | 8,334 | 8,315 |
| $Na_2O$ | 7,055 | 6,905 | 7,107 | 7,385 | 7,323 | 7,377 |
| $K_2O$ | 0,169 | 0,366 | 0,188 | 0,181 | 0,200 | 0,215 |
| TOTAL | 99,06 | 99,09 | 99,22 | 100,12 | 99,65 | 99,53 |
| Si | 2,5927 | 2,5823 | 2,6081 | 2,6077 | 2,6015 | 2,6068 |
| Al | 1,3826 | 1,3924 | 1,3741 | 1,3717 | 1,3797 | 1,3707 |
| Fe | 0,0065 | 0,0107 | 0,0000 | 0,0002 | 0,0000 | 0,0000 |
| Mn | 0,0002 | 0,0001 | – | – | – | – |
| Mg | 0,0017 | 0,0073 | – | – | – | – |
| Ca | 0,4169 | 0,4137 | 0,4056 | 0,4006 | 0,4019 | 0,4016 |
| Na | 0,6202 | 0,6077 | 0,6226 | 0,6413 | 0,6391 | 0,6448 |
| K | 0,0097 | 0,0212 | 0,0108 | 0,0103 | 0,0115 | 0,0123 |
| TOTAL | 5,0309 | 5,0359 | 5,0214 | 5,0321 | 5,0339 | 5,0363 |

| Grain | 2D | 2E | 3A | 3B | 3C | 3D |
|---|---|---|---|---|---|---|
| $SiO_2$ | 57,670 | 58,035 | 57,552 | 58,518 | 58,180 | 58,298 |
| $Al_2O_3$ | 25,961 | 26,180 | 25,987 | 25,884 | 25,937 | 25,950 |
| FeO | 0,000 | 0,000 | 0,000 | 0,000 | 0,000 | 0,000 |
| CaO | 8,479 | 8,506 | 8,438 | 8,355 | 8,195 | 8,349 |
| $Na_2O$ | 7,254 | 7,159 | 7,252 | 7,361 | 7,394 | 7,499 |
| $K_2O$ | 0,195 | 0,189 | 0,192 | 0,219 | 0,210 | 0,204 |
| TOTAL | 99,56 | 100,07 | 99,42 | 100,33 | 99,91 | 100,30 |
| Si | 2,5993 | 2,6003 | 2,5974 | 2,6147 | 2,6102 | 2,6078 |
| Al | 1,3794 | 1,3829 | 1,3827 | 1,3635 | 1,3718 | 1,3685 |
| Fe | 0,0000 | 0,0000 | 0,0000 | 0,0000 | 0,0000 | 0,0000 |
| Ca | 0,4095 | 0,4083 | 0,4080 | 0,4000 | 0,3939 | 0,4002 |
| Na | 0,6339 | 0,6220 | 0,6347 | 0,6378 | 0,6432 | 0,6504 |
| K | 0,0112 | 0,0108 | 0,0110 | 0,0125 | 0,0120 | 0,0116 |
| TOTAL | 5,0335 | 5,0246 | 5,0340 | 5,0286 | 5,0314 | 5,0388 |

Table A2-15: Microprobe analyses of zoned plagioclase grains, in pelitic gneiss specimen HA1036. All grains are in contact with garnet. Analyses A represent rim compositions while analyses C in grains 1,2,3 and 5 refer to core composition. In case of grain 4, analysis G was recorded in the core of the grain. A,B,C,D etc. are spot analyses along a traverse from rim to core. Ionic proportions on the basis of 8 oxygens.

| Grain | 1A | 1B | 1C | 2A | 2B | 2C | 3A |
|---|---|---|---|---|---|---|---|
| $SiO_2$ | 52,170 | 49,719 | 50,062 | 51,121 | 50,880 | 50,675 | 52,404 |
| $Al_2O_3$ | 30,187 | 31,128 | 31,584 | 30,393 | 30,840 | 30,275 | 29,795 |
| FeO | 0,204 | 0,477 | 0,119 | 0,399 | 0,085 | 1,027 | 0,588 |
| MnO | 0,001 | 0,012 | 0,002 | 0,013 | 0,098 | 0,014 | 0,022 |
| MgO | 0,007 | 0,249 | 0,037 | 0,203 | 0,094 | 0,690 | 0,233 |
| CaO | 13,208 | 13,969 | 14,728 | 13,377 | 14,186 | 12,976 | 12,613 |
| $Na_2O$ | 4,324 | 3,183 | 3,193 | 3,937 | 3,573 | 3,804 | 4,372 |
| $K_2O$ | 0,110 | 0,382 | 0,122 | 0,107 | 0,097 | 0,149 | 0,083 |
| TOTAL | 100,21 | 99,12 | 99,84 | 99,55 | 99,85 | 99,61 | 100,11 |
| Si | 2,3670 | 2,2916 | 2,2873 | 2,3388 | 2,3216 | 2,3235 | 2,3797 |
| Al | 1,6147 | 1,6914 | 1,7013 | 1,6394 | 1,6590 | 1,6365 | 1,5952 |
| Fe | 0,0077 | 0,0183 | 0,0045 | 0,0152 | 0,0032 | 0,0393 | 0,0223 |
| Mn | 0,0000 | 0,0004 | 0,0000 | 0,0004 | 0,0038 | 0,0005 | 0,0008 |
| Mg | 0,0005 | 0,0171 | 0,0025 | 0,0138 | 0,0064 | 0,0471 | 0,0157 |
| Ca | 0,6421 | 0,6899 | 0,7210 | 0,6557 | 0,6935 | 0,6375 | 0,6137 |
| Na | 0,3804 | 0,2845 | 0,2829 | 0,3492 | 0,3161 | 0,3382 | 0,3849 |
| K | 0,0063 | 0,0224 | 0,0071 | 0,0062 | 0,0056 | 0,0087 | 0,0048 |
| TOTAL | 5,0190 | 5,0161 | 5,0070 | 5,0192 | 5,0097 | 5,0316 | 5,0176 |

| Grain | 3B | 3C | 4A | 4B | 4C | 4D |
|---|---|---|---|---|---|---|
| $SiO_2$ | 50,474 | 50,324 | 51,610 | 52,194 | 50,904 | 50,464 |
| $Al_2O_3$ | 31,222 | 31,589 | 30,267 | 30,184 | 30,704 | 31,531 |
| FeO | 0,091 | 0,092 | 0,393 | 0,240 | 0,217 | 0,142 |
| MnO | 0,015 | 0,008 | 0,028 | 0,005 | — | — |
| MgO | 0,000 | 0,007 | 0,075 | 0,002 | — | — |
| CaO | 14,721 | 14,574 | 12,903 | 12,897 | 13,365 | 12,701 |
| $Na_2O$ | 3,408 | 3,340 | 4,270 | 4,468 | 4,225 | 3,599 |
| $K_2O$ | 0,076 | 0,148 | 0,063 | 0,123 | 0,092 | 1,009 |
| TOTAL | 100,01 | 100,08 | 99,61 | 100,11 | 99,50 | 99,44 |
| Si | 2,3024 | 2,2932 | 2,3563 | 2,3696 | 2,3302 | 2,3128 |
| Al | 1,6790 | 1,6971 | 1,6291 | 1,6156 | 1,6570 | 1,7037 |
| Fe | 0,0034 | 0,0035 | 0,0150 | 0,0090 | 0,0083 | 0,0054 |
| Mn | 0,0005 | 0,0003 | 0,0011 | 0,0001 | — | — |
| Mg | 0,0000 | 0,0005 | 0,0051 | 0,0001 | — | — |
| Ca | 0,7195 | 0,7116 | 0,6312 | 0,6274 | 0,6555 | 0,6237 |
| Na | 0,3014 | 0,2951 | 0,3780 | 0,3934 | 0,3750 | 0,3199 |
| K | 0,0044 | 0,0086 | 0,0036 | 0,0071 | 0,0054 | 0,0589 |
| TOTAL | 5,0109 | 5,0101 | 5,0199 | 5,0227 | 5,0315 | 5,0247 |

Table A2-15:

(Continued)

| Grain | 4E | 4F | 4G | 5A | 5B | 5C |
|---|---|---|---|---|---|---|
| $SiO_2$ | 50,792 | 50,731 | 51,306 | 54,106 | 50,533 | 50,215 |
| $Al_2O_3$ | 30,942 | 31,338 | 30,942 | 29,142 | 31,255 | 31,387 |
| FeO | 0,092 | 0,077 | 0,101 | 0,255 | 0,067 | 0,119 |
| CaO | 13,934 | 14,295 | 14,061 | 11,304 | 14,300 | 14,442 |
| $Na_2O$ | 3,841 | 3,698 | 3,923 | 5,559 | 3,702 | 3,486 |
| $K_2O$ | 0,134 | 0,093 | 0,119 | 0,078 | 0,070 | 0,078 |
| TOTAL | 99,73 | 100,23 | 100,45 | 100,44 | 99,93 | 99,73 |
| Si | 2,3202 | 2,3071 | 2,3272 | 2,4383 | 2,3054 | 2,2962 |
| Al | 1,6664 | 1,6803 | 1,6547 | 1,5483 | 1,6811 | 1,6921 |
| Fe | 0,0035 | 0,0029 | 0,0038 | 0,0096 | 0,0025 | 0,0045 |
| Ca | 0,6820 | 0,6965 | 0,6834 | 0,5458 | 0,6990 | 0,7076 |
| Na | 0,3402 | 0,3260 | 0,3450 | 0,4858 | 0,3275 | 0,3091 |
| K | 0,0078 | 0,0054 | 0,0069 | 0,0045 | 0,0041 | 0,0045 |
| TOTAL | 5,0205 | 5,0185 | 5,0213 | 5,0325 | 5,0199 | 5,0144 |

TABLE A2-16: Microprobe analyses of zoned plagioclase grains in pelitic gneiss specimen HA1026. All grains are in contact with garnet and analyses A represent rim compositions while analyses E refer to core compositions in grains 1 and 3. For grain 2, analysis C was recorded in the core of the grain. A,B,C, D etc. are spot analyses along a traverse from grain rim to core. Ionic proportions on the basis of 8 oxygens.

| Grain | 1A | 1B | 1C | 1D | 1E | 2A | 2B |
|---|---|---|---|---|---|---|---|
| $SiO_2$ | 55,212 | 57,436 | 57,238 | 56,704 | 56,810 | 56,839 | 56,839 |
| $Al_2O_3$ | 27,910 | 27,270 | 27,263 | 26,870 | 26,965 | 27,120 | 26,602 |
| FeO | 0,686 | 0,121 | 0,046 | 0,039 | 0,040 | 0,223 | 0,070 |
| CaO | 10,221 | 8,979 | 9,666 | 9,469 | 9,400 | 9,542 | 9,163 |
| $Na_2O$ | 5,656 | 6,638 | 6,502 | 6,417 | 6,425 | 6,580 | 6,587 |
| $K_2O$ | 0,063 | 0,199 | 0,097 | 0,187 | 0,243 | 0,169 | 0,171 |
| TOTAL | 99,74 | 100,64 | 100,81 | 99,68 | 99,88 | 100,47 | 99,43 |
| Si | 2,4978 | 2,5614 | 2,5516 | 2,5564 | 2,5561 | 2,5468 | 2,5676 |
| Al | 1,4885 | 1,4338 | 1,4328 | 1,4281 | 1,4303 | 1,4326 | 1,4167 |
| Fe | 0,0259 | 0,0045 | 0,0017 | 0,0014 | 0,0014 | 0,0083 | 0,0026 |
| Ca | 0,4954 | 0,4290 | 0,4617 | 0,4574 | 0,4532 | 0,4581 | 0,4435 |
| Na | 0,4961 | 0,5740 | 0,5620 | 0,5610 | 0,5606 | 0,5717 | 0,5770 |
| K | 0,0036 | 0,0113 | 0,0055 | 0,0107 | 0,0139 | 0,0096 | 0,0098 |
| TOTAL | 5,0077 | 5,0142 | 5,0156 | 5,0153 | 5,0159 | 5,0274 | 5,0174 |

| Grain | 2C | 3A | 3B | 3C | 3D | 3E |
|---|---|---|---|---|---|---|
| $SiO_2$ | 56,836 | 57,031 | 57,484 | 56,940 | 56,844 | 56,872 |
| $Al_2O_3$ | 27,067 | 27,167 | 27,299 | 27,198 | 26,901 | 27,061 |
| FeO | 0,047 | 0,238 | 0,118 | 0,038 | 0,034 | 0,047 |
| CaO | 9,497 | 9,097 | 8,051 | 9,425 | 9,313 | 9,549 |
| $Na_2O$ | 6,387 | 6,516 | 6,491 | 6,501 | 6,561 | 6,454 |
| $K_2O$ | 0,181 | 0,289 | 0,856 | 0,112 | 0,163 | 0,098 |
| TOTAL | 100,01 | 100,34 | 100,30 | 100,21 | 99,81 | 100,08 |
| Si | 2,5535 | 2,5552 | 2,5718 | 2,5521 | 2,5585 | 2,5532 |
| Al | 1,4337 | 1,4350 | 1,4398 | 1,4371 | 1,4275 | 1,4322 |
| Fe | 0,0018 | 0,0089 | 0,0044 | 0,0014 | 0,0012 | 0,0017 |
| Ca | 0,4571 | 0,4367 | 0,3859 | 0,4526 | 0,4491 | 0,4593 |
| Na | 0,5564 | 0,5660 | 0,5631 | 0,5650 | 0,5726 | 0,5618 |
| K | 0,0103 | 0,0165 | 0,0488 | 0,0064 | 0,0093 | 0,0056 |
| TOTAL | 5,0130 | 5,0185 | 5,0141 | 5,0149 | 5,0186 | 5,0143 |

TABLE A2-17: Microprobe analyses of alkali feldspar in pelitic gneiss specimens from the granulite facies. The analyses were obtained by the method outlined in Appendix I C. Ionic proportions on the basis of 8 oxygens.

| Sample No. | HA1026 | HA164 | HA681 | HA841 | HA143 | HA632 | HA505 |
|---|---|---|---|---|---|---|---|
| $SiO_2$ | 64,773 | 65,627 | 65,767 | 65,183 | 65,036 | 65,000 | 65,505 |
| $Al_2O_3$ | 18,597 | 18,904 | 18,869 | 18,768 | 18,672 | 18,494 | 18,744 |
| $FeO, Fe_2O_3$ | 0,006 | 0,000 | 0,000 | 0,051 | 0,008 | 0,005 | 0,021 |
| CaO | 0,220 | 0,302 | 0,115 | 0,184 | 0,395 | 0,337 | 0,558 |
| $Na_2O$ | 1,313 | 1,842 | 1,925 | 1,708 | 2,237 | 2,635 | 3,114 |
| $K_2O$ | 14,614 | 14,202 | 14,009 | 14,063 | 12,779 | 12,913 | 12,608 |
| TOTAL | 99,52 | 100,87 | 100,68 | 99,96 | 99,13 | 99,38 | 100,55 |
| Si | 2,9905 | 2,9854 | 2,9923 | 2,9896 | 2,9928 | 2,9908 | 2,9802 |
| Al | 1,0123 | 1,0138 | 1,0121 | 1,0148 | 1,0130 | 1,0032 | 1,0054 |
| Fe | 0,0002 | 0,0000 | 0,0000 | 0,0019 | 0,0003 | 0,0001 | 0,0008 |
| Ca | 0,0108 | 0,0147 | 0,0056 | 0,0090 | 0,0195 | 0,0166 | 0,0272 |
| Na | 0,1175 | 0,1625 | 0,1698 | 0,1519 | 0,1996 | 0,2350 | 0,2747 |
| K | 0,8608 | 0,8242 | 0,8131 | 0,8229 | 0,7503 | 0,7580 | 0,7319 |
| TOTAL | 4,9924 | 5,0009 | 4,9931 | 4,9904 | 4,9756 | 5,0041 | 5,0203 |

TABLE A2-18: Microprobe analyses of hercynite-spinel solid solutions in pelitic gneiss specimens from the granulite facies terrane. Ionic proportions on the basis of 4 oxygens.

| Sample No. Grain | HA505 1 | HA505 2 | HA505 3 | HA681 1 | HA681 2 | HA681 3 | HA1036 1 | HA841 1 |
|---|---|---|---|---|---|---|---|---|
| $SiO_2$ | 0,047 | 0,028 | 0,388 | 0,010 | 0,019 | 0,011 | 0,012 | 0,011 |
| $TiO_2$ | 0,009 | 0,033 | 0,025 | 0,043 | 0,008 | 0,003 | - | 0,000 |
| $Al_2O_3$ | 59,368 | 56,944 | 56,430 | 60,406 | 59,985 | 57,660 | 56,308 | 55,338 |
| $Cr_2O_3$ | 0,457 | 0,273 | 0,345 | 0,604 | 0,795 | 0,712 | 0,431 | 0,581 |
| $FeO, Fe_2O_3$ | 28,615 | 34,219 | 34,933 | 27,374 | 26,972 | 31,216 | 33,945 | 36,888 |
| MnO | 0,226 | 0,294 | 0,239 | 0,153 | 0,117 | 0,149 | 0,211 | 0,105 |
| MgO | 11,143 | 7,517 | 6,981 | 11,520 | 11,397 | 9,721 | 6,533 | 4,805 |
| CaO | 0,000 | 0,004 | 0,010 | 0,000 | 0,001 | 0,052 | 0,009 | 0,008 |
| $Na_2O$ | - | - | - | - | - | - | - | - |
| $K_2O$ | - | - | - | - | - | - | - | - |
| TOTAL | 99,86 | 99,31 | 99,35 | 100,11 | 99,29 | 99,52 | 97,45 | 97,74 |
| Si | 0,0012 | 0,0007 | 0,0110 | 0,0002 | 0,0005 | 0,0003 | 0,0003 | 0,0003 |
| Ti | 0,0001 | 0,0007 | 0,0005 | 0,0008 | 0,0001 | 0,0000 | - | 0,0000 |
| Al | 1,9127 | 1,9017 | 1,8892 | 1,9270 | 1,9279 | 1,8932 | 1,9182 | 1,9091 |
| Cr | 0,0098 | 0,0061 | 0,0077 | 0,0129 | 0,0171 | 0,0156 | 0,0098 | 0,0134 |
| Fe | 0,6539 | 0,8106 | 0,8296 | 0,6195 | 0,6149 | 0,7271 | 0,8203 | 0,9028 |
| Mn | 0,0052 | 0,0070 | 0,0057 | 0,0034 | 0,0026 | 0,0035 | 0,0051 | 0,0025 |
| Mg | 0,4538 | 0,3173 | 0,2954 | 0,4646 | 0,4630 | 0,4035 | 0,2813 | 0,2095 |
| Ca | 0,0000 | 0,0001 | 0,0003 | 0,0000 | 0,0000 | 0,0015 | 0,0002 | 0,0002 |
| Na | - | - | - | - | - | - | - | - |
| K | - | - | - | - | - | - | - | - |
| TOTAL | 3,0372 | 3,0445 | 3,0398 | 3,0288 | 3,0267 | 3,0451 | 3,0355 | 3,0383 |

TABLE A2-19 Microprobe analyses of garnets in calc-silicate rocks. *indicates specimens collected in the granulite facies terrane. All other specimens are from the upper amphibolite facies terrane. Ionic proportions on the basis of 12 oxygens. The analyses have been corrected for $Fe^{+3}$ by the method outlined in Appendix I D.

| Sample No. | HA1101 | HA1094 | HA1094 | HA1097 | HA1097 | HA1148 | HA1087 | HA1087 | HA1087 | HA1093 | HA1093 | HA1093 |
|---|---|---|---|---|---|---|---|---|---|---|---|---|
| Grain | 1 | 1 | 2 | 1 | 2 | 1 | 1 | 2 | 3 | 1 | 2 | 3 |
| $SiO_2$ | 35.523 | 37.074 | 37.230 | 37.621 | 37.822 | 35.042 | 36.474 | 36.620 | 36.456 | 35.944 | 36.303 | 36.156 |
| $TiO_2$ | 0.864 | 0.568 | 0.538 | 0.420 | 0.689 | 1.159 | 0.618 | 0.536 | 0.503 | 0.714 | 0.528 | 0.527 |
| $Al_2O_3$ | 7.120 | 9.597 | 9.870 | 10.498 | 12.225 | 6.909 | 7.210 | 7.202 | 7.218 | 6.147 | 7.082 | 6.941 |
| $Fe_2O_3$ | 22.041 | 18.078 | 17.596 | 16.784 | 14.675 | 21.881 | 20.840 | 20.821 | 21.079 | 22.667 | 21.497 | 21.492 |
| FeO | 3.516 | 1.332 | 1.482 | 0.975 | 0.629 | 0.438 | 4.334 | 4.545 | 4.144 | 3.954 | 4.131 | 3.993 |
| MnO | 0.608 | 0.276 | 0.282 | 0.430 | 0.399 | 0.780 | 0.492 | 0.308 | 0.552 | 0.822 | 0.952 | 0.878 |
| MgO | 0.153 | 0.171 | 0.140 | 0.139 | 0.211 | 0.367 | 0.110 | 0.136 | 0.119 | 0.093 | 0.104 | 0.102 |
| CaO | 31.046 | 33.420 | 33.367 | 33.865 | 34.591 | 32.608 | 30.100 | 30.129 | 30.381 | 30.157 | 30.173 | 30.146 |
| $Na_2O$ | - | 0.000 | - | 0.000 | - | - | 0.078 | - | - | 0.001 | - | - |
| $K_2O$ | - | 0.020 | - | 0.008 | - | - | 0.003 | - | - | 0.019 | - | - |
| TOTAL | 100.87 | 100.54 | 100.51 | 100.74 | 101.24 | 99.18 | 100.30 | 100.30 | 100.45 | 100.52 | 100.77 | 100.23 |
| Si | 2.9045 | 2.9698 | 2.9779 | 2.9886 | 2.9644 | 2.8949 | 2.9839 | 2.9928 | 2.9782 | 2.9567 | 2.9648 | 2.9682 |
| Ti | 0.0531 | 0.0342 | 0.0324 | 0.0251 | 0.0406 | 0.0720 | 0.0380 | 0.0329 | 0.0309 | 0.0442 | 0.0324 | 0.0325 |
| Al | 0.6862 | 0.9061 | 0.9306 | 0.9830 | 1.1294 | 0.6728 | 0.6952 | 0.6938 | 0.6950 | 0.5960 | 0.6817 | 0.6716 |
| $Fe^{+3}$ | 1.3562 | 1.0898 | 1.0592 | 1.0033 | 0.8656 | 1.3603 | 1.2830 | 1.2805 | 1.2959 | 1.4030 | 1.3211 | 1.3277 |
| $Fe^{+2}$ | 0.2404 | 0.0893 | 0.0991 | 0.0648 | 0.0413 | 0.0302 | 0.2965 | 0.3106 | 0.2832 | 0.2720 | 0.2822 | 0.2742 |
| Mn | 0.0421 | 0.0187 | 0.0191 | 0.0289 | 0.0265 | 0.0546 | 0.0341 | 0.0213 | 0.0382 | 0.0573 | 0.0659 | 0.0611 |
| Mg | 0.0186 | 0.0204 | 0.0167 | 0.0165 | 0.0247 | 0.0452 | 0.0134 | 0.0166 | 0.0145 | 0.0114 | 0.0127 | 0.0125 |
| Ca | 2.7200 | 2.8686 | 2.8598 | 2.8826 | 2.9051 | 2.8865 | 2.6385 | 2.6385 | 2.6595 | 2.6580 | 2.6405 | 2.6518 |
| Na | - | 0.0000 | - | 0.0000 | - | - | 0.0124 | - | - | 0.0002 | - | - |
| K | - | 0.0020 | - | 0.0008 | - | - | 0.0003 | - | - | 0.0046 | - | - |
| TOTAL | 8.0211 | 7.9989 | 7.9948 | 7.9936 | 7.9976 | 8.0165 | 7.9957 | 7.9870 | 7.9954 | 8.0034 | 8.0013 | 7.9996 |

| Sample No. | HA1140 | HA1140 | HA1140 | HA1132 | HA1132 | *HA1013 | *HA1013 | *HA1152 | *HA1152 | *HA459 | *HA459 |
|---|---|---|---|---|---|---|---|---|---|---|---|
| GRAIN | 1 | 2 | 3 | 1 | 2 | 1 | 2 | 1 | 2 | 1 | 2 |
| $SiO_2$ | 35.995 | 36.162 | 36.051 | 35.978 | 35.804 | 36.219 | 36.286 | 37.200 | 37.212 | 36.536 | 36.493 |
| $TiO_2$ | 0.800 | 0.763 | 0.742 | 0.753 | 0.968 | 0.750 | 0.655 | 0.551 | 0.756 | 0.894 | 0.864 |
| $Al_2O_3$ | 7.233 | 6.996 | 7.171 | 5.898 | 5.655 | 6.727 | 6.572 | 10.788 | 10.497 | 7.111 | 7.144 |
| $Fe_2O_3$ | 21.167 | 21.315 | 21.160 | 23.022 | 23.328 | 21.712 | 21.829 | 16.245 | 16.533 | 21.150 | 21.255 |
| FeO | 4.875 | 4.567 | 5.351 | 3.766 | 3.532 | 3.522 | 3.668 | 2.288 | 2.175 | 1.084 | 1.322 |
| MnO | 0.816 | 0.770 | 0.833 | 0.372 | 0.359 | 1.717 | 1.973 | 0.693 | 0.610 | 0.583 | 0.600 |
| MgO | 0.121 | 0.110 | 0.115 | 0.146 | 0.151 | 0.107 | 0.120 | 0.179 | 0.185 | 0.217 | 0.193 |
| CaO | 29.557 | 29.786 | 29.145 | 30.597 | 30.731 | 29.859 | 29.445 | 32.408 | 32.400 | 32.688 | 32.598 |
| $Na_2O$ | 0.030 | - | - | - | - | 0.000 | - | - | - | 0.000 | - |
| $K_2O$ | 0.000 | - | - | - | - | 0.000 | - | - | - | 0.000 | - |
| TOTAL | 100.59 | 100.47 | 100.57 | 100.53 | 100.53 | 100.61 | 100.55 | 100.35 | 100.37 | 100.26 | 100.47 |
| Si | 2.9479 | 2.9630 | 2.9557 | 2.9577 | 2.9467 | 2.9663 | 2.9766 | 2.9734 | 2.9862 | 2.9701 | 2.9641 |
| Ti | 0.0493 | 0.0470 | 0.0458 | 0.0466 | 0.0599 | 0.0462 | 0.0404 | 0.0331 | 0.0225 | 0.0547 | 0.0528 |
| Al | 0.6982 | 0.6757 | 0.6930 | 0.5715 | 0.5486 | 0.6494 | 0.6354 | 1.0164 | 0.9929 | 0.6814 | 0.6840 |
| $Fe^{+3}$ | 1.3046 | 1.3143 | 1.3055 | 1.4243 | 1.4448 | 1.3381 | 1.3475 | 0.9771 | 0.9984 | 1.2939 | 1.2992 |
| $Fe^{+2}$ | 0.3339 | 0.3130 | 0.3669 | 0.2589 | 0.2431 | 0.2413 | 0.2517 | 0.1529 | 0.1460 | 0.0737 | 0.0898 |
| Mn | 0.0566 | 0.0534 | 0.0578 | 0.0259 | 0.0250 | 0.1191 | 0.1371 | 0.0469 | 0.0415 | 0.0401 | 0.0413 |
| Mg | 0.0148 | 0.0134 | 0.0141 | 0.0179 | 0.0185 | 0.0131 | 0.0147 | 0.0213 | 0.0221 | 0.0263 | 0.0234 |
| Ca | 2.5938 | 2.6151 | 2.5604 | 2.6952 | 2.7101 | 2.6203 | 2.5882 | 2.7756 | 2.7860 | 2.8474 | 2.8371 |
| Na | 0.0048 | - | - | - | - | 0.0000 | - | - | - | 0.0000 | - |
| K | - | - | - | - | - | 0.0000 | - | - | - | 0.0000 | - |
| TOTAL | 8.0039 | 7.9949 | 7.9992 | 7.9980 | 7.9967 | 7.9938 | 7.9916 | 7.9967 | 7.9956 | 7.9876 | 7.9917 |

TABLE A2-20: Microprobe analyses of clinopyroxenes in calc-silicate rocks. *indicates specimens collected in the granulite facies terrane. All other specimens are from the upper amphibolite facies terrane. Ionic proportions on the basis of 6 oxygens.

| Grain | HA1101 | HA1094 | HA1097 | HA1087 | HA1093 | HA1140 | HA1132 | HA1013* | HA1152* | HA459* |
|---|---|---|---|---|---|---|---|---|---|---|
| $SiO_2$ | 45,458 | 51,403 | 50,536 | 46,271 | 46,662 | 45,252 | 46,159 | 49,644 | 49,231 | 49,290 |
| $TiO_2$ | 0,377 | 0,037 | 0,021 | 0,264 | 0,237 | 0,334 | 0,296 | 0,094 | 0,121 | 0,094 |
| $Al_2O_3$ | 4,760 | 1,666 | 1,250 | 4,050 | 4,050 | 4,469 | 4,950 | 1,990 | 2,558 | 2,656 |
| $FeO,Fe_2O_3$ | 21,498 | 12,954 | 11,017 | 23,238 | 21,384 | 23,306 | 20,559 | 17,847 | 16,628 | 16,441 |
| MnO | 0,262 | 0,185 | 0,344 | 0,220 | 0,351 | 0,351 | 0,194 | 1,070 | 0,551 | 0,551 |
| MgO | 5,173 | 10,045 | 11,981 | 3,908 | 4,790 | 3,809 | 5,081 | 6,552 | 7,183 | 7,876 |
| CaO | 22,090 | 24,075 | 24,019 | 22,277 | 22,315 | 22,096 | 22,283 | 22,958 | 24,125 | 23,133 |
| $Na_2O$ | 0,527 | 0,348 | 0,365 | 0,692 | 0,640 | 0,467 | 0,845 | 0,532 | 0,070 | 0,577 |
| $K_2O$ | 0,005 | 0,003 | 0,021 | 0,021 | 0,000 | 0,000 | 0,010 | 0,000 | 0,000 | 0,000 |
| TOTAL | 100,15 | 100,72 | 99,55 | 100,94 | 100,43 | 100,08 | 100,38 | 100,69 | 100,47 | 100,62 |
| Si | 1,8183 | 1,9531 | 1,9339 | 1,8495 | 1,8578 | 1,8282 | 1,8322 | 1,9383 | 1,9159 | 1,9114 |
| Ti | 0,0113 | 0,0010 | 0,0006 | 0,0079 | 0,0071 | 0,0101 | 0,0088 | 0,0027 | 0,0035 | 0,0027 |
| Al | 0,2244 | 0,0746 | 0,0563 | 0,1908 | 0,1900 | 0,2128 | 0,2316 | 0,0915 | 0,1173 | 0,1214 |
| Fe | 0,7191 | 0,4116 | 0,3526 | 0,7768 | 0,7120 | 0,7874 | 0,6824 | 0,5827 | 0,5412 | 0,5332 |
| Mn | 0,0088 | 0,0059 | 0,0111 | 0,0074 | 0,0118 | 0,0120 | 0,0065 | 0,0354 | 0,0181 | 0,0181 |
| Mg | 0,3083 | 0,5688 | 0,6833 | 0,2328 | 0,2842 | 0,2293 | 0,3005 | 0,3812 | 0,4166 | 0,4551 |
| Ca | 0,9467 | 0,9801 | 0,9849 | 0,9541 | 0,9519 | 0,9565 | 0,9477 | 0,9605 | 1,0060 | 0,9612 |
| Na | 0,0408 | 0,0256 | 0,0271 | 0,0536 | 0,0494 | 0,0366 | 0,0650 | 0,0403 | 0,0053 | 0,0434 |
| K | 0,0002 | 0,0001 | 0,0010 | 0,0010 | 0,0000 | 0,0000 | 0,0005 | 0,0000 | 0,0000 | 0,0000 |
| TOTAL | 4,0786 | 4,0213 | 4,0512 | 4,0744 | 4,0647 | 4,0734 | 4,0758 | 4,0332 | 4,0244 | 4,0468 |

TABLE A2-21: Microprobe analyses of plagioclase in calc-silicate rocks. Ionic proportions on the basis of 8 oxygens. * indicates specimens collected in the granulite facies terrane. (Z) represents core compositions of zoned plagioclase grains.

| Specimen | HA1093 | (Z) HA1093 | HA1093 | HA1094 | HA1132 | (Z) HA1101 | (Z) HA1101 | HA1101 | HA1101 |
|---|---|---|---|---|---|---|---|---|---|
| Grain | 1 | 2 | 3 | 1 | 1 | 2 | 3 | 4 | 5 |
| $SiO_2$ | 49,558 | 53,145 | 48,809 | 44,950 | 54,565 | 54.622 | 54,595 | 48,934 | 48,596 |
| $Al_2O_3$ | 31,543 | 29,585 | 31,676 | 34,504 | 27,900 | 28,036 | 27.917 | 31,773 | 31,929 |
| FeO | 0,288 | 0,253 | 0,185 | 0,231 | 0,292 | 0,324 | 0,303 | 0,370 | 0,367 |
| MnO | 0,000 | 0,000 | 0,000 | 0,000 | 0,000 | - | - | - | - |
| MgO | 0,014 | 0,011 | 0,000 | 0,028 | 0,002 | - | - | - | - |
| CaO | 15,740 | 13,041 | 15,947 | 19,392 | 11,256 | 11,445 | 11,162 | 15,851 | 16,182 |
| $Na_2O$ | 2,840 | 4,575 | 2,690 | 0,803 | 5,715 | 4,735 | 4,932 | 2,416 | 2,313 |
| $K_2O$ | 0,086 | 0,185 | 0,054 | 0,000 | 0,128 | 0,405 | 0,412 | 0,123 | 0,102 |
| TOTAL | 100,07 | 100.79 | 99,36 | 99,91 | 99,86 | 99,56 | 99,32 | 99,47 | 99,49 |
| Si | 2,2676 | 2,3970 | 2,2502 | 2,0820 | 2,4745 | 2,4798 | 2,4841 | 2,2527 | 2,2392 |
| Al | 1,7016 | 1,5731 | 1,7217 | 1,8842 | 1,4917 | 1,5006 | 1,4975 | 1,7244 | 1,7345 |
| Fe | 0,0110 | 0,0095 | 0,0071 | 0,0089 | 0,0110 | 0,0123 | 0,0115 | 0,0142 | 0,0141 |
| Mn | 0,0000 | 0,0000 | 0,0000 | 0,0000 | 0,0000 | - | - | - | - |
| Mg | 0,0009 | 0,0007 | 0,0000 | 0,0019 | 0,0001 | - | - | - | - |
| Ca | 0,7717 | 0,6302 | 0,7878 | 0,9624 | 0,5470 | 0,5567 | 0,5441 | 0,7819 | 0,7989 |
| Na | 0,2519 | 0,4001 | 0,2404 | 0,0722 | 0,5025 | 0,4168 | 0,4351 | 0,2157 | 0,2067 |
| K | 0,0050 | 0,0106 | 0,0031 | 0,0000 | 0,0074 | 0,0235 | 0,0239 | 0,0072 | 0,0060 |
| TOTAL | 5,0100 | 5,0217 | 5,0107 | 5,0119 | 5,0345 | 4,9899 | 4,9966 | 4,9964 | 4,9997 |

| Specimen | HA1148 | HA1148 | HA1087 | HA1087 | HA1140 | HA1140 | HA1140 | * HA1152 |
|---|---|---|---|---|---|---|---|---|
| Grain | 1 | 2 | 1 | 2 | 1 | 2 | 3 | 1 |
| $SiO_2$ | 44,025 | 44,135 | 48,174 | 48,192 | 46,059 | 46,860 | 46,966 | 44,389 |
| $Al_2O_3$ | 34,668 | 34,639 | 32,417 | 32,555 | 33,001 | 33,322 | 33,415 | 35,244 |
| FeO | 0,509 | 0,428 | 0,466 | 0,415 | 0,409 | 0,426 | 0,423 | 0,372 |
| MnO | 0,016 | - | 0,000 | 0,000 | 0,000 | 0,013 | 0,026 | 0,000 |
| MgO | 0,000 | - | 0,017 | 0,008 | 0,039 | 0,035 | 0,026 | 0,027 |
| CaO | 19,480 | 19,622 | 16,789 | 16,817 | 18,209 | 17,559 | 17,551 | 19,845 |
| $Na_2O$ | 0,420 | 0,366 | 2,195 | 2,187 | 1,493 | 1,611 | 1,593 | 0,412 |
| $K_2O$ | 0,018 | 0,020 | 0,091 | 0,085 | 0,080 | 0,066 | 0,074 | 0,015 |
| TOTAL | 99,13 | 99,21 | 100,15 | 100,26 | 99,29 | 99,89 | 100,07 | 100,30 |
| Si | 2,0585 | 2,0614 | 2,2115 | 2,2092 | 2,1436 | 2,1608 | 2,1613 | 2,0511 |
| Al | 1,9111 | 1,9074 | 1,7543 | 1,7594 | 1,8107 | 1,8115 | 1,8128 | 1,9199 |
| Fe | 0,0199 | 0,0167 | 0,0178 | 0,0159 | 0,0159 | 0,0164 | 0,0162 | 0,0143 |
| Mn | 0,0006 | - | 0,0000 | 0,0000 | 0,0000 | 0,0005 | 0,0010 | 0,0000 |
| Mg | 0,0000 | - | 0,0011 | 0,0005 | 0,0026 | 0,0024 | 0,0018 | 0,0018 |
| Ca | 0,9759 | 0,9820 | 0,8258 | 0,8260 | 0,9085 | 0,8676 | 0,8654 | 0,9825 |
| Na | 0,0380 | 0,0332 | 0,1953 | 0,1944 | 0,1347 | 0,1440 | 0,1421 | 0,0369 |
| K | 0,0010 | 0,0012 | 0,0053 | 0,0050 | 0,0047 | 0,0039 | 0,0043 | 0,0009 |
| TOTAL | 5,0054 | 5,0020 | 5,0116 | 5,0107 | 5,0207 | 5,0073 | 5,0054 | 5,0078 |

Table A2-22: Microprobe analyses of amphibole in calcium and magnesium-rich rocks. Ionic proportions on the basis of 23 oxygens. Both specimens are from the granulite facies terrane.

| Specimen | HA997 | HA997 | HA1150 |
|---|---|---|---|
| Grain | 1 | 2 | 1 |
| $SiO_2$ | 55,562 | 55,802 | 50,742 |
| $TiO_2$ | 0,110 | 0,095 | 1,020 |
| $Al_2O_3$ | 1,211 | 0,931 | 7,354 |
| $Cr_2O_3$ | - | - | - |
| FeO | 5,904 | 5,446 | 4,466 |
| MnO | 0,268 | 0,282 | 0,056 |
| MgO | 21,390 | 21,794 | 20,887 |
| CaO | 13,002 | 13,061 | 13,222 |
| $Na_2O$ | 0,235 | 0,168 | 1,085 |
| $K_2O$ | 0,142 | 0,107 | 0,677 |
| TOTAL | 97,82 | 97,69 | 99,51 |
| Si | 7,7578 | 7,7833 | 7,0057 |
| Ti | 0,0115 | 0,0099 | 0,1058 |
| Al | 0,1993 | 0,1532 | 1,1970 |
| Cr | - | - | - |
| Fe | 0,6894 | 0,6353 | 0,5157 |
| Mn | 0,0317 | 0,0333 | 0,0066 |
| Mg | 4,4511 | 4,5303 | 4,2977 |
| Ca | 1,9452 | 1,9520 | 1,9560 |
| Na | 0,0638 | 0,0454 | 0,2906 |
| K | 0,0254 | 0,0191 | 0,1192 |
| TOTAL | 15,1755 | 15,1623 | 15,4947 |

TABLE A2-23: Microprobe analyses along a traverse across a zoned plagioclase grain in calc-silicate specimen HA 1101. Ionic proportions on the basis of 8 oxygens.

| Grain | 1A | 1B | 1C | 1D | 1E | 1F | 1G | 1H | 1I | 1J |
|---|---|---|---|---|---|---|---|---|---|---|
| $SiO_2$ | 48.221 | 49.162 | 50.284 | 53.239 | 54.246 | 54.461 | 53.820 | 50.004 | 49.256 | 48.857 |
| $TiO_2$ | - | - | - | - | - | - | - | - | - | - |
| $Al_2O_3$ | 31.681 | 31.392 | 31.525 | 29.385 | 29.033 | 28.844 | 29.251 | 31.486 | 32.305 | 32.667 |
| FeO,$Fe_2O_3$ | 0.359 | 0.387 | 0.365 | 0.307 | 0.307 | 0.319 | 0.325 | 0.350 | 0.368 | 0.398 |
| MnO | 0.002 | - | - | - | - | - | - | - | - | - |
| MgO | 0.000 | - | - | - | - | - | - | - | - | - |
| CaO | 16.590 | 15.887 | 15.492 | 12.891 | 12.140 | 11.883 | 12.554 | 15.516 | 16.053 | 16.413 |
| $Na_2O$ | 2.242 | 2.532 | 2.879 | 4.113 | 4.494 | 4.673 | 4.334 | 2.800 | 2.481 | 2.181 |
| $K_2O$ | 0.070 | 0.126 | 0.147 | 0.301 | 0.341 | 0.329 | 0.328 | 0.151 | 0.115 | 0.089 |
| TOTAL | 99.16 | 99.48 | 100.69 | 100.23 | 100.56 | 100.51 | 100.61 | 100.31 | 100.58 | 100.60 |
| Si | 2.2328 | 2.2639 | 2.2842 | 2.4104 | 2.4424 | 2.4522 | 2.4256 | 2.2804 | 2.2436 | 2.2261 |
| Ti | - | - | - | - | - | - | - | - | - | - |
| Al | 1.7295 | 1.7042 | 1.6883 | 1.5685 | 1.5412 | 1.5311 | 1.5542 | 1.6928 | 1.7348 | 1.7547 |
| Fe | 0.0139 | 0.0149 | 0.0138 | 0.0116 | 0.0115 | 0.0120 | 0.0122 | 0.0133 | 0.0140 | 0.0152 |
| Mn | 0.0000 | - | - | - | - | - | - | - | - | - |
| Mg | 0.0000 | - | - | - | - | - | - | - | - | - |
| Ca | 0.8231 | 0.7839 | 0.7540 | 0.6254 | 0.5857 | 0.5733 | 0.6062 | 0.7582 | 0.7835 | 0.8013 |
| Na | 0.2013 | 0.2261 | 0.2536 | 0.3611 | 0.3923 | 0.4079 | 0.3787 | 0.2476 | 0.2191 | 0.1926 |
| K | 0.0041 | 0.0074 | 0.0085 | 0.0173 | 0.0196 | 0.0189 | 0.0188 | 0.0088 | 0.0066 | 0.0051 |
| TOTAL | 5.0051 | 5.0007 | 5.0027 | 4.9945 | 4.9930 | 4.9957 | 4.9960 | 5.0013 | 5.0018 | 4.9953 |

Table A2-24: Microprobe analyses of epidote and zoisite in calc-silicate rock specimen HA1148. Ionic proportions on the basis of 25 oxygens. The epidote analysis has been corrected for $Fe^{+3}$ by the method outlined in Appendix I D.

| | Epidote | Zoisite |
|---|---|---|
| $SiO_2$ | 37,388 | 39,450 |
| $TiO_2$ | 0,174 | 0,000 |
| $Al_2O_3$ | 23,643 | 33,307 |
| $Fe_2O_3$ | 13,187 | - |
| FeO | - | 0,279 |
| MnO | 0,078 | 0,018 |
| MgO | 0,013 | 0,000 |
| CaO | 23,726 | 24,264 |
| TOTAL | 98,21 | 97,32 |
| Si | 5,9446 | 6,0119 |
| Ti | 0,0208 | 0,0000 |
| Al | 4,4310 | 5,9840 |
| $Fe^{+3}$ | 1,5779 | - |
| $Fe^{+2}$ | - | 0,0355 |
| Mn | 0,0105 | 0,0024 |
| Mg | 0,0031 | 0,0000 |
| Ca | 4,0422 | 3,9620 |
| TOTAL | 16,0301 | 15,9960 |

TABLE A2-25: Microprobe analyses of coexisting minerals in ultramafic rock specimen HA 601. Ionic proportions were computed on the following basis: hornblende - 23 oxygens; olivine - 4 oxygens; orthopyroxene - 6 oxygens; spinel - 4 oxygens. The spinel analyses have been corrected for $Fe^{+3}$ by the method outlined in Appendix I D.

| Grain | MAGNESIO-HORNBLENDE | | HYALOSIDERITE | | | BRONZITE | | | SPINEL | | |
|---|---|---|---|---|---|---|---|---|---|---|---|
| | 1 | 2 | 1 | 2 | 3 | 1 | 2 | 3 | 1 | 2 | 3 |
| $SiO_2$ | 46,155 | 46,505 | 37,135 | 37,371 | 37,222 | 52,626 | 52,538 | 52,809 | 0,030 | 0,043 | 0,026 |
| $TiO_2$ | 1,146 | 1,160 | 0,016 | 0,018 | 0,015 | 0,150 | 0,148 | 0,141 | 0,070 | 0,063 | 0,066 |
| $Al_2O_3$ | 13,250 | 13,455 | 0,000 | 0,000 | 0,000 | 2,809 | 3,190 | 3,145 | 59,766 | 59,345 | 58,468 |
| $Cr_2O_3$ | - | - | - | - | - | 0,083 | 0,069 | 0,068 | 2,636 | 2,854 | 2,970 |
| $Fe_2O_3$ | - | - | - | - | - | - | - | - | 4,180 | 4,126 | 4,829 |
| FeO | 8,047 | 8,086 | 28,603 | 28,643 | 28,610 | 16,402 | 16,424 | 16,616 | 20,815 | 20,595 | 21,083 |
| MnO | 0,136 | 0,138 | 0,374 | 0,378 | 0,406 | 0,377 | 0,362 | 0,355 | 0,189 | 0,183 | 0,190 |
| MgO | 16,157 | 16,333 | 33,856 | 34,290 | 34,263 | 27,295 | 26,520 | 26,763 | 13,596 | 13,587 | 13,163 |
| CaO | 12,506 | 12,390 | 0,017 | 0,027 | 0,020 | 0,000 | 0,552 | 0,542 | 0,002 | 0,022 | 0,032 |
| $Na_2O$ | 0,827 | 0,818 | - | - | - | 0,145 | 0,000 | 0,000 | - | - | - |
| $K_2O$ | 0,087 | 0,100 | - | - | - | 0,004 | 0,000 | 0,000 | - | - | - |
| TOTAL | 98,31 | 98,99 | 100,00 | 100,73 | 100,54 | 99,89 | 99,80 | 100,44 | 101,28 | 100,82 | 100.83 |
| Si | 6,5266 | 6,5257 | 0,9968 | 0,9953 | 0,9937 | 1,9089 | 1,9083 | 1,9071 | 0,0008 | 0,0011 | 0,0007 |
| Ti | 0,1219 | 0,1224 | 0,0003 | 0,0003 | 0,0003 | 0,0040 | 0,0040 | 0,0038 | 0,0014 | 0,0013 | 0,0013 |
| Al | 2,2089 | 2,2259 | 0,0000 | 0,0000 | 0,0000 | 0,1201 | 0,1366 | 0,1339 | 1,8598 | 1,8554 | 1,8384 |
| Cr | - | - | - | - | - | 0,0023 | 0,0019 | 0,0019 | 0,0550 | 0,0599 | 0,0626 |
| $Fe^{+3}$ | - | - | - | - | - | - | - | - | 0,0830 | 0,0824 | 0,0969 |
| $Fe^{+2}$ | 0,9517 | 0,9490 | 0,6421 | 0,6380 | 0,6387 | 0,4975 | 0,4989 | 0,5018 | 0,4596 | 0,4569 | 0,4704 |
| Mn | 0,0163 | 0,0165 | 0,0084 | 0,0085 | 0,0091 | 0,0116 | 0,0111 | 0,0108 | 0,0042 | 0,0041 | 0,0043 |
| Mg | 3,4050 | 3,4156 | 1,3544 | 1,3611 | 1,3632 | 1,4755 | 1,4356 | 1,4404 | 0,5351 | 0,5372 | 0,5234 |
| Ca | 1,8949 | 1,8630 | 0,0004 | 0,0007 | 0,0005 | 0,0000 | 0,0214 | 0,0209 | 0,0001 | 0,0006 | 0,0009 |
| Na | 0,2268 | 0,2225 | - | - | - | 0,0102 | 0,0000 | 0,0000 | - | - | - |
| K | 0,0157 | 0,0179 | - | - | - | 0,0002 | 0,0000 | 0,0000 | - | - | - |
| TOTAL | 15,3682 | 15,3590 | 3,0028 | 3,0042 | 3,0059 | 4,0308 | 4,0182 | 4,0210 | 2,9990 | 2,9989 | 2,9989 |

TABLE A2-26 Microprobe analyses of coexisting garnet and pyroxene in specimen HA 990. Ionic proportions were computed on the following basis:
garnet - 12 oxygens, pyroxene - 6 oxygens, pyroxenoid - 6 oxygens.
The garnet analysis has been recalculated to allow for $Fe^{+3}$ by the method outlined in Appendix I D.

| Sample No. | Garnet | Ferroaugite | Pyroxmangite |
|---|---|---|---|
| $SiO_2$ | 36,304 | 48,554 | 46,598 |
| $TiO_2$ | 0,013 | 0,017 | 0,016 |
| $Al_2O_3$ | 18,063 | 0,640 | 0,061 |
| $Cr_2O_3$ | 0,004 | 0,000 | 0,010 |
| $Fe_2O_3$ | 4,319 | - | - |
| FeO | 16,173 | 20,989 | 29,626 |
| MnO | 16,977 | 6,039 | 16,733 |
| MgO | 0,586 | 5,124 | 3,024 |
| CaO | 7,326 | 18,081 | 3,601 |
| $Na_2O$ | - | 0,152 | 0,025 |
| $K_2O$ | - | 0,083 | 0,022 |
| TOTAL | 99,77 | 99,68 | 99,72 |
| Si | 2,9825 | 1,9664 | 1,9870 |
| Ti | 0,0008 | 0,0005 | 0,0005 |
| Al | 1,7491 | 0,0305 | 0,0030 |
| Cr | 0,0004 | 0,0000 | 0,0003 |
| $Fe^{+3}$ | 0,2670 | - | - |
| $Fe^{+2}$ | 1,1112 | 0,7109 | 1,0566 |
| Mn | 1,1814 | 0,2071 | 0,6044 |
| Mg | 0,0718 | 0,3092 | 0,1922 |
| Ca | 0,6449 | 0,7847 | 0,1645 |
| Na | - | 0,0119 | 0,0021 |
| K | - | 0,0042 | 0,0012 |
| TOTAL | 8,0091 | 4,0259 | 4,0123 |

TABLE A2-27: Microprobe analyses of biotite in metapelite specimen HA164. Analyses marked (*) are rim compositions of biotites not enclosed by garnet and the remaining analyses refer to rim compositions of biotite grains completely enclosed by garnet. All grains are in contact with garnet. Ionic proportions on the basis of 11 oxygens.

| GRAIN | 1* | 2* | 3* | 4* | 5 | 6 | 7 | 8 | 9 |
|---|---|---|---|---|---|---|---|---|---|
| $SiO_2$ | 38,386 | 38,229 | 38,193 | 38,567 | 37,933 | 37,754 | 38,199 | 38,329 | 38,223 |
| $TiO_2$ | 3,414 | 3,678 | 3,315 | 3,214 | 3,787 | 4,490 | 5,243 | 3,939 | 3,633 |
| $Al_2O_3$ | 18,408 | 18,274 | 18,264 | 17,750 | 17,934 | 17,808 | 17,600 | 18,087 | 18,533 |
| FeO | 11,897 | 11,283 | 13,077 | 11,593 | 11,033 | 11,872 | 11,215 | 11,235 | 11,165 |
| MnO | 0,043 | 0,040 | 0,043 | 0,031 | 0,054 | 0,067 | - | - | - |
| MgO | 15,785 | 15,712 | 13,693 | 16,322 | 15,999 | 14,930 | 15,812 | 16,305 | 16,272 |
| CaO | 0,033 | 0,043 | 0,188 | 0,027 | 0,032 | 0,026 | 0,016 | 0,024 | 0,024 |
| $Na_2O$ | 0,067 | 0,106 | 0,263 | 0,082 | 0,117 | 0,189 | 0,256 | 0,120 | 0,126 |
| $K_2O$ | 9,276 | 9,816 | 9,505 | 9,412 | 9,394 | 9,247 | 8,811 | 9,624 | 9,410 |
| TOTAL | 97,31 | 97,18 | 96,54 | 97,00 | 96,28 | 96,38 | 97,15 | 97,66 | 97,39 |
| Si | 2,7419 | 2,7377 | 2,7718 | 2,7634 | 2,7354 | 2,7303 | 2,7242 | 2,7280 | 2,7226 |
| Ti | 0,1834 | 0,1980 | 0,1809 | 0,1732 | 0,2054 | 0,2442 | 0,2812 | 0,2108 | 0,1946 |
| Al | 1,5502 | 1,5429 | 1,5626 | 1,4993 | 1,5247 | 1,5183 | 1,4797 | 1,5178 | 1,5563 |
| Fe | 0,7107 | 0,6757 | 0,7936 | 0,6947 | 0,6654 | 0,7180 | 0,6689 | 0,6688 | 0,6651 |
| Mn | 0,0026 | 0,0024 | 0,0026 | 0,0018 | 0,0032 | 0,0041 | - | - | - |
| Mg | 1,6804 | 1,6768 | 1,4810 | 1,7430 | 1,7195 | 1,6091 | 1,6805 | 1,7295 | 1,7273 |
| Ca | 0,0025 | 0,0033 | 0,0146 | 0,0020 | 0,0024 | 0,0020 | 0,0012 | 0,0018 | 0,0018 |
| Na | 0,0092 | 0,0147 | 0,0370 | 0,0113 | 0,0163 | 0,0265 | 0,0354 | 0,0166 | 0,0174 |
| K | 0,8453 | 0,8968 | 0,8800 | 0,8603 | 0,8642 | 0,8532 | 0,8016 | 0,8739 | 0,8551 |
| TOTAL | 7,7268 | 7,7488 | 7,7246 | 7,7495 | 7,7370 | 7,7061 | 7,6731 | 7,7475 | 7,7408 |

TABLE A2-28: Microprobe analyses of garnet in metapelite specimen HA164. The analyses refer to rim compositions of garnet at the contact with biotite. Ionic proportions on the basis of 12 oxygens.

| GRAIN | 1 | 2 | 3 | 4 | 5 | 6 | 7 | 8 | 9 |
|---|---|---|---|---|---|---|---|---|---|
| $SiO_2$ | 37,852 | 37,786 | 37,662 | 37,829 | 37,705 | 37,811 | 37,313 | 37,862 | 37,503 |
| $TiO_2$ | 0,057 | 0,095 | 0,081 | 0,068 | 0,047 | - | - | - | - |
| $Al_2O_3$ | 21,842 | 21,858 | 21,876 | 21,833 | 21,977 | 21,784 | 21,566 | 22,041 | 21,861 |
| FeO | 30,723 | 31,017 | 31,057 | 31,543 | 30,603 | 32,544 | 33,231 | 31,804 | 32,268 |
| MnO | 1,438 | 1,399 | 1,456 | 1,479 | 1,379 | 1,737 | 1,839 | 1,743 | 1,601 |
| MgO | 6,537 | 6,613 | 6,518 | 6,184 | 6,652 | 5,334 | 4,504 | 5,441 | 5,702 |
| CaO | 1,162 | 1,157 | 1,156 | 1,160 | 1,144 | 1,115 | 1,139 | 1,285 | 1,197 |
| $Na_2O$ | 0,000 | 0,008 | 0,004 | 0,006 | 0,000 | 0,000 | 0,027 | 0,083 | 0,018 |
| $K_2O$ | 0,057 | 0,125 | 0,086 | 0,044 | 0,012 | 0,051 | 0,021 | 0,049 | 0,029 |
| TOTAL | 99,67 | 100,06 | 99,90 | 100,15 | 99,52 | 100,37 | 99,64 | 100,31 | 100,18 |
| Si | 2,9813 | 2,9698 | 2,9664 | 2,9766 | 2,9716 | 2,9848 | 2,9832 | 2,9817 | 2,9641 |
| Ti | 0,0034 | 0,0056 | 0,0048 | 0,0040 | 0,0027 | - | - | - | - |
| Al | 2,0281 | 2,0253 | 2,0313 | 2,0254 | 2,0420 | 2,0273 | 2,0328 | 2,0463 | 2,0370 |
| Fe | 2,0237 | 2,0388 | 2,0457 | 2,0758 | 2,0171 | 2,1485 | 2,2220 | 2,0946 | 2,1329 |
| Mn | 0,0959 | 0,0931 | 0,0971 | 0,0986 | 0,0920 | 0,1161 | 0,1245 | 0,1112 | 0,1072 |
| Mg | 0,7673 | 0,7746 | 0,7651 | 0,7252 | 0,7814 | 0,6275 | 0,5366 | 0,6385 | 0,6716 |
| Ca | 0,0980 | 0,0974 | 0,0975 | 0,0978 | 0,0966 | 0,0943 | 0,0975 | 0,1084 | 0,1013 |
| Na | 0,0000 | 0,0012 | 0,0007 | 0,0010 | 0,0000 | 0,0000 | 0,0043 | 0,0127 | 0,0028 |
| K | 0,0057 | 0,0125 | 0,0086 | 0,0044 | 0,0012 | 0,0051 | 0,0021 | 0,0049 | 0,0029 |
| TOTAL | 8,0039 | 8,0188 | 8,0177 | 8,0092 | 8,0050 | 8,0040 | 8,0035 | 8,0039 | 8,0202 |

TABLE A2-29: Microprobe analyses along a traverse across a garnet grain in specimen HA 1041. Ionic proportions on the basis of 12 oxygens.

| Grain | 1A | 1B | 1C | 1D | 1E | 1F | 1G | 1H | 1I |
|---|---|---|---|---|---|---|---|---|---|
| $SiO_2$ | 36,847 | 37,030 | 37,321 | 37,550 | 37,670 | 37,868 | 37,816 | 37,787 | 37,450 |
| $TiO_2$ | - | - | - | - | - | - | - | - | - |
| $Al_2O_3$ | 21,527 | 21,705 | 21,673 | 21,785 | 21,848 | 21,941 | 22,014 | 21,014 | 21,876 |
| $FeO,Fe_2O_3$ | 32,719 | 31,729 | 31,355 | 30,657 | 30,259 | 30,247 | 30,132 | 30,109 | 29,552 |
| MnO | 3,318 | 3,044 | 3,008 | 2,949 | 2,872 | 2,877 | 2,925 | 2,919 | 2,926 |
| MgO | 4,097 | 4,723 | 5,128 | 5,754 | 5,925 | 6,158 | 6,191 | 6,290 | 6,177 |
| CaO | 1,313 | 1,337 | 1,380 | 1,381 | 1,382 | 1,330 | 1,318 | 1,258 | 1,278 |
| $Na_2O$ | 0,000 | - | - | - | - | - | - | - | - |
| $K_2O$ | 0,023 | - | - | - | - | - | - | - | - |
| TOTAL | 99,84 | 99,57 | 99,86 | 100,07 | 99,95 | 100,42 | 100,39 | 100,38 | 99,26 |
| Si | 2,9583 | 2,9617 | 2,9686 | 2,9679 | 2,9735 | 2,9725 | 2,9682 | 2,9659 | 2,9692 |
| Ti | - | - | - | - | - | - | - | - | - |
| Al | 2,0376 | 2,0466 | 2,0324 | 2,0300 | 2,0331 | 2,0304 | 2,0371 | 2,0371 | 2,0447 |
| Fe | 2,1969 | 2,1224 | 2,0858 | 2,0265 | 1,9975 | 1,9856 | 1,9780 | 1,9765 | 1,9594 |
| Mn | 0,2256 | 0,2062 | 0,2027 | 0,1974 | 0,1920 | 0,1912 | 0,1944 | 0,1941 | 0,1965 |
| Mg | 0,4902 | 0,5630 | 0,6078 | 0,6778 | 0,6969 | 0,7204 | 0,7242 | 0,7358 | 0,7298 |
| Ca | 0,1130 | 0,1145 | 0,1176 | 0,1169 | 0,1169 | 0,1118 | 0,1109 | 0,1058 | 0,1086 |
| Na | 0,0000 | - | - | - | - | - | - | - | - |
| K | 0,0023 | - | - | - | - | - | - | - | - |
| TOTAL | 8,0242 | 8,0148 | 8,0151 | 8,0169 | 8,0101 | 8,0123 | 8,0131 | 8,0154 | 8,0085 |

| Grain | 1J | 1K | 1L | 1M | 1N | 1O | 1P | 1Q |
|---|---|---|---|---|---|---|---|---|
| $SiO_2$ | 37,653 | 37,779 | 37,704 | 37,703 | 37,636 | 37,435 | 37,673 | 37,606 |
| $TiO_2$ | - | - | - | - | - | - | - | - |
| $Al_2O_3$ | 21,882 | 21,929 | 22,010 | 21,884 | 22,009 | 21,962 | 21,859 | 21,885 |
| $FeO,Fe_2O_3$ | 29,760 | 30,305 | 30,265 | 30,441 | 30,377 | 30,792 | 31,507 | 32,159 |
| MnO | 2,891 | 2,924 | 2,922 | 2,898 | 2,924 | 2,955 | 3,028 | 3,079 |
| MgO | 6,090 | 6,082 | 5,984 | 5,877 | 5,734 | 5,578 | 5,031 | 4,613 |
| CaO | 1,307 | 1,360 | 1,405 | 1,446 | 1,387 | 1,441 | 1,400 | 1,312 |
| $Na_2O$ | - | - | - | - | - | - | - | - |
| $K_2O$ | - | - | - | - | - | - | - | - |
| TOTAL | 99,58 | 100,38 | 100,29 | 100,25 | 100,06 | 100,16 | 100,50 | 100,65 |
| Si | 2,9761 | 2,9692 | 2,9660 | 2,9700 | 2,9691 | 2,9588 | 2,9758 | 2,9747 |
| Ti | - | - | - | - | - | - | - | - |
| Al | 2,0390 | 2,0319 | 2,0412 | 2,0324 | 2,0470 | 2,0465 | 2,0355 | 2,0409 |
| Fe | 1,9672 | 1,9919 | 1,9911 | 2,0055 | 2,0042 | 2,0354 | 2,0814 | 2,1275 |
| Mn | 0,1936 | 0,1946 | 0,1947 | 0,1933 | 0,1954 | 0,1978 | 0,2025 | 0,2063 |
| Mg | 0,7174 | 0,7124 | 0,7016 | 0,6899 | 0,6741 | 0,6570 | 0,5923 | 0,5438 |
| Ca | 0,1106 | 0,1145 | 0,1184 | 0,1221 | 0,1172 | 0,1220 | 0,1185 | 0,1112 |
| Na | - | - | - | - | - | - | - | - |
| K | - | - | - | - | - | - | - | - |
| TOTAL | 8,0042 | 8,0148 | 8,0133 | 8,0136 | 8,0073 | 8,0178 | 8,0063 | 8,0047 |

TABLE A2-30 Microprobe analyses of biotite in semipelitic gneiss - specimen HA 1041. Ionic proportions on the basis of 11 oxygens.

| Grain | 1A | 1B | 1C | 1D | 1E | 2 CORE | 3 CORE | 4A |
|---|---|---|---|---|---|---|---|---|
| $SiO_2$ | 36,509 | 36,378 | 36,629 | 36,557 | 36,865 | 36,575 | 36,675 | 36,438 |
| $TiO_2$ | 4,176 | 4,141 | 4,201 | 4,049 | 4,005 | 4,139 | 4,176 | 4,264 |
| $Al_2O_3$ | 16,837 | 16,651 | 16,773 | 16,863 | 16,748 | 16,792 | 16,695 | 17,018 |
| $FeO,Fe_2O_3$ | 15,223 | 15,267 | 14,852 | 14,801 | 14,938 | 15,118 | 14,874 | 15,263 |
| MnO | 0,052 | 0,039 | 0,049 | 0,042 | 0,055 | 0,063 | 0,062 | 0,061 |
| MgO | 14,214 | 14,135 | 14,098 | 14,291 | 14,186 | 14,176 | 14,194 | 13,773 |
| CaO | 0,029 | 0,022 | 0,047 | 0,032 | 0,032 | 0,028 | 0,014 | 0,033 |
| $Na_2O$ | 0,172 | 0,139 | 0,152 | 0,159 | 0,129 | 0,140 | 0,155 | 0,152 |
| $K_2O$ | 9,384 | 9,310 | 9,474 | 9,479 | 9,521 | 9,551 | 9,552 | 9,488 |
| TOTAL | 96,60 | 96,08 | 96,27 | 96,27 | 96,48 | 96,58 | 96,40 | 96,49 |
| Si | 2,6912 | 2,6965 | 2,7049 | 2,6992 | 2,7163 | 2,6973 | 2,7063 | 2,6906 |
| Ti | 0,2315 | 0,2308 | 0,2333 | 0,2248 | 0,2219 | 0,2295 | 0,2317 | 0,2368 |
| Al | 1,4632 | 1,4551 | 1,4602 | 1,4679 | 1,4548 | 1,4599 | 1,4524 | 1,4815 |
| Fe | 0,9385 | 0,9464 | 0,9172 | 0,9140 | 0,9205 | 0,9324 | 0,9179 | 0,9425 |
| Mn | 0,0032 | 0,0024 | 0,0031 | 0,0026 | 0,0034 | 0,0039 | 0,0039 | 0,0038 |
| Mg | 1,5616 | 1,5614 | 1,5516 | 1,5726 | 1,5578 | 1,5581 | 1,5610 | 1,5157 |
| Ca | 0,0023 | 0,0017 | 0,0037 | 0,0025 | 0,0025 | 0,0022 | 0,0011 | 0,0026 |
| Na | 0,0246 | 0,0199 | 0,0217 | 0,0228 | 0,0184 | 0,0200 | 0,0221 | 0,0217 |
| K | 0,8826 | 0,8804 | 0,8926 | 0,8930 | 0,8950 | 0,8986 | 0,8993 | 0,8938 |
| TOTAL | 7,7991 | 7,7952 | 7,7887 | 7,7998 | 7,7909 | 7,8024 | 7,7963 | 7,7895 |

| Grain | 4B | 4 CORE | 5A | 5B | 5C | 5D | 5E | 5F |
|---|---|---|---|---|---|---|---|---|
| $SiO_2$ | 36,383 | 36,809 | 36,336 | 36,349 | 36,455 | 36,223 | 36,211 | 36,295 |
| $TiO_2$ | 4,275 | 4,245 | 4,407 | 4,369 | 4,409 | 4,439 | 4,461 | 4,407 |
| $Al_2O3$ | 16,924 | 16,912 | 16,919 | 16,805 | 16,882 | 16,835 | 16,929 | 16,952 |
| $FeO,Fe_2O_3$ | 15,049 | 15,002 | 15,974 | 15,949 | 15,743 | 15,692 | 16,286 | 15,794 |
| MnO | 0,051 | 0,063 | 0,086 | - | - | - | - | - |
| MgO | 13,657 | 14,032 | 13,413 | 13,411 | 13,423 | 13,542 | 13,163 | 13,523 |
| CaO | 0,022 | 0,013 | 0,013 | 0,020 | 0,012 | 0,014 | 0,022 | 0,019 |
| $Na_2O$ | 0,161 | 0,137 | 0,109 | 0,161 | 0,167 | 0,139 | 0,133 | 0,099 |
| $K_2O$ | 9,361 | 9,409 | 9,319 | 9,359 | 9,404 | 9,483 | 9,244 | 9,330 |
| TOTAL | 95,88 | 96,62 | 96,57 | 96,42 | 96,49 | 96,37 | 96,45 | 96,42 |
| Si | 2,6993 | 2,7071 | 2,6877 | 2,6931 | 2,6939 | 2,6849 | 2,6848 | 2,6863 |
| Ti | 0,2385 | 0,2348 | 0,2451 | 0,2434 | 0,2452 | 0,2474 | 0,2487 | 0,2452 |
| Al | 1,4802 | 1,4662 | 1,4754 | 1,4679 | 1,4718 | 1,4711 | 1,4798 | 1,4790 |
| Fe | 0,9337 | 0,9227 | 0,9881 | 0,9882 | 0,9736 | 0,9727 | 1,0098 | 0,9776 |
| Mn | 0,0032 | 0,0039 | 0,0054 | - | - | - | - | - |
| Mg | 1,5101 | 1,5379 | 1,4786 | 1,4809 | 1,4794 | 1,4959 | 1,4545 | 1,4916 |
| Ca | 0,0017 | 0,0010 | 0,0010 | 0,0016 | 0,0009 | 0,0011 | 0,0017 | 0,0015 |
| Na | 0,0232 | 0,0195 | 0,0156 | 0,0231 | 0,0239 | 0,0199 | 0,0191 | 0,0142 |
| K | 0,8860 | 0,8827 | 0,8794 | 0,8846 | 0,8873 | 0,8968 | 0,8744 | 0,8809 |
| TOTAL | 7,7765 | 7,7763 | 7,7768 | 7,7832 | 7,7784 | 7,7903 | 7,7732 | 7,7766 |

TABLE A2-31: Microprobe analyses of mean garnet grain cores in semipelitic biotite-garnet gneiss. The number of analyses on which the mean is based is indicated in brackets. Ionic proportions on the basis of 12 oxygens.

| Sample No. | HA559 (5) | HA735 (4) | HA1041 (5) | HA1081 (5) |
|---|---|---|---|---|
| $SiO_2$ | 37,472 | 38,094 | 37,715 | 37,413 |
| $TiO_2$ | - | 0,033 | - | - |
| $Al_2O_3$ | 21,866 | 22,051 | 21,945 | 21,633 |
| FeO | 31,748 | 30,415 | 29,960 | 32,659 |
| MnO | 1,094 | 0,315 | 2,908 | 1,256 |
| MgO | 6,276 | 7,883 | 6,181 | 5,172 |
| CaO | 1,154 | 1,465 | 1,298 | 1,931 |
| $Na_2O$ | - | - | - | 0,018 |
| $K_2O$ | - | - | - | 0,000 |
| TOTAL | 99,61 | 100,26 | 100,01 | 100,08 |
| Si | 2,9645 | 2,9644 | 2,9704 | 2,9681 |
| Ti | - | 0,0019 | - | - |
| Al | 2,0393 | 2,0230 | 2,0377 | 2,0233 |
| Fe | 2,1006 | 1,9794 | 1,9733 | 2,1669 |
| Mn | 0,0733 | 0,0208 | 0,1940 | 0,0844 |
| Mg | 0,7400 | 0,9141 | 0,7255 | 0,6116 |
| Ca | 0,0978 | 0,1221 | 0,1095 | 0,1641 |
| Na | - | - | - | 0,0029 |
| K | - | - | - | 0,0000 |
| TOTAL | 8,0155 | 8,0257 | 8,0104 | 8,0213 |

TABLE A2-32: Microprobe analyses along a traverse across a garnet grain in specimen HA 1081. Ionic proportions on the basis of 12 oxygens.

| Grain | 1A | 1B | 1C | 1D | 1E | 1F | 1G | 1H | 1I |
|---|---|---|---|---|---|---|---|---|---|
| $SiO_2$ | 36,850 | 37,167 | 37,529 | 37,439 | 37,326 | 37,471 | 37,374 | 37,534 | 37,358 |
| $TiO_2$ | - | - | - | - | - | - | - | - | - |
| $Al_2O_3$ | 21,229 | 21,528 | 21,547 | 21,619 | 21,617 | 21,671 | 21,723 | 21,669 | 21,483 |
| $FeO,Fe_2O_3$ | 34,746 | 33,792 | 33,501 | 32,790 | 32,574 | 32,775 | 32,626 | 32,765 | 32,553 |
| MnO | 1,550 | 1,457 | 1,344 | 1,263 | 1,282 | 1,227 | 1,253 | 1,252 | 1,267 |
| MgO | 3,694 | 4,323 | 4,800 | 5,109 | 5,154 | 5,190 | 5,260 | 5,195 | 5,063 |
| CaO | 1,951 | 1,906 | 1,904 | 1,923 | 1,893 | 1,911 | 1,923 | 1,977 | 1,950 |
| $Na_2O$ | 0,025 | 0,016 | 0,015 | 0,027 | 0,025 | 0,000 | 0,032 | 0,022 | 0,013 |
| $K_2O$ | 0,005 | 0,000 | 0,014 | 0,000 | 0,000 | 0,000 | 0,000 | 0,000 | 0,000 |
| TOTAL | 100,05 | 100,19 | 100,65 | 100,17 | 99,87 | 100,24 | 100,19 | 100,41 | 99,69 |
| Si | 2,9630 | 2,9653 | 2,9718 | 2,9692 | 2,9673 | 2,9680 | 2,9615 | 2,9683 | 2,9755 |
| Ti | - | - | - | - | - | - | - | - | - |
| Al | 2,0123 | 2,0249 | 2,0115 | 2,0213 | 2,0260 | 2,0236 | 2,0292 | 2,0202 | 2,0173 |
| Fe | 2,3365 | 2,2548 | 2,2187 | 2,1749 | 2,1657 | 2,1711 | 2,1620 | 2,1671 | 2,1685 |
| Mn | 0,1055 | 0,0985 | 0,0901 | 0,0848 | 0,0863 | 0,0823 | 0,0841 | 0,0839 | 0,0855 |
| Mg | 0,4426 | 0,5140 | 0,5664 | 0,6039 | 0,6106 | 0,6126 | 0,6212 | 0,6123 | 0,6011 |
| Ca | 0,1681 | 0,1629 | 0,1615 | 0,1634 | 0,1612 | 0,1622 | 0,1632 | 0,1675 | 0,1664 |
| Na | 0,0039 | 0,0025 | 0,0023 | 0,0041 | 0,0040 | 0,0000 | 0,0050 | 0,0034 | 0,0021 |
| K | 0,0005 | 0,0000 | 0,0014 | 0,0000 | 0,0000 | 0,0000 | 0,0000 | 0,0000 | 0,0000 |
| TOTAL | 8,0330 | 8,0233 | 8,0242 | 8,0221 | 8,0216 | 8,0201 | 8,0265 | 8,0231 | 8,0167 |

| Grain | 1J | 1K | 1L | 1M | 1N | 1O | 1P | 1Q | 1R |
|---|---|---|---|---|---|---|---|---|---|
| $SiO_2$ | 37,398 | 37,288 | 37,438 | 37,505 | 37,308 | 37,297 | 37,148 | 37,127 | 36,743 |
| $TiO_2$ | - | - | - | - | - | - | - | - | - |
| $Al_2O_3$ | 21,444 | 21,515 | 21,591 | 21,703 | 21,498 | 21,725 | 21,537 | 21,479 | 21,464 |
| $FeO,Fe_2O_3$ | 32,882 | 33,667 | 32,995 | 32,922 | 32,871 | 33,101 | 33,218 | 33,770 | 34,198 |
| MnO | 1,308 | 1,349 | 1,331 | 1,325 | 1,379 | 1,420 | 1,432 | 1,476 | 1,588 |
| MgO | 5,015 | 4,388 | 4,912 | 4,945 | 4,621 | 4,756 | 4,578 | 4,066 | 3,558 |
| CaO | 1,970 | 1,911 | 2,005 | 1,999 | 1,929 | 1,911 | 1,893 | 1,852 | 1,900 |
| $Na_2O$ | 0,026 | 0,021 | 0,058 | 0,001 | 0,015 | 0,012 | 0,046 | 0,001 | 0,017 |
| $K_2O$ | 0,000 | 0,000 | 0,000 | 0,000 | 0,000 | 0,000 | 0,000 | 0,000 | 0,001 |
| TOTAL | 100,04 | 100,14 | 100,33 | 100,40 | 99,62 | 100,22 | 99,85 | 99,77 | 99,47 |
| Si | 2,9732 | 2,9724 | 2,9691 | 2,9696 | 2,9794 | 2,9629 | 2,9664 | 2,9745 | 2,9642 |
| Ti | - | - | - | - | - | - | - | - | - |
| Al | 2,0098 | 2,0219 | 2,0187 | 2,0258 | 2,0240 | 2,0347 | 2,0275 | 2,0287 | 2,0414 |
| Fe | 2,1863 | 2,2445 | 2,1884 | 2,1800 | 2,1954 | 2,1992 | 2,2184 | 2,2627 | 2,3073 |
| Mn | 0,0881 | 0,0911 | 0,0894 | 0,0888 | 0,0932 | 0,0956 | 0,0968 | 0,1001 | 0,1085 |
| Mg | 0,5942 | 0,5213 | 0,5806 | 0,5834 | 0,5500 | 0,5631 | 0,5448 | 0,4855 | 0,4277 |
| Ca | 0,1678 | 0,1632 | 0,1703 | 0,1695 | 0,1650 | 0,1627 | 0,1619 | 0,1589 | 0,1642 |
| Na | 0,0040 | 0,0033 | 0,0090 | 0,0002 | 0,0023 | 0,0019 | 0,0072 | 0,0002 | 0,0027 |
| K | 0,0000 | 0,0000 | 0,0000 | 0,0000 | 0,0000 | 0,0000 | 0,0000 | 0,0000 | 0,0001 |
| TOTAL | 8,0238 | 8,0181 | 8,0259 | 8,0177 | 8,0096 | 8,0205 | 8,0233 | 8,0111 | 8,0165 |

TABLE A2-33: Microprobe analyses of biotite in semipelitic gneiss - specimen HA 1081. Ionic proportions on the basis of 11 oxygens.

| Grain | 1A | 1B | 1C | 2A | 2B | 2C | 3A | 3B |
|---|---|---|---|---|---|---|---|---|
| $SiO_2$ | 34.396 | 34.998 | 34.987 | 34.865 | 34.992 | 34.920 | 35.005 | 34.947 |
| $TiO_2$ | 3.309 | 3.445 | 3.399 | 3.598 | 3.631 | 3.602 | 3.679 | 3.651 |
| $Al_2O_3$ | 17.426 | 17.434 | 17.706 | 17.001 | 17.272 | 17.375 | 17.558 | 17.573 |
| $FeO,Fe_2O_3$ | 20.840 | 21.112 | 20.380 | 21.163 | 20.603 | 20.882 | 20.794 | 20.888 |
| MnO | 0.046 | 0.034 | 0.030 | 0.030 | 0.021 | 0.025 | 0.026 | 0.031 |
| MgO | 10.603 | 10.255 | 10.070 | 10.016 | 10.210 | 10.010 | 10.054 | 10.009 |
| CaO | 0.013 | 0.020 | 0.001 | 0.024 | 0.009 | 0.014 | 0.000 | 0.004 |
| $Na_2O$ | 0.079 | 0.075 | 0.099 | 0.103 | 0.058 | 0.073 | 0.071 | 0.096 |
| $K_2O$ | 9.257 | 9.555 | 9.487 | 9.485 | 9.548 | 9.447 | 9.593 | 9.621 |
| TOTAL | 95.97 | 96.93 | 96.16 | 96.28 | 96.35 | 96.35 | 96.78 | 96.82 |
| Si | 2.6301 | 2.6519 | 2.6609 | 2.6627 | 2.6616 | 2.6582 | 2.6522 | 2.6491 |
| Ti | 0.1903 | 0.1963 | 0.1944 | 0.2066 | 0.2077 | 0.2062 | 0.2096 | 0.2081 |
| Al | 1.5709 | 1.5574 | 1.5876 | 1.5307 | 1.5488 | 1.5593 | 1.5683 | 1.5704 |
| Fe | 1.3327 | 1.3379 | 1.2963 | 1.3516 | 1.3106 | 1.3294 | 1.3176 | 1.3242 |
| Mn | 0.0029 | 0.0022 | 0.0019 | 0.0019 | 0.0013 | 0.0015 | 0.0017 | 0.0020 |
| Mg | 1.2083 | 0.1580 | 1.1414 | 1.1400 | 1.1574 | 1.1356 | 1.1352 | 1.1307 |
| Ca | 0.0011 | 0.0016 | 0.0000 | 0.0019 | 0.0007 | 0.0011 | 0.0000 | 0.0003 |
| Na | 0.0117 | 0.0110 | 0.0146 | 0.0152 | 0.0086 | 0.0107 | 0.0105 | 0.0141 |
| K | 0.9031 | 0.9237 | 0.9205 | 0.9241 | 0.9265 | 0.9174 | 0.9273 | 0.9304 |
| TOTAL | 7.8515 | 7.8404 | 7.8183 | 7.8352 | 7.8237 | 7.8199 | 7.8228 | 7.8298 |

| Grain | 3C | 3D | 3E | 3F | 4A | 4B | 4C |
|---|---|---|---|---|---|---|---|
| $SiO_2$ | 35.096 | 35.011 | 34.979 | 34.908 | 35.026 | 35.241 | 35.184 |
| $TiO_2$ | 3.523 | 3.485 | 3.502 | 3.391 | 3.687 | 3.730 | 3.688 |
| $Al_2O_3$ | 17.500 | 17.644 | 17.714 | 17.907 | 17.794 | 17.586 | 17.676 |
| $FeO,Fe_2O_3$ | 20.592 | 20.419 | 20.815 | 20.489 | 20.345 | 20.288 | 20.431 |
| MnO | 0.041 | 0.056 | 0.050 | 0.028 | 0.025 | 0.027 | 0.026 |
| MgO | 10.107 | 10.262 | 10.186 | 10.256 | 10.363 | 10.294 | 10.355 |
| CaO | 0.012 | 0.018 | 0.011 | 0.032 | 0.013 | 0.000 | 0.000 |
| $Na_2O$ | 0.065 | 0.090 | 0.092 | 0.110 | 0.136 | 0.123 | 0.090 |
| $K_2O$ | 9.507 | 9.426 | 9.449 | 9.477 | 9.355 | 9.435 | 9.495 |
| TOTAL | 96.44 | 96.41 | 96.80 | 96.60 | 96.74 | 96.72 | 96.94 |
| Si | 2.6642 | 2.6558 | 2.6478 | 2.6442 | 2.6452 | 2.6612 | 2.6533 |
| Ti | 0.2011 | 0.1988 | 0.1993 | 0.1932 | 0.2094 | 0.2118 | 0.2091 |
| Al | 1.5662 | 1.5779 | 1.5808 | 1.5991 | 1.5842 | 1.5656 | 1.5715 |
| Fe | 1.3073 | 1.2954 | 1.3177 | 1.2980 | 1.2849 | 1.2813 | 1.2885 |
| Mn | 0.0026 | 0.0036 | 0.0032 | 0.0018 | 0.0016 | 0.0017 | 0.0016 |
| Mg | 1.1434 | 1.1602 | 1.1491 | 1.1578 | 1.1662 | 1.1585 | 1.1638 |
| Ca | 0.0010 | 0.0014 | 0.0009 | 0.0026 | 0.0010 | 0.0000 | 0.0000 |
| Na | 0.0095 | 0.0133 | 0.0136 | 0.0162 | 0.0200 | 0.0180 | 0.0131 |
| K | 0.9207 | 0.9122 | 0.9125 | 0.9158 | 0.9013 | 0.9089 | 0.9135 |
| TOTAL | 7.8166 | 7.8190 | 7.8254 | 7.8290 | 7.8141 | 7.8075 | 7.8150 |

# APPENDIX III. LOCALITY MAP FOR SPECIMENS ANALYSED BY ELECTRON MICROPROBE.

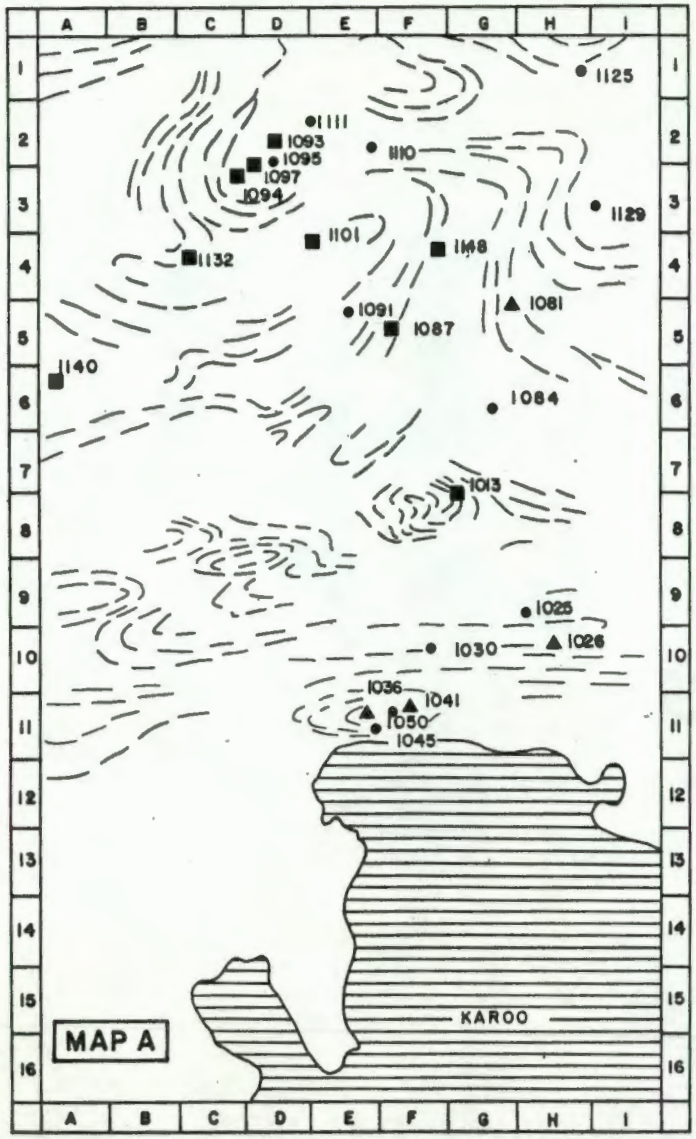


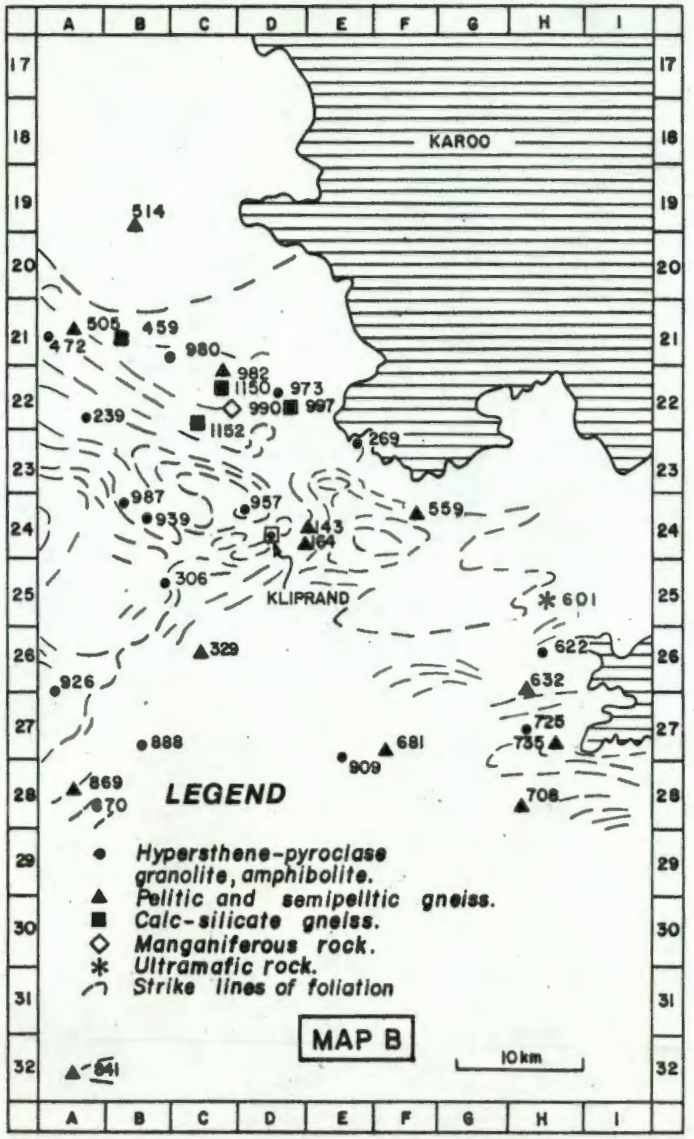

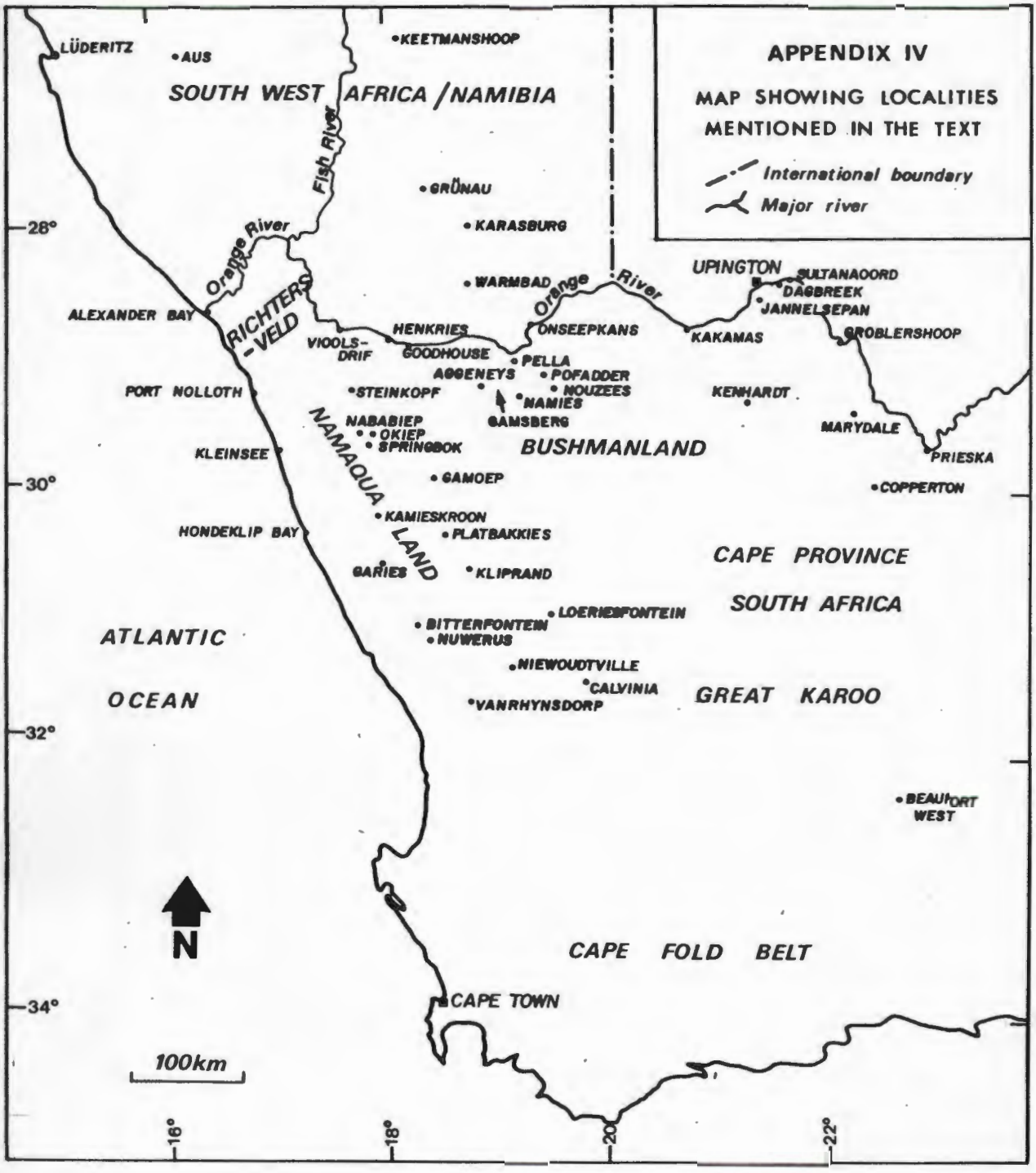
APPENDIX IV
MAP SHOWING LOCALITIES MENTIONED IN THE TEXT
International boundary
Major river
LÜDERITZ
AUS
KEETMANSHOOP
SOUTH WEST AFRICA / NAMIBIA
Fish River
GRÜNAU
KARASBURG
Orange River
28°
WARMBAD
Orange River
UPINGTON
SULTANAOORD
DAGBREEK
JANNELSEPAN
ALEXANDER BAY
RICHTERS-VELD
HENKRIES
ONSEEPKANS
KAKAMAS
GROBLERSHOOP
VIOOLS-DRIF
GOODHOUSE
PELLA
AGGENEYS
POFADDER
PORT NOLLOTH
STEINKOPF
NOUZEES
NAMIES
KENHARDT
NABABIEP
GAMSBERG
MARYDALE
OKIEP
SPRINGBOK
BUSHMANLAND
KLEINSEE
PRIESKA
NAMAQUA LAND
30°
GAMOEP
COPPERTON
KAMIESKROON
HONDEKLIP BAY
PLATBAKKIES
CAPE PROVINCE
SOUTH AFRICA
GARIES
KLIPRAND
LOERIESFONTEIN
BITTERFONTEIN
ATLANTIC
NUWERUS
OCEAN
NIEWOUDTVILLE
CALVINIA
GREAT KAROO
VANRHYNSDORP
32°
BEAUFORT WEST
N
CAPE FOLD BELT
34°
CAPE TOWN
100km
16°
18°
20°
22°

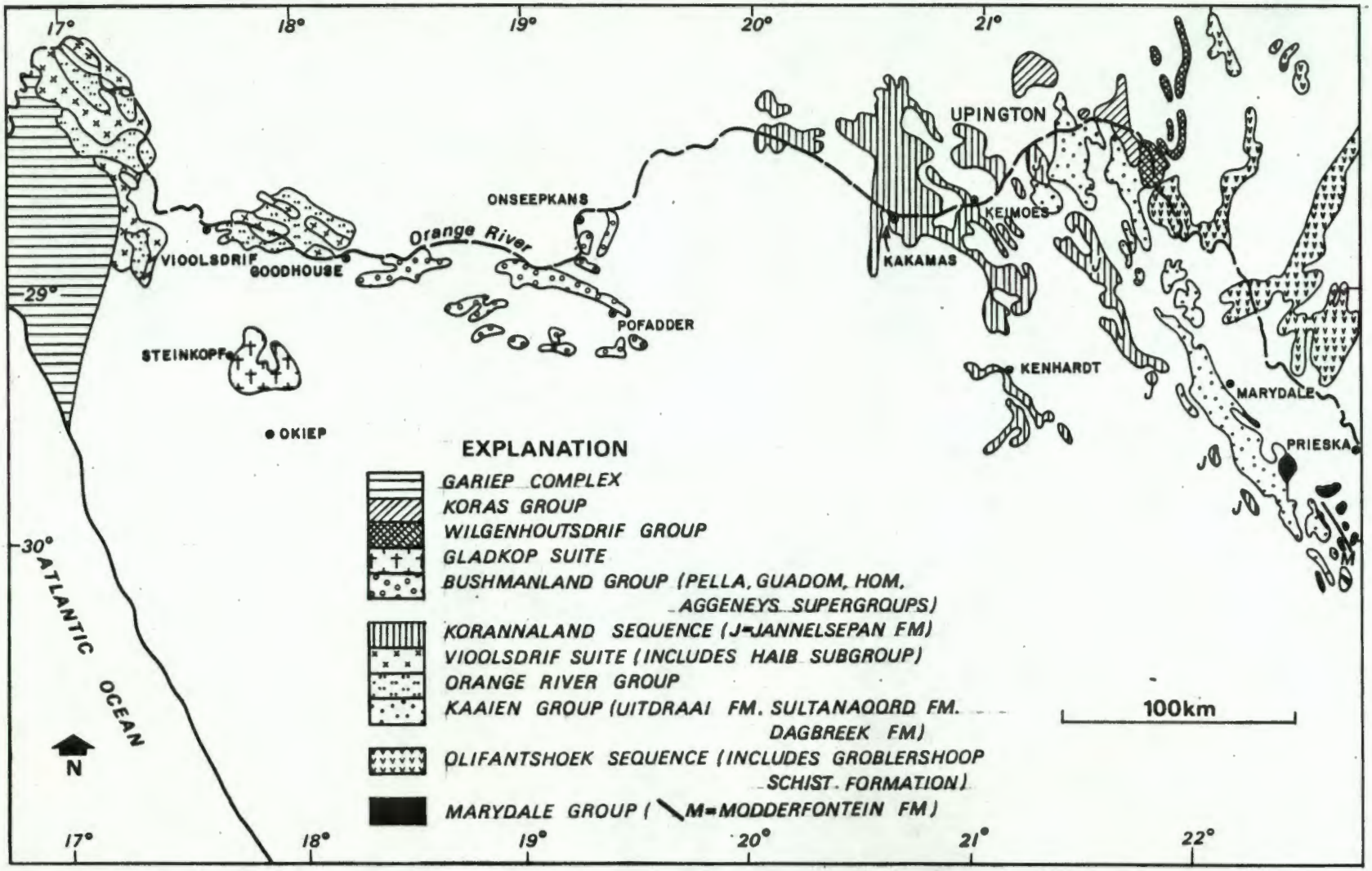


**APPENDIX V. SKETCH MAP SHOWING THE DISTRIBUTION OF LITHOSTRATIGRAPHIC UNITS MENTIONED IN THE TEXT.**

Plate 1 Ophthalmic migmatite. The "augen" structures are composed of coarse quartzo-feldspathic segregations and are surrounded by thin melanosomes resembling eyelids. Farm Aasvogel Kop (403).

Plate 2 Euhedral garnet porphyroblasts surrounded by leucocratic quartzo-feldspathic "haloes" in a semipilitic gneiss. Farm Roode Kloof (14).

Plate 3 Stromatic migmatite displaying boudinage structures. Farm Daauws (404).

Plate 4 Stromatic migmatite with isoclinally folded leucosomes sandwiched between planar leucosomes. Farm Daauws (404).

Plate 5 Three generations of leucosomes in a semipelitic gneiss. Farm Kamas (405).

Plate 6 Agmatite with slightly rotated angular fragments surrounded by garnetiferous leucosomes. The spotted appearance of the leucosomes is caused by garnet porphyroblasts. Farm Tafelberg (64).

Plate 7 Schlieric migmatite. Numerous large garnet porphyroblasts in the leucosomes account for the spotted nature of this rock. Farm Aasvogel Kop (403).

Plate 8 $D_3$ minor fold generated by flexural slip-type deformation. Farm Obeeb (8).

BUT 84/2504

# KLIPRAND AREA

## MAP A

## NORTH SHEET

ANNEXURE 1

# GEOLOGICAL MAP OF THE AREA AROUND AND NORTH OF KLIPRAND

SCALE 1:100 000

0 1 2 3 4 5 6 7 8 9 10 km

KEY

- Farm boundary
- Farm name
- Farmhouse settlement.
- Main Road.
- Trigonometrical beacon
- Pan.
- Drainage Channel.
- Lithological contact.
- Limit of outcrop
- Intrusive relationship
- Established fault
- Inferred or concealed fault
- Strike and dip of foliation/gneissic banding
- Vertical foliation
- Strike and dip of bedding
- Direction and plunge of mineral lineation
- Horizontal mineral lineation
- Lineation on foliation
- Lines of strike ex aerial photographs
- Prominent lineaments ex aerial photographs
- Mylonite zones
- Finely refoliated rock
- Mine or prospect (Cu-copper)

LOCALITY MAP

SWA/NAMIBIA — Upington, Vioolsdrif, Orange River, Pofadder, Aggeneys, Springbok, AREA MAPPED, Prieska, Garies, Kliprand, Bitterfontein, REPUBLIC OF SOUTH AFRICA, Cape Town

Mapped and compiled by H. M. Albat. Drawn by Mrs R. M. E. Kovats 1982. Colour separation by Ms v.d. Meiracker & R. M. E. Kovats 1983. Precambrian Research Unit, Department of Geology, University of Cape Town. ©

(META)SEDIMENTARY & (META)VOLCANIC ROCKS

- Superficial deposits (unconsolidated sand, calcrete, alluvium and surface (k = kaolinised rock).
- Shale, carbonaceous shale, sandstone, diamictite, tillite and arkose with boulders (includes dolerite sills).
- Shale (Phyllite), sandstone, grit, conglomerate, minor carbonate rocks.
- White feldspathic quartzite and conglomerate.

PRETECTONIC MOKOLIAN GNEISSES

- Calc-silicate gneiss.
- Ditto (subcrop).
- Semipelitic biotite-garnet gneiss, pelitic gneiss, calc-silicate gneiss and hypersthene-pyroclase granolite.
- Marble, minor quartzite, calc-silicate gneiss.
- Aluminous (pelitic) gneiss.
- Pelitic gneiss with hypersthene.
- Semipelitic pink quartzo-feldspathic gneiss (minor cordierite, garnet, sillimanite and hercynite), migmatitic gneiss.
- Quartz - biotite - muscovite schist, quartz-muscovite schist.
- Semipelitic biotite-garnet-bearing migmatite, minor feldspathic quartzite, aluminous gneiss, calc-silicate gneiss, hypersthene-pyroclase granolite and iron formation.
- Metaquartzite.
- Feldspathic quartzite, locally ferruginous.
- Migmatitic biotite-garnet gneiss, graphitic quartzite, hypersthene-pyroclase granolite, aluminous quartzo-feldspathic gneiss and iron formation.
- White quartz-feldspar-garnet rock.
- Undifferentiated pink gneiss.
- Ditto (subcrop).
- Quartzo-feldspathic gneiss (with ... content).
- Pink gneiss.
- Pink quartzo-feldspathic gneiss with minor altered amphibole.
- Migmatitic quartzo-feldspathic gneiss.
- Plagioclase-quartz-biotite gneiss with small quartz augen.
- Iron formation.
- Amphibolite.
- Granolite.

INTRUSIVE ROCKS

| | | |
|---|---|---|
| TERTIARY TO RECENT | | |
| CRETACEOUS | | Diatreme (possible and confirmed kimberlite pipe). Olivine – melilite basalt. |
| CARBONIFEROUS TO JURASSIC | KAROO SEQUENCE | Karoo dolerite. |
| NAMIBIAN | NAMA GROUP | |

SYNTECTONIC MOKOLIAN INTRUSIVE ROCKS

- Major quartz vein.
- Various dyke rocks (frequently sheared)
- Klein-Lieslap megacrystic charno-enderbite.
- Klein Matjesfontein alkali feldspar granite-gneiss.
- Roode Kloof granite-gneiss.
- Burtons Puts megacrystic granite-gneiss.
- Daauws megacrystic granite-gneiss.
- Uilklip megacrystic granite-gneiss.
- Megacrystic leucocratic granite-gneiss.
- Lepel megacrystic granite-gneiss.
- Banke megacrystic granodiorite-gneiss.
- Klein Banken megacrystic granodiorite-gneiss.
- Ekstensie megacrystic granodiorite-gneiss.
- Karagas hornblende-quartz monzonite-gneiss.
- Kliprand charnockite suite; charnockite, charno-enderbite, minor pyroxene monzonite and monzo-norite.
- Olivine-bearing mafic and ultramafic bodies.
- Obees ultramafic body (hornblende + olivine + orthopyroxene + spinel)
- Bosluis and Nuwefontein basic bodies.
- Augen gneiss and streaky quartzo-feldspathic gneiss.
- Ditto (subcrop).
- Undifferentiated grey gneiss (includes para- and orthogneiss).

NOT IN STRATIGRAPHIC ORDER

MOKOLIAN — NAMAQUALAND METAMORPHIC COMPLEX

BUT 84/2504

# KLIPRAND AREA

MAP B

SOUTH SHEET

ANNEXURE 2

30°15'S

18°45'E

18°30'E

19°00'E

31°00'S

Platbakkies
Ons
Groenvlei
Stofvlei
Graslaagte
Spioenkop
Langpan
Roolmond
Gannalaagte
Bitterfontein
Gannaputs
Dabidas
Klipfontein
Kliprand
Kamas
Oubees
Daauws
Langberg
Kokerboomkraal
Grootklip
Bloubok
Sout
Rietmond
Vaalkoppie
Kleinlieslaap
Kobeep
Wielspoor
Warmvlool
Tafelberg
Rietkloof
Uilklip
Kruispad
Dassiepis
Ekstensie
Slagkop
Vaaldam
Droehout
Witklip

PLAT-BAKKIES 388
DAAS DAAP 378
SKIMMELKOP 377
ZWART RAND 375
ROODE MOND 392
SARAIP 393
ZAND VLEI 390
SPION KOP 391
LANG PAN 395
PLATT PENS 394
BURTONS PUTS 408
ALEWYN FONTEIN 389
BANKE 409
BOVENSTE VLEI 398
GANNA LAAGTE 397
BITTER FONTEIN 396
DABIDAS 407
MATJES-FTN. 5
MIDDEL POST 3
KLEIN MATJESFONTEIN 2
NUWE-FONTEIN 6
ONDERSTE VLEI 399
UITVAL 400
PREEK STOEL KOP 401
DOOD DRINK 406
KAMAS 405
OBEES 402
OBEES 8
RIETMOND 24
HAARBEEN 23
UITKYK 9
KOKER BOOM KRAAL 13
DAAUWS 404
AASVOGEL KOP 403
LANGE BERG 271
ROODE KLOOF 14
KLIPPLAAT 328
KAMABOOS 22
LIESLAP 21
WARM VLOOL 20
WIELSPOOR 73
DE PUT 66
GROOT KLIP 16
TAFELBERG 64
TAFELBERG EXT. 1
TAFELBERG EXT. 2 67
UILKLIP 65
ROODE WAL 74
SAMUELSVLAKTE 81
ZUID GROOT KLIP 18
ROODE SLOOT VLAKTE 123
WOLVE GRAV WATER 330
KRUISPAD 72
LEEUW KUIL 75
BUSHMANS GRAAF WATER 68
KLEIN BANKEN 59
BANKEN 58
BRANDEWYNS KRAAL 69
STEENKAMPS KRAAL 70
NABEEP 102
MELKBOSCH VLAKTE 71
77 ZOOVOORBY
DUIKER VLAKTE 78
KALK GAT VLAKTE 84
KANAKIES 332
BEEST VLAKTE 80
SPRINGBOK VLAKTE 82
DROOGE HOUTS BERG FLATS A 331
ALEWYNS VLAKTE 79
LOT B DROOGE HOUTSBERG VLAKTE 83
KLEIN GRAAF WATER 333
EEN KOKER BOOM VLAKTE 76
VLERMUIS 31°00'S GAT 104

SPRINGBOK
BITTERFONTEIN
LOERIESFONTEIN
VANRHYNSDORP
POFADDER

BUT 84/2504

ANNEXURE 3

MAP B